COINAGE COMPLEXES IN C-C AND C-N BOND-FORMING REACTIONS

Ángel Luis Mudarra Alonso

UNIVERSITAT ROVIRA i VIRGILI

Coinage Metal Complexes in C–C and C–N Bond-forming Reactions

ÁNGEL LUIS MUDARRA ALONSO

DOCTORAL THESIS
2019

UNIVERSITAT ROVIRA I VIRGILI
COINAGE COMPLEXES IN C-C AND C-N BOND-FORMING REACTIONS
Ángel Luis Mudarra Alonso

UNIVERSITAT ROVIRA I VIRGILI
COINAGE COMPLEXES IN C-C AND C-N BOND-FORMING REACTIONS
Ángel Luis Mudarra Alonso

Ángel Luis Mudarra Alonso

Coinage Metal Complexes in C–C and C–N Bond-forming Reactions

DOCTORAL THESIS

Supervised by Prof. Feliu Maseras Cuní and Dr. Mónica Helvia Pérez Temprano

Institut Català d'Investigació Química (ICIQ)

UNIVERSITAT ROVIRA i VIRGILI

Tarragona, 2019

UNIVERSITAT ROVIRA I VIRGILI
COINAGE COMPLEXES IN C-C AND C-N BOND-FORMING REACTIONS
Ángel Luis Mudarra Alonso

ICIQ - Institut Català d'Investigació Química

Avgda., Països Catalans 16,

43007 Tarragona (Spain)

Prof. Feliu Maseras Cuní and Dr. Mónica Helvia Pérez Temprano, group leaders at the Institute of Chemical Research of Catalonia,

We STATE that the present study, entitled “Coinage Metal Complexes in C–C and C–N Bond-forming Reactions”, presented by Ángel Luis Mudarra Alonso to award the degree of Doctor, has been carried out under our supervision at the Institut Català d´Investigació Química (ICIQ) and that it fulfills all the requirements to be eligible for the International Doctor Distinction.

Tarragona, November 26th, 2019.

Doctoral Thesis Supervisors

Prof. Feliu Maseras Cuní

Dr. Mónica Helvia Pérez Temprano

UNIVERSITAT ROVIRA I VIRGILI
COINAGE COMPLEXES IN C-C AND C-N BOND-FORMING REACTIONS
Ángel Luis Mudarra Alonso

Como la trucha al trucho

Como el helado al cucurucho

Como la madera al serrucho

Como la escopeta al cartucho

Como la lechuza al lechuzo

…

A mi familia de su Mudarrilla

UNIVERSITAT ROVIRA I VIRGILI
COINAGE COMPLEXES IN C-C AND C-N BOND-FORMING REACTIONS
Ángel Luis Mudarra Alonso

“Desde que te vi venir, dije: a por la burra viene”

Amparo Alonso Maraver, canción popular

UNIVERSITAT ROVIRA I VIRGILI
COINAGE COMPLEXES IN C-C AND C-N BOND-FORMING REACTIONS
Ángel Luis Mudarra Alonso

Acknowledgments

The presented work has been carried out with the support of the following institutions:

UNIVERSITAT ROVIRA I VIRGILI
COINAGE COMPLEXES IN C-C AND C-N BOND-FORMING REACTIONS
Ángel Luis Mudarra Alonso

PUBLICATIONS

Publications arising from this work:

1. "*Catalytic Nitrene Transfer To Alkynes: A Novel and Versatile Route for the Synthesis of Sulfinamides and Isothiazoles*"
   Rodríguez, M. R.; Beltrán, A.; Mudarra, Á. L.; Álvarez, E.; Maseras, F.; Díaz-Requejo, M. M.; Pérez, P. J. *Angew. Chem. Int. Ed.* **2017**, *56*, 12842.

2. *"New Vistas in Transmetalation with Discrete "$AgCF_3$" Species: Implications in Pd-Mediated Trifluoromethylation Reactions"*
   Martínez de Salinas, S.; Mudarra, Á. L.; Benet-Buchholz, J.; Parella, T.; Maseras, F.; Pérez-Temprano, M. H. *Chem. Eur. J.* **2018**, *24*, 11895.
   Special Issue: 7th EuCheMS Chemistry Congress

3. *"Beyond the traditional roles of Ag in catalysis: the transmetalating ability of organosilver(I) species in Pd-catalysed reactions"*
   Mudarra, A. L.; Martínez de Salinas, S.; Pérez-Temprano, M. H. *Org. Biomol. Chem.* **2019**, *17*, 1655.
   Special Issues: Catalysis & biocatalysis in OBC & New Talent

4. *"Exploring the role of coinage metallates in trifluoromethylation: a combined experimental and theoretical study"*
   Martínez de Salinas, S.; Mudarra, Á. L.; Odena, C.; Belmonte, M. M.; Benet-Buchholz, J.; Maseras, F.; Pérez-Temprano, M. H. *Chem. Eur. J.* **2019**, *25*, 9390.
   Special Issue: OMCOS 20, Heidelberg

5. *"Nucleophilic Trifluoromethylation Reactions Involving Copper(I) Species: From Organometallic Insights to Scope"*
   Mudarra, Á. L.; Martínez de Salinas, S.; Pérez-Temprano, M. H. *Synthesis*, **2019**, *51*, 2809.
   Special Issue: Future Stars in Organic Chemistry

6. *"Sustainable knowledge-driven approaches in transition metal catalyzed Transformations"*
   Mudarra, Á. L., Sanjosé-Orduna, J., Martínez de Salinas, S., Pérez-Temprano, M.H. *ChemSusChem* **2019**, *12*, 2882.
   Special Issue: Sustainable Organic Synthesis

UNIVERSITAT ROVIRA I VIRGILI
COINAGE COMPLEXES IN C-C AND C-N BOND-FORMING REACTIONS
Ángel Luis Mudarra Alonso

TABLE OF CONTENTS

ABBREVIATIONS AND ACRONYMS -1-
A PERSONAL CONNECTION. From Tartessos to C–C and C–N bond-forming reactions -3-
ABSTRACT -5-
CHAPTER 1. *General introduction and objectives* -7-
1.1. Coinage metals as additives in organic synthesis -7-
1.2. Bimetallic dual catalysis -8-
1.3. Transmetalation step -12-
1.4. Trifluoromethylation reactions -15-
1.5. General objectives -18-
CHAPTER 2. *Unexpected cooperation in a bimetallic dual Rh/Cu catalytic system: DFT and microkinetic simulation as interrogating tools* -19-
2.1. Introduction -19-
2.1.1. Cu-containing oxidants in oxidative coupling systems -21-
2.1.2. Theoretical approach to discriminate mechanisms in complex systems -28-
2.2. Objectives -32-
2.3. Results and discussion -33-
2.3.1. Model system and computational methods -33-
2.3.2. Mechanistic investigation on the Cu^{I}-catalyzed denitrogenative reductive formation of imine from α-aryl vinyl azide -34-
2.3.3. Evaluation of the system using $[(Cp)Rh(OAc)_2]$ as active catalyst -37-
2.3.4. Evaluation of the system using $[(Cp)Rh(Cl)_2]$ as active catalyst -40-
2.3.5 Evaluation of $[(Cp)Rh(Cl)_2]$ and $[Cu(OAc)_2]_2$ as reals catalysts -44-
2.3.6. Evaluation of the regioselectivity when using *m*-bromo-substituted α-phenyl vinyl azides -52-
2.4. Conclusions -55-
2.5. Computational Appendix -56-
2.5.1. DFT calculations -56-
2.5.2. Microkinetic modeling -61-
2.6 References and notes -78-
CHAPTER 3. N*ew vistas in transmetalation with discrete Ag-CF_3 species: implications in Pd-mediated trifluoromethylation reactions* -81-
3.1. Introduction -81-
3.1.1. Thermolysis of phosphine-stabilized $[(L)_nPd(Ar)(CF_3)]$ intermediate -83-
3.1.2. Challenges associated to the formation of $[(L)_nPd(Ar)(CF_3)]$ intermediate -90-
3.1.3. Pd-catalyzed nucleophilic trifluoromethylation of aromatic acyl fluorides -95-
3.1.4. Trifluoromethylsilver(I) nucleophiles as transmetalating candidates -96-
3.2. Objectives -98-
3.3. Results and discussion -99-
3.3.1. Evaluating CF_3-containing transmetalating agents using a model system -99-
3.3.2. Translation to a productive system in the C–C bond formation: [(Xantphos)Pd(Ph)(I)] -110-
3.4. Conclusions -121-
3.5. Appendixes -122-
3.5.1. Experimental appendix -122-
3.5.2. Computational details -151-
3.6. References and notes -153-
CHAPTER 4. *Mechanistic studies on the transmetalation step in Pd/Ag bimetallic systems* -157-
4.1. Introduction -157-
4.1.1. Pd/Ag-catalyzed decarboxylative coupling reactions -158-

4.1.2. Pd-catalyzed/Ag-mediated C–H activation reactions -164-
4.1.3. Pd-catalyzed/Ag-catalyzed or mediated difluoromethylation reactions -170-
4.2. Objectives -172-
4.3. Results and discussion -173-
4.3.1. Selection of the model reaction -173-
4.3.2. Evaluation the group exchange using a neutral species (**1a**) in equilibrium with an ionic part (**1b**) -174-
4.3.3. Evaluation the group exchange when using an ionic species (**2**). -187-
4.4. Conclusions -200-
4.5. Appendixes -201-
4.5.1. Experimental appendix -201-
4.5.2. Computational appendix -227-
4.6 References and notes -240-
CHAPTER 5. *Exploring bis-(trifluoromethyl) coinage metallates landscape: a combined experimental and theoretical study* -243-
5.1. Introduction -243-
5.1.1. Bis-(trifluoromethyl) aurates -243-
5.1.2. Bis-(trifluoromethyl) argentates -244-
5.1.3. Bis-(trifluoromethyl) cuprates -247-
5.1.4. Bis-(trifluoromethyl) cuprates associated to *in situ* generated (trifluoromethyl) copper(I) species -248-
5.1.5. Bis-(trifluoromethyl) cuprates from the equilibrium of well-defined trifluoromethyl copper(I) species -255-
5.1.6. Recent advances on the reactivity of different trifluoromethylation protocols -259-
5.2. Objectives -261-
5.3. Results and discussion -26-
5.3.1. Synthesis, characterization and theoretical analysis of different $[Cs][M(CF_3)_2]$ -26-
5.3.2. Reactivity of $[Cs][M(CF_3)_2]$ -266-
5.3.3. Mechanistic investigations on the reaction of $[Cs][Cu(CF_3)_2]$ with aryl halides -271-
5.4. Conclusions -280-
5.5. Appendixes -281-
5.5.1. Experimental appendix -281-
5.5.2. Computational appendix -293-
5.6. References and notes -305-
CHAPTER 6. *General conclusions* -309-

ABBREVIATIONS AND ACRONYMS

In this Dissertation, we have used the standard abbreviations and acronyms for the "Guideline of Authors" of the Journal of Organic Chemistry. For ease of reading, the meaning of abbreviations and acronyms are specified the first time that appear in each Chapters. Additional abbreviations and acronyms use in this manuscript are listed as follows:

AI	Alkyne Insertion
anhyd	anhydrous
Bc	Bathocuproine
Brettphos	2-(dicyclohexylphosphino)-3,6-dimethoxy-2',4',6'-triisopropyl-1,1'-biphenyl
CMD	Concerted Metalation-Deprotonation
Cp	Cyclopentadienyl
Cp*	*1,2,3,4,5*-pentamethylcyclopentadienyl
dfmpe	1,2-bis(trifluoromethyl)ethane
dppbz	1,2-bis(diphenylphosphino)benzene)
dppe	1,2-bis(diphenylphosphino)ethane
dppf	1,1'-bis(diphenylphosphino)ferrocene
dppp	1,2-bis(diphenylphosphino)propane
D'BPF	1,1'-bis(di-tert-butylphosphine)ferrocene
HAT	Hydrogen Atom Transfer
KBBs	knowledge building blocks
KIE	Kinetic Isotopic Effect
MI	Migratory Insertion
MS	Molecular Sieve
Nu	Nucleophile
OA	Oxidative Addition
OAc	Acetate
OIRE	Oxidatively Induced Reductive elimination
ORTEP	Oak Ridge Thermal Ellipsoid Plot
Phen	Phenantroline
PhINTs	[N-(p-Toluensulfonyl)imino]phenyliodinane
RC	Reaction Coordinate
RE	Reductive Elimination
ref.	Reference
Ruphos	2-(dicyclohexylphosphino)-2',6'-diisopropoxybiphenyl)
SIMes	1,3-bis(2,4,6-trimethylphenyl)-4,5-dihydroimidazol-2-ylidene
SIPr	1,3-bis(2,6-diisopropylphenyl)imidazol-2-ylidene
'Bu-bpy	4,4'-di-tert-butyl-2,2'-bipyridyl
TM	Transition Metal
TMEDA	N,N'-tetramethylethylene diamine
Transm	Transmetalation
Xantphos	4,5-bis(diphenylphosphino)-9,9-dimethylxanthene
βHE	β Hydride Elimination

A PERSONAL CONNECTION. FROM TARTESSOS TO C–C and C–N BOND-FORMING REACTIONS

If we went back to the ancient Greek History, we would realize that the history of the Iberian Peninsula – especially the Southwest region – is extremely tied to the coinage metals: copper, silver and gold. Through Herodotus, considered the father of occidental history, we know that in 630 B.C., Kolaios of Samos reached an unknown land where metals were abundant. Those territories were part of Tartessos, considered by some the first civilization in Western Europe. Historical and archeological evidences locate Tartessos in the riverbank of the Río Tinto, namelly where Huelva city is nowadays. This civilization became a pivotal trading partner for Phoenicians and Greeks and vestiges of this intense activities still remain, for instance, archeological sites as "Tejada la Vieja" and treasures as "Tesoro del Carambolo". The "Tejada la Vieja" site is located in the current town of Escacena del Campo (Huelva), where a few years later the author of this thesis was born.

Figure 1. Left: Tartessian settlement of "Tejada la Vieja", Escacena del Campo (Huelva). Right: Tesoro del Carambolo, Seville Archeological Museum.

Interestingly, in hardly 6 km from the archeological site of "Tejada la Vieja", we can find "Tejada la Nueva" or Itvci which flourished in Romans times. At this very moment, we encounter another civilization cunning enough to take advantages of the abundance of metals in the southwest of Iberian Peninsula: the Romans. Important mines such as Riotinto, which were initially used by Tartessians, were inherited and fully exploited by Romans thanks to innovative pieces of engineering (see Figure 2). This mine has been providing coinage metals from Tartessian times and, up to date, it has been key for the development of the area.

Another fact that attaches the history of Huelva to the coinage metals is the discovery of America. From Palos de la Frontera harbor, precisely, again, in Río Tinto, Christopher Columbus departed pursuing a sailing route to Far East and resulting in the discovery of the New World. From this moment on, Guadalquivir River became a trading port with the Americas, and so

Seville turned into one of the most prosperous cities in the world, mainly thanks to mainly the trading of gold.

Figure 2. Left: Coin as proof of this splendor of Itvci in Roman age. Middle: Riotinto Mines, currently under working conditions (Minas de Río Tinto, Huelva). Right: Reconstruction of a Roman waterwheel using original pieces from Riotinto mines (Huelva Museum).

Nowadays, the relationship of my hometown to the coinage metals is far beyond the trading and their uses as raw materials. In the 1970s, an important industrialization of the zone prospered and, with it, the development of a wide array of chemical transformations. In this regard, copper, silver and gold have been further used as catalyst of specific chemical processes. In particular, significant advances have been achieved by the group of Prof. Pedro J. Pérez, at the Universidad de Huelva, that studies the catalytic activity of coinage metals for the construction of new C–C and C–N bonds. The growing interest on this area is the fundamental linkage between the historical importance of coinage metals in my hometown and my PhD research topic.

Here below, we will describe our research projects involving coinage metals in different chemical transformations. Preceding the research part *per se*, we include the general abstract and objectives of the thesis. Then, the results are presented into four different chapters. Each research chapter contains five sections including an introduction of the research topic, the pursued objectives, the discussion of the results, the concluding remarks and, finally, an appendix explaining the followed procedures. A final chapter collects the general conclusions.

ABSTRACT

Organometallic coinage metals complexes have been proven to be key reactive species for promoting a variety of organic transformations, such as those involved in C–C and C–N bond forming reaction. Gaining a better understanding on the operational mechanism of coinage metal complexes on these reactions will provide fundamental knowledge, and more importantly, pave the way for the improvement and development of a wide array of chemical transformations. This approach of harnessing fundamental insights is the basis of knowledge-driven research in Chemistry. It fits nicely with the current effort in modern chemistry to achieve more efficient and sustainable processes, which can help address the pressing societal demands on chemical industry.

In the course of this Dissertation, and after a general introduction (**Chapter 1**), we will go through four different chapters which encompass the reactivity of coinage metal complexes both as co-catalyst in oxidative coupling reactions, a hot topic in organic synthesis, and as organometallic nucleophiles, allowing us to study not only the organometallic aspects of these species but also their implications in some organic reactions. A brief overview on each specific topic will introduce the reader into the corresponding chapter.

Chapter 2, entitled "*Unexpected cooperation in a bimetallic dual Rh/Cu catalytic system: DFT and microkinetic simulation as interrogating tools*", is a purely computational study on the Rh/Cu-catalyzed synthesis of isoquinolines by coupling of α-aryl vinyl azides and alkynes as case study reaction of bimetallic dual catalysis in oxidative coupling. We were able to fully characterize this reaction mechanism which perfectly explains the experimental outcomes. To do so, we used an iterative research of the potential routes by combining both DFT calculations and microkinetic modeling going from a simple model to a much more complex one. In this way, the previously accepted mechanistic proposal of two independent cycles connected by a redox step is replaced by a single catalytic cycle where both Rh and Cu catalysts cooperate simultaneously.

Chapter 3, entitled "*New vistas in transmetalation with discrete Ag-CF_3 species: implications in Pd-mediated trifluoromethylation reactions*", discloses the potential of trifluoromethyl silver(I) species as organometallic nucleophiles to overcome neglected side-reactions in the context of $Pd^{0/II}$-catalyzed nucleophilic trifluoromethylation of aryl halides. Although it had been assumed that reductive elimination is the challenging step in these transformation, a close look into the literature reveals that transmetalation side reactions are competitive with the reductive

elimination, precluding the organic product formation. We were able to synthetize and characterize new trifluoromethyl silver(I) complexes which were proved to be compatible with the "catalytic" trifluoromethylation of aryl halides by circumventing unproductive transmetalation side reactions. This work was published in *Chem. Eur. J.* **2018**, 24, 11895.

Chapter 4, entitled "*Mechanistic studies on the transmetalation step in Pd/Ag bimetallic systems*", presents a combination of experimental and computational study on the transmetalation reaction between aryl-Pd(II) complexes and trifluoromethyl silver(I) complexes. Over the last decade, it has been revealed that silver salts can play a role as a C–H activation promoter or decarboxylating agent, generating organosilver(I) species. These nucleophiles can promote innovative transformations by reacting with Pd^{II} intermediates through a transmetalation step. Despite the growing interest on the field, little information has been gathered either from an experimental or computational point of view in these systems. We studied the stoichiometric transmetalation reaction between aryl-Pd(II) complexes and "$Ag(CF_3)$" species revealing the remarkable influence of the ancillary ligand on the silver complex in the transmetalation mechanism. The unprecedented mechanistic proposals are a direct consequence the linear geometry of silver(I) complexes. Part of the introduction of this chapter was published as a review in *Org. Biomol. Chem.* **2019**, 17, 1655.

Chapter 5, entitled "*Exploring bis-(trifluoromethyl) coinage metallates landscape: a combined experimental and theoretical study*", reveals the access to a family of bis-(trifluoromethyl) metallates complexes, $[Cs][M(CF_3)_2]$ (M = Cu, Ag, Au), and the study of their chemical behavior. We were able to prepare the different coinage metal salts, being particular challenging the access of the copper ate-type complex due to its instability. We were able to study the reactivity patterns of these bis-(trifluoromethyl) metallates towards different electrophiles, paying special attention to the potential role of the cuprates in the trifluoromethylation of aryl halides. By combining kinetic experiments, DFT calculations and microkinetic modeling, we stablished that these ate-type cuprates are not innocent spectators in trifluoromethylation reactions playing an essential role as CF_3^- reservoir. These results were published in *Chem. Eur. J.* **2019**, *25*, 9390. An account about the involvement of copper(I) species in nucleophilic trifluoromethylation reactions was published in *Synthesis*, **2019**, 51, 2809.

CHAPTER 1. GENERAL INTRODUCTION AND OBJECTIVES

1.1. Coinage metals as additives in organic synthesis

Over the past two decades, transition-metal (TM) have played a key role in tackling some of the major problems that our world faces, such as climate change, energy conversion, or human health, by improving the efficiency of key chemical transformations, *i.e.* C–C and C–N bond-forming reactions. Most of these advances have been accomplished based on trial-and-error experiments or serendipitous discoveries and the rational design of chemical transformations based on knowledge-driven approaches has been an underestimated strategy.[1] However, its extension could induce a paradigm shift in terms of sustainability by saving time, resources, *etc*.

In this regard, understanding reaction mechanisms could be of extreme importance. Typically, reaction mechanisms are studied *a posteriori* in order to describe a successful transformation. However, the study of the mechanism is becoming an *a priori* tool, for reaction design. In this venue, both computational and experimental approaches have been essential for consolidating this field. In the last years, computational methods have shown their tremendous capability, not only for predicting catalyst performance, but also for improving their efficiency.[2] Moreover, experimental mechanistic study can also facilitate the sustainable development of TM-catalyzed transformations by, for instance, using key reaction intermediates as knowledge building blocks (KBBs). The foundation of this is based on the next concept: the success or failure of a completely chemical process relies on the performance of the reaction intermediates involved in each elementary step that constitutes the catalytic cycle. This may seem obvious, but, surprisingly, it is often overlooked and can be a game changer for inefficient transformations.

In this regard, we focused our attention on a specific group of transition metals: group 11 (Cu, Ag and Au, also known as coinage metals). The coinage metals are ubiquitous in relevant C–C and C–N bond-forming reactions not only as catalyst or promoters but also they are crucial, yet unexpected, additives under certain conditions.[3] Despite the importance of this, there is still a shortage of fundamental knowledge on the operational mechanism of key coinage metal complexes in specific reactions. In particular, little attention has been paid to their behavior when

1 Sanjosé-Orduna, J.; Mudarra, Á. L.; Martínez de Salinas, S.; Pérez-Temprano, M. H. *ChemSusChem*, **2019**, *12*, 2882.

2 a) Sigman, M. S.; Harper, K. C.; Bess, E. N.; Milo, A. *Acc. Chem. Res*. **2016**, *49*, 1292. b) Poree, C.; Schoenebeck, F. *Acc. Chem. Res*. **2017**, *50*, 605. c) Reid, J. P.; Sigman, M. S. *Nat. Rev. Chem*. **2018**, *2*, 290. d) Meyer, T. H.; Finger, L. H.; Gandeepan, P.; Ackermann L. *Trends Chem.* **2019**, *1*, 63.

3 For copper in C-C and C-N bond-forming reactions, see: a) Ley, S. V.; Thomas, A. W. *Angew. Chem. Int. Ed*. **2003**, *42*, 5400. For silver in C-C and C-N bond-forming reactions, see: b) Weibel, J.-M.; Blanc, A.; Pale, P. *Chem. Rev*. **2008**, *108*, 3149. For silver in C-C bond-forming reactions, see: c) Jiménez-Núñez, E.; Echavarren, A. M. *Chem. Rev*. **2008**, *108*, 3326. For the unexpected, yet essential, role of coinage metals in different transformations, see: d) Mudarra, Á. L.; Martínez de Salinas, S.; Pérez-Temprano, M. H. *Synthesis* 2019, *51*, 2809 and references therein. e) Funes-Ardoiz, I.; Maseras, F. *ACS Catal*. **2018**, *8*, 1161.

playing roles as important as catalysts in bimetallic dual catalysis or as mediator in the transmetalation event in cross-coupling reactions. Scarce of information can be also found in the context of trifluoromethylation reactions. In what follows, we will introduce briefly each aforementioned reactions.

1.2. Bimetallic dual catalysis

Catalysis is a cornerstone in modern synthetic chemistry. It accelerates a thermodynamically-feasible reaction. These transformations rely on a catalyst-induced replacement of the reaction mechanism for an alternative one with a lower barrier. In other words, the catalyst activates a substrate in a way that decreases the energy barrier for the whole chemical process (**Int I** to the left in Figure 1.1). The study of catalytic processes, especially from a mechanistic perspective, has allowed not only to discover unprecedented reactions but also to control the selectivity of a wide array of previously described ones. In this venue, catalyst design has supported the creation of sophisticate homogeneous catalysts that afford reactions as important as cross-coupling reactions.[4]

Despite the advances in catalysis design, still now, the most powerful catalysts on the Earth are enzymes, which come from Nature. It has been shown that a number of enzymes are able to harness the cooperation of multiple active sites in challenging transformations, being unique examples of synergistic effects.[5] Nevertheless, this concept of cooperation did not emerge as a convenient approach in homogenous catalysis until the past few years when the use of synergistic catalysis has proved to be a burgeoning alternative for the creation of a wide range of different C–C and C–X bonds.[6] In contrast to traditional catalysis, these systems operate through the parallel generation of reactive intermediates from different catalysts which react to finally allow the formation of the desired product (**Int I** and **Int II** to the right in Figure 1.1).

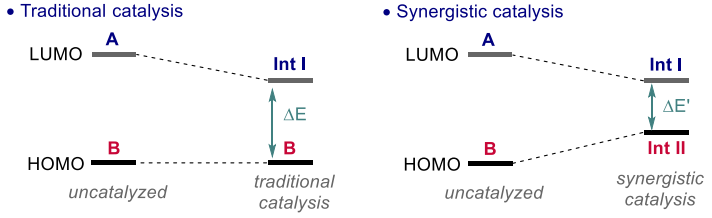

Figure 1.1. Comparison of the substrate activation when operating traditional catalysis versus the activation when operating synergistic catalysis. HOMO = Highest Occupied Molecular Orbital, LUMO = Lowest Unoccupied Molecular Orbital.

4 In 2010, Heck, Negishi and Suzuki were awarded with the Nobel Prize for the development of cross-coupling reactions. Further discussion can be found below.

5 a) van den Beuken, E. K.; Feringa, B. L. *Tetrahedron* **1998**, *54*, 12985. b) Strater, N.; Lipscomb, W. N.; Klabunde, T.; Krebs, B. *Angew. Chem., Int. Ed. Engl.*, **1996**, *35*, 2024.

6 a) Allen, A. E.; MacMillan, D. W. C. *Chem. Sci.*, **2012**, *3*, 633 and references therein. According to MacMillan definition, synergistic catalysis consists of two independent catalytic cycles that activate the substrates and the activated intermediates react to yield the product. There is a lack of consensus on the definition of these systems but we think that MacMillan definition is an appropriate starting point. Besides, in the aforementioned report, other cases of multi-catalyst systems are defined. b) Pye, D. R.; Mankad, N. P. *Chem. Sci.*, **2017**, *8*, 1705.

The formally most simple general mechanistic picture of synergistic catalysis can be described as two independent cycles that are interlaced by a common point where the two aforementioned key intermediates react allowing the final product formation, **Int I** and **Int II** in Scheme 1.1.

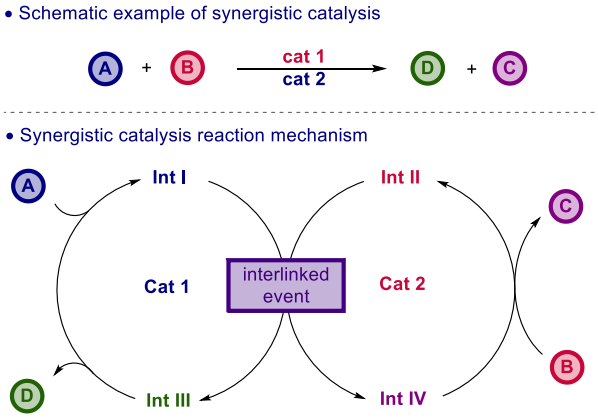

Scheme 1.1. General mechanistic proposal for synergistic catalytic transformations.

Among the synergistic catalytic systems, bimetallic dual catalysis[7] is emerging as a powerful tool for the creation of chemical complexity. In these systems, the potential of two discrete metal catalysts, **cat 1** and **cat 2** (Scheme 1.1), is exploited to activate different substrates, providing an interesting alternative not only for the improvement of known transformation but also for the discovery of new ones. For instance, in 2006, Goossen *et al.* disclosed an important and representative example of bimetallic dual catalytic transformation: Pd/Cu-catalyzed decarboxylative cross-coupling reactions (Scheme 1.2).[8]

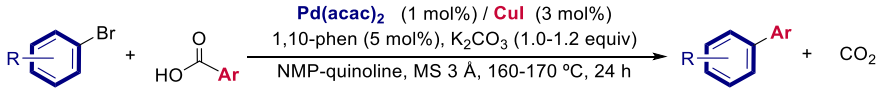

Scheme 1.2. General protocol for the Pd/Cu-catalyzed decarboxylative cross-coupling reaction of aryl bromides and benzoic acids. acac = acetilacetonate, phen = phenantroline, NMP = N-methyl-2-pyrrolidone.

The proposed reaction mechanism of this transformation consists of two independent catalytic cycles, connected by a transmetalation step, where each metal catalyst activates a different substrate. On the one hand, a palladium(0) species activates the aryl halide to form a

7 We selected "bimetallic dual catalysis" term for referring to synergistic catalytic systems where two different and discrete metal catalysts allow the formation of product through the formation of reactive intermediates. It should be mentioned that there is a lack of consensus for referring this multi-catalyst reactions. Although we agree with the definition of synergistic catalysis used by MacMillan, we also think that the term "synergistic" could be somehow ambiguous term. For that reason, we think that a convenient alternative should include "bimetallic catalysis", in accordance with Espinet review (Pérez-Temprano, M. H.; Casares, J. A.; Espinet, P. *Chem. Eur. J.* **2012**, *18*, 1864) but including "dual" to reinforce that there are two catalytic cycle and it is not about a bimetallic dinuclear catalyst or, as it is proposed to be named, bifunctional catalyst (ref. 6).

8 Goossen, L. J.; Deng G.; Levy, L. M. *Science*, **2006**, *313*, 662.

[(L)$_n$Pd(Ar)(X)] species (**I**) through a oxidative addition step. On the other hand, copper(I) species simultaneously generates an *in situ* arylcopper(I) complex (**II**) by decarboxylation of the carboxylic acid derivative. Then, the transmetalation step interlinks both catalytic cycles. The resulting biarylpalladium(II) complex (**III**) undergoes the reductive elimination step, affording the cross-coupling product along with a Pd(0) catalyst. Remarkably, this approach avoids the use of stoichiometric amounts of isolated organometallic nucleophilic partner, necessary in traditional cross-coupling reactions, which can be toxic, difficult to handle and/or instable.[9]

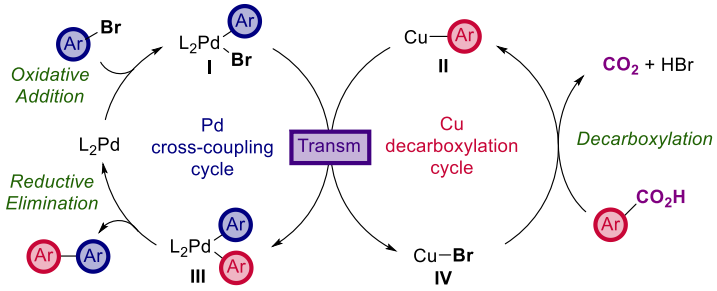

Scheme 1.3. Proposed mechanism for Pd/Cu-catalyzed decarboxylative cross-coupling reaction of aryl halides and benzoic acids.

The success of bimetallic dual catalysis relies on the kinetic compatibility of each and every elementary step involved in both catalytic cycles. Therefore, understanding the full mechanistic picture is fundamental for introducing rational modifications on those systems. Nevertheless, these mechanistic investigations are scarce across the literature likely due to the complexity of studying two metal catalyst simultaneously from an experimental point of view. In this regard, density functional theory (DFT) calculations are becoming a fundamental to tool for digging into the reaction mechanism intricacies of different catalytic systems in an accurate way.[10] Yet these calculations are not common for the full characterization of the mechanism of bimetallic dual catalytic systems,[11] especially in the context of oxidative coupling reactions.

Oxidative coupling reactions are becoming an important and greener alternative to classical cross-coupling reactions in the context of C–C bond-forming reactions. This approach allows,

9 a) Lennox, A. J. J.; Lloyd-Jones, G. C. *Chem. Soc. Rev*. **2014**, *43*, 412. b) Cordovilla, C.; Bartolomé, C.; Martínez-Ilarduya, J. M.; Espinet, P. *ACS Catal.* **2015**, *5*, 3040.

10 For representative examples of DFT calculations in understanding reaction mechanisms, see: a) Lin, Z. *Acc. Chem. Res.* **2010**, *43*, 602. b) Sameera, W. M. C.; Maseras, F. *WIREs Comput. Mol. Sci. 2*, **2012**, 375. c) Max, G.-M.; Braga, A. A. C.; Lledós, A.; Ujaque, G.; Maseras, F. *Acc. Chem. Res.* **2013**, *46*, 2626. d) Jover, J.; Fey, N. *Chem. Asian J*. **2014**, *9*, 1714. e) Sperger, T.; Sanhueza, I. A.; Kalvet, I.; Schoenebeck, F. *Chem. Rev.* **2015**, *115*, 9532. f) Sperger, T.; Sanhueza, I. A.; Schoenebeck, F. *Acc. Chem. Res*. **2016**, *49*, 1311. g) Poree, C.; Schoenebeck, F. *Acc. Chem. Res.* **2017**, *50*, 605. For representative examples of DFT calculations that accurately reproduce experimental results, see: i) McMullin, C. L.; Jover, J.; Harvey, J. N.; Fey, N. *Dalton Trans*. **2010**, *39*, 10833. j) Fey, N.; Ridgway, B. M.; Jover, J.; McMullin, C. L.; Harvey, J. N. *Dalton Trans.* **2011**, *40*, 11184. k) Peng, Q.; Duarte, F.; Paton, R. S. *Chem. Soc. Rev.* **2016**, *45*, 6093. l) Liu, Z.; Patel, C.; Harvey, J. N.; Sunoj, R. B. *Phys. Chem. Chem. Phys.* **2017**, *19*, 30647.

11 a) Fromm, A.; van Wüllen, C.; Dagmar, H.; Goossen, L. J. *J. Am. Chem. Soc.* **2014**, *136*, 10007. b) Kalek, M.; Himo, F. *J. Am. Chem. Soc.* **2017**, *139*, 10250.

for instance, the functionalization of C–H bonds, catalyzed by rhodium, palladium or ruthenium,[12] preventing the use of pre-functionalized starting materials.[13]

The formation of a C–C bond from a C–H activation event implies the formal oxidation of the substrates. Therefore, a simultaneous reduction must occur to guarantee the electroneutrality of the reaction. This issue is overcome by the use of stoichiometric amounts of an oxidant, which accepts the electrons from the substrate. Ideally, molecular oxygen (O_2) is the most convenient oxidant since it is low cost and environmentally friendly. In fact, if it is applied to oxidative coupling reactions involving hydrocarbons, the process turns greener from an environmental point of view since the only waste product is H_2O.

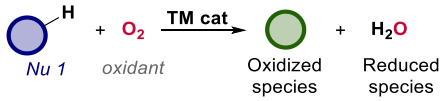

Scheme 1.4. General representation of a TM-catalyzed oxidative coupling reaction using molecular oxygen as terminal oxidant to yield water as waste product.

However, the generalized use of molecular oxygen by its own as ultimate oxidant is still an unresolved challenge. Instead, two alternatives are often applied: i) the use of stoichiometric amounts of other external oxidants, transforming the reaction in a non-green alternative[12] or ii) the use of a catalytic amounts of a redox active co-catalyst which ensures the electron flow from the substrates to the molecular oxygen. These co-catalysts are commonly metal-based salts of copper.

In this venue, in 2007, Miura and Satoh reported the Rh/Cu-catalyzed reaction of benzoic acids with alkynes under air.[14] It consists on the creation of a new C–C and C–O bonds catalyzed by a [(Cp*)Rh^{III}] species resulting in the formation of the isocumarin product and water as waste product in the presence of a copper(II) co-catalyst. Since, no product formation was observed under air without the copper, this salt is acting as a co-catalyst and, therefore, the reaction is an example of bimetallic dual catalysis. From a mechanistic point of view, the authors proposed that the reaction occurs thanks to the synchronization, shown in Scheme 1.5, of two independent catalytic cycles: the rhodium and the copper cycle. The rhodium cycle starts with the regioselective C–H activation of the *o*-position of the aromatic carboxylic acid by a rhodium(III)

12 For representative examples of Rh-catalyzed oxidative coupling reactions, see: a) Satoh, T.; Miura, M. *Chem. Eur. J.* **2010**, *16*, 11212. b) Colby, D. A.; Tsai, A. S.; Bergman, R. G.; Ellman, J. A. *Acc. Chem. Res.* **2012**, *45*, 814. c) Song, G.; Wang, F.; Li, X. *Chem. Soc. Rev.* **2012**, *41*, 3651. For representative examples of Pd-catalyzed oxidative coupling reactions, see: d) Lyons, T. W.; Sanford, M. S. *Chem. Rev.* 2010, *110*, 1147 e) Le Bras, J.; Muzart, J. *Chem. Rev.* 2011, *111*, 1170. For representative examples of Ru-catalyzed oxidative coupling reactions, see: f) Arockiam, P. B.; Bruneau, C.; Dixneuf, P. H. *Chem. Rev*. **2012**, *112*, 5879. g) Ackermann, L. *Acc. Chem. Res*. **2014**, *47*, 281.

13 Liu, C.; Zhang, H.; Shi, W.; Lei, A. *Chem. Rev.* **2011**, *111*, 1780. We should emphasize that oxidative coupling is an immense field of study and, for ease of reading, we exclusively focused our discussion only in oxidative coupling reaction which involves substrates bearing C-H bonds susceptible of being activated.

14 Ueura, K.; Satoh, T.; Miura, M. *Org. Lett*. **2007**, *9*, 1407.

complex (**V**) to afford a rhodacycle intermediate (**VI**).[15] Then, this intermediate **VI** evolves through the alkyne insertion (AI) step to a seven membered-ring metallacycle (**VII**), which further undergoes the reductive elimination step. This affords the organic product along with Rh(I) complex. Then, the interconnection between both cycles allows the reoxidation of [(Cp*)Rh^{I}] species (**VIII**) by the Cu^{II} complexes (**IX**), giving rise to [(Cp*)Rh^{III}] and Cu^{I} (**X**) complexes. The copper cycle consists of the reoxidation of the Cu^{I} to Cu^{II} utilizing molecular oxygen and acetic acid. In this case, it is noteworthy that the interlinked event consists of the exchange of both electrons and ligands between both metal catalysts. In sharp contrast, the transmetalation step in bimetallic dual catalyzed cross-coupling reactions, which interlinks both cycle, is generally proposed to be a redox neutral event (see *infra*).

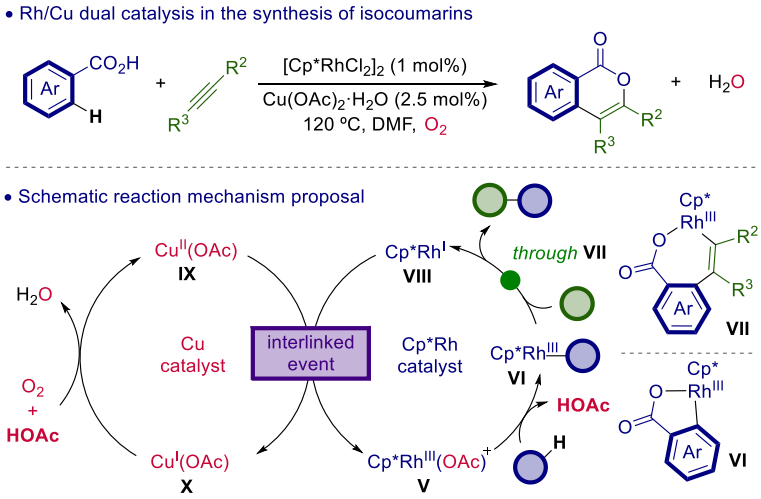

Scheme 1.5. Above: general protocol for the Rh/Cu-catalyzed coupling of benzoic acids with alkynes under air to yield isocumarin derivatives (ref. 14). Below: Mechanistic proposal for the Rh/Cu-catalyzed coupling reaction.

Although bimetallic dual catalysis in the context of oxidative coupling is a hot topic from a synthetic point of view, there is a lack of understanding when concerning the effects of coinage metal additives such as silver and copper complexes as well as the complete characterization of the full mechanistic picture.

1.3. Transmetalation step

In 2010, Heck, Negishi and Suzuki were awarded with the Nobel prize in Chemistry for developing palladium-catalyzed cross-coupling reactions in organic synthesis. *"This chemical tool has vastly improved the possibilities for chemists to create sophisticated chemicals, for*

15 Although in the original report is not proposed the acetate to promote the C–H activation, this species is proposed in the literature: Li, L.; Brennessel, W. W.; Jones, W. D. *Organometallics* **2009**, *28*, 3492.

example carbon-based molecules as complex as those created by nature itself", as stated in the press release from the Royal Swedish Academy of Science.[16]

These classical cross-coupling reactions allow the formation of new C–C bonds by the reaction of an organic electrophile with an organometallic nucleophile, normally catalyzed by a palladium complex (Scheme 1.6).[17,18]

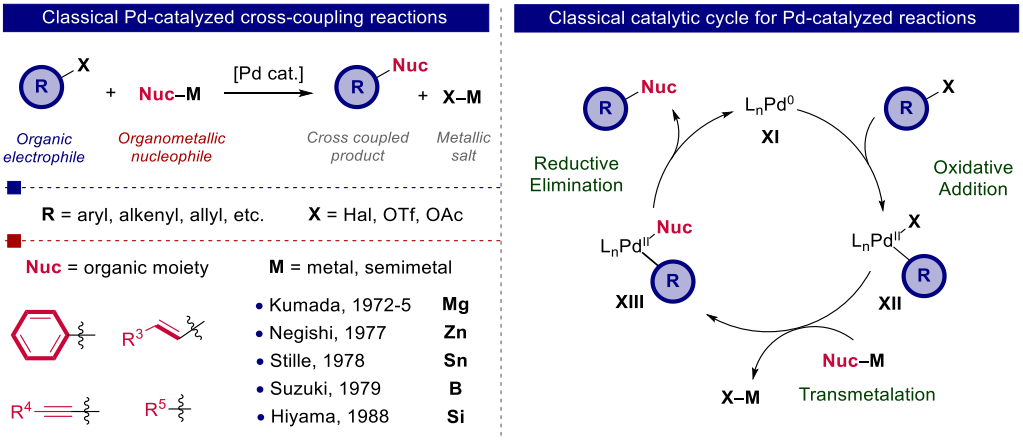

Scheme 1.6. Classical Pd-catalyzed cross-coupling reactions. Left: Pd-catalyzed cross-coupling reaction using different organometallic nucleophiles. Right: Most-accepted catalytic cycle for classical Pd-catalyzed cross-coupling reactions.

These reactions are generally proposed to proceed through a mechanism (see Scheme 1.6) that involves three elementary steps: oxidative addition (OA), transmetalation (Transm) and reductive elimination (RE).[19] The oxidative addition step implies a formal oxidation of the Pd(0) catalyst by a organopalladium(II) halide (or pseudohalide), and results in intermediate **XII**. The oxidative addition rate of the organohalide to Pd(0) is generally faster for weaker C–X bonds (I > Br > Cl).[20] Next, the transmetalation step occurs (Scheme 1.6). This redox neutral event involves the transfer of an organic moiety from the organometallic nucleophile to the Pd(II) intermediate, which entails the creation of a new Pd–C bond. Depending on the nature of the

16 https://www.nobelprize.org/prizes/chemistry/2010/press-release

17 Seechurn, C. C. C. J.; Kitching, M. O.; Colacot T. J.; Snieckus, V. *Angew. Chem., Int. Ed.*, **2012**, *51*, 5062.

18 Other important cross-coupling reactions do not involve a pre-formed organometallic nucleophile such as Sonogashira and Heck reactions. Sonogashira reaction involves the in-situ formation of the nucleophile by reaction of the copper co-catalyst with a terminal alkyne. In contrast, Heck reactions use alkene as nucleophiles instead of organometallic species In this case, the transmetalation step is replaced by a migratory-insertion step followed by a β-hydride elimination. See ref. 17.

19 Echavarren, A. M.; Homs, A., Mechanistic Aspects of Metal-Catalyzed C,C– and C,X–Bond Forming Reactions. In *Metal-Catalyzed Cross-Coupling Reactions and More*, Wiley-VCH Verlag GmbH & Co. KGaA: **2014**; pp 1–64.

20 a) Barrios-Landeros, F.; Carrow, B. P.; Hartwig, J. F. *J. Am. Chem. Soc.* **2009**, *131*, 8141. b) McMullin, C. L.; Jover, J.; Harvey, J. N.; Fey, N. *Dalton Trans*. **2010**, *39*, 10833.

metal[21] in this organometallic species, there are different cross-coupling reactions: Stille (Sn), Negishi (Zn), Kumada (Mg), *etc*.[22] Finally, the catalytic cycle is closed by the reductive elimination step (Scheme 1.6). This event allows the generation of the new C–C bond, affording the reaction product and a regenerated palladium(0) species which can start over the catalytic cycle (Scheme 1.6). The reductive elimination rate of the organic product is inversely proportional to the bond dissociation energy of the Pd–C bonds.[23]

Among all the aforementioned elementary steps, the transmetalation event is the least known from a mechanistic point of view. This is because the reaction pathway of the transmetalation step may depend on the used nucleophile. Organometallic coinage metal complexes have been described as nucleophiles, for example, in the Sonogashira cross-coupling reaction, which is an example of the aforementioned bimetallic dual catalytic systems.[24] Recently, coinage metal additives have been also proposed to be active in many other transformations such as C–H bond activation.[3d,3e] This is particularly outstanding in the case of silver additives.

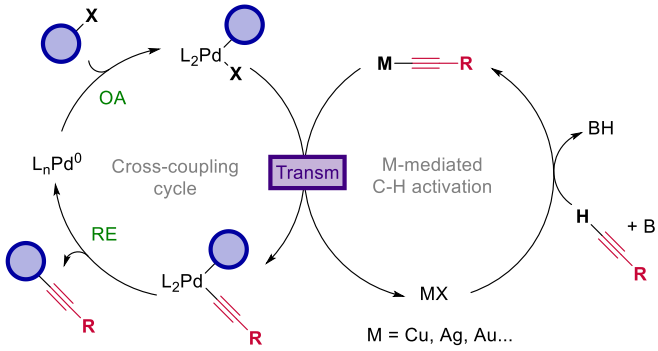

Scheme 1.7. Bimetallic dual catalysis for the Pd/coinage metal-catalyzed Sonogashira cross-coupling reaction. B = base.

21 Understand "metal" as if including boron and silicon main group elements. Species bearing a C–M bond where M is boron or silicon atom, are also considered organometallic species.

22 Kumada reactions involve the use of an organomagnesium: a) Yamamura, M.; Moritani, I.; Murahashi, S.-I. J. Organomet. Chem. 1975, 91, 39. b) Knappke, C. E. I.; von Wangelin, A. *J. Chem. Soc. Rev.*, 2011, *40*, 4948. Negishi reactions involve the use of organozincate: c) King, A. O.; Okukado, N.; Negishi, E.-I. *J.C.S. Chem. Comm.* 1977, 683. e) Haas, D.; Hammann, J. M.; Greiner, R.; Knochel, P. *ACS Catal.* 2016, *6*, 1540. Stille reactions imply the use of organostannanes: f) Milstein, D.; Stille, J. K. *J. Am. Chem. Soc.*, **1978**, *100*, 3636. g) Cordovilla, C.; Bartolomé, C.; Martínez-Ilarduya, J. M.; Espinet, P. *ACS Catal.* **2015**, *5*, 3040. Suzuki reactions involve the use of organoborane: h) Miyaura, N.; Yamada, K.; Suzuki, A. *Tetrahedron Lett.* **1979**, 3437. i) Miyaura, N.; Suzuki, A. *Chem. Rev.* **1995**, *95*, 2457. Hiyama reactions use organosilicon compounds: j) Hatanaka, Y.; Hiyama, T. *J. Org. Chem.* **1988**, *53*, 920. k) Nakao, Y.; Hiyama, T. *Chem. Soc. Rev.*, **2011**, *40*, 4893.

23 Hartwig, J. F. *Inorg. Chem.* 2007, *46*, 1936.

24 Copper: a) Sonogashira, K. *J. Organomet. Chem*. **2002**, *653*, 46. Silver: b) Y. Yamamoto, *Chem. Rev*. **2008**, *108*, 3199. Gold: c) Lauterbach, T.; Livendahl, M.; Rosellón, A.; Espinet, P.; Echavarren, A. M. *Org. Lett.* **2010**, *12*, 3006.

Silver salts are one of the most widely used additives in transition metal catalyzed transformations in promoting halide scavenger and/or reoxidation reactions.[25,26] Over the years, these additives have been considered to be mere spectators during the catalytic transformation. Nevertheless, this concept is evolving since it has been unveiled that they can be key for the activation of organic moieties in different transition metal catalyzed transformations, affording organosilver(I) complexes. The reactivity of these species have been specially harnessed – intentionally or unintentionally – in Pd-catalyzed C–C bond-forming reactions, a pivotal transformation for synthetic organic chemistry. The mechanistic intricacies of Pd/Ag systems, namely the transmetalation step, are completely unexplored.

1.4. Trifluoromethylation reactions

The trifluoromethyl group is a prevalent motif in pharmaceuticals, agrochemicals and materials because of its unique capacity to change physical, chemical and biological properties of organic molecules. The CF_3 group has such different characteristics that some authors proposed it to be considered as a different functional group and not as a substituted methyl group.[27] This is because this group exhibits an extraordinary electronegativity (similar to chlorine) and a considerable size (similar to isopropyl group).[27] Besides, it reacts with transition metals to afford the α-fluoride elimination, unknown for the methyl group.[28] Regarding the bio-activity, one of the characteristics of the CF_3 moiety is its lipophilicity. The incorporation of this moiety into a given drug can enhance its bioavailability since it can easily penetrate into the body and reach its site of action.[29] Examples of drugs bearing CF_3 group are Prozac®, Januvia® and Celebrex®. Interestingly, their synthetic routes involved starting material which already contain the trifluoromethyl group installed.

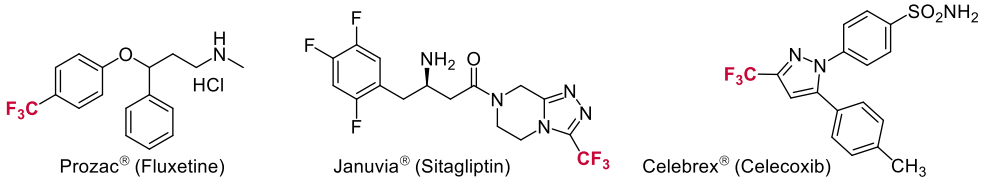

Figure 1.2. Top-selling CF_3-containing drugs.

25 Wender, P. A. in Silver in Organic Chemistry, ed. Harmata, M.; Weibel, J.-M.; Blanc, A.; Pale, P. John Wiley&Sons, **2010**, Ch. 10, 285.

26 For selected examples of silver salts as halide scavenger, see: a) Weibel, J.-M.; Blanc, A.; Pale, P. *Chem. Rev*. **2008**, *108*, 3149. b) Homs, A.; Escofet, I. Echavarren, A. M. *Org. Lett*., **2013**, *15*, 5782. c) Arroniz, C.; Denis, J. G.; Ironmonger, A.; Rassias G.; Larrosa, I. *Chem. Sci*., **2014**, *5*, 3509. For selected examples of silver salts as oxidant, see: a) Mijs, W. J.; Jong, C. R. H. I. *Organic Synthesis by Oxidation with Metal Complexes*, Plenum Press, New York, **1986**. b) Hull, K. L.; Sanford, M. S.; *J. Am. Chem. Soc*. **2007**, *129*, 11904; c) Naodovic, M.; Yamamoto, H. *Chem. Rev*., **2008**, *108*, 3132.

27 Furuya, T.; Kamlet, A. S.; Ritter, T. *Nature*, **2011**, *473*, 470.

28 Ferguson, D. M.; Bour, J. R.; Canty, A. J.; Kampf, J. W.; Sanford, M. S. *J. Am. Chem. Soc.* **2017**, *139*, 11662.

29 Purser, S.; Moore, P. R.; Swallow, S.; Gouverneur, V. *Chem. Soc. Rev*., **2008**, *37*, 320.

Currently, the large-scale manufacturing of trifluoromethylated aromatic compounds is mainly based on the Swarts method, disclosed approx. 120 years ago.[30] This synthetic approach consists of the formation of α,α,α-triflurotoluene from α,α,α-trichlorotoluene which is obtained by chlorination of toluene (Scheme 1.8). The required harsh reaction conditions precludes the use of functionalized starting materials.[31] Additionally, this route is not environmentally friendly neither efficient from an atom-economy perspective.

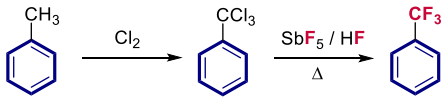

Scheme 1.8. The Swarts reaction for the synthesis of α,α,α-triflurotoluene from toluene.

For this reason, the chemical community has devoted its efforts towards the development of alternative methodologies for facilitating the formation of C–CF_3 bonds using transition metal complexes as catalysts or mediators. Thus, the trifluoromethyl group has been introduced into the organic scaffolds as a nucleophile, electrophile or a radical depending on the trifluoromethylating agent (Scheme 1.9).

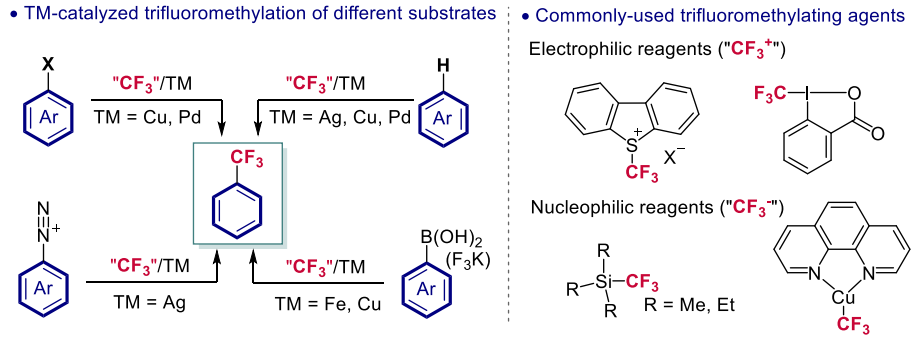

Scheme 1.9. To the left: Trifluoromethylation reaction of different substrates enabled by TM-catalysis. To the right: Different electrophilic and nucleophilic reagents used for the trifluoromethylation reactions. Radical CF_3 sources are not presented.

In this regard, coinage metals have been also exploited in the incorporation of the trifluoromethyl group into a wide array of substrates.[32] For example, it is remarkable the potential of copper as catalyst in nucleophilic trifluoromethylation reactions of aryl halides.[3d,31] In fact, a trifluoromethyl copper(I) complex, called "trifluoromethylator", is commercially available as nucleophilic CF_3 source (Scheme 1.9).[33]

30 Swarts, F. *Bull. Acad. R. Med. Belg*. **1892**, *24*, 309.
31 Tomashenko, O. A.; Grushin, V. V. *Chem. Rev.* **2011**, *111*, 4475 and references therein.
32 Chen, P.; Liu, G. *Synthesis*, **2013**, *45*, 2919.
33 https://www.sigmaaldrich.com/catalog/product/aldrich/777692?lang=es&region=ES

Despite the potential of coinage metal complexes as reactive species in trifluoromethylation reactions, there is still a lack of fundamental understanding on their chemical behavior, principally regarding bis-(trifluoromethyl) coinage metallates.

1.5. General objectives

The main scientific objective of this Thesis is to gain a better understanding of the operational mechanism of coinage metal complexes in an array of organic transformations, namely those involved in C–C and C–N bond forming reaction. We particularly aim to:

- Understand the full mechanistic picture underlying the Rh/Cu dual catalytic system in the context of oxidative coupling reactions.

- Get insight into the transmetalation event in Pd/Ag bimetallic systems in the context of C–C bond-forming reactions.

- Understand the behavior of bis-(trifluoromethyl) coinage metallates as potential nucleophiles in the creation of C–CF_3 bonds.

Each chapter of this PhD Thesis manuscript contains a more detailed description of the specific objectives.

CHAPTER 2. UNEXPECTED COOPERATION IN A BIMETALLIC DUAL Rh/Cu CATALYTIC SYSTEM: DFT AND MICROKINETIC SIMULATION AS INTERROGATING TOOLS.

2.1. Introduction

Bimetallic dual catalysis has shown to be essential for the greener formation of C–C and C–N bonds in the context of oxidative coupling. It allows the use of inexpensive and non-toxic molecular oxygen (O_2) as terminal oxidant producing water as waste product, as discussed in Chapter 1.[1] Another green alternative is the use of an organic molecule that simultaneously plays a role as both oxidant and substrate. This is the case of the Rh/Cu-catalyzed synthesis of isoquinolines from α-aryl vinyl azides and internal alkynes (Scheme 2.1) under nitrogen atmosphere.[2] In 2011, Chiba *et al.* proposed the use of the azide, which is reduce to an imine intermediate, as an oxidant for the regeneration of the copper catalyst.

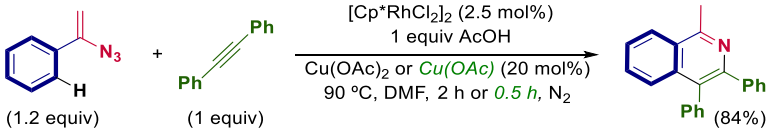

Scheme 2.1. Example of the scope of Rh/Cu-catalyzed synthesis of isoquinolines from α-aryl vinyl azides and internal alkynes. AcO = acetate.

Preliminary mechanistic studies pointed out that both metals centers were necessary in catalytic amounts for the reaction to proceed. When the authors used NaOAc instead of copper acetates, not product formation was observed. This indicates that copper is not simply providing acetates to the reaction. Also, copper(II) acetate could not be the terminal oxidant since it is added in catalytic amounts. In this regard, when using molecular oxygen as terminal oxidant, the reaction does not evolve. Thus, neither the copper(II) or the oxygen are the stoichiometric oxidants in the reactions. The authors proposed that copper(I) can catalyze a denitrogenative reductive formation of imine from α-aryl vinyl azide, meaning that the substrate itself is the stoichiometric oxidant. In fact, α-phenyl vinyl azide in the presence of copper(I) acetate and acetic acid gave rise to acetophenone, the putative intermediate the hydrolysis of the imine.

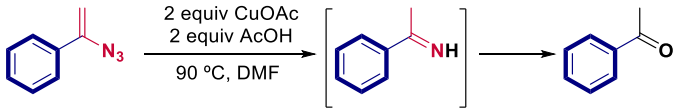

Scheme 2.2. Reaction of the α-phenyl vinyl azide under reductive conditions using of copper(I) acetate and acetic acid to yield acetophenone, a putative intermediate of the imine.

1 Another environmentally friendly and low cost alternative is the use of electricity as oxidant (Meyer, T. H.; Finger, L. H.; Gandeepan, P.; Ackermann L. *Trends Chem.* **2019**, *1*, 63).

2 Wang, Y.-F.; Toh, K. K.; Lee, J.-Y.; Chiba, S. *Angew. Chem. Int. Ed.* **2011**, *50*, 5927.

The proposed general mechanistic picture of this transformation is much complex (Scheme 2.3). The authors proposed two interconnected catalytic cycles: the copper and the rhodium cycle. On the one hand, copper(I) species catalyzes the cleavage of the N–N bond of the azide to yield the iminyl copper(II) radical intermediate, **I**.[3] Then, this intermediate evolves to form Cu^{II} aza-enolate complex (**III**) which, after protonation, yields the corresponding imine (**IV**). Thus, initial Cu^{I} catalyst is oxidized to Cu^{II} and the α-aryl vinyl azide is reduced to the corresponding imine. On the other hand, the Rh^{III} catalyst reacts with the *in situ* formed imine to afford the oxidative coupling reactions through C–H activation (**VI**), alkyne insertion (**VII**) and reductive elimination steps (Scheme 2.3). This sequence of events yield the corresponding organic product (**VIII**) and Rh^{I} species. Subsequently, this Rh^{I} species is proposed to react with the Cu^{II} intermediate to recover the initial formal oxidation state of both metals center, restarting both cycles again. Apart from this, scarce information is provided in the original report about the stoichiometry composition of the reactive intermediates, especially regarding the denitrogenative reductive formation of the imine which is key for the success of the whole catalytic transformation.

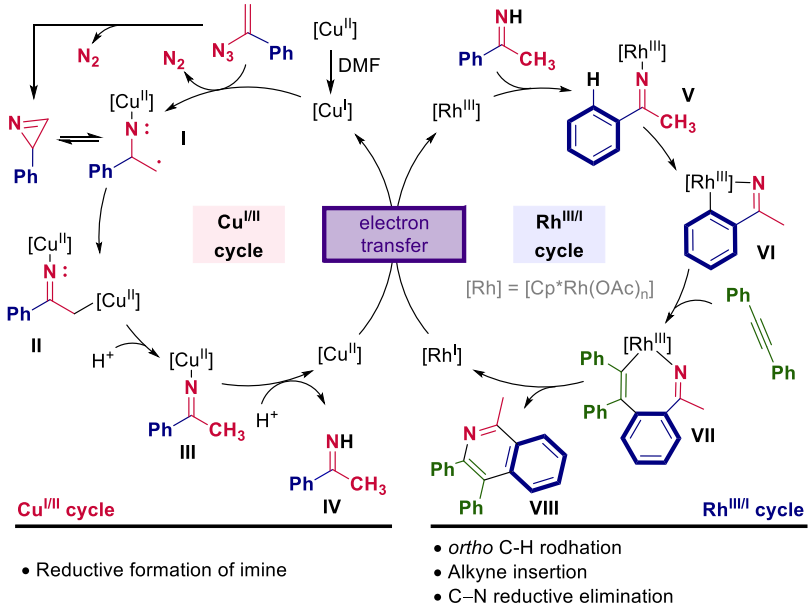

Scheme 2.3. Original mechanistic proposal for the Rh/Cu-catalyzed synthesis of isoquinolines from α-aryl vinyl azides and internal alkynes.

They also found that α-(*m*-substituted aryl) vinyl azides as substrates gave rise to the formation of regioisomeric mixtures (Scheme 2.4) where the C–H bond in *p*-position to the substituent (product **IX**) was preferentially cleavage. This outcome was rationalized on the basis

[3] It should be noticed that the authors also employ $[Cu(OAc)_2]$ to set up the coupling. It is well-known that Cu^{II} species can be reduced to Cu^{I} in DMF, allowing the initiation of the Cu^{I}-catalyzed transformation.

of this position is less sterically demanding.[Error! Bookmark not defined.] More insights into the origin of this selectivity could shed light into the selective creation of C–C and/or C–N bond bonds.

Scheme 2.4. Regioselective formation of isoquinolines when using α-(*m*-bromo-substituted phenyl) vinyl azide and diphenylacetylene under the standard reaction conditions.

The proposal described above for the Rh/Cu-catalyzed synthesis of isoquinolines from α-aryl vinyl azides and internal alkynes (Scheme 2.3) is similar to the accepted one when molecular oxygen is used as final external oxidant (**Error! Reference source not found.**). The particular difference relies on the used stoichiometric oxidant: molecular oxygen or a substrate that will be reduced and later modified during the catalysis. This approach is particularly interesting since it allows two chemical transformation in one-pot: the reduction and the functionalization of the substrate.

The reaction mechanism of this complex bimetallic dual catalytic system has not been further explored and there are uncertainties about the nature of the intermediates and the regioselectivity when using *m*-bromo-substituted substrates. Indeed, as we will discuss in the next section, the mechanistic scenario of this transformation could be even more complex than initially assumed due to unexpected cooperation between both metals.

2.1.1. **Cu-containing oxidants in oxidative coupling systems**

Many oxidative coupling reactions employs of stoichiometric amounts of metal-based salts for the catalyst regeneration.[Error! Bookmark not defined.] Interestingly, it has been recently proved that these oxidants, especially copper species, can have a relevant impact on the control of the selectivity and/or the efficiency of catalytic transformations.[4] In other words, the oxidants are not a mere electron sinks in oxidative coupling reactions and can play a role beyond the regeneration of the catalytically active species. Henceforth, we focused our attention on the non-

[4] For examples where copper is proposed to play a role beyond the catalyst recovery by DFT see: a) Jiang, J.; Ramozzi, R.; Morokuma, K. *Chem. Eur. J.* **2015**, *21*, 11158. b) Funes-Ardoiz, I.; Maseras, F. *Angew. Chem. Int. Ed.* **2016**, *55*, 2764. c) Funes-Ardoiz, I.; Maseras, F. *Chem. Eur. J.* **2018**, *24*, 12383. d) Jones, A. W.; Rank, C. K.; Becker, Y.; Malchau, C.; Funes-Ardoiz, I.; Maseras, F.; Patureau, F. W. *Chem. Eur. J.* **2018**, *24*, 15178. For examples where DFT calculations support that silver is not an innocent additive in oxidative coupling, see: e) Frasco, D. A.; Lilly, C. P.; Boyle, P. D.; Ison, E. A. *ACS Catal.* **2013**, *3*, 2421. f) Yang, Y.-F.; Cheng, G.-J.; Liu, P.; Leow, D.; Sun, T.-Y.; Chen, P.; Zhang, X.; Yu, J.-Q.; Wu, Y.-D.; Houk, K. N. *J. Am. Chem. Soc.* **2014**, *136*, 344. Examples of non-innocent role of oxidants in oxidative coupling catalysis have been reviewed by our group: g) Funes-Ardoiz, I.; Maseras, F. *ACS Catal.* **2018**, *8*, 1161. Experimental evidences of the role of the oxidants in oxidative coupling have been detected experimentally by our group, see: h) Sanjosé-Orduna, J.; Toro, J. M. S.; Pérez-Temprano, M. H. *Angew. Chem. Int. Ed.* **2018**, *57*, 11369.

innocent role of copper in different oxidative coupling transformation involving C–H activation event.

In 2008, Jones *et al.* studied the synthesis of isoquinolines salts through the oxidative C–H activation of different *N*-containing directing groups and alkynes as substrates. The reaction were mediated by the used of stoichiometric amounts of [(Cp*)Rh(Cl)$_2$].[5] As synthetic intermediate, they obtained the rhodacycle **XI** (Scheme 2.5). Then, the authors evaluated the influence of different oxidants in order to trigger the oxidative coupling of corresponding C–N bond. They found that $CuCl_2$ allowed the product formation and so they proposed a potential cooperation between Cu and Rh during the stoichiometric reductive elimination (RE) reaction. This pioneered proposal implied an oxidation of the Rh(III) species to a Rh(IV) by the Cu(II) salt. This high-valent rhodium species is prompted to afford the reductive elimination step more efficiently, affording a Rh(II) intermediate that is further oxidized by Cu(II) to the more stable [(Cp*)Rh(Cl)$_2$].

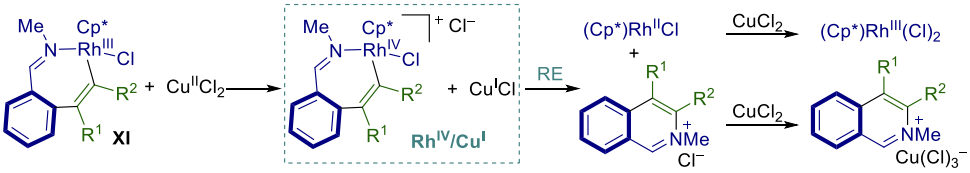

Scheme 2.5. Rh/Cu cooperation during the oxidative coupling event for the creation of the C–N bond formation proposed by Jones and co-workers.

Although it is beyond the scope of this Dissertation, it should be mentioned that this proposal is in line with the previous mechanistic picture proposed by Tilset *et al.* for the oxidatively induced reductive elimination (OIRE) from [(Cp*)Rh(PPh$_3$)(CH$_3$)$_2$] using electrolysis or ferrocenium hexafluorophosphate as chemical oxidant.[6] Recently, in this regard, it has been also proved that cyclometalated Ir, Rh and Ru complexes release the corresponding reductive elimination product upon chemical oxidation by silver salts or ferrocenium complexes.[7] Since, these reactions does not take place under heating, the authors propose that there is an oxidation of the metal complex prior to the reductive elimination (OIRE).

Regarding DFT calculations, one of the first mechanistic proposal considering explicitly [Cu(OAc)$_2$] species on the calculations was disclosed by Morokuma *et al.* in the Rh^{III}-catalyzed C–H activation of 8-methylquinoline,[4a] previously published by Song *et al*.[8] (Scheme 2.6). This reaction, which is not an oxidative coupling, consists of the creation of a new C–C bond between a C_{sp^3} and an alkyne through a Rh^{III} redox neutral catalytic cycle. Initially, in the experimental

5 Li, L.; Brennessel, W. W.; Jones, W. D. *J. Am. Chem. Soc*. **2008**, *130*, 12414.

6 Pedersen, A.; Tilset, M. *Organometallics* **1993**, *12*, 56.

7 a) Shin, K.; Park, Y.; Baik, M.-H.; Chang, S. *Nat. Chem*. **2018**, *10*, 218. b) Kim, J.; Shin, K.; Jin, S.; Kim, D.; Chang, S. *J. Am. Chem. Soc*. **2019**, *141*, 4137.

8 Liu, B.; Zhou, T.; Li, B.; Xu, S.; Song, H.; Wang, B. *Angew. Chem. Int. Ed*. **2014**, *53*, 4191.

report, copper(II) species was proposed to provide acetates as a base for the C–H activation step. In contrast to the experimental proposal, Morokuma *et al.* suggested that the acetate ligands coordinated to the copper(II) centers promoted an intermolecular C–H activation event on the Rh^{III} species (Scheme 2.6).

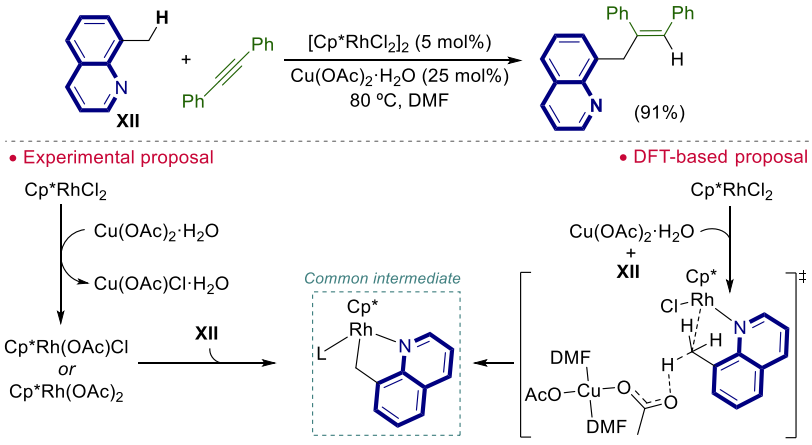

Scheme 2.6. Morokuma's case study using DFT calculations of the Rh^{III}-catalyzed C–H activation of 8-methylquinoline through redox neutral Rh catalytic cycle.

Yet interesting, the accuracy of these results have been questioned by Macgregor and co-workers due to the lack of diffuse functions in the basis set.[9]

In 2007, Miura and Satoh experimentally studied the influence of stoichiometric amounts of external oxidants in the chemoselectivity of the Rh-catalyzed oxidative coupling between benzoic acids and alkynes (Scheme 2.7).[10] On the one hand, when they used $[Cu(OAc)_2]$ as oxidant, product **XV** was exclusively observed in a 89% yield (Scheme 2.7). On the other hand, when using Ag(OAc), CO_2 extrusion takes places, giving rise to naphthalene derivative **XVI**, as the major product, along with product **XV**.

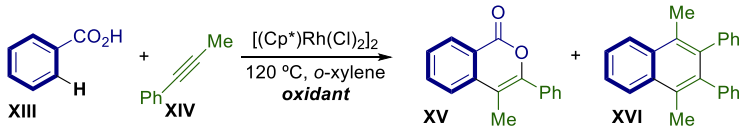

Scheme 2.7. Rh^{III}-catalyzed oxidative coupling between benzoic acid and alkyne using different metal-containing external oxidants.

The original mechanistic proposal is depicted in Scheme 2.8. The reaction starts with the formation of the five-membered rhodacycle intermediate **XVII** by a concerted metalation-deprotonation (CMD) event from $[(Cp^*)Rh(OAc)_2]$ intermediate.[Error! Bookmark not defined.,9] Once the C–H bond is cleavage, intermediate **XVII** undergoes alkyne insertion (AI) to form seven-

9 David, D. L.; Macgregor, S. A.; McMullin, C. L. *Chem. Rev*. **2017**, *117*, 8649.
10 Ueura, K.; Satoh, T.; Miura, M. *J. Org. Chem*. **2007**, *72*, 5362.

membered cyclometalated intermediate **XVIII**. At this point, this species can undergo two different transformations: a) direct reductive elimination, yielding product **XV** and [(Cp*)Rh^{I}] complex, and/or b) decarboxylation reaction forming intermediate **XIX** which further undergoes a sequence of alkyne insertion (AI) and reductive elimination that finally results in the formation of [(Cp*)Rh^{I}] species and the naphthalene derivative (**XVI**).

A common step for both pathways is the reoxidation of [(Cp*)Rh^{I}] species by the oxidant to generate the catalytically active Rh^{III} complex.

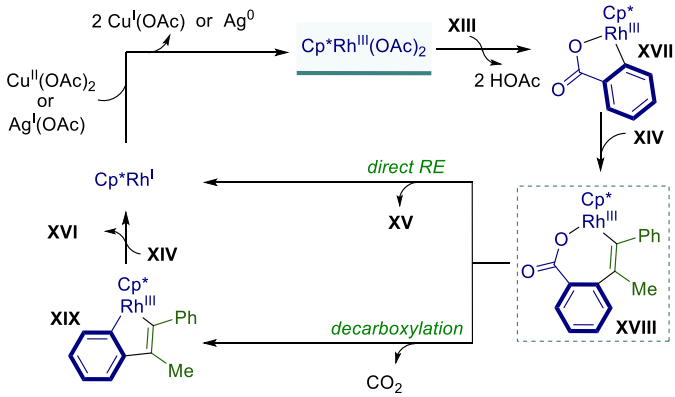

Scheme 2.8. Original mechanistic proposal by Miura and Satoh. Intermediate XXVII is the key intermediate controlling the chemoselectivity.

In 2016, our group undertook the study of the origin of the chemoselectivity for this reaction by performing calculations at the DFT level.[4b,c] To do so, *1,2,3,4,5*-pentamethylcyclopentadienyl ligand (Cp*) was approximated to cyclopentadienyl ligand (Cp) and a benchmarking of different functionals and basis sets was performed, showing that B97D represents properly the system with the least computational cost.[4b]

First, the authors investigated the C–H activation step of the benzoic acid. Regarding the widely proposed catalytically active [(Cp*)Rh(OAc)$_2$] species, the energy barrier for this step was 28.7 kcal·mol^{-1} above the reactants (**TS1**, Scheme 2.9), which is a high barrier. Then, they considered the potential participation of [Cu(OAc)$_2$] as a dimer in the form of [Cu(OAc)$_2$(H$_2$O)]$_2$ in the ortho rhodation. The copper(II) promoted the deprotonation of the benzoic acid to yield a benzoate moiety coordinated to the copper dimer, intermediate **XXI**. Henceforth, [(Cp*)Rh(Cl)$_2$] complex interacts with the copper moiety to give rise intermediate **XXII** which has the appropriate geometry for the concerted metalation-deprotonation (CMD). This transition state present a barrier of 28.0 kcal·mol^{-1}, suggesting that copper acetate can participate in the C–H activation step.

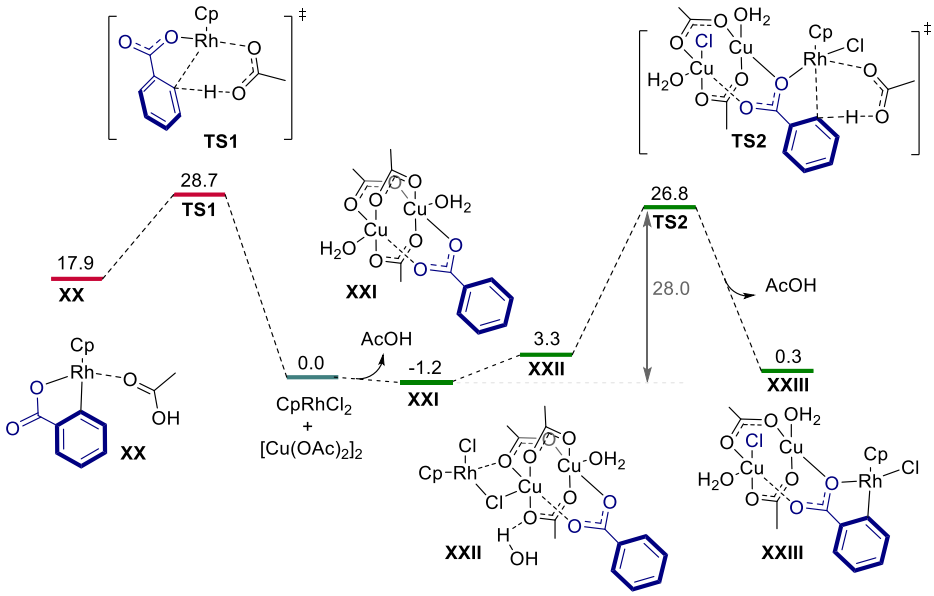

Scheme 2.9. C–H activation step for the Rh-catalyzed coupling of benzoic acid derivatives and alkynes in the presence of Cu(II) acetate. Free energies in kcal·mol^{-1}.

Regarding the observed experimental product distribution, our group considered **XVIII$_{Cp}$** species (Scheme 2.10) as previous intermediate to the chemoselectivity-determining transition states: the decarboxylation and the reductive elimination step (Scheme 2.10). Our group found that the CO_2 extrusion (**TS3**, Scheme 2.10) was favored versus the reductive elimination event (**TS4**, Scheme 2.10) from intermediate **XVIII$_{Cp}$**, leading to the exclusive formation of the naphthalene derivative **XVI**. Nonetheless, this result is in sharp contrast with the experimental results of the selective formation of isocumarin product **XV**. Further computational studies showed that Cu^{II} species, in the form of $[Cu(Cl)(OAc)(H_2O)]_2$ complex, can cooperate with rhodium catalyst and promote the reductive elimination event to generate exclusively product **XV**, explaining the experimental observation.[4b] The key intermediate **XXXI** consists of a trimetallic species where different ligands (carboxylate and chloride) are playing a role as bridging ligands between copper dimer and rhodium catalyst. Initially, the formal oxidation state of the metal centers can be represented by Cu^{II}–Cu^{II}–Rh^{III}. The reductive elimination from this adduct (**XXXI**) was only 0.6 kcal·mol^{-1} above the origin of energy (**TS5**, Scheme 2.10), much favored than **TS3** and **TS4**. Additionally, when studying in detail this reductive elimination event, they observed that the two electrons from the reductive elimination were transferred not only to the rhodium but also to the copper centers. This was proposed on the basis of the increase of spin density at the Rh metal center which indicates a partial reduction from Rh^{III} to Rh^{II} during the transition state. Finally, after the reductive elimination, the formal oxidation states of intermediate **XXXII** can be represented by Cu^{I}–Cu^{II}–Rh^{II}. Since both metals center are

electronically participating during the reductive elimination, this singular step was referred as cooperative reductive elimination (CRE).

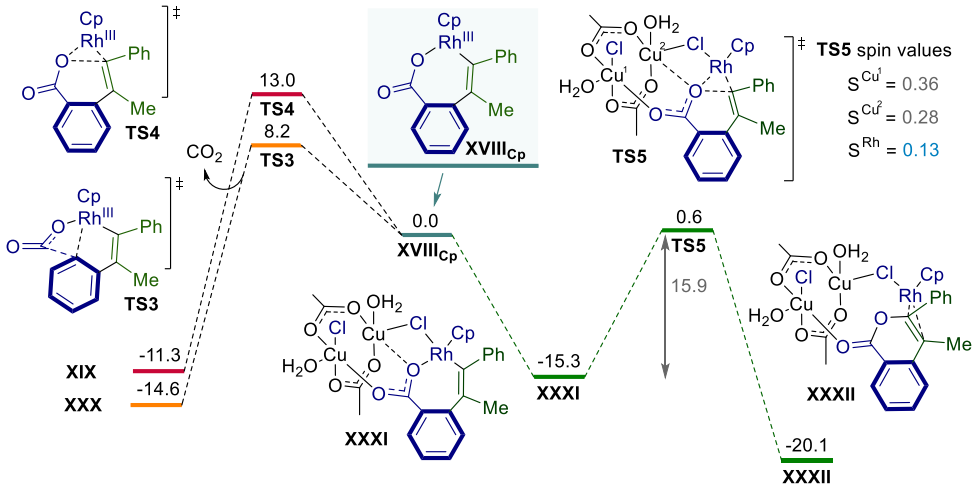

Scheme 2.10. Mechanistic divergence for explaining the exclusive formation of the C–O bond formation product, **XXV**, when using copper(II) acetate as external oxidant. Free energies in kcal·mol^{-1}.

When considering silver as oxidant for this system, the chemoselectivity-determining transition states were very close in energy, in line with the experimental formation of both the naphthalene and isocumarin derivatives. Interestingly, in this case, the carboxylate group remained attached to the rhodium center forming a slightly different intermediate prior the C–C or C–O bond-forming event compared to copper system (**XXXIII**, Scheme 2.11).[4c]

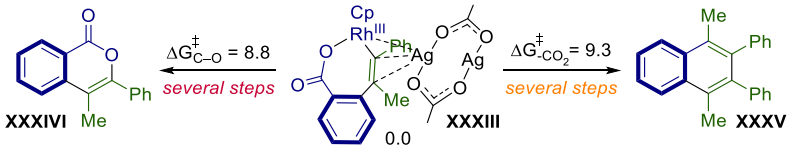

Scheme 2.11. Evaluation of the chemoselectivity-determining transition states: the decarboxylation or the reductive elimination from intermediate **XXXII**, which considered interaction between Rh^{III} intermediate and silver acetate oxidant. Free energies in kcal·mol^{-1}.

In this venue, endeavors of our group demonstrated that copper(II) acetate can play a crucial role in the reaction outcome, defining a new concept of reductive elimination: cooperative reductive elimination.

In 2018, our group in collaboration with Patureau group disclosed that this type of cooperation was not only restricted to Rh/Cu systems but it also appeared in Ru/Cu systems in the context of oxidative coupling.[4d] An experimental re-optimization of the reaction conditions for a previous report on a Ru/Cu co-catalyzed dehydrogenative homo-coupling of 9*H*-carbazoles at the C1 position[11] suggested that the Cu salt accelerated the coupling reaction. Further kinetic experiments pointed out the formation of a trinuclear Ru/Cu catalytically active species.[4d]

11 M.-L. Louillat; F. W. Patureau, *Org. Lett.* **2013**, *15*, 164.

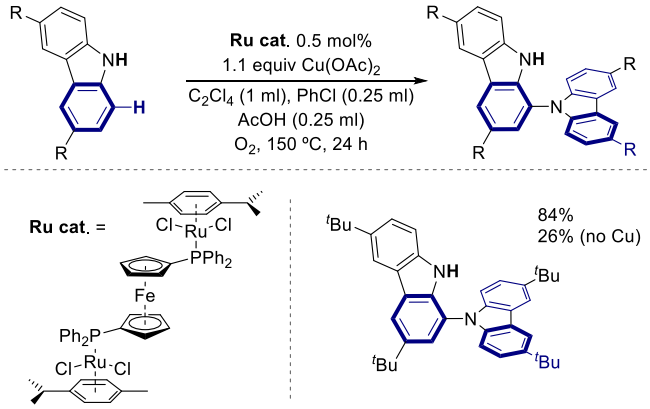

Scheme 2.12. General protocol for the dehydrogenative homo-coupling of 9*H*-carbazol derivatives.

DFT calculations supported this experimental evidence. First, the N–H activation takes place by the Cu(II) catalyst. Then, a trinuclear intermediate is formed by copper(II) and Rh(III) scaffolds, intermediate **XL**, that undergoes the C–H activation step through a very low barrier (**TS6**) to give rise intermediate **XLII**.[4d] Subsequently, the reductive elimination step from this trinuclear species (**TS7**) entails the formation of the organic product which remains coordinated to the Rh-Cu species. It is noteworthy that this transition state **TS7** involves a single electron transfer from the Rh^{III}–C bond (**XLII**) to the N atom that regenerates the Rh^{II} metal center and forms the corresponding C–N bond.

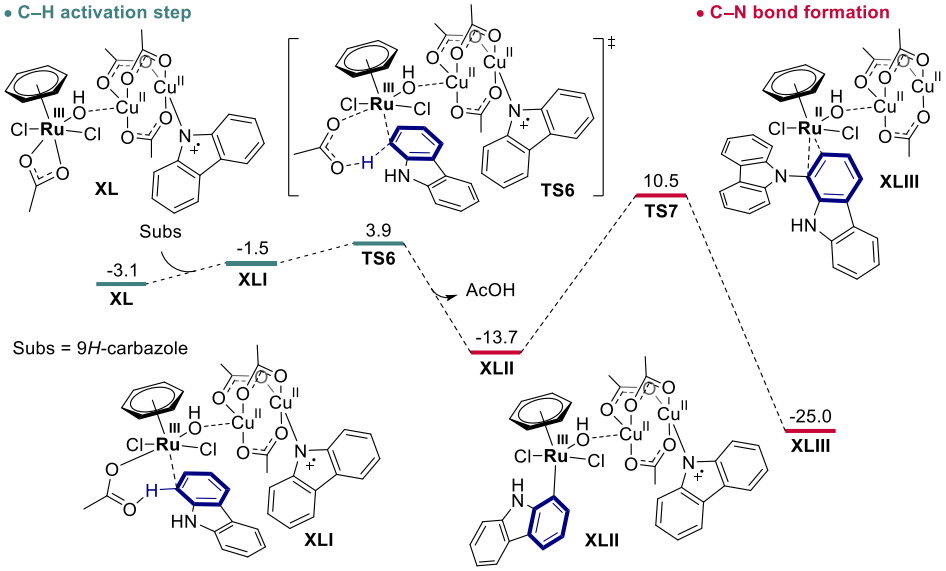

Scheme 2.13. Free energy profile for the C–H activation and reductive elimination steps of the Ru/Cu co-catalyzed dehydrogenative homo-coupling of 9*H*-carbazol derivative. The ligand in the Ru catalyst was simplified for benzene instead of *p*-cymene. Energies in kcal·mol^{-1}.

Hence, our group have shown that assumed reaction mechanisms in oxidative coupling reactions can be more complex than expected and, therefore, in some cases, the reaction outcome could be difficult to predict. Additionally, this reinforces that additives, reagents and/or co-catalysts can play an unexpected role in the reaction mechanism of catalytic transformations.[12] In this venue, we envisioned that this type of cooperation could be taking place in Rh/Cu-catalyzed synthesis of isoquinolines from α-aryl vinyl azides and alkynes, turning this bimetallic systems in an even more complex transformation from a mechanistic point of view.**Error! Bookmark not defined.**

2.1.2. **Theoretical approach to discriminate mechanisms in complex systems.**

A mechanistic proposal should explain each and every feature coming up from a given chemical transformation such as selectivity, side products, reaction rate, partial orders, reaction time, *etc*. Generally, DFT calculations have been used to explain these features based on the free energy of every intermediates and transition states that connect substrates and products, what is known as the free energy profile of the reaction. Firstly, the viability of a reaction is evaluated according to the obtained activation barrier. If the DFT-calculated activation barriers are below 20 kcal·mol^{-1}, the reaction should occur in a fast manner, while if the barrier is above 30 kcal·mol^{-1}, not product formation should be observed even under heating. Secondly, the discrimination between different reaction mechanisms relies on the assumption that the most plausible reaction mechanism is the lower in free energy profile. Apart from that, a DFT-calculated mechanistic proposal should be totally "corroborated" when the DFT-obtained free energy span[13] fully explains the experimental results. Ideally, thermodynamic or kinetic experimental data are important parameters to compare with DFT results but they are scarce in the literature as it is challenging to obtain.[14] In addition, another shortcoming of this approach is that issues as important as molecularity, concentration and temperature are negleted. These last variables are of special importance when considering complex systems as bimetallic dual catalytic transformations.

---

12 a) González-Pérez, A. B.; Álvarez, R.; Faza, O. N.; de Lera, Á. R.; Aurrecoechea, J. M. *Organometallics* **2012**, *31*, 2053. b) Mudarra, Á. L.; Martínez de Salinas, S.; Pérez Temprano, M. H. *Org. Biomol. Chem.* **2019**, *17*, 1655.

13 Kozuch, S.; Shaik, S. *Acc. Chem. Res.* **2011**, *44*, 101.

14 When lacking thermodynamic or kinetic information about a reaction, the selectivity of a reaction could be a reasonable criteria to evaluate the plausibility of a given mechanism since it is a consequence of the free energy difference between different mechanisms. For instance, it has been proved that for stereoselective processes, DFT calculation can explain the product distribution observed even if the description of activation energy height is not extremely accurate (ref. **Error! Bookmark not defined.**). However, mechanistic information can be missed if the criteria exclusively relies on the selectivity of the reaction.

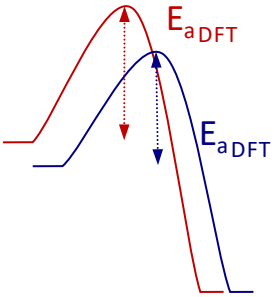

Figure 2.1. Ideal comparison of DFT-obtained free energy activation barrier and experimental one.

Alternatively, to discriminate between different reaction pathways, we envisioned to use an observable that is present across the literature: the reaction time. Importantly, reaction time is intimately tied to kinetic parameters and, therefore, as we will explain below, to the thermodynamic of the reaction. In other words, if we can predict the reaction time using DFT free energy values, we can validate mechanistic proposal directly by comparison with the experimental reaction time. This can be done by using microkinetic modeling. This tool allows the translation of the free energy profile of complex systems into the evolution of the concentration of the different species over time.[15] Additionally, this approach considers the neglected parameters when interpreting exclusively free energy profiles: molecularity, concentration and temperature.[Error! Bookmark not defined.b,17] Microkinetic modeling of DFT-calculated reaction mechanisms has been exploited in heterogeneous simulations[16] but it is still laying the ground for DFT-proposals in the field of homogeneous catalysis as has been recently described by Himo and *et al*. and Notestein, Nguyen and Broadbelt and co-coworkers.[Error! Bookmark not defined.b,17]

2.1.2.1. From activation barrier to reaction time in complex systems

In this section, we will briefly explain the transformation of the activation barrier to a predicted reaction time.

The macroscopic expression for the rate of a reaction as $n_aA + n_bB \rightarrow n_cC + n_dD$ is represented in eq. 1, which is known as rate law.

$$\text{rate} = -\frac{1}{n_a}\frac{d[A]}{dt} = -\frac{1}{n_b}\frac{d[B]}{dt} = \frac{1}{n_c}\frac{d[C]}{dt} = \frac{1}{n_d}\frac{d[D]}{dt} = k[A]^{n_a}[B]^{n_b} \quad (eq.\,1)$$

15 Besora, M.; Maseras, F. *Wiley Interdiscip. Rev.: Comput. Mol. Sci.* **2018**, *8*, e1372.

16 a) Li, Q.; García-Muelas, R.; López, N. *Nature Commun.* **2018**, *9*, 526. b) Rellán-Pineiro, M.; López, N. *ACS Sustainable Chem. Eng.* **2018**, *6*, 16169.

17 Yu, Y.; Zhu, Y.; Bhagat, M. N.; Raghuraman, A.; Hirsekorn, K. F.; Notestein, J. M.; Nguyen, S. T.; Broadbelt, L. J. *ACS Catal*. **2018**, *8*, 11119.

where [X] is the concentration of the species X, n_x is the stoichiometric coefficient of X in the reaction and *k* is the rate constant of the reaction. The transition state theory relates the rate constant with the activation free energy, $\Delta G^{\ddagger}$, through the Eyring-Polanyi equation, eq. 2.

$$k = \kappa(T)\frac{K_B T}{h}(c^0)^{1-m} e^{\left(\frac{-\Delta G^{\ddagger}}{RT}\right)} \quad (\text{eq. } 2)$$

where k is the rate constant, κ is the transmission faction, K_B is the Boltzmann's constant, T is the temperature, h is the Planck's constant, c^0 is a pressure- and temperature-dependent concentration factor that accounts the standard state (1 mol·l^{-1}), m is the number of reactants, $\Delta G^{\ddagger}$ is the activation free energy and R is the ideal gas constant. The value of the transmission fraction is assumed to be 1 in homogeneous catalysis

It should be noticed that the integration of the rate law (eq. 1) would provide the evolution of the concentration of the different species over time. This means that it is possible to connect DFT-calculated $\Delta G^{\ddagger}$ values, through the rate constant, with the evolution of the concentration of a species over time. In the case of an elementary reaction, the integration of the rate law can be a straightforward task and it can be resolved even analytically. However, most of the processes, especially in catalysis, are multistep reaction network whose differential equation systems are not obvious to resolve. To do so, microkinetic modeling are performed. It consists of a set of elementary reactions, whose rate constants are known, that connect the substrates with the products. The numerical resolution of the corresponding differential equation system affords the evolution of the concentration of the different species over time by using a given initial concentration. There are software that perform the resolution of this complex mathematical problem with a minimum computational cost such as COPASI.[18]

2.1.2.2. **Workflow for the discrimination between mechanisms**

We will consider the plausibility of a proposed mechanism for our bimetallic dual catalytic system if it completely explains two observables: the reaction time and the experimental selectivity. If the DFT-obtained reaction time or selectivity for a given reaction model are not representative of the experimental ones, this model will be reconsidered and an alternative one will be calculated. This iterative process may allow us to finally obtain a mechanistic proposal that fulfills all the experimental observations. Moreover, this search process would provide us a critical vision on the different assumed approximations for modeling oxidative coupling reactions.

[18] Hoops, S.; Sahle, S.; Gauges, R.; Lee, C.; Pahle, J.; Simus, N.; Singhal, M.; Xu, L.; Mendes, P.; Kummer, U. *Bioinformatics*, **2006**, *22*, 3067.

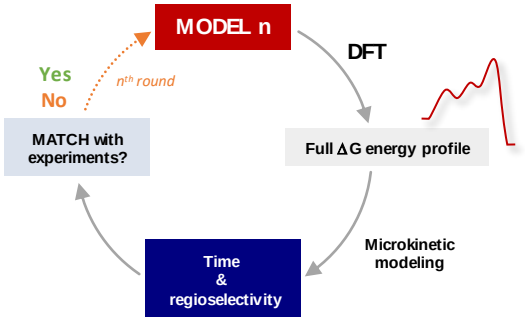

Figure 2.2. Workflow for the evaluation of the different reaction mechanisms based on a combination of DFT calculations and microkinetic modeling of the reaction model.

2.2. Objectives

Bimetallic dual catalytic systems in oxidative coupling reactions have been rarely explored from a mechanistic point of view. The general mechanistic proposal consists of two independent catalytic cycles which activate the corresponding substrates in concert. The interlinked step, in those systems, allows the transference of electrons and ligands between both catalysts.

In this venue, we focused our attention on the Rh/Cu-catalyzed synthesis of isoquinolines from α-aryl vinyl azides and internal alkynes. The current mechanistic proposal for this system implies the reductively activation of the azide by a Cu^{I} catalyst, forming Cu^{II}, while the Rh^{III} catalyst affords the oxidative coupling reactions through C–H activation, alkyne insertion and reductive elimination steps, yielding Rh^{I} species. The Rh^{III} and Cu^{I} catalysts are regenerated by reaction of Cu^{II} with Rh^{I}. Apart from this seminal proposal, there is not further discussion on the complete characterization of reaction mechanism of this kind of systems, by DFT, in the literature. Based on our previous knowledge on similar systems, we envisioned that these catalytic cycles may not be as independent as it is expected.

We decided to evaluate the DFT-obtained mechanisms by using microkinetic modeling due to the complexity of the system. Thus, we can use the DFT-predicted reaction time to compare with experimental reaction times and so validate our calculated mechanism. Moreover, the obtained route has also to explain the observed regioselectivity of the reaction.

This study not only aims to describe the energy profile of this particular system and explore the most plausible mechanism, but also to analyze in detail some common simplifications that have been widely assumed in theoretical investigations of complex catalytic cycles, especially in oxidative coupling reactions. To do so, the following points are pursued:

- Systematic study of the potential reaction mechanisms for the Rh/Cu-catalyzed synthesis of isoquinolines from α-aryl vinyl azides and internal alkynes.

- Evaluate the plausibility of the different reaction mechanisms by using microkinetic modeling.

- Reexamine the proposed reaction mechanism, if necessary, until it is able to explain the experimental reaction time (30 min when using CuOAc) and regioselectivity (in Scheme 2.4).

2.3. Results and discussion

2.3.1. Model system and computational methods.

We carried out DFT calculations using the B97D functional with a double-ζ plus polarization and diffuse basis set in DMF as solvent (see Computational Appendix for more details). The selection of the functional was based on previously benchmarking studies on similar systems.[4b] The model substrates are shown in Figure 2.3 for each case study.

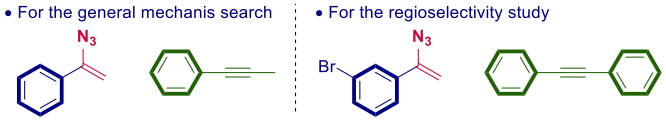

Figure 2.3. Model substrates for the mechanistic study using DFT calculations.

Regarding the catalysts, we investigated the speciation of copper acetate and rhodium(III) complexes in solution. We found that copper acetates, regardless if it is copper(I) or copper(II), tend to form dimeric species while the rhodium(III) dimer leads to the spontaneous formation of two monomeric complexes. For this reason, we will consider the monomeric form of the rhodium catalyst and the dimeric species of copper for the further mechanistic studies.

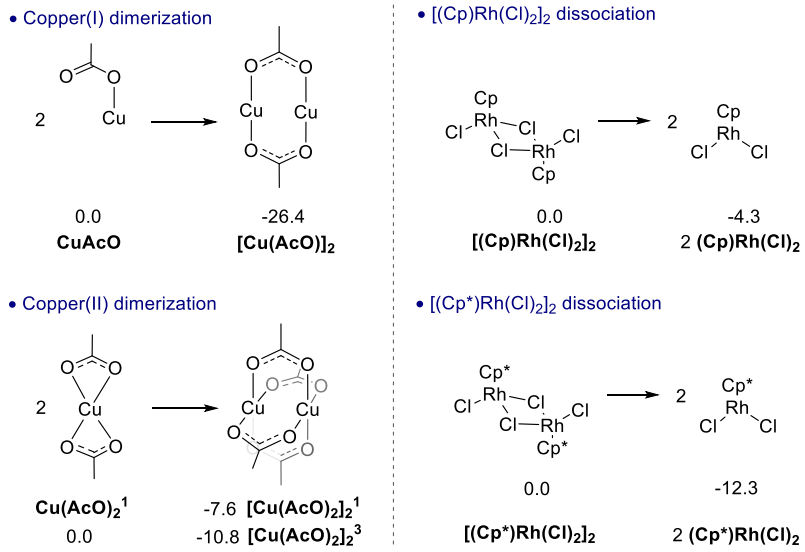

Scheme 2.14. Speciation of the catalyst in the reaction media calculated by DFT. The results show the dimerization of copper and the formation of monomers from rhodium(III) catalyst. Free energies in kcal·mol^{-1}.

2.3.2. **Mechanistic investigation on the Cu^{I}-catalyzed denitrogenative reductive formation of imine from α-aryl vinyl azide**

We started our investigations by studying the denitrogenative reduction of the α-phenyl vinyl azide. It is proposed that these substrate type spontaneously undergo the nitrogen extrusion at high temperatures to yield *2H*-azirine compounds.[Error! Bookmark not defined.] In our system, the thermally driven nitrogen extrusion reaction presents a barrier of 27.3 kcal·mol^{-1}, which does not agree with the experimental reaction time of 30 min (Scheme 2.15). Thus, we hypothesized that the reaction could be catalytically driven by the rhodium or copper metal complexes. When considering, Rh^{III} we observe a slightly decrease on the nitrogen extrusion barrier of 1.3 kcal·mol^{-1}, which is a small difference (Scheme 2.15). In sharp contrast, when considering [Cu(OAc)]$_2$, as a dimer, the activation barrier decreases in 5.5 kcal·mol^{-1} (21.8 kcal·mol^{-1}). This transition state, **TS I1-I4^1**, evolves towards the formation of a new N–C bond affording a *2H*-azirine organic moiety coordinated to the Cu^{I} dimer, **I4^1**. This step is irreversible due to the very exergonic dinitrogen extrusion (Scheme 2.15).

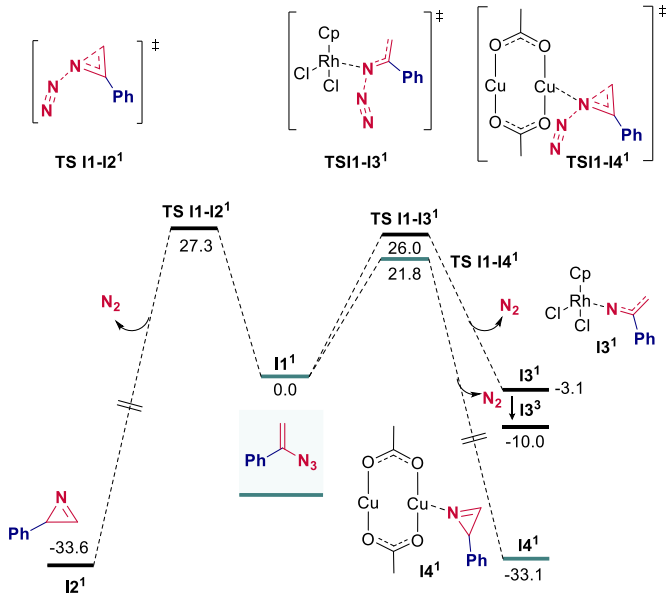

Scheme 2.15. Different pathways for the formation of *2H*-azirine from vinyl nitrene. The most favorable pathway is colored in turquoise for ease of reading. The superscript is the multiplicity of the calculation being 1 a singlet state and 3 a triplet state. The reference point of energy was all the species in solution.

We next investigated the reductive transformation of this *2H*-azirine intermediate catalyzed by copper(I). First, we found that the most favorable pathway consists of an initial ring opening of the 2*H*-azirine through the homolytic C–N bond cleavage (**TS-I4-I5^{OSS}**) to generate a new double C–C bond in **I5^{OOS}**, an open shell singlet intermediate. This step along with the

subsequent transformations is depicted in Scheme 2.16. Intermediate **I5^{OSS}** can easily undergo a multiplicity exchange from open-shell-singlet (OSS) to triplet state, giving rise intermediate **I6^{3}**. The barrier for this transformation is 24.0 kcal·mol^{-1}. Interestingly, **I5^{3}** collapse in **I6^{3}** by the coordination of the β-carbon to one of the copper centers. Then, the consecutive coordination of two molecules of acetic acid to form **I8^{3}** was found favorable and necessary to afford the subsequent protonation reactions.

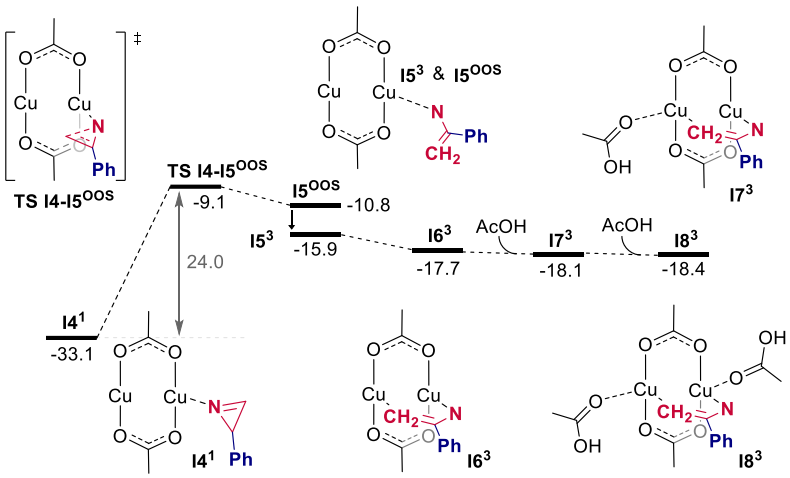

Scheme 2.16. Free energy profile for the ring opening of the 2*H*-azirine to afford the imidyl copper complex, **I8^{3}**. Energies in kcal·mol^{-1}.

In terms of electron flow, the Cu^{I}-Cu^{I} moiety in **I4^{1}** is oxidized to a triplet Cu^{II}-Cu^{I}-N^{radical} intermediate (**I8^{3}**). This was supported by analysis of the single-occupied molecular orbitals (SOMO) and the spin density distribution in **I8^{3}**. The analysis of the frontier molecular orbitals indicates that the unpaired electrons are mainly delocalized on the N and C atoms in the organic moiety but stabilized by some contribution of the metal centers (Figure 2.4).

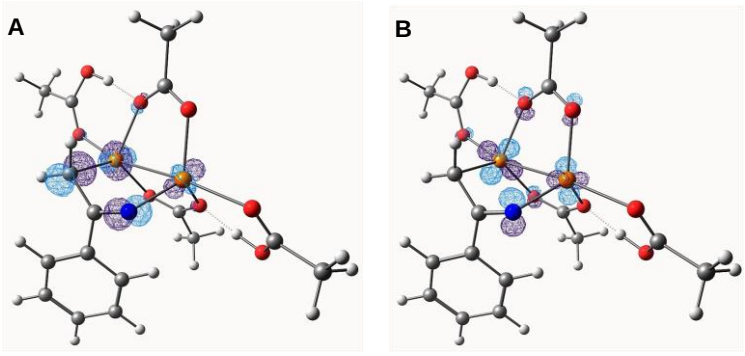

Figure 2.4. SOMO analysis of **I8^{3}** intermediate. A) Highest (left) energy single-occupied molecular orbital (SOMO) of I5^{3} (isosurface = 0.09). B) Highest (right) energy single-occupied molecular orbital (SOMO-1) of **I8^{3}** (isosurface = 0.09). Color code: carbon (gray), white (hydrogen), blue (nitrogen), orange (copper), red (oxygen).

Regarding the spin density, which represents the electron density of radical species, we found that one of the unpaired electrons is mainly located on the nitrogen atom while the other is delocalized among the C and the Cu atoms, indicating that a partial oxidation of the copper atoms has already taken place due to the homolytic cleavage of the C–N bond.

Next, we envisioned to evaluate the reduction of the imidyl moiety to the imine intermediate. This reaction proved to happen in a sequential fashion. First, a Hydrogen Atom Transfer (HAT) reaction takes place from the acetic acid to the nitrogen atom attached to copper (**TS I8-I9^3**, Scheme 2.17). This step involves a formal reduction of the imidyl moiety and, subsequently, a partial oxidation of the copper dimer. This was supported by the spin density evolution on the copper dimer and the substrate from **I8^3** and **I9^3**. Intermediate **I9** showed to be stable in triplet and single electronic state.

Then, a second HAT (**TS I10-I11^3**) from the acetic acid to the methylidene takes place generating a Cu^{II} dimer and the imine, **I11^3**. It should be noticed that the first HAT entails the protonation of the nitrogen atom instead of the methylidene group in contrast with what has been proposed in the literature.[Error! Bookmark not defined.] In fact, this reaction exhibited a higher energy barrier and so it is disfavored (**TS I8-I10^3**).

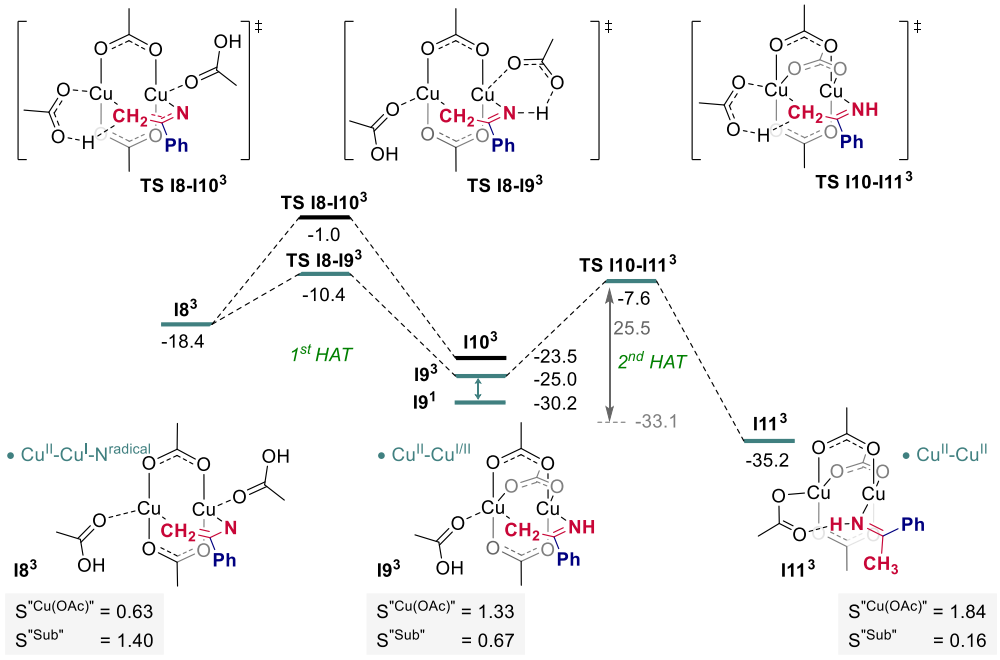

Scheme 2.17. Free energy profile of the reductive activation of the substrate by $[CuOAc]_2$. Energies in kcal·mol^{-1}. Spin densities values of **I8^3**, **I9^3** and **I11^3** intermediates are represented. The corresponding intermediate has been considered as two fragments: the copper dimer moiety ($S^{"Cu(OAc)"}$) and the substrate ($S^{"Sub"}$).

The analysis of the evolution of the spin density throughout the reduction of the 2*H*-azirine intermediate to the imine (Scheme 2.17) allowed us to assign the oxidation number of the copper along the transformation. Initially, as mentioned above, **I8^3** can be described as a Cu^{II}-Cu^{I}-$N^{radical}$ complex. After the first HAT, the spin density on the copper moiety increases indicating that **I9^3** can be rather described by Cu^{II}-$Cu^{I/II}$ complex. Finally, the second HAT affords **I11^3** which corresponds to a Cu^{II}-Cu^{II} species. In Figure 2.5, we can see the evolution of this spin density during the subsequent HAT reactions that involve the copper oxidation and substrate reduction.

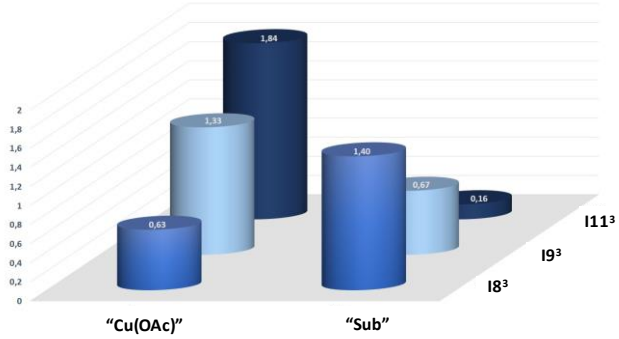

Figure 2.5. Spin density evolution on the reaction coordinate. Intermediates have been considered as two fragments: the copper fragment and the N-containing substrate fragment.

Thus, copper(I) catalyzed the denitrogenative reduction of the α-phenyl vinyl azide where the two protonation of the imidyl intermediate involves a formal oxidation of the Cu(I) to Cu(II), affording the corresponding imine. This reaction was proved to occur experimentally (Scheme 2.2).

2.3.3. **Evaluation of the system using [(Cp)Rh(OAc)$_2$] as active catalyst**

Once the substrate has been activated by the copper(I) complex into the corresponding imine, we addressed the exploration of the Rh^{III}/Rh^{I} catalytic cycle, described in the Introduction of this Chapter (Scheme 2.3). The original mechanistic proposal assumed that the catalytically active species of the oxidative C–H coupling reactions is the complex [(Cp*)Rh(OAc)$_2$] originated from the pre-catalyst [(Cp*)Rh(Cl)$_2$]$_2$ (Scheme 2.2). We started our DFT investigation using this proposal as starting point assuming the simplification of the Cp* ligand by Cp, a common approximation in DFT calculations regarding oxidative coupling.[4b,4c]

The most favorable mechanism is depicted in Scheme 2.18. Initially, the imine intermediate coordinated to the copper(II) complex, **I11^3**, can exergonically coordinate to the rhodium diacetate species to form **I13^1**. The next step, regarding the original proposal, is the deprotonation of the N–H at intermediate **I13^1** to give rise **I14^1** complex. We assumed a fast equilibrium between both the protonated (**I13^1**) and deprotonated species (**I14^1**) since we did not find any transition state for this step in an inner sphere fashion. Once **I14^1** is formed, the

vacancy generated by the released HOAc allows the C–H activation event *via* concerted metalation-deprotonation (CMD) transition state, **TS I14-I15^1**, encompassing the formation of rhodacycle **I11^1** through an overall free energy barrier of 20.6 kcal·mol^{-1}. Intermediate **I15^1** has a weakly coordinated HOAc that is easily exchanged by 1-phenyl-1-propyne to form **I16^1**.

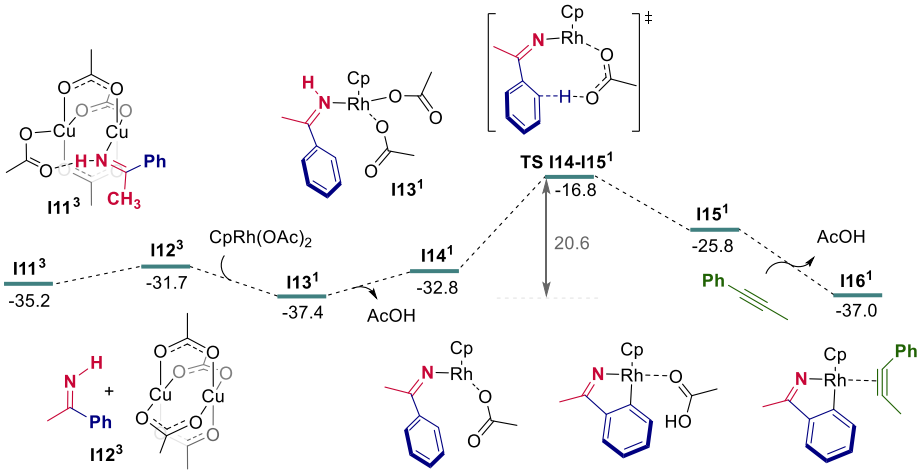

Scheme 2.18. Free energy profile for the C-H activation of the imine intermediate catalyzed by [CpRh(OAc)$_2$] assuming the current literature proposal. Energies in kcal·mol^{-1}.

Henceforth, a downhill cascade of low barrier events from **I16^1** ends up in the corresponding **I19^1** product *via* alkyne insertion (**TS I16-I17^1**) and reductive elimination (**TS I17-I18^1**) steps (Scheme 2.19). Finally, the initial catalyst is regenerated by the oxidation of the Rh^{I} to Rh^{III} and the concomitant reduction of Cu^{II} to Cu^{I}.

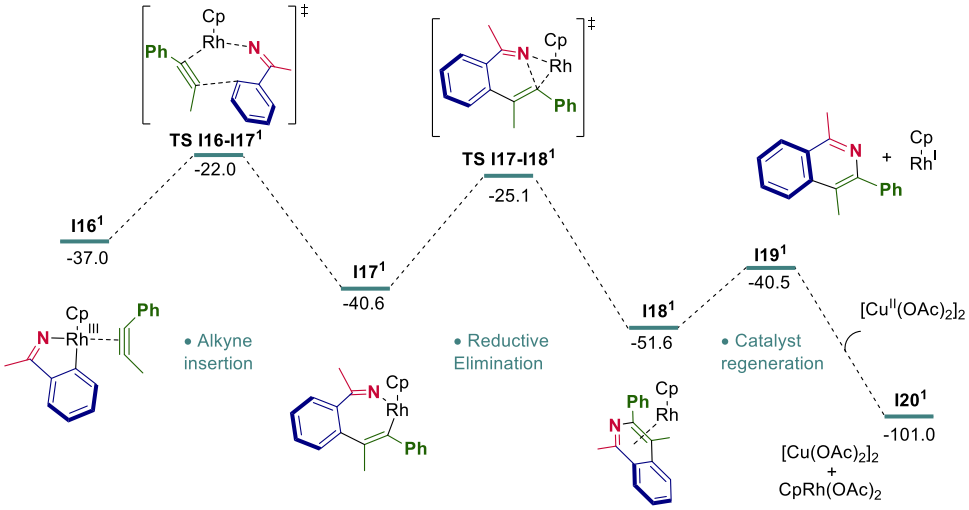

Scheme 2.19. Free energy profile for the alkyne insertion, reductive elimination and catalyst regeneration starting from **I16^1** when considering [(Cp)Rh(OAc)$_2$] as catalyst. Energies in kcal·mol^{-1}.

Once evaluated both potential cycles, the copper cycle and the rhodium cycle, the reaction profile that we obtained for the so-far proposal shows that the highest barrier of a single step is 24.0 kcal·mol^{-1}, corresponding to the *2H*-azirine ring opening (**TS I4-I5^{OSS}**, Scheme 2.16). The rate determining states are **I4^{1}** and **TS I10-I11^{3}** being the free energy span 25.5 kcal·mol^{-1} (Scheme 2.17).[13] Therefore, the reaction could be accessible at 90 ºC.

2.3.3.1. Microkinetic modeling of model 1

The aforementioned profiles, the Cu-catalyzed formation of the imine and the catalyzed oxidative coupling of the imine by [(Cp)Rh(OAc)$_2$], do not provide any further information apart from the feasibility of the reaction at that temperature on the basis of the free energy span of the catalytic transformation. As explained in the Introduction, we envisioned that we could employ a predicted reaction time based on the DFT calculations to evaluate if this mechanism could be representative of the real system. To do so, we use microkinetic modeling.

A set of fourteen reversible and irreversible elementary reactions were considered regarding the obtained free energy profiles for this model 1. For ease of reading, the complete description of the microkinetic model is in the Appendix. The initial concentrations for the microkinetic modeling, according to the experimental conditions and the speciation of each catalyst, are 0.20 M for the alkyne, 0.24 M for the azide, 0.02 M for the copper(I) and 0.0104 M for the rhodium(III) catalyst as a monomer. Catalyst decomposition or inconspicuous side reactions have not been considered and a 100% of conversion is expected for all the reactions.

Regarding this, when performing the microkinetic simulation, we obtained a predicted reaction time of 21 hours for achieving the complete conversion of the alkyne substrate. In sharp contrast, experimentally, the reaction is finished in 30 min when copper(I) acetate is used. Thus, we concluded that this mechanistic proposal (model 1) is too simplistic to accurately reproduce the experimental observations.

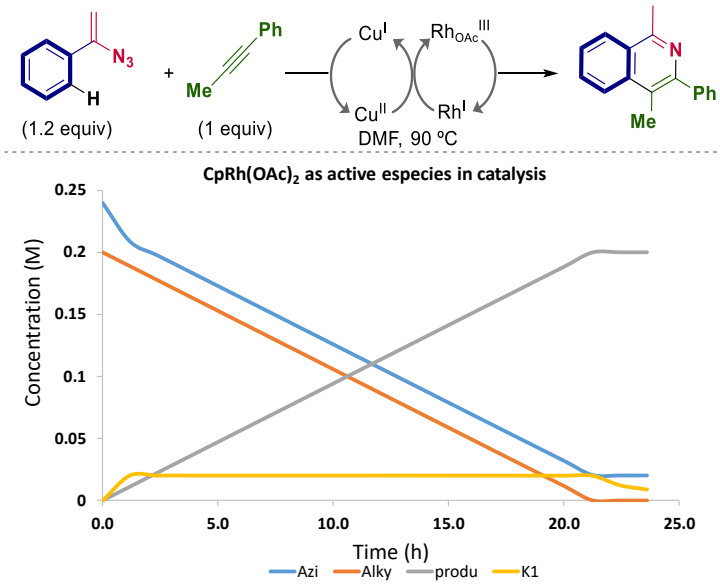

Scheme 2.20. Evolution of the concentration of substrates and products over time according to microkinetic modeling of the mechanistic proposal of model 1. K1 is I41.

2.3.4. **Evaluation of the system using [(Cp)Rh(Cl)$_2$] as active catalyst**

In previous studies, our group has showed that the formation of [(Cp)Rh(OAc)$_2$] is not trivial when there are not good acetate donors in the reaction mixture.[4b,4c] Indeed, based on our current DFT results (Scheme 2.21), the formation of this species seems to be highly unlikely to happen since the exchange of the chlorides from the Rh^{III} pre-catalyst and the acetates from copper(II) for this system is highly endergonic by 21.5 kcal·mol^{-1} per rhodium center.

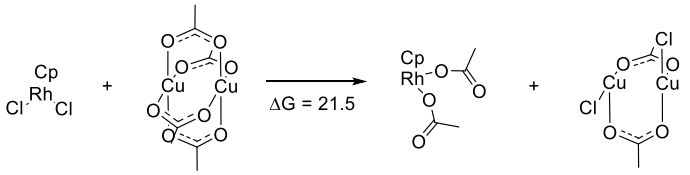

Scheme 2.21. Acetate-for-chloride ligand exchange between the [(Cp)Rh(Cl)$_2$] catalyst and copper(II) acetate, [Cu(OAc)$_2$]$_2$.

Thus, we recalculated the Rh$^{III/I}$ cycle for the original proposal (Scheme 2.2) starting directly from the experimentally used Rh^{III} pre-catalyst: [(Cp)Rh(Cl)$_2$]. This monomer, in DMF as solvent, is exergonically formed by -4.2 kcal·mol^{-1} from the corresponding dimer, as shown in Scheme 2.14. The reaction of [(Cp)Rh(Cl)$_2$] with **I11^3** is slightly endergonic by 1.1 kcal·mol^{-1} forming **I17^3** intermediate (Scheme 2.22). This species can evolve towards the formation of cationic Rh^{III} complex **I19^1** and **I18^3** as side product. Interestingly, the C–H activation step through CMD transition state **TS I19-I20^1** from this cationic species (**I19^1**) is 4.6 kcal·mol^{-1} lower in energy than

the neutral one described above (**TS I14-I15^1**). We also explored the deprotonation of the imine moiety at different stages of the Rh mechanism, but it was found to be prohibitively higher in energy (**I22^1**). Once the C–H activation step has taken place, 1-phenyl-1-propyne can easily displace the HOAc ligand in **I20^1** to form **I21^1**.

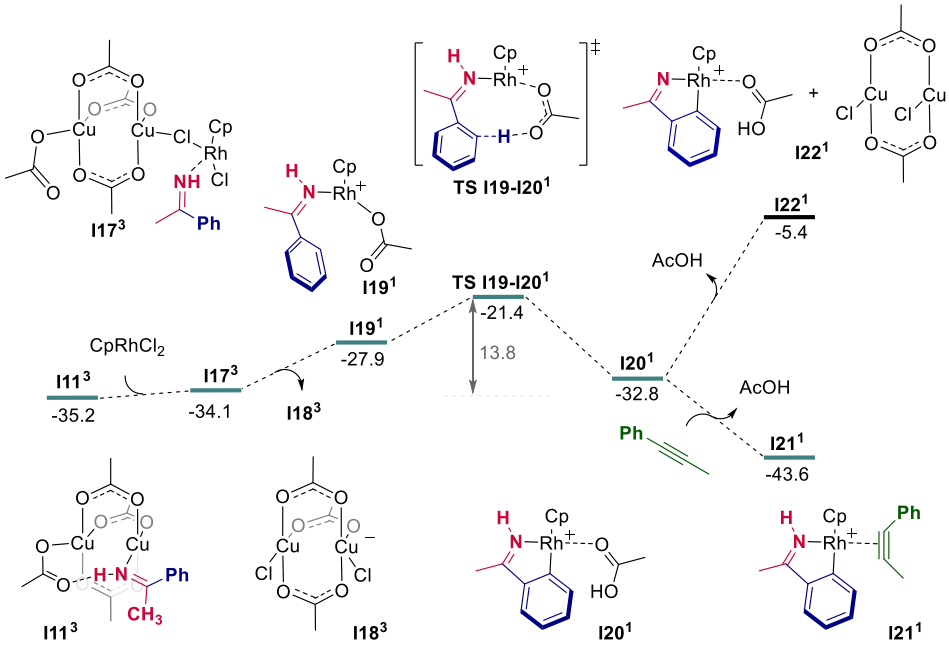

Scheme 2.22. Free energy profile for the C–H activation step starting from **I11^1** when considering [(Cp)Rh(Cl)$_2$] as catalyst. Energies in kcal·mol^{-1}.

Then, we explored the regioselectivity of the alkyne insertion (Scheme 2.23). The insertion of the carbon bearing the methyl group close to the phenyl ring of the imine, **TS I21-I22^1**, is much more favorable than the insertion of the alkyne with the phenyl group pointing to the aromatic ring in the imine, **TS I21-I23^1**. This difference of 4.5 kcal·mol^{-1} perfectly match with the experimental selective regioselectivity. As it occurs in related systems the different steric-demand of each substituent allows to explain the observe selectivity.[4c] In **TS I21-I22^1**, the small methyl group has a negligible steric hindrance over the imine during the C–C bond formation. On the other hand, in **TS I21-I23^1**, the C–C bond formation is hampered by the perpendicular disposition of the phenyl group in the alkyne and the aromatic ring in the imine. This steric hindrance is reflected on the elongation of the C–C bond distance during the transition state and, consequently, in the hindered formation of **I23^1** (to the left in Scheme 2.23). We also corroborated this by performing NCIplot[19] analysis. In Scheme 2.23 to the right, we can see how

19 a) Contreras-Garcia, J.; Johnson, E.; Keinan, S.; Chaudret, R.; Piquemal, J.-P.; Beratan, D.; Yang, W. *J. Chem. Theor. Comp.* **2011**, *7*, 625. b) Johnson, E. R.; Keinan, S.; Mori-Sanchez, P.; Contreras-Garcia, J.; Cohen, A J.; Yang, W. *J. Am. Chem. Soc.* **2010**, *132*, 6498.

the interaction between the aromatic ring in the imine moiety has a mainly repulsive interaction (upper part) while the methyl group has a small favorable interaction with the aromatic ring (lower part).

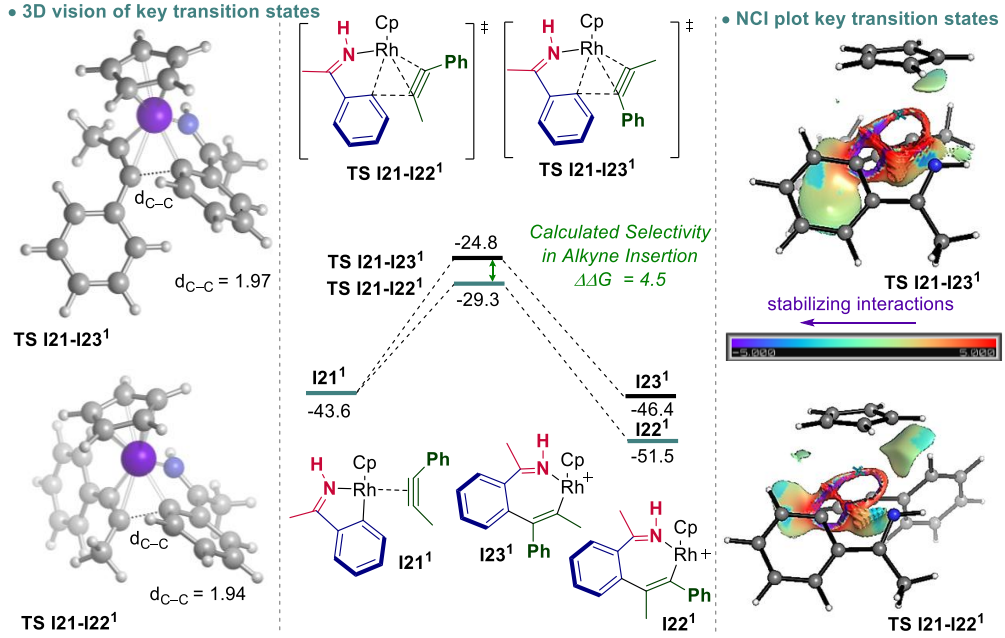

Scheme 2.23. Regioselectivity of the alkyne insertion step. Left: 3D representation of the corresponding transition states. Color code: gray (carbon), white (hydrogen), purple (rhodium), blue (nitrogen). Middle: Free Energy profile in kcal·mol^{-1}. Right: NCIplot representation of both transition states. For the calculation, the transition state was divided in two different fragments: the alkyne substrate and the remaining atoms that form the rhodacycle. Color code: gray (carbon), white (hydrogen), blue (nitrogen).

Once studied the regioselectivity of the alkyne insertion step, we further investigated the successive steps for the completion of the catalytic cycle. Through a low activation barrier, **I22^1** rhodacycle undergoes reductive elimination to form intermediate **I24^1** which contains the reductive elimination product attached to a Rh^I metal center (Scheme 2.24). Interestingly, the C–N bond-forming reductive elimination was found to be slightly endergonic. Yet the process is accelerated by the catalyst regeneration which showed to be a downhill succession of ligand exchange and electron transfer reactions. The deprotonation of the organic substrate coordinated to the Rh^I species, **I24^1**, by the Cu^{II} salt, **I18^3**, affords exergonically intermediate **I25^3**. Subsequently, this intermediate releases a molecule of AcOH to form **I26^3** which, through SET process or MECP, finally regenerates both Rh and Cu catalysts (**I27^1**).

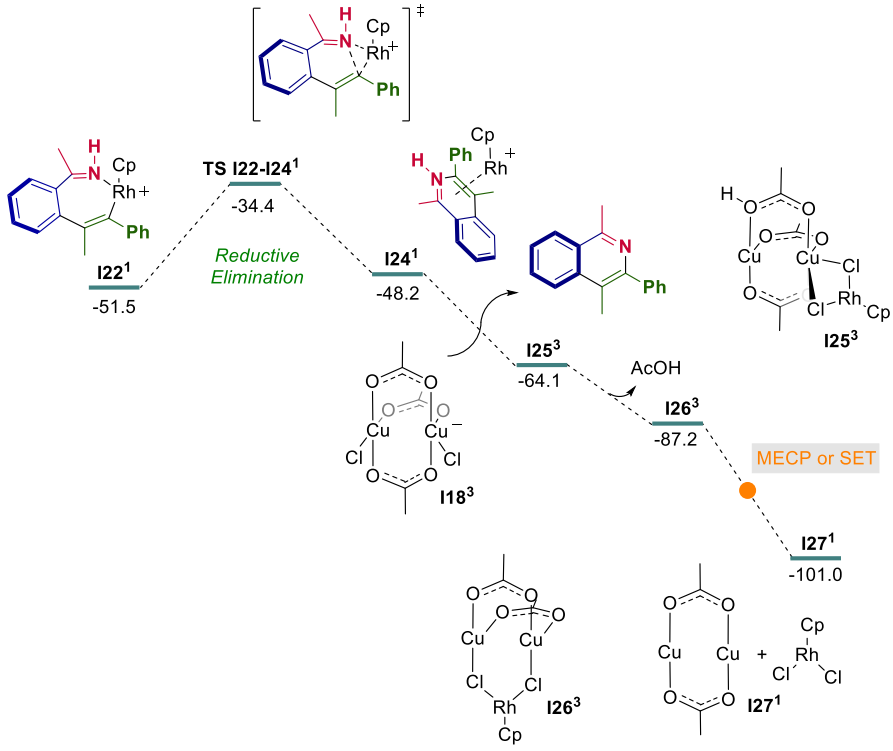

Scheme 2.24. Free energy profile for the reductive elimination step and subsequent catalyst regeneration starting from **I22**[1] when considering [(Cp)Rh(Cl)$_2$] as catalyst. Energies in kcal·mol^{-1}.

2.3.4.1. **Microkinetic modeling of model 2**

This new profile is qualitatively similar to the previous one, but considering the hampered formation of [(Cp)Rh(OAc)$_2$] in the reaction media, this cationic route should be preferred rather than the aforementioned neutral one. Again, in comparison to model 1, the highest barrier of a single step is related to the opening of the *2H*-azirine and the free energy span of the catalytic reaction is 25.5 kcal·mol^{-1}. When surveying this model 2 to microkinetic modeling, it also fails to reproduce the experimental outcome since the predicted reaction time remains unchanged at around 21 hours.

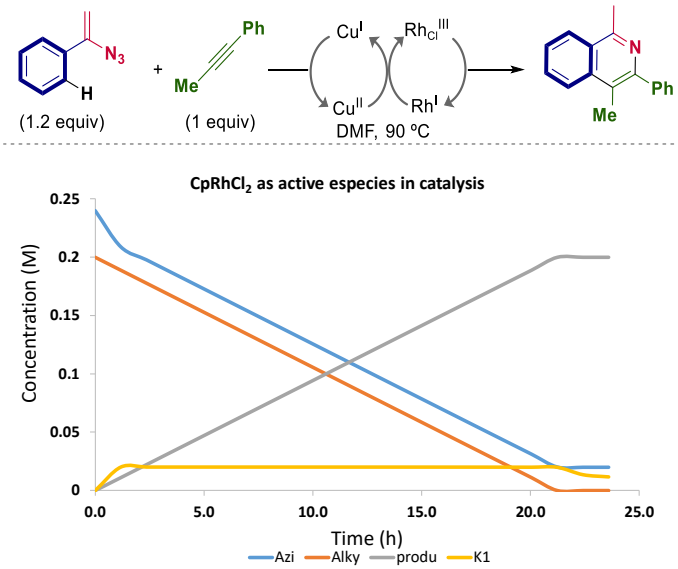

Scheme 2.25. Evolution of the concentration of substrates and products over time according to microkinetic modeling of the mechanistic proposal of model 2. K1 is **I4**[1].

2.3.5. Evaluation of [(Cp)Rh(Cl)$_2$] and [Cu(OAc)$_2$]$_2$ as reals catalysts

Bimetallic dual catalysis homogeneous catalytic systems are becoming a new paradigm in the development of unprecedented reaction modes but the direct cooperation between the different catalysts in those systems is still vastly unexplored. Recently, several studies have shown that cooperative mechanisms are critical for the deeply understanding of reaction outcomes.[Error! Bookmark not defined.,Error! Bookmark not defined.,Error! Bookmark not defined.,4] Following these ideas, we systematically explored the potential crossing points of the Cu-based and Rh-based catalytic cycle in the most kinetically relevant steps beyond the catalyst regeneration. We hypothesized that this cooperation, although computationally demanding, may be key to accurately describe the selected experimental observables. For clarity, we divided the mechanistic analysis in both initial proposed cycles of Scheme 2.3 in the Introduction: the reductive activation of the substrate ($Cu^{I/II}$ cycle) and the oxidative coupling of the imine intermediate ($Rh^{III/I}$ cycle).

2.3.5.1. Study of the participation of Rh(III) catalyst in the Cu-cycle

We first surveyed the influence of [(Cp)Rh(Cl)$_2$] coordination to intermediate **I4**[1], formed after the nitrogen extrusion process described previously (Scheme 2.16). The 2*H*-azirine as ligand in the so-formed **I28**[1] intermediate shows a slightly exergonic coordination to the rhodium metal center (Scheme 2.26). This facilitates the cleavage of the C–N bond of the *2H*-azirine (**TS I28-I29**[1]) to form **I30**[3] intermediate prior the coordination of two molecules of acetic acid. The barrier

for the C–N cleavage dramatically decreases by 10.5 kcal·mol^{-1} in comparison to the barrier for the Cu-alone cycle described above (**TS I4-I5^{OSS}**, Scheme 2.16). Then, we evaluated the hydrogen atom transfer (HAT) from the acetates to the activated imidyl moiety. The first HAT to the nitrogen takes place through a complex transition state, **TS I30-I31^3**, where rhodium is attached to nitrogen and a chloride ligand is bridging Cu and Rh metal centers, stabilizing the transition state by 9.0 kcal·mol^{-1} respect **TS I8-I9^3** in the Cu-alone mechanism. This reaction step generates **I31^3** intermediate that subsequently undergoes a second HAT, affording **I17^3**. In this case, the chloride again bridges the rhodium and copper metal centers, favoring the transfer of the hydrogen atom.

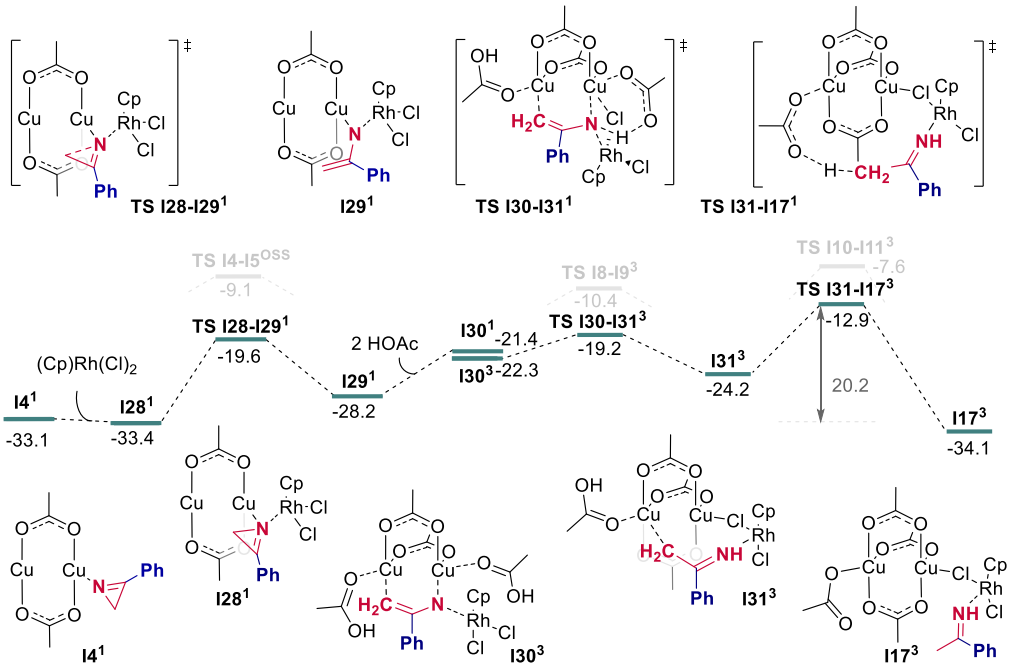

Scheme 2.26. Free energy profile of the Rh/Cu co-catalyzed reductive activation of the substrate. Energies in kcal·mol^{-1}.

Thus, as we can see in Scheme 2.26, the overall reduction of the 2*H*-azirine intermediate to the corresponding imine is much favorable when considering the formation of trinuclear Cu-Cu-Rh species. In view of this, we aimed at getting insights on this particular trinuclear catalyst. First, we analyzed the molecular orbitals of one of the key intermediates for the transformation, **I30^3**. In Figure 2.6, we can see how one of the two unpaired electrons of this triplet state intermediate is located mainly over a copper atom, which can be considered Cu^{II}, and the other

unpaired electron is shared between the nitrogen, copper and rhodium atoms. To certain extent, this suggests that the rhodium complex could stabilized the radical nitrogen in the imidyl moiety.

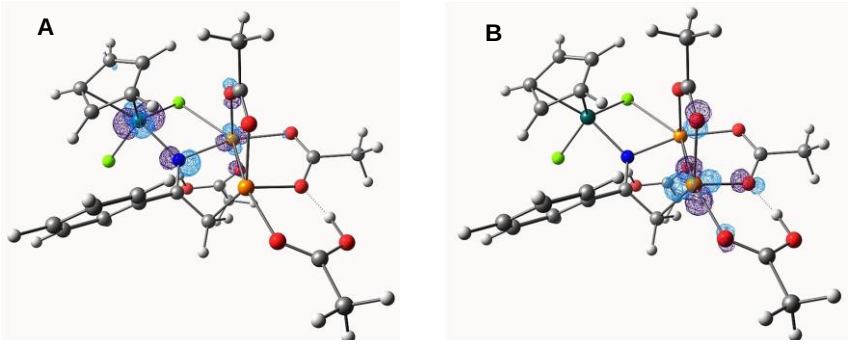

Figure 2.6. SOMO analysis of **I30^3** intermediate. A) Highest (left) energy single-occupied molecular orbital (SOMO) of **I30^3** (isosurface = 0.09). B) Highest (right) energy single-occupied molecular orbital (SOMO-1) of **I30^3** (isosurface = 0.09). Color code: carbon (gray), white (hydrogen), blue (nitrogen), orange (copper), red (oxygen), light green (chloride), turquoise (rhodium).

We then evaluated the spin density evolution during the overall reduction of the substrate. In Figure 2.7, we can see how the unpaired electrons in **I30^1** and **I31^1** are almost equally distributed between the copper moiety and the substrate but stabilized, to certain extent, by the rhodium metal center. This is slightly different from **I8^3**, in the Cu-alone cycle, where the spin density was mainly located on the substrate moiety. We hypothesized that if Rh is actively participating in the oxidation of the copper and the reduction of the substrate, its electron density should experiment some changes during the HAT. For this reason, we focused our attention on the spin density distribution during the formal oxidation from Cu$^{I/II}$ to Cu^{II}, **TS I31-I17^3**, the second HAT.

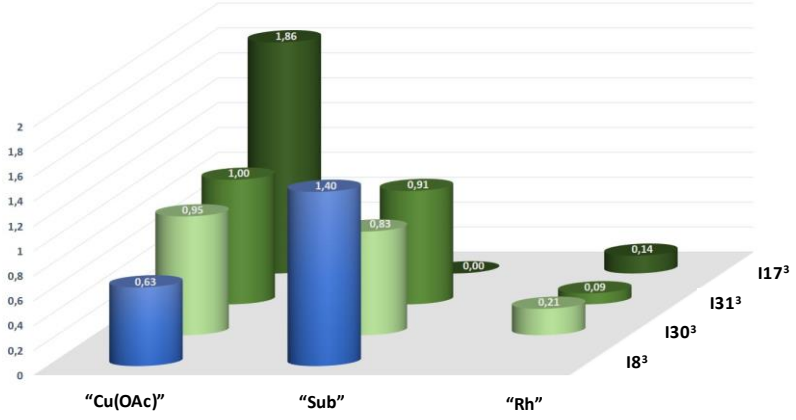

Figure 2.7. Spin density evolution along the reaction coordinate of the substrate reduction. Three different fragments (Cu, Rh, Substrate) are considered in intermediates **I30^3**, **I31^3** and **I17^3**. **I8^3** is shown for comparison. Further details regarding the definition of the fragments can be found in the Appendix.

Interestingly, when we analyzed the spin density distribution in **TS I31-I17^3**, we found that there is an accumulation of spin density in both copper and rhodium centers prior to the final oxidation of the copper. This is an additional proof that supports the key influence of rhodium in the electronic structure of the intermediates to facilitate the oxidation of the copper centers and, therefore, the reduction of the substrate.

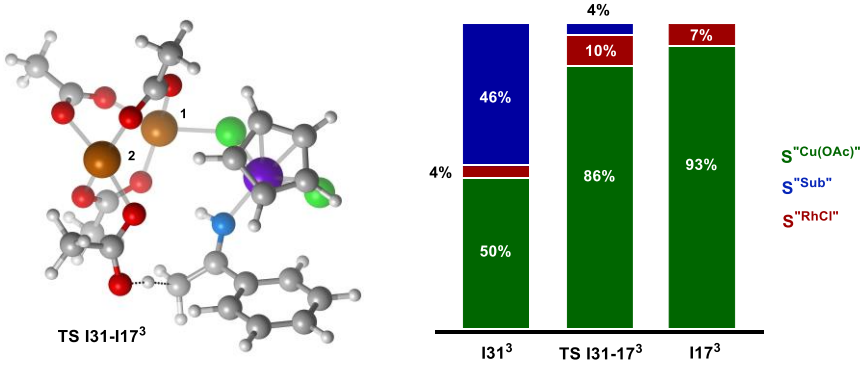

Figure 2.8. Evolution of the spin density along the reaction coordinate of the second HAT when considering the formation of trinuclear Cu-Cu-Rh species in percentage. RC = Reaction coordinate.

To the best of our knowledge, this is the first example where rhodium can not only cooperate in the copper catalytic cycle entailing a considerable decrease of the activation barriers but also facilitating the oxidation of the copper from Cu^{I} to Cu^{II}.

2.3.5.2. **Study of the participation of Cu(II) catalyst in the Rh-cycle**

Encouraged by the influence of Rh in the Cu cycle, we wondered if the cooperation could exist during the C–H activation event from **I17^3**, as it has been demonstrated in other similar cases.[4b-d] In this system, the cooperative C–H activation, depicted in Scheme 2.27, was found to be around 10 kcal·mol^{-1} higher in energy compared to the C-H activation from the cationic rhodacycle **I19^3** (Scheme 2.22).

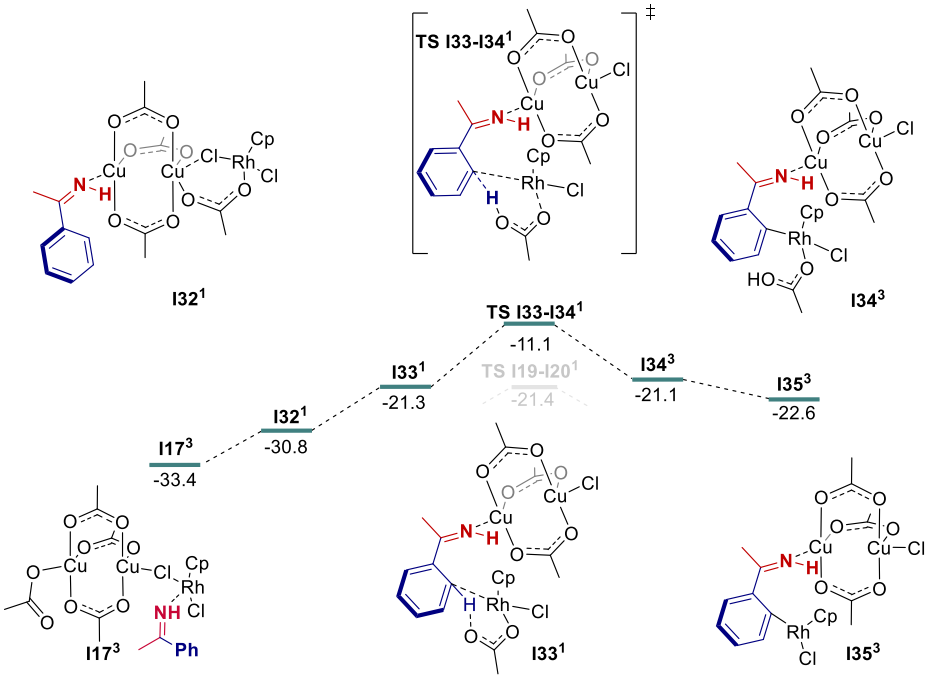

Scheme 2.27. Free energy profile for the cooperative C–H activation. Energies in kcal·mol^{-1}.

This means that the system would evolved through the described-above cationic mechanism to selectively form intermediate **I22^1**, as simplified in Scheme 2.28, instead through the cooperative C–H activation pathway. A reasonable explanation for this issue is the polarity of the reaction media (DMF) which favors the formation of ionic species. From **I22^1**, we then explored the reductive elimination as a monometallic or a cooperative step. Among the different options analyzed (see Computational Appendix for further details), we were able to find a cooperative reductive elimination (CRE) pathway (**TS I36-I37^3**) lower in 4.8 kcal·mol^{-1} than the Rh-alone system (Scheme 2.28). Interestingly, the bridging chloride between Rh and Cu centers is key for the transition state stabilization, which was also demonstrated in the oxidative coupling of benzoic acid and alkyne catalyzed by Rh/Cu dual system previously.[4b]

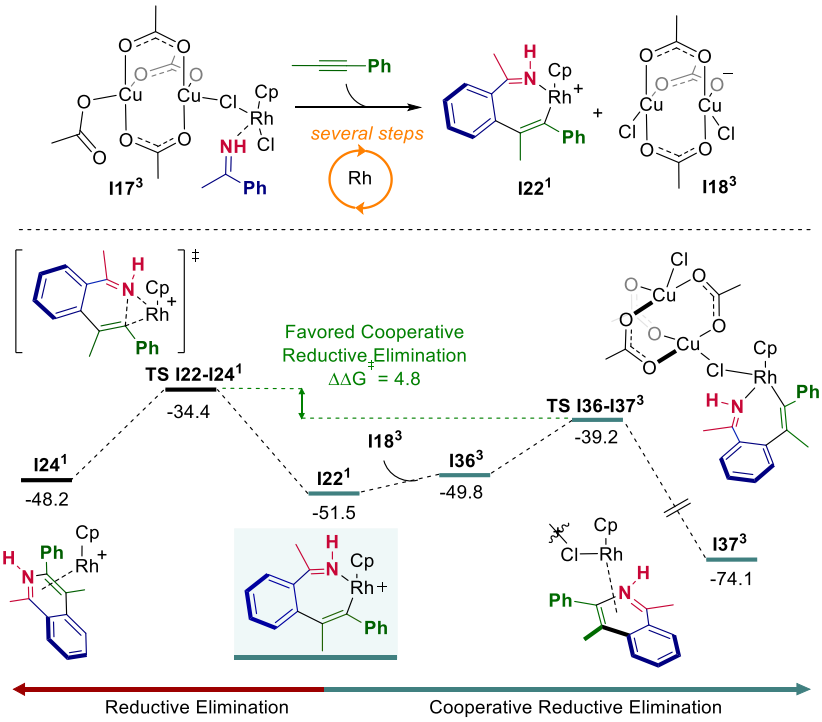

Scheme 2.28. Above: Summary of previously commented steps for the formation of **I22¹** from **I17³**. Below: Free energy profile of the Rh/Cu cooperative reductive elimination *vs* the Rh-alone catalyzed pathway. Energies in kcal·mol^{-1}.

To further analyze the nature of the CRE transition state, we studied the evolution of the spin densities during the reaction coordinate. During C–N bond formation, two electrons are released from the organic part to the catalyst and in the CRE one is received by the Rh center and the other by the Cu dimer (Figure 2.9). In this system, we observed an increment of the spin density over the Rh atom that indicates the reduction of Rh^{III} to Rh^{II}, while the spin density on the copper dimer is decreasing, confirming the reduction of the copper dimer from Cu^{II} to Cu^{I} (the delocalization of the spin density in the copper dimer impedes the formal electron assignment). Thus, the electronic structure of the metals in **I37³** can be represented as Rh^{II}-$Cu^{I/II}$-$Cu^{I/II}$.

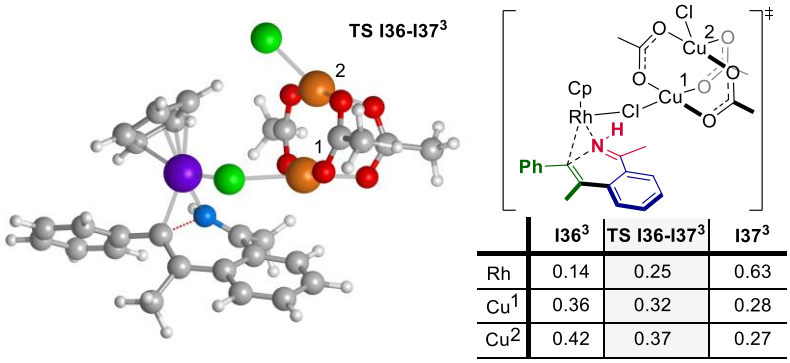

	I36³	TS I36-I37³	I37³
Rh	0.14	0.25	0.63
Cu¹	0.36	0.32	0.28
Cu²	0.42	0.37	0.27

Figure 2.9. 3D/2D structure of **TS I36-I37³** and spin density evolution along the cooperative C–N bond-forming reductive elimination step. Color code: gray (carbon), white (hydrogen), blue (nitrogen), purple (rhodium), orange (copper), red (oxygen), light green (chloride).

Intermediate, **I37³**, Rh^{II}-$Cu^{I/II}$-$Cu^{I/II}$, smoothly evolves toward the regeneration of the initial Rh^{III}-Cu^{I}-Cu^{I} oxidation state (Scheme 2.29). The exclusion of Rh^{I} during the catalytic cycle was further confirmed here by analyzing the different pathways for the regeneration of the catalysts. The separation of intermediate **I39³** in Rh^{I} and Cu^{II}-Cu^{II} moieties were 54.1 kcal·mol^{-1} above the formation of analogous Rh^{II} and $Cu^{I/II}$–$Cu^{I/II}$ intermediates, **I41²** (Scheme 2.29). The overall reaction is exergonic in -101.0 kcal·mol^{-1}.

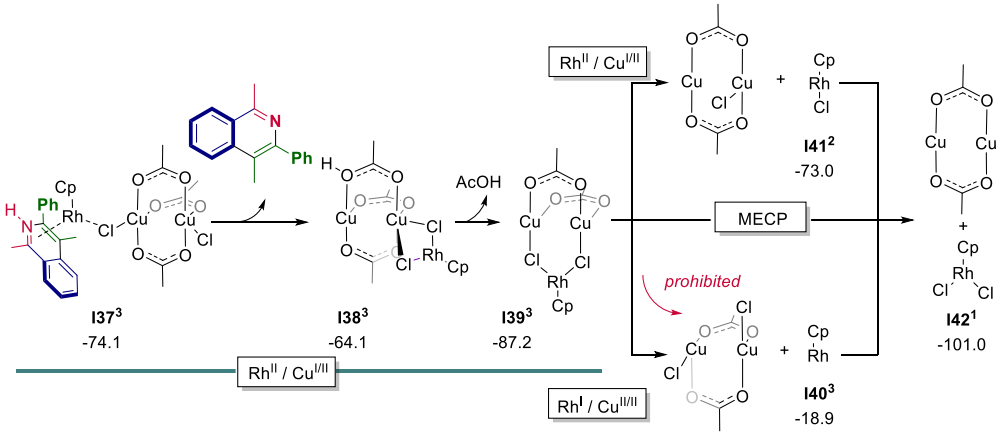

Scheme 2.29. Catalyst regeneration considering trinuclear Cu-Cu-Rh species as active species for the reductive elimination step. Free energies in kcal·mol^{-1}.

2.3.5.3. **Microkinetic modeling of model 3**

Once we have identified the influence of Rh^{III} in the copper cycle and Cu^{II} dimer in the rhodium cycle, we constructed a more complex microkinetic model taking into account this simultaneous cooperation. Interestingly, we found that the simulated reaction is over in less than 15 min (Scheme 2.30). This value is directly comparable to the experimental reaction time value

of 30 min when they use CuOAc as co-catalyst. In contrast, the so-far considered mechanisms predicted a reaction time of 21 hours. This way, we believed that this is an undoubtable evidence of the importance of tricky cooperation in bimetallic dual catalytic systems.

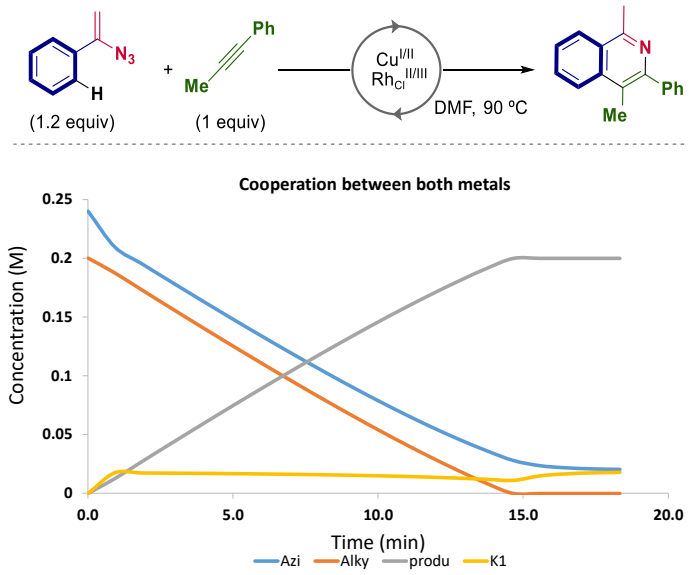

Scheme 2.30. Evolution of the concentration of substrates and products over time according to microkinetic modeling of the mechanistic proposal of model 3, the cooperative mechanistic proposal. K1 is $\mathbf{I4^1}$.

The aforementioned agreement of this model 3 with the experimental data implies a change in the mechanistic proposal of this Rh/Cu-catalyzed bimetallic system. DFT calculations show that both catalytic cycles collapse in a single cycle where the catalytically active species can be a copper dimer, a rhodium-copper adduct and a rhodium complex (Scheme 2.31). In this regard, the oxidation state of the Rh was proved to be either three or two being highly disfavored the proposed Rh^{I} species.

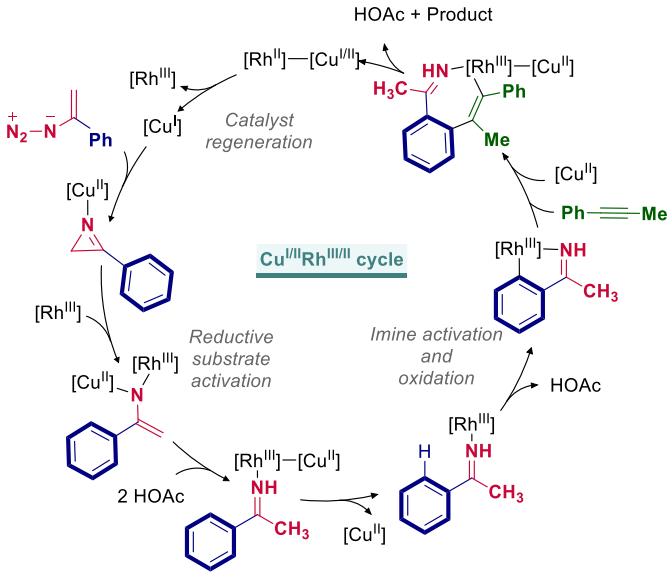

Scheme 2.31. Current proposal for the cooperative Rh/Cu-catalyzed synthesis of isoquinoline derivatives formation from α-phenyl vinyl azides and terminal alkynes.

2.3.6. Evaluation of the regioselectivity when using m-bromo-substituted α-phenyl vinyl azides

Inspired by the potential of the combination of microkinetic simulations and DFT calculations to critically analyze a theoretically-proposed reaction mechanism, we aimed to dig into on the prediction of the regioselectivity when using *meta*-substituted substrates, namely bromo-substituted. These substrates have two different *ortho*-positions that can be activated *via* CMD (Scheme 2.32). Experimentally, the activation of the *p*- position (in orange, Scheme 2.32) to the bromide is preferred and so product **XX** is favored over product **XXI**.

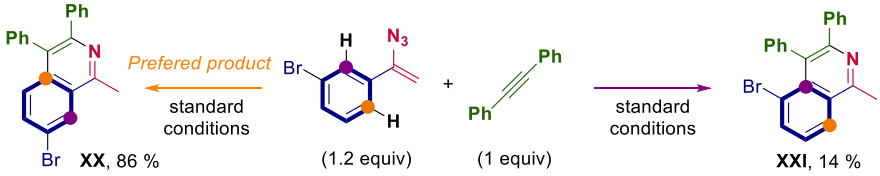

Scheme 2.32. Regiodivergent formation of isoquinolines by Rh/Cu-catalyzed coupling of azides and alkynes reported by Chiba *et al*. (ref.**Error! Bookmark not defined.**). The reaction was carried out under the standard conditions defined in Scheme 2.4.

According to our mechanism, the reaction regioselectivity would be determined by the C–H activation and alkyne insertion (AI) steps, which irreversibly generate the 7-membered ring rhodacycle. When we calculated the competitive reactions, using Br as substituent and Cp ligand as simplified model of the real ligand, the C–H activation step appeared to be the highest-in-energy and irreversible event in the free energy profile of both isomers. In this context, as

depicted in Scheme 2.33, product **XXI** is favored by a difference of 0.5 kcal·mol^{-1} respect to product **XX**. According to the Boltzmann distribution, a 66.8% of product **XXI** should be obtained. However, this does not explain the experimental outcome of the favored formation of product **XX** and, therefore, the model failed in the correct description of the reaction regioselectivity.

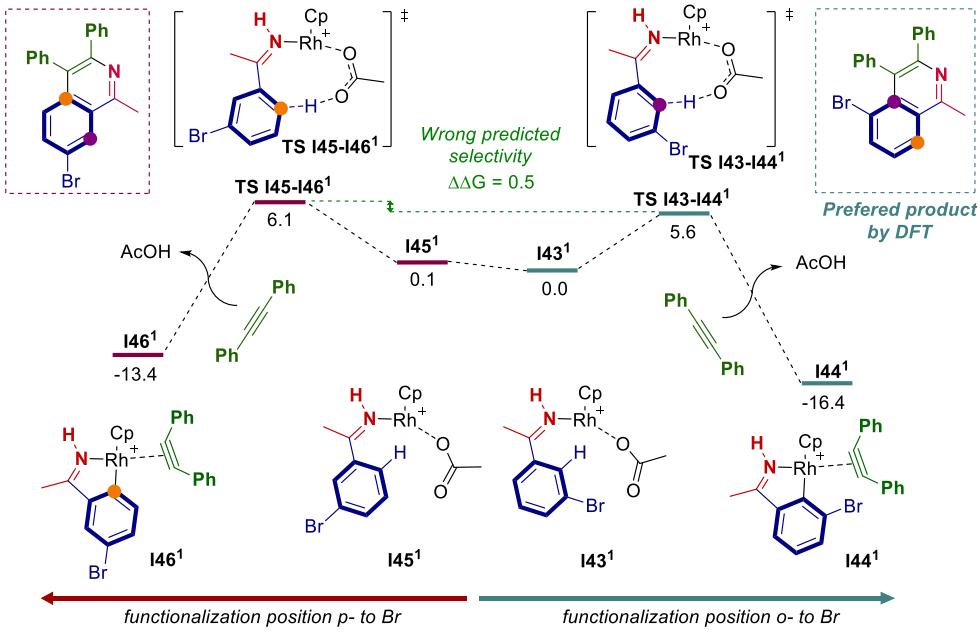

Scheme 2.33. Simplified free energy profile for the regioselectivity study of the C−H activation and alkyne insertion for *meta*-bromo-substituted vinyl azide. All the reaction steps can be found in the Appendix. The exchange of the alkyne by the acetic acid entails several steps but not represented for clarity.

We then hypothesized that the steric effects of the Cp* ligand would be crucial for the regioselectivity of the reaction, especially in the sterically-demanding alkyne insertion step. Thus, we moved from [(Cp)Rh(Cl)$_2$] to [(Cp*)Rh(Cl)$_2$], going from the model ligand to the experimentally used one. In this new scenario, depicted in Scheme 2.34, we observed that the alkyne insertion barriers turned to be competitive with the C–H activation. Hence, this system is governed by a Curtin-Hammett situation. For the formation of product **XX**, the determining step is the C–H activation step while for the formation of product **XXI**, the alkyne insertion is the most energy-demanding step. The relative similar barriers of both steps and the different first-order and second-order elementary steps hampers the direct application of the Eyring-TST to estimate the product ratio. When microkinetic modelling was used, the predicted ratio of the regioisomers was found to be 82% of product **XX** and 18% of product **XXI**. Excellent agreement was then encountered with the experimentally observed ratio of 86% for product **XX** and 14% for product **XXI**.

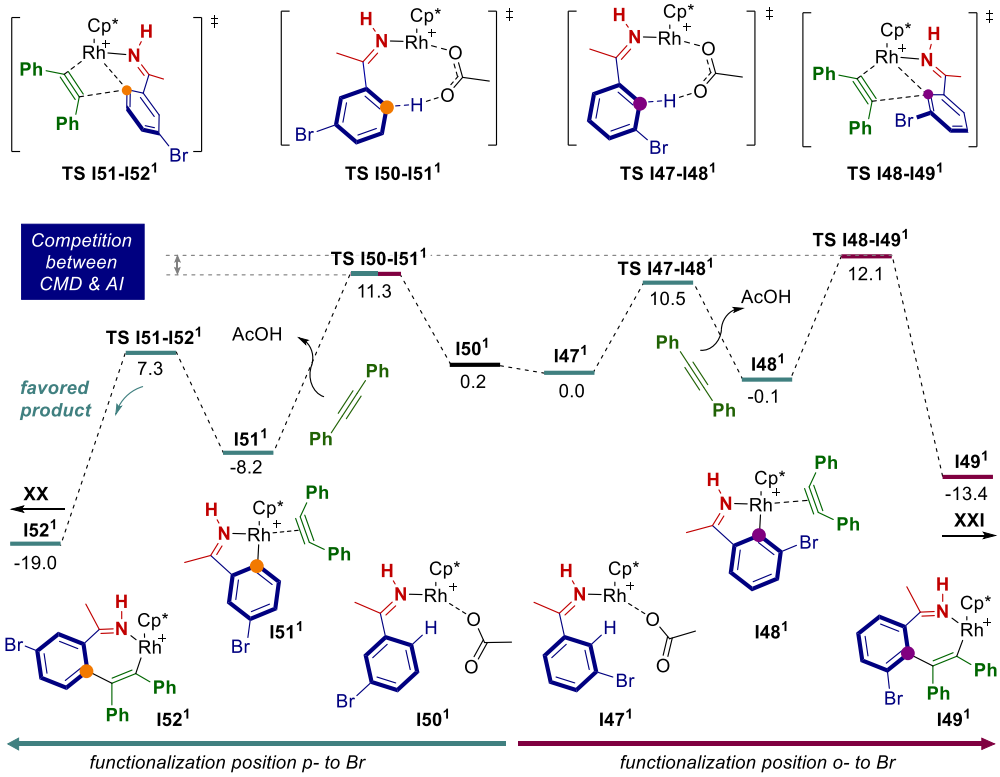

Scheme 2.34. Simplified free energy profile for the regioselectivity study of the C−H activation and alkyne insertion for *meta*-bromo-substituted vinyl azide using the real catalyst [(Cp*)Rh] complex. All the reaction steps can be found in the Appendix. The exchange of the alkyne by the acetic acid entails several steps but not represented for clarity. CMD = concerted metalation-deprotonation, AI = alkyne insertion.

Interestingly, this iterative search for the reaction mechanism using the combination of DFT and microkinetic analysis leads to a perfect description of the regioselectivity of the reaction.

2.4. Conclusions

In summary, in Chapter 2, we have evaluated different mechanistic scenarios using DFT calculations for the Rh/Cu-catalyzed coupling of α-vinyl azides with alkynes affording isoquinoline derivatives as case study bimetallic system. To do so, we have used a systematic approach, starting from a widely used simple model, assuming the generation of a well-defined catalytic active species, and increasing the complexity of the model up to three times to successfully describe all the factors that underline the reaction. Simultaneously, every mechanistic proposal has been surveyed on the basis of an observable that is present in almost all the manuscripts in the literature, the reaction time. If the predicted reaction time by the microkinetic simulation does not represent the experimental value, the model is revisited. This iterative approach conducted our initial model to a much more complex one that satisfies the experimental reaction time. In addition, we successfully reproduced the experimentally observed regioselectivity, calculating the relative ratio using a microkinetic model of the most complex mechanistic approximation.

In this regard, we proposed a mechanism for this system which involves the simultaneous cooperation of both metal centers during the whole catalytic transformation, in contrast with the two independent catalytic cycles assumed for bimetallic dual catalyzed oxidative coupling. This unexpected outcome remarks the importance of combining DFT calculations and microkinetic modeling in complex reaction networks to critically evaluate mechanistic proposals that, despite being reasonable, could not be representative of the system. Moreover, the research could end up in the discovery of reaction mechanisms which have thus far been overlooked in the literature.

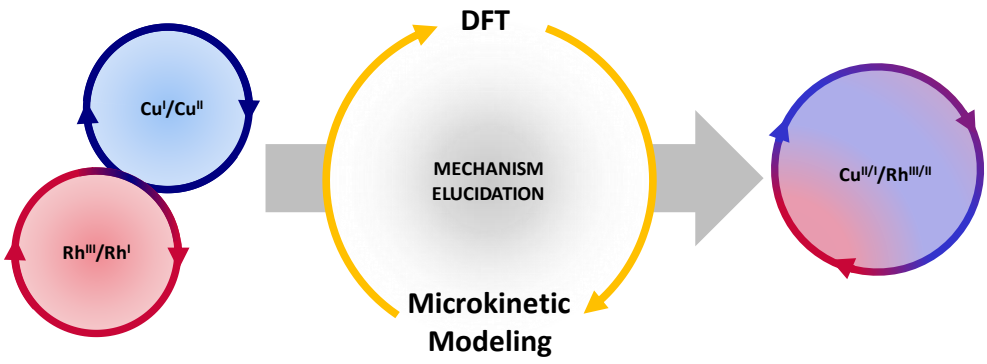

Figure 2.10. Graphical summary of Chapter 2.

2.5. Computational Appendix

2.5.1. DFT calculations

DFT calculations were carried out with the B97D functional,[20] using the Gaussian09 software package.[21] Two different basis sets were used. In basis set I, LANL2DZ (with the associated pseudopotential)[22] for Cu, Rh and Br and 6-31G(d)[23] for the remaining atoms were considered. In basis set II, the basis set for Cu and Rh was expanded to LANL2TZ-f,[24] for Br was expanded to LANL2DZ-dp[5] and for all remaining atoms was expanded to 6-311++G(d,p).[25] Basis set I was used for all geometry optimizations and frequency calculations, while basis set II was used to refine the potential energy values. All calculations, including geometry optimizations, were carried out with an implicit solvation model (Solvent Model Density, SMD)[26] simulating *N,N*-dimethylformamide (ε = 37.219), without symmetry restrictions. Free energy corrections were calculated in solution at 298.15 K and 1 atm. The analysis of vibrational frequency calculations allowed us to stablish the nature either as intermediate (without imaginary frequencies) or transition state (an imaginary frequency related to the reaction coordinate).

The connectivity of transition states and the intermediates was confirmed by relaxation of the transition states using limited step-size during the optimization. The connectivity between open-shell-singlet transition state and close-shell-singlet intermediate, was confirmed by scanning the potential energy surface to ensure that S^2 is increasing from zero while the transformation is occurring (Scheme A2.2).

---

20 Grimme, S. *J. Comp. Chem.* **2006**, 27, 1787.

21 Gaussian 09, Revision D.01, Frisch, M. J.; Trucks, G. W.; Schlegel, H. B.; Scuseria, G. E.; Robb, M. A.; Cheeseman, J. R.; Scalmani, G.; Barone, V.; Mennucci, B.; Petersson, G. A.; Nakatsuji, H.; Caricato, M.; Li, X.; Hratchian, H. P.; Izmaylov, A. F.; Bloino, J.; Zheng, G.; Sonnenberg, J. L.; Hada, M.; Ehara, M.; Toyota, K.; Fukuda, R.; Hasegawa, J.; Ishida, M.; Nakajima, T.; Honda, Y.; Kitao, O.; Nakai, H.; Vreven, T.; Montgomery, Jr., J. A.; Peralta, J. E.; Ogliaro, F.; Bearpark, M.; Heyd, J. J.; Brothers, E.; Kudin, K. N.; Staroverov, V. N.; Keith, T.; Kobayashi, R.; Normand, J.; Raghavachari, K.; Rendell, A.; Burant, J. C.; Iyengar, S. S.; Tomasi, J.; Cossi, M.; Rega, N.; Millam, J. M.; Klene, M.; Knox, J. E.; Cross, J. B.; Bakken, V.; Adamo, C.; Jaramillo, J.; Gomperts, R.; Stratmann, R. E.; Yazyev, O.; Austin, A. J.; Cammi, R.; Pomelli, C.; Ochterski, J. W.; Martin, R. L.; Morokuma, K.; Zakrzewski, V. G.; Voth, G. A.; Salvador, P.; Dannenberg, J. J.; Dapprich, S.; Daniels, A. D.; Farkas, O.; Foresman, J. B.; Ortiz, J. V.; Cioslowski, J.; Fox, D. J. Gaussian, Inc., WallingfordCT, **2013**.

22 a) Hay, P. J.; Wadt, W. R. *J. Chem. Phys.* **1985**, 82, 270. b) Hay, P. J.; Wadt, W. R. *J. Chem. Phys.* **1985**, 82, 284. c) Hay, P. J.; Wadt, W. R. *J. Chem. Phys*. **1985**, 82, 299.

23 a) Hehre, W. J.; Ditchfield, R.; Pople, J. A. *J. Chem. Phys*. **1972**, 56, 2257. b) Hariharan, P. C.; Pople, J. A. *Theoret. Chimica Acta.* **1973**, 28, 213. c) Francl, M. M.; Petro, W. J.; Hehre, W. J.; Binkley, J. S.; Gordon, M. S.; DeFrees, D. J.; Pople, J. A. *J. Chem. Phys.* **1982**, 77, 3654.

24 Taken from EMSL Basis Set Library: a) Feller, D. *J. Comp. Chem.* **1996**, 17, 1571. b) Schuchardt, K. L.; Didier, B. T.; Elsethagen, T.; Sun, L.; Gurumoorthi, V.; Chase, J.; Li, J.; Windus, T. L. *J. Chem. Inf. Model*. **2007**, *47*, 1045.

25 a) Krishnan, R.; Binkley, J. S.; Seeger, R.; Pople, J. A. *J. Chem. Phys.* **1980**, 72, 650. b) McLean, A. D.; Chandler, G. S. *J. Chem. Phys*. **1980**, 72, 5639.

26 Marenich, S. A. V.; Cramer, C. J.; Truhlar, D. G. *J. Phys. Chem. B*, **2009**, 113, 6378.

Reported energies are free energies in solution, refined by potential energies from basis set II. When specific properties were needed, say spin densities, values from single points calculations (basis set II) were considered.

The single assumed simplification was the substitution of the *1,2,3,4,5*-pentamethylcyclopentadienyl (Cp*) ligand on the rhodium catalyst by cyclopentadienyl (Cp) to save computational time. However, the study of the regioselectivity for *meta*-substituted vinyl azides was carried out using the complete ligand.

2.5.1.1. Alternative N-C bond cleavage from the 2*H*-azirine

We considered, as alternative intermediate for the C-N bond cleavage of the 2*H*-azirine, the coordination of two molecules of acetic acid to the copper(I) complex bearing the azirine coordinated, forming A4 intermediate. However, the intermediates were higher in energy respect to the favored mechanism (**Scheme 2.16** and **Scheme 2.17** in the main text).

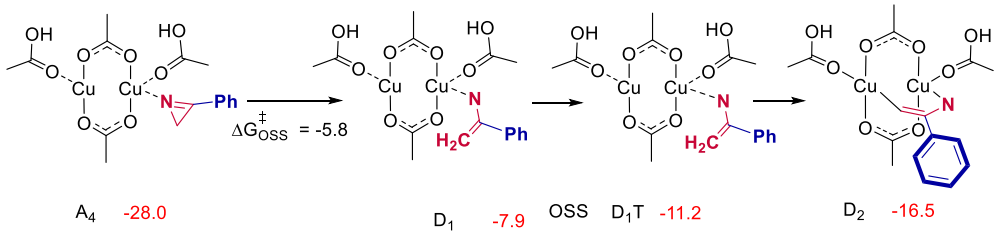

Scheme A2.1. Evaluation of the ring opening of the 2*H*-azirine considering the previous coordination of two acetic acid molecules. Energies in kcal·mol^{-1}.

2.5.1.2. Calculation on the connectivity of I4^{1} and I5^{OSS}

The connectivity between the closed-shell-singlet and the open-shell-singlet intermediates was confirmed by scanning the potential energy surface from **I4^{1}** intermediate to **I5^{OOS}** intermediate (Scheme 2.17) and examining the S^2 value during the reaction coordinate. The S^2 value varies from zero in **I4^{1}** to almost one in **I5^{OSS}** while the C−N distance increases (Scheme A2.2). This supports that the bond cleavage is homolytic.

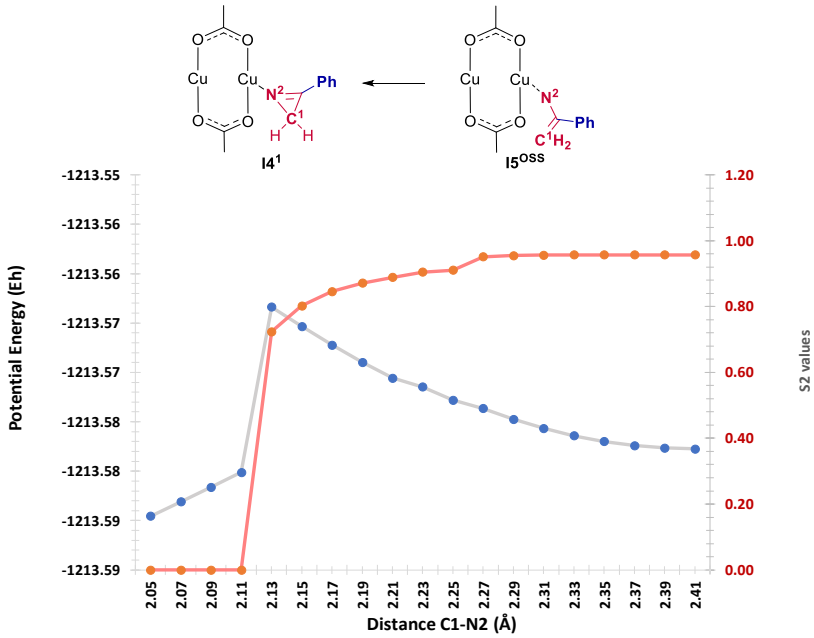

Scheme A2.2. Variation of spin density (S^2) and the potential energy surface (Hartree) during the reaction coordinate C–N bond.

2.5.1.3. Fragments for analyzing the spin density evolution in the multimetallic mechanism.

Selected fragments for checking the evolution of the spin density during the reduction of the substrate after the C–N bond cleavage. In Figure A2.1, **I30³** is shown as an example.

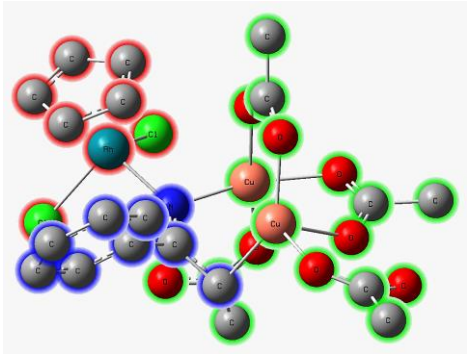

Figure A2.1. 3D representation of intermediate **I30³**. The considered as substrate fragment is highlighted in blue; in green, the copper fragment and, in red, the rhodium fragment.

2.5.1.4. C–N bond-forming reductive elimination alternatives

Different mechanisms for the reductive elimination step were considered. The reductive elimination from the neutral seven-membered rhodacycle **I55¹** is not likely to happen. The generation of a Rh(I) complex bearing two anionic ligands (Cp and chloride) together with the

potential steric hindrance of the chloride make difficult the reductive elimination. The reductive elimination step happens from **I27^3** since the barrier is 4.8 kcal/mol lower in energy than the barrier from the cationic rhodium complex, **I22^1** (Scheme A2.3).

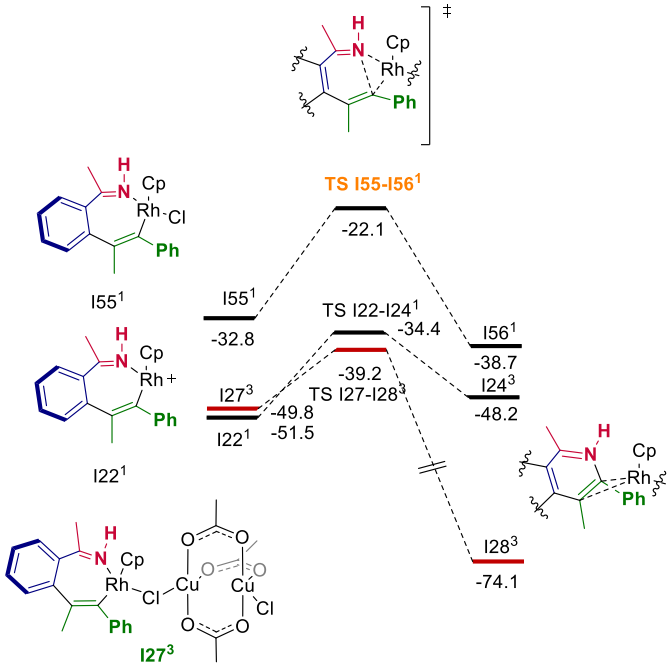

Scheme A2.3. Different possibilities for reductive elimination step. Energies in kcal·mol^{-1}.

2.5.1.5. **Regioselectivity study using Cp as ancillary ligand on the Rh catalyst**

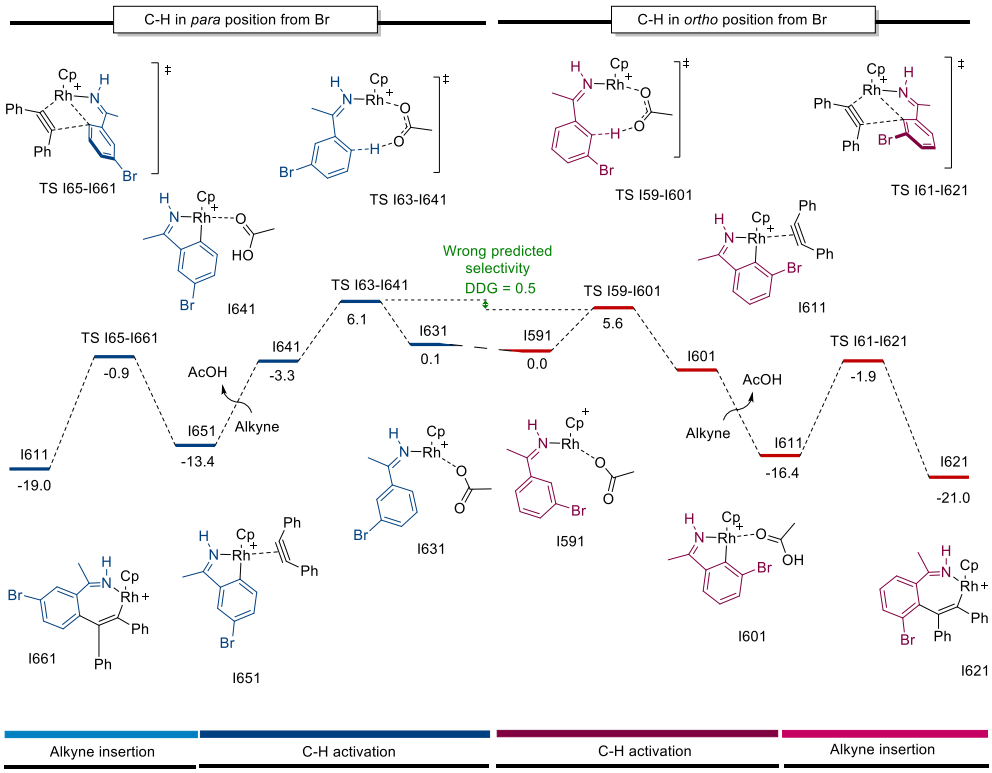

Scheme A2.4. Complete free energy profile for the regioselectivity study of the C−H activation and alkyne insertion for *meta*-bromo-substituted vinyl azide using [(Cp)Rh] complex as model of the real catalyst. The scale has been reduced for clarity. Energies in kcal·mol^{-1}.

2.5.1.6. **Regioselectivity study using Cp* as ancillary ligand on the Rh catalyst**

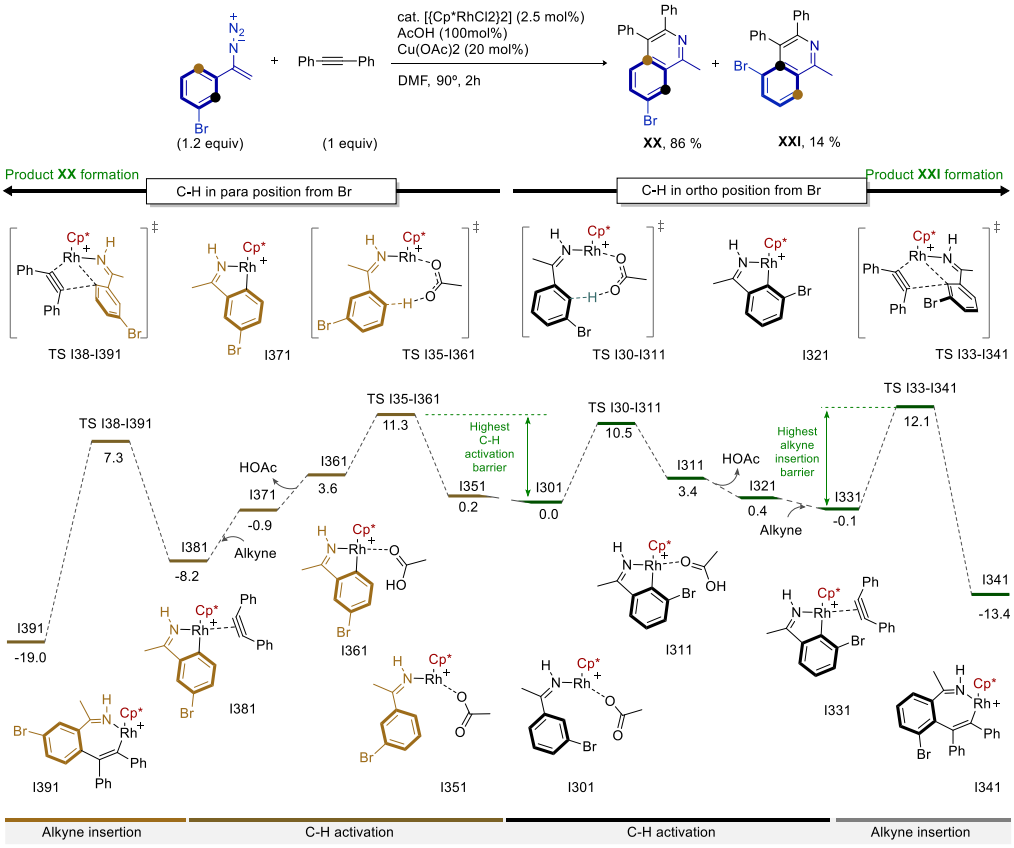

Scheme A2.5. Complete free energy profile for the regioselectivity study of the C−H activation and alkyne insertion for *meta*-bromo-substituted vinyl azide using the real catalyst [(Cp*)Rh] complex. The scale has been reduced for clarity. Energies in kcal·mol^{-1}.

2.5.2. **Microkinetic modeling**

We used COPASI 4.22 (Build 170) program package[18] for the microkinetic modeling. Deterministic method (LSODA) was used for the integration of the time-course simulation of the concentration of each species. Relative tolerance and absolute tolerance were fixed to $1{\cdot}10^{-13}$ and $1{\cdot}10^{-18}$, respectively. In the following sections, the considered elementary steps, free energy and rate constants for each kinetic model are specified. It should be mentioned that the considered elementary steps are bimolecular or unimolecular. COPASI software is not compatible with the resolution of trimolecular reactions.

The coordination or decoordination of ligands (i.e. ligand exchange reactions) that have been considered barrierless in the free energy surface in the aforementioned reactions, will be considered under diffusion-control for the microkinetic analysis. To do so, the rate constants for

a diffusion control reaction is calculated using the Stokes-Einstein equation with the Smoluchowski relation.[15] This means that the diffusion rate constant for a associative bimolecular elementary reaction is approximately defined by *eq.* 1 in L/(mol·s), where K_B is the Boltzmann constant, T is the temperature, η is the viscosity of the solvent at the given temperature and N_a, the Avogadro number.

$$k_{diff} = \frac{8K_B \cdot T}{3\eta} \cdot 1000N_a \quad (eq.1)$$

Regarding that the viscosity of DMF at 353.15 K is 0.47 mPa·s.[27] the conversion of the so-obtained diffusion rate constant to free energy using the Eyring equation is 3.9 kcal·mol^{-1} at 323.15 K. In the microkinetic model, this direct rate constant is assumed for all the associative processes whose equilibrium has a free energy difference $\Delta G < 4.4$ kcal·mol^{-1}. If the free energy difference is bigger than 4.4 kcal·mol^{-1} for a given associative process, the intermediate is considered as kinetically irrelevant and the barrier is taken from the next transition state. The reverse rate constant for these processes were calculated based on the equilibrium constants.

As mentioned in the main text, the initial concentrations for the microkinetic modeling, according to the experimental conditions and the speciation of each catalyst, are 0.20 M for the alkyne, 0.24 M for the azide, 0.02 M for the copper(I) and 0.0104 M for the rhodium(III) catalyst as a monomer. We expected a 100% of conversion for all the reactions since in the microkinetic models catalyst decomposition or inconspicuous side reactions are not contemplated.

2.5.2.1. Kinetic model of the reaction considering [(Cp)Rh(OAc)$_2$] as the catalytically active specie in the C–H activation and alkyne insertion.

Reactant(s)	Product(s)	Barrier ΔΔG	Rate Constant (k)		Corrected Barrier ΔΔG	Rate Constant (k)
Cu + Azi	K1+ N2	21.8	5.67E-01		21.8	5.67E-01
K1 + N2	Cu + Azi	54.9	6.69E-21		54.9	6.69E-21
K1	K2	24.0	2.69E-02		24	2.69E-02
K2	K1	8.6	5.02E+07		8.6	5.02E+07
K2 + AC	K2AC	0.0	7.56E+12		4.4	1.70E+10
K2AC	K2 + AC	0.4	4.34E+12		4.8	9.74E+09
K2AC + AC	K3	0.0	7.56E+12		4.4	1.70E+10
K3	K2AC + AC	0.3	4.98E+12		4.7	1.12E+10
K3	K4	8.0	1.15E+08		8.0	1.15E+08
K4	K3	19.8	9.07E+00		19.8	9.07E+00
K4	K5	22.6	1.87E-01		22.6	1.87E-01
K5	K4	27.6	1.87E-04		27.6	1.83E-04
K5 + RhOAc2	K6 + Cutwo	0.0	7.56E+12		4.4	1.70E+10
K6 + Cutwo	K5 + RhOAc2	2.2	3.58E+11		6.6	8.03E+08
K6	K7 + AC	4.7	1.12E+10		9.1	2.51E+07
K7 + AC	K6	0.0	7.56E+12		4.4	1.70E+10
K7	K8	15.9	2.02E+03		15.9	2.02E+03
K8	K7	8.9	3.31E+07		8.9	3.31E+07

[27] Bernal-Garcia, J. M.; Guzmas-Lopez, A.; Cabrales-Torres, A.; Estrada-Baltazar, A.; Iglesias-Silva, G. A. *J. Chem. Eng. Data*, **2008**, *53*, 1024.

K8 + Alky	K9 +AC	0.0	7.56E+12		4.4	1.70E+10
K9 + AC	K8 + Alky	11.2	1.37E+06		15.6	3.06E+03
K9	K10	15.0	7.04E+03		15	7.04E+03
K10	K9	18.6	4.79E+01		18.6	4.79E+01
K10	K11	15.4	4.04E+03		15.4	4.04E+03
K11	Rh + produ	11.2	1.37E+06		15.6	3.06E+03
Rh + produ	K11	0.0	7.56E+12		4.4	1.70E+10
Rh + Cutwo	RhOAc2 + Cu	0.0	7.56E+12		4.4	1.70E+10
RhOAc2 + Cu	Rh + Cutwo	63.7	3.37E-26		63.7	3.37E-26

Table A2.1. Calculated activation free energies and kinetic constant of kinetic model of the reaction considering [(Cp)Rh(OAc)$_2$] as the catalytically active specie. Free energies in kcal·mol^{-1}. For clarity the units of the rate constant is not shown in the table.

The data from Table A2.1 were used to perform the microkinetic analysis. The conditions for the analysis of the time course were 85000 seconds in 20 steps (4250 seconds of interval size). The results were recorded in Graph A2.1 and Table A2.2.

The following equations were used to perform the microkinetic study of the reaction considering the [(Cp)Rh(OAc)$_2$] as the catalytically active specie:

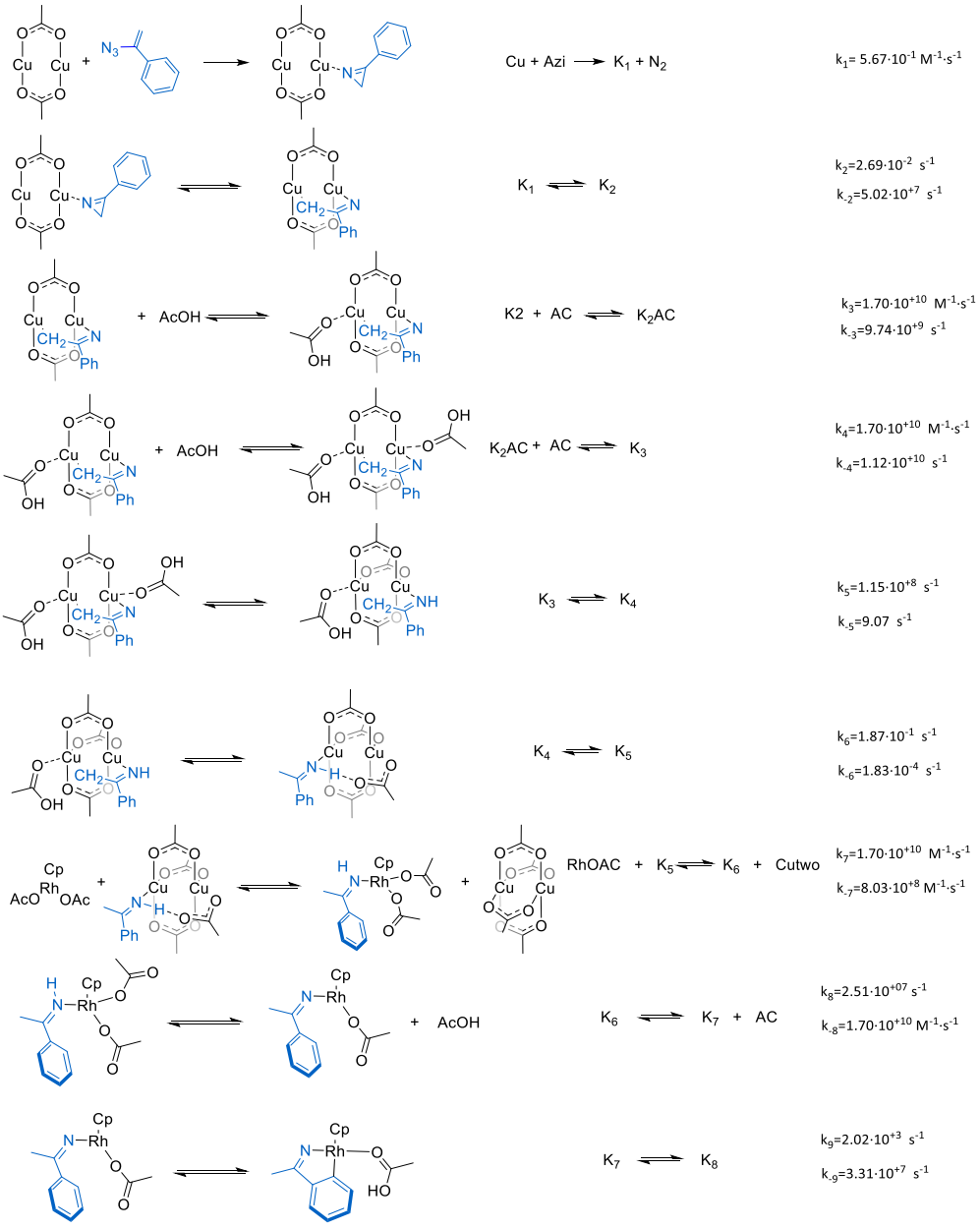
Cu + Azi → K1 + N2
k1= 5.67·10-1 M-1·s-1
K1 ⇌ K2
k2=2.69·10-2 s-1
k-2=5.02·10+7 s-1
K2 + AC ⇌ K2AC
k3=1.70·10+10 M-1·s-1
k-3=9.74·10+9 s-1
K2AC + AC ⇌ K3
k4=1.70·10+10 M-1·s-1
k-4=1.12·10+10 s-1
K3 ⇌ K4
k5=1.15·10+8 s-1
k-5=9.07 s-1
K4 ⇌ K5
k6=1.87·10-1 s-1
k-6=1.83·10-4 s-1
RhOAC + K5 ⇌ K6 + Cutwo
k7=1.70·10+10 M-1·s-1
k-7=8.03·10+8 M-1·s-1
K6 ⇌ K7 + AC
k8=2.51·10+07 s-1
k-8=1.70·10+10 M-1·s-1
K7 ⇌ K8
k9=2.02·10+3 s-1
k-9=3.31·10+7 s-1

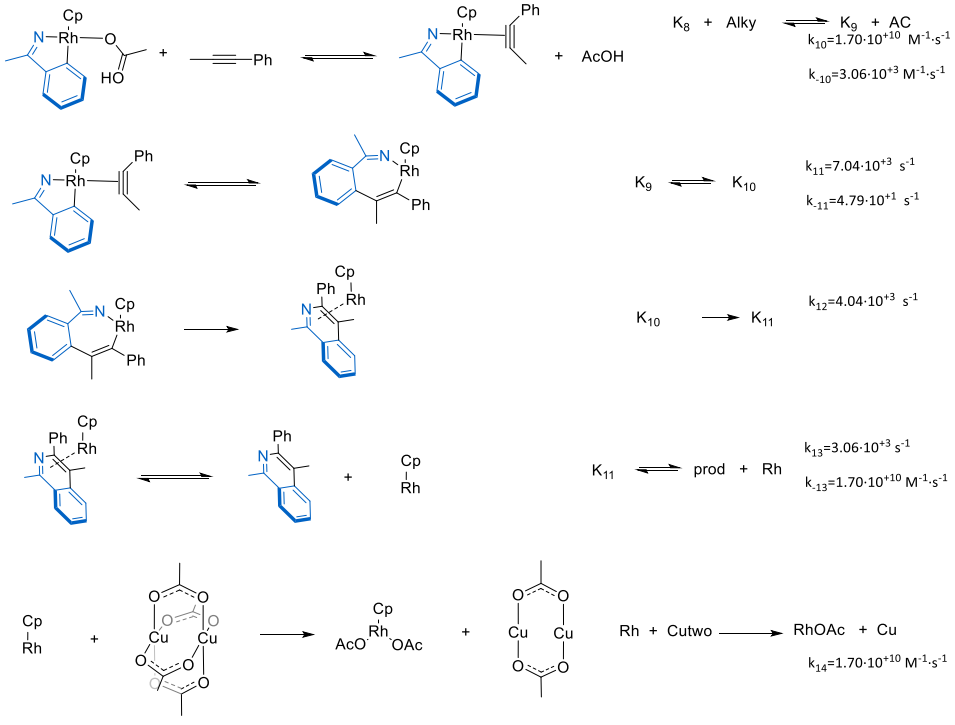

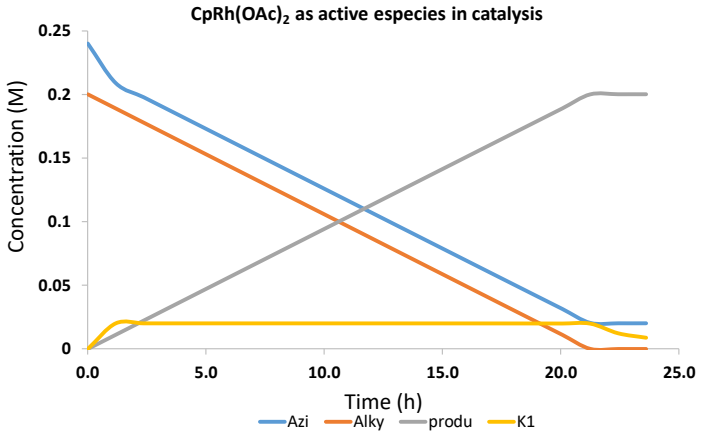

Graph A2.1. Evolution of the concentration of different species during the reaction considering [(Cp)Rh(OAc)$_2$] as catalyst.

Time(h)	AC	Cu	K2AC	K4	K10	K6	K8	K1	K11	K7	K3	Rh	K2	Azi	Alky	K9	Cutwo	K5	RhOAC	produ	N2
0.000	0.200	0.020	0.000	0.000	0.000	0.000	0.000	0.00	0.000	0.000	0.000	0.000	0.000	0.24	0.20	0.000	0.000	0.000	0.01	0.00	0.00
1.18	0.20	2.21E-05	3.71E-12	1.40E-05	6.48E-10	1.78E-07	8.87E-16	0.02	2.99E-06	1.31E-09	1.13E-12	4.85E-11	1.06E-11	0.21	0.19	3.76E-10	3.17E-06	2.58E-12	0.01	0.01	0.03
2.36	0.20	2.33E-05	3.71E-12	1.40E-05	6.48E-10	1.78E-07	9.43E-16	0.02	4.27E-06	1.31E-09	1.13E-12	3.46E-11	1.06E-11	0.20	0.18	3.76E-10	4.45E-06	3.61E-12	0.01	0.02	0.04
3.54	0.20	2.47E-05	3.71E-12	1.40E-05	6.48E-10	1.78E-07	1.01E-15	0.02	5.25E-06	1.31E-09	1.13E-12	2.83E-11	1.06E-11	0.19	0.17	3.76E-10	5.43E-06	4.40E-12	0.01	0.03	0.05
4.72	0.20	2.63E-05	3.71E-12	1.40E-05	6.48E-10	1.78E-07	1.08E-15	0.02	6.08E-06	1.31E-09	1.13E-12	2.46E-11	1.06E-11	0.18	0.16	3.76E-10	6.26E-06	5.08E-12	0.01	0.04	0.06
5.90	0.20	2.81E-05	3.71E-12	1.40E-05	6.48E-10	1.78E-07	1.16E-15	0.02	6.81E-06	1.31E-09	1.13E-12	2.20E-11	1.06E-11	0.16	0.14	3.76E-10	6.99E-06	5.67E-12	0.01	0.06	0.08
7.08	0.20	3.01E-05	3.71E-12	1.40E-05	6.48E-10	1.78E-07	1.26E-15	0.02	7.47E-06	1.32E-09	1.13E-12	2.01E-11	1.06E-11	0.15	0.13	3.76E-10	7.65E-06	6.21E-12	0.01	0.07	0.09
8.26	0.20	3.25E-05	3.71E-12	1.40E-05	6.48E-10	1.78E-07	1.37E-15	0.02	8.07E-06	1.32E-09	1.13E-12	1.87E-11	1.06E-11	0.14	0.12	3.76E-10	8.25E-06	6.71E-12	0.01	0.08	0.10
9.44	0.20	3.52E-05	3.71E-12	1.40E-05	6.48E-10	1.79E-07	1.51E-15	0.02	8.63E-06	1.32E-09	1.13E-12	1.75E-11	1.06E-11	0.13	0.11	3.76E-10	8.81E-06	7.18E-12	0.01	0.09	0.11
10.63	0.20	3.85E-05	3.71E-12	1.40E-05	6.47E-10	1.79E-07	1.68E-15	0.02	9.16E-06	1.32E-09	1.13E-12	1.65E-11	1.06E-11	0.12	0.10	3.76E-10	9.34E-06	7.62E-12	0.01	0.10	0.12
11.81	0.20	4.24E-05	3.71E-12	1.40E-05	6.47E-10	1.80E-07	1.89E-15	0.02	9.66E-06	1.33E-09	1.13E-12	1.56E-11	1.06E-11	0.11	0.09	3.76E-10	9.84E-06	8.05E-12	0.01	0.11	0.13
12.99	0.20	4.72E-05	3.71E-12	1.40E-05	6.47E-10	1.80E-07	2.15E-15	0.02	1.01E-05	1.33E-09	1.13E-12	1.49E-11	1.06E-11	0.10	0.08	3.76E-10	1.03E-05	8.46E-12	0.01	0.12	0.14
14.17	0.20	5.32E-05	3.71E-12	1.40E-05	6.47E-10	1.81E-07	2.51E-15	0.02	1.06E-05	1.34E-09	1.13E-12	1.43E-11	1.06E-11	0.09	0.07	3.76E-10	1.08E-05	8.87E-12	0.01	0.13	0.15
15.35	0.20	6.10E-05	3.71E-12	1.40E-05	6.47E-10	1.82E-07	3.02E-15	0.02	1.10E-05	1.34E-09	1.12E-12	1.37E-11	1.06E-11	0.08	0.06	3.76E-10	1.12E-05	9.28E-12	0.01	0.14	0.16
16.53	0.20	7.14E-05	3.70E-12	1.40E-05	6.46E-10	1.83E-07	3.77E-15	0.02	1.14E-05	1.35E-09	1.12E-12	1.32E-11	1.06E-11	0.06	0.04	3.75E-10	1.16E-05	9.71E-12	0.01	0.16	0.18
17.71	0.20	8.61E-05	3.70E-12	1.40E-05	6.46E-10	1.86E-07	5.02E-15	0.02	1.18E-05	1.37E-09	1.12E-12	1.28E-11	1.06E-11	0.05	0.03	3.75E-10	1.20E-05	1.02E-11	0.01	0.17	0.19
18.89	0.20	1.08E-04	3.70E-12	1.39E-05	6.45E-10	1.91E-07	7.52E-15	0.02	1.22E-05	1.41E-09	1.12E-12	1.24E-11	1.06E-11	0.04	0.02	3.75E-10	1.24E-05	1.08E-11	0.01	0.18	0.20
20.07	0.20	1.46E-04	3.69E-12	1.39E-05	6.44E-10	2.08E-07	1.50E-14	0.02	1.26E-05	1.53E-09	1.12E-12	1.20E-11	1.06E-11	0.03	0.01	3.74E-10	1.28E-05	1.21E-11	0.01	0.19	0.21
21.25	0.20	2.21E-04	3.68E-12	1.39E-05	6.04E-10	5.04E-06	2.20E-12	0.02	1.05E-05	3.72E-08	1.12E-12	9.47E-12	1.05E-11	0.02	0.00	3.51E-10	1.56E-05	3.57E-10	0.01	0.20	0.22
22.43	0.18	3.72E-25	2.09E-12	7.30E-06	1.18E-248	7.03E-03	3.44E-09	0.01	0.00E+00	5.63E-05	5.86E-13	0.00E+00	6.51E-12	0.02	0.00	6.79E-249	7.09E-03	7.12E-04	0.00	0.20	0.22
23.61	0.18	4.39E-46	1.45E-12	4.90E-06	0.00E+00	8.79E-03	4.46E-09	0.01	0.00E+00	7.31E-05	3.90E-13	0.00E+00	4.67E-12	0.02	0.00	0.00E+00	8.86E-03	2.39E-03	0.00	0.20	0.22

Table A2.2. Evolution of the concentration of different species during the reaction considering [(Cp)Rh(OAc)$_2$] as catalyst.

2.5.2.2. Kinetic model of the reaction considering [(Cp)Rh(Cl)$_2$] as the catalytically active specie in the C−H activation and alkyne insertion.

Reactant(s)	Product(s)	Barrier ΔΔG	Rate Constant (k)		Corrected Barrier ΔΔG	Rate Constant (k)
Cu + Azi	K1 + N2	21.8	5.67E-01		21.8	5.67E-01
K1 + N2	Cu + Azi	54.9	6.69E-21		54.9	6.69E-21
K1	K2	24.0	2.69E-02		24	2.69E-02
K2	K1	8.6	5.02E+07		8.6	5.02E+07
K2 + AC	K2AC	0.0	7.56E+12		4.4	1.70E+10
K2AC	K2 + AC	0.4	4.34E+12		4.8	9.74E+09
K2AC + AC	K3	0.0	7.56E+12		4.4	1.70E+10
K3	K2AC + AC	0.3	4.98E+12		4.7	1.12E+10
K3	K4	8.0	1.15E+08		8.0	1.15E+08
K4	K3	19.8	9.07E+00		19.8	9.07E+00
K4	K5	22.6	1.87E-01		22.6	1.87E-01
K5	K4	27.6	1.83E-04		27.6	1.83E-04
RhCl2 + K5	K12 + CuCl2n	7.3	1.40E+09		11.7	1.05E+06
K12 + CuCl2n	RhCl2 + K5	0.0	7.56E+12		4.4	1.70E+10
K12	K13	6.5	9.22E+08		6.5	9.22E+08
K13	K12	11.4	1.03E+06		11.4	1.03E+06
K13 + Alky	K14 + AC	0.0	7.56E+12		4.4	1.70E+10
K14 + AC	K13 + Alky	10.6	3.14E+06		15	7.04E+03
K14	K15	14.1	2.45E+04		14.1	2.45E+04
K15	K14	22.2	3.26E-01		22.2	3.26E-01
K15	K16	17.1	3.83E+02		17.1	3.83E+02
K16	K15	13.8	3.71E+04		13.8	3.71E+04
K16 + CuCl2n	produ + KA	0.0	7.56E+12		4.4	1.70E+10
KA	KB + AC	0.0	7.56E+12		4.4	1.70E+10
KB	Cu + RhCl2	0.0	7.56E+12		4.4	1.70E+10

Table A2.3. Calculated activation free energies and rate constant of kinetic model of the reaction considering [(Cp)Rh(Cl)$_2$] as the catalytically active specie. Free energies in kcal·mol^{-1}. For clarity the units of the rate constant is not shown in the table.

The data from Table A2.3 were used to perform the microkinetic analysis. The conditions for the analysis of the time course were 85000 seconds in 20 steps (4250 seconds of interval size). The results were recorded in Graph A2.1 and Table A2.3.

The following equations were used to perform the microkinetic study of the reaction considering the [(Cp)Rh(Cl)$_2$] as the catalytically active specie:

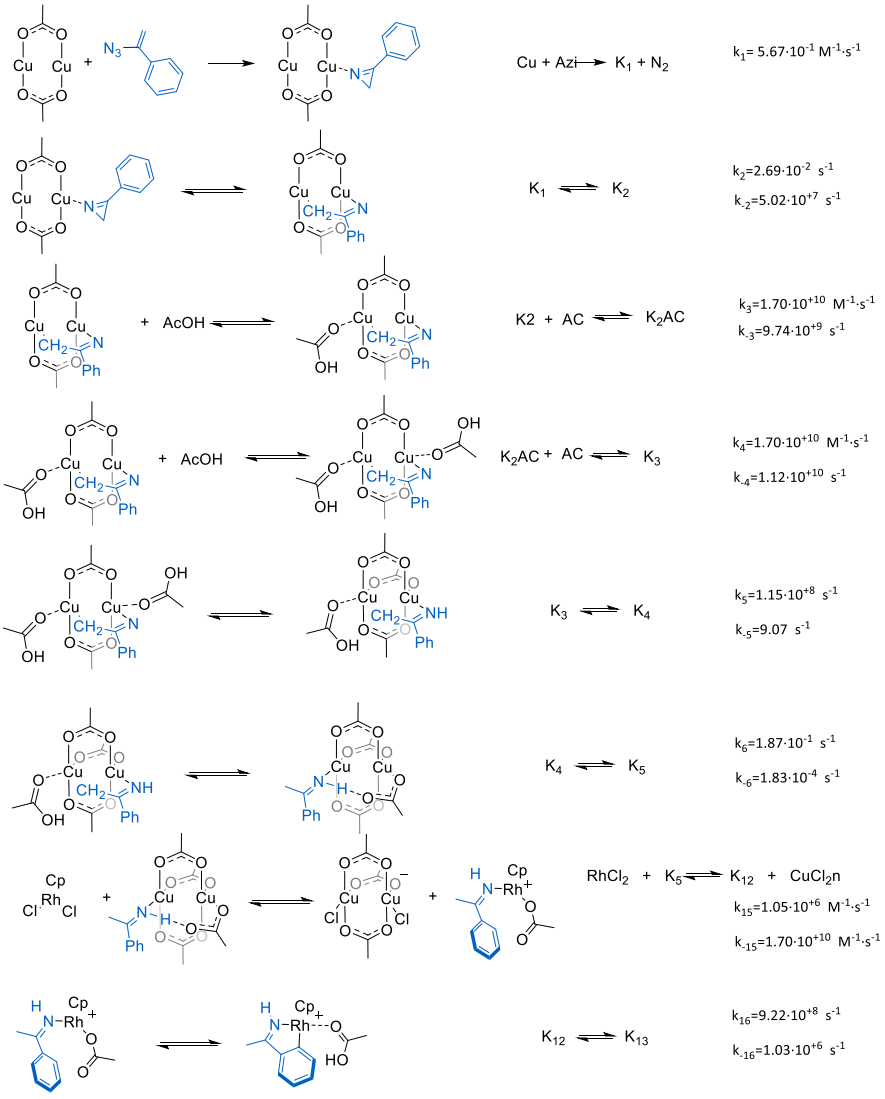
Cu + Azi → K1 + N2
k1= 5.67·10-1 M-1·s-1
K1 ⇌ K2
k2=2.69·10-2 s-1
k-2=5.02·10+7 s-1
K2 + AC ⇌ K2AC
k3=1.70·10+10 M-1·s-1
k-3=9.74·10+9 s-1
K2AC + AC ⇌ K3
k4=1.70·10+10 M-1·s-1
k-4=1.12·10+10 s-1
K3 ⇌ K4
k5=1.15·10+8 s-1
k-5=9.07 s-1
K4 ⇌ K5
k6=1.87·10-1 s-1
k-6=1.83·10-4 s-1
RhCl2 + K5 ⇌ K12 + CuCl2n
k15=1.05·10+6 M-1·s-1
k-15=1.70·10+10 M-1·s-1
K12 ⇌ K13
k16=9.22·10+8 s-1
k-16=1.03·10+6 s-1

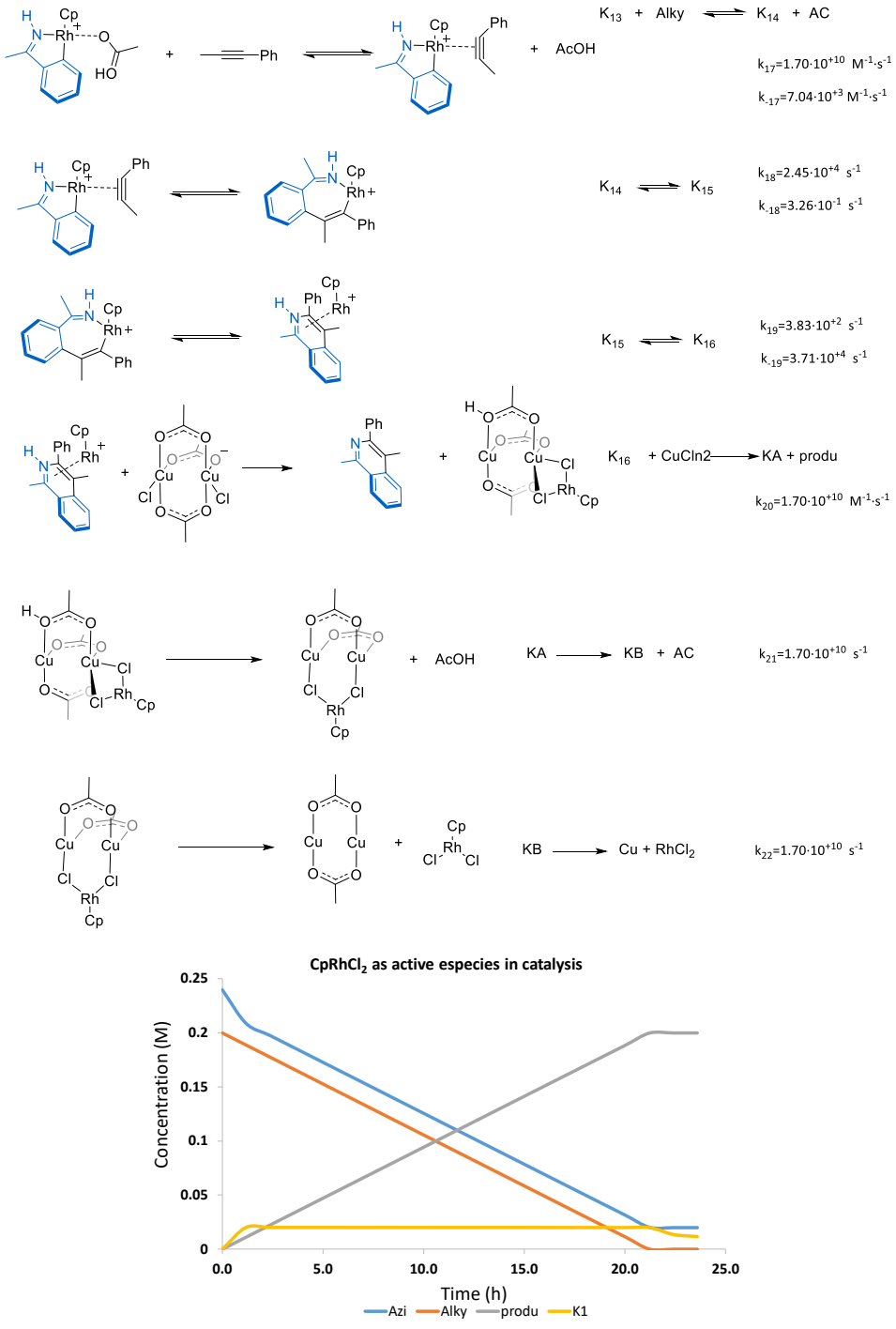

Graph A2.2. Evolution of the concentration of different species during the reaction considering $[(Cp)Rh(Cl)_2]$ as catalyst.

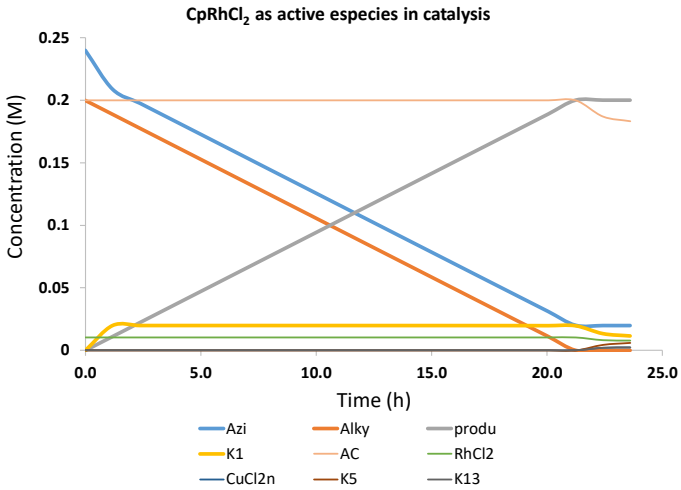

Graph A2.3. Evolution of the concentration of different species during the reaction considering [(Cp)Rh(Cl)$_2$] as catalyst considering other species.

Time (h)	AC	Cu	K2AC	K4	CuCl2n	K15	K13	K1	KA	K14	K5	KB	K16	Azi	Alky	K2	K3	RhCl2	N2	produ	K12
0.000	0.20	0.020	0.000	0.000	0.000	0.000	0.000	0.00	0.000	0.000	0.000	0.000	0.000	0.24	0.20	0.000	0.000	0.0104	0.00	0.00	0.000
1.18	0.20	2.21E-05	3.72E-12	1.40E-05	1.26E-07	1.25E-07	8.63E-16	0.02	1.54E-16	1.09E-10	8.02E-11	1.54E-16	1.22E-09	0.21	0.19	1.06E-11	1.13E-12	0.0104	0.03	0.01	2.85E-15
2.36	0.20	2.34E-05	3.72E-12	1.40E-05	1.26E-07	1.25E-07	9.17E-16	0.02	1.54E-16	1.09E-10	8.02E-11	1.54E-16	1.22E-09	0.20	0.18	1.06E-11	1.13E-12	0.0104	0.04	0.02	2.85E-15
3.54	0.20	2.47E-05	3.71E-12	1.40E-05	1.26E-07	1.25E-07	9.78E-16	0.02	1.54E-16	1.09E-10	8.02E-11	1.54E-16	1.22E-09	0.19	0.17	1.06E-11	1.13E-12	0.0104	0.05	0.03	2.85E-15
4.72	0.20	2.63E-05	3.71E-12	1.40E-05	1.26E-07	1.25E-07	1.05E-15	0.02	1.54E-16	1.09E-10	8.02E-11	1.54E-16	1.22E-09	0.18	0.16	1.06E-11	1.13E-12	0.0104	0.06	0.04	2.85E-15
5.90	0.20	2.81E-05	3.71E-12	1.40E-05	1.26E-07	1.25E-07	1.13E-15	0.02	1.54E-16	1.09E-10	8.02E-11	1.54E-16	1.22E-09	0.16	0.14	1.06E-11	1.13E-12	0.0104	0.08	0.06	2.85E-15
7.08	0.20	3.01E-05	3.71E-12	1.40E-05	1.26E-07	1.25E-07	1.22E-15	0.02	1.54E-16	1.09E-10	8.02E-11	1.54E-16	1.22E-09	0.15	0.13	1.06E-11	1.13E-12	0.0104	0.09	0.07	2.85E-15
8.26	0.20	3.25E-05	3.71E-12	1.40E-05	1.26E-07	1.25E-07	1.33E-15	0.02	1.54E-16	1.09E-10	8.02E-11	1.54E-16	1.22E-09	0.14	0.12	1.06E-11	1.13E-12	0.0104	0.10	0.08	2.85E-15
9.44	0.20	3.52E-05	3.71E-12	1.40E-05	1.26E-07	1.25E-07	1.47E-15	0.02	1.54E-16	1.08E-10	8.02E-11	1.54E-16	1.22E-09	0.13	0.11	1.06E-11	1.13E-12	0.0104	0.11	0.09	2.85E-15
10.63	0.20	3.85E-05	3.71E-12	1.40E-05	1.26E-07	1.25E-07	1.63E-15	0.02	1.54E-16	1.08E-10	8.01E-11	1.54E-16	1.22E-09	0.12	0.10	1.06E-11	1.13E-12	0.0104	0.12	0.10	2.85E-15
11.81	0.20	4.24E-05	3.71E-12	1.40E-05	1.26E-07	1.25E-07	1.84E-15	0.02	1.54E-16	1.08E-10	8.01E-11	1.54E-16	1.22E-09	0.11	0.09	1.06E-11	1.13E-12	0.0104	0.13	0.11	2.85E-15
12.99	0.20	4.72E-05	3.71E-12	1.40E-05	1.26E-07	1.25E-07	2.10E-15	0.02	1.54E-16	1.08E-10	8.01E-11	1.54E-16	1.22E-09	0.10	0.08	1.06E-11	1.13E-12	0.0104	0.14	0.12	2.85E-15
14.17	0.20	5.33E-05	3.71E-12	1.40E-05	1.26E-07	1.25E-07	2.45E-15	0.02	1.54E-16	1.08E-10	8.01E-11	1.54E-16	1.22E-09	0.09	0.07	1.06E-11	1.13E-12	0.0104	0.15	0.13	2.85E-15
15.35	0.20	6.11E-05	3.71E-12	1.40E-05	1.26E-07	1.25E-07	2.94E-15	0.02	1.54E-16	1.08E-10	8.01E-11	1.54E-16	1.22E-09	0.08	0.06	1.06E-11	1.13E-12	0.0104	0.16	0.14	2.85E-15
16.53	0.20	7.15E-05	3.71E-12	1.40E-05	1.26E-07	1.25E-07	3.67E-15	0.02	1.54E-16	1.08E-10	8.00E-11	1.54E-16	1.22E-09	0.06	0.04	1.06E-11	1.12E-12	0.0104	0.18	0.16	2.85E-15
17.71	0.20	8.63E-05	3.70E-12	1.40E-05	1.26E-07	1.25E-07	4.90E-15	0.02	1.54E-16	1.08E-10	8.00E-11	1.54E-16	1.22E-09	0.05	0.03	1.06E-11	1.12E-12	0.0104	0.19	0.17	2.84E-15
18.89	0.20	1.09E-04	3.70E-12	1.39E-05	1.26E-07	1.25E-07	7.35E-15	0.02	1.53E-16	1.08E-10	7.99E-11	1.53E-16	1.22E-09	0.04	0.02	1.06E-11	1.12E-12	0.0104	0.20	0.18	2.85E-15
20.07	0.20	1.47E-04	3.69E-12	1.39E-05	1.26E-07	1.24E-07	1.47E-14	0.02	1.53E-16	1.08E-10	7.97E-11	1.53E-16	1.22E-09	0.03	0.01	1.06E-11	1.12E-12	0.0104	0.21	0.19	2.85E-15
21.25	0.20	2.05E-04	3.68E-12	1.39E-05	2.01E-05	0.00E+00	2.01E-05	0.02	0.00E+00	0.00E+00	2.98E-07	0.00E+00	4.29E-29	0.02	0.00	1.05E-11	1.12E-12	0.0104	0.22	0.20	2.84E-08
22.43	0.19	2.38E-25	2.35E-12	8.37E-06	2.17E-03	0.00E+00	2.16E-03	0.01	0.00E+00	0.00E+00	4.36E-03	0.00E+00	0.00E+00	0.02	0.00	7.20E-12	6.67E-13	0.0082	0.22	0.20	3.06E-06
23.61	0.18	2.89E-46	1.99E-12	6.98E-06	2.48E-03	0.00E+00	2.47E-03	0.01	0.00E+00	0.00E+00	5.91E-03	0.00E+00	0.00E+00	0.02	0.00	6.21E-12	5.52E-13	0.0079	0.22	0.20	3.49E-06

Table A2.4. Evolution of the concentration of different species during the reaction considering $[(Cp)Rh(Cl)_2]$ as catalyst.

2.5.2.3. Kinetic model of the reaction considering the multimetallic cooperation between copper and rhodium species.

Reactant(s)	Product(s)	Barrier ΔΔG	Rate Constant (k)		Corrected Barrier ΔΔG	Rate Constant (k)
Cu + Azi	K1 + N2	21.8	5.67E-01		21.8	5.67E-01
K1 + RhCl2	K17	0.0	7.56E+12		4.4	1.70E+10
K17	K1 + RhCl2	0.3	4.98E+12		4.7	1.12E+10
K17	K18	13.8	3.71E+04		13.8	3.71E+04
K18	K17	9.3	1.90E+07		9.3	1.90E+07
K18 + AC	K19	0.7	2.86E+12		4.4	1.70E+10
K19	K18 + AC	0.0	7.56E+12		5.1	6.42E+09
K19 + AC	K20	9.0	2.88E+07		9	2.88E+07
K20	K19 + AC	9.0	2.88E+07		9	2.88E+07
K20	K21	15.3	4.64E+03		15.3	4.64E+03
K21	K20	21.2	1.30E+00		21.2	1.30E+00
K21	K12 + CuCl2n	6.2	1.40E+09		10.6	3.14E+06
K12 + CuCl2n	K21	0.0	7.56E+12		4.4	1.70E+10
K12	K13	6.5	9.22E+08		6.5	9.22E+08
K13	K12	11.4	1.03E+06		11.4	1.03E+06
K13 + Alky	K14 + AC	0.0	7.56E+12		4.4	1.70E+10
K14 + AC	K13 + Alky	10.6	3.14E+06		15	7.04E+03
K14	K15	14.1	2.45E+04		14.1	2.45E+04
K15	K14	22.2	3.26E-01		22.2	3.26E-01
K15 + CuCl2n	K22	1.7	7.16E+11		4.4	1.70E+10
K22	K15 + CuCl2n	0.0	7.56E+12		2.7	1.79E+11
K22	K23	10.6	3.14E+06		10.6	3.14E+06
K23	K24 + produ	10.0	7.21E+06		14.4	1.62E+04
K24 + produ	K23	0.0	7.56E+12		4.4	1.70E+10
K24	K25 + AC	0.0	7.56E+12		4.4	1.70E+10
K25	Cu + RhCl2	0.0	7.56E+12		4.4	1.70E+10

Table A2.5. Calculated activation free energies and rate constant of kinetic model of the reaction considering the multimetallic cooperation. Free energies in kcal·mol^{-1}. For clarity the units of the rate constant is not shown in the table.

The data from Table A2.5 were used to perform the microkinetic analysis. The conditions for the analysis of the time course were 1100 seconds in 20 steps (55 seconds of interval size). The results were recorded in Graph A2.4, Graph A2.5 and Table A2.6. The following equations were used to perform the microkinetic study of the reaction considering the multimetallic cooperation:

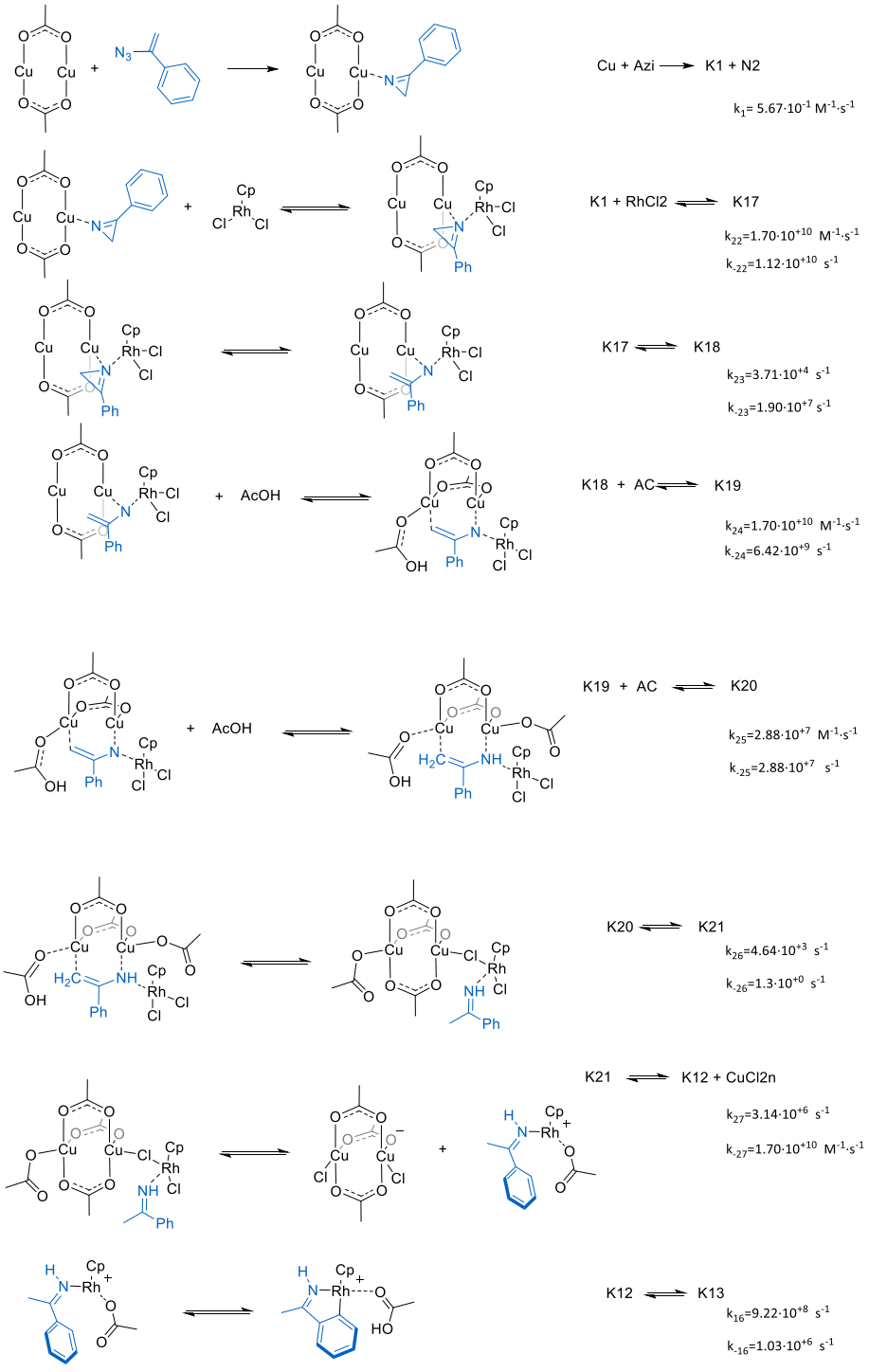
Cu + Azi → K1 + N2
k_1= 5.67·10^{-1} M^{-1}·s^{-1}
K1 + RhCl2 ⇌ K17
k_{22}=1.70·10^{+10} M^{-1}·s^{-1}
k_{-22}=1.12·10^{+10} s^{-1}
K17 ⇌ K18
k_{23}=3.71·10^{+4} s^{-1}
k_{-23}=1.90·10^{+7} s^{-1}
K18 + AC ⇌ K19
k_{24}=1.70·10^{+10} M^{-1}·s^{-1}
k_{-24}=6.42·10^{+9} s^{-1}
K19 + AC ⇌ K20
k_{25}=2.88·10^{+7} M^{-1}·s^{-1}
k_{-25}=2.88·10^{+7} s^{-1}
K20 ⇌ K21
k_{26}=4.64·10^{+3} s^{-1}
k_{-26}=1.3·10^{+0} s^{-1}
K21 ⇌ K12 + CuCl2n
k_{27}=3.14·10^{+6} s^{-1}
k_{-27}=1.70·10^{+10} M^{-1}·s^{-1}
K12 ⇌ K13
k_{16}=9.22·10^{+8} s^{-1}
k_{-16}=1.03·10^{+6} s^{-1}

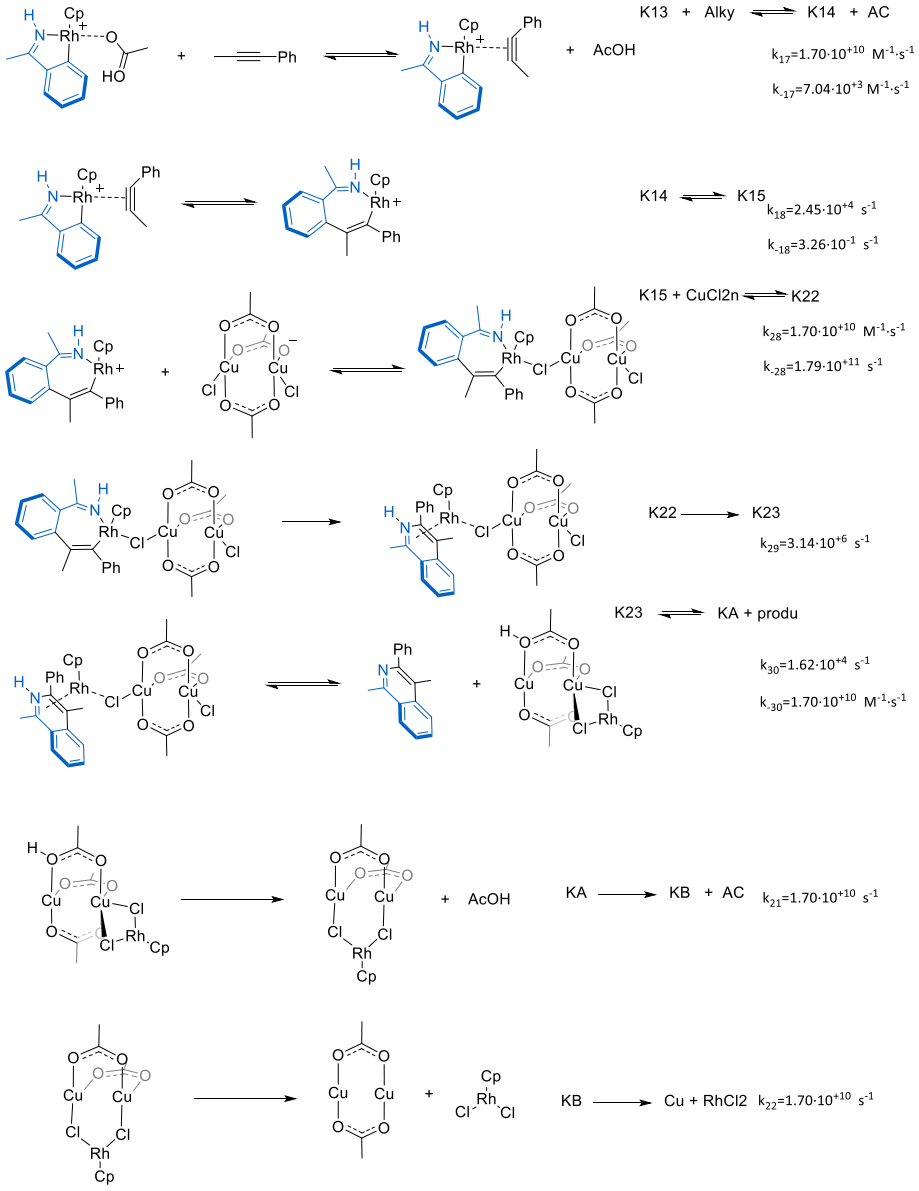
K13 + Alky ⇌ K14 + AC
$k_{17}=1.70\cdot10^{+10}$ $M^{-1}\cdot s^{-1}$
$k_{-17}=7.04\cdot10^{+3}$ $M^{-1}\cdot s^{-1}$
K14 ⇌ K15
$k_{18}=2.45\cdot10^{+4}$ s^{-1}
$k_{-18}=3.26\cdot10^{-1}$ s^{-1}
K15 + CuCl2n ⇌ K22
$k_{28}=1.70\cdot10^{+10}$ $M^{-1}\cdot s^{-1}$
$k_{-28}=1.79\cdot10^{+11}$ s^{-1}
K22 ⟶ K23
$k_{29}=3.14\cdot10^{+6}$ s^{-1}
K23 ⇌ KA + produ
$k_{30}=1.62\cdot10^{+4}$ s^{-1}
$k_{-30}=1.70\cdot10^{+10}$ $M^{-1}\cdot s^{-1}$
KA ⟶ KB + AC
$k_{21}=1.70\cdot10^{+10}$ s^{-1}
KB ⟶ Cu + RhCl2
$k_{22}=1.70\cdot10^{+10}$ s^{-1}

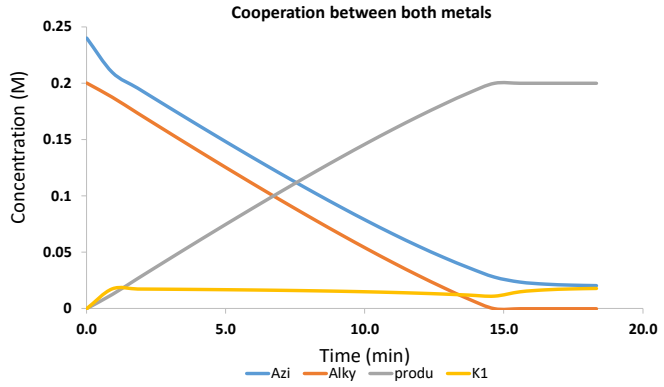

Graph A2.4. Evolution of the concentration of different species during the reaction considering the multimetallic cooperation.

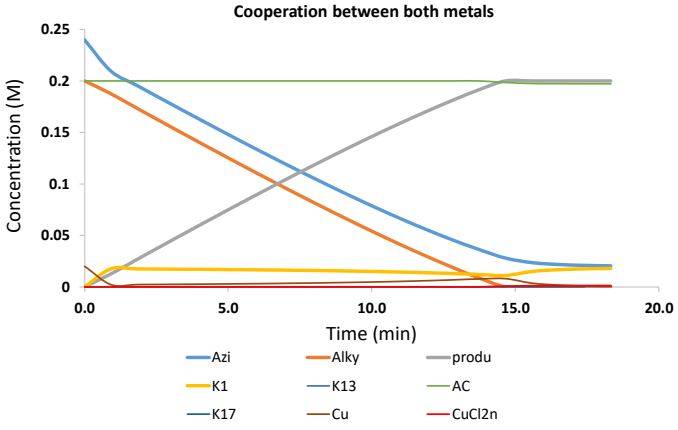

Graph A2.5. Evolution of the concentration of different species during the reaction considering the multimetallic cooperation considering other species.

Time(min)	AC	Cu	CuCl2n	K17	K19	K23	K13	K15	K21	KA	K1	K12	KB	K22	produ	K20	Azi	RhCl2	N2	Alky	K18	K14
0.0000	0.20	0.0200	0.0000	0.0000	0.0000	0.0000	0.0000	0.0000	0.0000	0.0000	0.0000	0.0000	0.0000	0.0000	0.0000	0.0000	0.24	0.0104	0.00	0.20	0.0000	0.0000
0.92	0.20	0.0022	6.42E-06	0.000027	2.79E-07	1.60E-08	8.59E-14	6.41E-06	1.74E-09	1.52E-14	0.0176	2.81E-13	1.52E-14	8.24E-11	0.01	5.58E-08	0.21	0.01012	0.03	0.19	5.27E-07	1.06E-08
1.83	0.20	0.0023	6.40E-06	0.000268	2.77E-07	1.61E-08	9.23E-14	6.39E-06	1.73E-09	1.51E-14	0.0174	2.79E-13	1.51E-14	8.18E-11	0.03	5.54E-08	0.20	0.01012	0.04	0.17	5.23E-07	1.06E-08
2.75	0.20	0.0024	6.37E-06	0.000266	2.75E-07	1.62E-08	9.96E-14	6.36E-06	1.71E-09	1.50E-14	0.0173	2.77E-13	1.50E-14	8.12E-11	0.04	5.49E-08	0.18	0.01013	0.06	0.16	5.19E-07	1.05E-08
3.67	0.20	0.0026	6.34E-06	0.000263	2.72E-07	1.62E-08	1.08E-13	6.33E-06	1.69E-09	1.48E-14	0.0171	2.74E-13	1.48E-14	8.04E-11	0.05	5.44E-08	0.17	0.01013	0.07	0.15	5.14E-07	1.04E-08
4.58	0.20	0.0028	6.31E-06	0.00026	2.69E-07	1.63E-08	1.18E-13	6.30E-06	1.68E-09	1.47E-14	0.0169	2.71E-13	1.47E-14	7.95E-11	0.07	5.38E-08	0.15	0.01013	0.09	0.13	5.08E-07	1.03E-08
5.50	0.20	0.0030	6.27E-06	0.000257	2.66E-07	1.63E-08	1.30E-13	6.26E-06	1.65E-09	1.45E-14	0.0167	2.68E-13	1.45E-14	7.85E-11	0.08	5.31E-08	0.14	0.01014	0.10	0.12	5.02E-07	1.01E-08
6.42	0.20	0.0033	6.22E-06	0.000253	2.62E-07	1.62E-08	1.45E-13	6.21E-06	1.63E-09	1.43E-14	0.0165	2.64E-13	1.43E-14	7.74E-11	0.10	5.24E-08	0.13	0.01014	0.11	0.10	4.94E-07	1.00E-08
7.33	0.20	0.0036	6.17E-06	0.000249	2.57E-07	1.61E-08	1.63E-13	6.16E-06	1.60E-09	1.40E-14	0.0162	2.59E-13	1.40E-14	7.60E-11	0.11	5.15E-08	0.11	0.01014	0.13	0.09	4.86E-07	9.83E-09
8.25	0.20	0.0039	6.10E-06	0.000244	2.52E-07	1.60E-08	1.86E-13	6.10E-06	1.57E-09	1.38E-14	0.0158	2.54E-13	1.38E-14	7.45E-11	0.12	5.04E-08	0.10	0.01015	0.14	0.08	4.76E-07	9.63E-09
9.17	0.20	0.0043	6.03E-06	0.000238	2.46E-07	1.58E-08	2.17E-13	6.02E-06	1.53E-09	1.34E-14	0.0154	2.48E-13	1.34E-14	7.27E-11	0.13	4.92E-08	0.09	0.01016	0.15	0.07	4.64E-07	9.39E-09
10.08	0.20	0.0048	5.94E-06	0.000231	2.39E-07	1.55E-08	2.60E-13	5.93E-06	1.49E-09	1.30E-14	0.0150	2.40E-13	1.30E-14	7.05E-11	0.15	4.77E-08	0.08	0.01016	0.16	0.05	4.51E-07	9.11E-09
11.00	0.20	0.0054	5.83E-06	0.000222	2.30E-07	1.51E-08	3.23E-13	5.82E-06	1.43E-09	1.25E-14	0.0144	2.32E-13	1.25E-14	6.79E-11	0.16	4.60E-08	0.07	0.01017	0.17	0.04	4.34E-07	8.78E-09
11.92	0.20	0.0060	5.70E-06	0.000212	2.20E-07	1.45E-08	4.29E-13	5.69E-06	1.37E-09	1.20E-14	0.0137	2.21E-13	1.20E-14	6.49E-11	0.17	4.39E-08	0.06	0.01018	0.18	0.03	4.15E-07	8.39E-09
12.83	0.20	0.0068	5.54E-06	0.0002	2.07E-07	1.39E-08	6.41E-13	5.53E-06	1.29E-09	1.13E-14	0.0130	2.09E-13	1.13E-14	6.12E-11	0.18	4.14E-08	0.05	0.01019	0.19	0.02	3.91E-07	7.92E-09
13.75	0.20	0.0078	5.34E-06	0.000186	1.93E-07	1.30E-08	1.31E-12	5.33E-06	1.20E-09	1.05E-14	0.0120	1.95E-13	1.05E-14	5.69E-11	0.19	3.85E-08	0.04	0.01021	0.20	0.01	3.64E-07	7.37E-09
14.67	0.20	0.0080	0.000668	0.00016	1.65E-07	7.88E-57	6.67E-04	0.00E+00	5.68E-05	6.33E-63	0.0111	7.45E-07	6.33E-63	2.58E-59	0.20	3.27E-08	0.03	0.00951	0.21	0.00	3.13E-07	3.07E-61
15.58	0.20	0.0036	0.001069	0.000204	2.08E-07	0.00E+00	1.07E-03	0.00E+00	0.0001454	0.00E+00	0.0150	1.19E-06	0.00E+00	0.00E+00	0.20	4.12E-08	0.02	0.00898	0.22	0.00	3.98E-07	0.00E+00
16.50	0.20	0.0018	0.001126	0.000225	2.30E-07	0.00E+00	1.12E-03	0.00E+00	0.0001614	0.00E+00	0.0167	1.26E-06	0.00E+00	0.00E+00	0.20	4.54E-08	0.02	0.00889	0.22	0.00	4.40E-07	0.00E+00
17.42	0.20	0.0009	0.001151	0.000235	2.40E-07	0.00E+00	1.15E-03	0.00E+00	0.0001688	0.00E+00	0.0175	1.28E-06	0.00E+00	0.00E+00	0.20	4.74E-08	0.02	0.00884	0.22	0.00	4.59E-07	0.00E+00
18.33	0.20	0.0005	0.001164	0.00024	2.45E-07	0.00E+00	1.16E-03	0.00E+00	0.0001725	0.00E+00	0.0179	1.30E-06	0.00E+00	0.00E+00	0.20	4.84E-08	0.02	0.00882	0.22	0.00	4.69E-07	0.00E+00

Table A2.6. Evolution of the concentration of different species during the reaction considering the multimetallic cooperation.

The experimental time reaction for this process has been reported to be 30 minutes. It should be noted that when the multimetallic cooperation is considered, the predicted reaction time by the microkinetic model is close to 15 minutes versus almost 21 hours for the previously proposed reaction mechanism.

2.5.2.4. Microkinetic model to study the regioselectivity of the C−H activation and alkyne insertion for *Br-meta*-substituted vinyl azides.

The following equations were used to perform the microkinetic study of the selectivity:

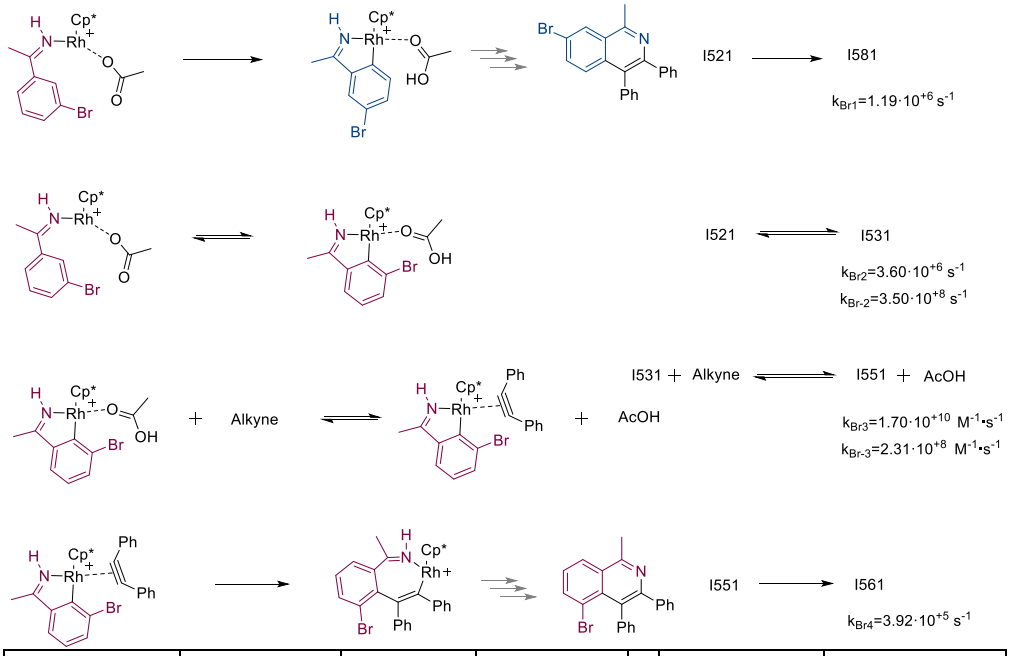

Reactant(s)	Product(s)	Barrier ΔΔG	Rate Constant (k)		Corrected Barrier ΔΔG	Rate Constant (k)
I52[1]	I58[1]	11.3	1.19E+06		11.3	1.19E+06
I52[1]	I53[1]	10.5	3.60E+06		10.5	3.60E+06
I53[1]	I52[1]	7.2	3.50E+08		7.2	3.50E+08
I53[1] + Alkyne	I55[1] + AcOH	0.0	7.56E+12		4.4	1.70E+10
I55[1] + AcOH	I53[1] + Alkyne	3.1	1.03E+11		7.5	2.31E+08
I55[1]	I56[1]	12.1	3.92E+05		12.1	3.92E+05

Table A2.7. Calculated activation free energies and rate constant of kinetic model of the regioselectivity when considering [(Cp*)Rh(Cl)$_2$] as catalyst for *m*-substituted substrates. Free energies in kcal·mol^{-1}. For clarity the units of the rate constant is not shown in the table.

We used an initial concentration for **I52[1]** of 0.0104 M and deterministic (LSODA) method was used for the integration. We obtained using this microkinetic model 81.7 % of the product from **I61[1]** versus 18.3 % of the product from **I56[1]**. Experimentally, they observe 86 % and 14 %, respectively. The reaction mechanism that we have studied for this system can perfectly explain the observe regioselectivity.

2.6. REFERENCES

1. Another environmentally friendly and low cost alternative is the use of electricity as oxidant (Meyer, T. H.; Finger, L. H.; Gandeepan, P.; Ackermann L. *Trends Chem.* **2019**, *1*, 63).

2. Wang, Y.-F.; Toh, K. K.; Lee, J.-Y.; Chiba, S. *Angew. Chem. Int. Ed*. **2011**, *50*, 5927.

3. It should be noticed that the authors also employ [$Cu(OAc)_2$] to set up the coupling. It is well-known that Cu^{II} species can be reduced to Cu^{I} in DMF, allowing the initiation of the Cu^{I}-catalyzed transformation.

4. For examples where copper is proposed to play a role beyond the catalyst recovery by DFT see: a) Jiang, J.; Ramozzi, R.; Morokuma, K. *Chem. Eur. J.* **2015**, *21*, 11158. b) Funes-Ardoiz, I.; Maseras, F. *Angew. Chem. Int. Ed.* **2016**, *55*, 2764. c) Funes-Ardoiz, I.; Maseras, F. *Chem. Eur. J.* **2018**, *24*, 12383. d) Jones, A. W.; Rank, C. K.; Becker, Y.; Malchau, C.; Funes-Ardoiz, I.; Maseras, F.; Patureau, F. W. *Chem. Eur. J.* **2018**, *24*, 15178. For examples where DFT calculations support that silver is not an innocent additive in oxidative coupling, see: e) Frasco, D. A.; Lilly, C. P.; Boyle, P. D.; Ison, E. A. *ACS Catal*. **2013**, *3*, 2421. f) Yang, Y.-F.; Cheng, G.-J.; Liu, P.; Leow, D.; Sun, T.-Y.; Chen, P.; Zhang, X.; Yu, J.-Q.; Wu, Y.-D.; Houk, K. N. *J. Am. Chem. Soc.* **2014**, *136*, 344. Examples of non-innocent role of oxidants in oxidative coupling catalysis have been reviewed by our group: g) Funes-Ardoiz, I.; Maseras, F. *ACS Catal*. **2018**, *8*, 1161. Experimental evidences of the role of the oxidants in oxidative coupling have been detected experimentally by our group, see: h) Sanjosé-Orduna, J.; Toro, J. M. S.; Pérez-Temprano, M. H. *Angew. Chem. Int. Ed*. **2018**, *57*, 11369.

5. Li, L.; Brennessel, W. W.; Jones, W. D. *J. Am. Chem. Soc*. **2008**, *130*, 12414.

6. Pedersen, A.; Tilset, M. *Organometallics* **1993**, *12*, 56.

7. a) Shin, K.; Park, Y.; Baik, M.-H.; Chang, S. *Nat. Chem*. **2018**, *10*, 218. b) Kim, J.; Shin, K.; Jin, S.; Kim, D.; Chang, S. *J. Am. Chem. Soc*. **2019**, *141*, 4137.

8. Liu, B.; Zhou, T.; Li, B.; Xu, S.; Song, H.; Wang, B. *Angew. Chem. Int. Ed*. **2014**, *53*, 4191.

9. David, D. L.; Macgregor, S. A.; McMullin, C. L. *Chem. Rev*. **2017**, *117*, 8649.

10. Ueura, K.; Satoh, T.; Miura, M. *J. Org. Chem*. **2007**, *72*, 5362.

11. M.-L. Louillat; F. W. Patureau, *Org. Lett*. **2013**, *15*, 164.

12. a) González-Pérez, A. B.; Álvarez, R.; Faza, O. N.; de Lera, Á. R.; Aurrecoechea, J. M. *Organometallics* **2012**, *31*, 2053. b) Mudarra, Á. L.; Martínez de Salinas, S.; Pérez Temprano, M. H. *Org. Biomol. Chem.* **2019**, *17*, 1655.

13. Kozuch, S.; Shaik, S. *Acc. Chem. Res.* **2011**, *44*, 101.

14. When lacking thermodynamic or kinetic information about a reaction, the selectivity of a reaction could be a reasonable criteria to evaluate the plausibility of a given mechanism since it is a consequence of the free energy difference between different mechanisms. For instance, it has been proved that for stereoselective processes, DFT calculation can explain the product distribution observed even if the description of activation energy height is not extremely accurate (ref. **Error! Bookmark not defined.**). However, mechanistic information can be missed if the criteria exclusively relies on the selectivity of the reaction.

15. Besora, M.; Maseras, F. *Wiley Interdiscip. Rev.: Comput. Mol. Sci.* **2018**, *8*, e1372.

16. a) Li, Q.; García-Muelas, R.; López, N. *Nature Commun.* **2018**, *9*, 526. b) Rellán-Pineiro, M.; López, N. *ACS Sustainable Chem. Eng.* **2018**, *6*, 16169.

17. Yu, Y.; Zhu, Y.; Bhagat, M. N.; Raghuraman, A.; Hirsekorn, K. F.; Notestein, J. M.; Nguyen, S. T.; Broadbelt, L. J. *ACS Catal*. **2018**, *8*, 11119.

18. Hoops, S.; Sahle, S.; Gauges, R.; Lee, C.; Pahle, J.; Simus, N.; Singhal, M.; Xu, L.; Mendes, P.; Kummer, U. *Bioinformatics*, **2006**, *22*, 3067.

19. a) Contreras-Garcia, J.; Johnson, E.; Keinan, S.; Chaudret, R.; Piquemal, J.-P.; Beratan, D.; Yang, W. *J. Chem. Theor. Comp.* **2011**, *7*, 625. b) Johnson, E. R.; Keinan, S.; Mori-Sanchez, P.; Contreras-Garcia, J.; Cohen, A J.; Yang, W. *J. Am. Chem. Soc.* **2010**, *132*, 6498.

20. Grimme, S. *J. Comp. Chem.* **2006**, 27, 1787.

21. Gaussian 09, Revision D.01, Frisch, M. J.; Trucks, G. W.; Schlegel, H. B.; Scuseria, G. E.; Robb, M. A.; Cheeseman, J. R.; Scalmani, G.; Barone, V.; Mennucci, B.; Petersson, G. A.; Nakatsuji, H.; Caricato, M.; Li, X.; Hratchian, H. P.; Izmaylov, A. F.; Bloino, J.; Zheng, G.; Sonnenberg, J. L.; Hada, M.; Ehara, M.; Toyota, K.; Fukuda, R.; Hasegawa, J.; Ishida, M.; Nakajima, T.; Honda, Y.; Kitao, O.; Nakai, H.; Vreven, T.; Montgomery, Jr., J. A.; Peralta, J. E.; Ogliaro, F.; Bearpark, M.; Heyd, J. J.; Brothers, E.; Kudin, K. N.; Staroverov, V. N.; Keith, T.; Kobayashi, R.; Normand, J.; Raghavachari, K.; Rendell, A.; Burant, J. C.;

Iyengar, S. S.; Tomasi, J.; Cossi, M.; Rega, N.; Millam, J. M.; Klene, M.; Knox, J. E.; Cross, J. B.; Bakken, V.; Adamo, C.; Jaramillo, J.; Gomperts, R.; Stratmann, R. E.; Yazyev, O.; Austin, A. J.; Cammi, R.; Pomelli, C.; Ochterski, J. W.; Martin, R. L.; Morokuma, K.; Zakrzewski, V. G.; Voth, G. A.; Salvador, P.; Dannenberg, J. J.; Dapprich, S.; Daniels, A. D.; Farkas, O.; Foresman, J. B.; Ortiz, J. V.; Cioslowski, J.; Fox, D. J. Gaussian, Inc., WallingfordCT, **2013**.

22. a) Hay, P. J.; Wadt, W. R. *J. Chem. Phys.* **1985**, 82, 270. b) Hay, P. J.; Wadt, W. R. *J. Chem. Phys.* **1985**, 82, 284. c) Hay, P. J.; Wadt, W. R. *J. Chem. Phys*. **1985**, 82, 299.

23. a) Hehre, W. J.; Ditchfield, R.; Pople, J. A. *J. Chem. Phys*. **1972**, 56, 2257. b) Hariharan, P. C.; Pople, J. A. *Theoret. Chimica Acta.* **1973**, 28, 213. c) Francl, M. M.; Petro, W. J.; Hehre, W. J.; Binkley, J. S.; Gordon, M. S.; DeFrees, D. J.; Pople, J. A. *J. Chem. Phys.* **1982**, 77, 3654.

24. Taken from EMSL Basis Set Library: a) Feller, D. *J. Comp. Chem.* **1996**, 17, 1571. b) Schuchardt, K. L.; Didier, B. T.; Elsethagen, T.; Sun, L.; Gurumoorthi, V.; Chase, J.; Li, J.; Windus, T. L. *J. Chem. Inf. Model*. **2007**, *47*, 1045.

25. a) Krishnan, R.; Binkley, J. S.; Seeger, R.; Pople, J. A. *J. Chem. Phys.* **1980**, 72, 650. b) McLean, A. D.; Chandler, G. S. *J. Chem. Phys*. **1980**, 72, 5639.

26. Marenich, S. A. V.; Cramer, C. J.; Truhlar, D. G. *J. Phys. Chem. B*, **2009**, 113, 6378.

27. Bernal-Garcia, J. M.; Guzmas-Lopez, A.; Cabrales-Torres, A.; Estrada-Baltazar, A.; Iglesias-Silva, G. A. *J. Chem. Eng. Data*, **2008**, *53*, 1024.

CHAPTER 3. NEW VISTAS IN TRANSMETALATION WITH DISCRETE Ag-CF_3 SPECIES: IMPLICATIONS IN Pd-MEDIATED TRIFLUOROMETHYLATION REACTIONS.

3.1. Introduction

Each and every one of the elementary steps (OA, Transmet., RE) in the conventional catalytic cycle of cross-coupling reactions have been proposed to be the rate limiting step depending on the reaction conditions. A well-known sluggish elementary step in Pd-catalyzed cross-coupling reaction is C–CF_3 bond-forming reductive elimination from organo-Pd(II) complexes (Scheme 3.1).[1] As mentioned in Chapter 1, the incorporation of this substituent has received great attention among the synthetic community due to its unique capability to modify the physicochemical and/or biological properties of high-value molecules and organometallic scaffolds.[2]

Due to the lack of applicability of Swarts method, previously discussed, the chemical community has devoted its efforts towards the development of alternative methodologies for facilitating the formation of C–CF_3 bonds. Among them, copper-mediated nucleophilic trifluoromethylation reactions of aryl halides, which will be discussed in Chapter 5, has exhibited great potential (Scheme 3.1).[3]

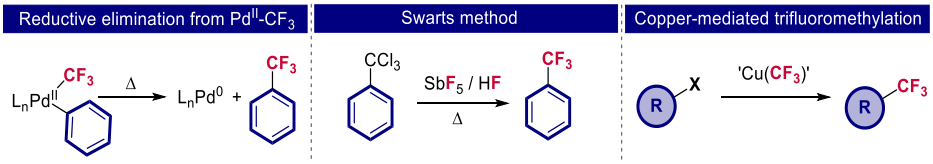

Scheme 3.1. Representative methods for introducing CF_3 moieties in organic scaffolds. Left: C–C bond-forming reductive elimination form organo-Pd(II) complexes. Middle: Swarts reaction for the conversion of α,α,α-trichlorotoluene into α,α,α-trifluorotoluene. Right: copper-mediated trifluoromethylation reaction of organohalides.

In the context of palladium catalysis, Sanford and co-workers have described the access to high-valent palladium(IV) species to surmount the hampered reductive elimination from the aforementioned organo-Pd(II) complexes. These electron-deficient palladium compounds

1 Although this topic will be covered below in the discussion, a flavor of the limitation in the reductive elimination in organo-Pd(II)-CF_3 complexes can be found in: a) Grushin, V. V.; Marshall, W. J. *J. Am. Chem. Soc.* **2006**, *128*, 4632. b) Grushin, V. V.; Marshall, W. J. *J. Am. Chem. Soc.* **2006**, *128*, 12644. c) Cho, E. J.; Senecal, T. D.; Kinzel, T.; Zhang, Y.; Watson, D. A.; Buchwald, S. L. *Science* **2010**, *328*, 1679.

2 For selected reviews: a) McClinton, M. A.; McClinton, D. A. *Tetrahedron* **1992**, *48*, 6555. b) Schlosser, M. *Angew. Chem. Int. Ed.* **2006**, *45*, 5432. c) Orsi, D. L.; Altman, R. A. *Chem. Commun*. **2017**, *53*, 7168.

3 Mudarra, A. L.; Martínez de Salinas, S.; Pérez-Temprano, M. H. *Synthesis* **2019**, *51*, 2809 and references therein.

(Figure 3.1) can undergo unprecedented C–CF_3 bond-forming reductive elimination under mild reaction conditions.[4] Nevertheless, this transformation will not be discussed herein since it is beyond the scope of this Dissertation.

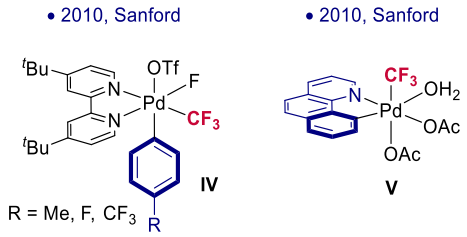

Figure 3.1. Trifluoromethyl complexes of palladium(IV) involved in C_{sp^2}-CF_3 bond-forming reaction.

Resuming the $Pd^{0/II}$ systems, a more intuitive strategy to circumvent the sluggish reductive elimination event from an organo-Pd(II) complexes involves the modification of the ligand attached to the palladium catalyst. Despite the efforts, only six different phosphine ligands have been reported to facilitate the C–CF_3 bond-forming reaction (Figure 3.2).[1,5] The use of these ligands has been rationalized based on the stero-electronic effects and ligand denticity. Among them, only the monodentate phosphine ligands have proved to be compatible with catalysis in a greater or lesser extent.[1c,5b] In this vein, it is remarkable that there is not a single version of Pd-catalyzed nucleophilic trifluoromethylation of aryl halides using bidentate phosphine ligands. The reason is that, besides the expected challenging reductive elimination, an array of generally-neglected competitive and unproductive side reactions hampers the product formation.[1a,6] As we will discuss, these side reactions have been also proposed to be present in systems involving monodentate phosphine ligands.

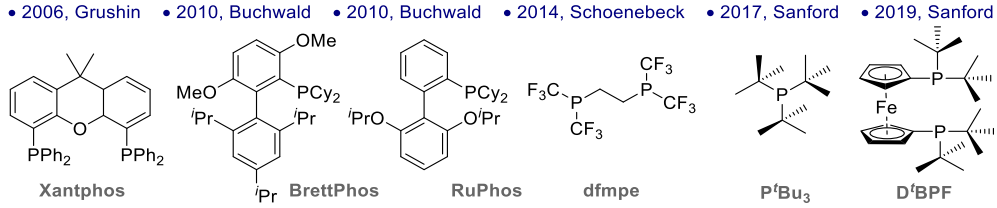

Figure 3.2. Productive ligands in high-yielding aryl–CF_3 reductive elimination at organo-Pd(II) complexes.

Here below, we will discuss the fundamental studies involving the thermolysis of well-defined phosphine-stabilized aryl-Pd-CF_3 complexes and some side reactions associated to these

4 a) Ball, N. D.; Kampf, J. W.; Sanford, M. S. *J. Am. Chem. Soc.* **2010**, *132*, 2878. b) Ye, Y.; Ball, N. D.; Kampf, J. W.; Sanford, M. S. *J. Am. Chem. Soc.* **2010**, *132*, 14682. c) Ball, N. D.; Gary, J. B.; Ye, Y.; Sanford, M. S. *J. Am. Chem. Soc*. **2011**, *133*, 7577.

5 a) Nielsen, M. C.; Bonney, K. J.; Schoenebeck, F. *Angew. Chem. Int. Ed.* **2014**, *53*, 5903. b) Ferguson, D. M.; Bour, J. R.; Canty, A. J.; Kampf, J. W.; Sanford, M. S. *J. Am. Chem. Soc.* **2017**, *139*, 11662 c) Ferguson, D. M.; Bour, J. R.; Canty, A. J.; Kampf, J. W.; Sanford, M. S. *Organometallics* **2019**, *38*, 519.

6 Bakhmutov, V. I.; Bozoglian, F.; Gómez, K.; González, G.; Grushin, V. V.; Macgregor, S. A.; Martin, E.; Miloserdov, F. M.; Novikov, M. A.; Panetier, J. A.; Romashov, L. V. *Organometallics* **2012**, *31*, 1315.

processes. Then, we will discuss the challenges associated to access key aryl-Pd-CF_3 complexes from [$(L)_nPd(Ar)(I)$] through commonly-used synthetic approaches.

3.1.1. **Thermolysis of phosphine-stabilized [$(L)_nPd(Ar)(CF_3)$] intermediate**

As mentioned above, the formation of C–CF_3 bonds formation from isolated organo-Pd(II) complexes bearing different phosphine ligands have been pursued by different groups. In this regard, seminal reports from Hartwig and Grushin supported the challenges associated to the formation of C–CF_3 bonds formation from isolated organo-Pd(II) complexes bearing phosphine ligands (Figure 3.3).[1,7] In those seminal reports, only a moderate yield in the formation of $PhCF_3$ was obtained for the thermolysis of trifluoromethyl phenyl-Pd(II) complex bearing dppp (1,2-bis(diphenylphosphino)propane) as ancillary ligand at temperatures as high as 145 ºC.[1a] In 2006, Grushin reported the first example of high-yielding C–CF_3 bond-forming reductive elimination at a reasonable temperature (60-80 ºC) using Xantphos (4,5-bis(diphenylphosphino)-9,9-dimethylxanthene) as ligand.[1b]

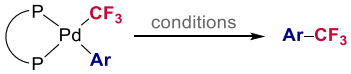

• 2004, Hartwig

ligand/**Ar**	product
dppbz/*o*-**Tol**	*o*-**Tol**–CF_3 (not observed)

conditions: 90-130 ºC, days, C_6H_6, PPh_3

• 2006, Grushin

ligand/**Ar**	product
dppp/**Ph**	60% **Ph**–CF_3
dppe/**Ph**	10% **Ph**–CF_3

conditions: 145 ºC, 64 h, xylenes

• 2006, Grushin

ligand/**Ar**	product
PPh_3/**Ph**	side reactions

conditions: 60 ºC, C_6H_6, 2 PhI

Figure 3.3. Selective examples of unproductive reductive elimination of Ar-CF_3 from isolated Pd(II)-CF_3 complexes. dppbz = 1,2-bis(diphenylphosphino)benzene), *o*-Tol = *ortho*-tolyl, dppp = 1,2-bis(diphenylphosphino)propane, dppe = 1,2-bis(diphenylphosphino)ethane.

From 2010 to nowadays, five additional phosphine ligands have been reported to induce a fast Ar–CF_3 bond formation: Brettphos (2-(dicyclohexylphosphino)-3,6-dimethoxy-2',4',6'-triisopropyl-1,1'-biphenyl),[1c] Ruphos (2-(dicyclohexylphosphino)-2',6'-diisopropoxybiphenyl),[1c] dfmpe (1,2-bis(trifluoromethyl)ethane),[5a] P^tBu_3,[5b] and D^tBPF (1,1'-bis(di-tert-butylphosphine)ferrocene).[5c]

Regarding other type of bidentate ligands, Sanford *et al.* reported that the reductive elimination of C–CF_3 bond is also challenging when using *N'N*-bidentate ligands for stabilizing the aryl-Pd(II) complexes even using harsh reaction conditions.[4a]

7 Culkin, D. A.; Hartwig, J. F. *Organometallics* **2004**, *23*, 3398.

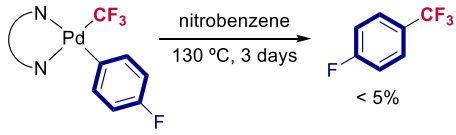

Scheme 3.2. Unproductive reductive elimination of Ar–CF_3 from isolated Pd(II)-CF_3 complexes stabilized by (N^N)-bidentate ligand. The (N^N) ligands tested were: TMEDA = N,N'-tetramethylethylene diamine, ^{t}Bu-bpy = 4,4'-di-tert-butyl-2,2'-bipyridyl.

Here below, we briefly describe the productive systems in the C–CF_3 bond-forming reaction. The section is classified according to the denticity of the given phosphine ligand attached to the palladium metal center.

3.1.1.1. Monodentate ligands

- **Buchwald phosphine ligands**

In 2010, Buchwald *et al.* disclosed for the first time a Pd-catalyzed nucleophilic trifluoromethylation reaction of aryl chlorides using Brettphos and RuPhos as ancillary ligands (Scheme 3.3).[1c] This methodology was shown to be compatible with a wide array of functional groups, affording the corresponding products in high yields. Additionally, the reductive elimination step was studied from an isolated aryl-Pd(II)-CF_3 intermediate **VII** (Scheme 3.3), showcasing that the Ar–CF_3 bond-forming reaction occurred in a facile manner at a reasonable temperature (80 ºC).[1c] Indeed, DFT calculations supported the feasibility of this process with an activation barrier of ≈ 22 kcal·mol^{-1} (22.6 kcal·mol^{-1}, from intermediate **VII**).[1c]

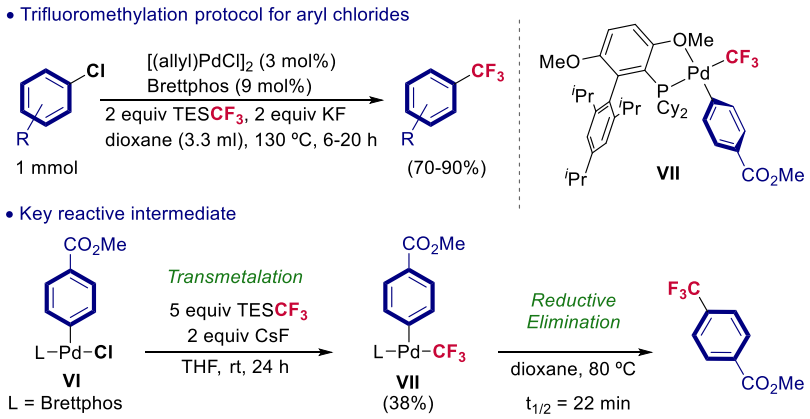

Scheme 3.3. Above: General Pd-catalyzed trifluoromethylation protocol of aryl chlorides using Brettphos. Below: Key isolated intermediate for mechanistic investigations.

Interestingly, product yields were eroded when using substrates such as aryl bromides or aryl triflates instead or aryl chlorides.[1c] It is well-known that those substrates are more reactive towards the oxidative addition than the corresponding aryl chloride and, therefore, organo-Pd(II)-

Br intermediates (**VI** bearing a Br in place of a Cl) may be formed in the reaction media. However, based on the obtained lower yields, the corresponding organo-Pd(II)-Br complex may be decomposing prior to achieving the remaining steps of the catalytic cycle (Transm. and RE). As it will be commented below, side reactions may be taking place during the stoichiometric transmetalation reaction but, potentially, to a less extent, during the catalytic cycle (page - 93 -).[6]

- **Tri-tert-butylphosphine, $^tBu_3P$**

Inspired by previous reports of Hartwig in the reductive elimination of C–N bond,[8] Sanford *et al.* hypothesized that three-coordinate aryl-Pd(II) complexes, bearing a single monodentate phosphine ligand, could promote the C–CF_3 bond-forming reductive elimination.[5b]

They undertook this study by performing DFT calculations on the potential mechanism underlying to the reductive elimination of the corresponding T-shaped [(L)Pd(Ar)(CF_3)] complex using $^tBu_3P$ as monodentate phosphine ligand. They found that two different mechanisms could explain the formation of the new C–C bond (Scheme 3.4). The first, orange in Scheme 3.4, implies the concerted formation of the C–CF_3 from **IX** through **TS1** with a high activation barrier of 27.0 kcal·mol^{-1}. The second one (green in Scheme 3.4) consists of a α-fluoride elimination (**TS2**) event followed by a phenyl migration[9] (**TS3**) to yield difluorobenzyl complex **X**. The highest activation barrier for this pathway, 24.7 kcal·mol^{-1}, is the reductive elimination of the fluoride with the difluorobenzyl moieties from intermediate **X**. Therefore, this route is much feasible (favored by 2.3 kcal·mol^{-1}) than the concerted reductive elimination route (Scheme 3.4).

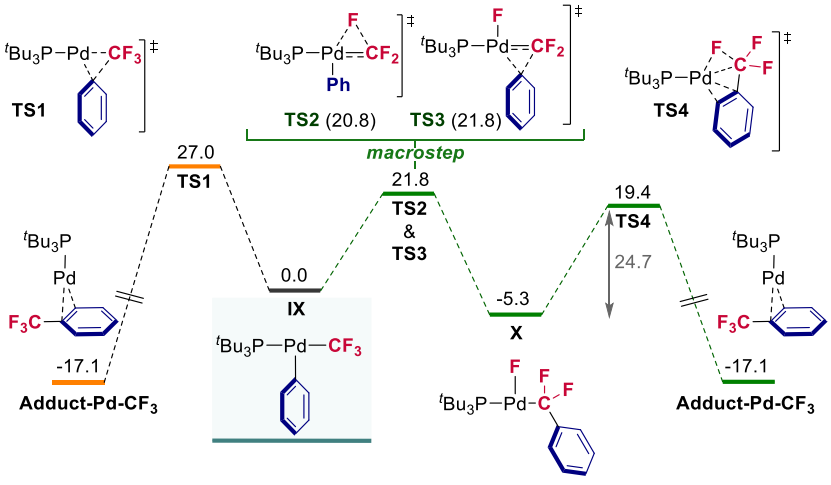

Scheme 3.4. DFT-calculated free energy profile for the reductive elimination mechanism of $PhCF_3$ from aryl-Pd(II) complex **IX**. Free energies in kcal·mol^{-1}.

8 a) Stambuli, J. P.; Incarvito, C. D.; Bühl, M; Hartwig, J. F. *J. Am. Chem. Soc.* **2004**, *126*, 1184. b) Yamashita, M.; Hartwig, J. F. *J. Am. Chem. Soc.* **2004**, *126*, 5344.

9 This process has been also described as a carbene insertion of the phenyl group. See Zhang, S.-L., Huang, L.; Sun L.-J. *Dalton Trans.* **2015**, *44*, 4613.

After the computational evaluation of the system, the stoichiometric reductive elimination event was experimentally studied from the isolated aryl-Pd(II) complex **IX** (Scheme 3.5). Complex **IX** affords the coupled product ($PhCF_3$) in 41% yield, in benzene after 5 min at 80 ºC, showing the efficiency of $^tBu_3P$ to induce the reductive elimination under mild conditions. In addition to $PhCF_3$, undesired side products were formed in moderate yield (**XII** and **XI**, Scheme 3.5). The authors rationalized that those side products appear as consequence of side transmetalation reactions between difluorobenzyl complex **X** and other organo-Pd(II) complexes (Scheme 3.5).

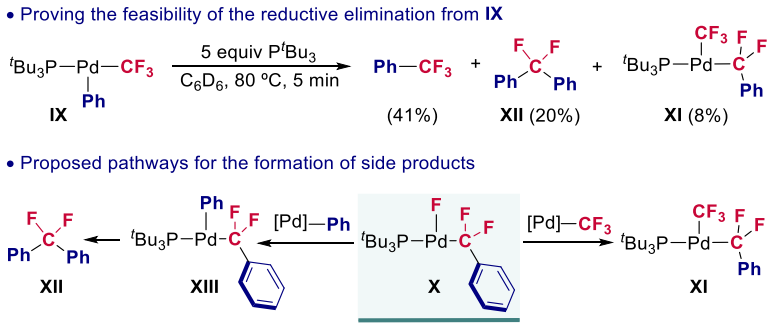

Scheme 3.5. Above: Reductive elimination from **IX**. Below: Proposed pathways for explaining the side products.

Consistent with the stoichiometric experiments, Pd(P^tBu_3)-catalyzed trifluoromethylation of 1-butyl-4-chlorobenzene (similar conditions of Buchwald system[1c]) resulted in the formation of the reductive elimination product **XIV** (22%, Scheme 3.6) along with difluorodiarylmethane **XV** as side product. This suggests that aforementioned side reactions may also happen under catalytic conditions.

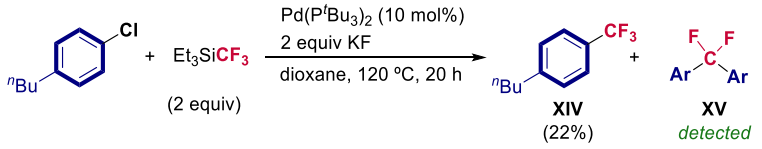

Scheme 3.6. Catalytic trifluoromethylation reaction of aryl chloride using [Pd(P^tBu_3)$_2$] as catalyst under previously described Buchwald conditions.

Collectively, these results show how the underlying mechanisms for elementary steps such as reductive elimination may be more complex than *a priori* assumed and can involve the formation of unexpected intermediates that undergo undesired side reactions.

3.1.1.2. **Bidentate ligands**

Once revisited the examples of monodentate phosphine ligands known to promote the reductive elimination of Ar–CF_3 bonds, we will briefly discuss the cases of bidentate phosphine ligands compatible with this transformation under mild conditions. As mentioned above, no catalytic examples of catalytic trifluoromethylation of aryl halides bearing these ligand-type phosphine ligands have been reported in the literature.

- **Xantphos phosphine ligand**

Seminal work by Grushin demonstrated for the first time the feasibility of Ph–CF_3 reductive elimination from an isolated aryl-Pd(II) intermediate bearing a phosphine ligand, [(Xantphos)Pd(Ph)(CF_3)] (**XVI**).[1b] The selection of this bidentate phosphine ligand was fundamentally based on its wide bite angle which would approximate both organic moieties (Ph and CF_3) in the Pd(II) complex and trigger the formation of the organic product.

Indeed, α,α,α-trifluorotoluene was generated in quantitative yield by heating a solution of **XVI** along with 1 equiv. of free phosphine ligand in benzene at 80 ºC (Scheme 3.7). The role of this additional phosphine ligand is to stabilize the Pd(0) formed after the reductive elimination in order to avoid side reactions.

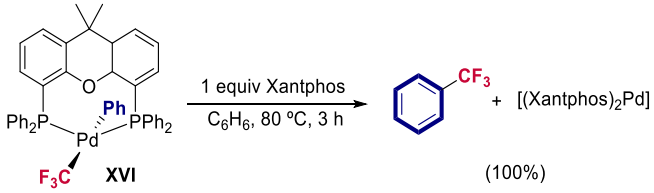

Scheme 3.7. Reductive elimination study from **XVI**.

It should be mentioned that the synthesis of **XVI** was not trivial using the conventional routes described to that date. The use of Ruppert-Prakash reagent (Me_3SiCF_3), along with an activating fluoride salt, resulted on the displacement of the phosphine ligand and generation of undesired products. In this regard, a reactive [(Xantphos)Pd(Ph)(F)] (**XVIII**, Scheme 3.8) complex was independently prepared from [(Xantphos)Pd(Ph)(I)] (**XVII**, Scheme 3.8) using AgF. That fluoride attached to the palladium, unlike the iodide, is able to activate Ruppert-Prakash reagent and, this way, generate **XVI** selectively. Further discussion about side reactions related to the access to **XVI**-type intermediates can be found along section 3.1.2.

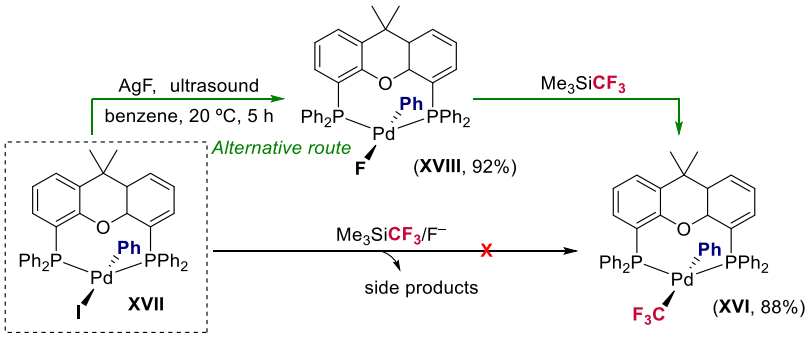

Scheme 3.8. Synthesis of XVI from the [(Xantphos)Pd(Ph)(I)] complex.

An additional side reaction from [(Xantphos)Pd(Ar)(CF_3)] intermediate is a intermolecular ligand scrambling between the aryl and the CF_3 groups (Scheme 3.9).[10] The thermal decomposition of this complex in benzene gave rise the corresponding C–CF_3 reductive elimination product and the formation of a biaryl organic compound (Scheme 3.9). This bimolecular reaction obviously depends on the concentration and it occurred in a reasonable yield at a concentration as high as 0.3 M so it is quite unlikely to happen in catalytic conditions.

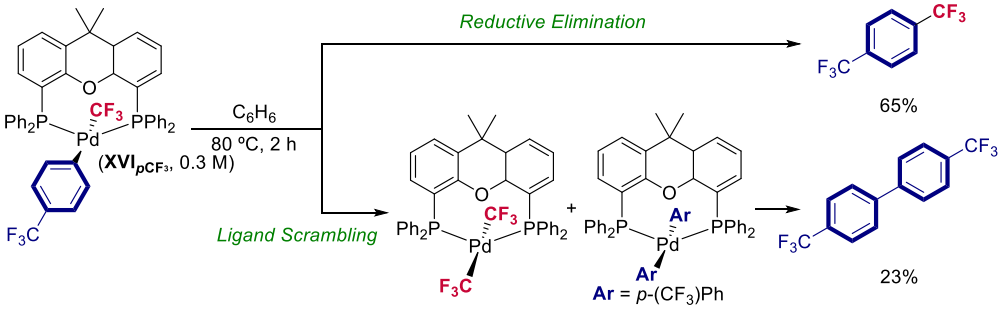

Scheme 3.9. Bimolecular ligand exchange between two molecules of **XVI**.

- **dfmpe (1,2-bis(trifluoromethyl)ethane), $(CF_3)_2PC_2H_4P(CF_3)_2$**

Between 2011 and 2014, Schoenebeck *et al.* employed DFT calculations for designing a new bidentate phosphine ligand that could promoted the Ph–CF_3 reductive elimination from Pd^{II} intermediate.[5a,11] Initially, they compared, theoretically, the efficiency of two synthetically accessible [$(L)_nPd(Ph)(CF_3)$] complexes bearing Xantphos and dppe as ancillary ligands. The former allowed the product release, whereas the latter required remarkably high temperature to afford $PhCF_3$ in low yield.[1a,1b] Schoenebeck's computational investigation revealed that, instead of the bite angle of the phosphine ligand, the critical feature for promoting the coupling was the electrostatic repulsion between the ligand substituents (R in Scheme 3.10) and the "to-be-eliminated" organic groups (Scheme 3.10). With this information in hand, they designed an

10 Zhang, S.-L.; Deng, Z.-Q. *Phys. Chem. Chem. Phys.* **2016**, *18*, 32664.
11 Anstaett, P.; Schoenebeck, F. *Chem. Eur. J.* **2011**, *17*, 12340.

unprecedented and experimentally efficient poly-(trifluoromethylated) bidentate phosphine ligand, $(CF_3)_2PC_2H_4P(CF_3)_2$ (dfmpe), with a narrow bite angle (dppe backbone) (Scheme 3.10).[5a] It should be mentioned that the reductive elimination may be also facilitated by the stabilization of the resulting Pd(0) as consequence of the electron-withdrawing nature of the poly-(trifluoromethylated) phosphine ligand. No further studies on the application of this phosphine ligand in catalysis has been reported.

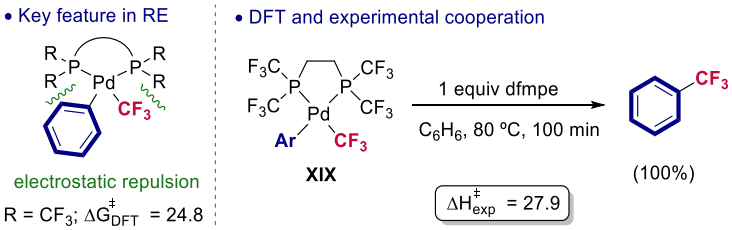

Scheme 3.10. Left: Electrostatic repulsion as key feature in the RE from aryl-Pd(II) complex. Right: Experimental evidence of the efficiency of the DFT-designed bidentate phosphine ligand (dfmpe).

- **Phosphine ligands derivate from Phosphinoferrocene scaffold**

In 2019, Sanford group disclosed a new bidentate phosphine ligand that facilitates the reductive elimination of $PhCF_3$ under mild conditions. In this work, the authors studied the influence of the bulkiness of the substituents at the phosphorous atoms of highly modular phosphinoferrocene-based ligands on the reductive elimination event from four different $[(L)Pd^{II}(Ph)(CF_3)]$ complexes (Scheme 3.11).[5c]

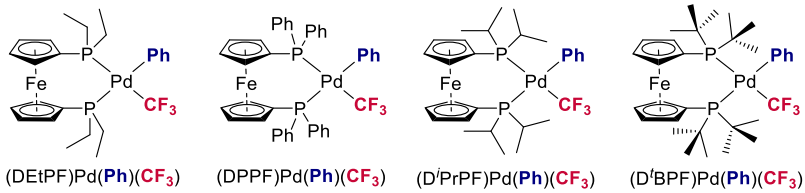

Scheme 3.11. Family of different phosphinoferrocene-ligated $Pd^{II}(Ph)(CF_3)$ complexes.

In accordance with previous DFT studies,[6] they were able to stablish a direct correlation between the use of more sterically-demanding substituents in the phosphine ligand and the rate of the C–CF_3 bond-forming reaction (Scheme 3.12).[5c] When using the bulkiest phosphine ligand, D^tBPF, bearing *tert*-butyl groups (Scheme 3.11), the product release occurred in high yield (82%) after 35 min at 80 ºC from the Pd(II) complex **XX** (Scheme 3.12) in the presence of 1 equiv of free phosphine.

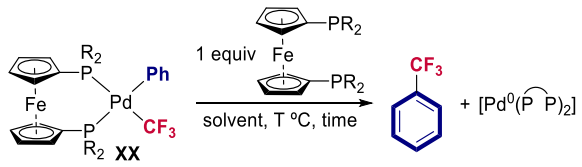

R	Solvent	T (°C)	time	Yield of $PhCF_3$(%)
Et	*p*-xylene	130	168 h	24
Ph	*p*-xylene	130	36 h	89
^{i}Pr	*p*-xylene	130	24 h	99
^{t}Bu	C_6D_6	80	35 min	82

Scheme 3.12. Reductive elimination study of $PhCF_3$ from different phosphinoferrocene-ligated Pd(II) complexes.

Additionally, they performed DFT calculations in order to study how the C–C bond formation occurred. They showed that the most plausible scenario involves a concerted C–C bond formation from intermediate **XX**. The authors also investigated a potential α-fluoride elimination/aryl migration sequence, previously proposed for $^{t}Bu_3P$ as ancillary ligand (Scheme 3.5), after the decoordination of one arm of the bidentate phosphine ligand. However this route showed to be incompatible with this type of bidentate ligand. This was further confirmed by the isolation of the corresponding difluorobenzyl palladium intermediate **XXI** (**Scheme 3.13**) which proved to be unproductive in the release of the trifluoromethylated organic product, $PhCF_3$ (Scheme 3.13).[5c]

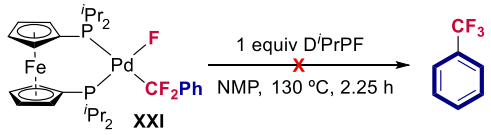

Scheme 3.13. Reductive elimination study at diflurobenzyl-Pd(II) complex **XXI**.

From a mechanistic point of view, this latter result implies a significant difference in the behavior of monodentate and bidentate phosphine ligands. While monodentate $P^{t}Bu_3$ phosphine ligands prompted the α-fluoride elimination/aryl migration sequence (**Scheme 3.4** and **Scheme 3.5**),[5b] bidentate $D^{t}BPF$ phosphine ligand favors the concerted formation of the C–CF_3 bond,[5c] preventing the formation of stable intermediates such as **X** (Scheme 3.5) or **XXI** (**Scheme 3.13**) that could give rise undesired side products.

3.1.2. **Challenges associated to the formation of $[(L)_nPd(Ar)(CF_3)]$ intermediate**

As mentioned above, the $Pd^{0/II}$ nucleophilic trifluoromethylation reactions are not hampered only for a challenging reductive elimination step but also for the existence of inherent side reactions in these reactive organometallic systems. We have already disclosed two different side reactions from isolated $[(L)_nPd(Ar)(CF_3)]$ intermediates: the ligand scrambling consequence of a α-fluoride elimination/aryl migration sequence (Scheme 3.5) and bimolecular ligand scrambling (**Scheme 3.9**).

In addition to the aforementioned undesired reactions from $[(L)_nPd(Ar)(CF_3)]$ complexes, two more side reactions have been proposed by Grushin in the formation of $[(L)_nPd(Ar)(CF_3)]$ intermediate from $[(L)_nPd(Ar)(I)]$, (**Scheme 3.14**):

a) The displacement of the phosphine ligand by CF_3 anions at the aryl-Pd(II) complexes (poly-(trifluoromethylation), **Scheme 3.14**).[6,12]

b) Ligand aryl/aryl scrambling between the aryl-Pd(II) halide complex ($[(L)_nPd(Ar)(X)]$, **XXII**) and aryl-Pd(II)-CF_3 complex ($[(L)_nPd(Ar)(CF_3)]$, **XXIII**) to yield reactive $[(L)_nPd(Ar)(Ar)]$ (**XXIV**) and $[(L)_nPd(X)(CF_3)]$ (**XXV**) (Scheme 3.14).[1b,6]

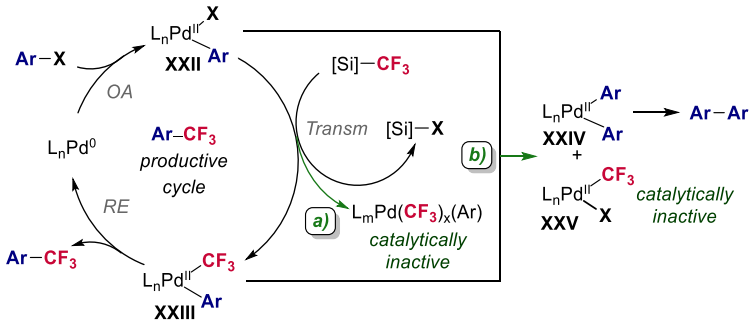

Scheme 3.14. Potential catalytic cycle for Pd-catalyzed nucleophilic trifluoromethylation reaction of aryl halides and described side reactions rendering catalytically inactive species (details in ref. 6).

Both side reactions are somehow related to the use of Ruppert-Prakash derivatives, R_3SiCF_3 (R = Me,[13] Et[1c,5b]), along with an activating agent (F^-), which are the most common CF_3 sources in nucleophilic trifluoromethylation protocols for both organic and organometallic scaffolds.[1c,5b,13] In the following sections, we will analyze the drawbacks of using R_3SiCF_3/F^- mixture as transmetalating agents and their potential relationship to the lack of Pd-based catalytic systems, especially, involving bidentate phosphine ligands.

3.1.2.1. Activation and decomposition pathway of Ruppert-Prakash reagent and derivatives

From a mechanistic point of view, the activation of R_3SiCF_3 species by F^- consists of the formation of CF_3-containing pentacoordinated silicon adducts $[R_3Si(F)(CF_3)]^-$ and $[R_3Si(CF_3)_2]^-$, as it has been probed by ^{19}F NMR spectroscopy (Scheme 3.15).[14] The latter $[R_3Si(CF_3)_2]^-$ species, under controlled reaction conditions, is able to deliver CF_3^- to the reaction

12 Naumann, D.; Kirij, N. V.; Maggiarosa, N.; Tyrra, W.; Yagupolskii, Y. L.; Wickleder, M. S. *Z. Anorg. Allg. Chem.* **2004**, *630*, 746.
13 Liu, X.; Xu, C.; Wang, M.; Liu, Q. *Chem. Rev.* **2015**, *115*, 683.
14 Maggiarosa, N.; Tyrra, W.; Naumann, D.; Kirij, N. V.; Yagupolskii, Y. L. *Angew. Chem. Int. Ed.* **1999**, *38*, 2252.

media. This CF_3 anion can be stabilized by incorporation into organic or organometallic electrophiles.[15]

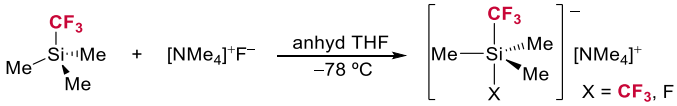

Scheme 3.15. Activation of Me_3SiCF_3 with fluoride salts. anhyd = anhydrous.

In the absence of stabilizing partners, the CF_3 anion tends to decompose though α-defluorination reaction into difluoromethyl carbene (:CF_2) and fluoride atoms (F^-), especially in the presence of Lewis acids such as K^+, Cs^+, *etc.* (from the activating fluoride salts).[15] Also, this CF_3 anion tends to form HCF_3 by any adventitious proton source.

In the context of Pd-catalyzed nucleophilic trifluoromethylation reactions based on the use of R_3SiCF_3/F^- mixture, this decomposition route implies that CF_3 anions could be consumed prior to the transmetalation step and, consequently, to its incorporation into the final product (**Scheme 3.14**).[16] Therefore, a stable but active CF_3-donating species is desired to prevent this decomposition pathway and ensure the CF_3 transfer towards the aryl-Pd(II) transient species.

3.1.2.2. Poly-(trifluoromethylation) of aryl-Pd(II) complexes by R_3SiCF_3/F^- mixtures.

Another intrinsic side reaction during the transmetalation step is the poly-(trifluoromethylation) of phosphine-ligated Pd(II) complexes by R_3SiCF_3/F^- mixtures (**Scheme 3.16**).[1b,12] The activation of the R_3SiCF_3 by F^- generates reactive "CF_3^-" species which unselectively reacts with aryl-Pd(II) complexes displacing not only the halide but also the stabilizing phosphine ligand (**Scheme 3.16**). As a result, catalytically inactive poly-(trifluoromethylated) palladium complexes are generated likely from both palladium complexes **XXII** and **XXIII** (Scheme 3.16).[17] As mentioned above, this was one of the mayor challenge for the synthesis of [(Xantphos)Pd(Ph)(CF_3)].

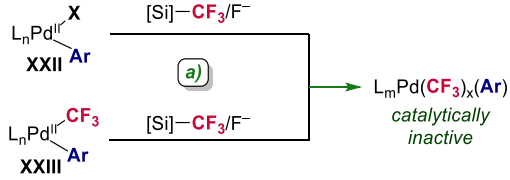

Scheme 3.16. Poly-(trifluoromethylation) reaction of **XXI** and **XXII** by activated R_3SiCF_3 species.

[15] Prakash, G. K. S.; Wang, F.; Zhang, Z.; Haiges, R.; Rahm, M.; Christe, K. O.; Mathew, T.; Olah, G. A. *Angew. Chem. Int. Ed*. **2014**, *53*, 11575.

[16] Similar behavior have been described for copper systems (Chapter 4, ref. **Error! Bookmark not defined.**)

[17] One could think that this side reaction may happen in Buchwald system (ref. 1c) and it could be also the reason why the transmetalation to form **VII** has such a lower yield (pag. - 6 -). However, we should take into account that under catalytic conditions, if the reductive elimination step is fast, the concentration of the transient Pd(II) **VII** species is very low and their poly-(trifluoromethylation) is unlikely to happen.

The employment of strongly chelating phosphine ligands can prevent this unselective transmetalation reaction but the resulting [(L)$_n$Pd(Ar)(CF$_3$)] complexes normally do not undergo the reductive elimination step.[1a] Thus, an alternative solution to overcome poly-(trifluoromethylation) side reactions is the use of a selective transmetalating agent toward the halide-for-CF$_3$ exchange which does not displace the phosphine ligand.

3.1.2.3. Ligand scrambling between [(L)$_n$Pd(Ar)(X)] (XXII) and [(L)$_n$Pd(Ar)(CF$_3$)] (XXIII)

In 2006, Grushin *et al.* reported the synthesis, characterization of different [(L)$_n$Pd(Ar)(CF$_3$)] palladium complexes, which are putative intermediates of Pd$^{0/II}$-catalyzed nucleophilic trifluoromethylation.[1a] The authors studied the C–CF$_3$ bond-forming reactions from [(dppe)Pd(Ph)(CF$_3$)] (**XIII$_{dppe}$**) in the presence of excess of iodobenzene, trying to mimic the formation of PhCF$_3$ under catalytic conditions. According to the hypothetic catalytic cycle, after the release of PhCF$_3$, the so-formed Pd(0) species should react with aryl halide to generate [(dppe)Pd(Ph)(I)] by oxidative addition. However, instead of this hypothetic scenario, the reaction of complex **XIII$_{dppe}$** with iodobenzene at 115 ºC in toluene yielded [(dppe)Pd(I)(CF$_3$)] (**XXV$_{dppe}$**) and homocoupling product, Ph–Ph (Scheme 3.17).

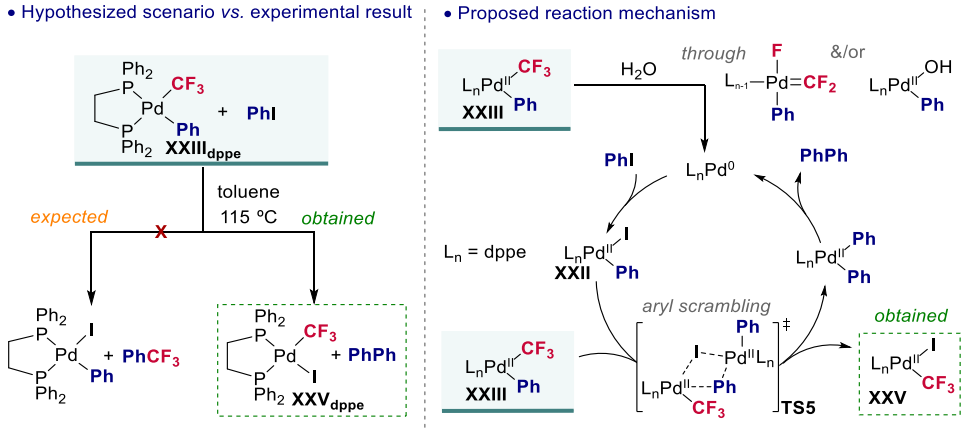

Scheme 3.17. Left: Initial experiment to get insights into potentially catalytic Pd$^{0/II}$ systems. Right: Proposed reaction mechanism for the unexpected experimental results.

After mechanistic studies, they proposed that adventitious water promotes the reduction of [(dppe)Pd(Ph)(CF$_3$)] (**XIII$_{dppe}$**) to a phosphine-stabilized Pd(0) complex that easily undergoes oxidative addition of iodobenzene – no reaction was observed under extremely anhydrous conditions.[1a] Next, the so-formed aryl-Pd(II) complex reacts with [(dppe)Pd(Ph)(CF$_3$)] complex (**XXV**) to yield the observed catalytically inactive [(dppe)Pd(I)(CF$_3$)] species (**XIII$_{dppe}$**). This ligand scrambling reaction is fundamentally a transmetalation reaction between both palladium complexes.

Same scenario was uncovered for [(Xantphos)Pd(Ph)(CF_3)] complex (**XVI**, Scheme 3.18).[1b] In this case, there was competition between the formation of the α,α,α-trifluorotoluene and [(Xantphos)Pd(I)(CF_3)] species (Scheme 3.18).

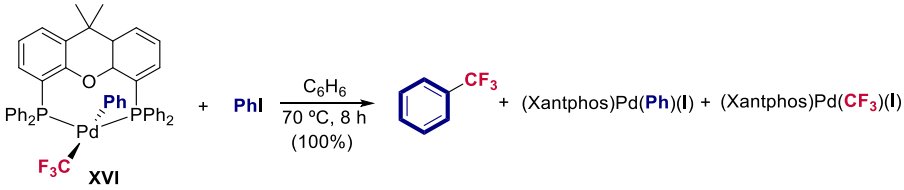

Scheme 3.18. Unselective reductive elimination from aryl-Pd(II)-CF_3 complex **XVI** in the presence of iodobenzene.

In 2012, Grushin *et al.* stated that this transmetalation reaction, which is a catalyst deactivation pathway, may be facilitated by "nucleophilic aid".[1a,6] This means that more polarizable halides (I > Br > Cl > F) increase the transmetalation rate between both palladium complexes (**XXII** and **XXIIII,** Scheme 3.17 and Scheme 3.19) either because it facilitates a potential "bridging", **TS5** in Scheme 3.17, or because it favors the generation of an coordinatively-unsaturated cationic palladium complex by decoordination of the halide.[1a,6,18] This hypothesis allowed them to explain the observed results by Buchwald and co-workers in catalysis when using aryl bromides or triflates as substrates in their catalytic system (pag. - 84 -).[1c,6] In this regard, a potential solution to prevent this bimolecular side reaction is minimizing the transient concentration of **XXII** and **XXIII** (Scheme 3.19). However, commonly, the reductive elimination event is the rate-limiting step of the catalytic cycle and accumulation of **XXIII** species is thus inevitable. On the other hand, the concentration of aryl-Pd(II) halide **XXII**, once it is formed, depends on the transmetalation event rate.

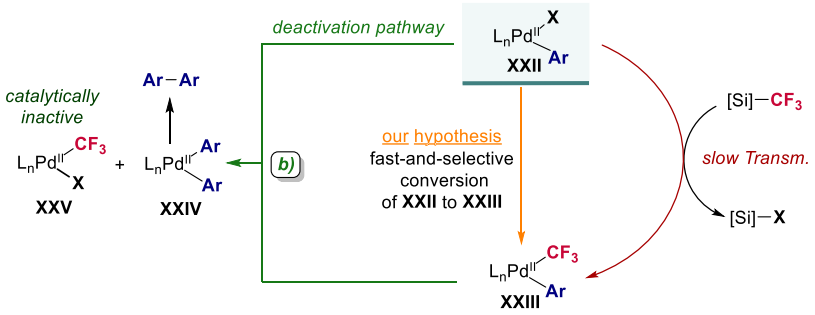

Scheme 3.19. Different transmetalation side reactions of aryl-Pd(II) complex **XXII** and R_3SiCF_3 or CF_3-cointaing Pd complex **XXIII**. The unselective poly-(trifluoromethylation) reactions of palladium complexes are not shown for clarity.

[18] Note that those arguments could be counterintuitive since a bridge mechanism for the transmetalation between Pd and another organometallic nucleophile, M–R, is well-known to be favored for more electrophilic palladium complexes (Cl > Br > I) (Casado, A.L.; Espinet, P. *J. Am. Chem. Soc.* **1998**, *120*, 8978). In the mechanism discussed above by Grushin this trend, since the electrophile is the Pd(II)–CF_3 complex, is difficult to predict and both mechanisms are proposed.

Nevertheless, the Ruppert-Prakash derivatives, activated by F^-, tend to react slowly.[19] Therefore, in a hypothetic catalytic scenario, the transient aryl-Pd(II) halide **XXII** can undergo two competitive transmetalation reactions (Scheme 3.19): the transmetalation reaction from activated R_3SiCF_3 to yield aryl-Pd(II)-CF_3 (red pathway in Scheme 3.19) and the transmetalation reaction from aryl-Pd(II)-CF_3 to yield $[(L)_nPd(CF_3)(I)]$ (**XXV**) and $[(L)_nPd(Ar)(Ar)]$ (**XXIV**) complexes (green pathway in Scheme 3.19). We envisioned that a rapid and selective CF_3-containing transmetalating agent could avoid catalyst deactivation pathways by reaction with the transient aryl-Pd(II) halide **XXII** and directly forming **XXIII**.

3.1.3. **Pd-catalyzed nucleophilic trifluoromethylation of aromatic acyl fluorides**

During the preparation of the work that will be described in Chapter 2, Schoenebeck *et al.* disclosed a method for circumventing the challenges associated to the transmetalation step in these systems.[20] Their approach consisted of moving from the widely-used aryl halides as starting materials to acyl fluorides.[21] This way, they achieved the use of Et_3SiCF_3 without exogenous activating agents.

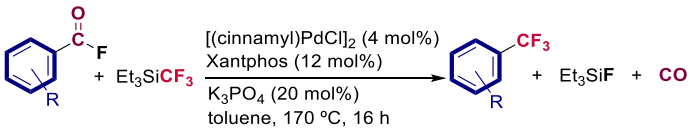

Scheme 3.20. General protocol for the Pd-catalyzed trifluoromethylation of aromatic acyl fluorides.

From a mechanistic point of view, acyl fluorides undergo oxidative addition to yield an PhCO-Pd(II) fluoride intermediate, **XXVI** (Scheme 3.21), which is crucial for the success of the whole catalytic transformation. Once this intermediate **XXVI** is formed, the Ruppert-Prakash derivative easily transfers the CF_3 moiety generating PhCO-Pd(II)-CF_3 intermediate **XXVII** without the necessity of the activating agent (F^-).[22] This feature overcomes different aforementioned challenges such as: decomposition of the CF_3 source by activation of the F^-, poly-(trifluoromethylation) of the aryl-Pd(II) complex by unselective R_3SiCF_3/F^- mixture and the ligand scrambling between **XXVI** and **XXVII** Pd(II) complexes due to the highly reactivity of the fluoride towards the Ruppert-Prakash reagents. The use of Pd–F species to activate Ruppert-Prakash

[19] For the synthesis of $[(L)_nPd(Ar)(CF_3)]$ complexes bearing tightly-binding phosphine ligands, 1 hour of reaction is needed at room temperature for the conversion of approx. 0.5 mmol of the corresponding $[(L)_nPd(Ar)(I)]$. This shows that the transmetalation reaction is not instantaneous. See ref 1a.

[20] Keaveney, S. T.; Schoenebeck, F. *Angew. Chem. Int. Ed.* **2018**, *57*, 4073.

[21] We should emphasize that this report and our study, enabling Xantphos in catalysis as a proof-of-concept, were published almost concomitantly as we will discuss in this Chapter 2. Basically, their initial approach was based on the modification of the substrate while our work consists of the search of a more efficient transmetalating agent to overcome potential side reactions.

[22] The role of the phosphate during the catalytic cycle is uncertain. They suggested that one of the role could be activating the Et_3SiCF_3 which is inconsistent with their mechanistic proposal since the Et_3SiCF_3 is supposed to be activated by Pd-F intermediates.

reagent was previously described to access the corresponding Pd-CF_3 complexes bearing relatively labile phosphine ligands such as Xantphos or PPh_3.[1b]

To close the catalytic cycle (Scheme 3.21), they proposed that after the formation of **XXVII** intermediate, a decarbonylation reaction followed by a reductive elimination event takes place to release the Ar–CF_3 product and carbon monoxide.

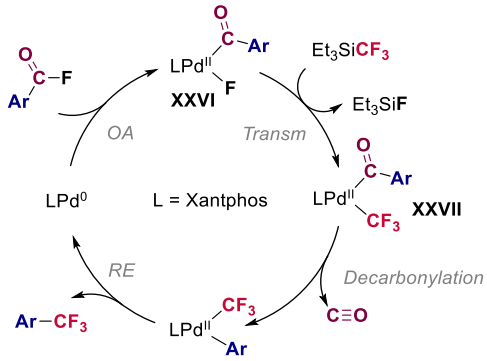

Scheme 3.21. Proposed catalytic cycle for the Pd-catalyzed decarbonylative trifluoromethylation of acyl flourides.

This was the first example of $Pd^{0/II}$-catalyzed nucleophilic trifluoromethylation reaction using a bidentate phosphine ligand (Xantphos).[20]

3.1.4. **Trifluoromethylsilver(I) nucleophiles as transmetalating candidates**

In 2014, Shen and co-workers described the synergistic cooperation between Pd and Ag as catalysts for the difluoromethylation of Ar–X (X = Br, I) with Me_3SiCF_2H.[23a] This catalytic Pd/Ag bimetallic system was designed by studying the feasibility of each elementary step of a previously-conceived catalytic cycle.[23] Thus, the stoichiometric reaction between the putative intermediates $[(L)_nPd(Ar)(X)]$ and $[(SIPr)Ag(CF_2H)]$ (SIPr = 1,3-bis(2,6-diisopropylphenyl)imidazol-2-ylidene) proved the viability of the transmetalation step (Scheme 3.22). This reaction proved to be selective and effective towards the I-for-CF_2H exchange and no side products were observed.

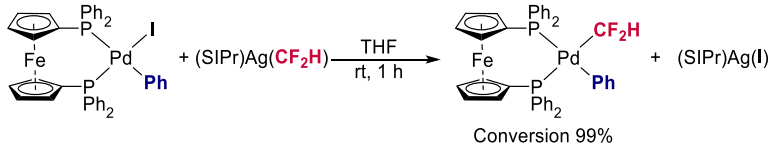

Scheme 3.22. Transmetalation reaction between $[(L)_nPd(Ar)(X)]$ and $[(SIPr)Ag(CF_2H)]$ as putative intermediate of the conceived catalytic cycle.

[23] a) Gu, Y.; Leng, X.; Shen, Q. *Nat. Commun.*, **2014**, *5*, 5405. b) Lu, C.; Gu, Y.; Wu, J.; Gu Y.; Shen, Q. *Chem. Sci.*, **2017**, *8*, 4848.

Apart from Shen's work, over the past few years, organosilver(I) species have demonstrated their potential as nucleophilic coupling partners in Pd-catalyzed transformations either as *in situ* generated species or as isolated compounds.[24] In the context of trifluoromethylsilver(I) nucleophiles, we found that there were already literature precedents of the use of *in situ* generated 'Ag(CF_3)' species as transmetalating agents for the synthesis of CF_3-containing organometallic complexes (Scheme 3.23).[25] Nevertheless, these species had never been explored as potential coupling partners.[26] More interestingly, it should be mentioned that these species are generated in polar solvents as a mixture of an ate-type complex, $[Ag(CF_3)_2]^-$ and neutral [(D)Ag(CF_3)] (D = solvent) species (Scheme 3.23).[27] This CF_3 exchange reaction by itself showcases the lability of the Ag–CF_3 bond, necessary for the transmetalation to happen in an efficient manner. The mayor downside of using *in situ* generated 'Ag(CF_3)' species as CF_3 shuttle is that the composition of the mixture can vary depending on the solvent, temperature, concentration, *etc.* For this reason, we focused our attention on well-defined and isolable trifluoromethyl organosilver(I) complexes.

In this regard, before the work described in this Chapter 2, there were only two examples of well-defined and isolable [(L)Ag(CF_3)] complexes: ([(SIPr)Ag(CF_3)][28] and [(BPhen)Ag(CF_3)],[26b] BPhen = bathophenanthroline) and only [(BPhen)Ag(CF_3)] was tested in a transmetalation reaction towards copper(I), not directly related to this Chapter 2.[26b]

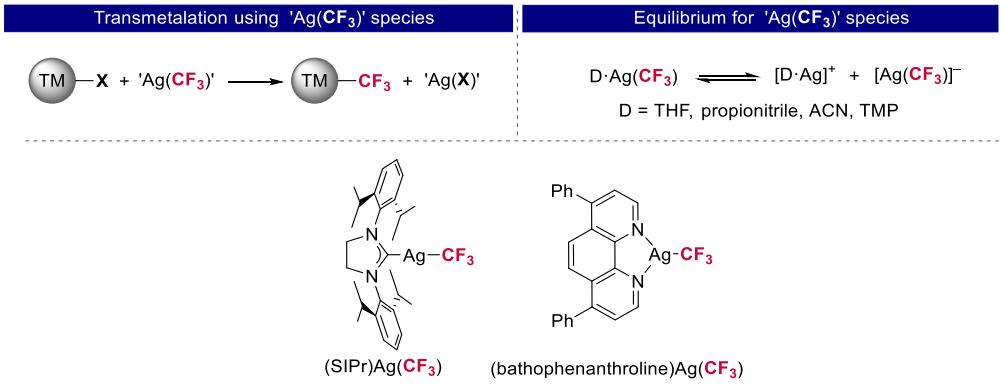

Scheme 3.23. Above left: Representation of the transmetalation reaction of transition metal halides with 'Ag(CF_3)' species. Above right: equilibrium of 'Ag(CF_3)' species in polar solvent. TMP = $(MeO)_3PO$. Below: Isolated trifluoromethylsilver(I) complexes previous to our investigation.

[24] Mudarra, Á. L.; Martínez de Salinas, S.; Pérez Temprano, M. H. *Org. Biomol. Chem.* **2019**, *17*, 1655.

[25] Homoleptic silver(I) complexes bearing perfluorinated aryl moieties have been also used as transmetalating agents to dimeric bis(halide)-Pd(II) complexes: a) Albéniz, A. C.; Espinet, P.; Martín-Ruiz, B. *Chem. Eur. J.* **2001**, *7*, 2481. b) Albéniz, A. C.; Espinet, P.; López-Cimas, O.; Martín-Ruiz, B. *Chem. Eur. J.* **2005**, *11*, 242.

[26] a) Tyrra, W. J. Fluorine Chem. **2001**, *112*, 149. b) Tyrra, W.; Naumann, D. *J. Fluorine Chem*. **2004**, 125, 823. c) Weng, Z.; Lee, R.; Jia, W.; Yuan, Y.; Wang, W.; Feng, X.; Huang, K.-W. *Organometallics* **2011**, 30, 3229. d) Hafner, A.; Bräse, S. *Angew. Chem. Int. Ed.* **2012**, *51*, 3713. e) Zhang; C.-P.; Wang, Huan; Klein, A.; Biewer, C.; Stirnat, K.; Yamaguchi, Y.; Xu, L.; Gomez-Benitez, V.; Vicic, D. A. *J. Am. Chem. Soc.* **2013**, *135*, 8141.

[27] Naumann, D.; Wessel, W.; Hahn, J.; Tyrra, W. *J. Organomet. Chem*. **1997**, *547*, 79.

[28] Tate, B. K.; Jordan, A. J.; Bacsa, J.; Sadighi, J. P. *Organometallics* **2017**, *36*, 964.

3.2. **Objectives**

Palladium-catalyzed nucleophilic trifluoromethylation reactions is a promising approach to introduce the exceptional CF_3 moiety into organic scaffolds. The development of this transformation, however, has been limited by the hampered reductive elimination of the C–CF_3 bond from organo-Pd(II) intermediates. Although there are phosphine ligands that promote this elementary step, only monodentate phosphine ligands have shown to be compatible with catalytic trifluoromethylation reactions.

The lack of catalytic examples employing bidentate phosphine ligands in catalytic trifluoromethylation reactions is not only a consequence of the challenging reductive elimination but also a result of unproductive side reactions such as politrifluoromethylation and/or mismatched transmetalation reactions of the organo-Pd(II) intermediates. The origin of these undesired reactions is related to unselective and inefficient transmetalation from activated R_3SiCF_3 reagents. We envisioned that the design of potentially more efficient and selective transmetalating agents based on silver could overcome these limitations.

In this context, the main objective of this Chapter 2 is to investigate the reactivity of Ag–CF_3 species as transmetalating agents in the context of $Pd^{0/II}$-catalyzed trifluoromethylation of aryl halides. To do so, the following points are pursued:

- Synthesis and characterization of well-defined and isolable "$AgCF_3$" complexes.
- Evaluation of those organosilver(I) complexes as transmetalating agents towards an model organo-Pd(II) halide as benchmark system.
- Evaluation of those organosilver(I) complexes as transmetalating agents in a productive system towards the formation of C–CF_3 bond using Xantphos as bidentate phosphine ligand.

3.3. Results and discussion

This section fundamentally divided into two parts. First, we use a palladium benchmark system to compare the transmetalating capability of different CF_3 nucleophilic sources including commercial ones and trifluoromethyl silver nucleophiles. The second part consists of translating the knowledge acquire from the palladium benchmark system into a productive system that can undergo C-CF_3 bond-forming reaction.

3.3.1. Evaluating CF_3-containing transmetalating agents using a model system

3.3.1.1. Selection of a palladium benchmark system

As described in the Introduction of this Chapter 2, apart from the high energy barrier associated to the C-CF_3 reductive elimination from Pd(II) specie, there are other identified challenges regarding the transmetalation step in $Pd^{0/II}$-mediated trifluoromethylation processes, namely when using the commonly-used CF_3^- sources. A potential solution for these usually ignored limitations would be the employment of a rapid and selective nucleophilic source towards the I-for-CF_3 exchange. To test this hypothesis, the first goal of this project was to define a [$(L)_nPd(Ar)(X)$] system that could enable the evaluation the transmetalating capability of different CF_3 sources.[29] We selected [(dppp)Pd(Ph)(I)][30] (**1**) as benchmark system for our initial investigation based on several considerations (Scheme 3.24). First, this aryl-Pd(II) complex contains a strong coordinating ligand that prevents the formation of the above mentioned inactive poly-(trifluoromethyl)palladium compounds (Scheme 3.16).[1a] Second, the resulting product [(dppp)Pd(Ph)(CF_3)] (**2**) does not undergo $PhCF_3$ coupling.[31]

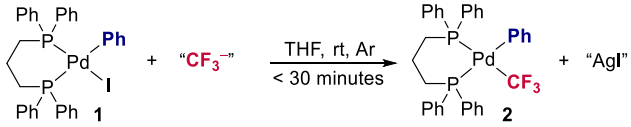

Scheme 3.24. Benchmark system for the transmetalation reaction.

In order to prevent the formation of undesired by-products related to long reaction times, we will target fast I-for-CF_3 exchanges (< 30 minutes).[32]

[29] Initially, we envisioned that the study of the transmetalation using [(Xantphos)Pd(Ph)(I)] complex to form [(Xantphos)Pd(Ph)(CF_3)] could be hampered by the formation of cis/trans isomers and/or eventual generation of the coupled product. Thus, we turned our attention on dppp, as a model bidentate phosphine ligand of Xantphos.

[30] The selection of the iodide as benchmark system was based on the discussion of Grushin in ref. 6 about the potential "nucleophilic aid" of some transmetalation side reactions. This means that the iodide palladium complexes are more prompted to undergo these undesired transformation and the transmetalating agent has to be effective enough to prevent these side reactions.

[31] It has been reported to yield a 60% yield at 145 ºC which will not be our working temperature.

[32] We selected THF as solvent to avoid solubility issues.

3.3.1.2. Commercially-available nucleophilic CF_3 sources as transmetalating agents towards the Pd benchmark system

As initial reference for our study, we aimed to stablish the transmetalating ability of different commercially available CF_3 sources. First, we tested the widely-used R_3SiCF_3 (R = Me,[13] Et[1c,5b]) in combination with a activating agent, a fluoride salt. The trifluoromethylation of [(dppp)Pd(Ph)(I)] (**1**) using different combinations of R_3SiCF_3/MF (Table 3.1) resulted in poor formation of **2**. The best result, a 19% yield, was observed for the combination of Me_3SiCF_3/CsF after 30 minutes. This shows the inefficiency of these mixtures as CF_3 nucleophilic sources.

We also tried as CF_3 shuttle to the aryl-Pd(II) complex a commercially available copper reagent, called Trifluoromethylator® ([(Phen)Cu(CF_3)]), developed by Hartwig and co-workers.[33] After 10 min, we only observed the desired product (**2**) in a 12% (entry 5, Table 3.1). Since the [(Phen)Cu(CF_3)] was not completely soluble, we run the reaction for longer reaction time. This reaction, after 16 h, yielded product **2** along with starting material **1** and several unknown products likely related to decomposition of **1** and/or **2** (Figure 3.4).

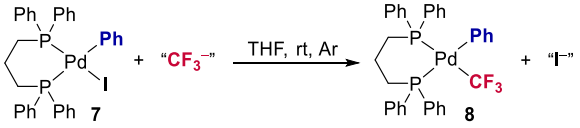

entry	CF_3 source (equiv)	Time (min)	(dppp)Pd(Ph)(CF_3) (**8**)(%)[a)]
1	Me_3SiCF_3/CsF (2/4)	30	19
2	Me_3SiCF_3/KF (2/4)	30	traces
3	Et_3SiCF_3/CsF (2/4)	30	0
4	Et_3SiCF_3/KF (2/4)	30	0
5	(Phen)Cu(CF_3) (1.5)	10	12

Table 3.1. Trifluoromethylation of the benchmark Pd-system and the corresponding trifluoromethyl source. The reactions were carried out at 0.01 M of Pd in a 5-ml crimped. [a)]The yield was measured by $^{31}P\{^1H\}$ NMR spectroscopy at –80 ºC to prevent the evolution of the reaction.

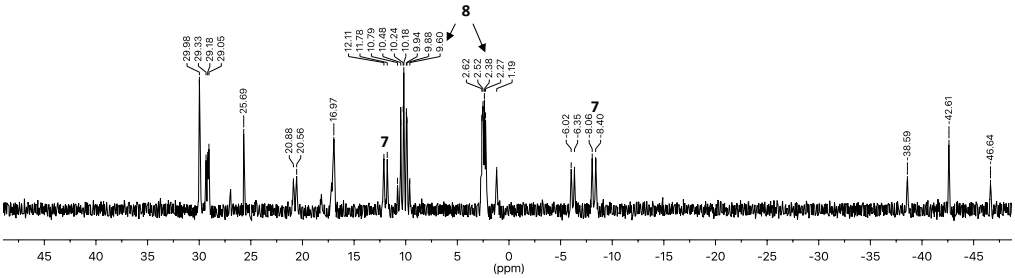

Figure 3.4. $^{31}P\{^1H\}$ NMR spectrum corresponding to reaction in entry 5, Table 3.1.

[33] Morimoto, H.; Tsubogo, T.; Litvinas, N. D.; Hartwig, J. F. *Angew. Chem. Int. Ed.* **2011**, *50*, 3793. The complex is commercially-available: https://www.sigmaaldrich.com/catalog/product/aldrich/777692?lang=es&region=ES.

3.3.1.3. NHC-Carbene trifluoromethylsilver(I) complexes

- **Synthesis and characterization of ([(SIPr)Ag(CF$_3$)].**

With these results as a reference, we then focused on the activity of one of the scarce examples of isolated trifluoromethylsilver(I) compounds reported in the literature to that date: [(SIPr)Ag(CF$_3$)] (**3**). The reported synthetic route consisted of the isolation of [(SIPr)Ag(O^{t}Bu)], a very sensible complex towards hydrolysis, and subsequent exposition to Me$_3$SiCF$_3$. We circumvent the isolation of [(SIPr)Ag(O^{t}Bu)] by its *in situ* generation from [(SIPr)Ag(Cl)] and NaO^{t}Bu in the presence of Me$_3$SiCF$_3$ (Scheme 3.25). The ^{1}H and ^{19}F NMR spectra of the corresponding complex were in accordance with the previously reported one.[28] Additionally, the structure of [(SIPr)Ag(CF$_3$)] was unambiguously confirmed by X-ray diffraction. It should be mentioned that during the synthesis of [(SIPr)Ag(CF$_3$)], very small amounts of [Ag(CF$_3$)$_2$]$^-$ were detected, likely formed by displacement of the NHC-carbene ligand.

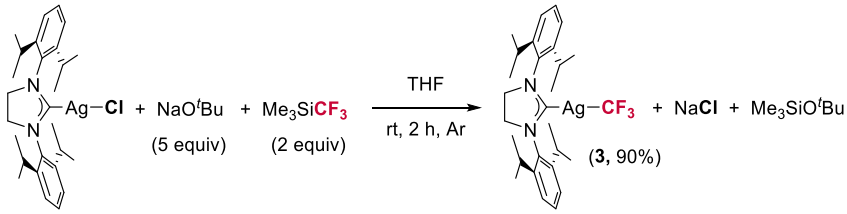

Scheme 3.25. Synthesis of [(SIPr)Ag(CF$_3$)] (**3**).

We also attempted to prepare another [(L)Ag(CF$_3$)], using L = SIMes (1,3-bis(2,4,6-trimethylphenyl)-4,5-dihydroimidazol-2-ylidene). During its formation, [Ag(CF$_3$)$_2$]$^-$ species was detected in the reaction media. Further experiments proved that this species was not in equilibrium with the neutral complex and the proportion of the ionic species depends on the synthetic approach. Therefore, we considered that the synthesis of this [(SIMes)Ag(CF$_3$)] was not reproducible enough to study its behavior as transmetalating agent.

- **Evaluation of ([(SIPr)Ag(CF$_3$)] in transmetalation towards the Pd benchmark system.**

The treatment of [(dppp)Pd(Ph)(I)] (**1**) with 1.5 equivalents of [(SIPr)Ag(CF$_3$)] (**3**) resulted in <5% yield of [(dppp)Pd(Ph)(CF$_3$)] (**2**) after 30 minutes, showing the poor capability for transferring the CF$_3$ group of this complex. This reaction also gave rise unknown products likely related to decomposition of the palladium complexes along time.

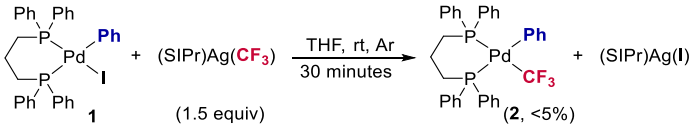

Scheme 3.26. Evaluation of the transmetalation reaction of **3** as transmetalating agent.

3.3.1.4. (N^N)-bidentate trifluoromethylsilver(I) complexes

- **Synthesis of previously described [(BPhen)Ag(CF$_3$)] complex**

We then focused our attention on [(L)Ag(CF$_3$)] where L is a bidentate nitrogen ligand. First of all, we attempted to investigate the reactivity of the previously described [(BPhen)Ag(CF$_3$)] complex (Scheme 3.27).[26b]

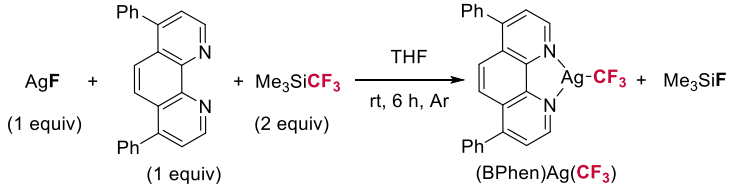

Scheme 3.27. Synthesis of [(BPhen)Ag(CF$_3$)] following the previously reported synthesis of Huang *et al.* (ref. 26b).

During its synthesis, following the reported reaction conditions, we detected the generation of an CF$_3$-containing anionic species, $[Ag(CF_3)_2]^-$, which were not mentioned in the original synthetic report.[34] We found that the concentration of this species depends on the polarity of the solvent, being more favored in DMF than in THF (**Figure 3.6**). This suggests that the anionic $[Ag(CF_3)_2]^-$ species is in equilibrium with the neutral [(BPhen)Ag(CF$_3$)]. In addition, we observed by ^{19}F NMR spectroscopy at room temperature the rapid decomposition of [(BPhen)Ag(CF$_3$)] into HCF$_3$ and other by-products (Figure 3.5 and Figure 3.6). The same outcomes were obtained for different (N^N)-bidentate ligands such as 1,10-phenanthroline (phen), 2,2'-bipyridyl (Bpy) or 4,4'-di-tert-butyl-2,2'-bipyridyl (^{t}Bu-bpy).

[34] This species was assigned on the basis of NMR spectroscopy. By ^{19}F NMR, it bears a very diagnostic coupling constant between silver and fluoride, as we will discuss further below.

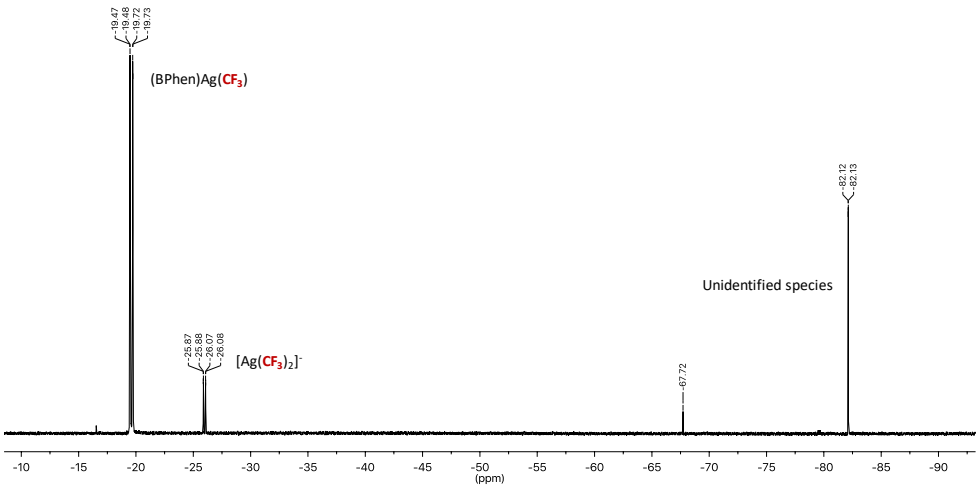

Figure 3.5. ^{19}F NMR spectra at room temperature in THF of the synthesis of [(BPhen)Ag(CF_3)].

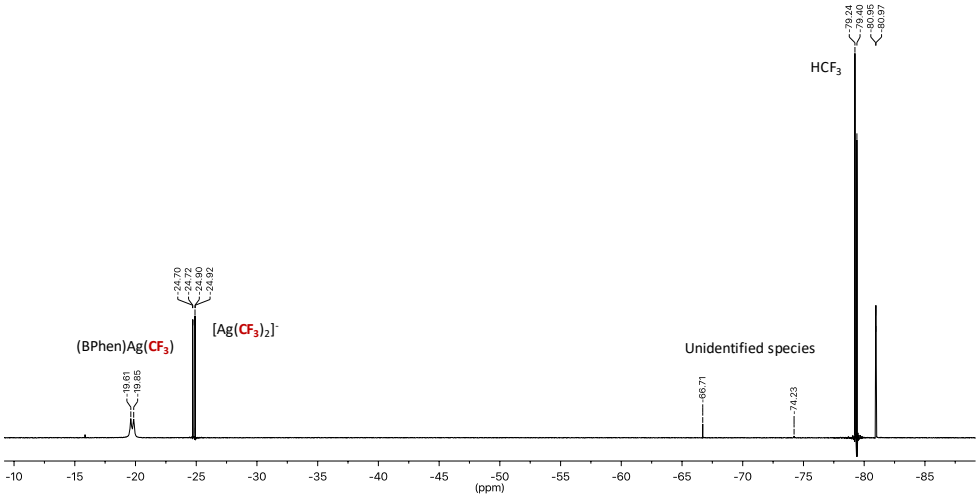

Figure 3.6. ^{19}F NMR spectra at room temperature in DMF of the synthesis of [(BPhen)Ag(CF_3)].

- **Synthesis and characterization of [(Bc)Ag(CF_3)]**

After some experimentation, we gratifyingly found a reliable synthesis of a stable [(*N^N*)Ag(CF_3)] complex (**4**) using bathocuproine (Bc) as ancillary ligand. In solution, **4** is an equilibrium of [(Bc)Ag(CF_3)] (**4a**) and [cat][Ag(CF_3)$_2$] (**4b**) as supported by NMR spectroscopy and ESI-MS.[35] In THF the proportion **4a**:**4b** is 98:2 and, in DMF, 66:34. In solid state, **4** can be stored during months at –30 ºC under inert atmosphere in the dark without any sign of decomposition. Additionally, we were able to crystalize the neutral species **4a** by slow diffusion

[35] Further experiments, which are discussed in the Appendix, confirmed **4** to be an equilibrium of **4a** and **4b** in polar solvents.

of hexane into a solution of tetrahydrofuran at room temperature, confirming the structure of this neutral species.

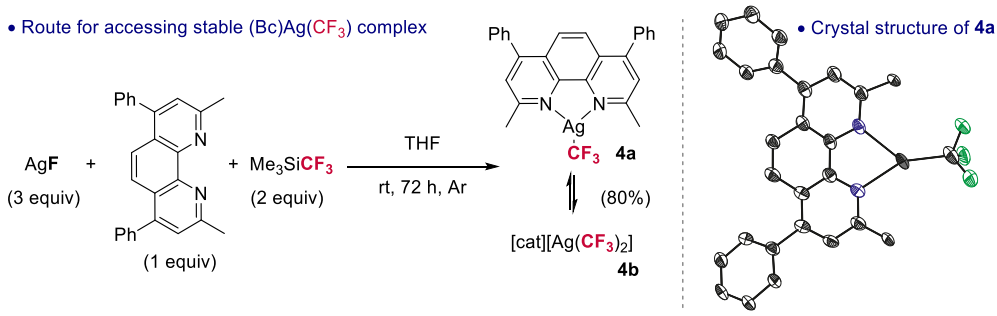

Scheme 3.28. Left: Synthesis of **4** as an equilibrium of **4a** and **4b** species. Right: ORTEP drawing (thermal ellipsoids set at 50% probability) of the structure of **4a**. Hydrogen atoms have been omitted for clarity.

By ^{19}F NMR spectroscopy, **4a** and **4b** present diagnostics signals. **4a** corresponds to two doublets around –21.84 ppm in THF. The observation of these two different doublets is a consequence of the coupling with the two isotopes of silver (^{109}Ag and ^{107}Ag, almost equally abundant, with spin = ½): $^{2}J_{^{109}Ag,F}$ = 122.3 Hz, $^{2}J_{^{107}Ag,F}$ = 107.0 Hz.[27,28,36] **4b** also appears as two doublets around –27.18 ppm in THF. In this case, the coupling constants, in accordance with literature precedents, are $^{2}J_{^{109}Ag,F}$ = 100.7 Hz and $^{2}J_{^{107}Ag,F}$ = 87.2 Hz.[36] These coupling constants were used to identify both species in further experiments.

At this point, we should mention that, although both **4a** and **4b** species are detected by ^{19}F NMR spectroscopy in polar solvents (THF or DMF), a single set of signals is observed by ^{1}H NMR spectroscopy. By analogy to related copper compounds,[37] we initially hypothesized that the structure of **4b** was [(Bc)$_2$Ag][Ag(CF$_3$)$_2$], whose cation should present by ^{1}H NMR spectra different signals from **4a**. However, the signals for the protons in **4a** and **4b** coalesce and hamper, therefore, the characterization of the cation for **4b**.[38] Intrigued by these results, we focused our attention on the characterization of the cation in **4b**.

[36] a) Tyrra, W. *Heteroat. Chem*. **2002**, *13*, 561. b) Zeng, Y.; Zhang, L.; Zhao, Y.; Ni, C.; Zhao, J.; Hu, J. *J. Am. Chem. Soc.* **2013**, *135*, 2955

[37] Morimoto, H.; Tsubogo, T.; Litvinas, N. D.; Hartwig, J. F. *Angew. Chem. Int. Ed.* **2011**, *50*, 3793.

[38] The addition of free bathocuproine to the equilibrium did not shift or modify the ^{1}H NMR spectroscopy signals. Therefore, in order to ensure that **4** was pure and free bathocuproine ligand was not present in the solid, we checked that the integration of a known amount of complex **4** by ^{19}F NMR spectra and the integration a known amount of internal standard (4,4'-diflurobiphenyl) correspond to the expected ratio according to the weight amounts.

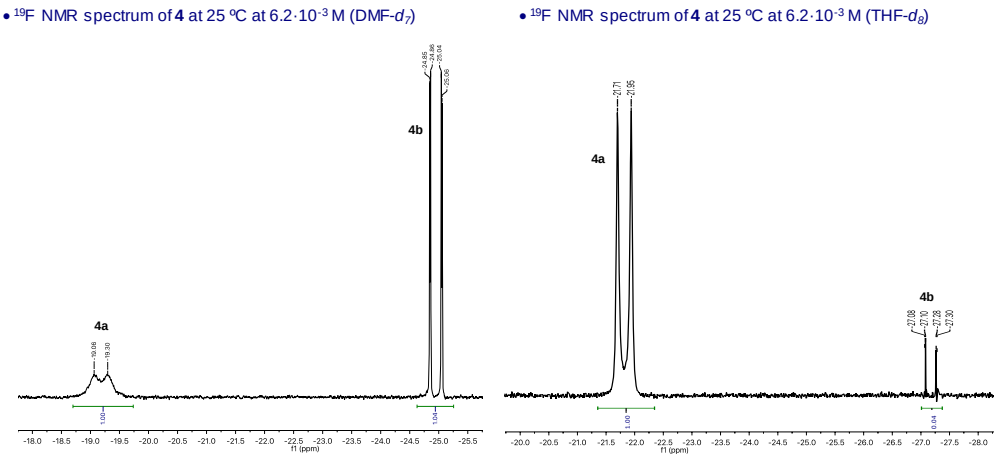

Figure 3.7. ^{19}F NMR spectra of **4** in different solvents (DMF-d_7 and THF-d_8).

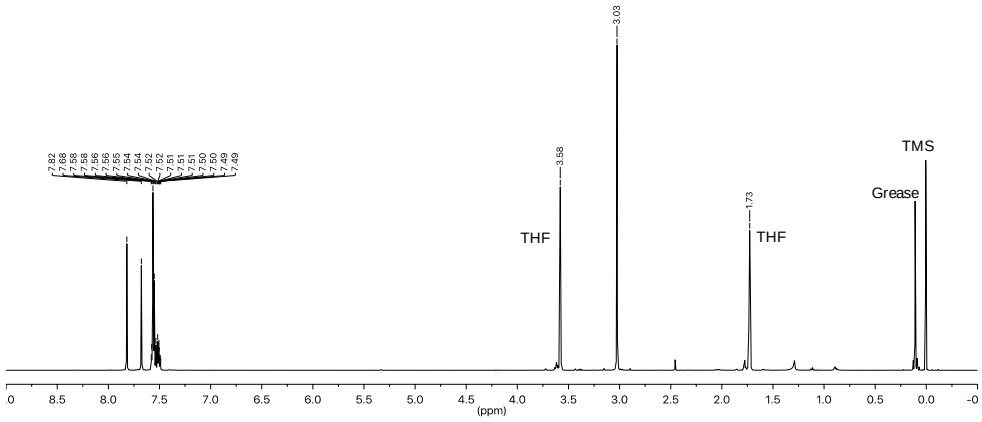

Figure 3.8. ^{1}H NMR spectra of **4** in THF-d_8.

○ Elucidation of the nature of the cation for **2b**

The elucidation of the nature of the counterpart of [Ag(CF$_3$)$_2$] anion (**2b**) in solution was investigated using NMR spectroscopy studies and DFT calculations. Although, herein, we briefly discuss how this cation was characterized, further details can be found in the Appendix.

In collaboration with Teodor Parella at Universitat Autònoma de Barcelona, we performed Diffusion-Ordered SpectroscopY (DOSY) ^{1}H NMR spectroscopy experiments. This NMR technique allows to obtain information about the size of a molecule. This is achieved through the application of electromagnetic field gradients on a given direction that allows to physically locate a molecule in that axis. Thus, it is possible to characterize the diffusion coefficient of a

molecule which is related to the molecular dimensions. If the molecule is approximated to a sphere, using the Stokes-Einstein equation (see Appendix), we can obtain the "radius" of the molecule under study. This value is called hydrodynamic radius and it can be used to discriminate between molecules that are different in size.

As mentioned above, the initially proposed structure for **4b** was $[(Bc)_2Ag][Ag(CF_3)_2]$ but it could not be identified by mono-dimensional ^1H NMR spectroscopy. To gain insights about the nature of the cation in **4b** (**4b-cat**), we aimed to evaluate its size by using DOSY ^1H NMR spectroscopy and compare it to an independently synthesized $[(Bc)_2Ag]$-containing species, $[(Bc)_2Ag][SbF_6]$ (**5**).[39] By DOSY ^1H NMR spectroscopy (Table 3.2), we observed that the hydrodynamic value of **5** is larger than for any species in **4** considering different solvents. We also compared the free bathocuproine and **4** and their values were comparable. We therefore discarded this $[(Bc)_2Ag][Ag(CF_3)_2]$ species to be part of the equilibrium.

	R_H (Å)		
Solvent	Free Bc	**5**	**4**
Benzene	4.37	7.60	4.08
THF	4.33	6.86	4.33
DMF	4.38	6.78	4.91

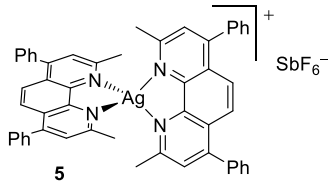

5

Table 3.2. Hydrodynamic radius of free bathocuproine, **4** and **5** obtained by DOSY ^1H NMR spectroscopy in different solvent.

Challenged by this unexpected outcome, we performed DFT studies.[40] Initial calculations supported the unlikely presence of $[(Bc)_2Ag][Ag(CF_3)_2]$ species in the equilibrium of **4**.[41] Given this, we considered a potential stabilization of **4b-cat** by solvent molecules. For the computational treatment of explicit solvent molecules, we used cluster/continuum model which is explained in detail in the Appendix.

Finally, after considering different cations and coordination modes, DFT calculations suggested that the most likely cation for **4b** is a structure that contains a silver center coordinated to a bathocuproine ligand along with two solvent molecules and a second bathocuproine ligand bound to the system through stabilizing π–π interactions.[42] In line with the DFT calculations, we observed the formation of [(Bc)Ag(THF)][SbF_6] upon exposure of **5** to THF.

[39] Further discussions about its synthesis is provide in the Appendix. We also achieved the synthesis of [(Bc)Ag(THF)][SbF_6] and it was evaluated as a potential cation candidate.

[40] These calculations were carried out with the ωB97-XD functional with a double-ζ plus polarization basis set in solvent (see Appendix for further details).

[41] As it is described in the Appendix, this equilibrium has associate a ΔG^0 of 16.2 kcal·mol^{-1} which is quite large for an equilibrium observable at room temperature by NMR spectroscopy.

[42] It should be mentioned that stabilizing π–π interactions are quite important in this system. Indeed, as it is described in the Appendix, **4a** as a dimer with π–π between the bathocuproine rings, is stabilized in 15.8 kcal·mol^{-1} below the separated monomers.

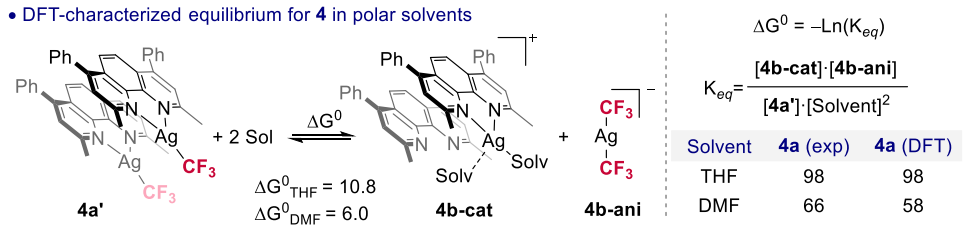

Solvent	4a (exp)	4a (DFT)
THF	98	98
DMF	66	58

Scheme 3.29. Left: Proposed equilibrium for **4** in polar solvents based on DFT calculations. Right: Equations for the calculation of the proportions of **4a** and **4b** in the equilibrium and comparison of DFT-calculated proportions and experimental ones.

This equilibrium, represented in Scheme 3.29, presents a ΔG^{o} value of 10.8 kcal·mol^{-1} in THF and 6.0 kcal·mol^{-1} in DMF. These values seem very large for species that are observed to be in equilibrium at room temperature by NMR spectroscopy. However, this is explained if we take into account the very different concentrations between the solvent and **4** (12.33 M for THF and 12.92 M for DMF).

- **Evaluation of 4 (4a/4b) in transmetalation towards the Pd benchmark system.**

We next investigated the reactivity of the mixture [(Bc)Ag(CF_3)] (**4a**) and [(Bc)$_2$Ag(THF)$_2$][Ag(CF_3)$_2$] (**4b**) in the transmetalation reaction towards the benchmark system (complex **1**). Interestingly, in contrast to **3**, the trifluoromethylation of [(dppp)Pd(Ph)(I)] (**1**) with 1.5 equivalents of **4** proceeded cleanly and quantitatively in 10 min to afford **2** (Table 3.4, entry 2).

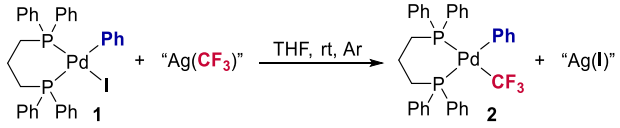

entry	"Ag(CF_3)" source (equiv)	Time (min)	(dppp)Pd(Ph)(CF_3) (%)[a)]
1	(SIPr)Ag(CF_3) (**3**) (1.5)	30	< 5
2	(Bc)Ag(CF_3) (**4**) (1.5)	10	100

Table 3.3. Trifluromethylation of the benchmark Pd-system and the corresponding trifluoromethylsilver(I) complex. The reactions were carried out at 0.01 M of Pd in a 5-ml crimped vial. [a)]The yield was measured by $^{31}P\{^{1}H\}$ NMR spectroscopy at –80 ºC to prevent the evolution of the reaction

3.3.1.5. "Ligandless" trifluoromethylsilver(I) complexes

Inspired by the extraordinary transmetalating ability of **4**, and prompted by its different behavior form **3**, we wondered whether [Ag(CF_3)$_2$]$^-$ could be a non-innocent spectator in **4** and participate as CF_3 shuttle. For this reason, we aimed at the synthesis and characterization of an analogous anion in **4b** but bearing a different stabilizing cation. This is interesting since the

synthesis, isolation and reactivity of the bis-(trifluoromethyl) argentates are unprecedented in the literature. We will resume this topic in Chapter 4.

- **Synthesis and characterization of [cat][Ag(CF$_3$)$_2$] complexes**

As shown in Scheme 3.30, [NBu$_4$][Ag(CF$_3$)$_2$] (**6$_{NBu4}$**) and [Cs][Ag(CF$_3$)$_2$] (**6$_{Cs}$**) were successfully synthetized. The reaction of AgOAc with 4 equiv of Me$_3$SiCF$_3$, in THF at room temperature, in the presence of 4 equiv of KF and 1 equiv of NBu$_4$OAc afforded a white crystalline solid, [NBu$_4$][Ag(CF$_3$)$_2$] (**6$_{NBu4}$**), in 83% isolated yield. Following a similar synthetic route, but using 2 equiv of CsF instead of the combination NBu$_4$OAc/KF, we synthesized [Cs][Ag(CF$_3$)$_2$] (**6$_{Cs}$**) in 85% yield as a yellow solid. Both salts were unambiguously characterized by NMR spectroscopy, ESI-MS and single crystal X-ray diffraction. No signs of decomposition of these complexes were observed when stored them for months at –30 ºC under inert atmosphere in the dark.

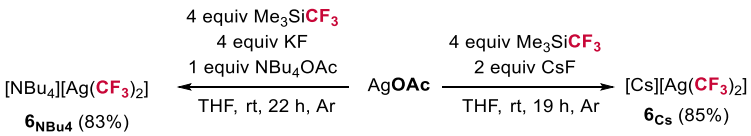

Scheme 3.30. Synthetic routes for accessing **6$_{NBu4}$** and **6$_{Cs}$** species.

Regarding the characterization by NMR spectroscopy, we will remark special features using **6$_{NBu4}$** as study case due to the quality of the spectra acquired. By ^{19}F NMR spectroscopy, diagnostic pattern of signals with a characteristic coupling constant was observed: two doublets with a coupling constants of $^2J_{^{109}Ag,F}$ = 100.5 Hz and $^2J_{^{107}Ag,F}$ = 87.0 Hz.[27,36] These values are in accordance with the values obtained for **4b**.

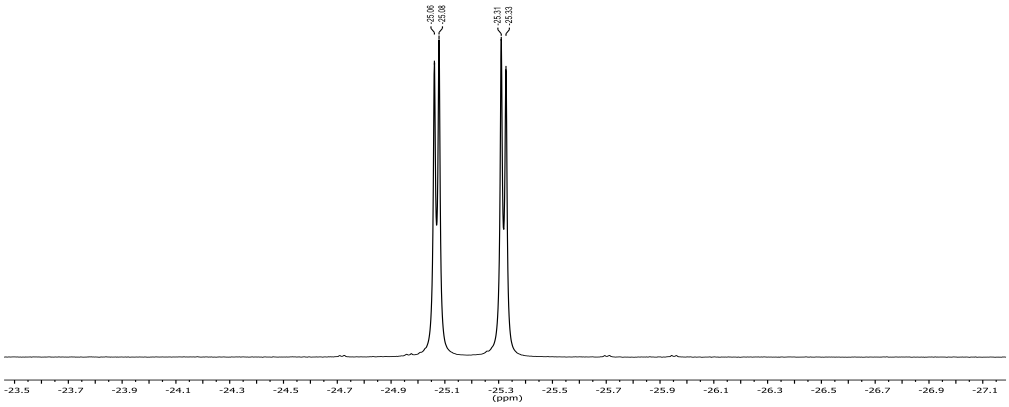

Figure 3.9. ^{19}F NMR spectrum at rt in THF of **6$_{NBu4}$** (acetone-*d$_6$*).

A more complex scenario was observed for the $^{13}C\{^{1}H\}$ NMR spectra corresponding to the CF_3 groups. In this case, the coupling of ^{13}C with the silver and the fluorine atoms, both active in NMR (spin = ½), affords two doublet quadruplet of quadruplets. We will explain this pattern in more detail. First, the three alpha fluorine atoms split the carbon signal into four ($^{1}J_{F,C}$ = 370.0 Hz). Then, the coupling with the silver (two isotopes and both active) splits the signal into two doublets ($^{1}J_{^{109}Ag,C}$ = 275.0 Hz and $^{1}J_{^{107}Ag,C}$ = 238 Hz). Finally, the fluorine atoms on the other carbon atom couple to the signal to yield a quartet ($^{3}J_{F,C}$ = 8.0 Hz, in green in Figure 3.10). This coupling could seem odd since both atom carbons are, in principle, chemically equivalent as a consequence of the symmetry of the molecule. However, from the NMR spectroscopy point of view, the measured ^{13}C nuclei, in low proportion, is able to "perceive" the ^{12}C nuclei magnetic environment as different and, consequently, the fluorine atoms are not equivalents.

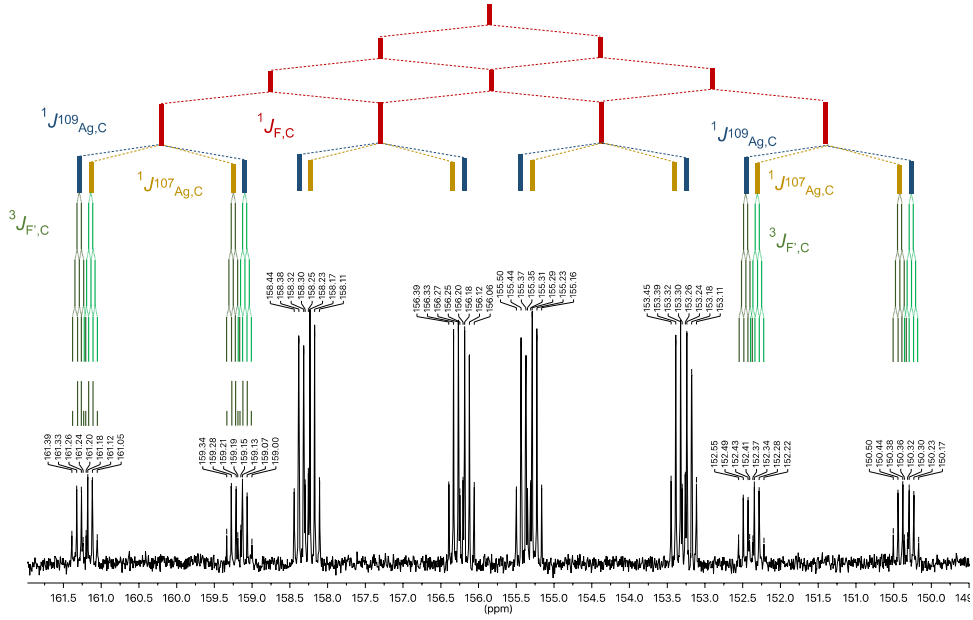

Figure 3.10. $^{13}C\{^{1}H\}$ NMR spectrum at room temperature in THF-d_8 of $\mathbf{6_{NBu4}}$. Corresponding splitting diagrams are shown above.

Considering the structure obtained by X-ray diffraction, it is worth mentioning the different bonding situation between these ionic species ($\mathbf{6_{NBu4}}$ and $\mathbf{6_{Cs}}$ in Scheme 3.18). The solid structure of $\mathbf{6_{NBu4}}$ shows a linear bis-(trifluoromethyl) argentate paired together with the NBu_4 cation. In sharp contrast, $\mathbf{6_{Cs}}$ presents a rather unique structure, with the silver atoms forming linear chains, and the cesium cations interacting with twelve different fluorine atoms. More details about the crystal of $\mathbf{6_{Cs}}$ will be disclose in Chapter 5.

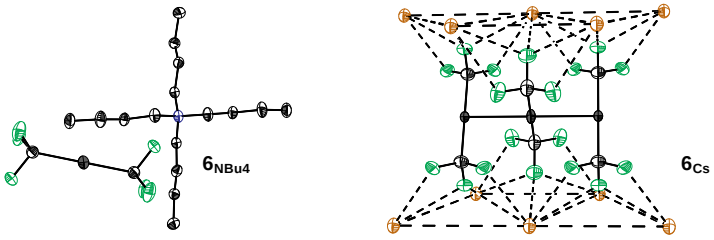

Figure 3.11. ORTEP drawing (thermal ellipsoids set at 50% probability) of the obtained X-ray structures of $\mathbf{6}_{NBu4}$ and $\mathbf{6}_{Cs}$.Hydrogen atoms have been omitted for clarity.

- **Evaluation of [cat][Ag(CF$_3$)$_2$] in transmetalation towards the Pd benchmark system.**

The reaction of **1** with 0.75 equivalents of [Cs][Ag(CF$_3$)$_2$] (**6$_{Cs}$**) resulted in the quantitative formation of **2** in 10 min along with [Cs][Ag(CF$_3$)(I)][43] (Table 3.4, entry 3). The reaction of [NBu$_4$][Ag(CF$_3$)$_2$] (**6$_{NBu4}$**), under the same conditions, arose a 93% yield (Table 3.4, entry 3). It should be mentioned that in this former case, along with [NBu$_4$][Ag(CF$_3$)(I)], we observed the formation of [NBu$_4$][Ag(CF$_3$)$_4$], decomposition product of **6$_{NBu4}$**.

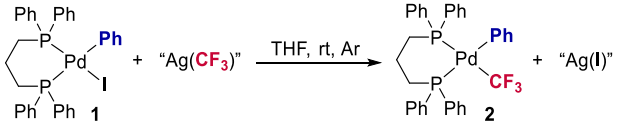

entry	"Ag(**CF$_3$**)" source (equiv)	Time (min)	(dppp)Pd(Ph)(CF$_3$) (%)[a)]
1	(SIPr)Ag(**CF$_3$**) (**3**) (1.5)	30	< 5
2	(Bc)Ag(**CF$_3$**) (**4**) (1.5)	10	100
3	[Cs][Ag(**CF$_3$**)$_2$] (**6$_{Cs}$**) (0.75)	10	100
4	[NBu$_4$][Ag(**CF$_3$**)$_2$] (**6$_{NBu4}$**) (0.75)	10	93

Table 3.4. Trifluoromethylation of the benchmark Pd-system and the corresponding trifluoromethylsilver(I) complex. The reactions were carried out at 0.01 M of Pd in a 5-ml crimped vial. [a)]The yield was measured by $^{31}P\{^1H\}$ NMR spectroscopy at –80 ºC to prevent the evolution of the reaction.

3.3.2. Translation to a productive system in the C–C bond formation: [(Xantphos)Pd(Ph)(I)]

As mentioned above, Grushin described the challenges associated to the synthesis of [(Xantphos)Pd(Ph)(CF$_3$)] (**8**) directly from [(Xantphos)Pd(Ph)(I)] (**9**).[1b] Encouraged by our previous results involving the benchmark system, we envisioned that trifluoromethyl silver nucleophiles could overcome these shortcomings. This way, we could access for the first time directly to PhCF$_3$ from **9** achieving two out of three "elementary" steps in a cross-coupling catalytic cycle: the transmetalation and the reductive elimination.

[43] The observed signal was assigned by ^{19}F NMR spectroscopy based on the previously reported chemical shift (see ref. 36a). This was also supported by the behavior of analogous trifluoromethyl copper(I) system: Agnes, K.; Movchun, V.; Rodima, T.; Dansauer, T.; Rusanov, E. B.; Leito, I.; Kaljurand, I.; Koppel, J.; Pihl, V.; Koppel, I.; Ovsjannikov, G.; Toom, L.; Mishima, M.; Medebielle, M.; Lork, E.; Röschenthaler, G.-V.; Koppel, I. A.; Kolomeitsev, A. A. *J. Org. Chem.* **2008**, *73*, 2607.

From this point on, we selected as reaction conditions the optimal ones reported by Grushin *et al*. to promote the reductive elimination from **8**, using benzene as solvent and in the presence of one additional equivalent of phosphine ligand. [1b,6]

3.3.2.1. In situ generation of $PhCF_3$ from [(Xantphos)Pd(Ph)(I)]

Following the same approach than the one described for our model system, we tested not only the transmetalating capability of the most efficient CF_3-containing silver complexes but also the performance of the widely-used R_3SiCF_3/F^- mixture. These results are shown in Table 3.5 and commented below.

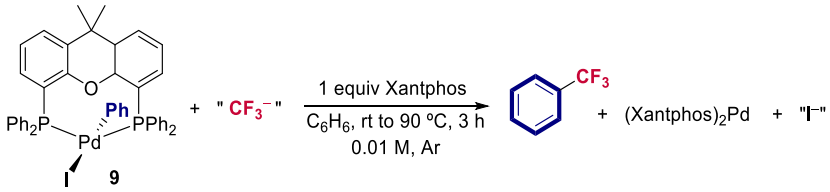

entry	CF_3^- source	Equiv.	$PhCF_3$ (%)[b]
1	(Bc)Ag(CF_3) (**4**)	1.50	70
2	[NBu_4][Ag(CF_3)$_2$] (**6**$_{NBu4}$)	0.75	42
3	[Cs][Ag(CF_3)$_2$] (**6**$_{Cs}$)	0.75	84
4	Me_3SiCF_3/CsF	2/4	14
5	Me_3SiCF_3/KF	2/4	0
6	Me_3SiCF_3/NBu_4F	2/4	4

Table 3.5. Transmetalating agent and product yield for the reaction shown above. The reactions were carried out in a 5-ml crimped vial under argon atmosphere. After heating 3 h with vigorous stirring, the reactions were filtered and, finally, the yield of the product was determined.

The reaction of [(Bc)Ag(CF_3)] (**4**) with **9** gave rise to a reasonable 70% yield of $PhCF_3$ product and an approximate 23% of [(Bc)Pd(CF_3)] as a result of ligand scrambling between the Xantphos and Bc ligand (entry 1 in Table 3.5; Figure 3.12). This indicates that the use of additional ancillary ligands for stabilizing the transmetalating agent can result in competition and depletion of the C–C bond-forming reaction. Thus, ligand-stabilized species as CF_3 source are not desirable under this reaction conditions.

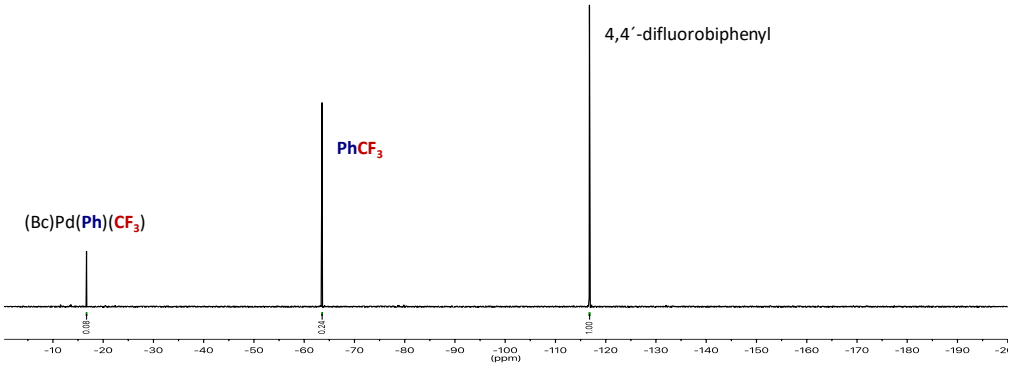

Figure 3.12. ^{19}F NMR spectrum 25 ºC in benzene (acetone-d_6) corresponding to reaction in entry 1, Table 3.5. The assigned signal as [(Bc)Pd(Ph)(CF_3)] (δ = –16.7 ppm) was based on the chemical shift of related species characterized in ref. 4c.

Next, we examined the reactivity of **9** with the bis-(trifluoromethyl) argentates: $\mathbf{6_{Cs}}$ and $\mathbf{6_{NBu4}}$. The tetrabutylammonium salt, $\mathbf{6_{NBu4}}$, gave rise to a moderate 42% of $PhCF_3$ (entry 2 in Table 3.5). This can be ascribed to unproductive pathways as the formation of poly-(trifluoromethyl) complexes and/or oxidation of $\mathbf{6_{NBu4}}$ to Ag(III) (**Figure 3.13**). In sharp contrast, the reaction of $\mathbf{6_{Cs}}$ with **9** yielded an excellent 84% product formation (entry 3 in Table 3.5). This result points out the capability of $\mathbf{6_{Cs}}$ for precluding the formation of side products that could potentially lead to dead-end routes under catalytic conditions using Xantphos as ligand (Figure 3.14).

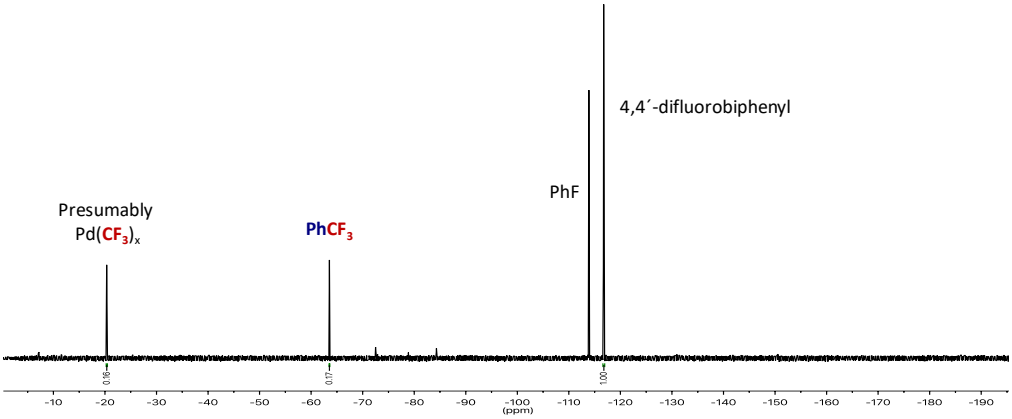

Figure 3.13. ^{19}F NMR spectrum 25 ºC in benzene (acetone-d_6) corresponding to reaction in entry 2 of Table 3.5. The assigned signal as [$Pd(CF_3)_x$] ($\delta \approx$ –20 ppm) was based on the chemical shift of related species characterized in ref. 12.

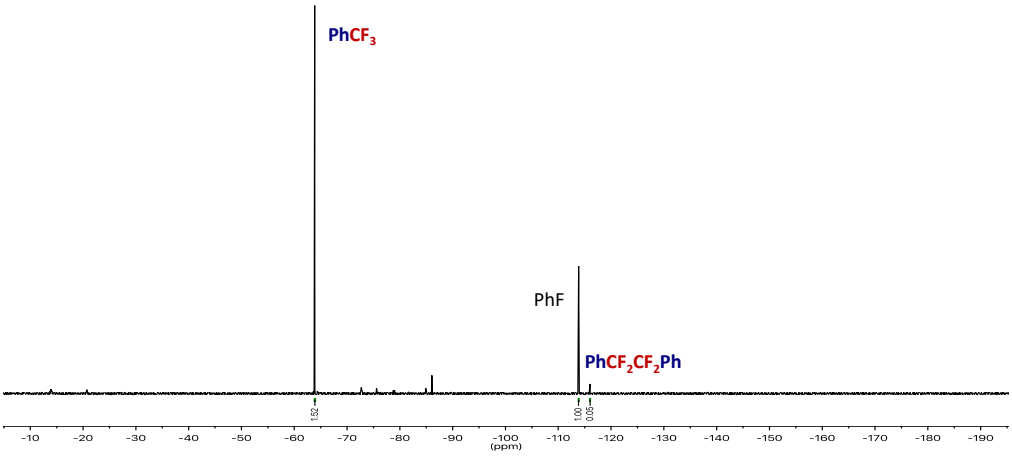

Figure 3.14. ^{19}F NMR spectrum 25 ºC in benzene (acetone-d_6) corresponding to reaction in entry 3, Table 3.5.

As we can see in entries 4-7 of Table 3.5, the widely-used Me_3SiCF_3/F^- mixture is not effective in the formation of $PhCF_3$ from [(Xantphos)Pd(Ph)(I)] (**9**). These experiments, however, provided interesting insights. In the case of using the combination Me_3SiCF_3/CsF, only a 14% of $PhCF_3$ is formed but complete consumption of the Me_3SiCF_3 is observed (Figure 3.15). The formation of HCF_3 suggests that this CF_3^- source decomposes prior to transferring the CF_3 moiety to **9** (as discussed in section 3.1.2.2). The combination of Me_3SiCF_3 with KF or NBu_4F were much less productive. In the former no product formation was observed likely due to solubility issues of the potassium salt. In the latter, full conversion of the Me_3SiCF_3 was observed along with a 4% of $PhCF_3$ and trifluoromethylated palladium complex (as discussed in section 3.1.2.1).

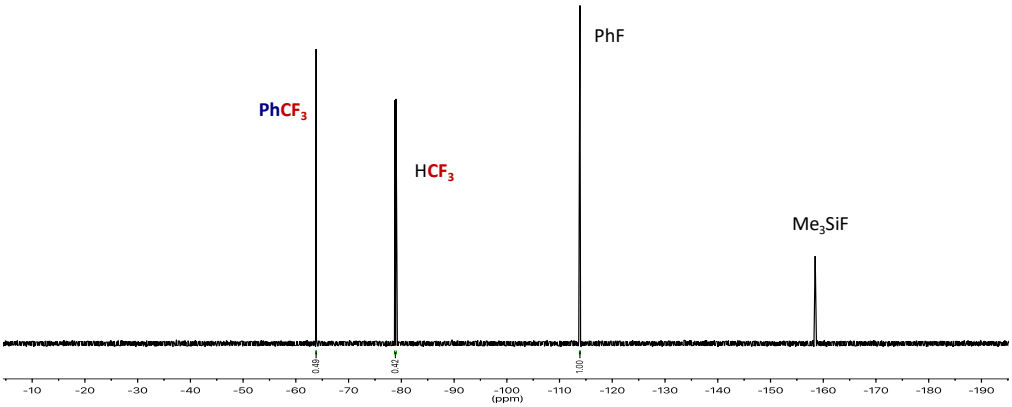

Figure 3.15. ^{19}F NMR spectrum corresponding to the stoichiometric trifluoromethylation of **9** using different CF_3 sources under standard conditions.

We also evaluated the influence of the deviation from the standard reaction conditions when using $\mathbf{6_{Cs}}$ as CF_3 shuttle but we did not observe any improvement of the yield in any case. The reductive elimination was determined to be reasonable fast: in 1 hour, a 69% of product formation was reached (entry 2, Table 3.6). Interestingly, polar and coordinating solvent are detrimental for the reaction to happen in a reasonable yield (entry 3, Table 3.6). The additional Xantphos ligand or the palladium complex was essential for the product formation.

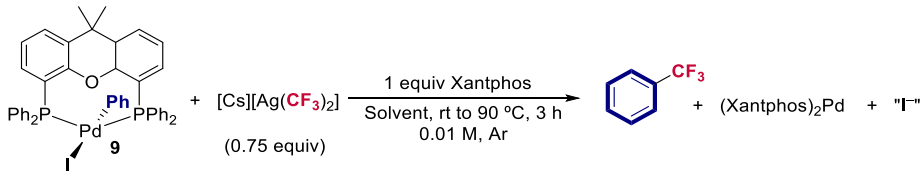

entry	Solvent	Additional deviation from standard conditions	$PhCF_3$ (%)[b)]
1	Benzene	-	84
2	Benzene	1 h, 90 ºC	69
3	THF	-	36
4	Benzene	No Xantphos	42
5	Benzene	No Pd complex	-
6	Benzene	No Xantphos nor Pd complex	-

Table 3.6. Deviation from standard conditions for the reaction between **9** and $\mathbf{6_{Cs}}$.

Collectively, these outcomes disclosed for the first time the one-pot transformation of **9** into the C–CF_3 coupling product. In other words, the possibility to perform two steps of the hypothetic catalytic cycle (transmetalation and reductive elimination) in a consecutive manner from [(Xantphos)Pd(Ph)(I)] complex, the intermediate formed after the oxidative addition step.

3.3.2.2. **Accessing [(Xantphos)Pd(Ph)(CF_3)] from [(Xantphos)Pd(Ph)(I)]**

With these results in hands, we aimed to have a proof of the direct formation of [(Xantphos)Pd(Ph)(CF_3)] (**8**) from [(Xantphos)Pd(Ph)(I)] (**9**) under the reaction conditions optimal for reductive elimination. To do so, we selected [Cs][Ag(CF_3)$_2$] (**6$_{Cs}$**) which was one of the best transmetalating agents in the benchmark palladium system. The reaction of **6$_{Cs}$** with **9** at room temperature in benzene gave rise to the near quantitatively formation of **8** after 10 min.[44]

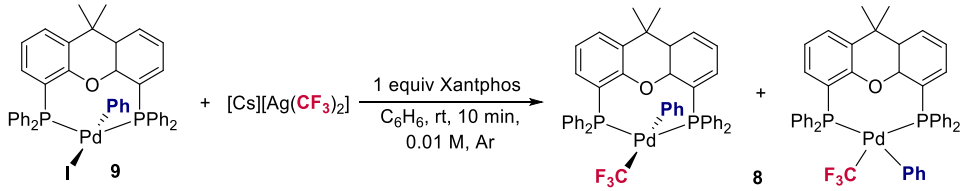

Scheme 3.31. Direct proof of the formation of intermediate **8** using **6$_{Cs}$** as CF_3 source.

Along with the product (*cis* and *trans* isomers), we also detected a small signals corresponding to unknown products (by $^{31}P\{^1H\}$ NMR spectroscopy) and other signals presumably related to the coordination of Xantphos ligand to Ag(CF_3) moiety ($\delta \approx -16$ ppm in ^{31}P NMR spectra and $\delta = -22.4$ ppm in ^{19}F NMR spectra, Figure 3.16 and Figure 3.17, respectively). The formation of the same complex was observed by mixing **6$_{Cs}$** and Xantphos under the same reaction conditions.

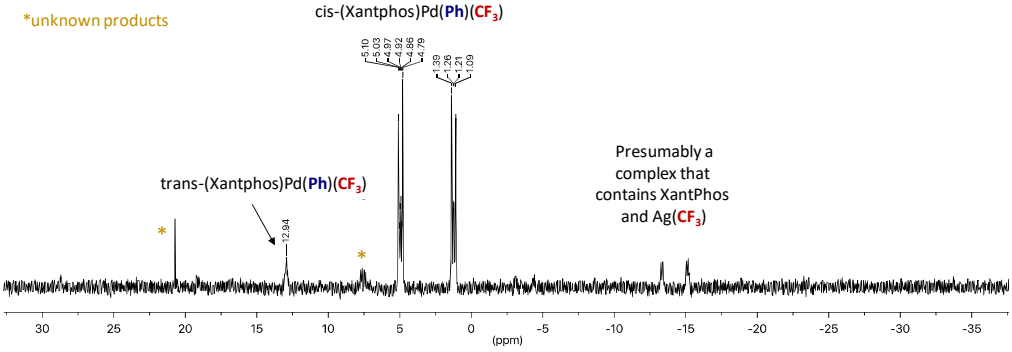

Figure 3.16. $^{31}P\{^1H\}$ NMR spectrum (ns = 1024) at –50 ºC in toluene (acetone-d_6) corresponding to reaction in Scheme 3.31.

[44] This reaction using the Ruppert-Prakash reagent along with the activating agent, does not yield product **9**.

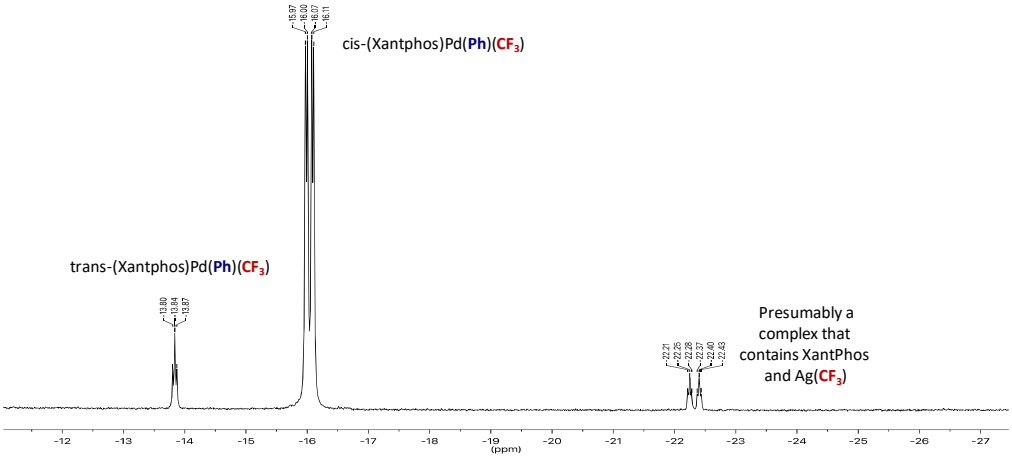

Figure 3.17. ^{19}F NMR spectrum (ns = 64) at -50 ºC in toluene (acetone-d_6) corresponding to reaction in Scheme 3.31.

3.3.2.3. Formation of $PhCF_3$ from PhI.

Based on the aforementioned promising data, we next examined the compatibility of **6_{Cs}**, the most productive transmetalating agent (**Table 3.5**), with all the elementary steps involved in the catalytic cycle under stoichiometric conditions in the presence of PhI (Scheme 3.32). Under the reaction conditions described in Scheme 3.32, we observed a 57% yield of $PhCF_3$ and, interestingly, a 10% of catalytically inactive [(Xantphos)Pd(CF_3)(I)] (**10**), as shown in Figure 3.18. According to Grushin proposal,[6] this product is a consequence of the reaction of [(Xantphos)Pd(Ph)(I)] (**9**) with [(Xantphos)Pd(Ph)(CF_3)] (**8**). This suggests that lower concentration of Pd is needed to prevent this undesired bimolecular reaction. After some screening of conditions, among them the decrease of the concentration, we found that product formation can be obtained in a 91% yield directly from PhI (30 equiv.) without the formation of catalytically inactive [(Xantphos)Pd(CF_3)(I)] (**10**) (Scheme 3.33).

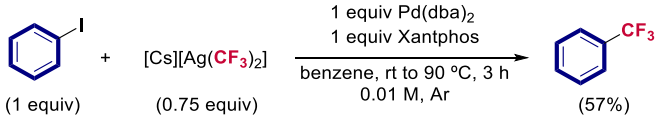

Scheme 3.32. Trifluoromethylation reaction of aryl iodide using **6_{Cs}** and stoichiometric amounts of [$Pd(dba)_2$], a common catalyst in cross-coupling reactions. dba = dibenzylideneacetone. The concentration is referred to the Pd complex ([Pd] = 0.01M).

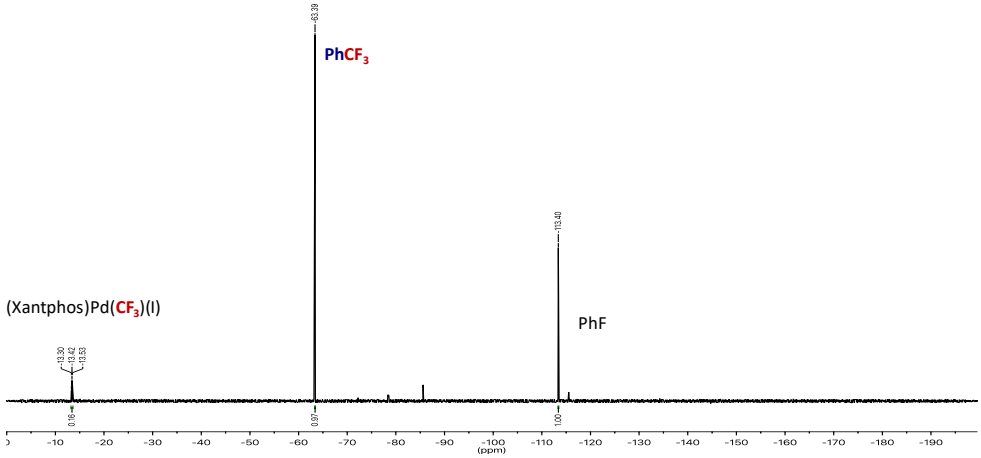

Figure 3.18. ^{19}F NMR spectrum corresponding to the stoichiometric trifluoromethylation of aryl iodide using **6**$_{Cs}$ and [Pd(dba)$_2$] 0.01M in benzene at 90 ºC after 3 hours.

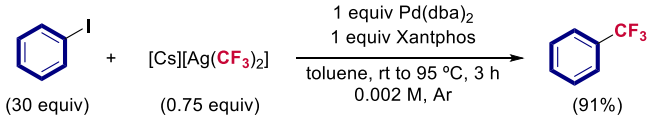

Scheme 3.33. Trifluoromethylation reaction of aryl iodide using **6**$_{Cs}$ and stoichiometric amounts of [Pd(dba)$_2$], a common catalyst in cross-coupling reactions. dba = dibenzylideneacetone. The concentration is referred to the Pd complex ([Pd] = 0.002 M), which is the limiting reagent.

The $^{31}P\{^1H\}$ NMR experiment shows mainly the oxidative addition product [(Xantphos)Pd(Ph)(I)] (Figure 3.19). This result clearly demonstrates the compatibility of **6**$_{Cs}$ as a CF_3 source in the Pd-mediated trifluoromethylation reactions. In other words, a fine tuning of the reaction conditions and the fast nucleophilic trifluoromethylating reagent **6**$_{Cs}$ do not lead to mismatched group exchanges, a sink for Pd in catalysis.

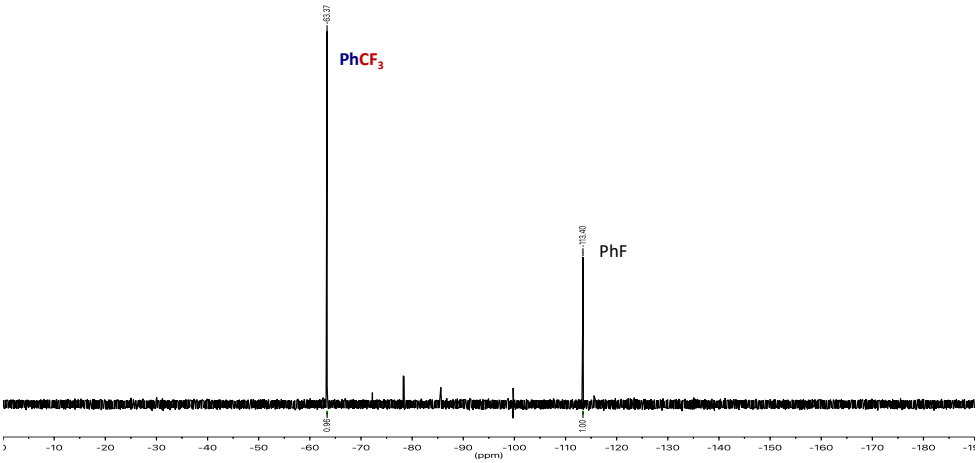

Figure 3.19. ^{19}F NMR spectrum corresponding to the stoichiometric trifluoromethylation of aryl iodide using **6Cs** and $[Pd(dba)_2]$ 0.002M in toluene at 95 ºC after 3 hours.

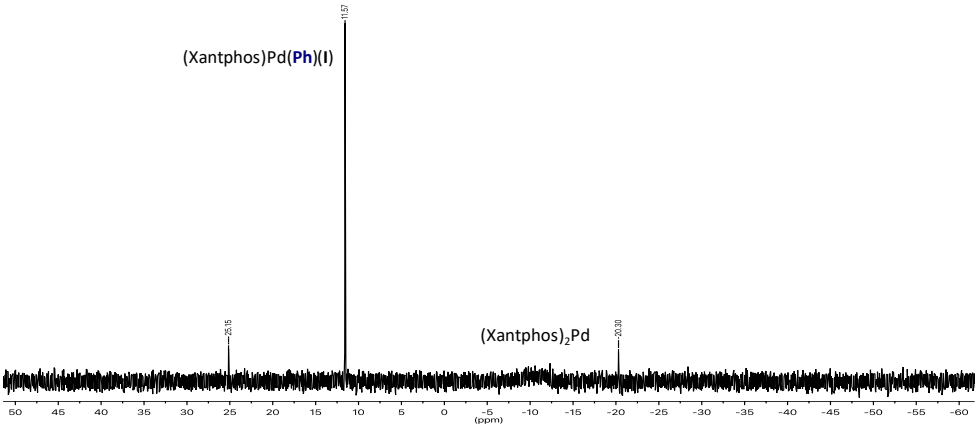

Figure 3.20. $^{31}P\{^1H\}$ NMR spectrum corresponding to the stoichiometric trifluoromethylation of aryl iodide using **6Cs** and $[Pd(dba)_2]$ 0.002M in toluene at 95 ºC after 3 hours.

3.3.2.4. Proof of concept of the viability of the $Pd^{0/II}$-catalyzed trifluoromethylation reaction of aryl halides using 6Cs as CF_3 source and its limitations.

Our experimental results show that, under stoichiometric conditions, **6Cs** is compatible with all the elementary events involved in a hypothetic $Pd^{0/II}$-catalyzed trifluoromethylation reaction of aryl halides under stoichiometric conditions. At this point, we wonder if we could show as a proof-of-concept that **6Cs** could enable the trifluoromethylation of aryl halides using Xantphos as bidentate phosphine ligand under catalytic amounts of palladium.

One of the mayor challenges of using **6Cs** in solution is the limited stability of this complex at the needed temperatures for the reductive elimination process (80 - 100 ºC). We envisioned that this issue could be partially circumvent by adding **6Cs** slowly to the reaction mixture. Once **6Cs** reaches the warm reaction mixture, the CF_3 moiety will be efficiently transferred to the Pd complex prior to decomposition. To avoid decomposition during the addition, we design an experimental setup that allowed the dropwise slow addition of a solution of **6Cs** ensuring the refrigeration up to the point when the drop is released (see Appendix).

Indeed, we can reach the formation of $PhCF_3$ in a 56% yield[45] by slow addition of **6Cs** under catalytic conditions in the presence of 60 equivalents of iodobenzene (Scheme 3.34). Taking into account that the catalyst amount is a 10 mol% per CF_3 transferred, the turnover number of this reaction is close to six. After the reaction by $^{31}P\{^1H\}$ NMR spectroscopy we observed [(Xantphos)Pd(Ph)(I)] (**9**) and signals that may correspond to oxidized phosphine ligand.

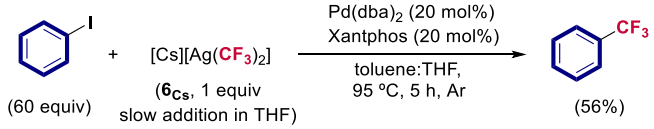

Scheme 3.34. Proof of the catalytic potential of $Pd^{0/II}$-catalyzed trifluoromethylation reaction of aryl iodide using **6Cs** as transmetalating agent. The results are calculated assuming the transfer of the two CF_3 moieties from **6Cs**.

- **Limitations of the system**

There is a substantial difference between the yield of the stoichiometric and the catalytic version of the trifluoromethylation reaction (Scheme 3.33 and Scheme 3.34). Obviously, catalytic conditions are quite different from the stoichiometric ones and diverse parameters have to be taken into account. For instance:

- Complex **6Cs** is only completely soluble in THF and DMF, where the reductive elimination is much more inefficient.[1a,1b,6] In toluene, **6Cs** decomposes with time at room temperature. This means that during the addition of the solution of **6Cs** in THF to the reaction mixture (toluene), the reductive elimination is becoming less efficient.

- Potential secondary reactions between Xantphos and complex **6Cs**, especially in polar solvents, can take place yielding Xantphos-silver complexes (Figure 3.16). This means that the increasing amount of silver during the addition can favor the competition between silver and palladium for the ancillary ligand.

Another interesting results come from the optimization of the reaction conditions of the catalytic proof-of-concept system. We tried the catalysis using one equivalent of a solid

[45] This yield is calculated respect to the initial amount of CF_3 moieties in **6Cs** which is the limiting reagent.

substrate, 4-iodoacetophenone (Scheme 3.35),[46] which was the limiting reagent (instead of the silver in Scheme 3.34). Interestingly, we observed the formation of two different products: 4-(trifluoromethyl)acetophenone and α,α,α-trifluorotoluene.

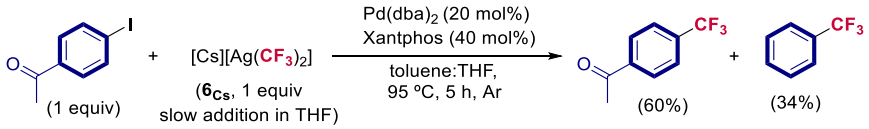

Scheme 3.35. Proof of the catalytic potential of $Pd^{0/II}$-catalyzed trifluoromethylation reaction of aryl iodide using $\mathbf{6_{Cs}}$ as transmetalating agent. Reaction yields considering the 4-iodoacetophenone as limiting reagent.

This suggests that the formation of this unexpected product ($PhCF_3$) is consequence of an additional, yet neglected, side reaction which can take place in the reaction media. This potential side reaction may be related to an aryl-aryl scrambling between aryl of the phosphine ligand attached to the palladium and the aryl moiety that comes from the oxidative addition events.[47] The proposed reaction mechanism for this aryl/aryl scrambling is depicted in Scheme 3.36 and entails an intramolecular reductive elimination/oxidative addition sequence *via* formation of a phosphonium salt intermediate.

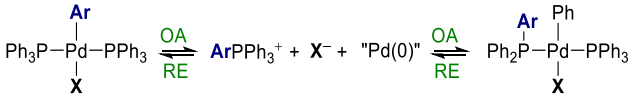

Scheme 3.36. Proposed mechanism for the aryl/aryl scrambling in phosphine-stabilized aryl-Pd(II) complexes.

The origin of this side reaction in our system is potentially related to the introduction of polar solvents (THF) to the reaction media. This suggests that the use of this solvent is detrimental and the origin of potential deactivation pathways.[48] As we will discuss in Chapter 3, this side reaction can be prevented by changing the aromatic substituents in the phosphine ligand by aliphatic ones. However, this means a design of a ligand that still has to promote the reductive elimination event.

Despite the moderate yields of the "catalytic" trifluoromethylation reactions and the above-mentioned downsides, these preliminary outcomes (Scheme 3.34 and Scheme 3.35) are the first "catalytic" examples of the trifluoromethylation of aryl halides using $Pd^{0/II}$ platform with a bidentate phosphine ligand. Further studies should be performed in this venue, especially involving the design of new transmetalating agents.

46 We thought that the small amounts of PhI, which is liquid, may be partially in the head space of the set up.

47 a) Goodson, F. E.; Wallow, T. I.; Novak, B. M. *J. Am. Chem. Soc.* **1997**, *119*, 12441. b) Grushin, V. V. *Organometallics* **2000**, *19*, 1888. c) Fiebig, L.; Schlörer, N.; Schmalz, H.-G.; Schäfer, M. *Chem. Eur. J.* **2014**, *20*, 4906.

48 To a lesser extent, this reaction can also take place in apolar solvents.

3.4. Conclusions

In summary, in Chapter 3, we have discussed the synthesis and characterization of several "$AgCF_3$"-containing complexes. The combination of several techniques including DOSY NMR spectroscopy and DFT calculations were key for the elucidation of the both components of the equilibrium of **4** in polar solvents (**4a**/**4b**). We also disclosed the unprecedented synthesis of $\mathbf{6}_{Cs}$ and $\mathbf{6}_{NBu4}$.

Moreover, the synthetized trifluoromethylsilver(I) compounds were compared to commercially available nucleophilic CF_3 sources towards a benchmark aryl-Pd(II) complex bearing a strong coordinating phosphine ligand, dppp. This study showed the exceptional transmetalating activity of some of the well-defined silver complexes (**4**, $\mathbf{6}_{Cs}$, $\mathbf{6}_{NBu4}$) versus the commercially available sources and other "$AgCF_3$" complexes (**3**). All the gathered information from the benchmark system was then translated to a C–CF_3 bond-forming productive system, [(Xantphos)Pd(Ph)(I)] (**9**). Hence, we overcome the challenges associated to the transmetalation for the formation of [(Xantphos)Pd(Ph)(CF_3)] (**8**) or directly the formation of Ph–CF_3 product. The compatibility of the silver species with all the steps of an hypothetic catalytic cycle allow us to design, as proof-of-concept, a catalytic version of $Pd^{0/II}$-catalyzed trifluoromethylation reaction of phenyl iodide using Xantphos as ancillary ligand for the first time.

This work reinforces that not only the reductive elimination can be challenging in Pd-catalyzed trifluoromethylation reactions but also undesired transmetalation side reactions. Thus, we proved how the transmetalation event can be decisive in enabling or preventing the product formation. We think that all the gathered knowledge during this project would provide an initial platform for the design of new transmetalating agents and the development of new methodologies.

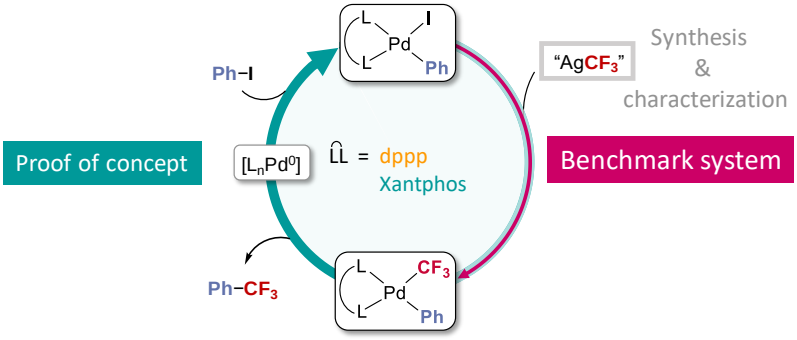

Figure 3.21. Graphical summary of the Chapter 3.

3.5. Appendixes

3.5.1. Experimental appendix

3.5.1.1. General procedures

All reactions were conducted in an argon-filled glovebox (mBraun Unilab 4420) with concentrations of O_2 and H_2O < 0.1 ppm or oven-dried glassware (at 100 ºC overnight and cooled under vacuum prior use) using Schlenk techniques under argon atmosphere (otherwise mentioned). NMR spectra were obtained on a Bruker 400 MHz, a 500 MHz or a 500 MHz with cryoprobe spectrometers equipped with probeheads capable of producing gradients in the z direction with a maximum strength of 53.5 G·cm^{-1}. ^{1}H, ^{13}C, ^{19}F and ^{31}P NMR chemical shifts are reported in parts per million (ppm), relative to tetramethylsylane (TMS) for ^{1}H and ^{13}C with the residual solvent peak used as an internal reference, relative to $CFCl_3$ (Freon) for ^{19}F and relative to 85% H_3PO_4 for ^{31}P. In the ^{19}F and ^{31}P NMR spectra registered in non-deuterated solvents, a coaxial tube containing acetone-d_6 or dimethylsulfoxide-d_6 was used to maintain the lock ^{2}H signal. Multiplicities are reported as follows: singlet (s), doublet (d), broad doublet (bd), doublet of doublets (dd), doublet of quadruplets (dq), triplet (t), quadruplet (q), doublet of quadruplet of quadruplets (dqq) and multiplet (m). ^{19}F NMR yields for stoichiometric reductive elimination studies were obtained on a Bruker 400 MHz spectrometer using fluorobenzene (–113.4 ppm) or 4,4'-difluorobenzene (–116.8 ppm) as internal standard with 32 scans for data acquisition. All diffusion ^{1}H and ^{19}F NMR experiments were carried out on dilute solutions (about 2 mg of product dissolved in 0.6 ml of the corresponding solvent for compound **4**) at 25 ºC to minimize the effect of different solution viscosities for different samples, which were confirmed from the diffusion coefficient value of the residual solvent signal taken as internal reference. To check the presence and effective suppression of deleterious convection effects, a test LEDBP experiment was recorded for the first sample with and without sample rotation, and the results were compared to data obtained from double-stimulated echo sequence.[49] Thus, we decided to run DOSY experiments for all samples using the double-stimulated echo sequence incorporating bipolar gradient pulses and a longitudinal eddy current delay (dstegp3s in the Bruker library) and without sample rotation. The gradient strength was linearly incremented in 16 steps from 2% up to 95% of the maximum gradient strength. Diffusion times and gradient pulse durations were optimized for each experiment in order to achieve a 95% decrease in the resonance intensity at the largest gradient amplitude; typically, diffusion times (Δ) of 150 ms and bipolar rectangular gradient pulses (δ) of 1.0 were employed. The longitudinal eddy current delay was held constant to 5 ms, whereas the gradient pulse recovery time was set to 100 μs. Data were processed with the standard DOSY program included into the Bruker TOPSPIN software package. The accuracy of the measurements was confirmed by obtaining the same

[49] Esturau, N.; Sanchez-Ferrando, F.; Gavin, J. A.; Roumestand, C.; Delsuc, M. A.; Parella, T. *J. Magn. Reson.* **2001**, *153*, 48.

experimental ^{1}H and ^{19}F diffusion coefficient value from two different ^{1}H and ^{19}F measurements of same NMR sample. The estimation of the hydrodynamic radius was performed according to the Stokes-Einstein equation using the viscosities values of $6 \cdot 10^{-4}$ kg·(m·s)$^{-1}$ (THF), $4.6 \cdot 10^{-4}$ kg·(m·s)$^{-1}$ (benzene) and $7.9 \cdot 10^{-4}$ kg·(m·s)$^{-1}$ (DMF) at 25 ºC.[50] High Resolution Mass Spectrometry (HRMS) data was recorded on a LCT-Premier (Waters) or a MicroTOF Focus (Bruker Daltonics) mass spectrometers using ESI ionization technique and dichloromethane or tetrahydrofuran as solvent.

The details for the X-ray structure determination can be found in page - 147 -.

3.5.1.2. Materials and methods

Bathocuproine (Bc), Bathophenantroline (BPhen), 1,3-Diisopropylimidazolinium chloride (SIPr · HCl), iodobenzene, fluorobenzene, 4,4'-difluorobiphenyl, Me_3SiCF_3, Et_3SiCF_3, [(Phen)Cu(CF_3)], [Pd(PPh_3)$_4$], [Pd(dba)$_2$], 1,3-bis(diphenylphosphino)propane (dppp) and Xantphos were used without further purification directly as received from the commercial supplier, and stored under inert gas and/or low temperature when required. If necessary, the solvents (Hexane, THF, CH_2Cl_2, toluene, Et_2O) were used from a solvent purification system *pure-solv* (SPS-400, Innovative Technology) and stored under argon over activated 4 Å molecular sieves. Anhydrous benzene and cyclohexane were used without further purification Deuterated solvents (C_6D_6, THF-d_8, DMF-d_7, CD_2Cl_2) were stored under argon over activated molecular sieves 4 Å. [(Xantphos)Pd(Ph)(I)],[1b] [(dppp)Pd(Ph)(I)][1a] and [(SIPr)AgCl][51] were synthesized according to previous literature procedures. All the silver complexes are light-sensitive, so the reactions are performed in the dark to be preserved from light to avoid photodecomposition.

3.5.1.3. Modified synthesis of [(SIPr)Ag(CF_3)] (3)

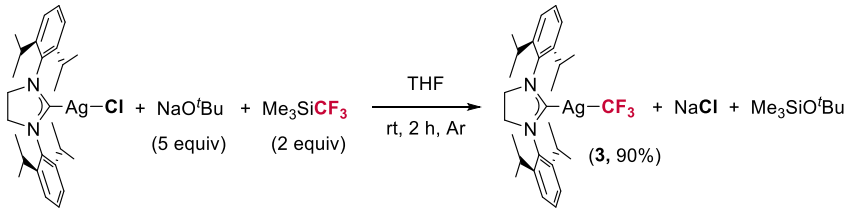

Scheme A3.1.Synthesis of **1**.

Complex **3** was prepared by a modification of the reported procedure.[28] In an argon atmosphere glovebox, SIPrAgCl[51] (100 mg, 0.18 mmol, 1 equiv) and NaO^{t}Bu (90.0, 0.9 mmol, 5 equiv) were added to an oven-dried Schlenk and 20 ml of THF were added. A solution of Me_3SiCF_3 (67 µL, 0.45 mmol, 2 equiv) in THF (5 ml) was added dropwise and the solution was

[50] Lide, D. R. (**2004**), CRC Handbook of Chemistry and Physics, 85th Edition, CRC Press, Boca Raton, FL.
[51] Fremont, P. De; Scott, N. M.; Stevens, E. D.; Ramnial, T.; Lightbody, O. C.; Macdonald, C. L. B.; Clyburne, J. A. C.; Abernethy, C. D.; Nolan, S. P. *Organometallics* **2005**, *24*, 6301.

stirred 2 h at room temperature outside the glovebox. After that, the solution was filtered through a celite pad and the solvent was removed under reduced pressure. The residue was precipitated in a mixture of THF: hexane (1 ml: 15 ml) and the white solid was dried under vacuum to afford **3**. Yield: (95.7 mg; 90%). The ^{1}H and ^{19}F NMR spectra are in accordance with the previously reported one.[28] The complex must be stored at –30 ºC under inert atmosphere to avoid decomposition.

3.5.1.4. **Synthesis and characterization of [(Bc)Ag(CF$_3$)] (2)**

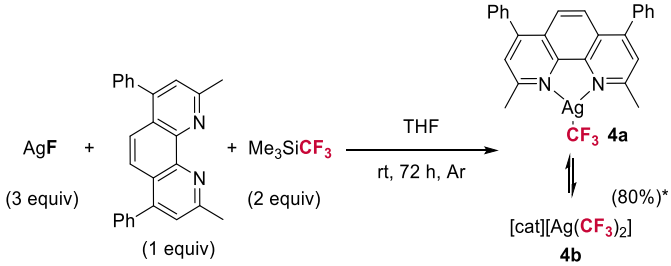

Scheme A3.2. Synthesis of **4**.

In an argon atmosphere glovebox, AgF (130 mg, 1.02 mmol, 2 equiv) and Bathocuproine (173 mg, 0.48 mmol, 1 equiv) were added to an oven-dried Schlenk containing a magnetic stir bar. The Schlenk flash was capped with a septum. Then, THF (30 ml) was added and the mixture was stirred at room temperature for 30 min. In parallel, a solution of Me_3SiCF_3 (0.15 ml, 1.0 mmol, 2 equiv.) in THF (5 ml) was prepared and it was added dropwise to the silver suspension and the mixture was stirred for 24 h. After that, the solution was filtered through cannula to other Schlenk with AgF (65 mg, 0.51 mmol, 1 equiv.) previously weighted in the glovebox. The solution was left stirring for 48 h at rt. After that, the solution was filtered through cannula and the solvent was removed under reduced pressure. The solid residue was washed with hexane (2 x 10 ml) and the white-yellow solid was dried under vacuum to afford **4** (206.3 mg, 80% yield). The complex can be stored indefinitely at –30 ºC under inert atmosphere in the dark for months without any sign of decomposition.

Characterization in THF: ^{1}H NMR (500 MHz, THF-d_8, 25 ºC): δ 7.82 (s, 2H), 7.68 (s, 2H), 7.58–7.49 (m, 10H), 3.03 (s, 6H). **$^{13}C\{^{1}H\}$ NMR** (126 MHz, THF-d_8, 25 ºC): δ 159.72, 150.63, 145.88, 139.01, 130.67, 129.65, 125.80, 125.51, 124.07, 27.01. No signal for *C*F$_3$ was observed due to the low signal-to-noise ratio. **^{19}F NMR** (470 MHz, THF-d_8, 25 ºC): δ –21.84 (2d, $^{2}J_{^{109}Ag,F}$ = 122.3 Hz, $^{2}J_{^{107}Ag,F}$ = 107.0 Hz, **2a**), –27.18 (2d, $^{2}J_{^{109}Ag,F}$ = 100.7 Hz, $^{2}J_{^{107}Ag,F}$ = 87.2 Hz, **2b**). **HRMS-electrospray (-) in tetrahydrofuran** (m/z): $[M]^-$ calcd. for C_2AgF_6, 244.8955 and 246.8952; found 244.8962 and 246.8965. **Characterization in DMF:^{1}H NMR** (500 MHz, DMF-d_7, 25 ºC):

δ 7.97 (s, 2H), 7.86 (s, 2H), 7.73 - 7.60 (m, 10H), 3.02 (s, 6H). **$^{13}C\{^{1}H\}$ NMR** (126 MHz, DMF-d_7, 25 ºC): δ 160.15, 151.78, 143.80, 138.12, 130.95, 130.33, 130.10, 126.82, 126.25, 124.78, 28.20. No signal for *C*F$_3$ was observed due to the low signal-to-noise ratio. **^{19}F NMR** (470 MHz, DMF- d_7, 25 ºC): δ –19.19 (broad, **2a**), –24.98 (2d, $^{2}J_{^{109}Ag,F}$ = 98.7 Hz, $^{2}J_{^{107}Ag,F}$ = 84.6 Hz, **2b**). **Characterization in benzene: ^{1}H NMR** (500 MHz, C_6D_6, 25 ºC): δ 7.52 (s, 2H), 7.31 - 7.10 (m, 10H, overlapping peaks with C_6D_6), 6.93 (s, 2H), 2.81 (s, 6H, C*H*$_3$). **$^{13}C\{^{1}H\}$ NMR** (126 MHz, C_6D_6, 25 ºC): δ 158.61, 148.55, 146.48, 138.85, 129.98, 128.68, 128.35, 124.96, 124.03, 123.17, 26.10. No signal for *C*F$_3$ was observed due to the low signal-to-noise ratio. **^{19}F NMR** (470 MHz, C_6D_6, 25 ºC): δ –19.24 (bd).

3.5.1.5. Studying the dynamic behavior of 4 (4a/4b) and characterization of the cation for 4b

- **Analyzing the behavior of 4 (4a/4b) in different solvent.**

The first evidence of the equilibrium between **4a** and **4b** came from the solvent dependence of the proportion of each species. In this regard, NMR samples of **4** at a concentration of $6.2 \cdot 10^{-3}$ M in different solvents (THF, DMF and benzene) were prepared at room temperature inside the glovebox. In THF and DMF, **4** generated a mixture of the neutral [(Bc)Ag(CF_3)] (**4a**) and the ionic [cat][Ag(CF_3)$_2$] (**4b**) in different proportions while, in benzene, we exclusively observed [(Bc)Ag(CF_3)] (**4a**) (Table A3.1).

This supports that **4** (as **4a** and **4b**) is an equilibrium and that **4b** is an ionic species which concentration is favored in more polar solvents.

Solvent	ε (D) 20 ºC**	4a*	4b
Benzene	2.28	100	-
THF	7.52	98	2
DMF	38.52	66	34

Table A3.1. Different proportions between **4a** and **4b** of **4** in different solvents at the same concentration. **The value has been obtained from ref. 52. *The ratio between species **4a** and **4b** was taken directly by the integration of the corresponding signals in ^{19}F NMR spectroscopy 25 ºC

- **Further investigations on the behavior of 4 (4a/4b): the addition of free ligand.**

We also wondered if the addition of free ligand would result in the splitting of different signals by ^{1}H NMR spectroscopy. However, as we can see in Figure A3.1, the additional free ligand do not affect the ^{1}H NMR spectrum of the equilibrium. This suggests that this free ligand could somehow participate in the chemical exchange process.

52 https://www.organicdivision.org/wp-content/uploads/2016/12/organic_solvents.html

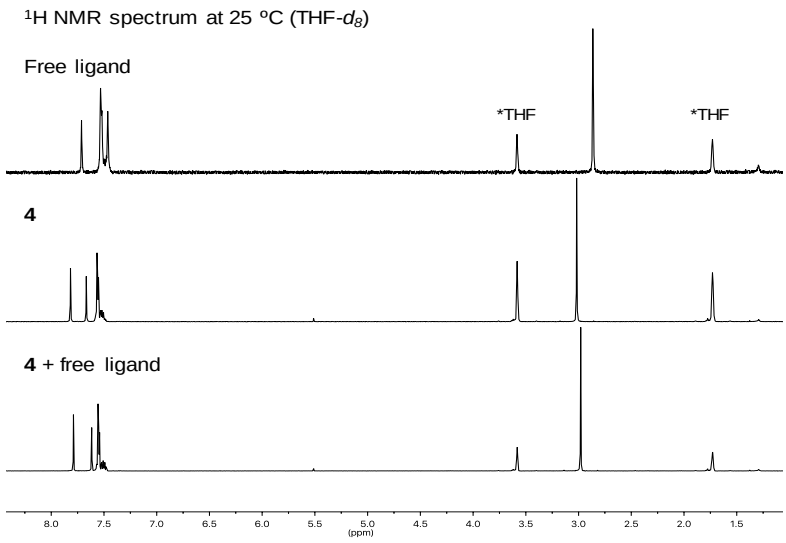

Figure A3.1. ^{1}H NMR spectra at room temperature in THF-d_8 of free ligand, **4** complex (**4a**/**4b**) and the addition of free ligand to **4** in solution.

- **^{19}F NMR 2D EXSY experiment of 4 (4a/4b)**

A simple way of confirming the chemical equilibrium between **4a** and **4b** in solution by NMR spectroscopy is performing 2D EXSY (Exchange SpectroscopY). This two-dimensional experiment uses the scheme of commonly-known 2D NOESY (Nuclear Overhauser Effect Spectroscopy) experiment and offer information about dynamic processes such as chemical or conformational exchanges that are slow in the NMR time scale.[53] From a practical point of view, 2D EXSY spectra provide cross-peaks for separated signals that are involved in a dynamic process such as chemical exchange (chemical equilibrium).

We used 2D ^{19}F EXSY experiments of **4** in THF and DMF in order to see if there are cross-peaks for the signals assigned to **4a** and **4b**.

[53] Perrin, C. L.; Dwyer, T. J. *Chem. Rev.* **1990**, *90*, 935.

• EXSY ^{19}F NMR spectrum of **4** at 25 ºC (DMF-d_7) • EXSY ^{19}F NMR spectrum of **4** at 25 ºC (THF-d_8)

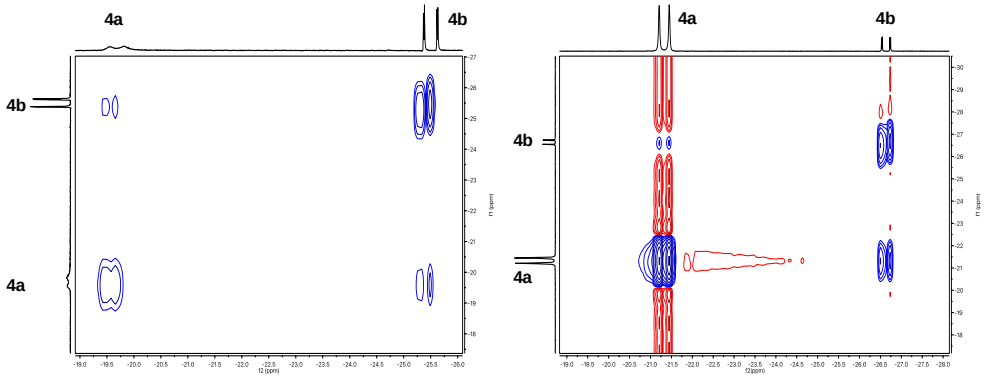

Figure A3.2. EXSY ^{19}F spectra showing the cross-peaks corresponding to the chemical exchange between **4a** and **4b**.

- **NMR line-shape analysis of** 4 **(**4a*/*4b**)**

NMR line-shape analysis is based on the fact that the shape of the NMR signal is related to the rate of the exchange processes. For example, a fast dynamic process at a given temperature may result on a broad signal in a NMR spectrum. Since the rate of an exchange process depends on the temperature, the shape of the NMR signal can be modified by varying the temperature of the experiment (broadening, coalescence and sharpening). This line-shape analysis is quite useful when certain signals coalesce as result of a fast dynamic exchange at a given temperature. We wonder if this is the case of the single set of signals of **4** by ^{1}H NMR spectrum.

In this regard, ^{19}F NMR and ^{1}H NMR spectra of a solution of **4** ($6\cdot10^{-3}$ M) in THF-d_8 were recorded at an array of different temperatures from 25 ºC to –90 ºC.[54] Once reached the lowest temperature, the spectra were recorded while increasing the temperature up to 25 ºC again. Remarkably, for both ^{1}H and ^{19}F NMR spectra (Figure A3.3 and Figure A3.4), the pattern of the signals remained invariable and no splitting in the signals of the ^{1}H NMR spectra was observed.

Collectively, these results suggest that there are different regimes for the ^{1}H-involving equilibrium between **4a** and **4b** and the ^{19}F-involving one. The rearrangement of the bathocuproine ligands is presumably involved in a fast-dynamic exchange process faster than the ^{1}H NMR time scale, giving rise to one set of signals by ^{1}H NMR spectroscopy even at low temperature. On the other hand, the trifluoromethyl group exchange is likely a slow-dynamic process that allows the detection of both different species by ^{19}F NMR spectroscopy.

[54] Prepared in the glovebox at room temperature.

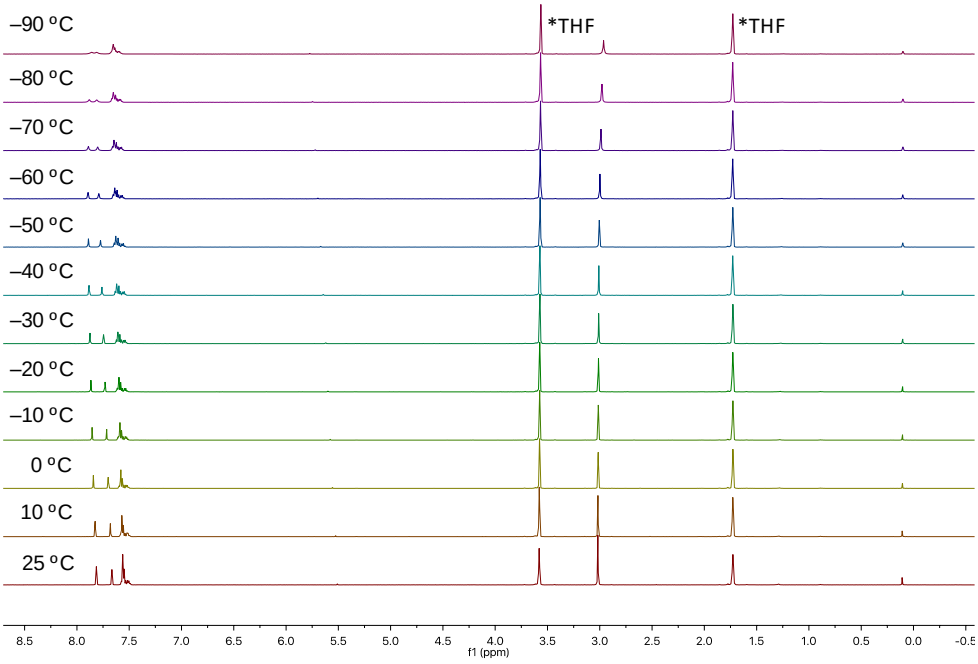

Figure A3.3. Variable temperature ^{1}H NMR spectrum of **4** (THF-d_8).

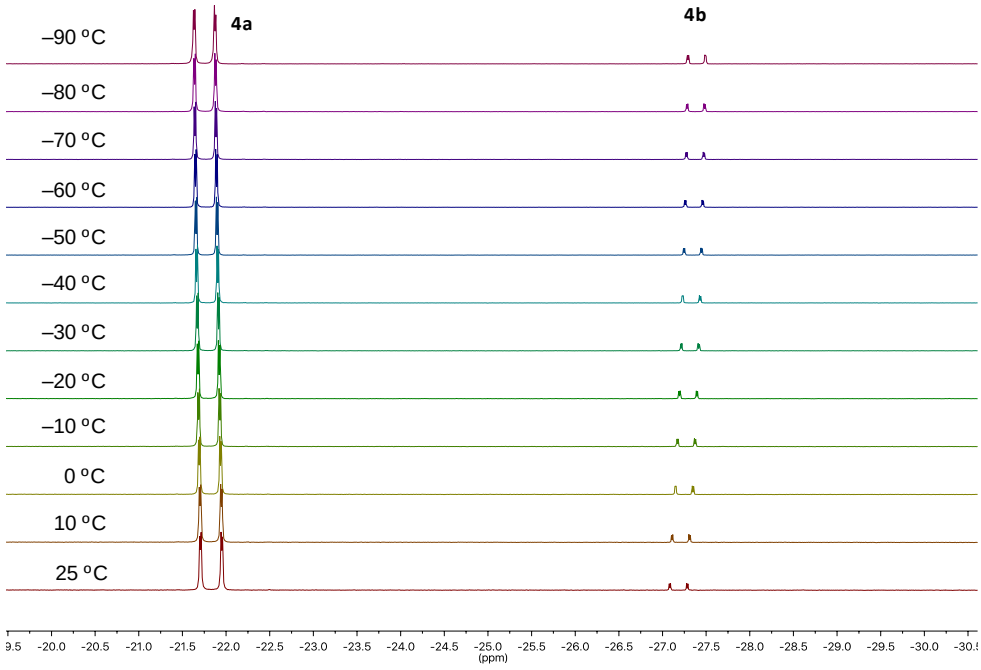

Figure A3.4. Variable temperature ^{19}F NMR spectrum of **4** (THF-d_8).

- **Independent synthesis of plausible cations for 4b**

Although the above-mentioned experiments confirms that **4a**/**4b** is an equilibrium and explain the observations by ^{1}H and ^{19}F NMR spectroscopy, no information is provided about the nature of the cation in [cat][Ag(CF_3)$_2$] (**4b**). For this reason, we aimed at the independent synthesis and characterization of potentially related cations to [cat][Ag(CF_3)$_2$] (**4b**). Initially, we hypothesized that the structure of this salt (**4b**) was [(Bc)$_2$Ag][Ag(CF_3)$_2$], by analogy to related copper compounds.[55]

- Synthesis and characterization of [(Bc)$_2$Ag][SbF_6] (**5**)

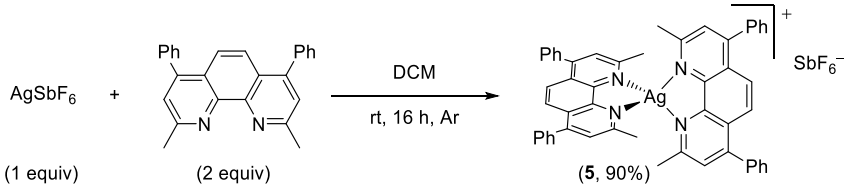

Scheme A3.3. Synthesis of **5**.

In an argon atmosphere glovebox, $AgSbF_6$ (50 mg, 0.15 mmol, 1 equiv.) and bathocuproine (108 mg, 0.30 mmol, 2 equiv.) were added to an oven-dried Schlenk containing a magnetic stir

[55] Morimoto, H.; Tsubogo, T.; Litvinas, N. D.; Hartwig, J. F. *Angew. Chem. Int. Ed.* **2011**, *50*, 3793.

bar. DCM (50 ml) was added and the mixture was stirred at room temperature overnight. After that, the solution was filtered through cannula and the mixture was concentrated to 5 ml and hexane was added to precipitate the product. The solid residue was washed with hexane (2 x 10 ml) and the white solid was dried under vacuum to afford **5** (144 mg, 90% yield).

Characterization in DCM: ^{1}H NMR (500 MHz, CD_2Cl_2, 25 ºC): δ 8.00 (s, 4H), 7.75 (s, 4H), 7.66–7.55 (m, 20H), 2.89 (s, 12H) ppm. **^{13}C{^{1}H} NMR** (126 MHz, CD_2Cl_2, 25 ºC): δ 158.66, 151.62, 143.53, 137.57, 130.12, 129.78, 129.50, 126.25, 125.85, 124.40, 28.25 ppm. **HRMS-electrospray in dichloromethane** (m/z): $[M]^+$ calcd. for $C_{52}H_{40}AgN_4$, 827.2304 and 829.2301; found 827.2319 and 829.2337. **Characterization in THF: ^{1}H NMR** (500 MHz, THF-*d*$_8$, 25 ºC): δ 8.05 (s, 4H), 7.92 (s, 4H), 7.69 - 7.54 (m, 20H), 2.94 (s, 12H) ppm. **^{13}C{^{1}H} NMR** (126 MHz, THF- *d*$_8$, 25 ºC): δ 159.45, 151.79, 143.64, 137.95, 130.35, 129.78, 129.53, 126.28, 126.16, 124.46, 27.73 ppm.

- Synthesis and characterization of $[(Bc)Ag(THF)][SbF_6]$

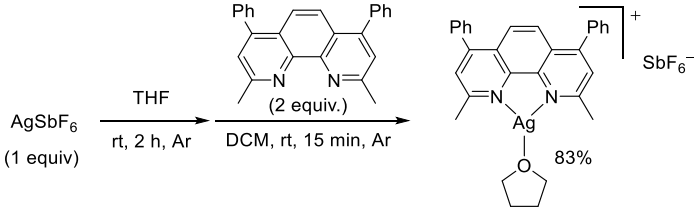

Scheme A3.4. Synthesis of $[(Bc)Ag(THF)][SbF_6]$.

In an argon atmosphere glovebox, $AgSbF_6$ (10 mg, 0.029 mmol, 1 equiv.) was dissolved in 10 ml of THF and the solution was stirred for 2 hours at room temperature. To this solution was added a solution of bathocuproine (10.4 mg, 0.029 mmol, 1 equiv.) in 1 ml of CH_2Cl_2 and the mixture was stirred 15 min at room temperature. Then, the mixture was concentrated to 1 ml and hexane was added to precipitate the product. The white solid was washed with hexane (2 x 5 ml) and it was dried under vacuum at low temperature to yield $[(Bc)Ag(THF)][SbF_6]$ (13 mg, 83% yield). The complex was stored at –32 ºC to avoid decomposition. We observe the formation of complex $[(Bc)Ag(THF)][SbF_6]$ after exposure of complex **5** to THF by single crystal X-ray diffraction.

Characterization in DCM: ^{1}H NMR (500 MHz, CD_2Cl_2, 25 ºC): δ 7.92 (s, 2H), 7.76 (s, 2H), 7.62–7.56 (m, 10H), 3.83 (m, 4H, THF), 3.03 (s, 6H, CH_3), 1.90 (m, 4H, THF) ppm. **^{13}C{^{1}H} NMR** (126 MHz, CD_2Cl_2, 25 ºC): δ 158.66, 152.10, 142.75, 137.40, 130.13, 129.63, 129.36, 126.24, 126.07, 124.41, 69.74, 28.77, 26.15 ppm.

- Comparison of [(Bc)Ag(THF)][SbF_6] and [$(Bc)_2Ag$][SbF_6] (**5**) by ^{1}H NMR spectroscopy

With a reliable route in hands to access to two candidates for the cation in [cat][$Ag(CF_3)_2$] (**4b**), $[(Bc)_2Ag]^+$ (cation in **5**) and $[(Bc)Ag(THF)]^+$, we decided to compare their ^{1}H NMR spectra in order to extract any valuable information. It is noteworthy that, the chemical shift of the aromatic part in [(Bc)Ag(THF)][SbF_6] and **5** complex is practically identical so we could not identify them as a hypothetical mixture using this technique. When comparing the ^{1}H NMR spectra of [(Bc)Ag(THF)][SbF_6] and **5** to **4**, we found that, although the chemical shift is slightly different,[56] the pattern of signals is quite similar so we can discard any of those cations to be present in the equilibrium as counterpart of **4b**.

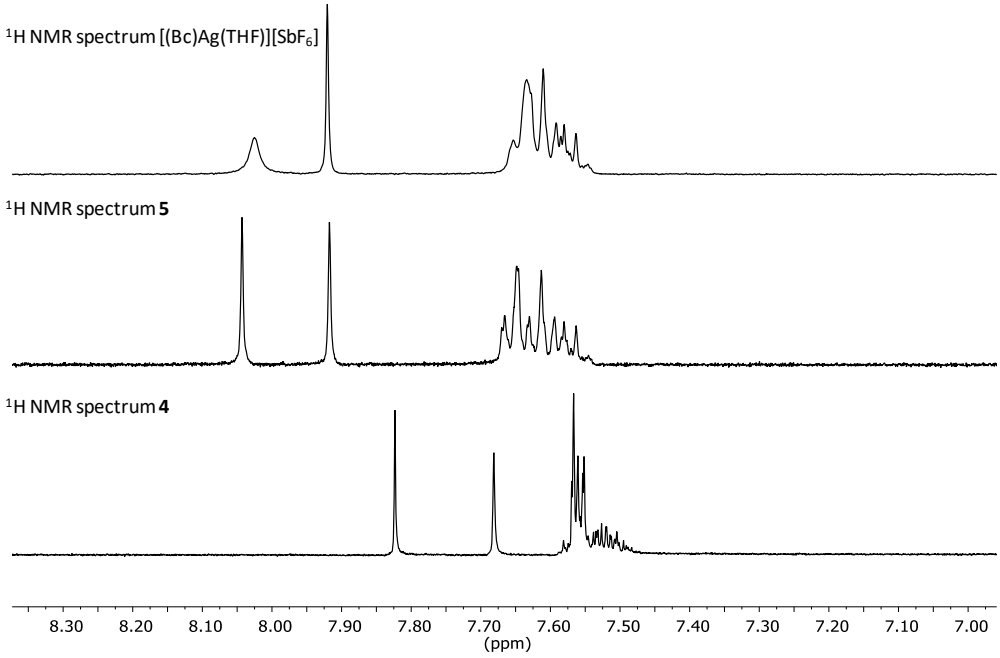

Figure A3.5. ^{1}H NMR spectra of **4**, **5** and [(Bc)Ag(THF)][SbF_6]. Only the aromatic signals in the complexes (from approx. 7 ppm to approx. 8.3 ppm) are shown.

- **^{1}H 2D DOSY experiments**

The unexpected striking nature of the cation of **4b** prompts us to utilize Diffusion-Ordered SpectroscopY (DOSY) ^{1}H and ^{19}F NMR spectroscopy experiments. As mentioned in the main text, this technique can be used to obtain the molecular size of a given molecule by NMR spectroscopy. Fundamentally, this experiment consist of the application of electromagnetic field gradients on a direction to physically locate a molecule in that axis and so characterize the

[56] Likely due to the different counter anion ($[SbF_6]^-$ *vs.* $[Ag(CF_3)_2]^-$).

diffusion coefficient. As a results, this allows to obtain a 2D plot with the chemical shift (δ) on the horizontal axis and logarithm of the diffusion coefficient (log(*D*)) on the vertical axis.[57]

The diffusion coefficient is related to the molecular dimensions through eq. 1, where K_B is the Boltzmann constant, T is the absolute temperature and f is the hydrodynamic friction coefficient. This is the component in the equation related to the size and shape of the molecule.

$$D = \frac{K_B \cdot T}{f} \qquad (\text{eq. } 1)$$

When ideally considering a spherical molecule, the hydrodynamic friction coefficient, f, is related to the viscosity of the solution, η, and the hydrodynamic radius of the sphere, R_H, through the Stokes equation (eq. 2).

$$f = 6\pi \cdot \eta(T) \cdot R_H \qquad (\text{eq. } 2)$$

The combination of both eq. 1 and eq. 2 gives the Stokes-Einstein equation (eq. 3) that shows how the diffusion coefficient inversely depends on the size of a molecule.

$$D = \frac{K_B \cdot T}{6 \cdot \eta(T) \cdot \pi \cdot R_H} \qquad (\text{eq. } 3)$$

We hypothesized that by measuring the diffusion coefficient (*D*) and so obtaining the hydrodynamic radius (R_H) of the different species in solution, it is possible to get insights into the structure of the non-intuitive cation of **4b**. To do so, all diffusion ^{1}H and ^{19}F NMR experiments were carried out on dilute solutions (approx. $6.2 \cdot 10^{-3}$ M) at 25 ºC to keep constant the viscosity of the different samples.[58] For comparison purposes, we selected two standards based on their size and potential participation in the investigated chemical equilibrium: free bathocuproine ligand (**Bc**) and $[(Bc)_2Ag][SbF_6]$ (**5**), as it contains independently the cation of the initially assumed.

[57] Claridge, T. D. W. Diffusion NMR spectroscopy. In *High-Resolution NMR Techniques in Organic Chemistry*, Elsevier Science: **2016**; pp 381-419.

[58] The values of the diffusion coefficient of the residual solvent signal, taken as internal reference, were used to validate our measurement, being these values approximately $D_{benzene} = 2.69 \cdot 10^{-9}$ $m^2 \cdot s^{-1}$ for benzene, $D_{THF} = 3.16 \cdot 10^{-9}$ $m^2 \cdot s^{-1}$ for THF and $D_{DMF} = 1.66 \cdot 10^{-9}$ $m^2 \cdot s^{-1}$ for DMF.

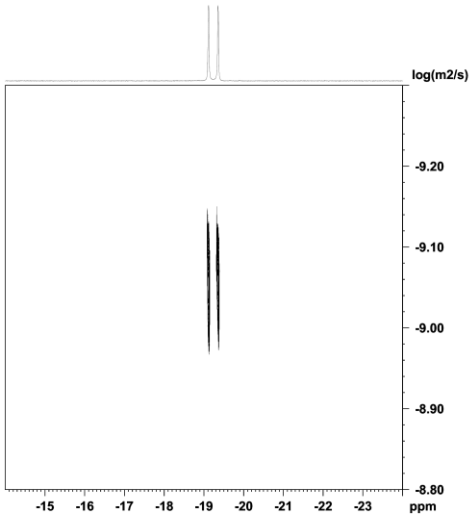

Figure A3.6. Example of ^{19}F 2D DOSY NMR experiment. In this case, it corresponds to a sample of **4** in benzene. Only signals corresponding to [(Bc)Ag(CF_3)] (**4a**) are observed.

	R_H (Å)				
	Free Bc	$[(Bc)_2Ag][SbF_6]$ (**5**)	Single set of signal, **2**	(Bc)Ag(CF_3) **4a**	[cat][Ag(CF_3)$_2$] **4b***
Solvent	^1H	^1H	^1H	^{19}F	^{19}F
Benzene	4.37	7.60	4.08	4.37	-
THF	4.33	6.86	4.33	4.13	3.36
DMF	4.38	6.78	4.91	4.38	2.14

Table A3.2. Comparison of hydrodynamic radii (R_H) between bathocuproine free ligand (**Bc**), complex **4** (**4a/4b** in polar solvents) and $[(Bc)_2Ag][SbF_6]$ (**5**).

Regarding the data shown in Table A3.2., we should mention that the hydrodynamic radius for the free bathocuproine, **4** and **4a** are practically the same. This indicates that, in solution, the approximated sphere for those species is qualitatively the same. Secondly, the hydrodynamic value of **4b** is larger in THF than in DMF. A reasonable explanation for this is that, in THF, **4b** can be considered as an ion-pair while, in DMF, they behave as independent ions. Thirdly, and more important, $[(Bc)_2Ag][SbF_6]$ (**5**) shows a significant larger R_H, by ^1H DOSY NMR, than the other species. This discards the presence of $[(Bc)_2Ag]^+$ cation as counterpart in **4b**. Hence, further investigations are needed to characterized the nature of the cation in [cat][Ag(CF_3)$_2$] (**4b**).

- **DFT calculations for the characterization of the cation for [cat][Ag(CF$_3$)$_2$] (2b)**

Challenged by this unexpected outcome, we performed DFT studies. These calculations were carried out with the ωB97-XD functional with a double-ζ plus polarization basis set in solvent (see Appendix for further details).

We started by computing **4a** in THF, and to our surprise, computations show a significant stabilizing interaction between neighboring molecules by π-π interactions, which prompts us to propose a dimeric structure for [(Bc)Ag(CF$_3$)]$_2$ (**4a'**), as shown in Scheme A3.5. The free energy of this dimer, which is stabilized by off-set π-π interactions[59] between the bathocuproine rings, is 15.8 kcal/mol below the separated monomers of **4a**. This species **4a'** was selected as origin of energy for the rest of the calculations.[60]

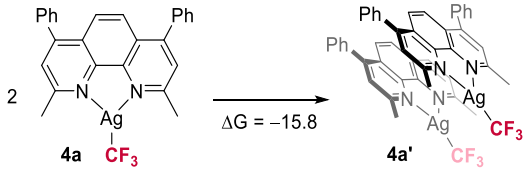

Scheme A3.5. Formation of the dimeric species **4a'**. Free energy in kcal·mol^{-1}.

Although we discarded the cation of **4b** to be related to the cation in [(Bc)$_2$Ag][Ag(CF$_3$)$_2$] by DOSY NMR spectroscopy, we studied if we could reach to the same conclusion by using DFT calculations.[55] As we can see in Scheme A3.6**Error! Reference source not found.**, **4b** with this cation is not stable enough to give rise an equilibrium observable by ^{19}F NMR spectroscopy at room temperature. We then considered the possibility of the solvent to be playing a role on the stabilization of the so-far unidentified cation.

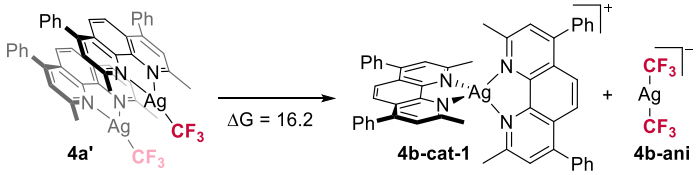

Scheme A3.6. Equilibrium between **4a'** and **4b** considering the cation in **5**. Free energy in kcal·mol^{-1}.

The introduction of explicit solvent molecules present some challenges from a computationally point of view, as we will discuss below.

[59] Martínez, C. R.; Iverson, B. L. *Chem. Sci.* **2012**, *3*, 2191.

[60] We used **4a'** and the interaction of a maximum of two bathocuproine ligands as models of a potentially more complex system. We are aware that these stabilizing π-π interactions could further facilitate the stabilization of other species such as trimer, tetramers, etc. both in reagents and in products.

- Application of the cluster/continuum model for the treatment of explicit solvent molecules

The computational prediction of the number of solvent molecules acting as ligand for a given solute is not trivial when explicit solvent molecules are used in the calculation.

The most obvious approach is the consideration of explicit solvent molecules as another discrete substrate/solute. However, a solvent molecule cannot be introduced in the system as independent and non-interacting entities, since these solvent molecules are not independent in the condensed phase. This entails an overestimation of the entropy of the solvent molecules in the calculation versus the real system.

In this regard, the main problem is the proper consideration of the effects, mainly entropic ones, associated to the transfer of a solvent molecule from the bulk of the solvent to the solute. A successful approach to overcome this problem is the application of a cluster/continuum model.[61,62] The fundamental idea of this approach relies on the identification and correction of the error associated to the treatment of explicit solvent molecules in a computed chemical process. To do so, we can assume that a good representation of the continuum bulk of the solvent is a sufficiently large cluster of solvent molecules. Ideally, the release of a molecule from the bulk of the solvent does not entail a modification of the global free energy of the system since the bulk is infinitely large respect to that punctual molecule. This process is represented by eq. 5, where *(Solv.)*$_n$ represents the bulk of the solvent as a cluster of a given number of molecules, *n*, and *x* is the number of molecules released from the cluster.

$$(Solv.)_n \rightarrow x\ Solv. + (Solv.)_{n-x} \quad \Delta G_5 \quad (\text{eq. } 5)$$

Nevertheless, the value obtained for ΔG_5 when using DFT techniques is different from zero and, in principle, negative. This value is not constant and depends on the number of solvent molecules considered in the cluster. Increasing the number of molecules of solvent involves a decrease of ΔG_5.[61a] This is a consequence of the minimization of the contribution of a punctual solvent molecule to the free energy (including entropic and enthalpic terms) and, in other words, the model is more representative of reality.

[61] a) Pliego, J. R.; Riveros, J. M. *J. Phys. Chem. A* **2001**, *105*, 7241. b) Bryantsev, V. S.; Diallo, M. S.; Goddard III, W. A. *J. Phys. Chem. B* **2008**, *112*, 9709. c) Marenich, A. V.; Ding, W.; Cramer, C. J.; Truhlar, D. G. *J. Phys. Chem. Lett.* **2012**, *3*, 1437. d) Ho, J.; Ertem, M. Z. *J. Phys. Chem. B* **2016**, *120*, 1319.

[62] a) del Pozo, J.; Pérez-Iglesias, M.; Álvarez, R.; Lledós, A.; Casares, J. A.; Espinet, P. *ACS Catal.* **2017**, *7*, 3575. b) Harvey, J. N.; Himo, F.; Maseras, F.; Pedrrin, L. *ACS Catal*. **2019**, *9*, 6803.

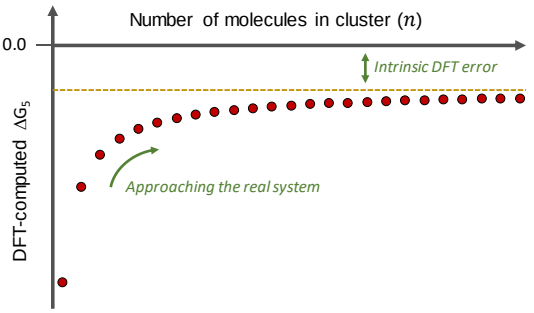

Figure A3.7. Expected behavior for the building of a cluster for the application of the cluster/continuum model for the calculation of the binding energy of the solvent.

Once the cluster is sufficiently large, ΔG_5 tends to an asymptotic value. This can be interpreted as the intrinsic error of using DFT theory in the treatment of eq. 5, which is inexorable. This intrinsic error arises from different sources:

- It can be attributed to the error of merging explicit and implicit models. In continuum models, the Gibbs energy contributions arising from the solvation procedure are included in the potential energy of the system. Thus, when combining this method with explicit solvent molecules there is an overcorrection of the entropic terms derived by the solvation procedure.
- Discrete interactions between the cluster and punctual solvent molecules (e.g. hydrogen bridge, π–π stacking, etc.) is inherent to the resolution of eq. 5 by using this method so a value different from zero is always expected to ΔG_5.
- Counterpoise error can be also playing a role as a source of error.
- Miscellaneous errors and difficult to assert.

How to apply the correction value to your own system?

Considering a process represented in eq. 4, in which a number of solvent molecules acting as ligand. In this equation, *M* represents a solute, *Solv.* is a solvent molecule and *x* is the number of solvent molecules involved in the coordination reaction. The coordination energy is defined by ΔG_4.

$$M + x\,Solv. \rightarrow M(Solv.)_x \quad \Delta G_4 \quad \text{(eq. 4)}$$

As mentioned above, this definition of coordination by DFT as an intrinsic error which is related to ΔG_5. We can correct the error in ΔG_4 by using ΔG_5 as follows in eq. 6:[63]

[63] From a practical point of view, *i.e.* the calculation of the equilibrium constants or the application of the translational correction, our system is described by eq. 4 but the free energy value is corrected and defined by ΔG_6. This is based on the assumption that the ΔG_5 associated to eq. 5 should be zero.

$$M + (Solv.)_n \rightarrow M(Solv.)_x + (Solv.)_{n-x} \quad \Delta G_6$$

$$\Delta G_6 = \Delta G_4 + \Delta G_5 \qquad \text{(eq. 6)}$$

Where ΔG_6 represents a closer value to the real system represent in eq. 4.

The only practical problem with this approach is the need to find an appropriate size for the solvent cluster. The building of the cluster should be done by the subsequent addition of solvent molecules to a solvent cluster till the asymptotic region is reached. In other words, when the energy variation of extracting a solvent molecule tends to a constant value. This can become a complex task due to the high number of conformations that a cluster can acquire. The systematic increase of solvent molecules of the cluster should minimize the conformational errors.

In our own system, the building of the cluster has been done by the subsequent addition of solvent molecules to a cluster of two molecules of THF or DMF. The free energy difference, ΔG_5, for eq. 5 is reported in Table A3.3. for THF, and in Table A3.4. for DMF.[64]

n(THF)	$\Delta G_{5(x=1)}$	$\Delta G_{5(x=2)}$
1	-	-
2	–8.2	-
3	–6.6	–14.8
4	–6.8	–13.4
5	–5.6	–12.4
6	–6.5	–12.2
7	–5.0	–11.6
8	–6.2	–11.2

Table A3.3. Free energy values (kcal·mol^{-1}) for the reaction in eq. 5 with THF as solvent.

n(DMF)	$\Delta G_{5(x=1)}$	$\Delta G_{5(x=2)}$
1	-	-
2	–6.4	-
3	–5.8	–12.2
4	–4.6	–10.4
5	–4.7	–9.3
6	–5.9	–10.6
7	–4.0	–9.9
8	–6.6	–10.6

Table A3.4. Free energy values (kcal·mol^{-1}) for the reaction in eq. 5 with DMF as solvent.

A cluster of seven solvent molecules ((Solv.)$_7$) was taken as the optimal choice for the representation of the bulk of the solvent as reactant (eq. 7).

$$M + (Solv.)_7 \rightarrow M(Solv.)_x + (Solv.)_{7-x} \quad \text{(eq. 7)}$$

[64] In these cases, the translational correction (from 1 atm. to 1M) was not applied to ΔG_5 values as we are only interested in the trend.

- Computed candidates for **4b-cat**.

We next analyzed possible forms of the cation in **4b** (**4b-cat**) as candidates (Scheme A3.7).

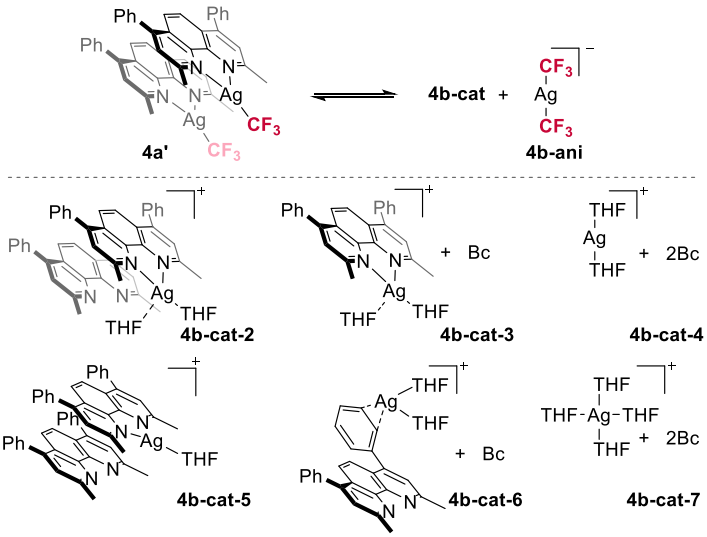

Scheme A3.7 Above: equilibrium of **4** in polar solvent. Below: Different cations considered as candidates.

The free energy differences associate to the equilibrium[65] of the different cations with **4a'** are shown in Table A3.5. The most favorable cationic form is by far **4b-cat-2**.

Plausible equilibrium	$\Delta G°$
4a' ↔ **4b-cat-2** + **4b-ani**	10.8
4a' ↔ **4b-cat-3** + **4b-ani**	26.2
4a' ↔ **4b-cat-4** + **4b-ani**	45.8
4a' ↔ **4b-cat-5** + **4b-ani**	18.3
2a' ↔ **4b-cat-6** + **4b-ani**	49.1
4a' ↔ **4b-cat-7** + **4b-ani**	36.8

Table A3.5. Free energy values for free ions equilibrium of **4a'** in THF. For clarity, Bc and THF molecules are not shown in the respective equilibria.

- Equilibrium concentrations from computed ΔG° value considering **4b-cat-2**

By definition, a chemical equilibrium is a dynamical process where the free energy, ΔG, of the system is zero. Taking this into account, we can obtain a relationship between the free energy and the equilibrium constant (eq. 8).

$$\Delta G = \Delta G° + Ln(K_{eq}) = 0 \quad (\text{eq. } 8)$$

Hence, having the equilibrium constant, we can obtain the concentrations of each species in the equilibrium (eq. 9).

[65] Standard conditions: 25 ºC and 1 M concentration of each reagent or product. We are aware that 1 M is not the standard state for the solvent, but this is taken into account when computing equilibrium concentrations.

$$\Delta G° = -Ln(K_{eq}) \quad (\text{eq. } 9)$$

As mentioned above, the most plausible cationic form based on DFT calculations is **2b-cat-2**. This equilibrium, represented in Scheme A3.8, present a $\Delta G°$ value of 10.8 kcal·mol^{-1} in THF and 6.0 kcal·mol^{-1} in DMF. These values seem very large for species that are observed to be in equilibrium at room temperature. This is however correct if we take into account the very different concentrations involved (12.33 M for THF and 12.92 M for DMF). We explain here below how we calculated the proportion of **2a** and **2b** in solution using the DFT-computed data.

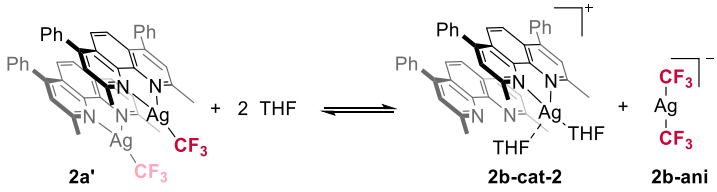

Scheme A3.8. Most favored cation (**2b-cat-2**) for the equilibrium of **2a'** and **2b-ani** in polar solvents.

The equilibrium constant in THF for the process depicted in Scheme A3.8 has a value of:

$$K_{eq,THF} = 1.1 \cdot 10^{-8}\ \text{M}^{-1}$$

The proportion in the equilibrium was calculated as follows:

2a'	+	2 THF	⇌	**2b-cat-2**	+	**2b-ani**
C_0		12.33		0		0
C_0 - x		12.33 - 2x		x		x

$$K_{eq,THF} = \frac{[\textbf{2b-cat-2}][\textbf{2b-ani}]}{[\textbf{2a'}][\textbf{THF}]^2} = \frac{x^2}{(C_0 - x)[\textbf{THF}]^2} \qquad (\text{eq. } 10)$$

Taking into consideration that the experimental initial concentration (C_0) of **2a** is 6.2·10^{-3} M (3.1·10^{-3} M, for the calculated dimer **2a'**) and the concentration of THF is constant (12.33 M), the value for *x* is 7.12·10^{-5} M, using eq. 10, and the proportion of **2a$_{DFT}$** is 98%.

When considering DMF as coordinating solvent, $\Delta G°$ is 6.0 kcal·mol^{-1} and the equilibrium constant for the previous equilibrium takes a value of 3.8·10^{-5} M^{-1}. The concentration of the solvent is 12.92 M and so the value of *x*, using eq. 10, is 2.28·10^{-3} M. The resulting proportion of **2a$_{DFT}$** in DMF is thus 58%.

As mentioned in the main text, a good agreement was found between our model system[60] and the experimental results for the equilibrium of **4** in polar solvents (Scheme 3.29).

The DFT-characterized cation allows us to explain some experimental results such as the observation of a single set of signals in ^{1}H NMR spectra. The stabilization of this cation by coordinating solvent (in high concentration) and the strong π–π interaction between bathocuproine ligands support the fast chemical exchange and the coalescence of the proton signals even a low temperature (Figure A3.3).

3.5.1.6. Synthesis and characterization of [NBu$_4$][Ag(CF$_3$)$_2$] (6$_{NBu4}$)

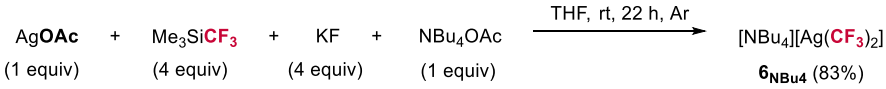

Scheme A3.9. Synthesis of **6$_{NBu4}$**.

In an argon atmosphere glovebox, a Schlenk was charged with AgOAc (50 mg, 0.29mmol, 1 equiv), NBu$_4$OAc (90.3 mg, 0.29 mmol, 1 equiv) and KF (67.4 mg, 1.16 mmol, 4 equiv) and dissolved in 20 ml of THF. A solution of Me$_3$SiCF$_3$ (171.5 µL, 1.16 mmol, 4 equiv) in 10 ml of THF was added and this mixture was stirred 22 h until the signal at –21.40 ppm (2d, $^{2}J_{^{109}Ag,F}$ = 132.8 Hz, $^{2}J_{^{107}Ag,F}$ = 115.1 Hz) ppm corresponding to [NBu4][Ag(CF3)(OAc)] had completely disappeared. The white suspension was filtered of at –20 ºC and the solution was then reduced to dryness under vacuum at this temperature. The white oil was recrystallized in a mixture of cold THF (1 ml) and cold hexane (20 ml) affording a crystalline white solid (**6$_{NBu4}$**, 120 mg, 83% yield). It was stored inside the glovebox at –32 ºC to avoid decomposition.

Characterization in THF: **^{1}H NMR** (500 MHz, DMF-*d*$_7$, 25 ºC): δ 3.25 (m, 8H, NC*H*2), 1.70 (m, 8H, NCH2C*H*2), 1.43 (m, 8H, NCH2CH2C*H*2), 1.02 (t, $^{3}J_{H,H}$= 7.4 Hz,12H, C*H*3) ppm. **^{13}C{^{1}H} NMR** (126 MHz, DMF-*d*$_7$, 25 ºC): δ 155.85 (dqq, $^{1}J_{^{109}Ag,C}$ = 275.0 Hz, $^{1}J_{C,F}$ = 370.0 Hz, $^{3}J_{C,F}$ = 8.0 Hz), 155.70 (dqq, $^{1}J_{^{107}Ag,C}$ = 238.0 Hz, $^{1}J_{C,F}$ = 370.0 Hz, $^{3}J_{C,F}$ = 8.0 Hz), 59.33 (broad triplet, N*C*H2), 24.61 (s, NCH2*C*H2), 20.82 (broad triplet, 8H, NCH2CH2*C*H2), 14.19 (s, CH3) ppm. In this particular case, the highly symmetric environment around ^{14}N allows the observation of the *J* couplings ^{13}C-^{14}N. **^{19}F NMR** (470 MHz, DMF- *d*$_7$, 25 ºC): δ –25.19 (2d, $^{2}J_{^{109}Ag,F}$ = 100.5 Hz, $^{2}J_{^{107}Ag,F}$ = 87.0 Hz) ppm. **HRMS-electrospray (-) in tetrahydrofuran** (m/z): [M]$^{-}$ calcd. for C$_2$AgF$_6$, 244.8955 and 246.8952; found 244.8950 and 246.8949.

3.5.1.7. Synthesis and characterization of [Cs][Ag(CF$_3$)$_2$] (6$_{Cs}$)

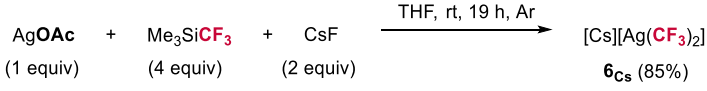

Scheme A3.10. Synthesis of **6$_{Cs}$**.

In an argon atmosphere glovebox, two duplicate reactions were carried out. The schlenks were charged equally with AgOAc (50 mg, 0.3 mmol) and CsF (73 mg, 0.49 mmol) and each one was dissolved in 30 ml of THF. A solution of Me_3SiCF_3 (142 µL, 1.04 mmol) in 10 ml of THF was added dropwise to each Schlenk and the mixtures were stirred overnight. After 16 h, inside the glovebox, a Schlenk was charged with CsF (108 mg, 0.71 mmol) and it was dissolved in 10 ml of THF. Outside the glovebox, each duplicate yellow suspension was filtered through cannula to the schlenk containing the CsF suspension and a solution of Me3SiCF3 (47 µL, 0.32 mmol) in 5 ml of THF was added dropwise to the schlenk. The mixture was stirred around 3 h until the reaction was completed and the signal of –21.15 ppm (2d, $^2J_{^{109}Ag,F}$ = 133.4 Hz, $^2J_{^{107}Ag,F}$ = 115.8 Hz) corresponding to [Cs][Ag(CF3)(OAc)] had completely disappeared. At this point, the resulting yellow suspension was filtered through cannula at –20 ºC and the solution was then reduced to dryness under vacuum at this temperature. The yellow oily residue was recrystallized in a mixture of cold THF (1 ml) and cold hexane (20 ml) and the resulting yellow solid was washed with cold hexane (2 x 10 ml). The yellow solid (**6_{Cs}**, 192 mg, 85% yield) was stored in the dark at –32 ºC to avoid decomposition.

Characterization in THF: **$^{13}C\{^1H\}$ NMR** (126 MHz, THF-d_8, 25 ºC): δ 154.10 (dqq, $^1J_{^{109}Ag,C}$ = 275.0 Hz, $^1J_{C,F}$ = 370.0 Hz, $^3J_{C,F}$ = 8.0 Hz), 152.09 (dqq, $^1J_{^{107}Ag,C}$ = 238.0 Hz, $^1J_{C,F}$ = 370.0 Hz, $^3J_{C,F}$ = 8.0 Hz) ppm. **^{19}F NMR** (470 MHz, THF-d_8, 25 ºC): δ –24.67 (2d, $^2J_{^{109}Ag,F}$ = 98.6 Hz, $^2J_{^{107}Ag,F}$ = 88.9 Hz) ppm. **HRMS-electrospray (-) in tetrahydrofuran** (m/z): $[M]^-$ calcd. for C_2AgF_6, 244.8955 and 246.8952; found 244.8970 and 246.8971.

3.5.1.8. Transmetalation reactions in the benchmark system

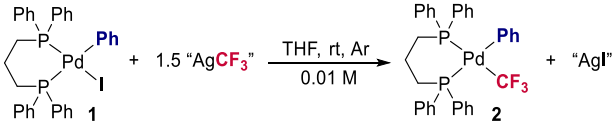

Scheme A3.11. General transmetalation reaction towards our benchmark palladium system.

- **Procedure for Me_3SiCF_3/MF (M = K or Cs)**

Inside the glovebox, a 5 ml-crimped vial containing a 12mmx3mm PTFE cylindrical stirrer was charged with Pd complex **1** (4.3 mg, 0.006 mmol) and CsF (1.4 mg, 0.009 mmol) or KF (0.5 mg, 0.009 mmol) and dissolved in 0.5 ml of THF. After that, Me_3SiCF_3 (100 µL of a 0.09 M stock solution in THF) were added and the heterogeneous mixture was left stirring at 1500 rpm the corresponding time at room temperature.

- **Initial procedure for (Phen)Cu(CF_3)**

Inside the glovebox, a 5 ml-crimped vial containing a 12mmx3mm PTFE cylindrical stirrer was charged with Pd complex **1** (4.3 mg, 0.006 mmol) and [(Phen)Cu(CF_3)] (2.8 mg, 0.009 mmol) and dissolved in 0.6 ml of THF. The heterogeneous mixture was left stirring at 1500 rpm the corresponding time at room temperature. The analysis of the reaction mixture is explained below.

- **Initial procedure for complexes 3 and 4**

Outside the glovebox, a 5 ml-crimped vial containing a 12mmx3mm PTFE cylindrical stirrer was charged with Pd complex **1** (4.3 mg, 0.006 mmol) and **3** (5.1 mg, 0.009 mmol) or **4** (4.8 mg, 0.009 mmol), purged under argon, dissolved in 0.6 ml of THF and left stirring at 1500 rpm the corresponding time at room temperature. The analysis of the reaction mixture is explained below.

- **Initial procedure for complexes 6**

"CF_3" sources [1.7 mg (**6_{Cs}**), 2.2 mg (**6_{NBu4}**), 0.0045 mmol] and Pd complex **1** (4.3 mg, 0.006 mmol) were weighted in a 5 ml-crimped vial containing a 12mmx3mm PTFE cylindrical stirrer inside the glovebox, dissolved in 0.6 ml of THF and left stirring at 1500 rpm the corresponding time at room temperature. The analysis of the reaction mixture is explained below.

- **NMR spectroscopy analysis of the reaction mixtures.**

After that, for all the procedures, the reactions were cooled at –80 ºC and transferred to different NMR tubes previously purged and cooled. All the ^{19}F (ns = 256) and $^{31}P\{^1H\}$ (ns = 1024) NMR experiments were measured at –80 ºC and each reaction was repeated at least three times, taking the average for the percentage of the product formed determined by $^{31}P\{^1H\}$ NMR. The NMR data is in accordance with the previously described [(dppp)Pd(Ph)(CF_3)][1a] the excess of the corresponding "$AgCF_3$" source and the different observed intermediates when it is the case.

3.5.1.9. Synthesis of [(Xantphos)Pd(Ph)(CF_3)] from [(Xantphos)Pd(Ph)(I)] using [Cs][Ag(CF_3)$_2$] (6Cs)

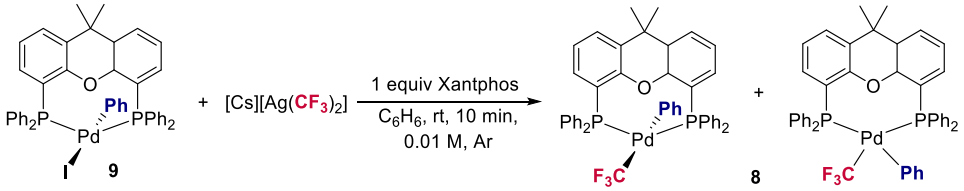

Scheme A3.12. Preparation of [(Xantphos)Pd(Ph)(CF_3)] (**8**) from [(Xantphos)Pd(Ph)(I)] (**9**) using [Cs][Ag(CF_3)$_2$] (**6$_{Cs}$**).

In a glovebox, a 5ml-crimped vial was charged with [(Xantphos)Pd(Ph)(I)] (**9**) (5.3 mg, 0.006 mmol), Xantphos (3.5 mg, 0.006 mmol) and (Cs)[Ag(CF3)2] (**6$_{Cs}$**) (1.7 mg, 0.0045 mmol), dissolved in benzene (0.6 ml) and stirred at room temperature during 10 min. After that, the bright yellow solution was transferred to a NMR tube and the solvent was evaporated. Next, 0.6 ml of toluene were added and ^{19}F NMR (ns = 64) and ^{31}P NMR (ns = 1024) spectra were measured at –50 ºC. The same reaction was repeated using Me_3SiCF_3/CsF mixture as CF_3^- source and no [(Xantphos)Pd(Ph)(CF_3)] complex (**8**) was observed.

3.5.1.10. Representative procedure for the reductive elimination study from [(Xantphos)Pd(Ph)(I)] and different trifluoromethylating agents.

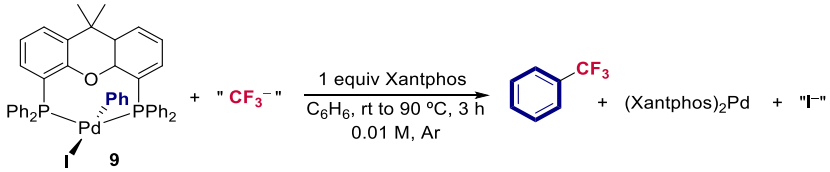

Scheme A3.13. Transmetalation reaction to **9** using different trifluoromethylating agents and one-pot reductive elimination.

In a glovebox, a 5ml-crimped vial was charged with [(Xantphos)Pd(Ph)(I)] (**9**) (5.3 mg, 0.006 mmol), Xantphos (3.5 mg, 0.006 mmol) and the corresponding trifluoromethyl source [**4** (4.8 mg, 0.009 mmol), **6$_{Cs}$** (1.7 mg, 0.0045 mmol), **6$_{NBu4}$** (2.2 mg, 0.0045 mmol)] or a combination of the fluoride source [CsF (3.6 mg, 0.024 mmol), KF (1.4 mg, 0.024 mmol), NBu_4F (24 µL of a 1 M solution in THF, 0.024 mmol)] with Me_3SiCF_3 (0.012 mmol, 100 µL of a 0.12 M stock solution in benzene). The reactions were dissolved in 0.6 ml of benzene (in case of MF/ Me_3SiCF_3 only 0.5 ml of benzene were added) and heated at 90 oC during 3 h. After that, each solution was filtered through a PTFE 13mm 0.2µm NSTR syringe filter and the internal standard was added; fluorobenzene (180 µL of a 0.06 M stock solution in cyclohexane) and/or 4,4'-difluorobiphenyl (250 µL of a 0.1 M stock solution in benzene). A ^{19}F NMR spectrum was acquired to determine

the yield of α,α,α-triflurotoluene and the different products obtained for the reaction. The experiments were performed at least duplicate. The yield was calculated taking the average of the different runs and it was determined by comparing the original mass of the sample **9** (limiting reactive) to its number of moles versus the amount of the internal standard.

3.5.1.11. Competency of [Cs][Ag(CF$_3$)$_2$] (**6$_{Cs}$**) as CF$_3^-$ source under relevant stoichiometric conditions.

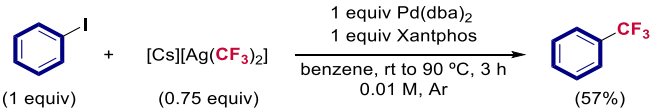

Scheme A3.14. First attempt in the study of the competency of [Cs][Ag(CF$_3$)$_2$] (**6$_{Cs}$**) with all the elementary steps under stoichiometric conditions.

In a glovebox, a 5ml-crimped vial containing a 12mmx3mm PTFE cylindrical stirrer was charged with [Pd(dba)$_2$] (3.4 mg, 0.006 mmol), Xantphos (3.5 mg, 0.006 mmol) and **6$_{Cs}$** (1.7 mg, 0.0045 mmol). The reaction was dissolved in 0.6 ml of benzene and PhI was added (10 µL of a 0.6 M stock solution in toluene, 0.006 mmol). The suspension was taken out of the glovebox and the mixture was heated at 90 ºC and stirred at 1200 rpm during 3 h. After that, the solution was filtered through a PTFE 13mm 0.2µm NSTR syringe filter and the internal standard was added: fluorobenzene (180 µL of a 0.06 M stock solution in cyclohexane). A ^{19}F NMR spectrum was acquired to determine the yield of α,α,α-triflurotoluene and the different products obtained for the reaction. The yield was determined by comparing the original mass of [Pd(dba)$_2$] (limiting reactive) to its number of moles against the internal standard. The reaction afforded a 57% of α,α,α-triflurotoluene and a 10% of the catalytically inactive [(Xantphos)Pd(CF$_3$)(I)].

After some screening of solvent, temperature and concentration, the best conditions, that we found, showed the compatibility of all the different steps and **6$_{Cs}$** in the Pd-mediated trifluoromethylation of phenyl iodide.

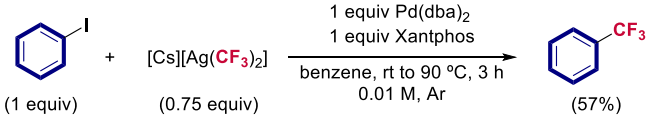

Scheme A3.15. Final conditions for proving the competency of [Cs][Ag(CF$_3$)$_2$] (**6$_{Cs}$**) with all the elementary steps under stoichiometric conditions.

In a glovebox, a 5ml-crimped vial containing a 12mmx3mm PTFE cylindrical stirrer was charged with [Pd(dba)$_2$] (3.4 mg, 0.006 mmol), Xantphos (3.5 mg, 0.006 mmol) and **6$_{Cs}$** (1.7 mg, 0.0045 mmol). The reaction was dissolved in 3 ml of toluene and PhI was added (30 µL, 0.18 mmol). The suspension was taken out of the glovebox and the mixture was heated at 95 ºC and

stirred at 1200 rpm during 3 h. After that, the solution was filtered through a PTFE 13mm 0.2µm NSTR syringe filter and an aliquot of 1 ml was added to a NMR tube together with the internal standard; fluorobenzene (100 µL of a 0.06 M stock solution in cyclohexane). A ^{19}F NMR spectrum was acquired to determine the yield of α,α,α-triflurotoluene and the different products obtained for the reaction. The experiment was performed in duplicate. The yield was calculated taking the average of the different runs and it was determined by comparing the original mass of $[Pd(dba)_2]$ (limiting reactive) to its number of moles against the internal standard. The reaction afforded a 91% of α,α,α-triflurotoluene and no catalytically inactive $[(Xantphos)Pd(CF_3)(I)]$.

3.5.1.12. Catalytic proof-of-concept

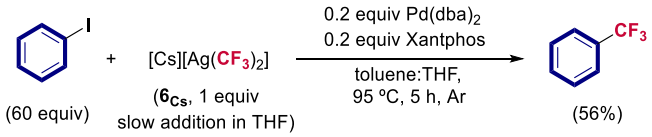

In a glovebox, a schlenk with a female joint ST/NS 29/32, a height of 19 cm and a diameter of 28 cm containing a 12mmx3mm PTFE cylindrical stirrer was charged with $[Pd(dba)_2]$ (1.8 mg, 0.003 mmol) and Xantphos (1.8 mg, 0.003 mmol) and covered with a septum of 30.7 mm. The solids were dissolved in 3 ml of toluene and PhI was added (105 µL, 0.9 mmol). At the same time, **6$_{Cs}$** (5.7 mg, 0.015 mmol) was weighted in a crimped vial, dissolved in 1 ml of THF and directly transferred to a syringe of 1 ml and 4.7 mm of diameter. The schlenk and the syringe were taken out of the glovebox. The solution in the schlenk was heated at 95 ºC and stirred at 1200 rpm during 5 min before the addition of the solution of **6$_{Cs}$** in THF started. The syringe containing the solution of **6$_{Cs}$** was placed in a syringe pump covered with aluminum foil. The needle was directly connected to a refrigerated piece of glass (0 ºC) with a small cavity inside (6 medium glass and 1.1 mm diameter) that directly aligns the end of the needle to the middle of the solution in the schlenk with a distance between them around 20 cm. Once the set-up is prepared, the solution of **6$_{Cs}$** in THF is pumped with a rate of 0.004 ml/min (around 4 h). When the addition is finished, the mixture is heated 30 min more and then, it is cooled during other 30 min. Afterwards, the solution was filtered through a PTFE 13mm 0.2µm NSTR syringe filter and an aliquot of 1 ml was added to a NMR tube together with the internal standard; fluorobenzene (100 µL of a 0.06 M stock solution in cyclohexane). A ^{19}F NMR spectrum was acquired to determine the yield of α,α,α-triflurotoluene and the different products obtained for the reaction. The yield was determined by comparing the original mass of $[Cs][Ag(CF_3)_2]$ (limiting reactive) to its number of moles against the internal standard taking into account that both CF_3 groups are

transferred. The reaction afforded a 56% of α,α,α-triflurotoluene and no catalytically inactive [(Xantphos)Pd(CF3)(I)].

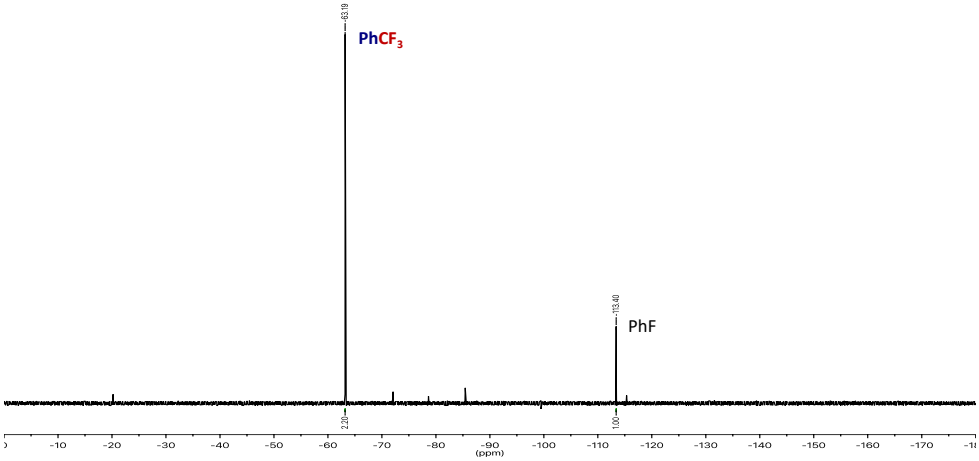

Figure A3.8. ^{19}F NMR spectrum corresponding to the catalytic trifluoromethylation of aryl iodide using **6**$_{Cs}$.

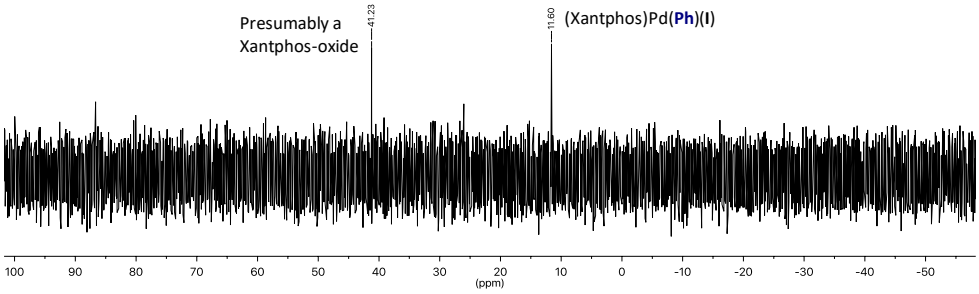

Figure A3.9. $^{31}P\{^{1}H\}$ NMR spectrum corresponding to the catalytic trifluoromethylation of aryl iodide using **6**$_{Cs}$.

- **Complete the setup for the catalysis.**

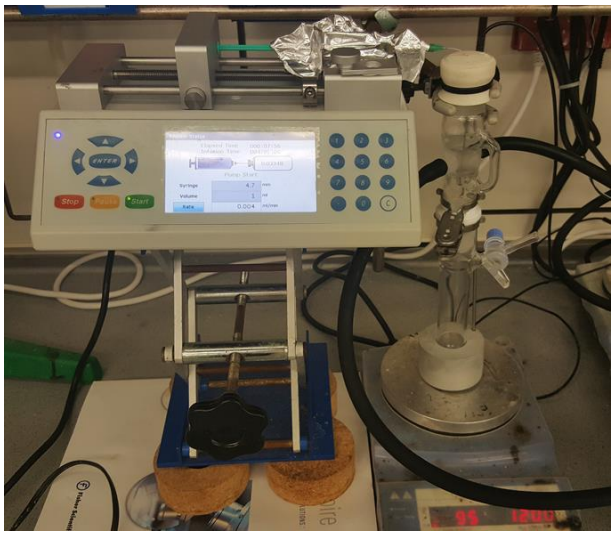

3.5.1.13. **X-ray structure determination for 3, 4a, 5, 6_{Cs}, 6_{NBu4}, and [(Bc)Ag(THF)][SbF_6].**

Crystal preparation: Crystals of **3**, **4a** and [(Bc)Ag(THF)][SbF_6] were grown by slow diffusion of hexane into solutions of tetrahydrofuran at room temperature. Crystals of **5** was grown by slow diffusion of hexane into solutions of dichloromethane at room temperature. Crystals of **6_{Cs}** were grown by slow diffusion of hexane into a solution of tetrahydrofuran at –32 ºC. Crystals of **6_{NBu4}** were grown by slow diffusion of heptane into a solution of tetrahydrofuran at –32 ºC. The measured crystals were prepared under inert conditions, immersed in perfluoropolyether as protecting oil on a glass slide before being mounted on a capton loop. The crystals were quickly handled before being mounted. Compound **6_{Cs}** and **6_{NBu4}** was crystallized at –32 ºC and the single crystal preparation was performed using dry ice CO_2 as preparation base for avoiding heating of the crystal and mounted at –173 ºC for measurement.

Data collection: Crystal structure determinations for samples **4a**, **5**, **6_{Cs}**, **6_{NBu4}** and [(Bc)Ag(THF)][SbF_6] were carried out using an Apex DUO Kappa 4-axis goniometer equipped with an APPEX 2 4K CCD area detector, a Microfocus Source E025 IuS using MoK_α radiation (0.71073 Å), Quazar MX multilayer Optics as monochromator and an Oxford Cryosystems low temperature device Cryostream 700 plus (T = –173 °C). Crystal structure determination for sample **3** was carried out using a Rigaku diffractometer equipped with a Pilatus 200K area detector, a Rigaku MicroMax-007HF microfocus rotating anode with MoK_α radiation, Confocal Max Flux optics and an Oxford Cryosystems low temperature device Cryostream 700 plus (T =

–183 ºC). Full-sphere data collection was used with ω and φ scans. *Software used:* Bruker Device: Data collection APEX-2[66], data reduction Bruker Saint[67]V/.60A and absorption correction SADABS[68] or TWINABS[69]. Rigaku device: Data collection and reduction with CrysAlisPro[70] and absorption correction with Scale3 Abspack scaling algorithm.[71]

Structure Solution and Refinement: Crystal structure solution was achieved using the computer program SHELXT.[72] Visualization was performed with the program SHELXle.[73] Missing atoms were subsequently located from difference Fourier synthesis and added to the atom list. Least-squares refinement on F2 using all measured intensities was carried out using the program SHELXL 2015.[74] All non-hydrogen atoms were refined including anisotropic displacement parameters. These data are provided free of charge by The Cambridge Crystallographic Data Centre. The corresponding code in the data base is shown in brackets next to the corresponding label in the next section.

Comments to the structures:

- **Structure for 3 *(CCDC 1588501)***

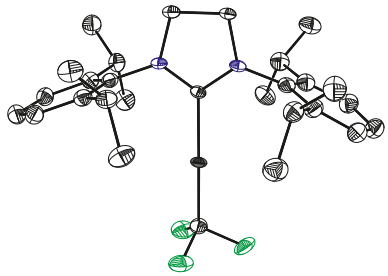

Figure A3.10. ORTEP drawing (thermal ellipsoids set at 50% probability) of the structure of **3**. Hydrogen atoms have been omitted for clarity.

The asymmetric unit of this compound contains two independent molecules of the metal complex. Both refined molecules are respectively disordered in two shifted positions with ratios of 84:16 and 69:31. The possibility to have a twin (β-angle of 90.84º which may emulate orthorhombic) was checked but the refinement was not successful. The structure is of moderate

66 Data collection with APEX II version v2013.4-1. Bruker (**2007**). Bruker AXS Inc., Madison, Wisconsin, USA.
67 Data reduction with Bruker SAINT version V8.30c. Bruker (**2007**). Bruker AXS Inc., Madison, Wisconsin, USA.
68 SADABS: V2014/5 Bruker (**2001**). Bruker AXS Inc., Madison, Wisconsin, USA. Blessing, Acta Cryst. (**1995**) A51 33-38.
69 TWINABS Version 2008/4 Bruker AXS; Blessing, *Acta Cryst.* (**1995**) A51 33.
70 Data collection and reduction with CrysAlisPro 1.171.39.12b (Rigaku OD, **2015**).
71 Empirical absorption correction using spherical harmonics implemented in Scale3 Abspack scaling algorithm, CrysAlisPro 1.171.38.37f (Rigaku OD, **2015**).
72 SHELXT; G. M. Sheldrick, *Acta Cryst*. **2015** A71, 3.
73 SHELXle; Huebschle, C. B.; Sheldrick, G. M.; Dittrich, B.; *J. Appl. Cryst.* **2011**, *44*, 1281.
74 SHELXL; Sheldrick, G. M. *Acta Cryst*. **2015** C71, 3. SHELXT.

quality due to the difficulties to find a measurable crystal (A- and B-alerts due to high residual electron densities are commented in the CIF-file).

- **Structure for 4a *(CCDC 1566841)***

The data collected for this structure (shown in **Scheme 3.28**) are of very low quality since the crystals are showing weak diffraction power and the typical signals of high mosaicity. A and B alerts are obtained in the check-cif related to low resolution, poor data to parameter ratio and low bond precision. The following comments were added into the CIF-file in relation to A and B-alerts: Several crystals of this sample where measured and no better dataset could be collected. The final data collected are showing weak diffraction power and the typical signals of high mosaicity. Although the low data quality, it was considered that the data were good enough for structure confirmation avoiding any deeper discussion about bond lengths and angles. The measured sample was formed by four crystals with a ratio of 29:29:22:20. The collected data for the crystals were processed with TWINABS taking into account overlapping reflections. We considered that the structure is publishable but only for structural identification.

- **Structure for 5 *(CCDC 1566842)***

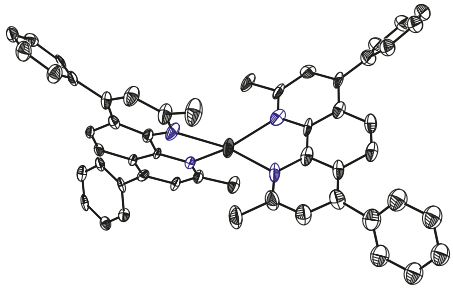

Figure A3.11. ORTEP drawing (thermal ellipsoids set at 50% probability) of the structure of **5**. Hydrogen atoms and hexafluoroantimoniate anion have been omitted for clarity.

The asymmetric unit contains two independent cationic molecules of the organometallic compound and two SbF_6 anions. The SbF_6 anions are highly disorder located in three positions. The major part of the aromatic rings at the cationic organometallic compound are disordered in two orientations. The measured crystals were showing a weak diffraction power. Different attempts were performed to collect a complete data set. The final dataset collected was measured on a rotating anode with long exposition time and it was considered of enough quality to confirm the structure.

- **Structure for [(Bc)Ag(THF)][SbF_6] *(CCDC 1566843)***

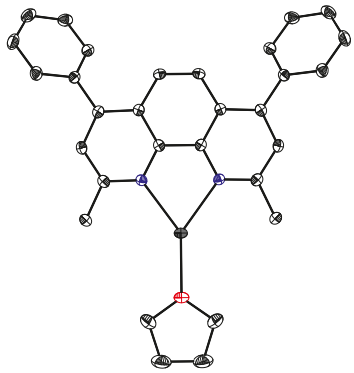

Figure A3.12. ORTEP drawing (thermal ellipsoids set at 50% probability) of the structure of [(Bc)Ag(THF)][SbF_6]. Hydrogen atoms and hexafluoroantimoniate anion have been omitted for clarity.

The asymmetric unit contains a half molecule of the metal complex which shows *Cs* symmetry (mirror plane) and half SbF_6 anion. The THF molecule coordinated to the metal complex is partially disordered in two orientations (ratio of disorder: 65:35).

- **Structure for 6_{Cs} *(CCDC 1566839)***

This structure is shown in Figure 3.11. The asymmetric unit contains half Cs-cation and two quarters of $Ag(CF_3)_2$ anions. All the CF_3 groups are disordered in a minimum of two orientations. The cesium cation is disordered in two positions with a ratio of 57:43. The measured sample is formed by a minimum of two crystals with a ratio of 86:14. The data collected were processed with TWINABS taking in account overlapping reflections. The structure could be refined in the space groups *C*2/m, *C*2 (as a racemic twin) and *C*m (as a twin) with similar results. Finally, the higher symmetrical space group C2/m was selected which also gave the slowest R1 value. Structure solutions were also found using a larger monoclinic unit cell (a:17.00 b:5.77 c:16.12 β:119.57 instead of a:16.12 b:5.77 c:8.35 β:117.60) but the statics were worse so that they were not further used. The selected structure in the space group *C*2/m is of excellent quality and it does not show any A- or B-alerts.

- **Structure for 6_{NBu4} *(CCDC 1588502)***

This structure is shown in Figure 3.11. The cation and the anion show *C*2-symmetry in the crystal packing and the asymmetric unit contains only half of each. The fluorine atoms of the CF_3-group are disordered in three orientations with a ratio of 46:44:10. The silver atom does not show any contact to neighboring silver atoms (7.89 Å). The fluorine atoms do not show any weak interaction and are highly disordered.

3.5.2. **Computational details**

A data set collection of computational results is available in the ioChem-BD repository[75] and can be accessed via DOI: 10.19061/iochem-bd-1-82. DFT calculations were performed with the ωB97-XD functional,[76] using the Gaussian09 package.[77] The basis set was SDD plus pseudopotential for silver,[78] and 6-31G(d)[79] for the remaining atoms. All geometry optimizations were carried out in solution without symmetry restrictions. Implicit solvent was modeled through the SMD method.[80] Calculations were carried out in two different solvents: THF (ε = 7.43) and DMF (ε = 37.22). Explicit solvent molecules were introduced when coordinating to the silver center. The number of required solvent molecules was decided through the application of a cluster continuum model, discussed in detail in the main text of this Chapter. All the energies presented are free energies in kcal·mol^{-1} at 25 ºC and 1 M, except for the selection of the cluster. The free energies provided by the standard Gaussian09 calculations at ideal gas concentrations were corrected by 1.895 kcal·mol^{-1} in steps with change of molecularity. We are aware that 1 M is not the standard state for the solvent, but this is taken into account when computing equilibrium concentrations.

[75] Álvarez-Moreno, M.; de Graaf, C.; López, N.; Maseras, F.; Poblet, J. M.; Bo, C. *J. Chem. Inf. Model*. **2015**, *55*, 95.

[76] Chai, J. D.; Head-Gordon, M. *Phys. Chem. Chem. Phys.* **2008**, *10*, 6615.

[77] Gaussian 09, Revision D.01, Frisch, M. J.; Trucks, G. W.; Schlegel, H. B.; Scuseria, G. E.; Robb, M. A.; Cheeseman, J. R.; Scalmani, G.; Barone, V.; Mennucci, B.; Petersson, G. A.; Nakatsuji, H.; Caricato, M.; Li, X.; Hratchian, H. P.; Izmaylov, A. F.; Bloino, J.; Zheng, G.; Sonnenberg, J. L.; Hada, M.; Ehara, M.; Toyota, K.; Fukuda, R.; Hasegawa, J.; Ishida, M.; Nakajima, T.; Honda, Y.; Kitao, O.; Nakai, H.; Vreven, T.; Montgomery, Jr., J. A.; Peralta, J. E.; Ogliaro, F.; Bearpark, M.; Heyd, J. J.; Brothers, E.; Kudin, K. N.; Staroverov, V. N.; Keith, T.; Kobayashi, R.; Normand, J.; Raghavachari, K.; Rendell, A.; Burant, J. C.; Iyengar, S. S.; Tomasi, J.; Cossi, M.; Rega, N.; Millam, J. M.; Klene, M.; Knox, J. E.; Cross, J. B.; Bakken, V.; Adamo, C.; Jaramillo, J.; Gomperts, R.; Stratmann, R. E.; Yazyev, O.; Austin, A. J.; Cammi, R.; Pomelli, C.; Ochterski, J. W.; Martin, R. L.; Morokuma, K.; Zakrzewski, V. G.; Voth, G. A.; Salvador, P.; Dannenberg, J. J.; Dapprich, S.; Daniels, A. D.; Farkas, O.; Foresman, J. B.; Ortiz, J. V.; Cioslowski, J.; Fox, D. J. Gaussian, Inc., WallingfordCT, **2013**.

[78] Andrae, D.; Haeussermann, U.; Dolg, M.; Stoll, H.; Preuss, H. *Theor. Chem. Accu.* **1990**, *77*, 123.

[79] a) Hehre, W. J.; Ditchfield, R.; Pople, J. A. *J. Chem. Phys.* **1972**, *56*, 2257. b) Dill, J. D.; Pople, J. A. *J. Chem. Phys.* **1975**, *62*, 2921. c) Francl, M. M.; Petro, W. J.; Hehre, W. J.; Binkley, J. S.; Gordon, M. S.; DeFrees, D. J.; Pople, A. J. *J. Chem. Phys.* **1982**, *77*, 3654.

[80] Marenich, A. V.; Cramer, C. J.; Truhlar, D. G. *J. Phys. Chem. B* **2009**, *113*, 6378.

Coinage Metal Complexes in C–C and C–N Bond-forming Reactions

Organosilver(I) species have previously demonstrated their potential as coupling partners in Pd-catalyzed transformations, but this ability is far from being fully exploited. Discrete Ag–CF3 complexes with a new silver ate complex, [Cs][Ag(CF3)2], have been employed in the highlighted paper. Their unique structure can tackle some usually overshadowed limitations related to the transmetalation step within the trifluoromethylation area.

3.6. REFERENCES AND NOTES

1. Although this topic will be covered below in the discussion, a flavor of the limitation in the reductive elimination in organo-Pd(II)-CF_3 complexes can be found in: a) Grushin, V. V.; Marshall, W. J. *J. Am. Chem. Soc.* **2006**, *128*, 4632. b) Grushin, V. V.; Marshall, W. J. *J. Am. Chem. Soc.* **2006**, *128*, 12644. c) Cho, E. J.; Senecal, T. D.; Kinzel, T.; Zhang, Y.; Watson, D. A.; Buchwald, S. L. *Science* **2010**, *328*, 1679.
2. For selected reviews: a) McClinton, M. A.; McClinton, D. A. *Tetrahedron* **1992**, *48*, 6555. b) Schlosser, M. *Angew. Chem. Int. Ed.* **2006**, *45*, 5432. c) Orsi, D. L.; Altman, R. A. *Chem. Commun*. **2017**, *53*, 7168.
3. Mudarra, A. L.; Martínez de Salinas, S.; Pérez-Temprano, M. H. *Synthesis* **2019**, *51*, 2809 and references therein.
4. a) Ball, N. D.; Kampf, J. W.; Sanford, M. S. *J. Am. Chem. Soc.* **2010**, *132*, 2878. b) Ye, Y.; Ball, N. D.; Kampf, J. W.; Sanford, M. S. *J. Am. Chem. Soc.* **2010**, *132*, 14682. c) Ball, N. D.; Gary, J. B.; Ye, Y.; Sanford, M. S. *J. Am. Chem. Soc*. **2011**, *133*, 7577.
5. a) Nielsen, M. C.; Bonney, K. J.; Schoenebeck, F. *Angew. Chem. Int. Ed.* **2014**, *53*, 5903. b) Ferguson, D. M.; Bour, J. R.; Canty, A. J.; Kampf, J. W.; Sanford, M. S. *J. Am. Chem. Soc.* **2017**, *139*, 11662 c) Ferguson, D. M.; Bour, J. R.; Canty, A. J.; Kampf, J. W.; Sanford, M. S. *Organometallics* **2019**, *38*, 519.
6. Bakhmutov, V. I.; Bozoglian, F.; Gómez, K.; González, G.; Grushin, V. V.; Macgregor, S. A.; Martin, E.; Miloserdov, F. M.; Novikov, M. A.; Panetier, J. A.; Romashov, L. V. *Organometallics* **2012**, *31*, 1315.
7. Culkin, D. A.; Hartwig, J. F. *Organometallics* **2004**, *23*, 3398.
8. a) Stambuli, J. P.; Incarvito, C. D.; Bühl, M; Hartwig, J. F. *J. Am. Chem. Soc.* **2004**, *126*, 1184. b) Yamashita, M.; Hartwig, J. F. *J. Am. Chem. Soc.* **2004**, *126*, 5344.
9. This process has been also described as a carbene insertion of the phenyl group. See Zhang, S.-L., Huang, L.; Sun L.-J. *Dalton Trans.* **2015**, *44*, 4613.
10. Zhang, S.-L.; Deng, Z.-Q. *Phys. Chem. Chem. Phys.* **2016**, *18*, 32664.
11. Anstaett, P.; Schoenebeck, F. *Chem. Eur. J.* **2011**, *17*, 12340.
12. Naumann, D.; Kirij, N. V.; Maggiarosa, N.; Tyrra, W.; Yagupolskii, Y. L.; Wickleder, M. S. *Z. Anorg. Allg. Chem*. **2004**, *630*, 746.
13. Liu, X.; Xu, C.; Wang, M.; Liu, Q. *Chem. Rev.* **2015**, *115*, 683.
14. Maggiarosa, N.; Tyrra, W.; Naumann, D.; Kirij, N. V.; Yagupolskii, Y. L. *Angew. Chem. Int. Ed.* **1999**, *38*, 2252.
15. Prakash, G. K. S.; Wang, F.; Zhang, Z.; Haiges, R.; Rahm, M.; Christe, K. O.; Mathew, T.; Olah, G. A. *Angew. Chem. Int. Ed*. **2014**, *53*, 11575.
16. Similar behavior have been described for copper systems (Chapter 4, ref. **Error! Bookmark not defined.**.
17. One could think that this side reaction may happen in Buchwald system (ref. 1c) and it could be also the reason why the transmetalation to form **VII** has such a lower yield (pag. - 84 -). However, we should take into account that under catalytic conditions, if the reductive elimination step is fast, the concentration of the transient Pd(II) **VII** species is very low and their poly-(trifluoromethylation) is unlikely to happen.
18. Note that those arguments could be counterintuitive since a bridge mechanism for the transmetalation between Pd and another organometallic nucleophile, M–R, is well-known to be favored for more electrophilic palladium complexes (Cl > Br > I) (Casado, A.L.; Espinet, P. *J. Am. Chem. Soc.* **1998**, *120*, 8978). In the mechanism discussed above by Grushin this trend, since the electrophile is the Pd(II)–CF_3 complex, is difficult to predict and both mechanisms are proposed.
19. For the synthesis of [$(L)_nPd(Ar)(CF_3)$] complexes bearing tightly-binding phosphine ligands, 1 hour of reaction is needed at room temperature for the conversion of approx. 0.5 mmol of the corresponding [$(L)_nPd(Ar)(I)$]. This shows that the transmetalation reaction is not instantaneous. See ref 1a.
20. Keaveney, S. T.; Schoenebeck, F. *Angew. Chem. Int. Ed.* **2018**, *57*, 4073.
21. We should emphasize that this report and our study, enabling Xantphos in catalysis as a proof-of-concept, were published almost concomitantly as we will discuss in this Chapter 2. Basically, their initial approach was based on the modification of the substrate while our work consists of the search of a more efficient transmetalating agent to overcome potential side reactions.

22. The role of the phosphate during the catalytic cycle is uncertain. They suggested that one of the role could be activating the Et_3SiCF_3 which is inconsistent with their mechanistic proposal since the Et_3SiCF_3 is supposed to be activated by Pd-F intermediates.

23. a) Gu, Y.; Leng, X.; Shen, Q. *Nat. Commun*., **2014**, *5*, 5405. b) Lu, C.; Gu, Y.; Wu, J.; Gu Y.; Shen, Q. *Chem. Sci.*, **2017**, *8*, 4848.

24. Mudarra, Á. L.; Martínez de Salinas, S.; Pérez Temprano, M. H. *Org. Biomol. Chem.* **2019**, *17*, 1655.

25. Homoleptic silver(I) complexes bearing perfluorinated aryl moieties have been also used as transmetalating agents to dimeric bis(halide)-Pd(II) complexes: a) Albéniz, A. C.; Espinet, P.; Martín-Ruiz, B. *Chem. Eur. J.* **2001**, *7*, 2481. b) Albéniz, A. C.; Espinet, P.; López-Cimas, O.; Martín-Ruiz, B. *Chem. Eur. J*. **2005**, *11*, 242.

26. a) Tyrra, W. J. Fluorine Chem. **2001**, *112*, 149. b) Tyrra, W.; Naumann, D. *J. Fluorine Chem*. **2004**, 125, 823. c) Weng, Z.; Lee, R.; Jia, W.; Yuan, Y.; Wang, W.; Feng, X.; Huang, K.-W. *Organometallics* **2011**, 30, 3229. d) Hafner, A.; Bräse, S. *Angew. Chem. Int. Ed.* **2012**, *51*, 3713. e) Zhang; C.-P.; Wang, Huan; Klein, A.; Biewer, C.; Stirnat, K.; Yamaguchi, Y.; Xu, L.; Gomez-Benitez, V.; Vicic, D. A. *J. Am. Chem. Soc.* **2013**, *135*, 8141.

27. Naumann, D.; Wessel, W.; Hahn, J.; Tyrra, W. *J. Organomet. Chem*. **1997**, *547*, 79.

28. Tate, B. K.; Jordan, A. J.; Bacsa, J.; Sadighi, J. P. *Organometallics* **2017**, *36*, 964.

29. Initially, we envisioned that the study of the transmetalation using [(Xantphos)Pd(Ph)(I)] complex to form [(Xantphos)Pd(Ph)(CF_3)] could be hampered by the formation of cis/trans isomers and/or eventual generation of the coupled product. Thus, we turned our attention on dppp, as a model bidentate phosphine ligand of Xantphos.

30. The selection of the iodide as benchmark system was based on the discussion of Grushin in ref. 6 about the potential “nucleophilic aid” of some transmetalation side reactions. This means that the iodide palladium complexes are more prompted to undergo these undesired transformation and the transmetalating agent has to be effective enough to prevent these side reactions.

31. It has been reported to yield a 60% yield at 145 ºC which will not be our working temperature.

32. We selected THF as solvent to avoid solubility issues.

33. Morimoto, H.; Tsubogo, T.; Litvinas, N. D.; Hartwig, J. F. *Angew. Chem. Int. Ed*. **2011**, *50*, 3793. The complex is commercially-available: https://www.sigmaaldrich.com/catalog/product/aldrich/777692?lang=es&region=ES.

34. This species was assigned on the basis of NMR spectroscopy. By ^{19}F NMR, it bears a very diagnostic coupling constant between silver and fluoride, as we will discuss further below.

35. Further experiments, which are discussed in the Appendix, confirmed **4** to be an equilibrium of **4a** and **4b** in polar solvents.

36. a) Tyrra, W. *Heteroat. Chem*. **2002**, *13*, 561. b) Zeng, Y.; Zhang, L.; Zhao, Y.; Ni, C.; Zhao, J.; Hu, J. *J. Am. Chem. Soc.* **2013**, *135*, 2955.

37. Morimoto, H.; Tsubogo, T.; Litvinas, N. D.; Hartwig, J. F. *Angew. Chem. Int. Ed.* **2011**, *50*, 3793.

38. The addition of free bathocuproine to the equilibrium did not shift or modify the ^1H NMR spectroscopy signals. Therefore, in order to ensure that **4** was pure and free bathocuproine ligand was not present in the solid, we checked that the integration of a known amount of complex **4** by ^{19}F NMR spectra and the integration a known amount of internal standard (4,4’-diflurobiphenyl) correspond to the expected ratio according to the weight amounts.

39. Further discussions about its synthesis is provide in the Appendix. We also achieved the synthesis of [(Bc)Ag(THF)][SbF_6] and it was evaluated as a potential cation candidate.

40. These calculations were carried out with the ωB97-XD functional with a double-ζ plus polarization basis set in solvent (see Appendix for further details).

41. As it is described in the Appendix, this equilibrium has associate a ΔG^0 of 16.2 kcal·mol^{-1} which is quite large for an equilibrium observable at room temperature by NMR spectroscopy.

42. It should be mentioned that stabilizing π–π interactions are quite important in this system. Indeed, as it is described in the Appendix, **4a** as a dimer with π–π between the bathocuproine rings, is stabilized in 15.8 kcal·mol^{-1} below the separated monomers.

43. The observed signal was assigned by ^{19}F NMR spectroscopy based on the previously reported chemical shift (see ref. 36a). This was also supported by the behavior of analogous trifluoromethyl copper(I) system: Agnes, K.; Movchun, V.; Rodima, T.; Dansauer, T.; Rusanov, E. B.; Leito, I.; Kaljurand, I.; Koppel, J.; Pihl, V.; Koppel, I.; Ovsjannikov, G.; Toom, L.; Mishima, M.; Medebielle, M.; Lork, E.; Röschenthaler, G.-V.; Koppel, I. A.; Kolomeitsev, A. A. *J. Org. Chem.* **2008**, *73*, 2607.

44. This reaction using the Ruppert-Prakash reagent along with the activating agent, does not yield product **9**.

45. This yield is calculated respect to the initial amount of CF_3 moieties in $\mathbf{6_{Cs}}$ which is the limiting reagent.

46. We thought that the small amounts of PhI, which is liquid, may be partially in the head space of the set up.

47. Goodson, F. E.; Wallow, T. I.; Novak, B. M. *J. Am. Chem. Soc.* **1997**, *119*, 12441. b) Grushin, V. V. *Organometallics* **2000**, *19*, 1888. c) Fiebig, L.; Schlörer, N.; Schmalz, H.-G.; Schäfer, M. *Chem. Eur. J.* **2014**, *20*, 4906.

48. To a lesser extent, this reaction can also take place in apolar solvents.

49. Esturau, N.; Sanchez-Ferrando, F.; Gavin, J. A.; Roumestand, C.; Delsuc, M. A.; Parella, T. *J. Magn. Reson.* **2001**, *153*, 48.

50. Lide, D. R. (**2004**), CRC Handbook of Chemistry and Physics, 85th Edition, CRC Press, Boca Raton, FL.

51. Fremont, P. De; Scott, N. M.; Stevens, E. D.; Ramnial, T.; Lightbody, O. C.; Macdonald, C. L. B.; Clyburne, J. A. C.; Abernethy, C. D.; Nolan, S. P. *Organometallics* **2005**, *24*, 6301.

52. https://www.organicdivision.org/wp-content/uploads/2016/12/organic_solvents.html

53. Perrin, C. L.; Dwyer, T. J. *Chem. Rev.* **1990**, *90*, 935.

54. Prepared in the glovebox at room temperature.

55. Morimoto, H.; Tsubogo, T.; Litvinas, N. D.; Hartwig, J. F. *Angew. Chem. Int. Ed.* **2011**, *50*, 3793.

56. Likely due to the different counter anion ($[SbF_6]^-$ *vs*. $[Ag(CF_3)_2]^-$).

57. Claridge, T. D. W. Diffusion NMR spectroscopy. In *High-Resolution NMR Techniques in Organic Chemistry*, Elsevier Science: **2016**; pp 381-419.

58. The values of the diffusion coefficient of the residual solvent signal, taken as internal reference, were used to validate our measurement, being these values approximately $D_{benzene} = 2.69 \cdot 10^{-9}$ $m^2 \cdot s^{-1}$ for benzene, $D_{THF} = 3.16 \cdot 10^{-9}$ $m^2 \cdot s^{-1}$ for THF and $D_{DMF} = 1.66 \cdot 10^{-9}$ $m^2 \cdot s^{-1}$ for DMF.

59. Martínez, C. R.; Iverson, B. L. *Chem. Sci.* **2012**, *3*, 2191.

60. We used **4a'** and the interaction of a maximum of two bathocuproine ligands as models of a potentially more complex system. We are aware that these stabilizing π-π interactions could further facilitate the stabilization of other species such as trimer, tetramers, etc. both in reagents and in products.

61. a) Pliego, J. R.; Riveros, J. M. *J. Phys. Chem. A* **2001**, *105*, 7241. b) Bryantsev, V. S.; Diallo, M. S.; Goddard III, W. A. *J. Phys. Chem. B* **2008**, *112*, 9709. c) Marenich, A. V.; Ding, W.; Cramer, C. J.; Truhlar, D. G. *J. Phys. Chem. Lett.* **2012**, *3*, 1437. d) Ho, J.; Ertem, M. Z. *J. Phys. Chem. B* **2016**, *120*, 1319.

62. a) del Pozo, J.; Pérez-Iglesias, M.; Álvarez, R.; Lledós, A.; Casares, J. A.; Espinet, P. *ACS Catal.* **2017**, *7*, 3575. b) Harvey, J. N.; Himo, F.; Maseras, F.; Pedrrin, L. *ACS Catal*. **2019**, *9*, 6803.

63. From a practical point of view, *i.e.* the calculation of the equilibrium constants or the application of the translational correction, our system is described by eq. 4 but the free energy value is corrected and defined by ΔG_6. This is based on the assumption that the ΔG_5 associated to eq. 5 should be zero.

64. In these cases, the translational correction (from 1 atm. to 1M) was not applied to ΔG_5 values as we are only interested in the trend.

65. Standard conditions: 25 ºC and 1 M concentration of each reagent or product. We are aware that 1 M is not the standard state for the solvent, but this is taken into account when computing equilibrium concentrations.

66. Data collection with APEX II version v2013.4-1. Bruker (**2007**). Bruker AXS Inc., Madison, Wisconsin, USA.

67. Data reduction with Bruker SAINT version V8.30c. Bruker (**2007**). Bruker AXS Inc., Madison, Wisconsin, USA.

68. SADABS: V2014/5 Bruker (**2001**). Bruker AXS Inc., Madison, Wisconsin, USA. Blessing, Acta Cryst. (**1995**) A51 33-38.

69. TWINABS Version 2008/4 Bruker AXS; Blessing, *Acta Cryst.* (**1995**) A51 33.

70. Data collection and reduction with CrysAlisPro 1.171.39.12b (Rigaku OD, **2015**).

71. Empirical absorption correction using spherical harmonics implemented in Scale3 Abspack scaling algorithm, CrysAlisPro 1.171.38.37f (Rigaku OD, **2015**).

72. SHELXT; G. M. Sheldrick, *Acta Cryst*. **2015** A71, 3.

73. SHELXle; Huebschle, C. B.; Sheldrick, G. M.; Dittrich, B.; *J. Appl. Cryst.* **2011**, *44*, 1281.

74. SHELXL; Sheldrick, G. M. *Acta Cryst*. **2015** C71, 3. SHELXT.

75. Álvarez-Moreno, M.; de Graaf, C.; López, N.; Maseras, F.; Poblet, J. M.; Bo, C. *J. Chem. Inf. Model*. **2015**, *55*, 95.

76. Chai, J. D.; Head-Gordon, M. *Phys. Chem. Chem. Phys.* **2008**, *10*, 6615.

77. Gaussian 09, Revision D.01, Frisch, M. J.; Trucks, G. W.; Schlegel, H. B.; Scuseria, G. E.; Robb, M. A.; Cheeseman, J. R.; Scalmani, G.; Barone, V.; Mennucci, B.; Petersson, G. A.; Nakatsuji, H.; Caricato, M.; Li, X.; Hratchian, H. P.; Izmaylov, A. F.; Bloino, J.; Zheng, G.; Sonnenberg, J. L.; Hada, M.; Ehara, M.; Toyota, K.; Fukuda, R.; Hasegawa, J.; Ishida, M.; Nakajima, T.; Honda, Y.; Kitao, O.; Nakai, H.; Vreven, T.; Montgomery, Jr., J. A.; Peralta, J. E.; Ogliaro, F.; Bearpark, M.; Heyd, J. J.; Brothers, E.; Kudin, K. N.; Staroverov, V. N.; Keith, T.; Kobayashi, R.; Normand, J.; Raghavachari, K.; Rendell, A.; Burant, J. C.; Iyengar, S. S.; Tomasi, J.; Cossi, M.; Rega, N.; Millam, J. M.; Klene, M.; Knox, J. E.; Cross, J. B.; Bakken, V.; Adamo, C.; Jaramillo, J.; Gomperts, R.; Stratmann, R. E.; Yazyev, O.; Austin, A. J.; Cammi, R.; Pomelli, C.; Ochterski, J. W.; Martin, R. L.; Morokuma, K.; Zakrzewski, V. G.; Voth, G. A.; Salvador, P.; Dannenberg, J. J.; Dapprich, S.; Daniels, A. D.; Farkas, O.; Foresman, J. B.; Ortiz, J. V.; Cioslowski, J.; Fox, D. J. Gaussian, Inc., WallingfordCT, **2013**.

78. Andrae, D.; Haeussermann, U.; Dolg, M.; Stoll, H.; Preuss, H. *Theor. Chem. Accu.* **1990**, *77*, 123.

79. a) Hehre, W. J.; Ditchfield, R.; Pople, J. A. *J. Chem. Phys.* **1972**, *56*, 2257. b) Dill, J. D.; Pople, J. A. *J. Chem. Phys.* **1975**, *62*, 2921. c) Francl, M. M.; Petro, W. J.; Hehre, W. J.; Binkley, J. S.; Gordon, M. S.; DeFrees, D. J.; Pople, A. J. *J. Chem. Phys.* **1982**, *77*, 3654.

80. Marenich, A. V.; Cramer, C. J.; Truhlar, D. G. *J. Phys. Chem. B* **2009**, *113*, 6378.

CHAPTER 4. MECHANISTIC STUDIES ON THE TRANSMETALATION STEP IN Pd/Ag BIMETALLIC SYSTEMS.

4.1. Introduction

A general mechanistic proposal in Pd/Ag bimetallic systems implies the connection of the canonical palladium cycle with organosilver(I) species **I** through a transmetalation step. In this step, the activated organic moiety is transferred from the silver to the Pd(II) intermediate **II**. Then, the so-formed organopalladium(II) complex **III** subsequently undergoes the reductive elimination event affording the formation of the organic product and Pd^0 catalyst (**IV**). A more general mechanistic picture is depicted in **Scheme 4.1** where the oxidative steps varies depending on the nature of the starting material.

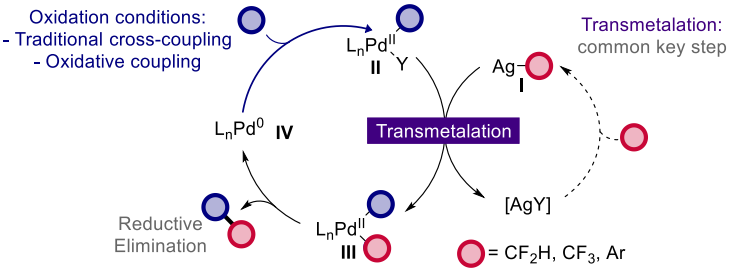

Scheme 4.1. Simplified version for the general proposal in the context of synergistic Pd/Ag bimetallic coupling reactions.

The synergy between Pd/Ag bimetallic couples for promoting the formation of C–C bonds, where organosilver(I) species transfer the organic moiety into the palladium cycle, is widely proposed in the literature (**Scheme 4.1**). Nevertheless, there is a dramatic lack of fundamental knowledge about its reaction mechanism, especially regarding the transmetalation step, being a drawback for the rational development of novel Pd/Ag bimetallic transformations. A reasonable approach for the mechanistic study would be the isolation of both the organo-Pd and organo-Ag species to study how the group exchange takes place. However, the isolation of both complexes is not always a straightforward task, especially when regarding the organosilver(I) species which are inherently thermo- and photo-sensitive and, in some cases, explosives.[1] This could be related to the scarce advances on the field.

Here below, we briefly discuss the Pd/Ag synergy in reactions as important as cross-coupling and oxidative coupling reactions, highlighting the scarce hints of mechanistic investigation that are provided in the literature.

[1] Schmidbaur, H.; Bayler, A. *Synthesis and Uses of Organosilver Compounds*, in *The Chemistry of Organic Derivatives of Gold and Silver* (Eds.: S. Patai. Z. Rappoport), Wiley, Chichester, **1999**, 211.

4.1.1. Pd/Ag-catalyzed decarboxylative coupling reactions

Decarboxylative coupling reactions enable the use of inexpensive and commercially available carboxylic acid derivatives as raw materials. In this context, the combination of Pd/Ag has shown to be fruitful for both cross-coupling and oxidative coupling reactions. The most accepted mechanistic proposes the silver salts to promote the decarboxylation reaction and, then, to transfer the nucleophilic moiety into the Pd-cycle.

4.1.1.1. Bimetallic Pd/Ag decarboxylative cross-coupling reactions

In 2006, Goossen proposed a new approach to form C–C bonds from stable, cheap and abundant pre-nucleophiles: benzoic acids.[2] Originally, this methodology was developed using Pd/Cu bimetallic couples to promote the reaction between *ortho*-nitro-substituted benzoic acids and aryl bromides (**Scheme 4.2**), as discussed in Chapter 1.

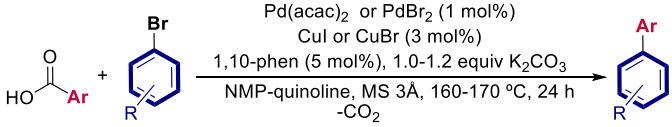

Scheme 4.2. Seminal protocol for the Pd/Cu-catalyzed decarboxylative C_{sp2}-C_{sp2} coupling reaction. acac = acetylacetonate, phen = phenantroline, NMP = 1-methyl-2-pyrrolidinone, MS = molecular sieve.

Shortly after, Goossen mentioned, for the first time, the use of silver salts as decarboxylating agents in this type of transformation (**Scheme 4.3**).[3] Concurrently, Wagner *et al*. described the use of super stoichiometric amounts of silver salts to promote the decarboxylation in Pd-catalyzed reactions (**Scheme 4.3**).[4] It was in 2010, when Goossen and co-workers described the formation of biaryls using aryl triflates and carboxylate salts, in the presence, for the first time, of catalytic amounts of palladium and silver.[5] As is shown in **Scheme 4.3**, this work proceeded under milder conditions, more than 40 °C below, compared to the previously reported analogous copper version.

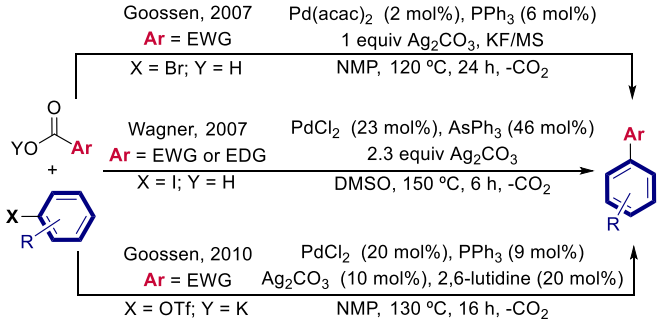

Scheme 4.3. Different protocols involving Pd/Ag bimetallic cooperation.

2 Goossen, L. J.; Deng, G.; Levy, L. M. *Science*, **2006**, *313*, 662.
3 Goossen, L. J.; Rodríguez, N.; Melzer, B.; Linder, C.; Deng, G.; Levy, L. M. *J. Am. Chem. Soc*. **2007**, *129*, 4824.
4 Becht, J. M.; Catala, C.; Le Drian, C.; Wagner, A. *Org. Lett*. **2007**, *9*, 1781.
5 Goossen, L. J.; Lange, P. P.; Rodríguez, N.; Linder, C. *Chem. Eur. J*. **2010**, *16*, 3906.

The proposed mechanism involves a transmetalation step from the arylsilver(I) species **V**, *in situ* generated through the CO_2 extrusion, to a aryl–Pd(II) complex **VI**, $[(L)_nPd(Ar)(X)]$, formed by oxidative addition of Ar–X to $[(L)_nPd^0]$ (**Scheme 4.4**). The resulting biarylpalladium(II) complex **VII** undergoes reductive elimination, affording the cross-coupling product along with the Pd^0 catalyst. In view of the complex mechanistic picture, Goossen and co-workers emphasized the necessity of a perfect match between all the elementary steps involved in both catalytic cycles.

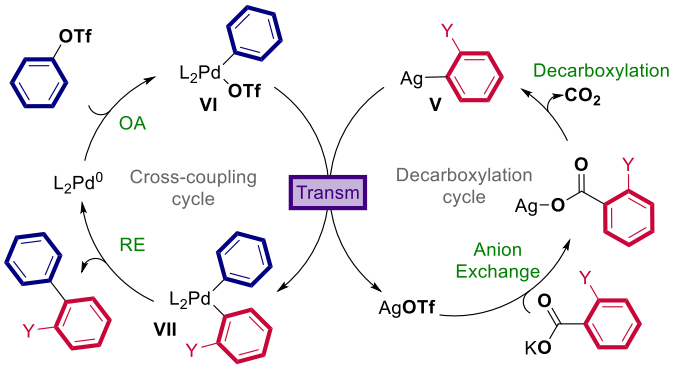

Scheme 4.4. Proposed catalytic cycle for the Pd/Ag-catalyzed decarboxylative synthesis of biaryls.

4.1.1.2. Bimetallic Pd/Ag decarboxylative oxidative coupling reactions

Oxidative coupling reactions, which involve the reaction of two nucleophilic partners under oxidative conditions, have become a greener alternative to traditional cross-coupling reactions.[6] They offer multiple advantages such as the employment of more readily available starting materials and the minimization of by-product formation. In this regard, organosilver(I) species have been proposed to be involved in the transmetalation step of the coupling or benzoic acids with different coupling partners as we will briefly describe below.

- **Pd-catalyzed/Ag-mediated decarboxylative Heck-type reaction**

In 2002, Myers *et al*. disclosed the first example of Pd-catalyzed decarboxylative Heck-type reactions between *ortho*-substituted benzoic acids and alkenes such as styrene, acrylates or cyclohexanone (**Scheme 4.5**).[7] In this seminal work, the authors proposed the silver salts to play a role as external oxidants. Additional mechanistic studies showed the capability of palladium species to promote the decarboxylation of electron-rich benzoic acids.[8]

6 Ackermann, L.; Vicente, R.; Kapdi, A. R. *Angew. Chem. Int. Ed*. **2009**, *48*, 9792.
7 Myers, A. G.; Tanaka, D.; Mannion, M. R. *J. Am. Chem. Soc*. **2002**, *124*, 11250.
8 Tanaka, D.; Romeril, S. P.; Myers, A. G. *J. Am. Chem. Soc*. **2005**, *127*, 10323.

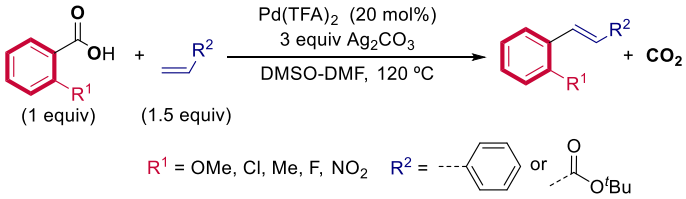

Scheme 4.5. Pd-catalyzed decarboxylative Heck-type reaction in the presence of silver salts reported by Myers ref 7. TFA = trifluoroacetate.

Regarding the potential active species during the catalysis, it is not possible to rule out the participation of silver in the decarboxylative event as Larrosa and Goossen pointed out.[9] Indeed, in 2016, an interesting report by Jana's group described a mechanistic divergence on the Pd-catalyzed decarboxylative Heck-type coupling reaction depending on the nature of the corresponding benzoic acid (**Scheme 4.6**).[10] The coupling of alkenes and electron-rich carboxylic acids proceeds using [Pd(TFA)$_2$] as catalyst and 1,4-benzoquinone as oxidant to afford the corresponding organic product. However, when using electron-poor benzoic acids, the authors did not observe product formation in the absence of silver. This suggested that providing the silver salts are not only play a role as external oxidants but also as mediators of the decarboxylative process.

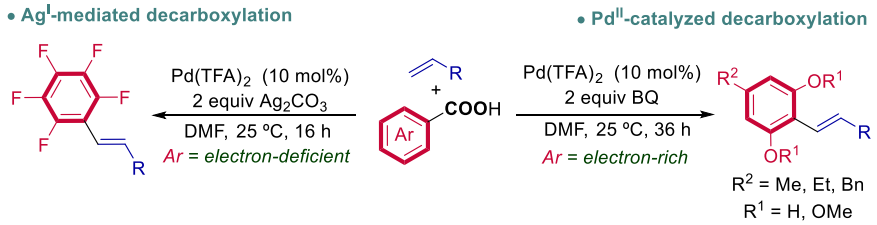

Scheme 4.6. Experimental proof of the potential participation of silver salts as decarboxylative mediator in Heck-type reactions. TFA = trifluoroacetate, BQ = 1,4-benzoquinone, Bn = bencyl.

Collectively, the current mechanistic proposal, especially when involving electron-poor moieties on the nucleophile, implies the Ag-promoted decarboxylation process to afford the organosilver(I) intermediate **VIII** that participates in the transmetalation step to a [(L)$_2$Pd^{II}(X)$_2$] intermediate (**IX**). The so-formed aryl-Pd(II) complex **X** undergoes a migratory insertion (MI) followed by β-hydride elimination (βHE), releasing the desired product (**Scheme 4.7**). The [(L$_2$Pd^{II}(H)(X)] intermediate **XI** undergoes a reductive elimination, regenerating palladium(0) which is re-oxidized by silver. In this case, the silver salt not only plays a role as decarboxylating agent but also as an external oxidant.

[9] a) Rodríguez, N.; Goossen, L. J. *Chem. Soc. Rev*. **2011**, *40*, 5030. b) Cornella, J.; Larrosa, I. *Synthesis* **2012**, *44*, 653.

[10] Hossian, A.; Bhunia, S. K.; Jana, R. *J. Org. Chem*. **2016**, *81*, 2521.

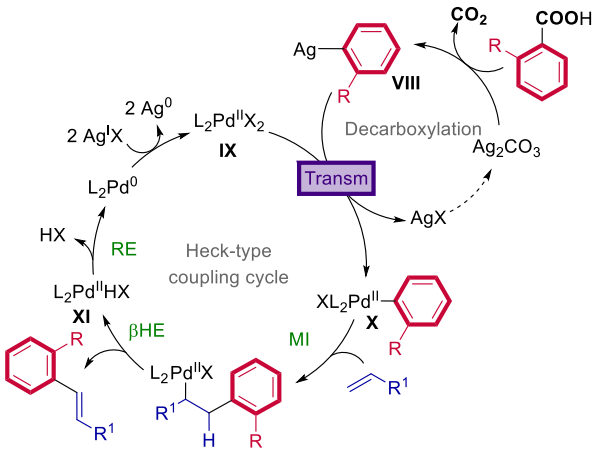

Scheme 4.7. Mechanistic proposal for the Pd-catalyzed/Ag-mediated decarboxylative Heck-type reaction.

- **Pd-catalyzed C-H activation and Ag-promoted decarboxylation in the C–COOH/C–H coupling**

In 2009, Glorius *et al.* published the first intramolecular example of an oxidative C–C coupling from C–COOH and C–H moieties. In this reaction, the organosilver nucleophile was proposed as a transmetalating agent to the Pd-cycle after the decarboxylation event (**Scheme 4.8**).[11,12]

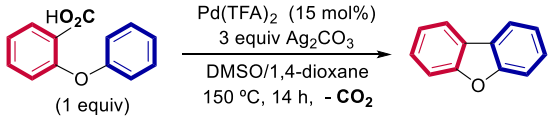

Scheme 4.8. Pd-catalyzed/Ag-mediated intramolecular direct arylation of carboxylic acids derivatives.

Subsequently, Larrosa described the intermolecular synthesis of C-3 arylated indoles *via* a Pd-catalyzed/Ag-mediated C–H activation/decarboxylation process.[13]

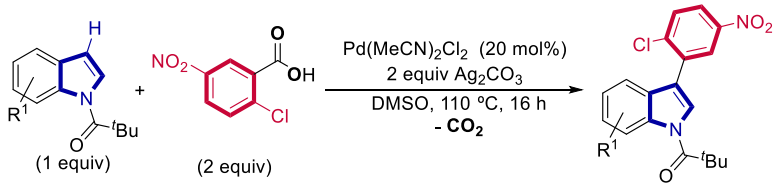

Scheme 4.9. Pd-catalyzed/Ag-mediated intermolecular C-3 arylation of indoles with benzoic acids.

In this transformation, while the silver salt mediates the decarboxylation process, the palladium catalyst performs the C–H bond activation step affording the corresponding Pd^{II} intermediate **XII**. This species is involved in the transmetalation step with the arylsilver(I) species

11 Wang, C.; Piel, I.; Glorius, F. *J. Am. Chem. Soc*. **2009**, *131*, 4194.

12 An analogous intermolecular version of this transformation was previously described by Crabtree, using microwave irradiation, but the potential role of the silver was not explicitly mentioned. Voutchkova, A.; Coplin, A.; Leadbeater, N. E.; Crabtree, R. H. *Chem. Commun.* **2008**, 6312.

13 Cornella, J.; Lu, P.; Larrosa, I. *Org. Lett*., **2009**, *11*, 5506.

(**Scheme 4.10**). As in the previously shown examples, subsequent reductive elimination releases the organic product.

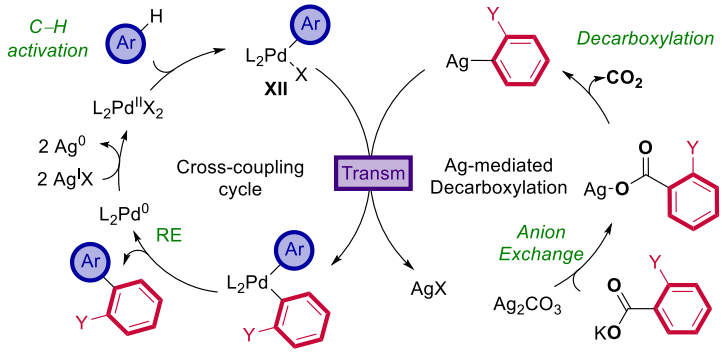

Scheme 4.10. Mechanistic proposal for the Pd-catalyzed/Ag-mediated intermolecular C-3 arylation of indoles with benzoic acids.

- **Pd-catalyzed/Ag-mediated decarboxylation reaction in the C–COOH/C–COOH coupling**

In 2010, Larrosa and co-workers described an alternative to the oxidative C–COOH/ C–H couplings based on the use of two carboxylic acid derivatives as pre-nucleophiles, which are decarboxylated by the silver salt and, then, coupled by the palladium catalyst after two consecutive transmetalations.[14] The authors could access symmetric biaryls in good to excellent yields using aromatic acids bearing an *ortho* electron-withdrawing substituent or an α heteroatom (**Scheme 4.11**). The nature of the group in the *ortho* position is key for favoring the transmetalation towards the Pd-cycle over undesired protodemetalation of the organosilver(I) species. This points out the importance of the efficiency of the group transfer between Pd and Ag metals for the outcome of the reaction.

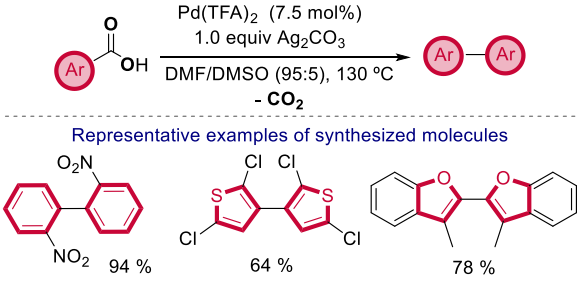

Scheme 4.11. Pd-catalyzed/Ag-mediated homocoupling reaction of aromatic carboxylic acids.

In this vein, Deng *et al*. introduced and Su *et al*. developed the concept of the Pd/Ag-catalyzed oxidative cross-coupling of two different carboxylic acids (**Scheme 4.12**).[15] In this asymmetric version of the aforementioned Larrosa's system, silver species promote the

[14] Cornella, J.; Lahlali H.; Larrosa, I. *Chem. Commun*. **2010**, *46*, 8276.

[15] a) Xie, K.; Wang, S.; Yang, Z.; Liu, J.; Wang, A.; Li, X.; Tan, Z.; Guo C.; Deng, W. *Eur. J. Org. Chem*. **2011**, 5787. b) Hu, P.; Shang Y.; Su, W. *Angew. Chem. Int. Ed*., **2012**, *51*, 5945.

decarboxylation of the carboxylic acid, the transfer the organic moiety and the reoxidation of the palladium complex while the palladium catalyst simply undergoes the coupling of both nucleophiles. This represents a remarkable platform to couple two pre-nucleophiles with different electronic properties from cheap and not activated functionalities.

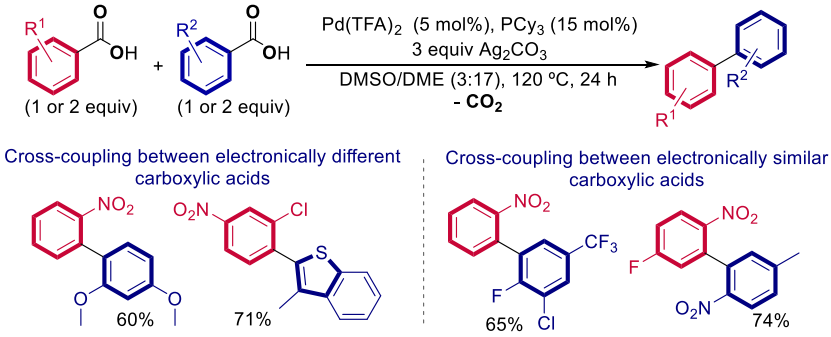

Scheme 4.12. Pd-catalyzed/Ag-mediated heterocoupling reaction of different aromatic carboxylic acids. TFA = trifluoroacetate, Cy = cyclohexyl, DME = 1,2-dimethoxyethane.

As is shown in **Scheme 4.13**, the palladium catalyst is a mere vehicle for the coupling of the two decarboxylated nucleophiles. It should be emphasized the kinetic compatibility of all the elementary steps involved in the catalytic cycle since no homocoupling and/or protodecarboxylative products are the main observed products.

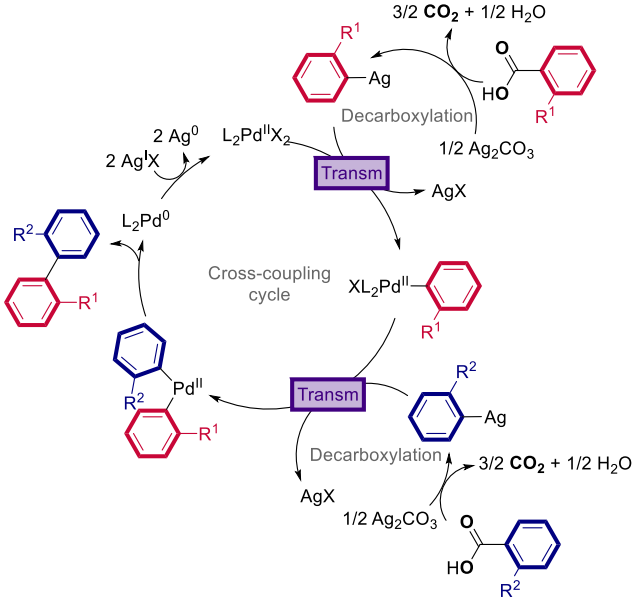

Scheme 4.13. Proposed mechanism for the Pd-catalyzed/Ag-mediated of the oxidative heterocoupling of benzoic acids.

4.1.2. **Pd-catalyzed/Ag-mediated C–H activation reactions**

Apart from promoting decarboxylative events, silver salts have been also proposed to activate C–H bonds in different organic substrates. In the context of Pd-catalyzed cross-coupling reactions, the first experimental proof of the capability silver salts as C–H activator is related to the Sonogashira type cross-coupling, mentioned in the general Introduction. This transformation consists of the coupling of different electrophiles with terminal alkynes, which are activated by a coinage metals as co-catalyst (Scheme 4.14).[16]

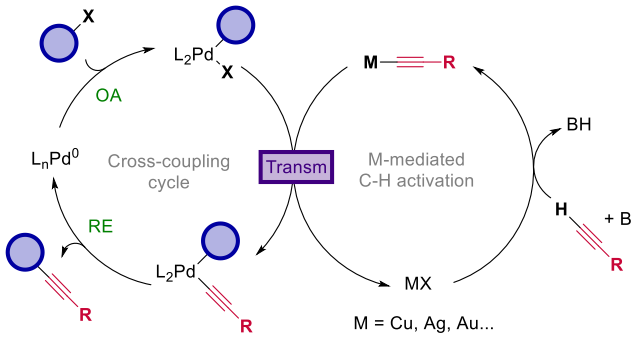

Scheme 4.14. General mechanistic proposal for the Pd/coinage metal-catalyzed Sonogashira cross-coupling reaction. B = base.

In 2001, Pale and co-workers showed that silver acetylides can react with *in situ* generated Pd^{II} intermediates to yield the corresponding C–C bond-forming reductive elimination product **XIII**.[17] The authors observed a dependence of the product formation on the solvent (Scheme 4.15). When using DMF as solvent, the reaction happens in a fast manner (5 min), while the yield decreases dramatically when using acetonitrile. According to Pale *et al*., this result shows that the transmetalation reaction is affected by the coordinating ability of the solvent since the oxidative addition event using vinyl triflates is supposed to be a fast process regardless the solvent used.[18]

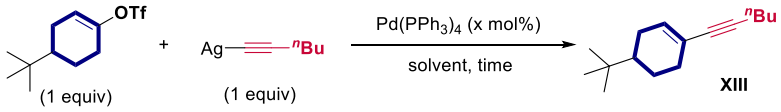

x cat. Pd	solvent	time	Yield **XIII** %
none	DMF	24 h	0
50 mol%	DMF	5 min	98
50 mol%	MeCN	1 h	15
50 mol%	Et_2O	4 h	37

Scheme 4.15. Cross-coupling reaction of vinyl triflates and silver acetylides in the presence of catalytic amounts of Pd^0 species. Indirect transmetalation study varying the reaction conditions.

[16] Copper: a) Sonogashira, K. *J. Organomet. Chem*. **2002**, *653*, 46. Silver: b) Y. Yamamoto, *Chem. Rev*. **2008**, *108*, 3199. Gold: c) Lauterbach, T.; Livendahl, M.; Rosellón, A.; Espinet, P.; Echavarren, A. M. *Org. Lett.* **2010**, *12*, 3006.

[17] Dillinger, S.; Bertus, P.; Pale, P. *Org. Lett.* **2001**, *3*, 1661.

[18] The authors explicitly mentioned the role of the coordinating ability of the solvent on stabilizing the specific silver acetylide used in the reaction. See ref. 17.

From this seminal report on, there has been a lack of stoichiometric studies that explore *per se* the transmetalation step in detail. In 2014, Albéniz *et al*. disclosed the synthesis of heterobimetallic Pd-Ag organometallic complexes using silver acetylenes derivatives as transmetalating agents (**Scheme 4.16**).[19] Although this reaction could have been considered as transmetalation model reaction for Sonogashira couplings, the study on the group exchange between both species was overlooked. It should be mentioned that the polymeric nature of the silver complex could hamper this analysis.

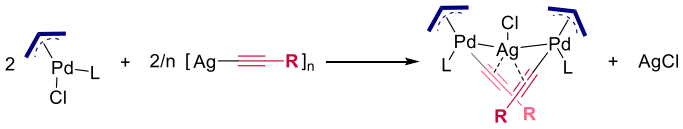

Scheme 4.16. Synthesis of heterobimetallic Pd–Ag complexes.

Apart from Sonogashira cross-coupling reactions, different research groups support the crucial role of silver species in other Pd-catalyzed reactions involving a C–H bond activation. In 2016, a pioneering study by Larrosa *et al*. on Pd-catalyzed arylation of $Cr(CO)_3$-complexed fluorobenzene revealed the efficient C_{sp2}–H activation of electron-deficient arenes by an *in situ* generated phosphine-ligated silver species [$(PPh_3)Ag(OCOAd)$] (**Scheme 4.17**).[20]

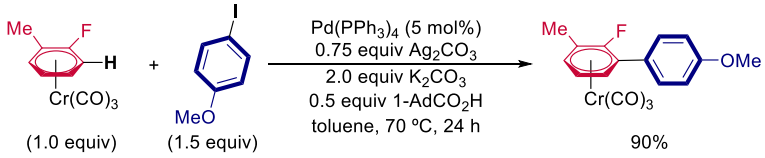

Scheme 4.17. Pd-catalyzed/Ag-mediated direct arylation of [(*m*-fluorotoluene)$Cr(CO)_3$] using *p*-iodoanisole. Ad = adamantyl.

Mechanistic investigations including H/D exchange, kinetic isotopic effect (KIE) and kinetic studies pointed out that the turnover-determining step of the whole catalytic process was the Ag-mediated C–H activation of the [(*m*-fluorotoluene)$Cr(CO)_3$] complex. Regarding the $Pd^{0/II}$-cycle, the transmetalation was proposed to be the slowest step since they were able to detect by NMR spectroscopy the *trans*-[$(PPh_3)_2Pd(OCOAd)$(*p*-(OMe)Ph)] complex (**XIV**), intermediate prior to the transmetalation.

They also performed stoichiometric experiments between the *trans*-[$(PPh_3)_2Pd(OCOAd)$(*p*-(OMe)Ph)] complex **XIV**, the resting state of the catalytic cycle, and the arene-Cr complex **XV** under different reaction conditions affording the coupling product in 72% yield in the presence of AgOCOAd, PPh_3 and an *p*-(trifluoromethyl)-iodobenzene. This is an indirect proof of the group exchange from the *in situ* generated [$(PPh_3)Ag$(arenyl-Cr)] complex to the Pd(II) intermediate.

[19] Meana, I.; Espinet, P.; Albéniz, A. C. *Organometallics* **2014**, *33*, 1.
[20] Whitaker, D.; Burés J.; Larrosa, I. *J. Am. Chem. Soc*. **2016**, *138*, 8384.

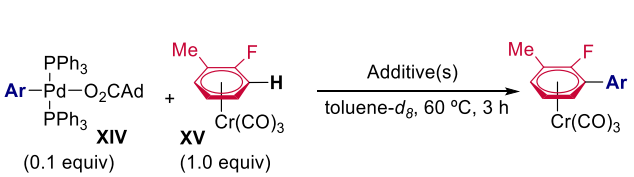

Additive(s) (equiv)	Yield
none	0%
K_2CO_3 (2)	0%
O_2	0%
Ag(OCOAd) (0.5), PPh_3 (0.5)	26%
Ag(OCOAd) (0.5), PPh_3 (0.5), *p*-$(CF_3)C_6H_4I$ (1.5)	72%

Scheme 4.18. Stoichiometric reaction of aryl-Pd(II) complex with the arene-Cr complex under different reaction conditions. Ad = adamantly.

Concurrently, the same group reported the critical effect of silver additives for the success of the selective β-arylation of thiophenes and benzo[*b*]thiophenes using iodoarenes as coupling partners. In this system, the silver salt was proposed to be essential for the activation the HFIP, which is transferred to aryl-Pd^{II} complex **XVI** affording intermediate **XVII**. This intermediate subsequently perform the C–H functionalization step(s).[21]

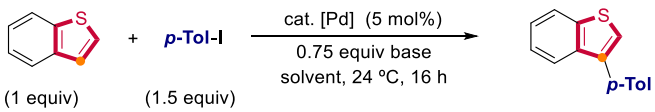

entry	base	cat. [Pd]	solvent	NMR yield (%)
1	Ag_2CO_3	$Pd(OAc)_2$	TFE	34
2	Ag_2CO_3	$Pd(OAc)_2$	HFIP	72
3	Ag_2CO_3	$Pd_2(dba)_3{\cdot}CHCl_3$	HFIP	92
4	K_2CO_3	$Pd_2(dba)_3{\cdot}CHCl_3$	HFIP	0
5	Ag_2CO_3	none	HFIP	0

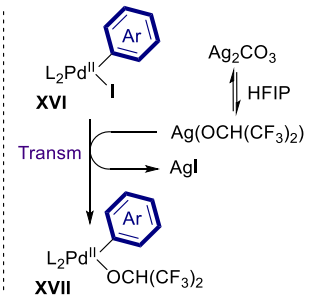

Scheme 4.19. Optimization of the reaction conditions for the Pd-catalyzed/Ag-mediated C-3 arylation of benzo[b]thiophenes using 4-iodoanisole as electrophilic coupling partner. Tol = tolyl, TFE = 1,1,1-trifluoroethanol, HFIP = 1,1,1,3,3,3-hexafluoroisopropan-2-ol, Ac = acetate, dba = dibenzylideneacetone.

Two years later, the same research group described the dependence of the regioselectivity of the aforementioned system on the Pd/Ag ratio.[22] As we can see in **Scheme 4.20**, a decrease on the Pd/Ag ratio shifted the exclusive arylation on C-3 position (**XVIII**) towards the preferentially arylation of the C-2 position of the substrate (**XIX**). Different mechanistic studies such as competition experiments and kinetic studies as well as H/D exchange and KIE experiments were gathered to support a cooperative bimetallic process for the C-2 functionalization. The regioselective swap is associated with the role of the silver additive to selectively activate the C-2–H bond (turquoise in **Scheme 4.20**) of the substrate which is further incorporated into the Pd-cycle through a transmetalation event. Interestingly, they observed a decrease on the C-2:C-3 regioselectivity when using *ortho*-substituted aryl iodides. This was attributed to a more challenging transmetalation step, due to steric hindrance of the aryl-Pd(II)

[21] Colletto, C.; Islam, S.; Juliá-Hernández, F.; Larrosa, I. *J. Am. Chem. Soc*. **2016**, *138*, 1677.
[22] Colletto, C.; Panigrahi, A.; Fernández-Casado, J.; Larrosa, I. *J. Am. Chem. Soc*., **2018**, *140*, 9638.

intermediate, that favors the formation of the non-desired product (**XVIII**). A common mechanistic picture for both transformations is shown in **Scheme 4.20**.

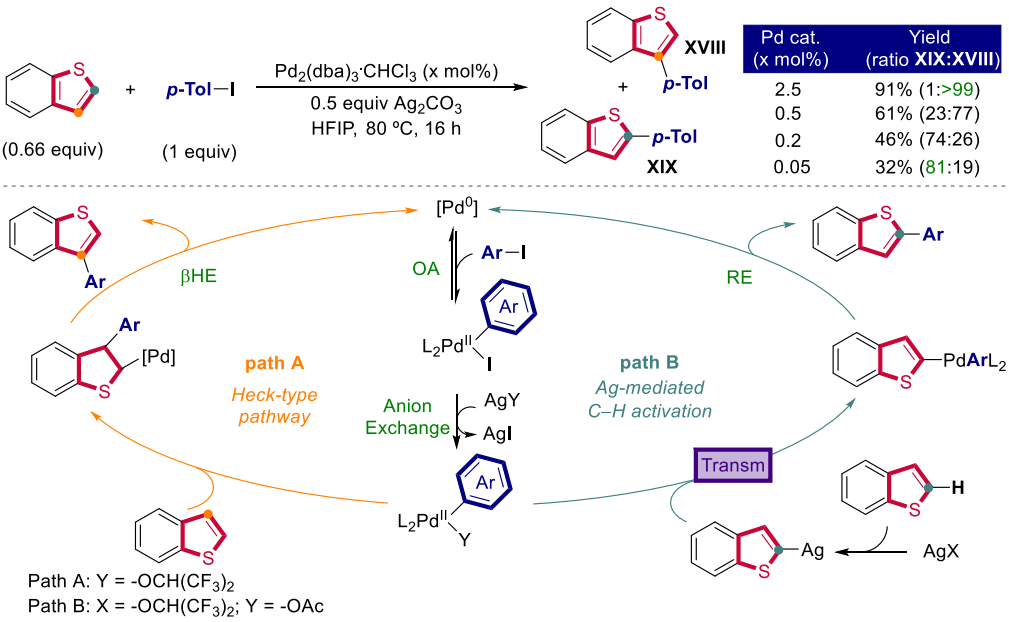

Scheme 4.20. Dependence of the regioselectivity on the Pd/Ag ratio for Pd-catalyzed/Ag-mediated C-3:C-2 arylation of benzo[b]thiophenes. Tol = tolyl, HFIP = 1,1,1,3,3,3-hexafluoroisopropan-2-ol, Ac = acetate, dba = dibenzylideneacetone.

Regarding the potential of silver salts to activate the C-2 position in thiophene rings, Sanford and co-workers reported the Pd^{II}-catalyzed/Ag-mediated oxidative dimerization of 2-alkylthiophenes (**Scheme 4.22**).[23] In this oxidative coupling system, silver is proposed to play multiple roles as C–H bond activator, nucleophilic transmetalating agent and external oxidant to regenerate the active Pd^{II} catalyst mirroring the mechanistic proposal in **Scheme 4.13**.

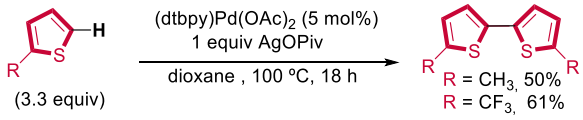

Scheme 4.21. Pd-catalyzed oxidative dimerization of 2-alkyl-thiophenes. dtbpy = 4,4'-di-tert-butyl-2,2'-bipyridyl, Piv = pivalate

Mechanistic studies demonstrated the capability of AgOPiv to activate the 5-position of 2-substituted thiophene derivatives through H/D exchange reactions, obtaining the corresponding deuterated molecules in 50-60% yield in the absence of palladium (**Scheme 4.22**).

[23] Lotz, M. D.; Camasso, N. M.; Canty, A. J.; Sanford, M. S. *Organometallics*, **2017**, *36*, 165.

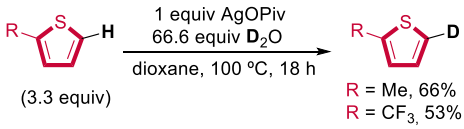

Scheme 4.22. H/D exchange reaction promoted by silver pivalate salt of 2-alkyl-thiophenes in deuterated water.

In the same work, the authors observed for the first time, by ^{19}F NMR spectroscopy, the stoichiometric *in situ* formation of $Ag(C_6F_5)$ via C–H activation of C_6F_5H using AgOPiv, proving the capability of silver to promote the C–H bond cleavage.[23] In addition, the authors demonstrated the feasible transfer of pentafluorophenyl groups from AgC_6F_5, synthesized independently, to $[(N^N)Pd(OAc)_2]$, producing the bis-(pentafluorophenyl)-palladium complex in high yields (**Scheme 4.23**). It is worth mentioning that the nature of the silver salt plays a crucial role in the outcome of the C–H activation step. When using silver salts such as AgX (X = PF_6, BF_4 or OTf) or different pivalates MOPiv (M = Cs, Na or NMe_4) only traces of Pd^{II}–(C_6F_5) species were observed (**Scheme 4.23**). DFT calculations were performed regarding the C–H activation but the reaction between Pd and Ag complexes were not theoretically contemplated.

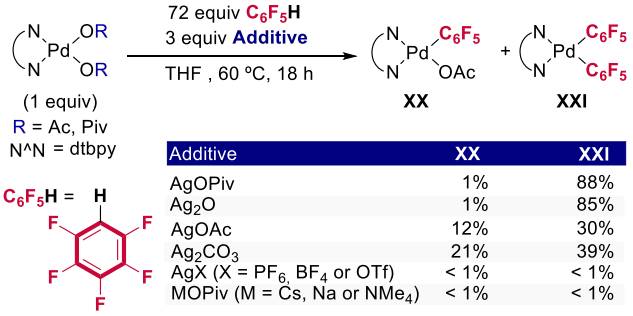

Additive	XX	XXI
AgOPiv	1%	88%
Ag_2O	1%	85%
AgOAc	12%	30%
Ag_2CO_3	21%	39%
AgX (X = PF_6, BF_4 or OTf)	< 1%	< 1%
MOPiv (M = Cs, Na or NMe_4)	< 1%	< 1%

Scheme 4.23. Effect of additives on the reaction of Pd complexes and C_6F_5H. Ac = acetate, Piv = pivalate, dtbpy = 4,4'-di-tert-butyl-2,2'-bipyridyl, OTf = triflate.

The same year, Hartwig and co-workers reported the selective formation of C_{sp2}–C_{sp3} bonds by palladium-catalyzed/silver-mediated allylation of monofluorobenzenes or non-fluorinated benzenes with allylic pivalates to form (E)-allylarenes (**Scheme 4.24**).[24]

[24] Lee, S. Y.; Hartwig, J. F. *J. Am. Chem. Soc*. **2016**, *138*, 15278.

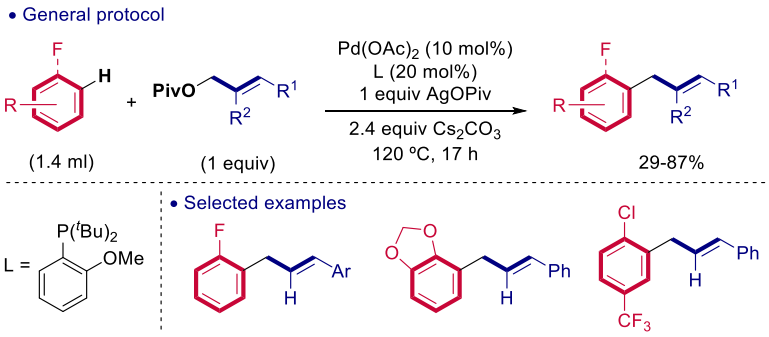

Scheme 4.24. General protocol for the Pd-catalyzed/Ag-mediated direct allylation of aryl C–H bonds. Piv = pivalate, Ac = acetate.

This work is particularly interesting since the authors were able not only to isolate and fully characterize for the first time a phosphine-ligated aryl silver(I) complex which is considered a key intermediate in this transformation, but also to establish its participation in the catalytic system by carrying out the stoichiometric reaction (**Scheme 4.25**). All the mechanistic data including H/D scrambling, KIE, *in situ* ^{31}P NMR spectroscopy and stoichiometric experiments are in accordance with a Pd/Ag synergistic system where the arylsilver(I) complex **XXII** is able to transmetalate an aryl group to a (π-allyl)palladium(II) pivalate species, **XXIII**. The so-formed (π-allyl)palladium-aryl complex **XXIV** undergoes a reductive elimination to yield the allylation product.

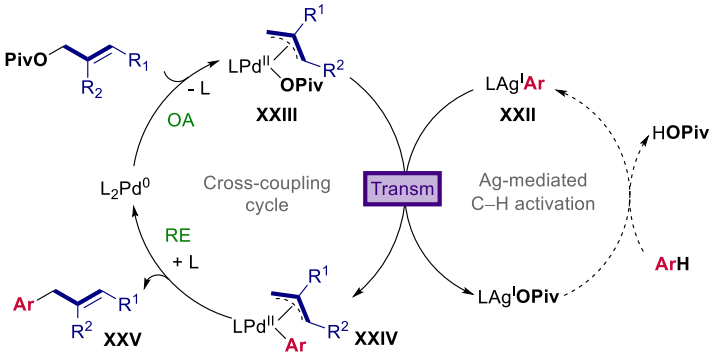

Scheme 4.25. Mechanistic proposal for the Pd-catalyzed/Ag-mediated direct allylation of aryl C–H bonds.

The synthesis of the proposed intermediates (**XXII'** and **XXIII**) involved in the transmetalation and the study of stoichiometric transmetalation affording the organic product (**XXV'**) reinforces the viability of this mechanism (**Scheme 4.26**).

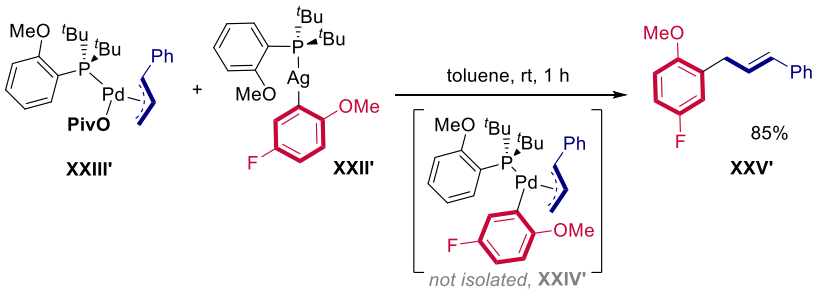

Scheme 4.26. Stoichiometric transmetalation study between both isolated Pd and Ag proposed intermediates.

4.1.3. **Pd-catalyzed/Ag-catalyzed or mediated difluoromethylation reactions**

Over the past few years, the scientific community has directed its efforts towards the development of rapid and efficient strategies to install perfluoroalkyl groups, CF_2H and CF_3 functional groups onto organic scaffolds due to their capability to induce changes in their physicochemical properties.[25,26] In this context, well-defined organometallic silver derivatives have demonstrated their great ability as transmetalating reagents in Pd-catalyzed cross-coupling reactions.[27]

In 2014, Shen *et al*. reported for the first time the Pd/Ag-catalyzed difluoromethylation of Ar–X (X = Br, I) using Me_3SiCF_2H.[28] This methodology turned to be widely compatible with different functional groups, other electrophilic coupling partners and it even was applied in the late-stage difluoromethylation of target molecules in medicinal chemistry (**Scheme 4.27**).[29]

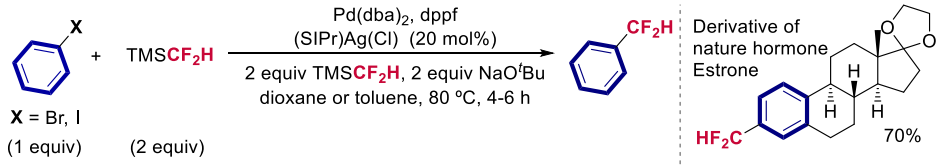

Scheme 4.27. General protocol for the Pd/Ag-catalyzed difluoromethylation of aryl halides. When X = Br, $[Pd(dba)_2]$ (5 mol%), dppf (10 mol%) in dioxane. When X = I, $[Pd(dba)_2]$ (7 mol%), dppf (14 mol%) in toluene. dppf = 1,1'-bis(diphenylphosphino)ferrocene.

The authors pointed out that the development of the whole catalytic procedure was based on the isolation of the Pd^{II} and Ag^{I} intermediates, using them to test the feasibility of each

[25] For selected reports regarding the CF_2H properties, see: Gillis, E. P.; Eastman, K. J.; Hill, M. D.; Donnelly D. J.; Meanwell, N. A. *J. Med. Chem.*, **2015**, *58*, 8315. For selected reports regarding the CF_3 properties, see: Schlosser, M. *Angew. Chem. Int. Ed.*, **2006**, *45*, 5432.

[26] For selected review on difluoromethylation, see: a) Feng, Z.; Xiao, Y.-L.; Zhang, X. *Acc. Chem. Res.*, **2018**, *51*, 2264. For selected review on trifluoromethylation, see: b) Furuya, T.; Kamlet A. S.; Ritter, T. *Nature*, **2011**, *473*, 470.; c) Tomashenko O. A.; Grushin, V. V. *Chem. Rev.*, **2011**, *111*, 4475.

[27] This topic is covered in detail in the Introduction of Chapter 2.

[28] Gu, Y.; Leng X.; Shen, Q. *Nat. Commun.*, **2014**, *5*, 5405.

[29] a) Lu, C.; Lu, H.; Wu, J.; Shen, H. C.; Hu, T.; Gu, Y.; Shen, Q. *J. Org. Chem.*, **2018**, *83*, 1077. b) Chang, D.; Gu, Y.; Shen, Q. *Chem. Eur. J.* **2015**, *21*, 6074. c) Lu, C.; Gu, Y.; Wu, J.; Gu Y.; Shen, Q. *Chem. Sci.*, **2017**, *8*, 4848.

elementary step in a theoretic catalytic cycle (**Scheme 4.28**). The experimental data suggest that the key step in this process is the transmetalation that connects the palladium and silver cycles.

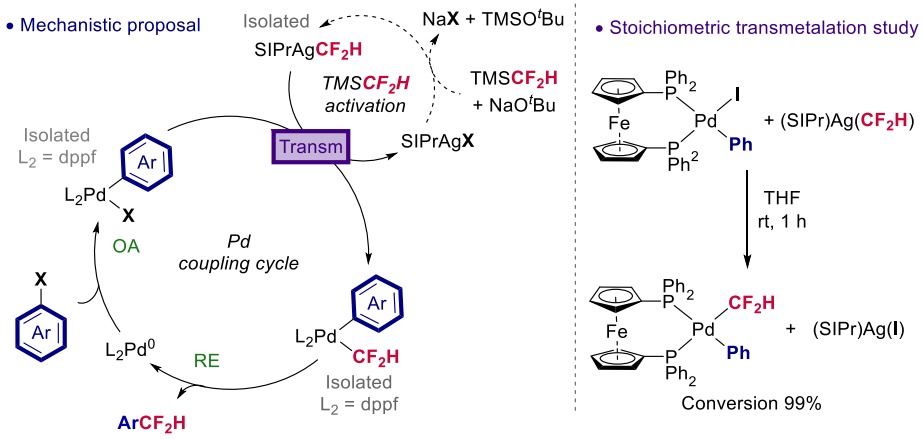

Scheme 4.28.To the left: proposed mechanism for the Pd/Ag-catalyzed difluoromethylation of aryl halides. To the right: stoichiometric study of the transmetalation by isolating the proposed intermediates in the catalytic cycle.

Further studies for the difluoromethylation of different electrophiles showed that two equivalents of a salt such as potassium bromide was beneficial for the reaction.[29b] The authors proposed that this salt contributes to the generation of a more stable Pd^{II}–Br species that improve the performance of the transmetalation step, highlighting the vital importance of the X-for-CF_2H exchange in the reaction outcome. As discussed in Chapter 2, an efficient transmetalation step in trifluoromethylation reactions is essential for the success or failure of the coupling process. The work presented in Chapter 2 reinforces the key role of silver nucleophiles in Pd-catalyzed cross-coupling reactions.

In conclusion, Pd/Ag bimetallic cooperation has led to the creation of a wide array of C–C bonds through different mechanistic routes which share a common transmetalation event. Although there are some seminal studies on this step including stoichiometric experiments of isolated intermediates, there is still a lack of fundamental knowledge on the mechanism that governs the transfer of the groups from organosilver(I) species to Pd(II) complexes.

4.2. **Objectives**

Palladium/silver bimetallic systems enable the creation of a wide array of C–C bonds not only in the context of cross-coupling reactions but also in oxidative coupling arena. A common mechanistic step in all these processes is the group exchange from an organosilver(I) species to an organo-Pd(II) intermediate – the transmetalation step – which basically allows the C–C bond-forming reductive elimination event. Despite its ubiquity, scarce pieces of information on the underlying reaction mechanism can be gathered from the literature, especially if considered stoichiometric experiments on the group transfer from the isolated complexes. This has been likely hampered by the inherent thermo- and photo-sensitivity of the organosilver(I) species and/or the direct formation of the organic product. This lack of fundamental knowledge on the transmetalation reaction mechanism is a drawback for the rational development of new Pd/Ag bimetallic transformations.

In this context, we envisioned the study of the transmetalation reaction mechanism in a model system from a organosilver(I) species to a organo-Pd(II) complex. To do so, the following points are pursued:

- Selection of the model system that allow us to study exclusively the transmetalation reaction using well-defined complexes and preventing side reactions such as the reductive elimination.

- Synthesis of organo-Pd(II) and organosilver(I) complexes regarding the selected model system.

- Evaluation of the group exchange by performing not only kinetic experiments but also DFT calculations.

4.3. Results and discussion

This section fundamentally divided into three parts. We undertake the discussion of the results by i) the selection of the model system that allowed us to prevent side reactions. Then, we will discuss the mechanistic investigations on the transmetalation step regarding, firstly, ii) a neutral silver complex in equilibrium with an ionic species and, secondly, iii) the reaction mechanism regarding exclusively ionic silver species.

4.3.1. Selection of the model reaction.

The study of the stoichiometric transmetalation reaction has intrinsic challenges especially due to the instability of organometallic nucleophiles and the inherent instability of the post-transmetalation intermediate species. Two different scenarios are likely to occur: a) an exergonic transmetalation event, which forms a more stable intermediate, or an endergonic process, forming a less stable intermediate. In both cases, the favored reductive elimination would push the reaction towards the product formation.

One strategy is the study of either both processes simultaneously (reductive elimination and transmetalation) or the retro-transmetalation reaction.[30] However, our goal is to study exclusively the transmetalation in the "direction" of the catalytic cycle, from the oxidative addition species to the species formed after the transmetalation and prior the reductive elimination. For this reason, we started our investigation choosing a system where reductive elimination is hampered and, moreover, the transmetalation is exergonic. We focused our attention, first, on the CF_3 moiety to be transferred to a Pd(II) complex since the strength of the Pd^{II}–CF_3 bond prevents the coupling. This manner, we could study the transmetalation independently from the reductive elimination.

The selection of the palladium complex was based on the representability of common intermediates in cross-coupling reactions. Thus, we addressed [(L)Pd(Ar)(X)] complexes, which are proposed to be intermediates formed after the oxidative addition step in $Pd^{0/II}$ catalytic cycles. Moreover, the modification of the aryl and the halide can provide some mechanistic information. As ligand, we focused our attention on bidentate phosphine ligand on the Pd complex which prevents the decoordination of the phosphine and increases its stability. During the synthesis of the Pd complexes, we realized that, especially when using electron-donating groups on the aryl moiety, there is scrambling between the phosphine ligand and the aryl moiety attached to the palladium (see Appendix). We then hypothesized that an electron-poor phosphine with a narrow bite angle could prevent this undesired side reaction. After some experimentation, we found that 1,2-bis(diphenylphosphino)benzene, dppbz, precludes the

[30] Pérez-Temprano, M. H.; Casares, J. A.; de Lera, Á. R.; Álvarez, R.; Espinet, P. *Angew. Chem. Int. Ed*. **2012**, *51*, 4917.

scrambling reaction. Moreover, we also hypothesized that the electro-steric characteristics of this ligand could decrease the transmetalation rate and so facilitate its study.

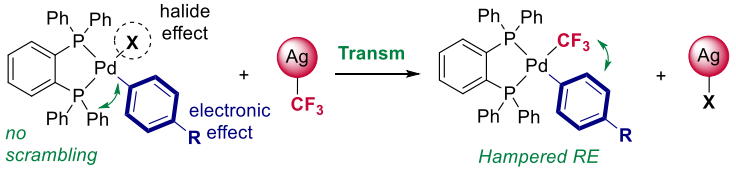

Scheme 4.29. Designed model system for the study exclusively the transmetalation reaction.

Regarding the silver nucleophile, two different well-defined systems were selected for the transmetalation study: a) $BcAgCF_3$ (**1a**/**1b**$_{Ag}$) and b) $[M][Ag(CF_3)_2]$ (**2**$_{Ag}$).[31][32] These complexes may be representative of silver species formed in catalytic conditions on the reaction media. For instance, bathocuproine ligand has been used in Pd-catalyzed decarboxylative coupling. The argentates have been proved to be effective in trifluoromethylation reactions and likely to be formed in solution.[33] The main interest of this project is to understand the transfer between groups and we think that CF_3 moiety is a perfect probe to do so.

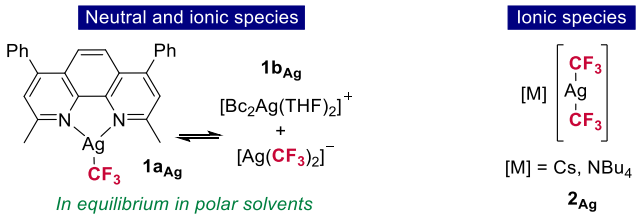

Scheme 4.30. Target trifluoromethyl silver(I) complexes as transmetalating agents.

4.3.2. Evaluation the group exchange using a neutral species (1a) in equilibrium with an ionic part (1b)

As discussed in Chapter 2, our group disclosed the potential of well-defined and isolable $[(Bc)Ag(CF_3)]$ species as transmetalating agents. In polar solvent, this species has been shown to be in equilibrium with an ionic part. This type of equilibrium has been detected for other neutral ligands such as phosphines or (N^N)-bidentate ligands.[34,32] Our special interest in this system lies in the systematic use of (N^N)-bidentate ligand type as auxiliary ligand for silver in bimetallic systems such as Pd/Ag catalyzed decarboxylative cross-coupling reactions.

[31] Martínez de Salinas, S.; Mudarra, A. L.; Benet-Buchholz, J.; Parella, T.; Maseras, F.; Pérez-Temprano, M. H. *Chem. Eur. J.* **2018**, 24, 11895.

[32] We discard the study of 'ligandless' $AgCF_3$ species because they are not well-defined and non-isolable. $[(SIPr)Ag(CF_3)]$ complex was tested in the transmetalation reaction but inconclusive results were obtained (see Appendix).

[33] Indeed, during the synthesis of $[(R)_3PAg(CF_3)]$ complexes, we observed an equilibrium with this ionic species and the neutral $[(R)_3PAg(CF_3)]$ one. This complex were not sufficiently stable to handle.

[34] Weng, Z.; Lee, R.; Jia, W.; Yuan, Y.; Wang, W.; Feng, X.; Huang, K.-W. *Organometallics* **2011**, 30, 3229.

We first studied the evolution of the different species during the transmetalation reaction of **1a**/**1b**$_{Ag}$ reaction at 10 ºC in THF using the [(dppbz)Pd(*p*-FPh)(I)] (**3**$_{Pd}$) as benchmark palladium complex (**Scheme 4.31**).

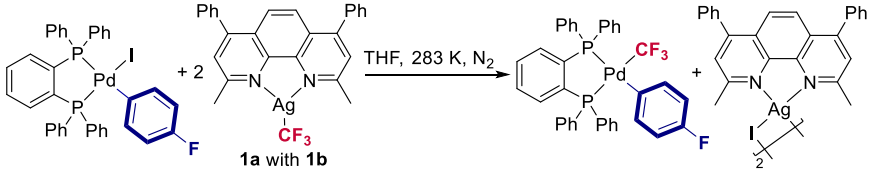

Scheme 4.31. Stoichiometric transmetalation reaction of [(Bc)Ag(CF_3)] and [(dppbz)Pd(*p*-FPh)(I)] in THF at 10 ºC.

Interestingly, the ionic part in equilibrium with the neutral species disappears while the product formation is taking place (**Error! Reference source not found.**). This could be related either to the potential transmetalation either from the neutral [(Bc)Ag(CF_3)] species or the ionic part, [$(Bc)_2Ag(THF)_2$][$Ag(CF_3)_2$]. During the reaction, precipitation of white crystals were observed corresponding to the dimer $[(Bc)Ag(I)]_2$.

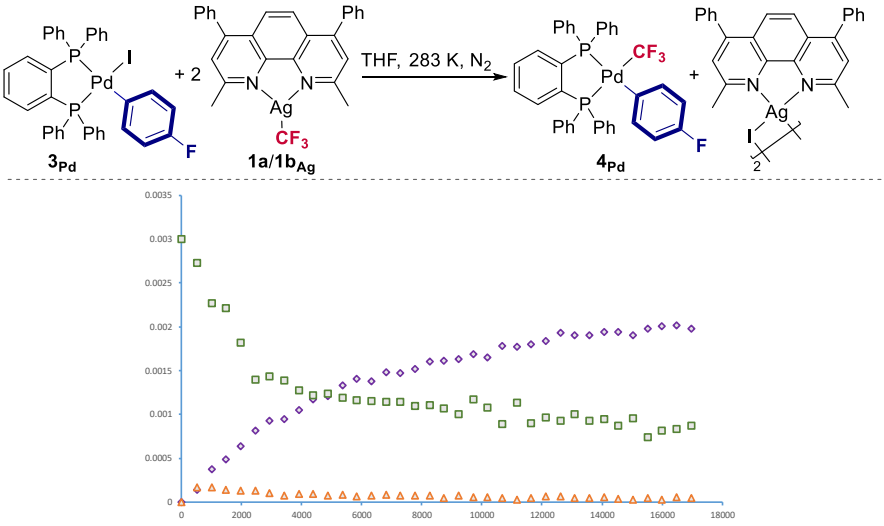

Scheme 4.32. Full profile (80%) of the reaction BcAgCF3 and [(dppbz)Pd(*p*-FPh)(I)] at 10°C.

4.3.2.1. **NMR spectroscopy kinetic studies**

To gain insights into the reaction mechanism we decided to study two different variables: a) the influence of the halide at the palladium complex on the transmetalation rate, and b) the influence of the substituent in *para* position in the aryl probe on the palladium complex.

- **Study of the effect of the halide on the transmetalation rate**

Different literature precedents proposed the transmetalation reaction to occur through either a concerted mechanism or a stepwise one depending on the capability of X to bridge or not the Pd metal center and the corresponding organometallic nucleophile.[35] Thus, depending on the reaction mechanism underlying the group transfer, the reaction rate trend for the different halides is proposed to be different. If the transmetalation is governed by a concerted transfer, the more electrophilic the Pd complex, the faster the transmetalation. It implies that the Pd(II)–Cl complex would undergo the transmetalation faster than the iodide. In contrast, if the transmetalation happens through a stepwise mechanism, the weaker the Pd–X bond, the faster the transmetalation. This makes the Pd(II)-I congener the more reactive complex.[36]

We started our comparison with the study of the transmetalation using aryl-Pd(II) complexes bearing different halide ligands at 10 ºC up to a 25% of ^{19}F NMR yield. In our case, the transmetalation reaction is faster for [(dppbz)Pd(*p*-FPh)(I)] than for the analogues with Br or Cl which may indicate that the cleavage of the Pd–X bond is involved in the rate determining step of the reaction.

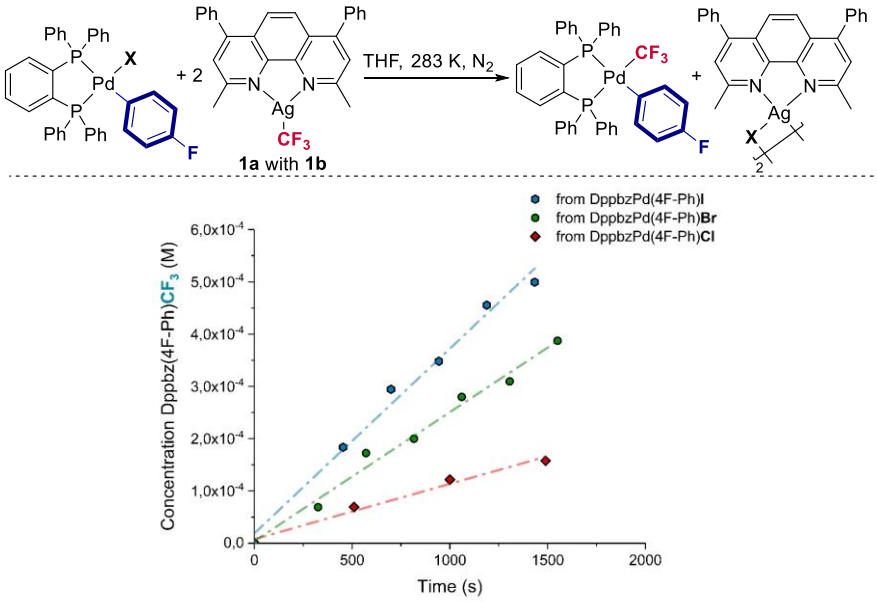

Scheme 4.33. Concentration evolution over time of complex [(dppbz)Pd(*p*-FPh)(X)] (**3$_{Pd}$**) bearing different halide ligands (X = I, Cl, Br) using [(Bc)Ag(CF_3)] (**1a**/**1b$_{Ag}$**)as transmetalating agent. This plot shows the dependence of the halide ligand on the transmetalation reaction at 0°C.

35 Casado, A.L.; Espinet, P. *J. Am. Chem. Soc.* **1998**, *120*, 8978.
36 Jagadeesan, R.; Velmurugan, G.; Venuvanalingam, P. *RSCAdv*. 2015, 5, 80661.

We then aimed at obtaining more information about the mechanism by modifying the electronic properties of the aryl probe on the palladium complexes.

- **Study of the effect of the electronic properties of the aryl moiety on the transmetalation rate. Hammett-plot study**

Hammett plot study is a fundamental tool for understanding reaction mechanisms. This allows us to obtain information as important as the accumulation of charges in the rate determining step of a reaction. The initial report was applied to the acid-base equilibrium of benzoic acid and stablishes a set of parameters that measures the influence of a given substituent *via* inductive effects to shift the acid-base equilibrium.[37]

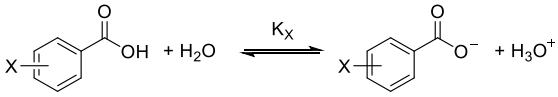

$$\log\left(\frac{K_x}{K_H}\right) = \rho \cdot \alpha_x \qquad (\text{eq. } 1)$$

Scheme 4.34. Acid-base equilibrium of benzoic acids in water.

where K_x is the acid-base equilibrium constant of different benzoic acids derivatives, K_H is the equilibrium constant for the benzoic acid, ρ is the slope of the linear relationship and σ_x is the sigma parameter stablished for a given substituent. By definition, the slope of the linear relationship for the equilibrium constants of benzoic acids and sigma values is +1. This means that reactions where a negative charge is created, as deprotonation of benzoic acid, would present a positive slope ($\rho > 1$) while a negative slope would be related to the generation of positive charge ($\rho < 1$). Apart from equilibrium constant, this concept can be also applied to the rate ratio of a given reaction with different substituents in the aromatic ring. In this case, it would provide information about the influence of the electronic effect of the aromatic ring on the rate determining transition state *via* inductive effects.

[37] Hammett, L. P. *Chem. Rev*. **1935**, *17*, 125.

Regarding the transmetalation reaction, different research groups have corroborate the role of the nucleophile by performing Hammett plot studies.[38] In our study, we the rate constant relationship was obtained by initial rate approach at 0 ºC. The so-achieved Hammett plot, depicted in **Figure 4.1**, shows a negative slope, ρ value, of -0.95. As discussed above, this value is related to the generation of a positive charge on the palladium complex during the rate determining transition state.

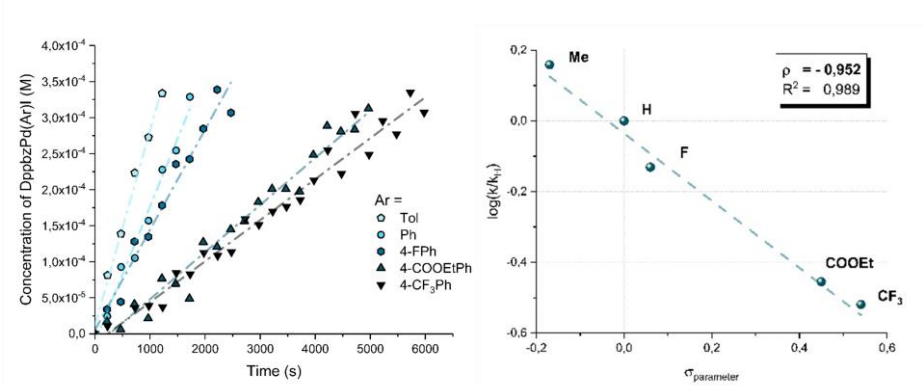

Figure 4.1. Dependence of the e-richness of the aryl moiety attached to the palladium complexes during the transmetalation reaction using [(Bc)Ag(CF_3)] at 0 ºC.

This result is however counterintuitive since the aryl-Pd(II) complex, which is supposed to be an electrophile in Pd-catalyzed cross-coupling catalytic cycle, is apparently behaving as a nucleophile according to the Hammett plot. [39]

Collectively, the halide dependence and Hammett plot study suggest that the rate determining step may be related to the generation of a positively-charged palladium species or transition state where the cleavage of the Pd–X is key.[40]

[38] a) Saito, S.; Oh-tani, S.; Miyaura, N. *J. Org. Chem.* **1997**, *62*, 8024. b) Zim, D.; Lando, V. R.; Dupont, J.; Monteiro, A. L. *Org. Lett*., **2001**, *3*, 3049. c) Jin, L.; Xin, J.; Huang, Z.; He, J.; Lei, A. *J. Am. Chem. Soc*. **2010**, *132*, 9607. d) Payard, P.-A.; Perego, L. A.; Ciofini, I.; Grimaud, L. *ACS Catal*. **2018**, *8*, 4812.

[39] It is assumed that the stronger the character of the electrophile, the faster the reaction with the nucleophile, in this case the silver nucleophile. However, this Hammett plot study shows that the less electrophilic the palladium complex, the faster the transmetalation. Scarce examples have been found to point out a potential nucleophilic nature of palladium complexes during the transmetalation reaction, see: Moriya, T.; Miyaura, M.; Suzuki, A. *SYNLETT*, **1994**, 149.

[40] Cationic palladium complexes have been proposed to be key for the transmetalation in several reports. In Negishi coupling: b) García-Melchor, M.; Fuentes, B.; Lledós, A.; Casares, J. A.; Ujaque, G.; Espinet, P. *J. Am. Chem. Soc*. **2011**, *133*, 13519. In Stille coupling: Nova, A.; Ujaque, G.; Maseras, F.; Lledós, A.; Espinet, P. *J. Am. Chem. Soc*. **2016**, *128*, 14571.

- **Solvent effect on the transmetalation rate**

The influence of the solvent in a given reaction is widely known to provide relevant information about the reaction mechanism. For instance, transformation that imply the generation of a charge are favored in more polar solvents that could stabilized the transition state or intermediate.[41] In our case, we envisioned that relevant information about the mechanism could be obtained using a more polar and coordinating solvent such as DMF. We hypothesized that the reaction would speed up if a polar transition state is governing the transformation or, in contrast, the reaction would slow down if the solvent gets coordinated during the transformation. Interestingly, the reaction of 1 equiv of complex **3**$_{Pd}$ with **1a**/**1b**$_{Ag}$ in DMF at room temperature does not finish in 24 hours while it is finished in less than 10 minutes in THF.[42]

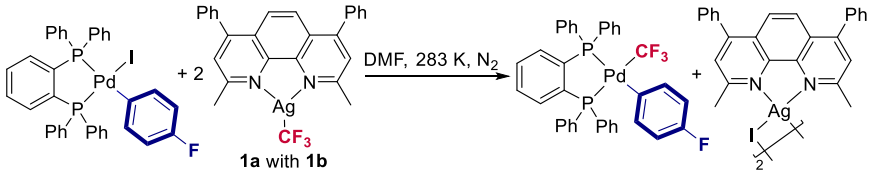

Scheme 4.35. Stoichiometric transmetalation reaction of [(Bc)Ag(CF_3)] and [(dppbz)Pd(*p*-FPh)(I)] in DMF at 35 ºC.

This experiment supports the generation of a cationic palladium complex stabilized by the coordination of solvent molecules. In this venue, we decided to run DFT calculations to get more information about the system.

4.3.2.2. Mechanistic investigation using DFT calculations.

DFT calculations were carried out with the ωB97xD functional with a double-ζ plus polarization basis set in THF continuum solvent. See Appendix for further details.

- **Analysis of the properties of aryl-Pd(II) complexes**

We first explored the characteristics of the different palladium complexes bearing different aryl groups which could be related to the obtained Hammett plot when studying the CF3 transfer from **1a**/**1b**$_{Ag}$. We found a correlation between the experimental Hammett plot and two different parameters: a) the energy of the HOMO orbital, which is located on the iodide atom for all palladium complexes regardless substitution pattern, and b) the partial charge of the iodide atom (see **Figure 4.2**). On the one hand, the more stable the HOMO, the slower the transmetalation. On the other hand, the less negatively charged the iodide, the slower the transmetalation. This

[41] Mayr, H.; Minegishi, S. *Angew. Chem. Int. Ed*. **2002**, *41*, 4493.
[42] Decomposition of the silver nucleophile was observed before achieving total conversion of the aryl-Pd(II) complex.

may seem counterintuitive since the more electrophilic the palladium complex, the slower the reaction with the nucleophile.

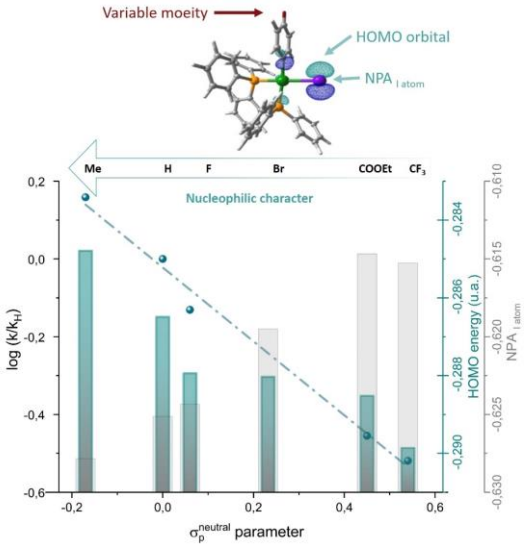

Figure 4.2. Key parameters related to the Hammett plot observed experimentally. Color code for 3D image: white (hydrogen), gray (carbon), orange (phosphorous), green (palladium), blue (fluorine), black (silver), purple (iodine), dark blue (nitrogen).

- **Mechanistic investigations on the free energy profile**

Once we discovered that the nucleophilic character of the palladium complex makes the reaction faster, we focus our efforts on studying the reaction mechanism of the transmetalation between [(dppbz)Pd(Ph)(I)] (**Pd-I**), as a model of **3$_{Pd}$**, and **1a**/**1b$_{Ag}$** as transmetalating agent. This mechanistic proposal should explain the transmetalation rate trends observed experimentally. To do so, we evaluated two different mechanistic possibilities based on the literature precedents: a) a concerted transmetalation where the CF_3-for-I exchange from the silver to the palladium happens in a simultaneous manner and b) a stepwise mechanism where the Pd–X bond cleavage happens prior to the transference of the CF_3.[43]

First, we considered that both species in the equilibrium, the neutral [(Bc)Ag(CF_3)] and [(Bc)$_2$Ag(THF)$_2$][Ag(CF_3)$_2$] may be potentially active in the transmetalation event. This equilibrium is defined by a free energy difference of 10.6 kcal·mol^{-1} and it was shown to be operative, despite the large free energy difference, by the coordination of two solvent molecules, in high concentration. The structure of the cation was previously described by our group.[40,44]

[43] For concerted and stepwise mechanism in transmetalation reactions: a) Ricci, A.; Angelucci, F.; Bassetti, M.; Lo Sterzo, C. *J. Am. Chem. Soc*. **2002**, *124*, 1060. b) Lennox, A. J. J.; Lloyd-Jones, G. C. *Angew. Chem. Int. Ed*. **2013**, *52*, 7362.

[44] Martínez de Salinas, S.; Mudarra, Á. L.; Benet-Buchholz, J.; Parella, T.; Maseras, F.; Pérez-Temprano, M. H. *Chem. Eur. J.* **2018**, *24*, 11895.

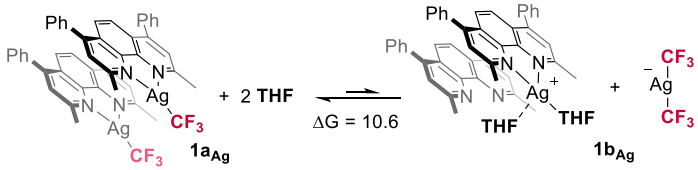

Scheme 4.36. Equilibrium of [(Bc)Ag(CF_3)] complex in THF. Energy in kcal·mol^{-1}.

After considering different alternatives by DFT (see Appendix), we found that the most plausible mechanisms are either a concerted transmetalation from the [(Bc)Ag(CF_3)] (path A) or a stepwise mechanism promoted by [(Bc)$_2$Ag(THF)$_2$][Ag(CF_3)$_2$] (path B). Both alternatives are compared here below.

Regarding the concerted mechanism from the neutral [(Bc)Ag(CF_3)] (path A), the irreversible halide-CF_3 exchange can be achieved by overcoming a relatively low barrier of 18.6 kcal/mol, **TS-I0-I4**, as we can see in **Scheme 4.37**. The located transition state consists of a metal-metal interaction between Pd and Ag where the CF_3 bridges both metal centers. Considering the halide, an Ag–I bond is created while an elongation of the Pd–I distance takes place. The Pd-I distance is close to the sum of the crystallographic Van der Waals radii (4.08 *vs.* 4.15 Å) (see **Scheme 4.37**)[45] so this transition state, **TS-I0-I4**, can be considered as a late transition state corresponding to a concerted yet asynchronous transfer of the iodide to the [(Bc)Ag(CF_3)] moiety.

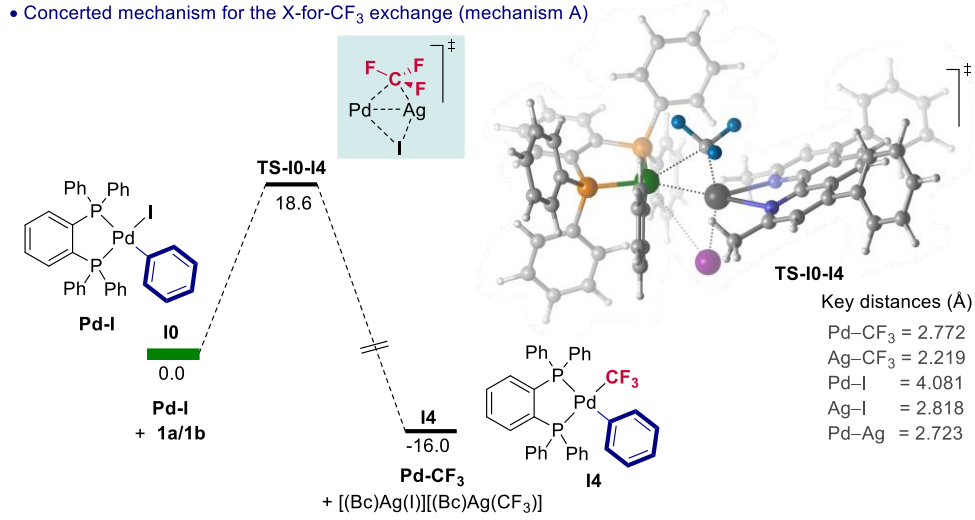

Scheme 4.37. DFT-calculated free energy profile for the I-for-CF_3 transfer through a concerted transition state. Energy in kcal·mol^{-1}. Color code for 3D image: white (hydrogen), gray (carbon), orange (phosphorous), green (palladium), blue (fluorine), black (silver), purple (iodine), dark blue (nitrogen).

45 Batsanov, S. S. *Inorg. Mater*. **2001**, 37, 1031.

Regarding the stepwise mechanism promoted by the ionic part of our system (path B), we first studied the potential dehalogenation by the cationic silver specie in equilibrium with the neutral $BcAgCF_3$. To do so, we evaluated the possibility to calculate a barrier for the dehalogenation considering a cationic silver complex without solvent molecules coordinated. However, this process proves to be barrierless (see Appendix). In order to have a representative barrier of the process, we considered a first decoordination of a molecule of THF from the cation. Then, this unstable cation is able to exchange the remaining THF solvent molecule by the iodide of the palladium complex through a low energy barrier (**TS-I0-I1**).[46] The dehalogenation process gives rise to a cationic palladium complex (**Pd-I**) and, subsequently, the formation of a neutral halide silver complex (**I1-Ag**) as we can see in **Scheme 4.38**. Once **I1-Ag** is formed, it can easily form a dimer and the irreversible precipitation of crystalline $[(Bc)Ag(I)]_2$ takes place. The irreversibility of the precipitation necessarily makes the process exergonic.

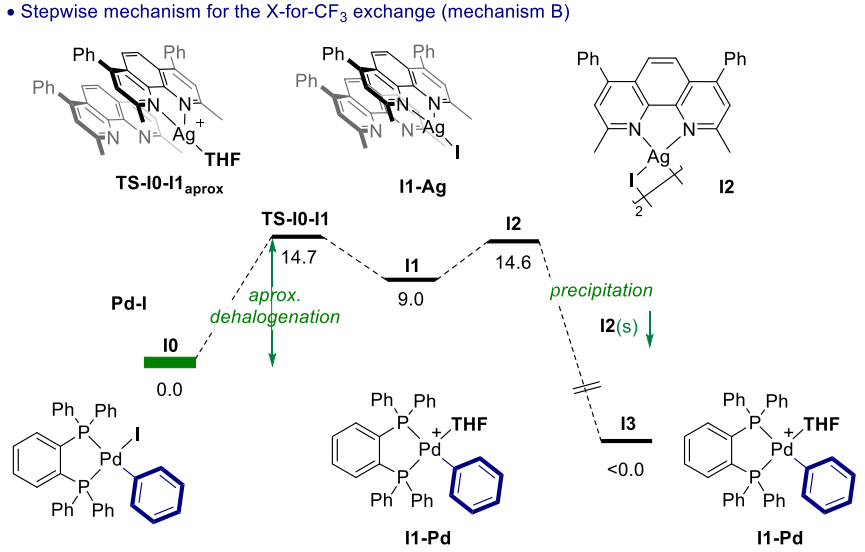

Scheme 4.38. DFT-calculated free energy profile for the I-for-CF_3 exchange through a previous dehalogenation step promoted by $[(Bc)_2Ag(THF)_2][Ag(CF_3)_2]$.

Once **I1-Pd** is formed, the transference of the CF_3 from the anionic species takes place from the bis-(trifluoromethyl) argentate through a very low barrier compared to the transfer from the neutral species (**Scheme 4.39**).

[46] This value corresponds to the generation of the cationic species with a single molecule of THF coordinated to the metal centre. This approximation allows us to get an estimated value for the dehalogenation process.

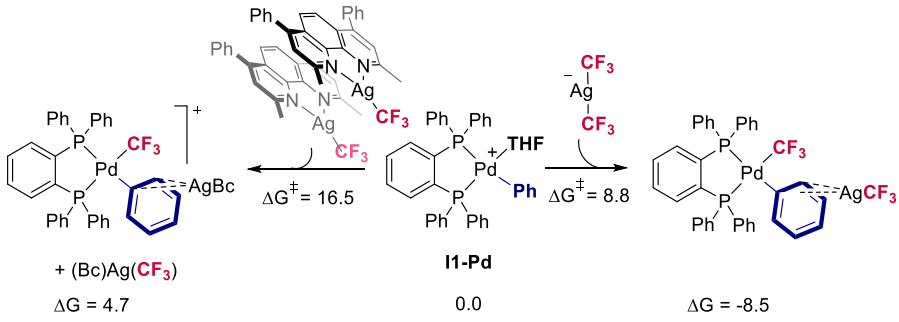

Scheme 4.39. CF_3 transfer to **I1-Pd** intermediate considering different silver species in the reaction media. Energies in kcal·mol^{-1}.

As we can see in **Scheme 4.40**, the Pd–I bond, which is cleavage by the cationic silver species in mechanism A, is stronger when the aryl probe is more electron-poor. This is due to the higher charge transfer from the iodide to the palladium due to the electron-withdrawing nature of the substituent.[36] If the dehalogenation is the rate determining step, as DFT calculation suggests, the electron-richer the substituent, the faster the transmetalation. This is in accordance with the experimental Hammett plot study.

Regarding the experimental halide trend, it can be explained in terms of relative stability of the formed species after the dehalogenation process in the stepwise mechanism (**I1-Ag** and **I2**). The formation of **I1-Ag-Cl** or **I2-Cl**, $[(Bc)Ag(Cl)]_2$, is not as favored as the formation of their iodide analogues, as we can see in **Scheme 4.40**. We assumed that this thermodynamic difference is reflected into the energy difference in the transition states for the dehalogenation and, therefore, into a slower transmetalation reaction.[47]

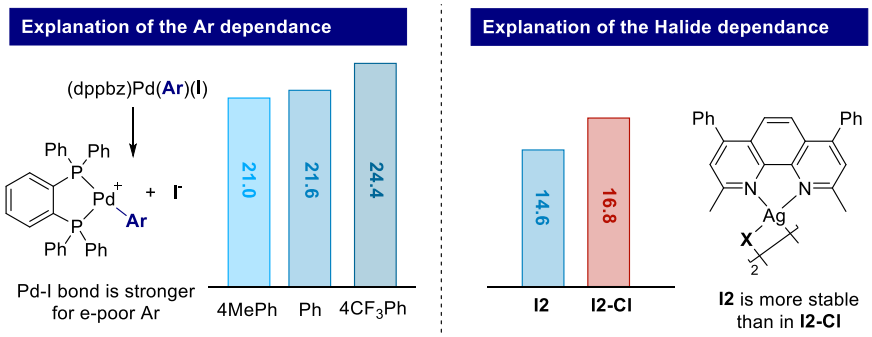

Scheme 4.40. To the left: Evaluation of the dehalogenation process using as model reaction the cleavage of the Pd-I bond. To the right, Evaluation of the formation of the chloride version of intermediate **I2** in **Scheme 4.38**.

According to our DFT calculations, when comparing **TS-I0-I4** and **TS-I0-I1**, the estimated barrier for the dehalogenation (mechanism B) is 3.9 kcal·mol^{-1} lower than the barrier for the

[47] We discarded that this trend is controlled by the solubility of the corresponding silver halide. If this was the case, we would not observe any influence of the substitution pattern on the aromatic moiety since the rate determining step would be related to the precipitation of the silver.

concerted mechanism (mechanism A). Therefore, the transmetalation is likely to happen through a stepwise mechanism where the cationic silver species is performing the dehalogenation event affording a short-lived cationic palladium complex. This is the most energy-demanding step and, here, the palladium complex is behaving as a nucleophile.

4.3.2.3. Intermediate elucidation and potential misleading pathway

Since experiments and calculations pointed out the potential intermediacy of a short-lived cationic palladium complex, we focused our efforts in the detection of this intermediate during the reaction. Attempts to detect the cationic palladium complex in the reaction media using [(dppbz)Pd(*p*-FPh)(I)] or electron richer aryl moieties were unsuccessful at low temperature even in a more coordinating solvent such as DMF. We envisioned that a palladium complex containing an electron richer phosphine could increase its stability and favors its detection. We evaluate the NBO partial charge of $[(dppbz)Pd(Ph)(THF)]^+$ *vs* $[(dppp)Pd(Ph)(THF)]^+$ by DFT and we observed a decrease in the charge of the palladium metal center when the dppp phosphine is attached (**Figure 4.3**).[48] In this regard, we carried out the transmetalation reaction using this phosphine ligand.

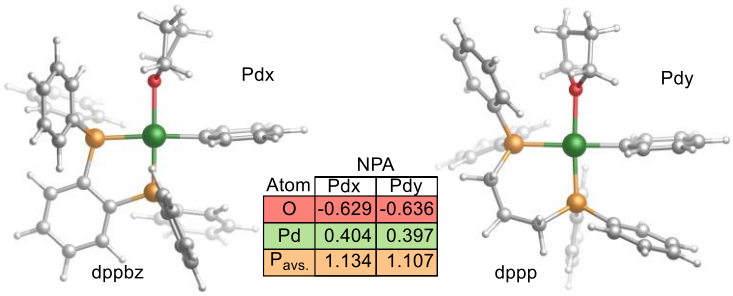

Figure 4.3. NPA values of the evaluated cationic palladium intermediates considering the stabilization by coordination of a THF solvent molecule. Color code for 3D image: white (hydrogen), gray (carbon), orange (phosphorous), green (palladium), red (oxygen).

When using [(dppp)Pd(Ph)(I)], we were able to detect in the reaction media the desired intermediate $[(dppp)Pd(Ph)(DMF)]^+$. The assignation of this intermediate was independently synthesized and characterized through the reaction of [(dppp)Pd(Ph)(I)] and $AgSbF_6$ in DMF (see **Scheme 4.41**).[49] As mentioned above, the transmetalation in DMF when using [(dppbz)Pd(*p*-FPh)(I)] is slower than in THF, likely due to a stabilization of this intermediate by solvent coordination.

[48] We only considered the phenyl group due to scrambling issues when using a substituted aryl group. This scrambling reaction, discussed in Chapter 2, allows the exchange between the aryl moiety on the palladium metal centre and the one on the phosphorous of the phosphine. See a) Goodson, F. E.; Wallow, T. I.; Novak, B. M. *J. Am. Chem. Soc.* **1997**, *119*, 12441. b) Grushin, V. V. *Organometallics* **2000**, *19*, 1888. c) Fiebig, L.; Schlörer, N.; Schmalz, H.-G.; Schäfer, M. *Chem. Eur. J.* **2014**, *20*, 4906.

[49] This cationic palladium complex was observed in DMF in the presence of silver as halide scavenger. It was not observed in the absence of silver.

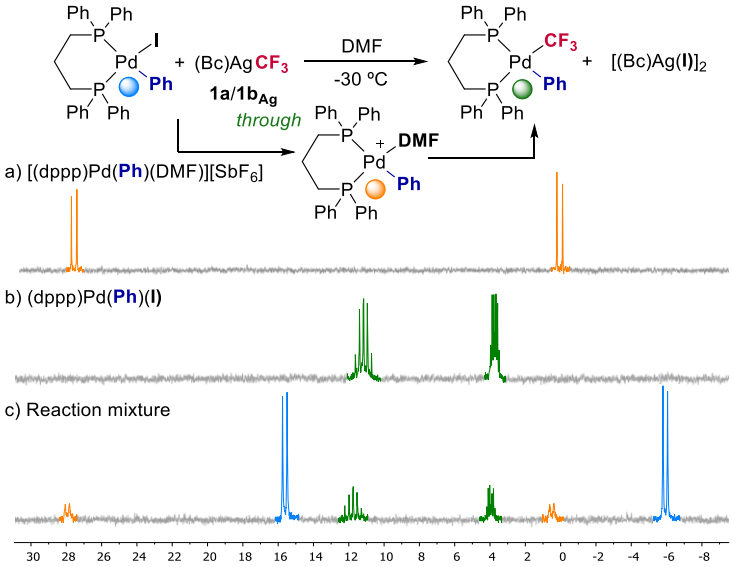

Scheme 4.41. Detection of the corresponding cationic palladium complex, $[(dppp)Pd(Ph)(DMF)]^+$, in the reaction media at low temperature.

Encourage by the potential of dppp to stabilize intermediates, we envisioned the detection of potential post-transmetalation species encompassing silver and palladium in a discrete complex (**Scheme 4.42**, **I-post**).[50] This intermediate could be formed by the reaction of the cationic palladium complex (**I1-Pd**) and $[(Bc)Ag(CF_3)]$ neutral species during the transmetalation reaction. Since the $[(dppp)Pd(Ph)(THF)][SbF_6]$ was not sufficiently stable to study this direct route for the hypothetic intermediate,[51] we envisioned that an alternative route could be the reaction of $[(dppp)Pd(Ph)(CF_3)]$ and a cationic silver complex, $[(Bc)Ag(THF)][SbF_6]$.

[50] a) Braunstein, P.; Frison, C.; Oberbeckmann-Winter, N.; Morise, X.; Messaoudi, A.; Bénard, M.; Rohmer, M.-M.; Welter, R. *Angew. Chem. Int. Ed*. **2004**, *43*, 6120. b) Heckenroth, M.; Kluser, E.; Neels, A.; Albrecht, M. *Angew. Chem. Int. Ed*. **2007**, *46*, 6293. c) Arias, A.; Forniés, J.; Fortuño, C.; Martín, A.; Mastrorilli, P.; Gallo, V.; Latronico, M.; Todisco, S. *Eur. J. Inorg. Chem*. **2014**, 1679.

[51] We observed decomposition of the expected compound even at low temperature in solution.

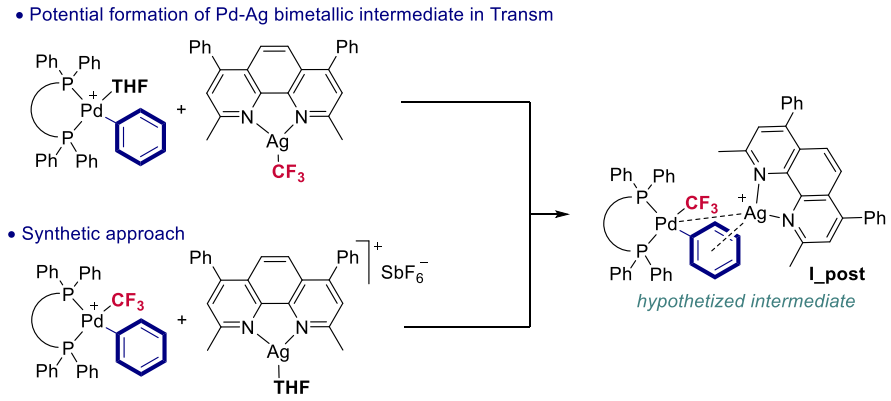

Scheme 4.42. Potential formation of a post-transmetalation intermediate with Pd and Ag in a discrete molecule and our synthetic approach for access it.

When running the experiments, neither **I_post** intermediate nor $BcAgCF_3$ species were not observed. This reinforces the irreversibility of the transmetalation reaction and the strength of the Pd–CF_3 bond compared to Ag–CF_3 bond. Unexpectedly, we detected a new palladium species that proved to be [(dppp)Pd(CF_3)$_2$]. We hypothesized that the presence of cationic silver species can promote the homocoupling reaction in Pd systems through, potentially, the formation of Ag–Ph intermediates.[52] In fact, this scrambling reaction was selective when using an excess of $AgSbF_6$ in toluene.

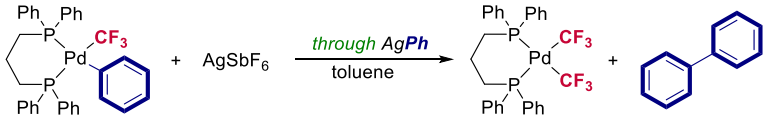

Scheme 4.43. Silver-promoted scrambling reaction for the formation of poly-(trifluoromethylated) palladium(II) complexes and biaryl product.

In view of this results, we think that this scrambling reaction could be a strong source of unselective pathways in catalysis when using silver salts and the reductive elimination is slow.[53] This is quite interesting since it points out that cationic silver species, although promote the dehalogenation, can scramble the ligands between palladium complexes and yield homocoupling. This side reaction is relevant for the understanding and development of silver nucleophiles in catalytic processes. The presence of cationic silver either in equilibrium or as counterion can deplete the efficiency in the transmetalation event by promoting side reactions.

[52] These intermediates has been proposed to be formed in catalytic conditions through C–H activation event (see ref. 24) or decarboxylation (even isolated, see: Baur, A.; Bustin, K. A.; Aguilera, E.; Petersen, J. L.; Hoover, J. M. *Org. Chem. Front.*, **2017**, *4*, 519.

[53] The formation of bis-(trifluoromethyl) Pd(II) complexes was observed in low yield during kinetic experiments when using dppp and [(Bc)Ag(CF_3)] as transmetalating agent, which contains a low amount of cationic silver species. This reinforces the potential of cationic silver species to scramble the ligands even at low concentration (in a 5% at the beginning of the reaction, according to the equilibrium).

The detection of the cationic palladium complex in the reaction media, along with the DFT free energy profile and the explanation of the Hammett plot and halide trend supports a stepwise mechanism for the transmetalation between Pd–halide complexes and [(Bc)Ag(CF_3)] in polar solvent. The overall transmetalation event can be understood as a sequential cleavage of Pd–halide bond, by a cationic silver species, and, subsequent, Pd–CF_3 bond formation by the anionic silver(I) species. The neutral [(Bc)Ag(CF_3)] has been shown to be unlikely to be directaly involve in the Pd/Ag group exchange in this reaction conditions.

4.3.3. Evaluation the group exchange when using an ionic species (2).

Given the potential of species such as [M][Ag(CF_3)$_2$] to transmetalate and the information acquired from the previous system, we wondered how this species transfer the organic moiety from silver to palladium. In contrast to [(Bc)Ag(CF_3)], this system is lacking a cationic silver species that can scavenger the halide from **3$_{Pd}$** and, therefore, the reaction mechanism may be different.

Experimentally, we focused our attention in the [Cs][Ag(CF_3)$_2$] (**2$_{Ag}$**) since it is the most efficient and stable than its NBu_4 analogue.[31] We studied the evolution of the reaction up to a 90% of conversion of the reaction at 15 ºC by $^{19}F\{^{31}P\}$ NMR spectroscopy.

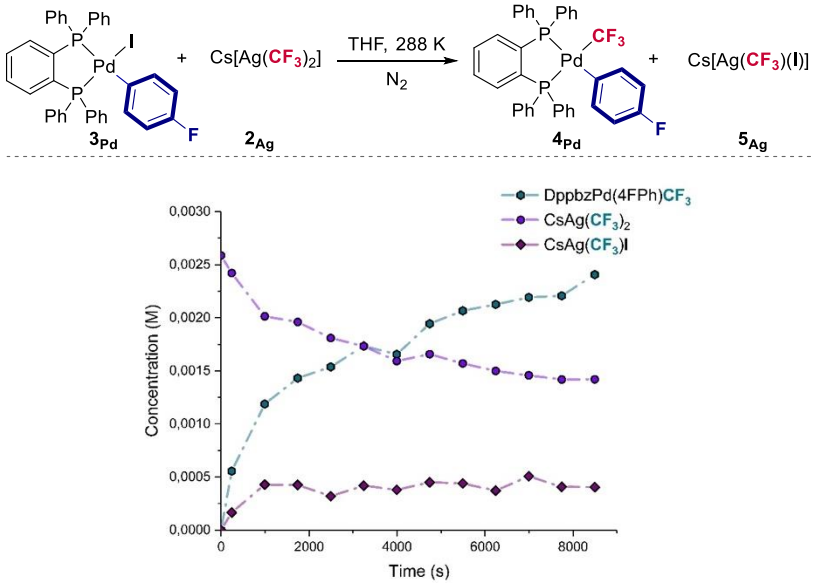

Scheme 4.44. Full profile for the transmetalation using [Cs][Ag(CF_3)$_2$] (**2$_{Ag}$**) and [(dppbz)Pd(*p*-FPh)(I)] (**3$_{Pd}$**) in THF at 15 ºC.

It should be noticed that [Cs][Ag(CF_3)(I)] (**5**$_{Ag}$) is observed during the transmetalation. Interestingly, the final concentration of this species is not the same than the palladium product suggesting that a Schlenck equilibrium could be operative in the reaction conditions.[54]

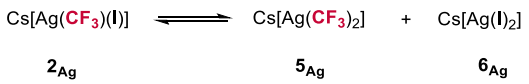

Scheme 4.45. Schlenck equilibrium for the bis-(trifluoromethyl) argentate in presence of the transmetalation reaction products.

4.3.3.1. NMR spectroscopy kinetic studies

As shown for the [(Bc)Ag(CF_3)] system, evaluating the effect of the halide ligand and the aryl probe at the palladium complex in the transmetalation reaction rate can provide essential insights about the potential mechanism.

- **Study of the effect of the halide and substituent on the aryl moiety on the transmetalation rate**

We started our investigation by studying the influence of the halide in the transmetalation reaction. We observed that the transmetalation between the argentate (**2**$_{Ag}$) and the palladium complex (3$_{Pd}$) at 10 ºC, is faster for the chloride palladium complex than the bromide or the iodide. This trend is contrary to the observed for the [(Bc)Ag(CF_3)] complex as transmetalating agent, suggesting that a different reaction mechanism may underlie to the transmetalation with **2**$_{Ag}$. A reasonable explanation is that, as in the cyclic mechanism of the Stille reaction, the transfer of the CF_3 group is occurring in a concerted manner.[35] Thus, the more electrophilic the palladium complex, the faster the attack of the nucleophile. This would mean that the silver complex, during the transmetalation reaction, donates electronic density to the palladium as the Pd–CF_3 bond is being created.

[54] These species can generate Cs[Ag(I)$_2$] and Cs[Ag(CF_3)$_2$]. It should be kept in mind that Cs[Ag(I)$_2$] could form CsI and AgI during the reaction. These species could precipitate.

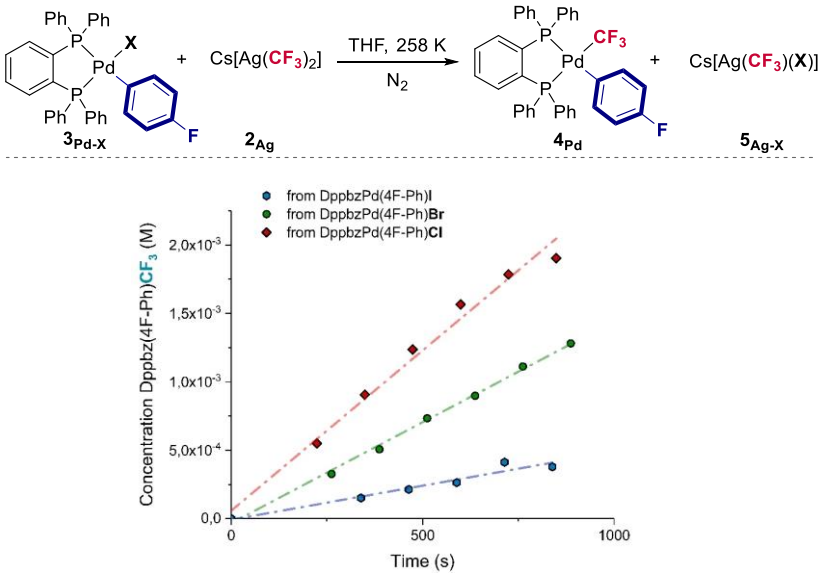

Scheme 4.46. Concentration evolution over time of complex [(dppbz)Pd(*p*-FPh)(X)] (**3**$_{Pd}$) bearing different halide ligands (X = I, Cl, Br) using [Cs][Ag(CF_3)$_2$] as transmetalating agent. This plot shows the dependence of the halide ligand on the transmetalation reaction at 0°C.

We then evaluated the influence of the substituent on the aryl group on the palladium complex. In this case, the transmetalation was faster for the more electron-rich aryls than the more electron-poor, in line with the results for **1a**/**1b**$_{Ag}$ as transmetalating agents. This result is in disagreement with the concerted mechanism that explains the trend of the halides.

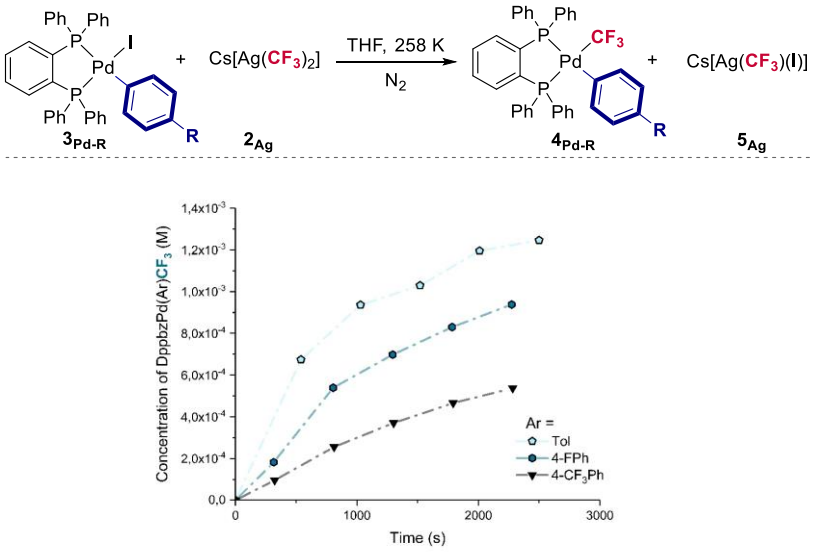

Scheme 3.47. Concentration evolution over time of complex [(dppbz)Pd(*p*-RPh)(X)] (**3$_{Pd}$**) bearing different substituents (R = Me, F, CF_3) using [Cs][Ag(CF_3)$_2$] as transmetalating agent. This plot shows the dependence of the halide ligand on the transmetalation reaction at 0°C.

- **Solvent effect on the transmetalation rate**

We then evaluated the influence of the solvent in the transmetalation rate when using **2$_{Ag}$** as transmetalating agent. To do so, we compare the performance when using THF, the study solvent, and DMF. When carrying out the transmetalation of **2$_{Ag}$** and **3$_{Pd}$** in DMF at 10 ºC, we did not observed product formation. We increased the temperature at 35 ºC and the reaction gave rise to a 10% of NMR yield after 1h. The reaction takes less than 10 min at room temperature in THF.[31] The decrease on the transmetalation rate may be again related to the coordination of the solvent.

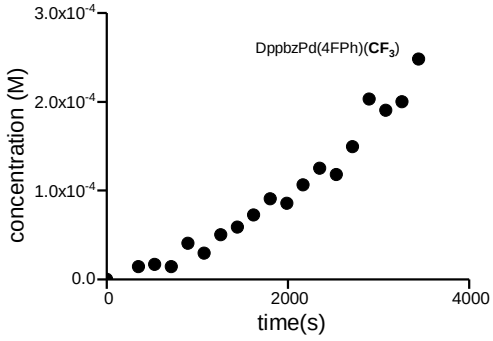

Scheme 4.48. Concentration evolution over time of complex [(dppbz)Pd(*p*-FPh)(CF_3)] using **3$_{Pd}$** and [Cs][Ag(CF_3)$_2$] as transmetalating agent in DMF at 35 ºC.

We also carried out a Hammett plot study in order to study if in DMF the rate determining step is associated to the accumulation of a positive charge. Indeed, we observed the same trend in both solvents.

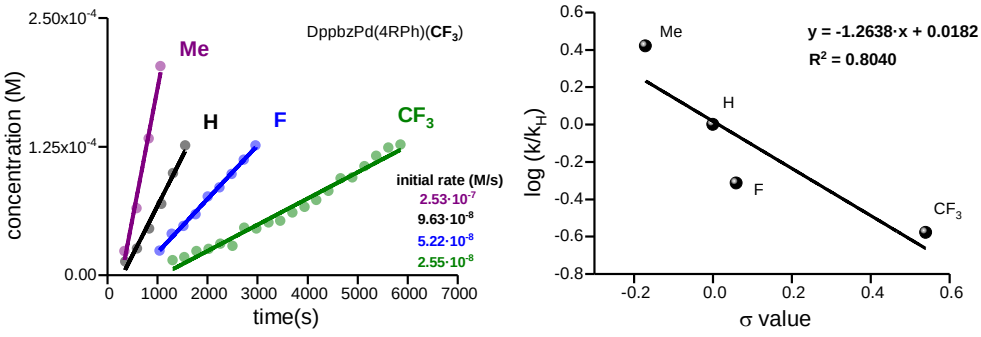

Scheme 4. 49. To the left: Concentration evolution over time of complex [(dppbz)Pd(*p*-RPh)(X)] (**3**$_{Pd}$) bearing different substituents (R = Me, H, F, CF_3) using [Cs][Ag(CF_3)$_2$] (**2**$_{Ag}$) as transmetalating agent in DMF. To the right: Hammett plot of the reaction in DMF.

It seems that the reaction mechanism for **2**$_{Ag}$ and **1a**/**1b**$_{Ag}$ share a common feature: the accumulation of a positive charge in the rate determining step of the reaction. However, there is still a lack of explanation for the trend observed when using different Pd–X complexes in THF. Interestingly in DMF, when comparing the transmetalation using [(dppbz)Pd(Ph)(I)] and [(dppbz)Pd(Ph)(Cl)], the reaction rates were similar. This points out that in DMF, the rate determining step of the reaction is not related to the halide abstraction.

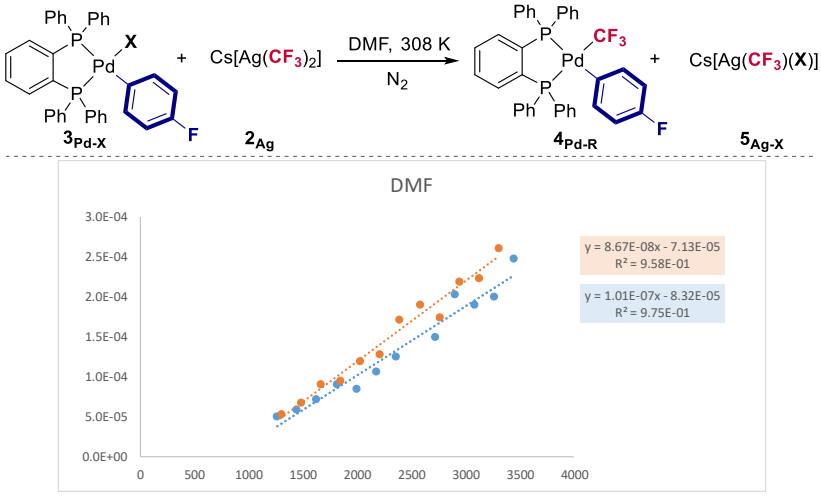

Scheme 4.50. Comparison of the reaction evolution of the stoichiometric transmetalation reaction of **2**$_{Ag}$ with **3**$_{Pd-X}$ complexes, where X = Cl or I.

Considering these results, we carried out DFT calculations to evaluate the most likely pathway.

4.3.3.2. DFT calculations for the evaluation of the system.

The DFT calculations were performed using the same method than for the [(Bc)Ag(CF3)] species. First, we tried to model the system using Cs as cation but issues such as coordination of solvent molecules were found. For this reason, we considered tetraethylammonium as a representative cation since experimental kinetic experiment using tetrabutylammonium shows that there is not a fundamental difference between their behaviors in the transmetalation reaction (see Appendix).

Once we established our model system, we evaluated two different mechanisms: a) a concerted mechanism where the halide could bridge both metals centers, which would be in accordance with the observed halide trend in THF, and b) a stepwise mechanism where a cationic palladium intermediate is formed, which would be in line with the observed tendency of the aryl substituents in THF.

When evaluating the concerted transmetalation mechanism, we first observed that the tetraethylammonium cation is necessary to stabilize this transition state in 10 kcal·mol^{-1},[55] yielding a neutrally-charged transition state between the palladium, **Pd-I**, and the silver argentate, [NEt_4][$Ag(CF_3)_2$] (TSXX). We found that, interestingly, the Pd–I bond distance is much more elongated than the Ag–I bond distance (3.71 *vs* 2.87 as can be seen **Scheme 4.40**). Therefore, **TS-I0-I7** can be considered a late transition state where the Pd–I bond is broken prior the CF_3 transference. In comparison with **TS-I0-I4**, the concerted mechanism for the [(Bc)Ag(CF_3)], all the key distances, which are fundamentally modified in the transition state, are shorter. This is probably due to the steric hindrance of the bathocuproine ligand. The fact that this process is mainly governed by the early cleavage of the Pd-halide bond makes that the version of this transition state for the chloride, which has a higher bond dissociation energy, is hampered (**Scheme 4.40**).[56]

[55] For further discussion on the nature of the transition states, see Appendix.
[56] The Ag–X bond in not been formed simultaneously to the cleavage of the Ag–CF_3 bond.

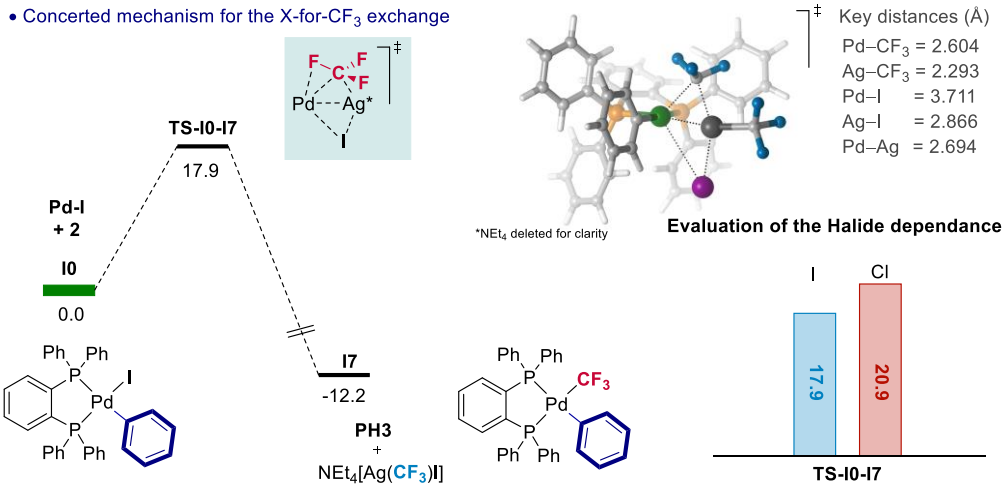

Scheme 4.51. DFT-calculated free energy profile for the I-for-CF_3 exchange through a concerted transition state considering $[NEt_4][Ag(CF_3)_2]$. Energies are in kcal·mol^{-1} at 25 ºC and 1 atm. Ag* denotes $Ag(CF_3)$. Color code for 3D image: white (hydrogen), gray (carbon), orange (phosphorous), green (palladium), blue (fluorine), black (silver), purple (iodine).

On the other side, we considered a stepwise mechanism for the ligand exchange between both metals. First, an exchange between the iodide in the palladium complex and the argentate anion was considered, forming NEt_4I and **I5**. This process is slightly endergonic. Interestingly, **I5** is not just an ion pair species since it exhibits a Pd–Ag bond as indicates the distance between both metals centers (2.712 Å), which may be key for its stabilization. Once this intermediate is formed, the transference of the CF_3 happens through a low-in-energy transition state (**TS-I5-I6**) forming the product and short-lived $[(THF)Ag(CF_3)]$. It can easily recombine with NEt_4I in the reaction media to form $[NEt_4][Ag(CF_3)(I)]$, which takes part in the Schlenck equilibrium. This stepwise mechanism is 7.1 kcal/mol more favorable than the concerted mechanism (**TS-I0-I7**). Again, the reaction for the chloride is supposed to be slower since the Pd–Cl bond is stronger than the Pd–I.

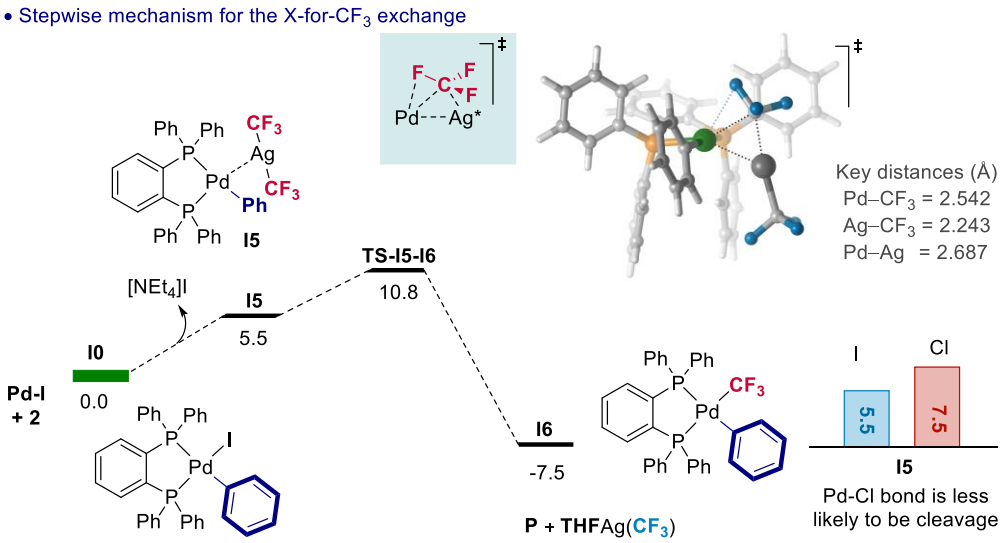

Scheme 4.52. DFT-calculated free energy profile for the I-for-CF_3 exchange through a stepwise mechanism considering $[NEt_4][Ag(CF_3)_2]$. Energies are in kcal·mol^{-1} at 25 ºC and 1 atm. Ag* denotes $Ag(CF_3)$. Color code for 3D image: white (hydrogen), gray (carbon), orange (phosphorous), green (palladium), blue (fluorine), black (silver), purple (iodine).

To further understand how the group exchange occurs, we analyzed the NPA partial charges during the reaction coordinate of this favorable stepwise mechanism. The first step of this sequential transformation consists of the cleavage of the Pd-I bond to form I5 intermediate. As we can see in **Scheme 4.53**, the NPA on the iodide atom evolves from -0.671 on the initial palladium complex to -0.981 in the NEt_4I salt. This is translated in a loss of charge on the palladium complex. Interestingly, during the transition state, both CF_3 moiety and silver donate electronic density to the palladium complex, recovering the initial NPA charge.

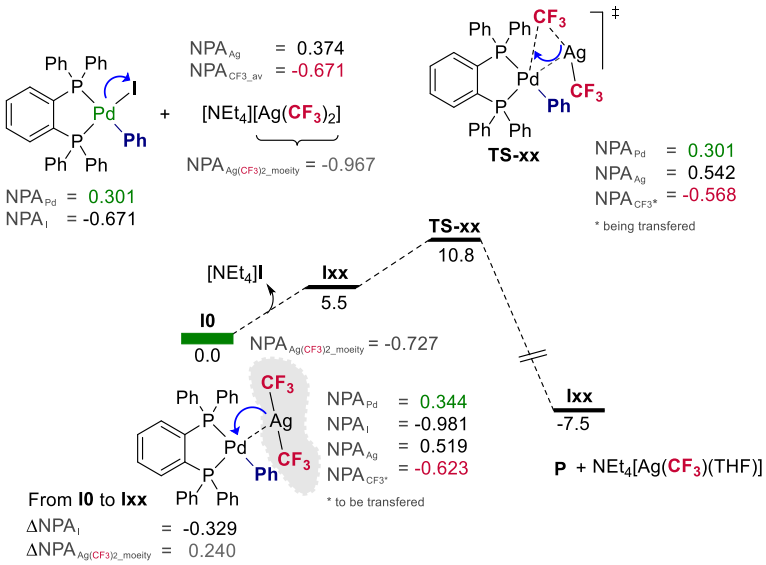

Scheme 4.53. DFT-calculated free energy profile for the I-for-CF_3 exchange through a stepwise mechanism considering $[NEt_4][Ag(CF_3)_2]$ along with the NPA values during the reaction coordinate. Energies in kcal·mol^{-1} at 25 ºC and 1 atm.

This means that, initially, the first step of the transmetalation would be favored for electron-rich substituents on the aryl group which would stabilize intermediate **I5**. However, during the CF_3 transfer *per se* (TS), there is a movement of charge from the silver and CF_3 group to the palladium center which would be favored for electron-withdrawing groups. Thus, the overall transmetalation event is a compromise between these two features, the formation of the cationic Pd center and the cleavage of the Ag–CF_3 bond. We evaluated the free energy profile for different substituents and we found that the most important contribution on the transmetalation is the formation of **I5** and, therefore, the transmetalation is favored for electron-rich Pd(II)-complexes. This is in agreement with the experimental observation.

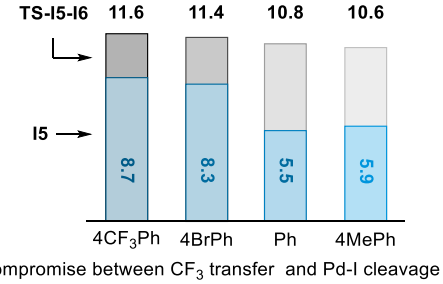

Scheme 4.54. Evaluation of the transmetalation reaction considering the stepwise mechanism for the reaction of different [(dppbz)Pd(Ar)(I)] complexes and $[NEt_4][Ag(CF_3)_2]$. Energies in kcal·mol^{-1} at 25 ºC and 1 atm.

Unfortunately, as mentioned above, this stepwise transmetalation mechanism does not explain the observe trend for the different Pd(II) halides. We hypothesized that [(THF)Ag(CF_3)] **I6**, which is formed after the transmetalation reaction, could directly scavenger the halogen from the palladium complex, instead of forming $[NEt_4][Ag(CF_3)(X)]$ from the reaction with NEt_4X, which may be in very low concentration. This could justify the experimental results since the formation of a new Ag–Cl bond is more favorable than the Ag–I bond and, therefore, the dehalogenation of [(dppbz)Pd(Ph)(Cl)] would be faster.

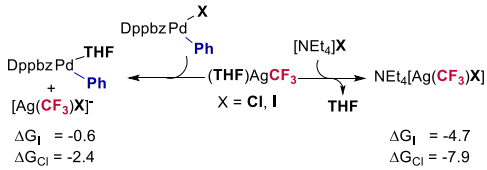

Scheme 4.55. Formation of the corresponding salts from [(THF)Ag(CF_3)] intermediate. Free energies in kcal·mol^{-1}.

As we can see in **Scheme 4.56**, this potential mechanism could be similar to a radical chain reaction mechanism. First, an initiation step formally generates a cationic palladium complex and negatively charged halide. The so-formed Pd complex would react with the argentate forming the product and [(THF)Ag(CF_3)] intermediate. This intermediate, which can be considered as the chain carrier, would react with [(dppbz)Pd(Ph)(Cl)], which is in a higher concentration than the corresponding X^-. This reaction, which would be considered as the propagation event, generates a cationic palladium complex which again reacts with $[Ag(CF_3)_2]^-$ species and forms the chain carrier, [(THF)Ag(CF_3)]. At this point, considering the contemplated mechanism, we envisioned that an induction period should be experimentally observed corresponding to the accumulation of [(THF)Ag(CF_3)].

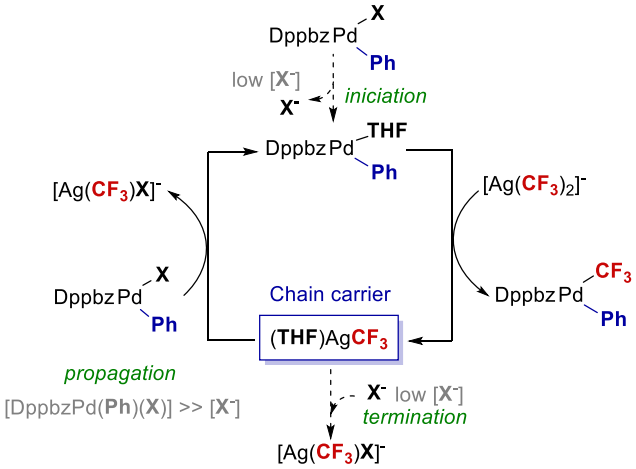

Scheme 4.56. Proposed chain mechanism for the transmetalation reaction when using $[Cs][Ag(CF_3)_2]$ species as transmetalating agents.

4.3.3.3. Experimental evaluation of the DFT proposal

With all this information in hand, we decided to perform different experiments that could support the DFT-calculated reaction mechanism and the chain transmetalation hypothesis. We envisioned that common-ion effect and low temperature kinetic could shed light on our hypothesis.

- **Common-ion effect**

According to the common-ion effect, a reversible dissociation reaction where an ion is formed is hampered by the external addition of that ion – common ion – to the reaction. This means that if the bis-(trifluoromethyl) argentate undergoes the transmetalation reaction through a stepwise mechanism where the dissociation of the halide occurs prior to the transfer of the CF_3, the addition of a halide salt to the reaction should slow down the transmetalation rate.

In this regard, we study the reaction using an excess of NBu_4I in the reaction media. No product formation was observed from the reaction of $\mathbf{2}_{Ag}$ and $\mathbf{3}_{Pd}$ after 1.5 h of reaction at 0 °C (a 30 % of product formation was formed at this time in the absence of the salt). The heteroleptic silver species was observed in the reaction media due to reaction of the salt and the homoleptic argentate.

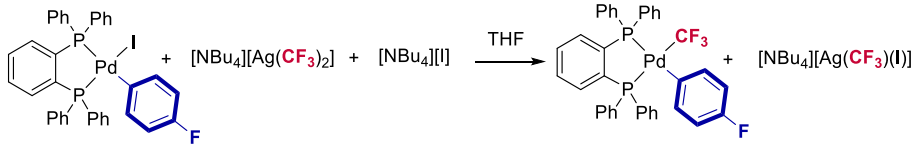

Scheme 4.57.

The same experiment at room temperature showed the formation of the corresponding product in a 100% yield overnight at room temperature. This experiment shows that the cleavage of the Pd–I bond is essential for the reaction to happen. If there is a common ion in the reaction media, that hampers the Pd–X dissociation, the transmetalation reaction is slower. Therefore, the concerted mechanism was ruled out, supporting our calculations.[57]

- **Low temperature NMR kinetic experiment**

We envisioned that if the aforementioned hypothesis of the transmetalation chain mechanism is right, and induction period corresponding to the generation of the more reactive [(THF)Ag(CF_3)] species should be observed at lower temperatures. To probe this, we run a kinetic experiment by ^{19}F NMR spectroscopy of the transmetalation of $\mathbf{2_{Ag}}$ and $\mathbf{3_{Pd}}$ at 0 ºC. Gratifyingly, it showed the existence of an induction period, supporting our hypothesis based on calculations.

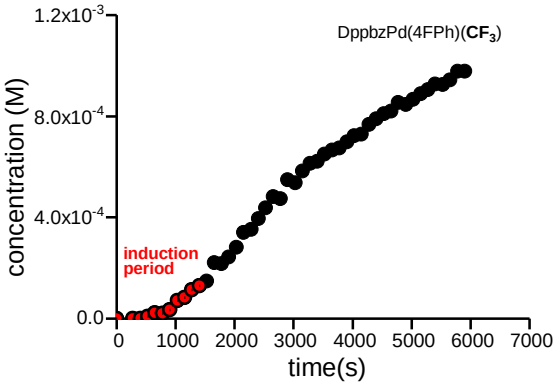

In summary, the transmetalation reaction when using [Cs][Ag(CF_3)] occurs *via* a stepwise mechanism where a short-lived cationic palladium complex is essentially generated by [(THF)Ag(CF_3)] transient species. The Hammett plot study indicates the generation of a positive charge supporting this proposal. In the case of DMF, the influence of the halide ligand is attenuated by its the high coordinating aptitude towards the palladium metal center. The

[57] No decomposition was observed when the salt was added to the $NBu_4Ag(CF_3)_2$, just formation of the corresponding heteroleptic argentate, NBu4Ag(CF3)I. This experiment suggests that the concerted mechanism is not likely to be operative.

Hammett study also points out the generation of a positive charge during the rate determining step. This is likely related to the decoordination of the solvent.

Interested by this unexpected role of the neutral silver species to promote the dehalogenation of the palladium complex as a “chain carrier”, we wondered if similar species proposed to be catalytically active could abstract the chloride ligand faster than the iodide from aryl-Pd(II) complexes. Indeed, based on DFT calculations, species such as [Ag–C≡CPh] and [Ag–(*o*-NO_2Ph)] follow the same thermodynamic trend. These results point out that neutral silver species, potentially formed in the catalytic reaction, can create a vacancy in the aryl-Pd(II)-Cl complex faster than in iodide one. This is important to keep in mind for the design of transmetalating agents.

4.4. Conclusions

In summary, in Chapter 3, we have discussed the stoichiometric mechanistic studies on the transmetalation step between aryl-Pd(II) complexes and trifluoromethyl silver(I) species. To do so, we have carried out kinetic experiments based on NMR spectroscopy and DFT calculations.

In this study, we have demonstrated the ancillary-ligand control of the transmetalation mechanism. When using the bathocuproine, a stepwise mechanism where a cationic silver complex abstracts the halide ligand from the palladium complex has been proposed. In the case of anionic ligand (CF_3), we suggested a much complex mechanism similar to a radical chain mechanism. The transmetalation reaction involves a stepwise sequence of halide abstraction/CF_3 transfer, where a “ligandless” silver species promote the halide abstraction.

The Hammett plot for the study of both silver nucleophiles showed an accumulation of a positive charge in the rate determining step. To certain extent, this could be counterintuitive since the silver nucleophile is reacting faster with an electron-richer palladium complex. A reasonable explanation is that the rate determining step is more related to the dehalogenation or the decoordination of the solvent than the CF_3 transfer *per se*. A short-lived cationic palladium complex is proposed to be a common intermediate in both systems. Indeed, we were able to characterize a putative intermediate of this cationic palladium complex using low temperate NMR spectroscopy and slightly modifications on the phosphine ligand attached to the palladium metal center.

This study not only suggests that the transmetalation step is not an elementary step in Pd/Ag bimetallic systems but also highlights its complexity giving rise to the definition of new transmetalation reaction mechanisms. The stepwise nature of the transmetalation using silver could be a source of undesired reactions in catalytic conditions.

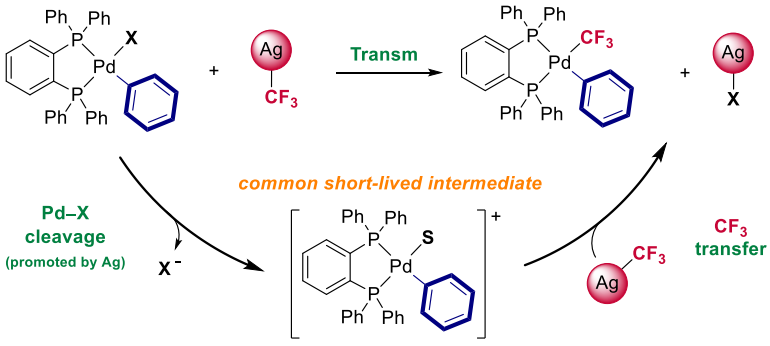

Figure 4.4. Graphical abstract of Chapter 4.

4.5. Appendixes

4.5.1. Experimental appendix

4.5.1.1. General procedures

All reactions were conducted in an argon-filled glovebox (mBraun Unilab 4420) with concentrations of O_2 and H_2O < 0.1 ppm or oven-dried glassware (at 100 ºC overnight and cooled under vacuum prior use) using Schlenk techniques under argon atmosphere (otherwise mentioned). NMR spectra were obtained on a Bruker 400 MHz, a 500 MHz or a 500 MHz with cryoprobe spectrometers equipped with probeheads capable of producing gradients in the z direction with a maximum strength of 53.5 G·cm^{-1}. ^{1}H, ^{13}C, ^{19}F and ^{31}P NMR chemical shifts are reported in parts per million (ppm), relative to tetramethylsylane (TMS) for ^{1}H and ^{13}C with the residual solvent peak used as an internal reference, relative to $CFCl_3$ (Freon) for ^{19}F and relative to 85% H_3PO_4 for ^{31}P. In the ^{19}F and ^{31}P NMR spectra registered in non-deuterated solvents, a coaxial tube containing acetone-d_6 or dimethylsulfoxide-d_6 was used to maintain the lock ^{2}H signal. Multiplicities are reported as follows: singlet (s), doublet (d), broad doublet (bd), doublet of doublets (dd), doublet of quadruplets (dq), triplet (t), quadruplet (q), doublet of quadruplet of quadruplets (dqq) and multiplet (m).

4.5.1.2. Materials and methods

Commercially available reagents AgF, AgOAc, Ag_2O, $AgSbF_6$, AgCl, AgBr, bathocuproine (Bc), bathophenantroline, 1,3-diisopropylimidazolinium chloride(SIPr· HCl), iodobenzene, 4-fluoroiodobenzene, 4-methyliodobenzene, 4-trifluoromethyliodobenzene, 4-methoxyiodobenzene, ethyl 4-iodobenzoate, fluorobenzene, 4,4'-difluorobiphenyl, $Pd(PPh_3)_4$, 1,3-bis(diphenylphosphino)propane (dppp), 1,2-bis(diphenylphosphino)ethane (dppe), 1,1'-bis(diphenylphosphino)ferrocene (dppf), bis(dicyclohexylphosphino)ethane (dCype), 1,2-Bis(diphenylphosphino)benzene (dppbz) were used without further purification directly as received from the commercial supplier, and stored under inert gas and/or low temperature when required. If necessary, the solvents (Hexane, THF, CH_2Cl_2, toluene, Et_2O) were used from a solvent purification system *pure-solv* (SPS-400, Innovative Technology) and stored under argon over activated 4 Å molecular sieves. Anhydrous benzene was used without further purification. Deuterated solvents (C_6D_6, THF-d_8, DMF- d_7, CD_2Cl_2) were stored under argon over activated molecular sieves 4 Å. For the synthesis of silver complexes, dpppPd(Ph)(I) and dpppPd(Ph)(CF_3) we followed previously reported protocols. All the silver complexes are light-sensitive, so the reactions were preserved from light to avoid photodecomposition.

4.5.1.3. Synthesis of oxidative addition Pd(II) complexes and characterization

- **Synthesis of $(PPh_3)_2Pd(Ar)(I)$**

The synthesis of $(PPh_3)_2Pd(Ar)(I)$ were carried out by oxidative addition of Pd(0) complex and aryl iodide in benzene according to the synthesis of the previously-synthetized $(PPh_3)_2Pd(4MePh)(I)$, $(PPh_3)_2Pd(Ph)(I)$ and $(PPh_3)_2Pd(4FPh)(I)$.[58,59] Outside the glove-box, an oven-dried Schlenk flask was charged with $(PPh_3)_4Pd$ complex (1 equiv., 0.043 M) and several argon/vacuum cycles were performed. Then, benzene was added to the Schlenk flask under vigorous stirring. After that, the corresponding aryl iodide (1.2 equiv.) was added. The yellowish suspension changes its color to a dark green/brown solution. The reaction evolved overnight to yield a suspension of the desired palladium complex. The solvent was partially removed under reduced pressure. The formed $(PPh_3)_2Pd(Ar)(X)$ was recrystallized by adding hexane. After filtration, the solid was washed several times with hexane till the free phosphine signal disappears in ^{31}P NMR spectroscopy. A white/yellowish powder is generally formed. Comparison with the previously reported NMR spectra confirmed the formation of the desired product.

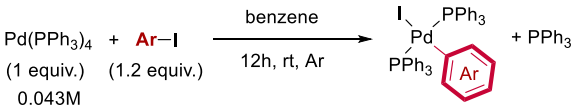

Scheme S1.

All the 31P NMR experiments of the obtained arylpalladium(II) complexes are in agreement with the previously described ones. $(PPh_3)_2Pd(4COOEtPh)(I)$, which was not previously reported, was characterized by NMR spectroscopy techniques and weight-spectrometry.

- Characterization of $(PPh_3)_2Pd(4COOEtPh)(I)$

^{1}H NMR (500 MHz, CD_2Cl_2, 25 ºC): δ 7.61 – 7.44 (m, 12H, *Ph*-phosphine), 7.43 – 7.33 (m, 6H, *para-Ph-phosphine*), 7.32 – 7.23 (m, 12H), 6.87-6.81 (m, 2H, *ortho*-4COOEt*Ph*), 6.80 – 6.74 (m, 2H, *meta*-4COOEt*Ph*), 4.20 (q, 2H, $COOCH_2CH_3$, $^2J_{H,H}$ = 7.1 Hz), 1.29 (t, 3H, $COOCH_2CH_3$, $^2J_{H,H}$ = 7.1 Hz). **$^{13}C\{^1H\}$ NMR** (126 MHz, CD_2Cl_2, 25 ºC): δ 170.86 (t, $^2J_{C,P}$ = 2.7 Hz, *ipso*-Pd), 167.66 (s, *C*OOEt), 136.22 (t, $^3J_{C,P}$ = 5.0 Hz, *ortho*-4COOEt*Ph*), 135.38 (t, $J_{C,P}$ = 6.0 Hz, *Ph*-phosphine), 132.36 (t, $^1J_{C,P}$ = 22.9 Hz, *ipso*-P-phosphine), 130.47 (s, *p-Ph*-phosphine),128.4-128.2 (overlapping signals, Ph-phospine, *meta*-4COOEt*Ph*), 124.9 (m, p-4COOEt*Ph*), 60.57 (s, $COOCH_2CH_3$), 14.70 (s,$COOCH_2CH_3$). **$^{31}P\{^1H\}$ NMR** (202 MHz, CD_2Cl_2, 25 ºC): δ 25.72 (s).

HRMS-electrospray (+) in MeOH (m/z): $[M-I]^+$ calcd for $C_{45}H_{39}O_2P_2{}^{106}Pd$, 779.1455; found 779.1451.

58 Munjanja, L.; Brennessel, W. W.; Jones, W. D. *Organometallics* **2015**, 34, 4574.
59 Kaspi, A. W.; Yahav-Levi, A.; Goldberg, I.; Vigalok, A. *Inorganic Chemistry*, **2008**, 47, 5.

- **Synthesis of $(PPh_3)_2Pd(4FPh)(X)$, X=Cl, Br**

The metathesis reaction was performed using the corresponding AgX salt.[60] Inside the glove-box, $(PPh_3)_2Pd(4FPh)(I)$ and the corresponding salt was added into an oven-dried Schlenk flask. Next, dichloromethane was added. The reaction was carried out overnight at room temperature covered by aluminum foil to prevent decomposition of the silver salt. The suspension was then filtered through celite under argon atmosphere. The solvent was removed under reduce pressure and the resulting white solid was washed with hexane.

- **Screening for the appropriate ligand to evaluate the electronic effects on the Pd(II) complexes during transmetalation.**

The synthesis for the (P^P)Pd(Ar)(I) complexes were performed by ligand exchange of the corresponding $(Ph_3P)_2Pd(Ar)(I)$ complexes and the corresponding bidentate phosphine ligand. The general procedure is described below. In an argon atmosphere glovebox, $(PPh_3)_2Pd(Ar)(I)$ complex (1 equiv., 0.024M) and the corresponding bidentate phosphine ligand (1.3 equiv.) were added to an oven-dried Schlenk flask. Then, benzene was added and the reaction was stirred overnight. The solution was concentrated and hexane was added to precipitate the product. The solid residue was washed with hexane to afford a fluffy and yellowish powder.

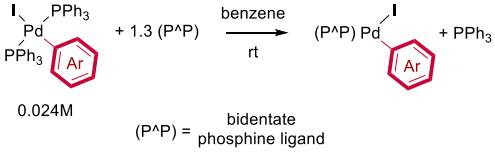

Reaction S 1

This reaction was peformed for the synthesis of dpppPd(4FPh)(I), dpppPd(4MePh)(I), dpppPd(4OMePh)(I), dppfPd(4FPh)(I), dppfPd(4OMePh)(I) and dppePd(4OMe)(I). The corresponding pure complexes were not obtained in any case as it was shown by ^{19}F or/and ^{31}P NMR spectroscopy. We believe that exchange between the aryls moieties on the phosphorous and the palladium is the source of the impurities.

[60] Ludwig, M.; Strömberg, S.; Svensson, M.; Åkermark, B. *Organometallics* **1999**, 18, 970.

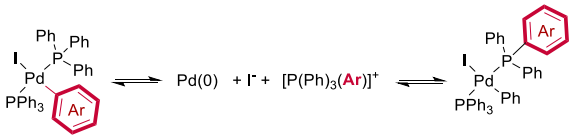

We hypothesized that 1,2-bis(dicyclohexylphosphino)ethane(dCype) or 1,2-Bis(diphenylphosphino)benzene (dppbz) ligands could overcome this limitation. On the one hand, dCype contains aliphatic substituents which could hamper this scrambling reaction. On the other hand, dppbz is a rigid and more electron-poor phosphine that can prevent the reorganization of the aryl groups, which is proposed to happen through a cationic palladium complex.[61] No scrambling was observed for dCypePd(4OMePh)(I) or dppbzPd(4MePh)(I) by ^{19}F and ^{31}P NMR spectroscopy. Finally, we chose dppbz ligand because it was economically more convenient.

- dpppPd(4FPh)(I)

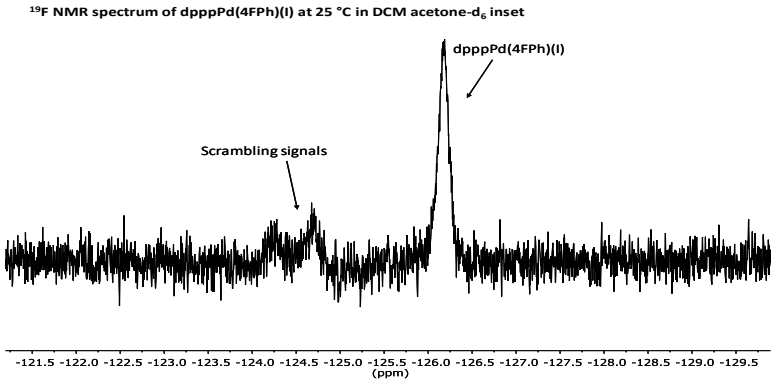

[61] Goodson, F. E.; Wallow, T. I.; Novak, B. M. *J. Am. Chem. Soc.*, **1997**, *119*, 12441.

$^{31}P\{^{1}H\}$ NMR spectrum of dpppPd(4FPh)(I) at 25 °C in DCM acetone-d_6 inset

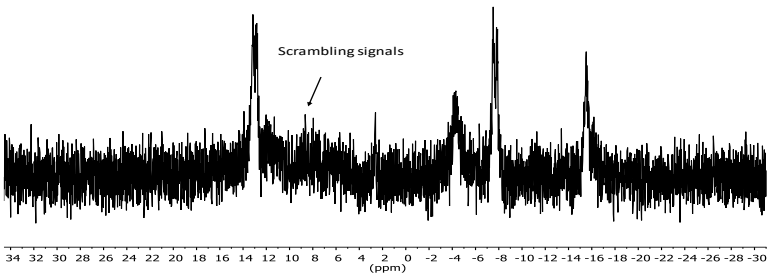

^{19}F NMR spectrum of dpppPd(4FPh)(I) at 25 °C in THF acetone-d_6 inset

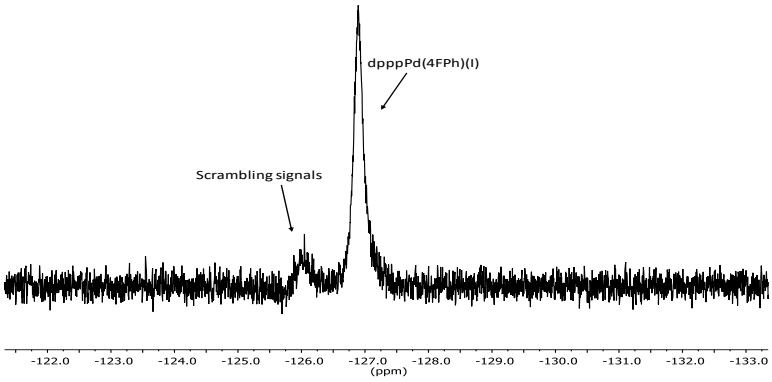

$^{31}P\{^{1}H\}$ NMR spectrum of dpppPd(4FPh)(I) at 25 °C in THF acetone-d_6 inset

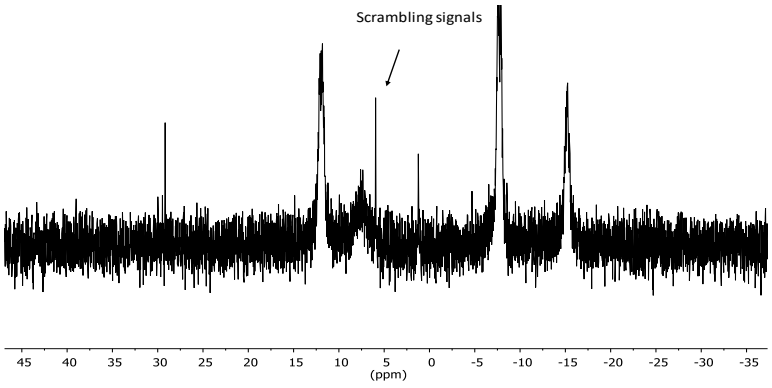

- dpppPd(4MePh)(I)

$^{31}P\{^{1}H\}$ NMR spectrum of dpppPd(4MePh)(I) at 25 °C in C_6D_6

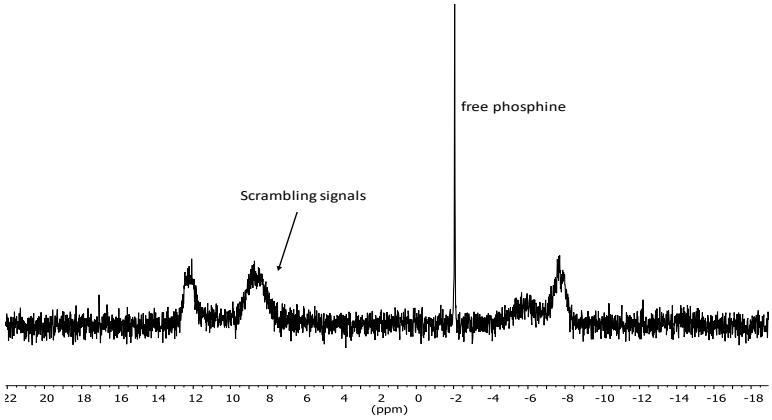

- dppfPd(4FPh)(I)

$^{31}P\{^{1}H\}$ NMR spectrum of dppfPd(4FPh)(I) at 25 °C in THF acetone-d_6 inset after heating 2h at 40 °C

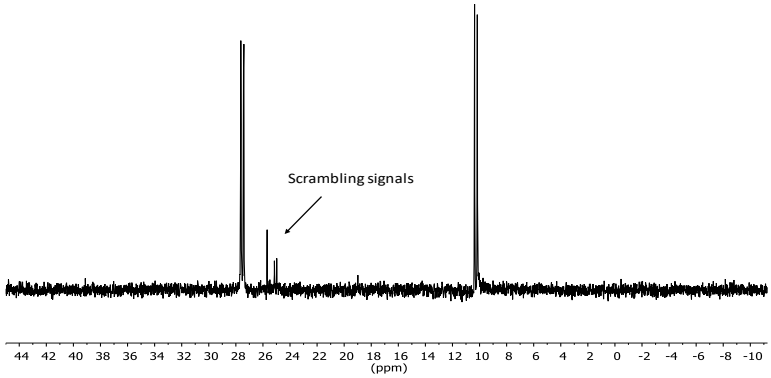

- dppfPd(4OMePh)(I)

$^{31}P\{^{1}H\}$ NMR spectrum of dppfPd(4OMePh)(I) at 25 °C in THF acetone-d_6 inset

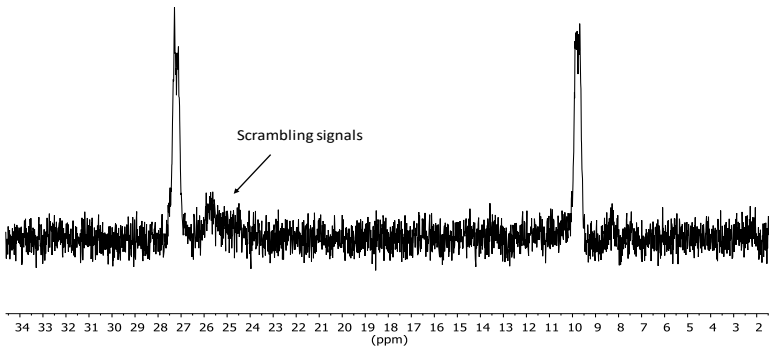

- dppePd(4OMe)(I)

$^{31}P\{^{1}H\}$ NMR spectrum of dppePd(4MePh)(I) at 25 °C in C_6D_6

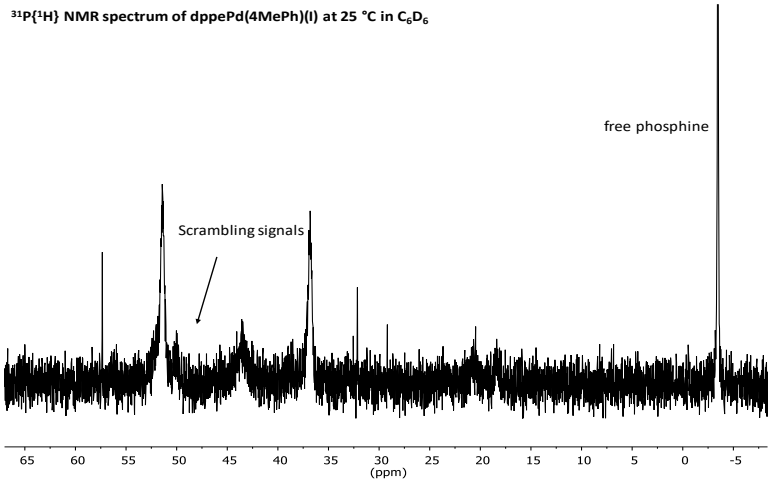

- dCypePd(4OMePh)(I)

$^{31}P\{^{1}H\}$ NMR spectrum of dCypePd(4OMePh)(I) at 25 °C in $CDCl_3$

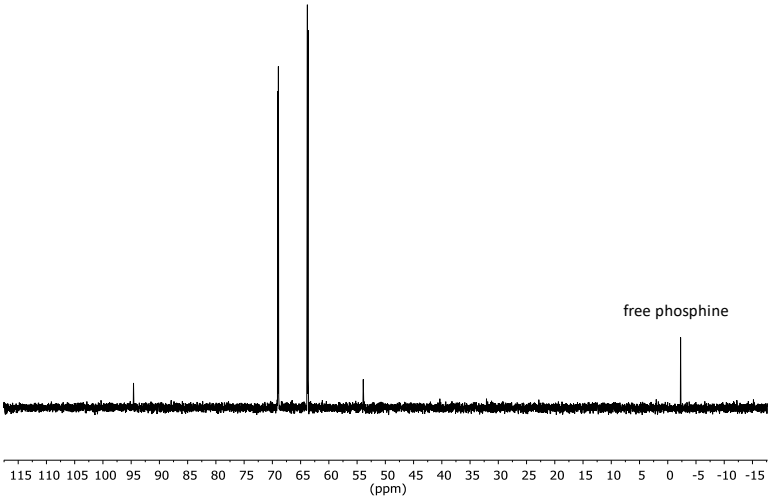

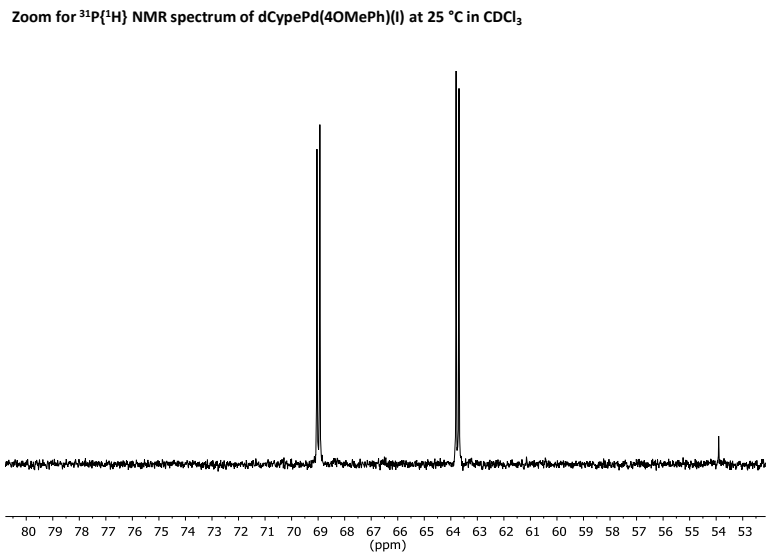

- **Synthesis and characterization of dppbzPd(Ar)(X)**

The synthesis for the dppbzPd(Ar)(X) complexes were performed by ligand exchange of the corresponding $(Ph_3P)_2Pd(Ar)(X)$ complexes and dppbz phosphine ligand, as it is reported for dppbzPd(4MePh)(I) and dppbzPd(4FPh)(I).[62] The general procedure is described below. In an argon atmosphere glovebox, $(PPh_3)_2Pd(Ar)(X)$ complex (1 equiv., 0.024M) and dppbz ligand (1.3 equiv.) were added to an oven-dried schlenk. Then, benzene was added and the reaction was stirred overnight. The solvent was partially removed under reduced pressure of the resulting suspension. The precipitated of the corresponding (P^P)Pd(Ar)(X) was recrystallized by adding hexane. After filtration, the solid was washed several times with hexane to afford a fluffy and yellowish powder.

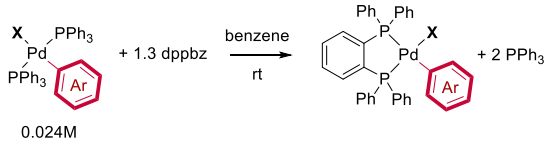

Reaction S2

- DppbzPd(4MePh)(I)

^{1}H NMR (500 MHz, CD_2Cl_2, 25 ºC): δ 7.75 – 7.42 (m, overlapping signals, 16H, *Ph*-phosphine), 7.32 – 7.25 (m, overlapping signals, 8H, *Ph*-phosphine), 6.82 (td, $^1J_{H,H}$ = 8.2, $^4J_{P,H}$ = 2.1 Hz, 2H, *ortho*-4Me*Ph*), 6.60 (m, 2H, *meta*-4Me*Ph*), 2.15 (s, 3H, 4*Me*Ph). **^{13}C{^{1}H} NMR** (126 MHz, CD_2Cl_2, 25 ºC): δ 151.22 (d, $^2J_{C,P}$ = 133.77 Hz, *ipso*-Pd), 144.38 (vt, $J_{C,P}$ = 46.71 Hz, *ipso*-P-backbone), 142.15 (dd, $J_{C,P}$ = 35.29 Hz, $J_{C,P}$ = 39.85 Hz, *ipso*-P-backbone), 138.03 (vt, 11.7

[62] a) Mann, G.; Baranano, D.; Hartwig, J. F.; Rheingold, A. L.; Guzei, I. A. *J. Am. Chem. Soc*. **1998**, *120*, 9205. b) Kaspi, A. W.; Yahav-Levi, A.; Goldberg, I.; Vigalok, A. *Inorganic Chemistry*, **2008**, *47*, 5.

Hz, *ortho*-4Me*Ph*), 134.84 (d, $J_{C,P}$ = 15.38 Hz), 134.49 (d, $J_{C,P}$ = 12.08 Hz), 134.30 (dd, $J_{C,P}$ = 1.83 Hz, $J_{C,P}$ = 16.43 Hz), 133.85 (d, $J_{C,P}$ = 11.56 Hz), 132.6 (m), 132.37 (broad dd), 132.27 (d, $J_{C,P}$ = 37.65 Hz, *ipso*-P), 132.00 (s), 131.28 (d, $J_{C,P}$ = 2.55 Hz), 131.1 (d, $J_{C,P}$ = 2.16 Hz), 129.96 (d, $J_{C,P}$ = 52.39 Hz, *ipso*-P), 129.00 (d, $J_{C,P}$ = 8.63 Hz), 128.93 (d, $J_{C,P}$ = 10.00 Hz), 128.68 (s), 128.04 (d, $J_{C,P}$ = 9.5 Hz, *meta*-4Me*Ph*), 20.93 (s, 4*Me*Ph). A carbon signal is missing probably due to overlapping. The multiplicity of the signals was deduced by performing $^{13}C\{^{1}H\}\{^{31}P\}$ NMR spectroscopy. **$^{31}P\{^{1}H\}$ NMR** (202 MHz, CD_2Cl_2, 25 ºC): δ 53.91 (d, 2P, $^{2}J_{P,P}$ = 27.3 Hz), 46.24 (d, 2P, $^{2}J_{P,P}$ = 27.3 Hz).

HRMS-electrospray (+) in ACN (m/z): $[M-I]^+$ calcd for $C_{36}H_{28}FP_2{}^{106}Pd$, 647.0680; found 647.0686.

- DppbzPd(Ph)(I)

^{1}H NMR (500 MHz, CD_2Cl_2, 25 ºC): δ 7.74 – 7.41 (m, 16H, *Ph*-phosphine), 7.32 – 7.25 (m, 8H, *Ph*-phosphine), 7.00 – 6.93 (t, 2H, *ortho*-*Ph*), 6.76 – 6.68 (m, 3H).**$^{13}C\{^{1}H\}$ NMR** (126 MHz, CD_2Cl_2, 25 ºC): δ 156.50 (d, $^{2}J_{C,P}$ = 143.5 Hz, , *ipso*-Pd), 144.47 (vt, 47.5 Hz), 142.45 (vt, $J_{C,P}$ = 39.9 Hz), 142.13 ($J_{C,P}$ = 40.0 Hz), 138.48 (vt, 3.2 Hz, *ortho*-4Me*Ph*), 135.00 (d, $J_{C,P}$ = 14.4 Hz), 134.67 (d, $J_{C,P}$ = 12.0 Hz), 134.46 (d, $J_{C,P}$ = 16.7 Hz), 133.96 (d, $J_{C,P}$ = 16.7 Hz), 132.7 – 132.1 (overlapping signals), 132.22 (s), 131.49 (d, $J_{C,P}$= 2.7 Hz), 131.31 (d, $J_{C,P}$= 2.3 Hz), 130.00 (d, $J_{C,P}$= 52.9 Hz), 129.4 – 129.0 (overlapping signals), 128.87 (s), 127.24 (d, $^{4}J_{C,P}$= 9.2 Hz, , *meta*-4Me*Ph*), 123.00 (s, *para*-4Me*Ph*).**$^{31}P\{^{1}H\}$ NMR** (202 MHz, CD_2Cl_2, 25 ºC): δ 54.01 (d, 2P, $^{2}J_{P,P}$ = 28.2 Hz), 46.20 (d, 2P, $^{2}J_{P,P}$ = 28.2 Hz).

HRMS-electrospray (+) in ACN (m/z): $[M-I]^+$ calcd for $C_{37}H_{31}P_2{}^{104}Pd$, 641.0936, and for $C_{37}H_{31}P_2{}^{106}Pd$, 643.0930; found 641.0919 and 643.0945, respectively.

a. **DppbzPd(4FPh)(I)**

^{1}H NMR (500 MHz, CD_2Cl_2, 25 ºC): δ 7.75 – 7.42 (m, 16H), 7.35 – 7.26 (m, 8H), 6.90 (m, 2H, *ortho*-4F-*Ph*), 6.53(m, 2H, *meta*-4F-*Ph*). **$^{13}C\{^{1}H\}$ NMR** (126 MHz, CD_2Cl_2, 25 ºC): δ 161.02 (dd, $^{2}J_{C,P}$ = 240.64 Hz, *J* = 3.50 Hz, *ipso*-Pd), 149.29 (dd, $^{1}J_{C,F}$ = 142.3 Hz, *J* = 3.50 Hz, *ipso*-F), 144.34 (d, $J_{C,P}$ = 46.4 Hz), 143.94 (d, $J_{C,P}$ = 46.4 Hz), 142.26 (d, $J_{C,P}$ = 35.7 Hz), 141.94 (d, $J_{C,P}$ = 35.7 Hz), 138.54 (m, *ortho*-4F-*Ph*), 134.85 (d, $J_{C,P}$ = 15.6 Hz), 134.49 (d, $J_{C,P}$ = 12 Hz), 134.3 – 133.9 (overlapping signals), 133.76 (d, $J_{C,P}$ = 11.8 Hz), 132.8 – 132.1 (overlapping signals), 132.04 (d, $J_{C,P}$ = 36.7 Hz), 131.49 (d, $J_{C,P}$ = 2.7 Hz), 131.24(d, $J_{C,P}$ = 2.2 Hz), 129.91 (s), 129.48 (s), 129.3 – 128.7 (overlapping signals), 113.65 (dd, *meta*-4F-*Ph*). **$^{31}P\{^{1}H\}$ NMR** (202

MHz, CD_2Cl_2, 25 ºC): δ 54.6 (d, 2P, $^2J_{P,P}$ = 26.2 Hz), 47.4 (d, 2P, $^2J_{P,P}$ = 26.2 Hz). **^{19}F NMR** (470 MHz, THF-d8, 25 ºC): δ -124.1 (m).

HRMS-electrospray (+) in MeOH (m/z): $[M-I]^+$ calcd for $C_{36}H_{28}FP_2{}^{104}Pd$, 645.0685; found 645.0693.

- DppbzPd(4COOEtPh)(I)

^{1}H NMR (500 MHz, CD_2Cl_2, 25 ºC): δ 7.76 – 7.42 (overlapping signals, m, 15H), 7.38 – 7.24 (overlapping signals, 11H), 7.14 (m, 2H, *ortho*-4COOEt-*Ph*), 4.24 (q, 2H, $^2J_{H,H}$ = .7.1 Hz, COOC*H*$_2$CH$_3$), 1.31 (t, 3H, , $^2J_{H,H}$ = .7.1 Hz, COOCH$_2$C*H*$_3$). **^{13}C{^{1}H} NMR** (126 MHz, CD_2Cl_2, 25 ºC): δ 167.75 (d, $^2J_{C,P}$ = 131.98 Hz, , *ipso*-Pd), 167.93 (s, *C*OOEt), 144.09 (d, $J_{C,P}$ = 45.9 Hz), 143.7 (d, $J_{C,P}$ = 46.5 Hz), 142.16 (d, $J_{C,P}$ = 35.9 Hz), 141.83 (d, $J_{C,P}$ = 35.42 Hz), 138.18 (s), 134.87 (d, $J_{C,P}$ = 15.46 Hz), 134.5 (d, $J_{C,P}$ = 12.3 Hz), 134.2 (d, $J_{C,P}$ = 16.7 Hz), 133.74 (d, $J_{C,P}$ = 12.0 Hz), 132.9 – 132.5 (overlapping signals), 132.07 (s), 131.76 (s), 131.58 (d, $J_{C,P}$ = 2.29 Hz), 131.29 (d, $J_{C,P}$ = 1.85 Hz), 129.67 (s), 129.4 – 128.9 (overlapping signals), 128.7 (s), 126.90 (d, $J_{C,P}$ = 2.29 Hz, *meta*-4COOEt-*Ph*), 60.54 (s, COO*C*H$_2$CH$_3$), 14.60 (s,COOCH$_2$*C*H$_3$). **^{31}P{^{1}H} NMR** (202 MHz, CD_2Cl_2, 25 ºC): δ 54.1 (d, 2P, $^2J_{P,P}$ = 26.7 Hz), 47.22 (d, 2P, $^2J_{P,P}$ = 26.7 Hz).

HRMS-electrospray (+) in MeOH (m/z): $[M+Na]^+$ calcd for $C_{39}H_{33}INaO_2P_2{}^{106}Pd$, 850.9942; found 850.9964.

- DppbzPd(4CF$_3$Ph)(I)

^{1}H NMR (500 MHz, CD_2Cl_2, 25 ºC): δ 7.75 – 7.63 (overlapping signals, m, 6H), 7.60 – 7.50 (overlapping signals, m, 4H), 7.49 – 7.43 (m, 6H), 7.33 – 7.25 (overlapping signals, m, 8H), 7.15 (m, 2H, *ortho*-4CF$_3$-*Ph*), 6.95 (m, 2H, *meta*-4CF$_3$-*Ph*). **^{13}C{^{1}H} NMR** (126 MHz, CD_2Cl_2, 25 ºC): δ 164.8 (d, $^2J_{C,P}$ = 135.1 Hz, , *ipso*-Pd), 144.0 (d, $J_{C,P}$ = 45.9 Hz), 143.6 (d, $J_{C,P}$ = 46.1 Hz), 142.1 (d, $J_{C,P}$ = 35.6 Hz), 141.8 (d, $J_{C,P}$ = 35.5 Hz), 138.12 (vt, $J_{C,P}$ = 3.0 Hz, *ortho*-4CF$_3$-*Ph*), 134.9 (d, $J_{C,P}$ = 15.2 Hz), 134.5 (d, $J_{C,P}$ = 12.0 Hz), 134.2 (d, $J_{C,P}$ = 2.0 Hz), 134.0 (d, $J_{C,P}$ = 2.2 Hz), 133.67 (d, $J_{C,P}$ = 12.1 Hz), 132.9 – 132.5 (overlapping signals), 131.95 (s), 131.6 (d, $J_{C,P}$ = 2.7 Hz), 131.3 (d, $J_{C,P}$ = 2.4 Hz), 129.7 (s), 129.3 – 128.9 (overlapping signals), 128.72 (s), 126.67 (s), 125.09 (s), 124.80 (s), 124.51 (s) 122.66 (dd, $J_{C,P}$ = 4.4 Hz, $J_{C,P}$ = 9.6 Hz, *meta*-4CF$_3$-*Ph*). **^{31}P{^{1}H} NMR** (202 MHz, CD_2Cl_2, 25 ºC): δ 54.6 (d, 2P, $^2J_{P,P}$ = 27.0 Hz), 47.3 (d, 2P, $^2J_{P,P}$ = 27.0 Hz). **^{19}F NMR** (470 MHz, THF-d8, 25 ºC): δ -62.07 (s).

HRMS-electrospray (+) in MeOH (m/z): $[M+Na]^+$ calcd for $C_{37}H_{28}F_3INaP_2{}^{104}Pd$, 844.9596; found 844.9554.

- DppbzPd(4FPh)(Br)

^{1}H NMR (500 MHz, CD_2Cl_2, 25 ºC): δ 7.75 – 7.68 (overlapping signals, 5H), 7.63 – 7.43 (overlapping signals, 11H), 7.36 – 7.12 (overlapping signals,8H), 6.90 (m, 2H, *ortho*-4F-*Ph*), 6.55 (t, 2H, *meta*-4F-*Ph*). **^{13}C{^{1}H} NMR** (126 MHz, CD_2Cl_2, 25 ºC): δ 161.08 (d, $^{2}J_{C,P}$ = 240.1 Hz, , *ipso*-Pd), 152.83 (dd, $^{1}J_{C,F}$ = 137.8 Hz, *J* = 2.9 Hz, *ipso*-F), 144.7 (d, $J_{C,P}$ = 47.3 Hz), 144.3 (d, $J_{C,P}$ = 47.3 Hz), 141.3 (d, $J_{C,P}$ = 33.8 Hz), 141.3 (d, $J_{C,P}$ = 33.9 Hz), 137.64 (m, *ortho*-4F-*Ph*), 134.72 (d, $J_{C,P}$ = 15.4 Hz), 134.29 (d, $J_{C,P}$ = 11.7 Hz), 133.80 (d, $J_{C,P}$ = 12.0 Hz), 132.7 – 132.5 (overlapping signals), 131.56 (d, $J_{C,P}$ = 2.7 Hz), 131.27 (d, $J_{C,P}$ = 2.5 Hz), 129.91 (s), 129.46 (s), 129.4 – 128.9 (overlapping signals), 113.78 (dd, *meta*-4F-*Ph*). **^{31}P{^{1}H} NMR** (202 MHz, CD_2Cl_2, 25 ºC): δ 56.68 (d, 2P, $^{2}J_{P,P}$ = 26.3 Hz), 46.73 (d, 2P, $^{2}J_{P,P}$ = 26.3 Hz). **^{19}F{^{1}H} NMR** (470 MHz, THF-d_8, 25 ºC): δ -123.43 (s).

HRMS-electrospray (+) in MeOH (m/z): $[M\text{-}Br]^+$ calcd for $C_{36}H_{28}FP_2{}^{106}Pd$, 647.0680; found 647.0686.

- DppbzPd(4FPh)(Cl)

^{1}H NMR (500 MHz, CD_2Cl_2, 25 ºC): δ 7.75 – 7.69 (overlapping signals, 4H), 7.62 – 7.42 (overlapping signals, 12H), 7.36 – 7.29 (m, 8H), 6.91 (m, 2H, *ortho*-4F-*Ph*), 6.55 (t, *J* = 9.7 Hz,2H, *meta*-4F-*Ph*). **^{13}C{^{1}H} NMR** (126 MHz, CD_2Cl_2, 25 ºC): δ 161.05 (d, $^{2}J_{C,P}$ = 239.9 Hz, , *ipso*-Pd), 154.23 (d, $^{1}J_{C,F}$ = 137.8 Hz, *ipso*-F), 144.96 (d, $J_{C,P}$ = 48.1 Hz), 144.4 (d, $J_{C,P}$ = 48.1 Hz), 140.77 (d, $J_{C,P}$ = 33.6 Hz), 140.44 (d, $J_{C,P}$ = 32.4 Hz), 137.2 (m, *ortho*-4F-*Ph*), 134.67 (d, $J_{C,P}$ = 14.9 Hz), 134.7 – 133.7 (overlapping signals), 132.7 – 132.5 (overlapping signals), 131.7 – 131.1 (overlapping signals), 129.92 (s), 129.5 – 128.6 (overlapping signals), 113.83 (m, *meta*-4F-*Ph*). **^{31}P{^{1}H} NMR** (202 MHz, CD_2Cl_2, 25 ºC): δ 56.79 (d, 2P, $^{2}J_{P,P}$ = 27.4 Hz), 46.54 (d, 2P, $^{2}J_{P,P}$ = 27.4 Hz). **^{19}F NMR** (470 MHz, THF-d_8, 25 ºC): δ -123.15 (m).

HRMS-electrospray (+) in MeOH (m/z): $[M\text{-}Cl]^+$ calcd for $C_{36}H_{28}FP_2{}^{104}Pd$ 645.0685; found 645.0671.

4.5.1.4. Synthesis and Characterization of dppbzPd(Ar)(CF_3)

The synthesis for the dppbzPd(Ar)(CF_3) complexes were performed by a transmetalation reaction from the corresponding dppbzPd(Ar)(Cl) complexes and (Cs)[Ag(CF_3)$_2$] complex. The general procedure is described below. In an argon atmosphere glovebox, (PPh_3)$_2$Pd(Ar)(Cl) complex (1 equiv., 0.01M) and the silver complex (0.55 equiv.) were added to an oven-dried vial. Both solids were dissolved in THF-d_8 and stirred at room temperature for 15 min. The solution was then filtered using a PTFE 13mm 0.2µm NSTR syringe filter and transfered to a NMR tube. The recorded NMR spectra are similar to the one previously described.[63]

[63] Culkin, D. A.; Hartwig, J. F. *Organometallics*, **2004**, 23, 3398.

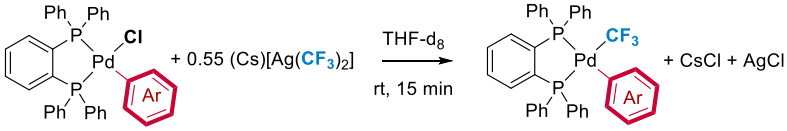

Reaction S3.

- **DppbzPd(4MePh)(CF_3)**

This complex has been previously reported.[63]

^{1}H NMR (500 MHz, THF-d_8, 25 ºC): 7.70 – 7.62 (m, 6H), 7.55 – 7.34 (m, 10H), 7.28 – 7.20 (m, 8H), 6.88 (t, *J* = 7.2 Hz, 2H, *ortho*-4Me-*Ph*), 6.52 – 6.48 (m, 2H, *meta*-4Me-*Ph*), 2.07 (s, 3H, 4*Me*-Ph). **^{31}P{^{1}H} NMR** (202 MHz, THF-d_8, 25 ºC): δ 48.2 – 47.2 (m). **^{19}F NMR** (470 MHz, THF-d_8, 25 ºC): δ -18.4 – -18.6 (m).

- **DppbzPd(Ph)(CF_3)**

^{1}H NMR (500 MHz, THF-d_8, 25 ºC): δ 7.70 – 7.61 (m, 6H), 7.57 – 7.34 (m, 10H), 7.28 – 7.19 (m, 8H), 7.01 (m, 2H, *ortho*-4F-*Ph*), 6.62 (overlapping signals, 3H, 4F-*Ph*). **^{31}P{^{1}H} NMR** (202 MHz, THF-d_8, 25 ºC): δ 48.3 – 47.4 (m). **^{19}F NMR** (470 MHz, THF-d_8, 25 ºC): δ -18.3 – -18.5 (m).

- **DppbzPd(4FPh)(CF_3)**

^{1}H NMR (500 MHz, THF-d_8, 25 ºC): δ 7.69 – 7.62 (m, 4H), 7.61 – 7.56 (m, 2H), 7.41 – 7.37 (m, 5H), 7.37 – 7.31 (m, 5H), 7.25 – 7.19 (m, 7H), 7.07 (m, 2H, *ortho*-4F-*Ph*), 6.52 (m, 3H, *meta*-4F-*Ph*). **^{31}P{^{1}H} NMR** (202 MHz, THF-d_8, 25 ºC): δ 48.7 – 47.7 (m). **^{19}F NMR** (470 MHz, THF-d_8, 25 ºC): δ -18.2 – -18.4 (m, 3F), -124.2 (m, 1F).

- **DppbzPd(4CF_3Ph)(CF_3)**

^{1}H NMR (500 MHz, THF-d_8, 25 ºC): δ 7.75 (m, 1H), 7.68 – 7.60 (m, 5H), 7.60 – 7.52 (m, 2H), 7.51 – 7.37 (m, 8H), 7.30 – 7.20 (m, 10H), 6.89 (m, 2H, 4CF_3*Ph*). **^{31}P{^{1}H} NMR** (202 MHz, THF-d_8, 25 ºC): δ 48.9 – 47.9 (m). **^{19}F NMR** (470 MHz, THF-d_8, 25 ºC): δ -18.5 – -18.7 (m, 3F), -62.45 (s, 3F).

4.5.1.5. In situ synthesis and characterization of cationic Pd intermediate

In an argon-filled glovebox, [dpppPd(Ph)(I)] complex (1 equiv., 10 mg, 0.0134 mmol) and $AgSbF_6$ (1 equiv, 4.79 mg, 0.0139 mmol) were separately added to two oven-dried vials. Then, 600 μl of DMF-d_7 was added to the Pd-containing vial and the solution was transferred to a screw-cap NMR tube. On the other hand, 300 μl of DMF-d_7 was added to the Ag-containing vial and this solution was transferred to a syringe, protected from air (with a septum).

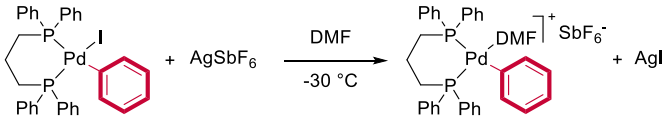

Reaction S4.

The NMR tube was introduced in a cooling bath (–80°C) and the syringe was wrapped in aluminum foil with dry ice. At low temperature, the silver solution was added into the NMR tube. The spectra showed the generation of a new cationic palladium complex stabilized by DMF at –30 °C. In the $^{31}P\{^{1}H\}$ NMR spectra, we can clearly observe the shift of the signals when comparing to dpppPdPhI in DMF-d_7. Monodimensional and bidimensional ^{1}H and ^{31}P NMR spectroscopy experiments could not provide direct information about the coordination of solvent molecules to the metal center. However, similar palladium complex that have been previously synthetized, [dpppPd(Ph)][PF_6] and [dpppPd(Ph)][BF_4] complexes in DMF, showed the same value for $^{2}J_{P,P}$ coupling constant that our complex.[60] We believe that the invariance of this value is related to the coordination of the solvent since those anions are weak coordinating ligands.

^{1}H NMR (500 MHz, DMF-d_7, -30 ºC): δ 7.90 – 7.82 (m, 3H), 7.68 – 7.58 (overlapping signals, 10H), 7.51 – 7.44 (m, 2H), 7.41 – 7.32 (overlapping signals, 6H), 7.03 (m, 2H), 6.64 (m, 2H), 3.08 (m, 2H), 2.93 – 2.85 (overlapping signals), 1.73 (m, 2H). **$^{31}P\{^{1}H\}$ NMR** (202 MHz, DMF-d_7, -30 ºC): δ 28.55 (d, 2P, $^{2}J_{P,P}$ = 50.4 Hz), 1.13 (d, 2P, $^{2}J_{P,P}$ = 50.4 Hz).

$^{31}P\{^{1}H\}$ NMR spectrum of [dpppPd(Ph)(DMF)][SbF_6] at -30°C in DMF-d_7

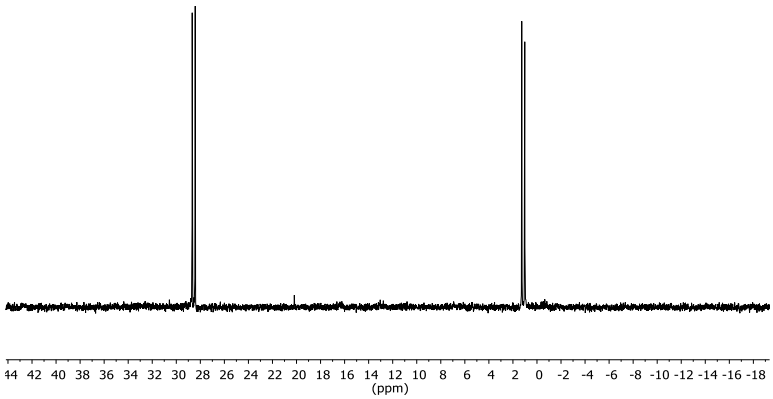

^{1}H NMR spectrum of [dpppPd(Ph)(DMF)][SbF_6] at -30°C in DMF-d_7

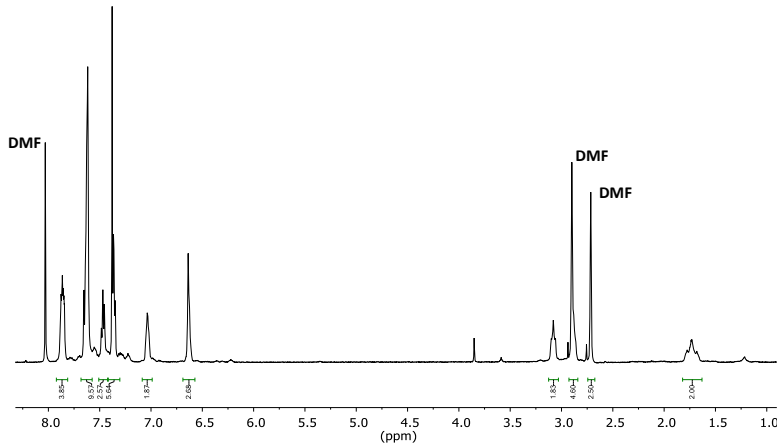

Comparison $^{31}P\{^{1}H\}$ NMR spectrum of dpppPd(Ph)(I) and [dpppPd(Ph)(DMF)][SbF_6] at -30°C in DMF-d_7

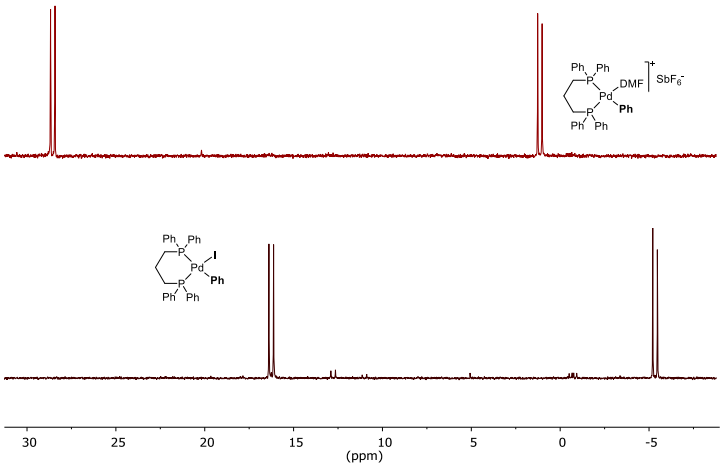

Comparison ^{1}H NMR spectrum of dpppPd(Ph)(I) and [dpppPd(Ph)(DMF)][SbF_6] at -30°C in DMF-d_7

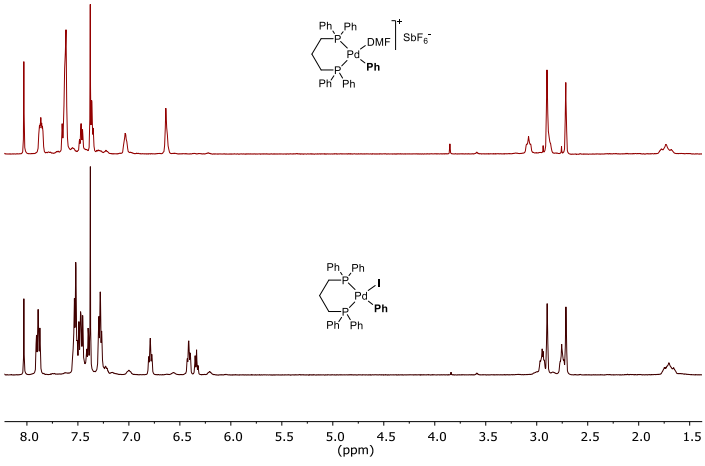

^{1}H-^{31}P HMBC NMR spectrum of [dpppPd(Ph)(DMF)][SbF_6] at -30°C in DMF-d_7

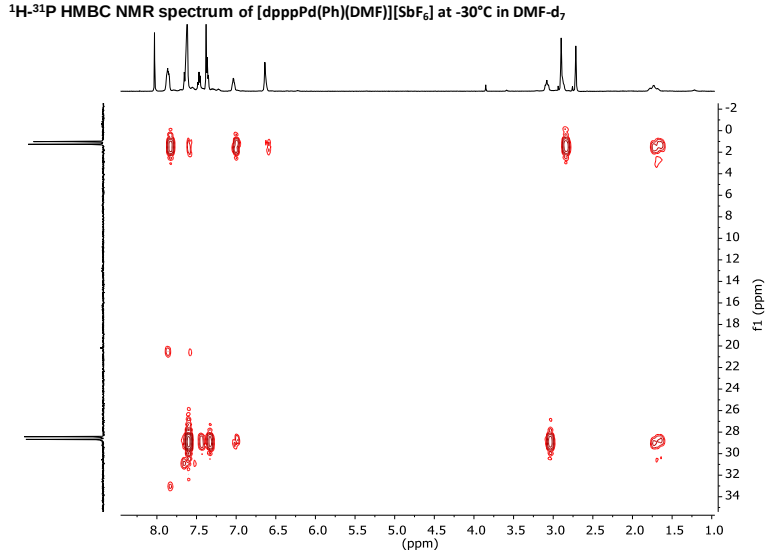

^{1}H-^{1}H NOESY NMR spectrum of [dpppPd(Ph)(DMF)][SbF_6] at -30°C in DMF-d_7

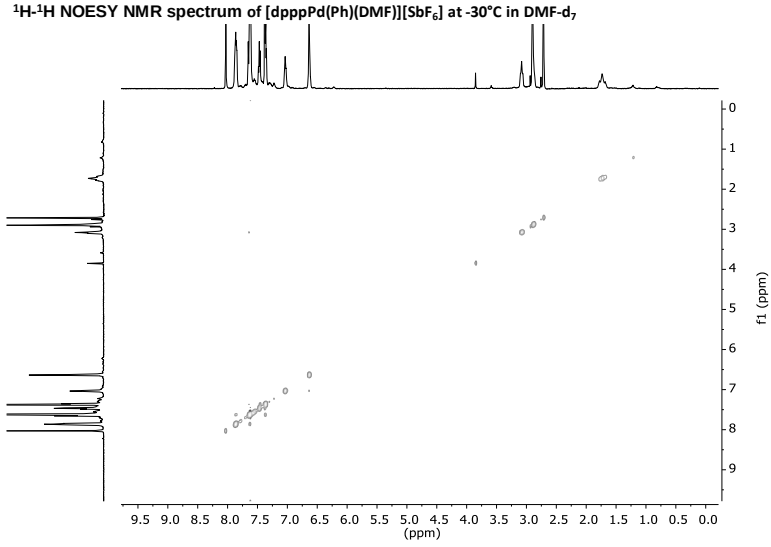

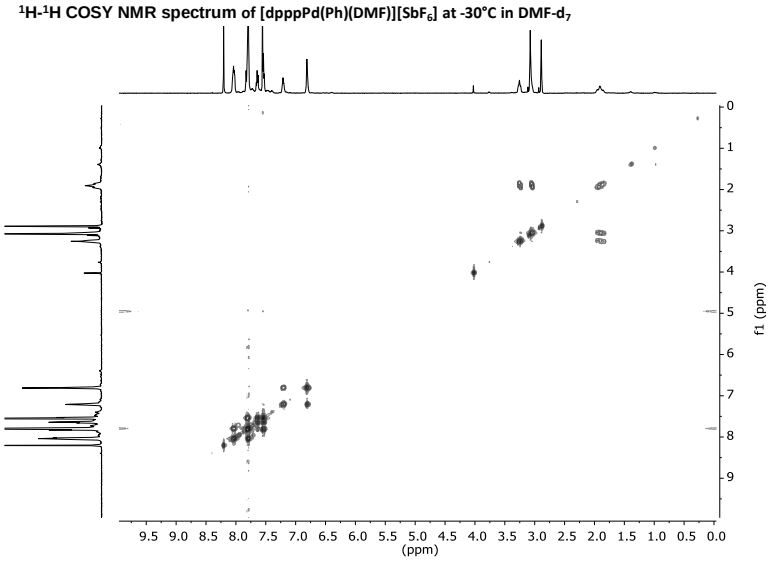

4.5.1.6. **Synthesis of PMe_3AgCF_3 complex and transmetalation study.**

We aimed at the synthesis of new silver complexes bearing monodentate phosphine ligands that could be representative of catalytic Pd/Ag systems. Although attempts to synthesize different well-defined PR_3AgCF_3 (R = Ph, Cy) complexes failed, we found a route to synthesize PMe_3AgCF_3 complex.

In an argon-filled glovebox, an oven-dried Schlenk flask was charged with AgF (50 mg, 0.40 mmol, 1 equiv.) and 5 ml of DCM. Then, $TMSCF_3$ reagent (60 μl, 0.40 mmol, 1 equiv.) was added to the so-formed suspension and was stirred for 5 min. After that, a solution of PMe_3 in toluene 1M (400 μl, 0.40 mmol, 1 equiv.) was added. The so-formed orange solution was filtered using a PTFE 13mm 0.2μm NSTR syringe filter after 15 min. The solvent was partially removed under reduced pressure outside the glovebox. Precipitation with hexane (20 ml) was then carried out. The so-obtained pale pink solid was stored in the glovebox at –32 °C. Further experiments showed that this solid is a mixture of silver neutral species, PMe_3AgCF_3, and the corresponding argentate, $[(PMe_3)Ag][Ag(CF_3)_2]$ in solution.

Reaction S5.

- DCM: (90% PMe_3AgCF_3, 10% $[(PMe_3)Ag][Ag(CF_3)_2]$)

^{1}H NMR (500 MHz, CD_2Cl_2, 25 ºC): δ 1.41 (d, $^{1}J_{H,P}$ = 7.9 Hz, 1H). **^{31}P{^{1}H} NMR** (203 MHz, CD_2Cl_2, 25 ºC): δ -32.86(s, br). **^{19}F NMR** (471 MHz, CD_2Cl_2, 25 ºC): δ -24.24 (2d, 6F, $^{2}J_{^{109}Ag,F}$ = 98.6 Hz, $^{2}J_{^{107}Ag,F}$ = 88.9 Hz), -26.65(d, br, 3F).

- THF: (95% PMe_3AgCF_3, 5% $[(PMe_3)Ag][Ag(CF_3)_2]$)

^{31}P{^{1}H} NMR (203 MHz, THF-d_8, 25 ºC): δ -31.93 (m). **^{19}F NMR** (471 MHz, THF-d_8, 25 ºC): δ -24.98 – -27.30 (br,6F), -26.06 (d, br, 3F).

PMe_3AgCF_3

^{31}P{^{1}H} NMR (203 MHz, THF-d_8, -80 ºC): δ -31.10 (2dq, $^{1}J_{^{109}Ag,P}$ = 496.31 Hz, $^{1}J_{^{107}Ag,P}$ = 430.77 Hz, $^{3}J_{P,F}$ = 20.4 Hz). **^{19}F NMR** (471 MHz, THF-d_8, -80 ºC): δ -29.08 (m).

$[(PMe_3)Ag][Ag(CF_3)_2]$)

^{31}P{^{1}H} NMR (203 MHz, THF-d_8, -80 ºC): δ -32.93 (2dd, $^{1}J_{^{109}Ag,P}$ = 580.30 Hz, $^{1}J_{^{107}Ag,P}$ = 506.40 Hz).**^{19}F NMR** (471 MHz, THF-d_8, -80 ºC): δ -26.67 (2d, $^{2}J_{^{109}Ag,F}$ = 96.97 Hz, $^{2}J_{^{107}Ag,F}$ = 86.96 Hz).

- **Study of the dependence of the equilibrium of PMe_3AgCF_3 with the temperature.**

In order to confirm that both species are in equilibrium, we run NMR spectroscopy experiments at different temperatures. The equilibrium was shifted towards the ionic species when decreasing the temperature. See experiments below.

^{19}F NMR spectrum of PMe_3AgCF_3 in THF-d_8 at different temperatures

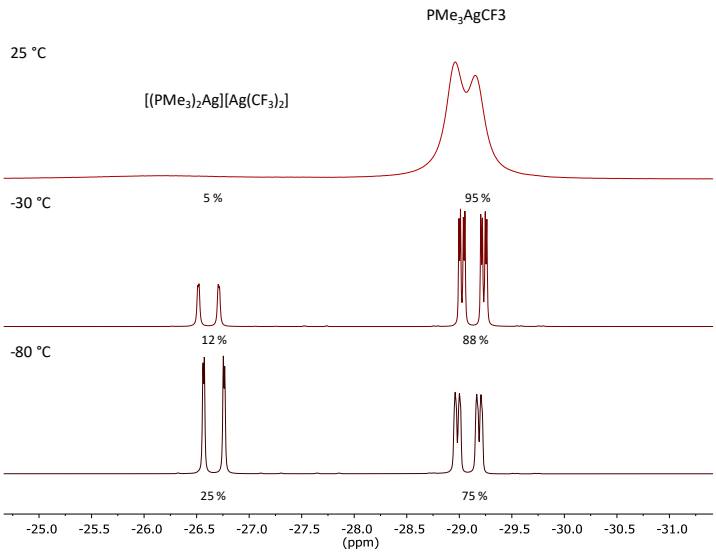

$^{31}P\{^1H\}$ NMR spectrum of PMe_3AgCF_3 in THF-d_8 at different temperature

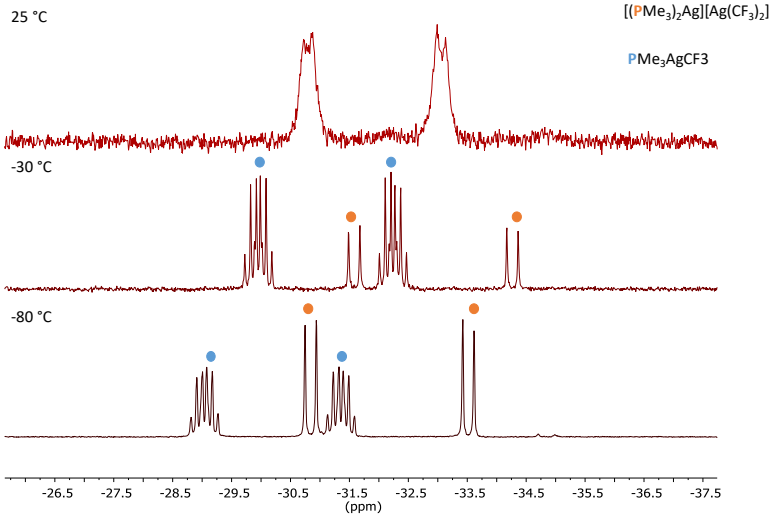

- **Transmetalation study of PMe_3AgCF_3 and dppbzPd(4FPh)(I).**

Under argon atmosphere, we weight the palladium and the silver compounds in two separate oven-dried crimped vials. Then, we added a solution of the internal standard, 4,4'-bifluorobiphenyl (4.0 mg, 0.021 mmol), dissolved in 300 µl of THF to the vial containing $PMe_3Ag(CF_3)$ complex (2.27 mg, $8.97 \cdot 10^{-3}$ mmol, 1.5 equiv.). This solution along the internal

standard was transferred to a screw-cap NMR tube previously charged with a DMSO-d_6 inset. On the other hand, to the second vial, containing the dppbzPd(4FPh)(I) palladium complex (4.65 mg, $6.00 \cdot 10^{-3}$ mmol, 1 equiv.), we added 300 μl of THF. This solution was transferred to a syringe, protected from air (with a septum). Both the NMR tube and the palladium-containing syringe were taken out the glove box. The NMR tube was introduced in a cooling bath (-80°C) and the syringe was wrapped in aluminum foil with dry ice. The transmetalation reaction was performed by combining both solutions at low temperature. The desired working temperature (25 °C) was previously set in the NMR instrument.

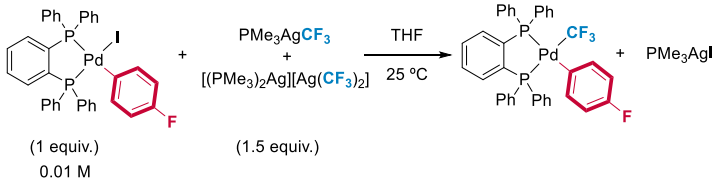

Reaction S6.

No dppbzPd(4FPh)(CF_3) product was observed after mixing both complexes. After 48h, small amount of the expected product is observed. However, the reaction is not selective to the formation of this compound and unidentified by-products are inherently formed. We believe that the phosphine ligand can block some position in the palladium complex and inhibit the transmetalation reaction.

$^{19}F\{^{1}H\}$ NMR spectrum of PMe_3AgCF_3 at 25 °C in THF

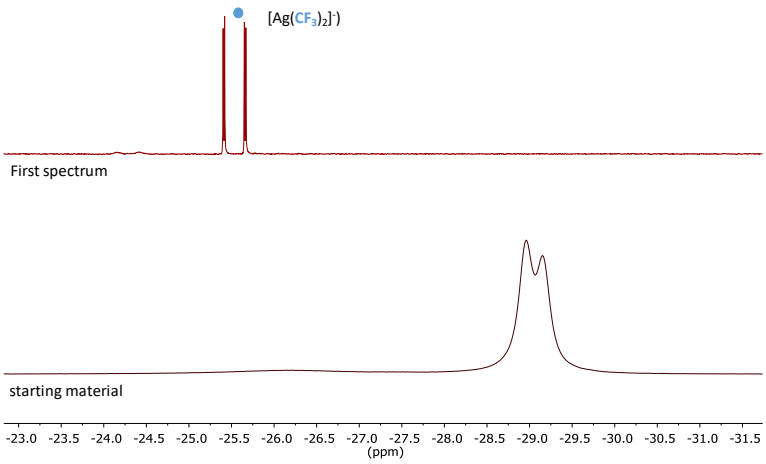

$^{31}P\{^{1}H\}$ NMR spectrum of the transmetalation using PMe_3AgCF_3 25 °C in THF

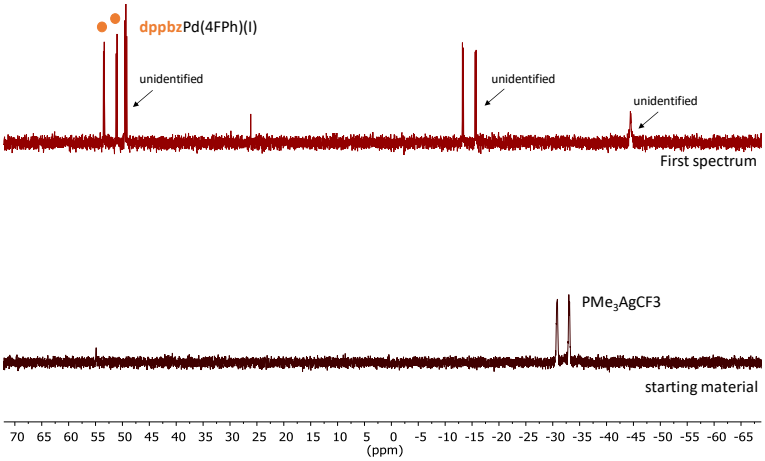

$^{19}F\{^{1}H\}$ NMR spectrum of PMe_3AgCF_3 at 25 °C in THF after 48h

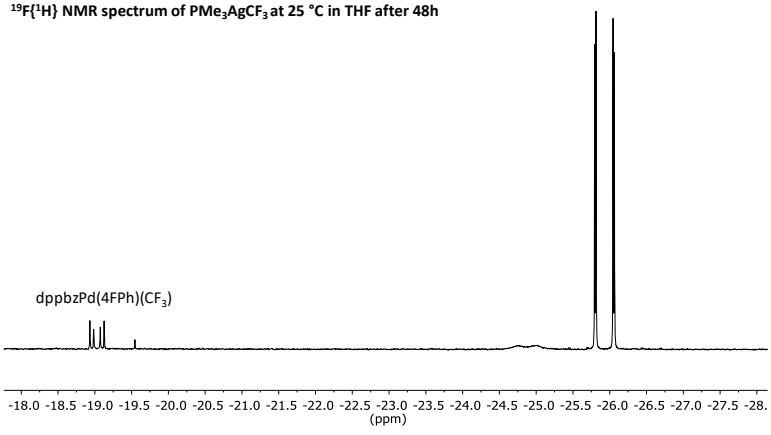

4.5.1.7. **Study of scrambling reaction when using cationic silver salts.**

With the aim of detecting a post-transmetalation intermediate where palladium and silver could be in a discrete molecule, we focused our attention on the reaction of [BcAg(THF)](SbF_6) and dpppPd(Ph)(CF_3). As we mentioned in the main text, the reaction does not yield any post-transmetalation intermediate but give rise to an unexpected side-product, dpppPd(CF_3)$_2$ complex. The experimental procedure for the detection and selective formation is described below.

Under argon atmosphere, we placed dpppPd(Ph)(CF_3) palladium complex (5mg, $7.52 \cdot 10^{-3}$ mmol, 1 equiv.) in a NMR tube, which previously contained an acetone-d_6 inset, and we dissolved it in 0.7 ml of THF. Then, [BcAg(THF)](SbF_6) silver complex (8.8 mg, $7.52 \cdot 10^{-3}$ mmol, 1 equiv.) was added.

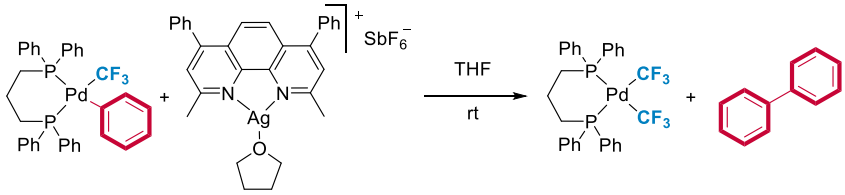

Reaction S7.

The same reaction was also performed in toluene. In both cases, dpppPd(CF_3)$_2$ was observed by NMR spectroscopy but, in toluene, the proportion of dpppPd(CF_3)$_2$ complex was higher.

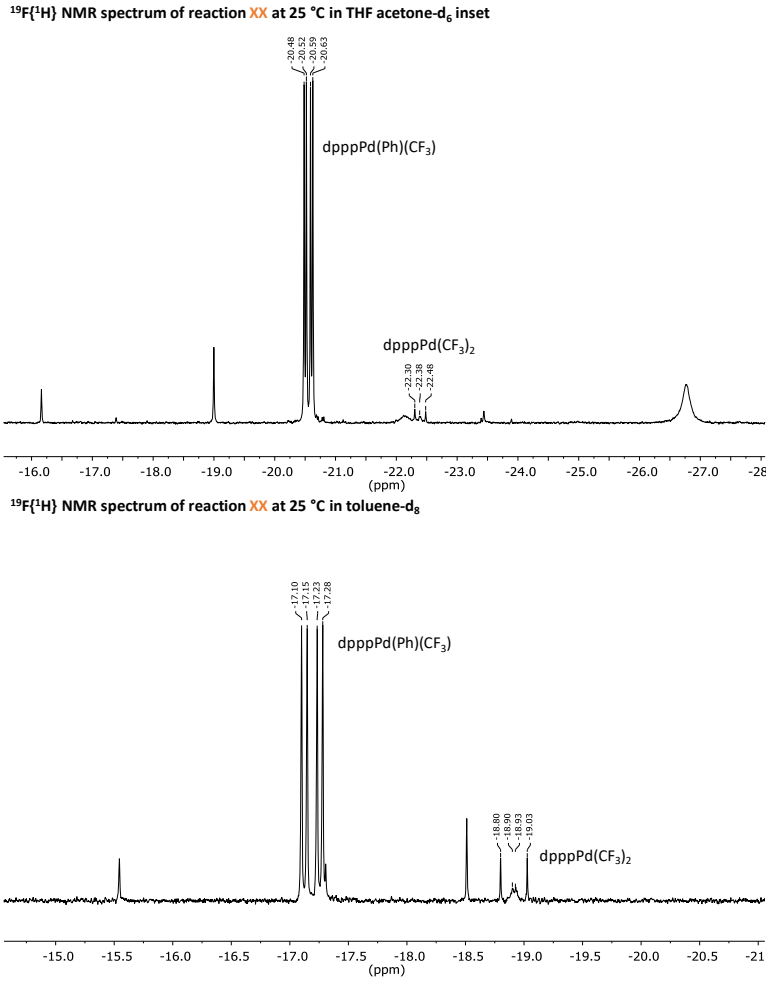

We envisioned that cationic silver salt without ancillary ligand could favor the formation of dpppPd(CF_3)$_2$. Indeed, the combination of dpppPd(Ph)(CF_3) palladium complex (4 mg, $6.01 \cdot 10^{-3}$ mmol, 1 equiv., 0.01M) and $AgSbF_6$ salt (2 mg, $5.82 \cdot 10^{-3}$ mmol, 1 equiv.) in a NMR tube yield a higher proportion of dpppPd(CF_3)$_2$.

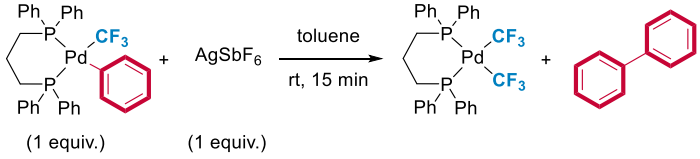

Reaction S8.

^{19}F NMR spectrum of reaction XX at 25 °C in toluene-d_8

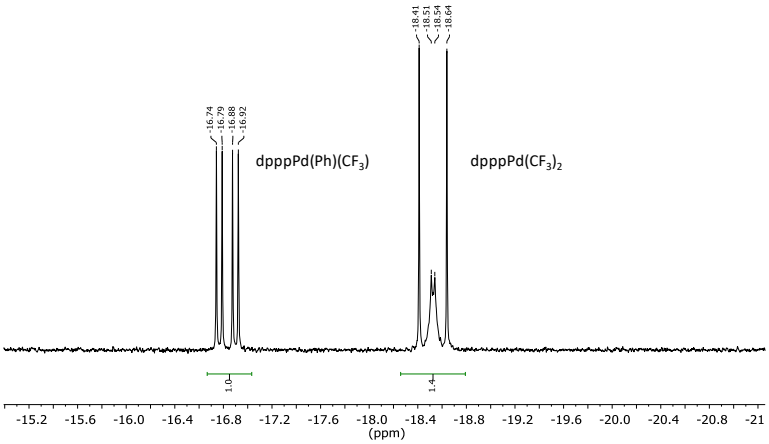

^{19}F NMR spectrum of reaction XX at 25 °C in toluene-d_8

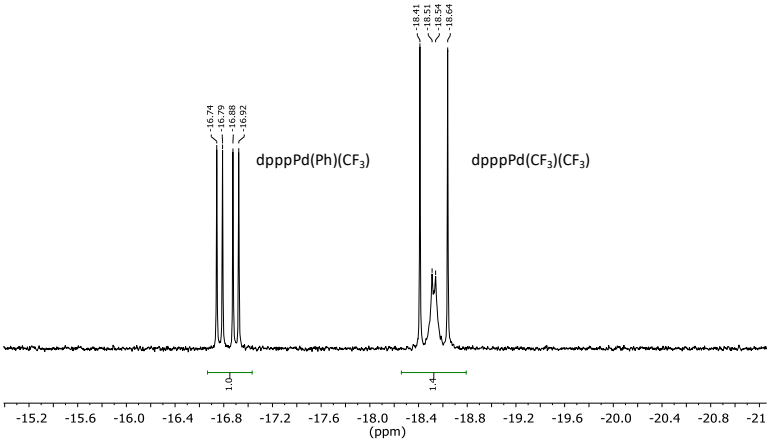

^{31}P{^{1}H} NMR spectrum of reaction XX at 25 °C in toluene-d_8

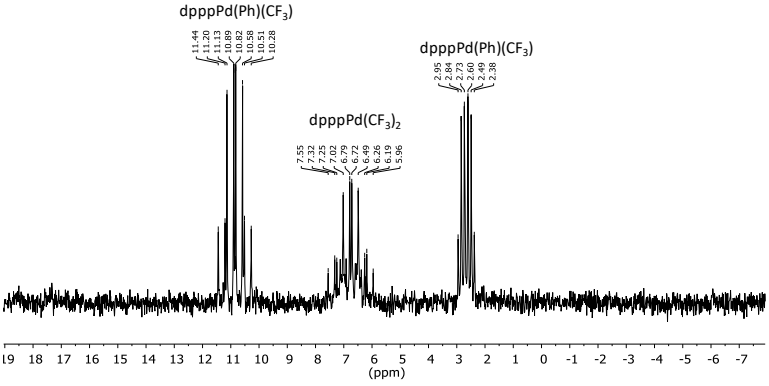

Finally, we were able to synthesize the desired dpppPd(CF_3)$_2$ palladium complex. The procedure is described below. We placed dpppPd(Ph)(CF_3) palladium complex (30 mg, 0.045 mmol, 1 equiv.), under argon atmosphere, in an oven-dried vial and we added 10 ml of toluene. Then, $AgSbF_6$ salt (30 mg, 0.087 mmol, 2 equiv.) was added. After 45 min stirring, the reaction mixture was filtered through a cannula and the red-brown residue was removed under reduced pressure. The obtained solid was analyzed by NMR spectroscopy in toluene-d_8. The structure was confirmed by X-ray diffraction.

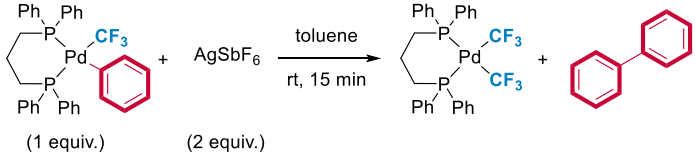

Reaction S9.

^{31}P{^{1}H} NMR (202 MHz, toluene-d8, 25 ^{o}C): δ 8.2 – 6.6 (m).**^{19}F NMR** (470 MHz, toluene-d8, 25 ^{o}C): δ -18.6 – -18.9 (m).

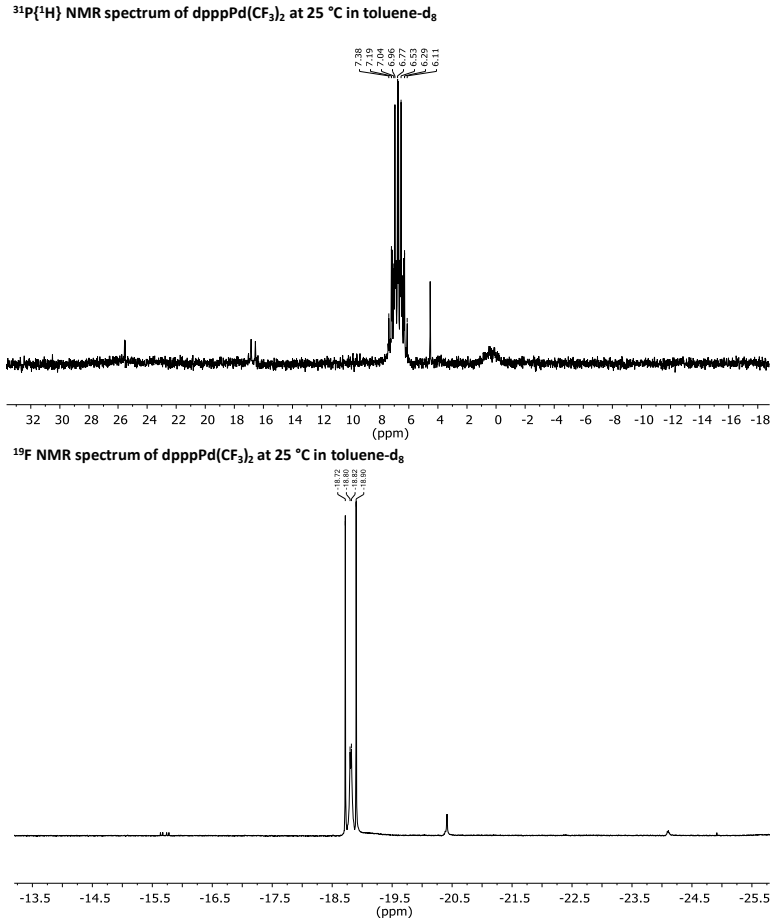

4.5.1.8. **Comparison of [Cs][Ag(CF$_3$)$_2$] and [NBu$_4$][Ag(CF$_3$)$_2$]**

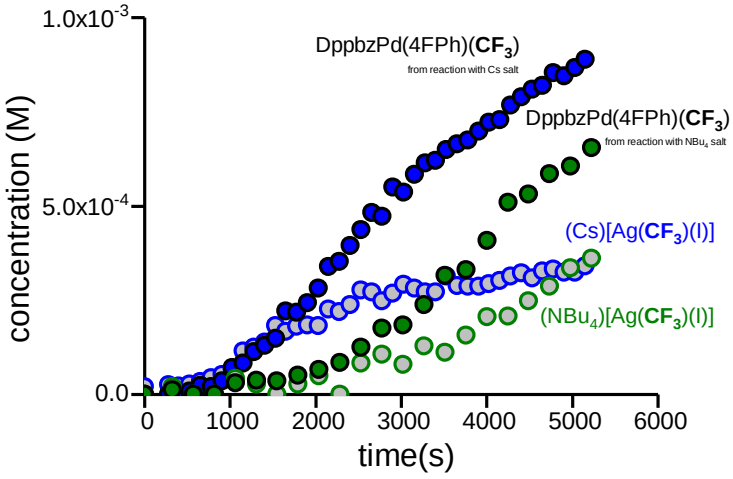

4.5.2. **Computational appendix**

4.5.2.1. **Computational details**

DFT calculations were performed with the ωB97-xD functional, using the Gaussian09 package.[64] Two basis set were used: basis set I for optimization and basis set II for energy refinement. Basis set I was SDD plus pseudopotential for silver, palladium, iodine and bromine, 6-31G(d,p) for the remaining atoms. Basis II was SDD plus pseudopotential for silver, palladium, iodine and bromine, 6-31++G(d,p) for the remaining atoms. All geometry optimizations were carried out in solution without symmetry restrictions. Implicit solvent was modeled through the SMD method. Calculations were carried out in THF (ε = 7.43). Explicit solvent molecules were introduced when coordinating to the silver or palladium centers. Details on the application of the coordination of the solvent molecules to the metal center considering cluster continuum model have been previously described. Cluster of n = 5, 6 and 7 molecules of THF, which were reported to be big enough to represent the asymptotic error associated to these calculations, were optimized at the used DFT level of the rest of the calculations. All the energies presented are free energies in kcal/mol at 25 ºC and 1 atm. NBO analysis of optimized structures was performed using version 6.0 of the software and basis set II. The general profile studies have

[64] Gaussian 09, Revision D.01, Frisch, M. J.; Trucks, G. W.; Schlegel, H. B.; Scuseria, G. E.; Robb, M. A.; Cheeseman, J. R.; Scalmani, G.; Barone, V.; Mennucci, B.; Petersson, G. A.; Nakatsuji, H.; Caricato, M.; Li, X.; Hratchian, H. P.; Izmaylov, A. F.; Bloino, J.; Zheng, G.; Sonnenberg, J. L.; Hada, M.; Ehara, M.; Toyota, K.; Fukuda, R.; Hasegawa, J.; Ishida, M.; Nakajima, T.; Honda, Y.; Kitao, O.; Nakai, H.; Vreven, T.; Montgomery, Jr., J. A.; Peralta, J. E.; Ogliaro, F.; Bearpark, M.; Heyd, J. J.; Brothers, E.; Kudin, K. N.; Staroverov, V. N.; Keith, T.; Kobayashi, R.; Normand, J.; Raghavachari, K.; Rendell, A.; Burant, J. C.; Iyengar, S. S.; Tomasi, J.; Cossi, M.; Rega, N.; Millam, J. M.; Klene, M.; Knox, J. E.; Cross, J. B.; Bakken, V.; Adamo, C.; Jaramillo, J.; Gomperts, R.; Stratmann, R. E.; Yazyev, O.; Austin, A. J.; Cammi, R.; Pomelli, C.; Ochterski, J. W.; Martin, R. L.; Morokuma, K.; Zakrzewski, V. G.; Voth, G. A.; Salvador, P.; Dannenberg, J. J.; Dapprich, S.; Daniels, A. D.; Farkas, O.; Foresman, J. B.; Ortiz, J. V.; Cioslowski, J.; Fox, D. J. Gaussian, Inc., WallingfordCT, **2013**.

been done using phenyl group in the palladium complexes and no other structural simplifications of the system has been assumed.

4.5.2.2. Analysis of the influence of the aryl moiety on the transmetalation rate by DFT

As mentioned in the main text, our first goal using DFT calculations for the $BcAgCF_3$ system was to find different parameters that would support the experimental observed trend. We found a trend between a) the HOMO, which is located on the iodide atom of the palladium complex; b) the NPA of the iodide atom and c) the energy difference for the heteroleptic cleavage or the Pd–**I** bond for the DppbzPd(**Ar**)(**I**) complexes. A good correlation was also found for the difference in potential energy

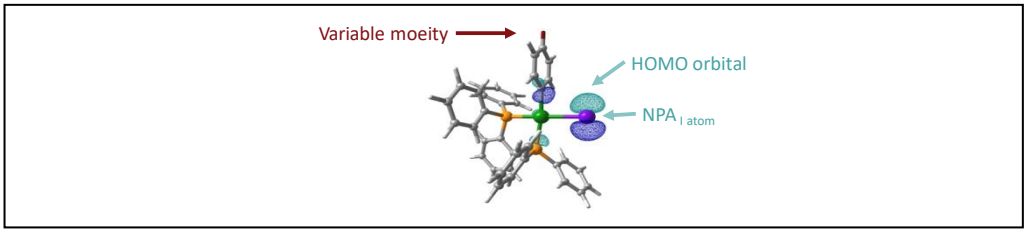

(ΔH) for reaction 1 with basis set I.

R	Hammett σ value	HOMO energy (u.a.)	NPA_{iodide}	ΔG reaction 1	$\Delta E_{basis\ set\ I}$ reaction 1	$-\Delta\Delta E^*_{basis\ set\ I}$ reaction 1
Me	-0.17	-0.28369	-0.62784	21.0	29.8	0.4
H	0.00	-0.28606	-0.62512	21.6	30.2	0.0
F	0.06	-0.28744	-0.62435	22.8	30.7	-0.5
Br	0.23	-0.28803	-0.61950	23.7	31.4	-1.2
COOEt	0.45	-0.28851	-0.61467	22.4	31.4	-1.2
CF_3	0.54	-0.28972	-0.61526	24.4	31.9	-1.7

Table S1. ***-DDE = -(ΔE_R-ΔE_H)**

As we can see, the HOMO energy of the palladium complexes, located on the iodide atom, is lower in energy as the electron-withdrawing nature of the substituent increases. This indicates a stabilization of this molecule and a low reactivity towards electrophiles. Regarding the NPA over the iodide atom, we can see how the electron-richness of the iodide decreases as the electron-withdrawing nature of the substituent increases. This is due to a mayor charge transfer from the iodide to the more electro-poor aryl substituent. Considering the spontaneous dehalogenation, we can observe how the Pd–**I** bond is stronger when more electron-withdrawing is the substituent in the aryl probe. Acceptable correlations were found for the HOMO energy (u.a.) and the Hammett σ values or NPA (iodide) and the Hammett σ values.

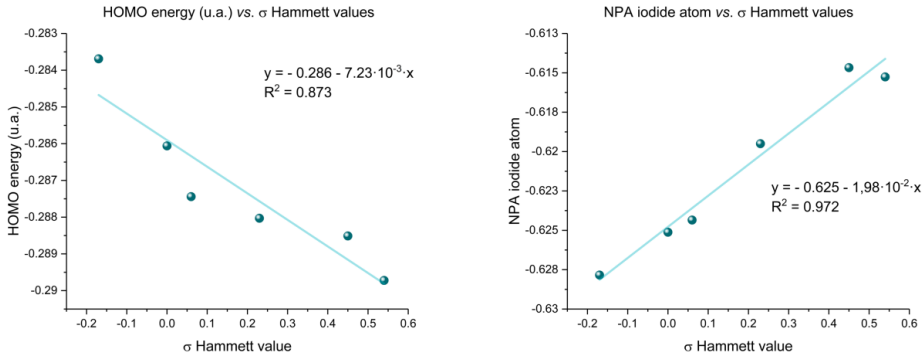

Figure S1. To the left, linear fitting for the HOMO energy (u.a.) obtained by DFT calculations and s Hammett values for the different Pd complexes. To the right, linear correlation for the NPA (Natural Population Analysis from NBO calculations) on the iodide atom and the σ Hammett values.

4.5.2.3. Evaluation of the most plausible mechanisms when considering $BcAgCF_3$ and DppbzPd(Ph)(I)

Concerted and stepwise mechanisms were studied considering exclusively the neutral part of the $BcAgCF_3$ equilibrium in polar solvents. As we can see in Figure SXX, the stepwise mechanism considering the $BcAgCF_3$ species has a high barrier for the transference of the CF_3 of 23.5 kcal/mol, transition state IX. This barrier is 4.9 kcal/mol higher than the barrier for the concerted transference (**TS-I0-I4**). Therefore, the $BcAgCF_3$ neutral species tends to transfer the CF_3 moiety through a concerted mechanism.

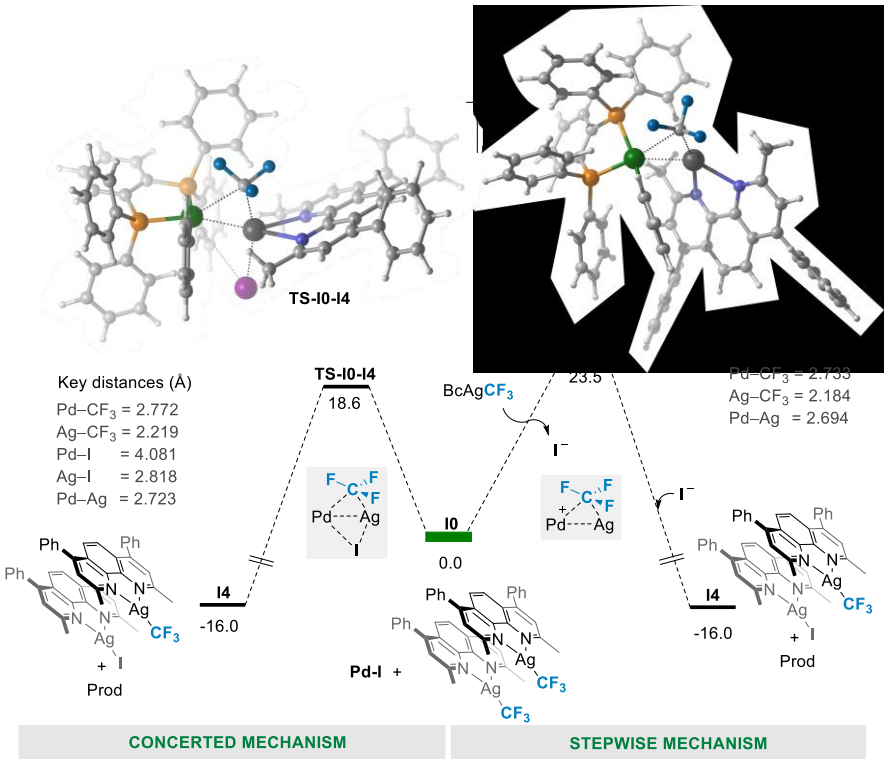

Figure S2. DFT energy profiles for the concerted and stepwise (from left to right) transference of the CF_3 moiety from silver to iodide palladium complexes considering exclusively the silver neutral species.

4.5.2.4. Evaluation of the most plausible mechanisms when considering $BcAgCF_3$ and DppbzPd(Ph)(Cl)

The same analysis performed for DppbzPd(**Ph**)(**I**) was carried out for DppbzPd(**Ph**)(**Cl**) complex considering exclusively the neutral part of the equilibrium, $BcAgCF_3$. As we can see, both transition states are higher than the corresponding TS's for their iodide analogues.

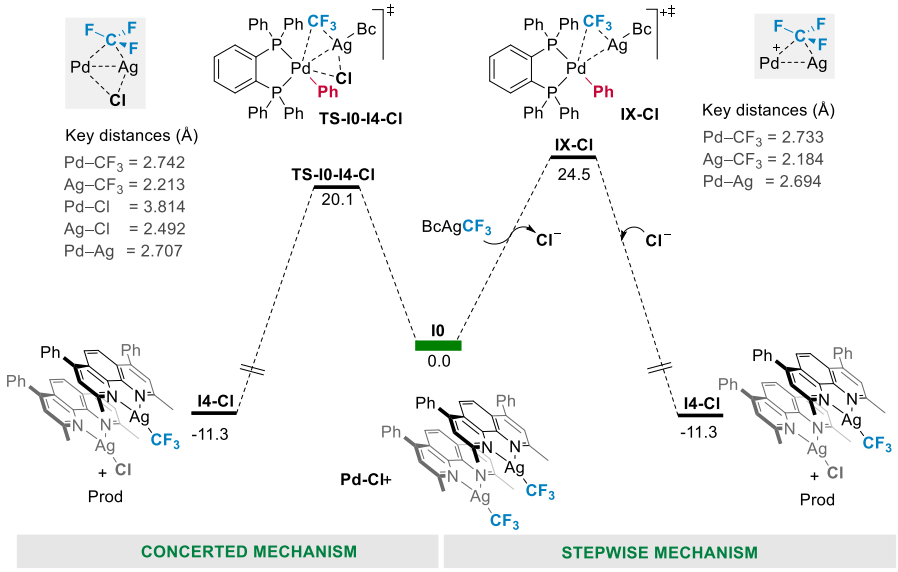

Figure S3. DFT energy profiles for the concerted and stepwise (from left to right) transference of the CF_3 moiety from silver to chloride palladium complexes considering exclusively the silver neutral species.

4.5.2.5. Evaluation of the most plausible mechanisms when considering $[Bc_2Ag(THF)_2][Ag(CF_3)_2]$ and DppbzPd(Ph)(I)

Two different scenarios were considered for the exclusive transmetalation by $[Bc_2Ag(THF)_2][Ag(CF_3)_2]$. On the one hand, a dehalogenation of the palladium complex by the cationic silver complex (**1b-cat**), right part of Figure S5b). On the other hand, a transference of the CF_3 moiety from the bistrifluoromethylargentate to the palladium without prior dehalogenation (left part of Figure S5b)). As we can see, the concerted transference is 20 kcal/mol higher in energy than the dehalogenation by the cationic silver species. Once the cationic palladium complex is formed and the silver(I) halide species is precipitate, the transference of the CF_3 from the argentate is very low in energy (8.8 kcal/mol) and more favorable than the transference from the neutral species.

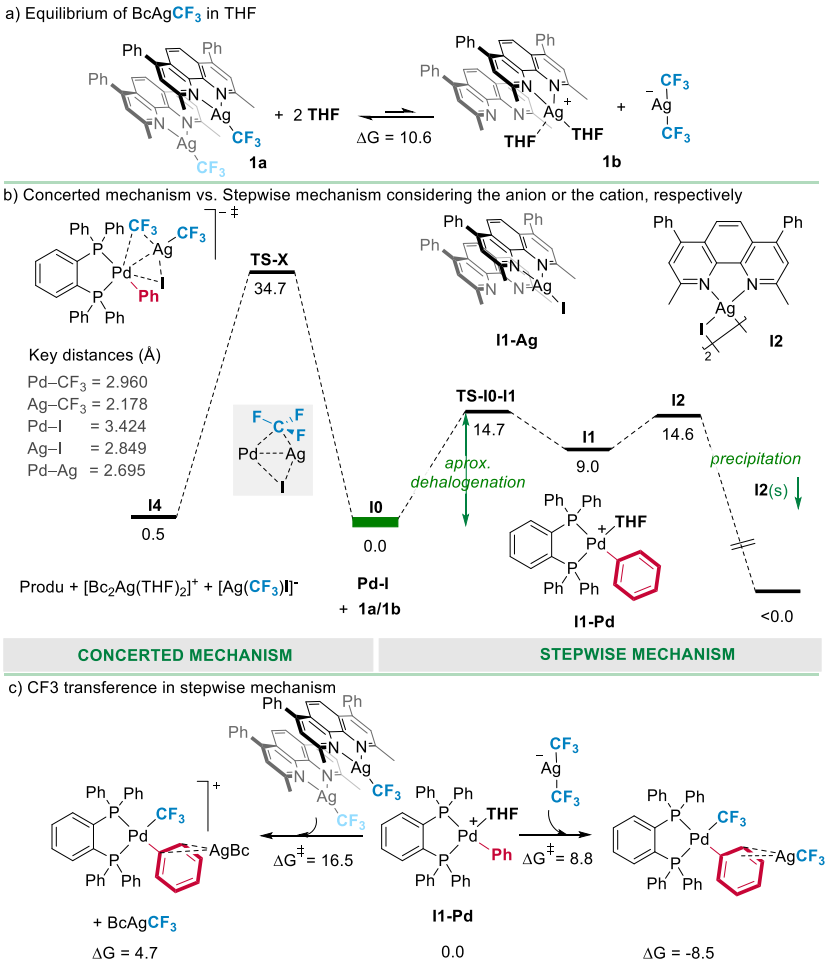

Figure S4. a) Previously described equilibrium in polar solvent (THF in this case) for the $BcAgCF_3$ complexes and its related free energy. b) DFT energy profiles for the concerted and stepwise (from left to right) transference of the CF_3 moiety from silver to iodide palladium complexes considering exclusively the silver ionic species (cation and anion). c) Comparison of the transference of the CF_3 moiety to the cationic palladium complex from the neutral silver species or the anionic one.

4.5.2.6. Evaluation of the most plausible mechanisms when considering [Bc2Ag(THF)2][Ag(CF3)2] and DppbzPd(Ph)(Cl)

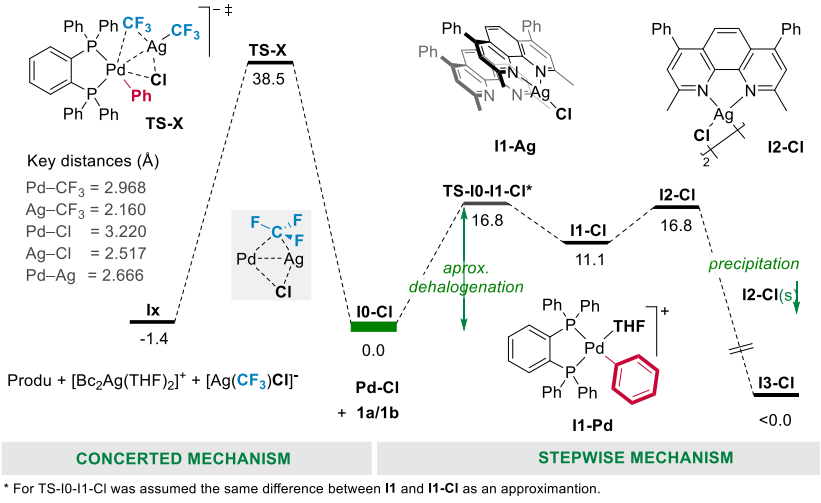

* For TS-I0-I1-Cl was assumed the same difference between **I1** and **I1-Cl** as an approximantion.

Figure S5. DFT energy profiles for the concerted and stepwise (from left to right) transference of the CF_3 moiety from silver to chloride palladium complexes considering exclusively the silver ionic species (cation and anion).

4.5.2.7. Evaluation of TS-I0-I1 for different DppbzPd(Ar)(I).

As we mentioned in the main text, the concerted transference of the CF_3 moiety through **TS-I0-I4** is faster for electron-rich aryl groups. This trend can be seen below in Figure S6.

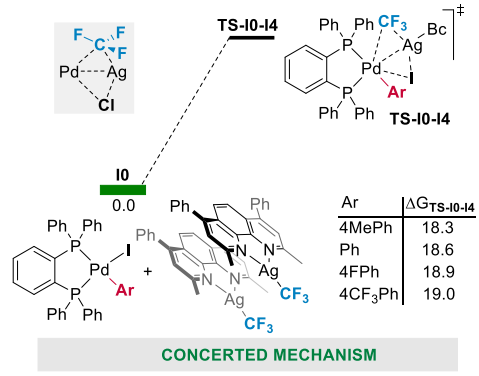

Figure S6. Evaluation of different DppbzPd(Ar)(I) towards the concerted transference of the CF_3 and I from silver to palladium complexes (TS-I0-I1).

4.5.2.8. Barrierless dehalogenation of DppbzPd(Ar)(I) when using [BcAg] cation.

The study of the dehalogenation of the palladium complex was performed by optimizing XX intermediate. This intermediate consists on the incorporation of a $[BcAg]^+$ moiety to

DppbzPd(**Ph**)(**I**). We can see in Figure S7 that the Pd-I bond distance is longer than the bond distance in the starting material. When we explore the potential energy surface by shortening this bond, we did not find a minimum in the surface. Therefore, this is a barrierless process.

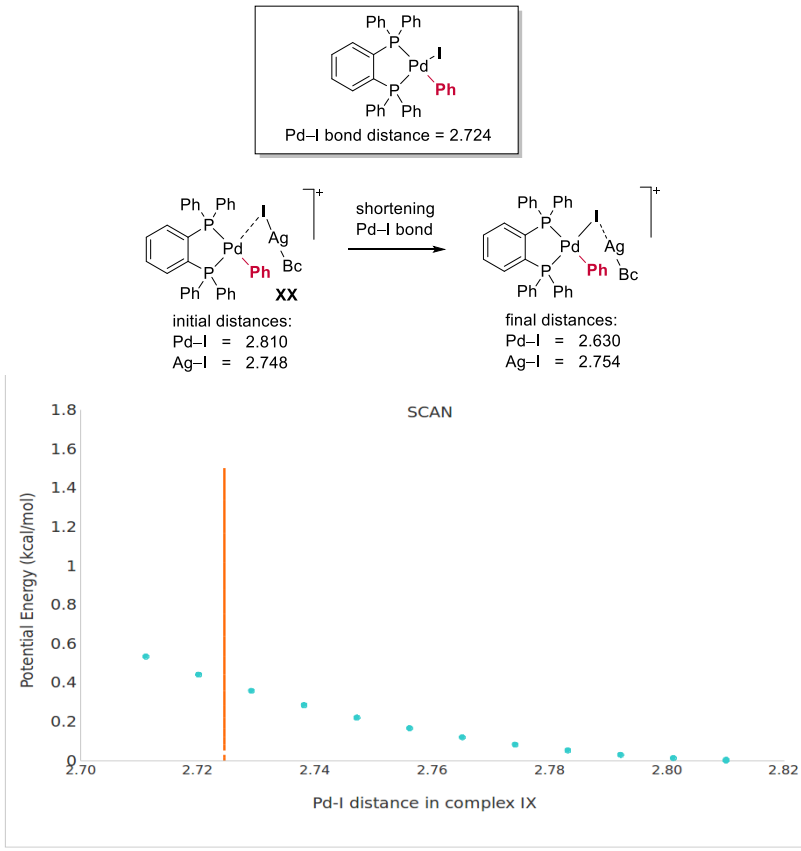

Figure S7. Schematic for the evaluated process and analysis of the potential energy surface corresponding to the shortening of the Pd–I bond in XX complex.

4.5.2.9. Evaluation of the most plausible mechanisms when considering DppbzPd(Ph)(I) and [NEt_4][$Ag(CF_3)_2$]. Anionic transition states.

We first studied the transmetalation from the argentate considering anionic transition states. As we can see, the concerted transition state (**TS-xx**) is unfavorable vs. a stepwise mechanism involving a prior reorganization of the iodide by the argentate (**TS-xx**), as we can see in Figure S8.

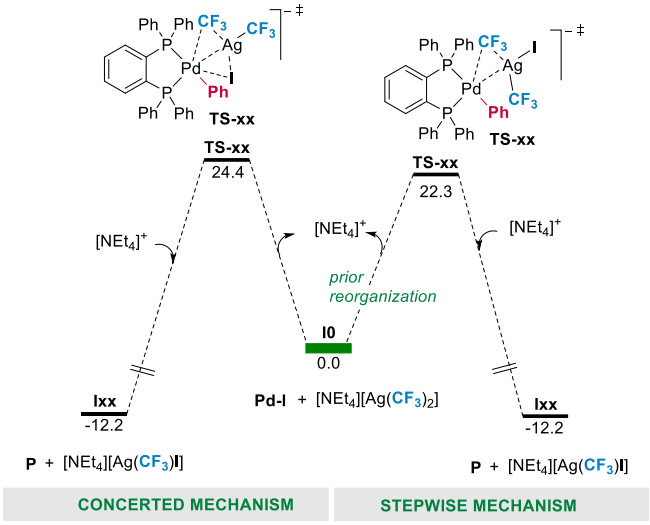

Figure S8. DFT free energy profiles for the concerted and stepwise, involving a prior reorganization, (from left to right) transference of the CF_3 moiety from argentate to iodide palladium complexes regarding anionic transition states.

4.5.2.10. Evaluation of the most plausible mechanisms when considering DppbzPd(Ph)(I) and [NEt$_4$][Ag(CF$_3$)$_2$]. Neutral transition states.

We carried out DFT calculations for the transmetalation from the argentate considering a potential stabilization of the species by the cation. As we can see, the neutral transition states are much more favored than the anionic ones (see Figure S8 and Figure S9). In this case, the concerted transition state (**TS-xx**) is much unfavorable than the stepwise mechanism (**TS-xx**) involving a prior reorganization of the iodide by the argentate (**Ixx**), as we can see in Figure S9. **TS-xx** is unfavoured compared to **TS-05-06** in the main text (Figure XX).

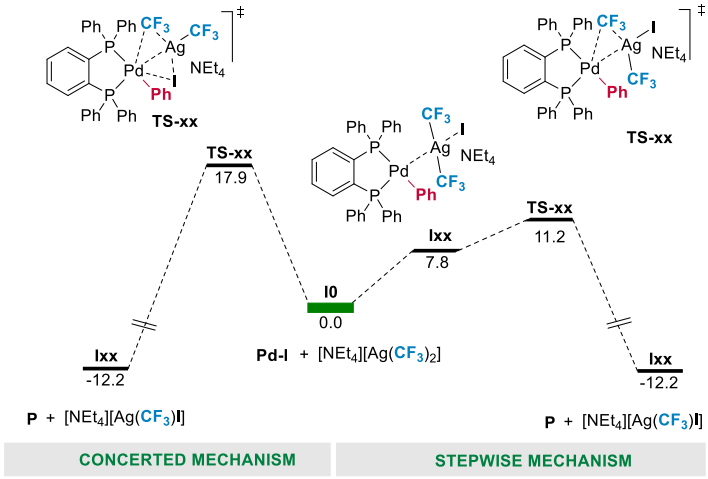

Figure S9. DFT free energy profiles for the concerted and stepwise, (from left to right) transference of the CF3 moiety from argentate to iodide palladium complexes regarding neutral transition states.

4.5.2.11. Evaluation of the most plausible mechanisms when considering DppbzPd(Ph)(I) and [NEt4][Ag(CF3)I].

The heteroleptic species, $[NEt_4][Ag(CF_3)I]$, were also evaluated towards the transmetalation reaction. In the most favourable pathways for the homoleptic argentate, $[NEt_4][Ag(CF_3)_2]$, the heteroleptic species showed to be less efficient in the transmetalation reaction, as we can see in Figure S10 (compared to left part of Figure S9 and Figure XX in the main text). TS-xx is 1.4 kcal/mol less favourable than **TS-05-06** in the main text. Heteroleptic species are less promted to transmetalated than homoleptic ones. However, both mechanism could be competing.

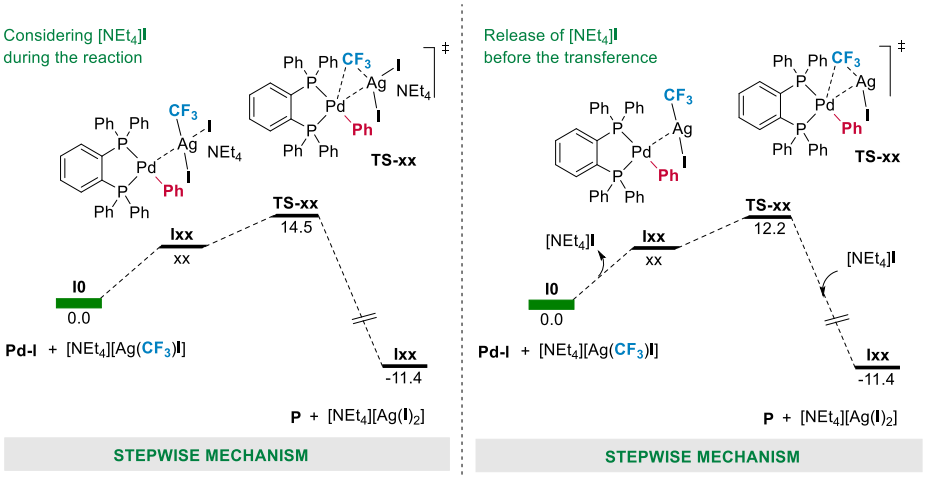

Figure S10. DFT free energy profiles for the stepwise transference of the CF_3 moiety from heteroleptic argentate to iodide palladium complexes regarding neutral transition states, regarding participation of the NEt_4I or not.

4.5.2.12. NBO analysis for the pathway mechanism through TS-05-06.

The most favourable pathway for the transmetalation when considering the argentate is a stepwise mechanism. There is a prior exchange of the iodide on the starting palladium complex by the argentate and, then, the transference of the CF_3 moiety happens through a very low barrier. The first step of this sequential transformation consists on the cleavage of the Pd-I bond. As we can see in Figure S12, the NPA on the iodide atom evolves from -0.671 on the initial palladium complex to -0.981 in the NEt_4I salt. This is translated in an increase of -0.329 of electronic density on the iodide and, therefore, a loss of the same amount on the palladium complex. This loss is compensated by the argentate (Ixx), which decrease its initial electron density.

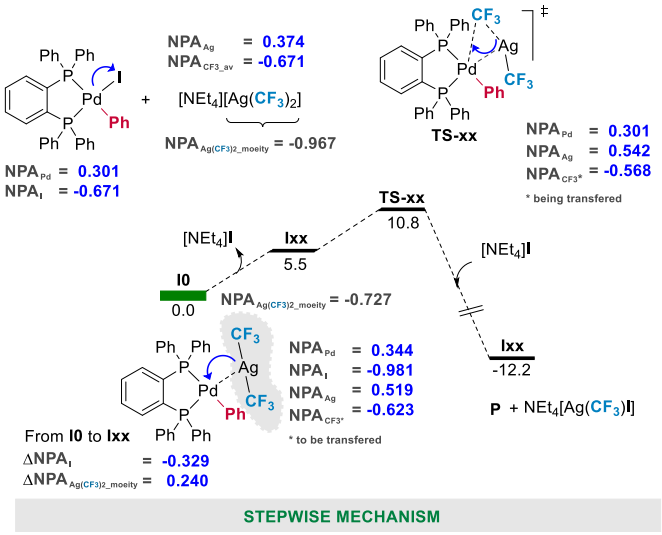

Figure S11. NBO analysis for the charge of selected atoms (NPA) during the stepwise mechanism involving the release of NEt_4I.

Fundamentally, the more electron-rich the aryl substituent, the more stable **Ixx** intermediate. Interestingly, during the transition state, both CF_3 moiety and silver donate electronic density to the palladium complex, recovering the initial NPA charge.

4.5.2.13. Evaluation of the most plausible mechanisms when considering DppbzPd(Ph)(Cl) and $[NEt_4][Ag(CF_3)_2]$. Neutral transition states.

As we can see in Figure S13, the neutral transition states when considering DppbzPd(Ph)(Cl) as starting material are higher than the corresponding for their iodide analogues.

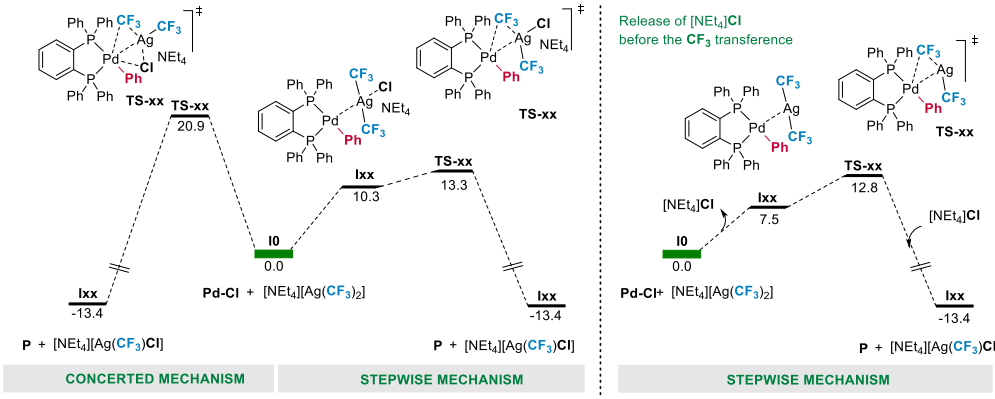

Figure S12. DFT free energy profiles for the concerted and stepwise, (from left to right), transference of the CF_3 moiety from argentate to chloride palladium complexes regarding neutral transition states.

4.5.2.14. Evaluation of the stepwise mechanisms when considering DppbzPd(Ph)(I) and [NEt4][Ag(CF3)2] and [NEt4][Ag(CF3)Cl].

As we can see in Figure S14, the heteroleptic species, [NEt4][Ag(CF3)Cl], when considering DppbzPd(Ph)(Cl) as starting material are less reactive than the corresponding for their iodide analogues

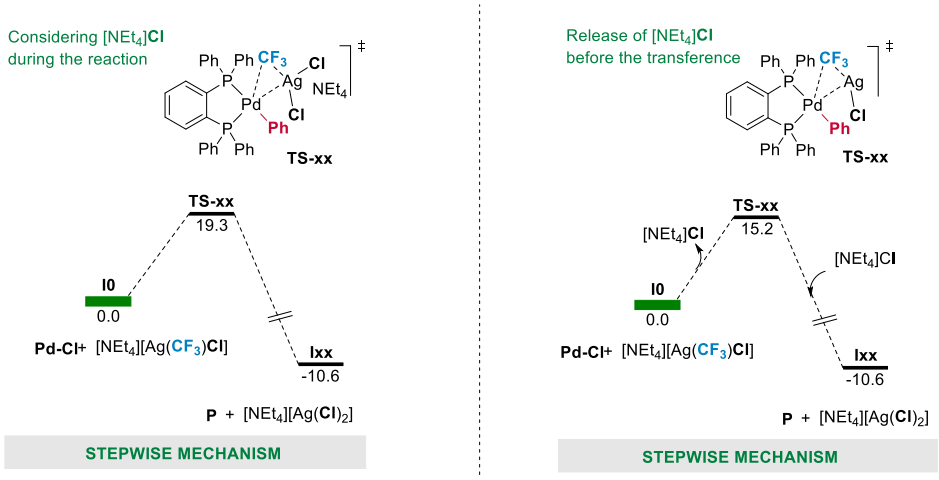

Figure S13. DFT free energy profiles for the stepwise transference of the CF_3 moiety from heteroleptic argentate to chloride palladium complexes regarding neutral transition states, regarding participation of the NEt_4Cl or not.

4.6. References and notes

1. Schmidbaur, H.; Bayler, A. *Synthesis and Uses of Organosilver Compounds*, in *The Chemistry of Organic Derivatives of Gold and Silver* (Eds.: S. Patai. Z. Rappoport), Wiley, Chichester, **1999**, 211.
2. Goossen, L. J.; Deng, G.; Levy, L. M. *Science*, **2006**, *313*, 662.
3. Goossen, L. J.; Rodríguez, N.; Melzer, B.; Linder, C.; Deng, G.; Levy, L. M. *J. Am. Chem. Soc*. **2007**, *129*, 4824.
4. Becht, J. M.; Catala, C.; Le Drian, C.; Wagner, A. *Org. Lett*. **2007**, *9*, 1781.
5. Goossen, L. J.; Lange, P. P.; Rodríguez, N.; Linder, C. *Chem. Eur. J*. **2010**, *16*, 3906.
6. Ackermann, L.; Vicente, R.; Kapdi, A. R. *Angew. Chem. Int. Ed*. **2009**, *48*, 9792.
7. Myers, A. G.; Tanaka, D.; Mannion, M. R. *J. Am. Chem. Soc*. **2002**, *124*, 11250.
8. Tanaka, D.; Romeril, S. P.; Myers, A. G. *J. Am. Chem. Soc*. **2005**, *127*, 10323.
9. a) Rodríguez, N.; Goossen, L. J. *Chem. Soc. Rev*. **2011**, *40*, 5030. b) Cornella, J.; Larrosa, I. *Synthesis* **2012**, *44*, 653.
10. Hossian, A.; Bhunia, S. K.; Jana, R. *J. Org. Chem*. **2016**, *81*, 2521.
11. Wang, C.; Piel, I.; Glorius, F. *J. Am. Chem. Soc*. **2009**, *131*, 4194.
12. An analogous intermolecular version of this transformation was previously described by Crabtree, using microwave irradiation, but the potential role of the silver was not explicitly mentioned. Voutchkova, A.; Coplin, A.; Leadbeater, N. E.; Crabtree, R. H. *Chem. Commun*. **2008**, 6312.
13. Cornella, J.; Lu, P.; Larrosa, I. *Org. Lett*., **2009**, *11*, 5506.
14. Cornella, J.; Lahlali H.; Larrosa, I. *Chem. Commun*. **2010**, *46*, 8276.
15. a) Xie, K.; Wang, S.; Yang, Z.; Liu, J.; Wang, A.; Li, X.; Tan, Z.; Guo C.; Deng, W. *Eur. J. Org. Chem*. **2011**, 5787. b) Hu, P.; Shang Y.; Su, W. *Angew. Chem. Int. Ed*., **2012**, *51*, 5945.
16. Copper: a) Sonogashira, K. *J. Organomet. Chem*. **2002**, *653*, 46. Silver: b) Y. Yamamoto, *Chem. Rev*. **2008**, *108*, 3199. Gold: c) Lauterbach, T.; Livendahl, M.; Rosellón, A.; Espinet, P.; Echavarren, A. M. *Org. Lett.* **2010**, *12*, 3006.
17. Dillinger, S.; Bertus, P.; Pale, P. *Org. Lett.* **2001**, *3*, 1661.
18. The authors explicitly mentioned the role of the coordinating ability of the solvent on stabilizing the specific silver acetylide used in the reaction. See ref. 17.
19. Meana, I.; Espinet, P.; Albéniz, A. C. *Organometallics* **2014**, *33*, 1.
20. Whitaker, D.; Burés J.; Larrosa, I. *J. Am. Chem. Soc*. **2016**, *138*, 8384.
21. Colletto, C.; Islam, S.; Juliá-Hernández, F.; Larrosa, I. *J. Am. Chem. Soc*. **2016**, *138*, 1677.
22. Colletto, C.; Panigrahi, A.; Fernández-Casado, J.; Larrosa, I. *J. Am. Chem. Soc*., **2018**, *140*, 9638.
23. Lotz, M. D.; Camasso, N. M.; Canty, A. J.; Sanford, M. S. *Organometallics*, **2017**, *36*, 165.
24. Lee, S. Y.; Hartwig, J. F. *J. Am. Chem. Soc*. **2016**, *138*, 15278.
25. For selected reports regarding the CF_2H properties, see: Gillis, E. P.; Eastman, K. J.; Hill, M. D.; Donnelly D. J.; Meanwell, N. A. *J. Med. Chem*., **2015**, *58*, 8315. For selected reports regarding the CF_3 properties, see: Schlosser, M. *Angew. Chem. Int. Ed*., **2006**, *45*, 5432.
26. For selected review on difluoromethylation, see: a) Feng, Z.; Xiao, Y.-L.; Zhang, X. *Acc. Chem. Res*., **2018**, *51*, 2264. For selected review on trifluoromethylation, see: b) Furuya, T.; Kamlet A. S.; Ritter, T. *Nature*, **2011**, *473*, 470.; c) Tomashenko O. A.; Grushin, V. V. *Chem. Rev.*, **2011**, *111*, 4475.
27. This topic is covered in detail in the Introduction of Chapter 2.
28. Gu, Y.; Leng X.; Shen, Q. *Nat. Commun*., **2014**, *5*, 5405.
29. a) Lu, C.; Lu, H.; Wu, J.; Shen, H. C.; Hu, T.; Gu, Y.; Shen, Q. *J. Org. Chem*., **2018**, *83*, 1077. b) Chang, D.; Gu, Y.; Shen, Q. *Chem. Eur. J*. **2015**, *21*, 6074. c) Lu, C.; Gu, Y.; Wu, J.; Gu Y.; Shen, Q. *Chem. Sci*., **2017**, *8*, 4848.

30. Pérez-Temprano, M. H.; Casares, J. A.; de Lera, Á. R.; Álvarez, R.; Espinet, P. *Angew. Chem. Int. Ed*. **2012**, *51*, 4917.

31. Martínez de Salinas, S.; Mudarra, A. L.; Benet-Buchholz, J.; Parella, T.; Maseras, F.; Pérez-Temprano, M. H. *Chem. Eur. J.* **2018**, 24, 11895.

32. We discard the study of 'ligandless' $AgCF_3$ species because they are not well-defined and non-isolable. [(SIPr)Ag(CF_3)] complex was tested in the transmetalation reaction but inconclusive results were obtained (see Appendix).

33. Indeed, during the synthesis of [$(R)_3PAg(CF_3)$] complexes, we observed an equilibrium with this ionic species and the neutral [$(R)_3PAg(CF_3)$] one. This complex were not sufficiently stable to handle.

34. Weng, Z.; Lee, R.; Jia, W.; Yuan, Y.; Wang, W.; Feng, X.; Huang, K.-W. *Organometallics* **2011**, 30, 3229.

35. Casado, A.L.; Espinet, P. *J. Am. Chem. Soc.* **1998**, *120*, 8978.

36. Jagadeesan, R.; Velmurugan, G.; Venuvanalingam, P. *RSCAdv*. 2015, 5, 80661.

37. Hammett, L. P. *Chem. Rev*. **1935**, *17*, 125.

38. a) Saito, S.; Oh-tani, S.; Miyaura, N. *J. Org. Chem.* **1997**, *62*, 8024. b) Zim, D.; Lando, V. R.; Dupont, J.; Monteiro, A. L. *Org. Lett*., **2001**, *3*, 3049. c) Jin, L.; Xin, J.; Huang, Z.; He, J.; Lei, A. *J. Am. Chem. Soc*. **2010**, *132*, 9607. d) Payard, P.-A.; Perego, L. A.; Ciofini, I.; Grimaud, L. *ACS Catal*. **2018**, *8*, 4812.

39. It is assumed that the stronger the character of the electrophile, the faster the reaction with the nucleophile, in this case the silver nucleophile. However, this Hammett plot study shows that the less electrophilic the palladium complex, the faster the transmetalation. Scarce examples have been found to point out a potential nucleophilic nature of palladium complexes during the transmetalation reaction, see: Moriya, T.; Miyaura, M.; Suzuki, A. *SYNLETT*, **1994**, 149.

40. Cationic palladium complexes have been proposed to be key for the transmetalation in several reports. In Negishi coupling: b) García-Melchor, M.; Fuentes, B.; Lledós, A.; Casares, J. A.; Ujaque, G.; Espinet, P. *J. Am. Chem. Soc*. **2011**, *133*, 13519. In Stille coupling: Nova, A.; Ujaque, G.; Maseras, F.; Lledós, A.; Espinet, P. *J. Am. Chem. Soc*. **2016**, *128*, 14571.

41. Mayr, H.; Minegishi, S. *Angew. Chem. Int. Ed*. **2002**, *41*, 4493.

42. Decomposition of the silver nucleophile was observed before achieving total conversion of the aryl-Pd(II) complex.

43. For concerted and stepwise mechanism in transmetalation reactions: a) Ricci, A.; Angelucci, F.; Bassetti, M.; Lo Sterzo, C. *J. Am. Chem. Soc*. **2002**, *124*, 1060. b) Lennox, A. J. J.; Lloyd-Jones, G. C. *Angew. Chem. Int. Ed*. **2013**, *52*, 7362.

44. Martínez de Salinas, S.; Mudarra, Á. L.; Benet-Buchholz, J.; Parella, T.; Maseras, F.; Pérez-Temprano, M. H. *Chem. Eur. J.* **2018**, *24*, 11895.

45. Batsanov, S. S. *Inorg. Mater*. **2001**, 37, 1031.

46. This value corresponds to the generation of the cationic species with a single molecule of THF coordinated to the metal centre. This approximation allows us to get an estimated value for the dehalogenation process.

47. We discarded that this trend is controlled by the solubility of the corresponding silver halide. If this was the case, we would not observe any influence of the substitution pattern on the aromatic moiety since the rate determining step would be related to the precipitation of the silver.

48. We only considered the phenyl group due to scrambling issues when using a substituted aryl group. This scrambling reaction, discussed in Chapter 2, allows the exchange between the aryl moiety on the palladium metal centre and the one on the phosphorous of the phosphine. See a) Goodson, F. E.; Wallow, T. I.; Novak, B. M. *J. Am. Chem. Soc.* **1997**, *119*, 12441. b) Grushin, V. V. *Organometallics* **2000**, *19*, 1888. c) Fiebig, L.; Schlörer, N.; Schmalz, H.-G.; Schäfer, M. *Chem. Eur. J.* **2014**, *20*, 4906.

49. This cationic palladium complex was observed in DMF in the presence of silver as halide scavenger. It was not observed in the absence of silver.

50. a) Braunstein, P.; Frison, C.; Oberbeckmann-Winter, N.; Morise, X.; Messaoudi, A.; Bénard, M.; Rohmer, M.- M.; Welter, R. *Angew. Chem. Int. Ed*. **2004**, *43*, 6120. b) Heckenroth, M.; Kluser, E.; Neels, A.; Albrecht, M. *Angew. Chem. Int. Ed*. **2007**, *46*, 6293. c) Arias, A.; Forniés, J.; Fortuño, C.; Martín, A.; Mastrorilli, P.; Gallo, V.; Latronico, M.; Todisco, S. *Eur. J. Inorg. Chem*. **2014**, 1679.

51. We observed decomposition of the expected compound even at low temperature in solution.

52. These intermediates has been proposed to be formed in catalytic conditions through C–H activation event (see ref. 24) or decarboxylation (even isolated, see: Baur, A.; Bustin, K. A.; Aguilera, E.; Petersen, J. L.; Hoover, J. M. *Org. Chem. Front*., **2017**, *4*, 519.

53. The formation of bis-(trifluoromethyl) Pd(II) complexes was observed in low yield during kinetic experiments when using dppp and [(Bc)Ag(CF_3)] as transmetalating agent, which contains a low amount of cationic silver species. This reinforces the potential of cationic silver species to scramble the ligands even at low concentration (in a 5% at the beginning of the reaction, according to the equilibrium).

54. These species can generate Cs[Ag(I)$_2$] and Cs[Ag(CF_3)$_2$]. It should be kept in mind that Cs[Ag(I)$_2$] could form CsI and AgI during the reaction. These species could precipitate.

55. For further discussion on the nature of the transition states, see Appendix.

56. The Ag–X bond in not been formed simultaneously to the cleavage of the Ag–CF_3 bond.

57. No decomposition was observed when the salt was added to the $NBu_4Ag(CF_3)_2$, just formation of the corresponding heteroleptic argentate, NBu4Ag(CF3)I. This experiment suggests that the concerted mechanism is not likely to be operative.

58. Munjanja, L.; Brennessel, W. W.; Jones, W. D. *Organometallics* **2015**, 34, 4574.

59. Kaspi, A. W.; Yahav-Levi, A.; Goldberg, I.; Vigalok, A. *Inorganic Chemistry*, **2008**, 47, 5.

60. Ludwig, M.; Strömberg, S.; Svensson, M.; Åkermark, B. *Organometallics* **1999**, 18, 970.

61. Goodson, F. E.; Wallow, T. I.; Novak, B. M. *J. Am. Chem. Soc*., **1997**, *119*, 12441.

62. a) Mann, G.; Baranano, D.; Hartwig, J. F.; Rheingold, A. L.; Guzei, I. A. *J. Am. Chem. Soc*. **1998**, *120*, 9205. b) Kaspi, A. W.; Yahav-Levi, A.; Goldberg, I.; Vigalok, A. *Inorganic Chemistry*, **2008**, *47*, 5.

63. Culkin, D. A.; Hartwig, J. F. *Organometallics*, **2004**, 23, 3398.

64. Gaussian 09, Revision D.01, Frisch, M. J.; Trucks, G. W.; Schlegel, H. B.; Scuseria, G. E.; Robb, M. A.; Cheeseman, J. R.; Scalmani, G.; Barone, V.; Mennucci, B.; Petersson, G. A.; Nakatsuji, H.; Caricato, M.; Li, X.; Hratchian, H. P.; Izmaylov, A. F.; Bloino, J.; Zheng, G.; Sonnenberg, J. L.; Hada, M.; Ehara, M.; Toyota, K.; Fukuda, R.; Hasegawa, J.; Ishida, M.; Nakajima, T.; Honda, Y.; Kitao, O.; Nakai, H.; Vreven, T.; Montgomery, Jr., J. A.; Peralta, J. E.; Ogliaro, F.; Bearpark, M.; Heyd, J. J.; Brothers, E.; Kudin, K. N.; Staroverov, V. N.; Keith, T.; Kobayashi, R.; Normand, J.; Raghavachari, K.; Rendell, A.; Burant, J. C.; Iyengar, S. S.; Tomasi, J.; Cossi, M.; Rega, N.; Millam, J. M.; Klene, M.; Knox, J. E.; Cross, J. B.; Bakken, V.; Adamo, C.; Jaramillo, J.; Gomperts, R.; Stratmann, R. E.; Yazyev, O.; Austin, A. J.; Cammi, R.; Pomelli, C.; Ochterski, J. W.; Martin, R. L.; Morokuma, K.; Zakrzewski, V. G.; Voth, G. A.; Salvador, P.; Dannenberg, J. J.; Dapprich, S.; Daniels, A. D.; Farkas, O.; Foresman, J. B.; Ortiz, J. V.; Cioslowski, J.; Fox, D. J. Gaussian, Inc., WallingfordCT, **2013**.

CHAPTER 5. EXPLORING BIS-(TRIFLUOROMETHYL) COINAGE METALLATES LANDSCAPE: A COMBINED EXPERIMENTAL AND THEORETICAL STUDY.

5.1. Introduction

Over the past years, trifluoromethyl organometallic compounds of coinage metals have received special attention due to their potential as reactive species in the synthesis of fluorinated scaffolds. Therefore, the organometallic community has devoted its efforts towards the isolation and characterization of these key species in order to better understand their reactivity.[1-3] In this context, the chemical behavior of ate-type complexes, [Cat][M(CF_3)$_2$] (M = Cu, Ag, Au), has not been fully explored and, in the case of copper, there is not even a selective route to access them.

5.1.1. Bis-(trifluoromethyl) aurates

The first example of an isolable bis-trifluoromethyl coinage metallate was reported by Mathur *et al.* in 2011. In this seminal report, the authors described the synthesis and characterization of well-defined Au(I) complexes, [NMe_4][Au(CF_3)$_2$].[1a] Initially, the reactivity of those complexes were studied for the synthesis of gold nanoparticles through hydrolysis in aqueous medium. Later on, Menjón *et al*. expanded the study of their reactivity using strong oxidant agents such as X_2 (X = Cl, Br, I), R^FI (R^F = CF_3 and *n*-Bu^F) and XeF_2 (Scheme 5.1) using another stabilizing cation, [PPh_4]$^+$. Those reactions gave rise to the formation of Au(III) complexes and have been deeply studied from a organometallic point of view.[1b,1c,1e]

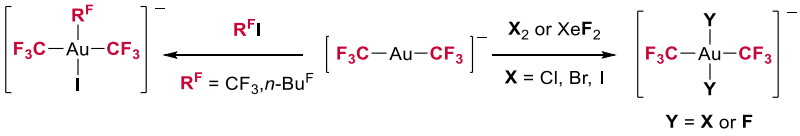

Scheme 5.1. State of the art in the reactivity of [PPh_4][Au(CF_3)$_2$] species.

However, further implications of these gold complexes in organic transformations have thus far lacking.

---

1 *For representative examples on the synthesis and reactivity of* AuCF_3 *complexes, see: a)* Zopes, D.; Kremer, S.; Scherer, H.; Belkoura, L.; Pantenburg, I.; Tyrra, W.; Mathur, S. *Eur. J. Inorg. Chem*. **2011**, 273. b) Gil-Rubio, J.; Vicente, J. *Dalton Trans*. **2015**, *44*, 19432 and references therein. c) Pérez-Bitrián, A.; Martínez-Salvador, S.; Baya, M.; Casas, J. M.; Martín, A.; Menjón, B.; Orduna, J. *Chem. Eur. J.* **2017**, *23*, 6919. d) Levin, M. D.; Chen, T. Q.; Neubig, M. E.; Hong, C. M.; Theulier, C. A.; Kobylianskii, I. J.; Janabi, M.; O'Neil, J. P.; Toste, F. D. *Science* **2017**, 356, 1272. e) Pérez-Bitrián, A; Baya, M.; Casas, J. M.; Martín, A.; Menjón, B.; Orduna, J. *Angew. Chem. Int. Ed*. **2018**, 57, 6517.

2 *For representative examples on the synthesis and reactivity of* AgCF_3 *complexes, see*: a) Tyrra, W.; Naumann, D. *J. Fluorine Chem*. **2004**, 125, 823. b) Weng, Z.; Lee, R.; Jia, W.; Yuan, Y.; Wang, W.; Feng, X.; Huang, K.-W. *Organometallics* **2011**, 30, 3229. c) Hafner, A.; Jung, N.; Bräse, S. *Synthesis* **2014**, 46, 1440. d) Tate, B. K.; Jordan, A. J.; Bacsa, J.; Sadighi, J. P. *Organometallics* **2017** 36 964. e) Martínez de Salinas, S.; Mudarra, A. L.; Benet-Buchholz, J.; Parella, T.; Maseras, F.; Pérez-Temprano, M. H. *Chem. Eur. J*. **2018**, 24, 11895. f) Joven-Sancho, D. Baya, M.; Martín, A.; Menjón, B. *Chem. Eur. J.* **2018**, 24, 13098.

3 *For representative examples on the synthesis and reactivity of* CuCF_3*, see:* Mudarra, A. L.; Martínez de Salinas, S.; Pérez-Temprano, M. H. *Synthesis* **2019**, *51*, 2809 and references therein.

5.1.2. **Bis-(trifluoromethyl) argentates**

Regarding silver, the first example of isolable silver ate-type complex, [cat][Ag(CF$_3$)$_2$], came from our group in 2018, as mentioned in Chapter 2. The study of the reactivity of this isolated complex was focused on the transmetalation reaction towards aryl-Pd(II) complexes.[2e] In this venue, their high efficiency as nucleophiles in the transmetalation event proved to be relevant for Pd-catalyzed nucleophilic trifluoromethylations.[2e] To that date, the reactivity of these species was not explicitly revealed. This is surprising since, as discussed in Chapter 2, silver argentates, [Ag(CF$_3$)$_2$]$^-$, are proposed to be part of *in situ* generated 'Ag(CF$_3$)' mixture[4] (Scheme 5.2, above left) which have been used in wide array of nucleophilic trifluoromethylation reactions. On one hand, 'Ag(CF$_3$)' species has been used from an organometallic perspective to introduce CF$_3$ groups in metal complexes *via* ligand metathesis reaction (Scheme 5.2, above right).[2a,2b,2e,5] On the other hand, several synthetic protocols have used these 'Ag(CF$_3$)' species to form a new C–CF$_3$ bonds by the trifluoromethylation of C–H aromatic bonds, alkenes and *in situ* generated arynes (Scheme 5.2).[6]

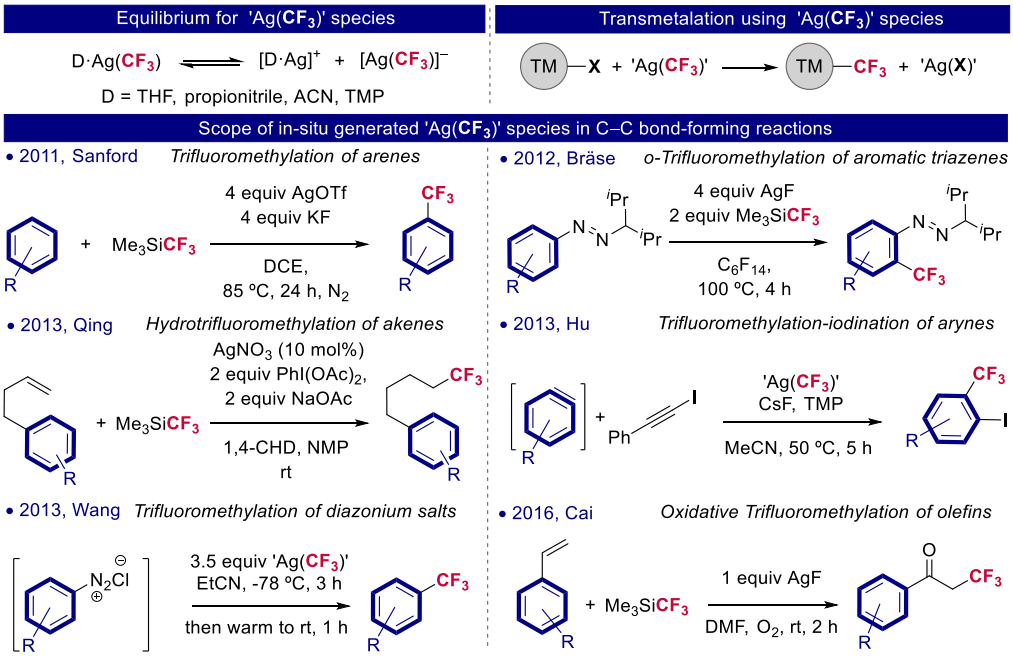

Scheme 5.2. Above left: equilibrium of 'Ag(CF$_3$)' species in polar solvent. TMP = (MeO)$_3$PO. Above right: Representation of the transmetalation reaction using 'Ag(CF$_3$)' species. Below: synthetic protocols for the formation of C–CF$_3$ bonds based on the formation of 'Ag(CF$_3$)' species. 1,4-CHD = 1,4-cyclohexadiene, NMP = 1-methyl-2-pyrrolidinone, TMP = (MeO)$_3$PO.

4 Naumann, D.; Wessel, W.; Hahn, J.; Tyrra, W. *J. Organomet. Chem*. **1997**, *547*, 79.

5 a) Hafner, A.; Bräse, S. *Angew. Chem. Int. Ed.* **2012**, *51*, 3713. b) Zhang; C.-P.; Wang, Huan; Klein, A.; Biewer, C.; Stirnat, K.; Yamaguchi, Y.; Xu, L.; Gomez-Benitez, V.; Vicic, D. A. *J. Am. Chem. Soc.* **2013**, *135*, 8141.

6 a) Ye, Y.; Lee, S. H.; Sanford, M. S. *Org. Lett.*, **2011**, *13*, 5464. b) Hafner, A.; Bräse, S. *Angew. Chem. Int. Ed.* **2012**, *51*, 3713. c) Wu, X.; Chu, L.; Qing, F.-L. *Angew. Chem. Int. Ed.* **2013**, *52*, 2198. d) Zeng, Y.; Zhang, L.; Zhao, Y.; Ni, C.; Zhao, J.; Hu, J. *J. Am. Chem. Soc.* **2013**, *135*, 2955. e) Wang, X.; Xu, Y.; Mo, F.; Ji, G.; Qiu, D.; Feng, J.; Ye, Y.; Zhang, S.; Zhang, Y.; Wang, J. *J. Am. Chem. Soc.* **2013**, *135*, 10330. f) Ye-bin Wu, Y.-b.; Guo-ping Lu, G.-p.; Yuan, T.; Xu, Z.-b. Wan, L.; Cai, C. *Chem. Commun*., **2016**, *52*, 13668.

The creation of $F_3C–X$ bond (X = O, N) has been also achieved using *in situ* generated trifluoromethyl silver(I) complexes under oxidant conditions.[7]

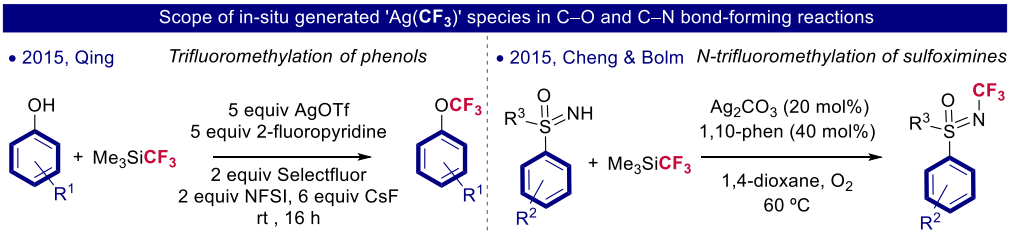

Scheme 5.3. Synthetic protocols based for the formation of $F_3C–X$ (X = O, N) bonds on the formation of '$Ag(CF_3)$' species under oxidative conditions. NFSI = *N*-Fluorobenzenesulfonimide, 1,10-phen = 1,10-phenantroline.

As described above, '$Ag(CF_3)$' species have been proposed to be a remarkable nucleophilic source of CF_3 moiety in different trifluoromethylation protocols. Despite that, regarding the mechanism, little pieces of information can be found and, generally, bis-(trifluoromethyl) argentates have been overlooked.

- **Mechanistic proposals for in situ generated '$Ag(CF_3)$' species in organic transformations**

Among the few mechanistic proposals for the participation of '$Ag(CF_3)$' in the reaction media, there is a number of reports that propose the '$Ag(CF_3)$' species as a source of free trifluoromethyl radicals ($\bullet CF_3$) and Ag(0).[6a,7] A different scenario was proposed for the trifluoromethylation-iodination of arynes reported by Hu in 2013 (Scheme 5.4).[6d] After studying the speciation of '$Ag(CF_3)$' complexes in the reaction media, their proposal establishes that a nucleophile attack of [(TMP)$Ag(CF_3)$] to the aryne happens giving rise to the carboargentation product, **I**. Then, this intermediate forms hydrogen bonds with TMP molecules, generating **II**. Once this happens, intermediate **II** undergoes deprotonation forming an anionic intermediate **III** that interacts with iodophenylacetylene and, subsequently, forms **IV**. Next, the aryl moiety attached to the silver metal center is proposed to perform an intramolecular nucleophilic attack to release the final product and silver phenylacetylide. They also considered a potential oxidative addition event from intermediate **IV**. In this scenario, the formation of different Ag(III) complexes during the oxidative addition may yield two different organic products through reductive elimination from **V** and **VI** intermediates (Scheme 5.4). They discarded this scenario on the basis of the observed selectivity of the reaction towards a single organic product. However, the oxidative addition may be somehow selective towards the formation of intermediate **V** and this route could not be completely discarded. Regarding $[Ag(CF_3)_2]^-$ complex, the authors proposed it as a potential deprotonating agent of TMP interacting with intermediate **II**.

7 a) Liu, J.-B.; Chen, C.; Chu, L.; Chen, Z.-H.; Xu, X.-H. Qing, F.-L. *Angew. Chem. Int. Ed.* **2015**, *54*, 11839. b) Teng, F.; Cheng, J.; Bolm, C. *Org. Lett.* **2015**, *17*, 3166.

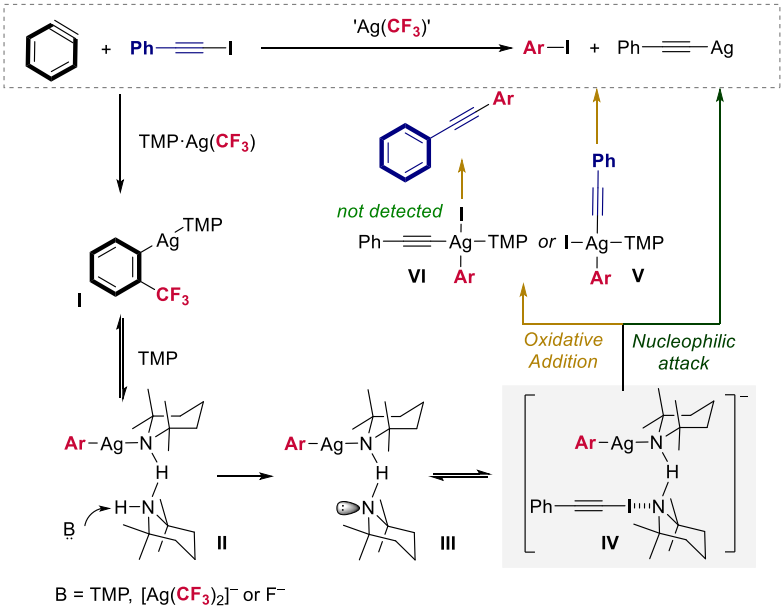

Scheme 5.4. Proposed mechanism for silver-mediated trifluoromethylation-iodination of arynes.

Mechanistic proposals that support $Ag^{I/III}$ scenarios can be found in the aforementioned synthetic protocols (Scheme 5.2 and Scheme 5.3). This is the case for the silver-mediated trifluoromethylation of aryldiazonium salts reported by Wang.[6e] Mechanistic investigations discarded radical mechanism and support a $Ag^{I/III}$ scenario where the diazonium salt performs oxidative addition to 'Ag(CF_3)' species, labeled as **VII** (Scheme 5.5). The authors do not specify the nature of this trifluoromethyl silver(III) species. The release of the organic product happens through a reductive elimination step (Scheme 5.5). Further computational studies on this system have been recently performed by Zhang. This work supports the oxidative addition/reductive elimination mechanism but, instead of a Ag(I) → Ag(III) event, dimeric species allow a transformation Ag(I)-Ag(I) → Ag(II)-Ag(II), generating intermediate **VIII**, as portrayed in Scheme 5.5.[8] A similar scenario was proposed by Ritter in the late-stage fluorination reactions of stannanes using silver salts as catalyst.[9]

8 Zhang, X. *Comput. Theor. Chem.* **2019**, *1158*, 15
9 Tang, P.; Furuya, T.; Ritter, T. *J. Am. Chem. Soc.* **2010**, *132*, 12150.

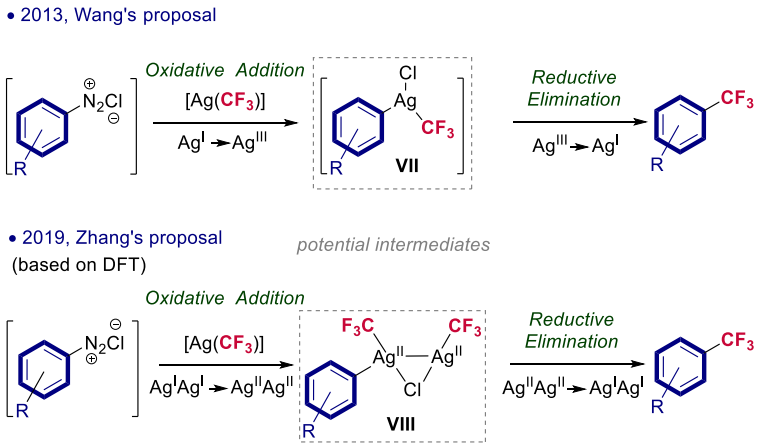

Scheme 5.5. Different oxidative addition/reductive elimination scenarios for silver-mediated trifluoromethylation of aryl diazonium salts.

Trifluoromethyl silver(III) species have been also proposed in the silver-mediated oxidative trifluoromethylation of phenols.[7a] In this case, the 'Ag(CF_3)' species reach a high oxidation state by the oxidant, Selectfluor, forming 'Ag(CF_3)(F)' species. Then, the exchange of the fluoride to phenoxide happens to afford the intermediate previous to the reductive elimination, 'Ag(CF_3)(OPh)'. No much information is provide about the nature of the contemplated species.

5.1.3. **Bis-(trifluoromethyl) cuprates**

As discussed, studies involving trifluoromethyl gold and silver complexes are not extremely mentioned in the literature. However, their copper analogous have been widely invoked as key species in nucleophilic trifluoromethylation reaction where a tremendous development has been achieved by the use of trifluoromethyl Cu(I) species.[3] In the reaction media, these copper species form an intricate mosaic of different 'Cu(CF_3)' complexes including homoleptic and/or heteroleptic cuprates, [cat][Cu(CF_3)X], X = halogen or CF_3. This behavior of 'Cu(CF_3)' in solution, along with their inherent instability, prevents the selective access to the cuprates and, therefore, the study of their potential implications in trifluoromethylation reactions.[3]

The aforementioned trifluoromethylation protocols can be classified according to the origin of the 'CuCF_3' species: (i) *in situ* generation or (ii) isolable and well-defined trifluoromethyl copper(I) complexes (Scheme 5.6). In both cases, bis-(trifluoromethyl) cuprates are widespread.

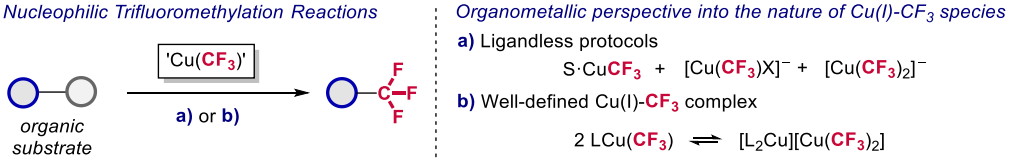

Scheme 5.6. Left: general representation for the incorporation of CF_3 moiety using trifluoromethyl copper(I) species. Right: ubiquity of homoleptic trifluoromethyl cuprate in different protocols. S = solvent.

Due to the relevance of 'Cu(CF_3)' species in trifluoromethylation reactions and the elusive role of the cuprates, the next sections will be dedicated to contextualize the stage of this field, paying special attention on mechanistic proposals.

5.1.4. Bis-(trifluoromethyl) cuprates associated to *in situ* generated (trifluoromethyl) copper(I) species

Many efforts have been devoted to the identification of the different species forming the nucleophilic 'Cu(CF_3)' mixture. Back in 1986, Burton *et al.* described that the *in situ* formed mixture of "ligandless" 'Cu(CF_3)' contained *elusive and complex species*.[10] Initially, the authors observed a "ligandless" 'Cu(CF_3)' species (δ = –28.8 ppm) by ^{19}F NMR spectroscopy when they performed the reaction between CuBr and [Cd(CF_3)(X)] in DMF at –50 °C. When this solution was warmed up, two additional 'Cu(CF_3)' species were detected (δ = –32.3 and –35.5 ppm). No further information was provided about the nature of the 'Cu(CF_3)' species. In 1989, the same research group performed further studies in order to provide a better understanding of the nature of the copper species involved in the "ligandless" 'Cu(CF_3)' mixture.[11] This was the first time that species such as [Cd(I)][Cu(CF_3)$_2$] or (Cd)[Cu(CF_3)(I)] (named in the paper as $CuCF_3$·L, L = cadmium iodide) were proposed to be part of the 'Cu(CF_3)' mixture. Although proposed, the different species were not characterized.

It was not until 2008, when Kolomitsev *et al.* confirmed that the term "ligandless" 'Cu(CF_3)' species had been an oversimplification and assigned the different signals observed by ^{19}F NMR spectroscopy.[12] During the *in situ* generation of 'Cu(CF_3)', they were able to observe its speciation in three different complexes: $CuCF_3$-solvent, [Cu(CF_3)$_2$]$^-$ and [Cu(CF_3)$_4$]$^-$ exhibiting three singlets in the ^{19}F NMR spectrum: –28.8 ppm; –32.3 ppm and –35.5 ppm, respectively. As mentioned above, exactly the same chemical shifts that Burton originally reported. In this venue, in 2011, for the first time, Goossen *et al.* characterized the heteroleptic cuprate [Cu(CF_3)(I)]$^-$ by ^{19}F NMR spectroscopy (δ = –28.14 ppm) (Scheme 5.7).[13]

In summary, "ligandless" 'Cu(CF_3)' mixture indicates a complex scenario where different species, including [Cu(CF_3)]$^-$ are potentially in equilibrium. In the next sections, we put together relevant information about the generation of these 'Cu(CF_3)' mixtures, their scope and relevant mechanistic proposals.

---

10 Wiemers, D. M.; Burton, D. J. *J. Am. Chem. Soc.* **1986**, *108*, 832 and references cited therein.

11 Willert-Porada, M. A.; Burton, D. J.; Baenziger, N. C. *J. Chem. Soc., Chem. Comm.* **1989**, *21*, 1633.

12 Agnes, K.; Movchun, V.; Rodima, T.; Dansauer, T.; Rusanov, E. B.; Leito, I.; Kaljurand, I.; Koppel, J.; Pihl, V.; Koppel, I.; Ovsjannikov, G.; Toom, L.; Mishima, M.; Medebielle, M.; Lork, E.; Röschenthaler, G.-V.; Koppel, I. A.; Kolomeitsev, A. A. *J. Org. Chem.* **2008**, *73*, 2607.

13 Knauber, T.; Arikan, F.; Röschenthaler, G.-V.; Goossen, L. J. *Chem. Eur. J.* **2011**, *17*, 2689.

5.1.4.1. Routes for accessing *in situ* 'Cu(CF_3)' species

The potential of the 'Cu(CF_3)' mixture to perform nucleophilic trifluoromethylation reactions has encouraged the organic and organometallic community to access them using different methods.[3] In Scheme 5.7, it is shown a classification of the different routes according to the nature of the source that provides the nucleophilic CF_3 moiety to the copper: i) fluoroform,[14] ii) trifluoromethylated organic sources as nucleophilic CF_3 synthons[15] and iii) trifluoromethyl organometallic complexes that act as CF_3 shuttle through a transmetalation step, being the metal center a transition metal,[16,10] post-transition metal[17] or semimetal.[18,13]

It should be mentioned that the exact nature of the 'Cu(CF_3)' mixture is generally overlooked since the main purpose of these works is the transference of the CF_3 to other substrates.

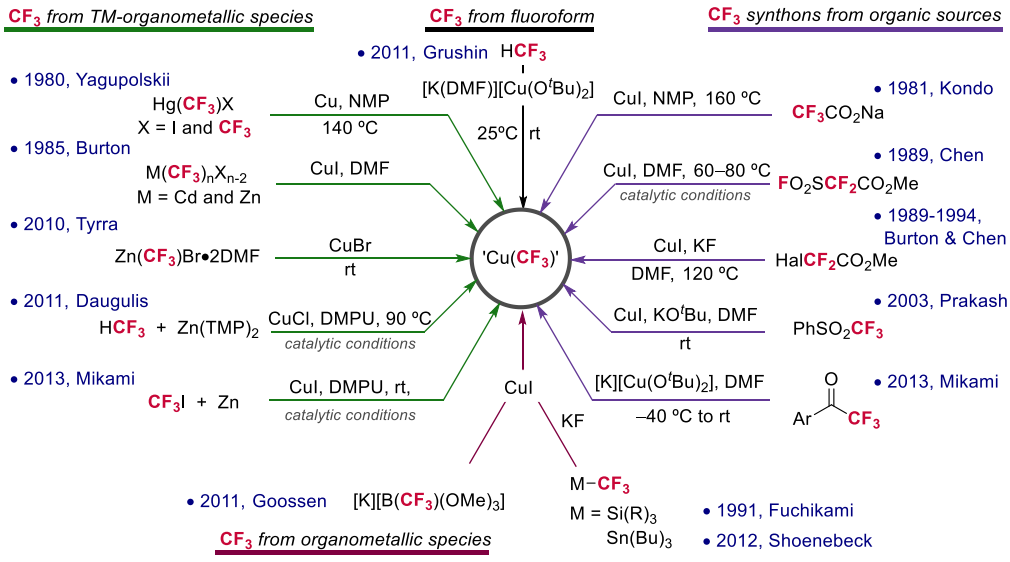

Scheme 5.7. Overview of the state of the art for the *in situ* synthesis of 'Cu(CF_3)' species. DMPU = 1,3-dimethyl-3,4,5,6-tetrahydro-2(1*H*)-pyrimidinone. Catalytic conditions means Cu in catalytic amounts. Hal = halogen.

14 Zanardi, A.; Novikov, M. A.; Martin, E.; Benet-Buchholz, J.; Grushin, V. V. *J. Am. Chem. Soc*. **2011**, *133*, 20901.

15 a) Matsui, K.; Tobita, E.; Ando, M.; Kondo, K. *Chem. Lett.* **1981**, 1719. b) Chen, Q.; Wu, S. *J. Chem. Soc., Chem. Commun.* **1989**, 705. c) MacNeil, J. G. Jr.; Burton, D. J. *J. Fluorine Chem.*, **1991**, *55*, 225. d) Duan, J-X.; Su, D-B.; Wu, J-P.; Chen, Q-Y. *J. Fluorine Chem.*, **1994**, *66*, 167. e) Prakash, G. K. S.; Hu, J.; Olah, G. A. *Org. Lett.* **2003**, *5*, 3253. f) Serizawa, H.; Aikawa, K.; Mikami, K. *Chem. Eur. J.* **2013**, *19*, 17692.

16 a) Kondratenko, N. V.; Vechirko, E. P.; Yagupolskii, L. M. *Synthesis* **1980**, 932. b) Kremlev, M. M.; Tyrra, W.; Mushta; A. I.; Naumann, D.; Yagupolskii, Y. Y. *J. Fluorine Chem.* **2010**, *131*, 212. c) Popov, I.; Lindeman, S.; Daugulis, O. *J. Am. Chem. Soc.* **2011**, *133*, 9286. d) Nakamura, Y.; Fujiu, M.; Murase, T.; Itoh, Y.; Serizawa, H.; Aikawa, K.; Mikami, K. *Beilstein J. Org. Chem.* **2013**, *9*, 2404.

17 Sanhueza, I. A.; Nielsen, M. C.; Ottiger, M.; Schoenebeck, F. *Helv. Chim. Acta* **2012**, *95*, 2231.

18 Urata, H.; Fuchikami, T. *Tetrahedron* **1991**, *32*, 91.

5.1.4.2. Scope of the trifluoromethylation reaction using *in situ* 'Cu(CF_3)' complexes.

In terms of scope, the *in situ* generated mixture has been proved to be able to trifluoromethylate aryl iodide,[10,14,15e,16d,19] α-diazo esters[20] and organometallic species affording (IPr)Cu(CF_3) and [(TMEDA)Pd(Ph)(CF_3)][19] in excellent yields. Interestingly, under oxidative conditions they have been used for the nucleophilic trifluoromethylation of boronic acids and terminal alkynes.[21] Scheme 5.8 displays the nucleophilic trifluoromethylation reactions where 'Cu(CF_3)' has been proved to be effective.

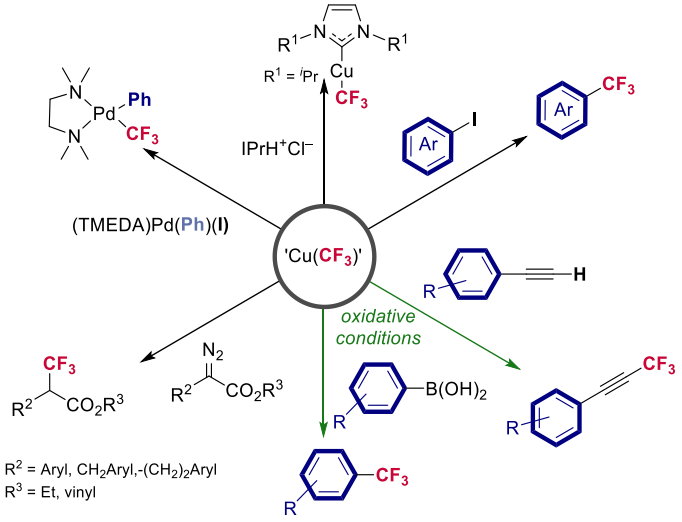

Scheme 5.8. General scope of the trifluoromethylation reactions using *in situ* generated 'Cu(CF_3)' species.

5.1.4.3. Proposed mechanisms in trifluoromethylation using 'Cu(CF_3)' mixture.

In 1988, pioneering work from Parker and co-workers uncovered the nucleophilic nature of transient $[Cu(CF_3)(I)]^-$ species by performing Hammett plot studies on the trifluoromethylation of different aryl halides.[22] From this point on, despite the tremendous development of Cu-mediated/catalyzed trifluoromethylation reactions, mechanistic proposals for these systems are not frequent in the literature. This has been principally hampered by the elusive nature of the species in the reaction media consequence of their dynamic behavior and their inherent instability. Interestingly, the sporadic examples that propose mechanistic aspects also examine the speciation of these 'Cu(CF_3)' complexes in the reaction media.

19 Lishchynskyi, A.; Novikov, M. A.; Martin, E.; Escudero-Adán, E. C.; Novák, P.; Grushin, V. V. *J. Org. Chem.* **2013**, *78*, 11126.

20 Hu, M.; Ni, C.; Hu, J. *J. Am. Chem. Soc.* **2012**, *134*, 15257.

21 a) Chu, L.; Qing, F.-L. *J. Am. Chem. Soc.* **2010**, *132*, 7262. b) Chu, L.; Qing, F.-L. *Org. Lett.* **2010**, *12*, 5060. c) Jiang, X.; Chu, L.; Qing, F.-L. *J. Org. Chem.* **2012**, *77*, 1251.

22 Carr, G. E.; Chambers, R. D.; Holmes, T. F.; Parker, D. G. *J. Chem. Soc., Perkin Trans. I* **1988**, *921*.

- **Mechanistic proposal for the functionalization of α-diazo esters.**

In 2012, Hu and co-workers reported the use of Me_3SiCF_3 in the preparation of 'Cu(CF_3)' for the trifluoromethylation of a wide variety of α-diazo esters (see Scheme 12a).[20] To gain insights into the reaction mechanism, the authors tentatively described the composition of 'Cu(CF_3)' mixture by ^{19}F NMR spectroscopy, identifying three different species in the reaction media (Cu(CF_3)-solvent, $[Cu(CF_3)_2]^-$ and $[Cu(CF_3)(I)]^-$ complexes. Their proposal involves the activation of $[Cu(CF_3)(I)]^-$ by water, which scavenges the I^-, forming a hydrated iodide ion, affording Cu(CF_3)-diazoester intermediate, where the N_2 extrusion takes place (Scheme XX). Their hypothesis was supported by the decrease on the reaction efficiency when less water (<10 equiv) was used or when external KI was added. Remarkably, the authors also noted that the amount of $[Cu(I)_2]^-$ can affect the chemical shift of $[Cu(CF_3)(I)]^-$ species. Thus, they suggested that a more appropriate way to denominate these species would be $\{[Cu(CF_3)(I)]_x\}^{x-}\{[Cu(I)_2]_y\}^{y-}$.

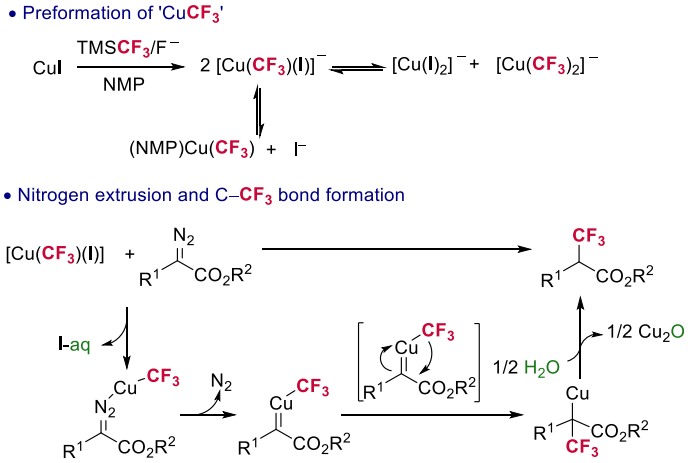

Scheme 5.9. Proposed reaction mechanism for the copper-mediated trifluoromethylation of α-diazo esters. aq = H_2O.

- **Mechanistic proposals in aerobic oxidative trifluoromethylation of terminal alkynes**

In 2013, Qing *et al*. reported the catalytic trifluoromethylation of boronic acids and terminal alkynes using Ruppert-Prakash reagent, Me_3SiCF_3, under oxidative conditions.[21] Therein, an important mechanistic hint was proved for these transformations. The reaction can be catalytic in copper if the addition of the CF_3 source to the reaction mixture is slow.[21c] They rationalized that slow addition prevents the decomposition of the silane before the CF_3 fragment is transferred to the copper center. Therefore, the recovering of the copper catalyst has to be sluggish. In this regard, same year, Maseras and Jover proposed, based on DFT calculations, that the reductive elimination from **X** may be the rate-limiting step of the oxidative

trifluoromethylation of alkynes, supporting the challenges associated to the catalyst recovering (Scheme 5.10).[23]

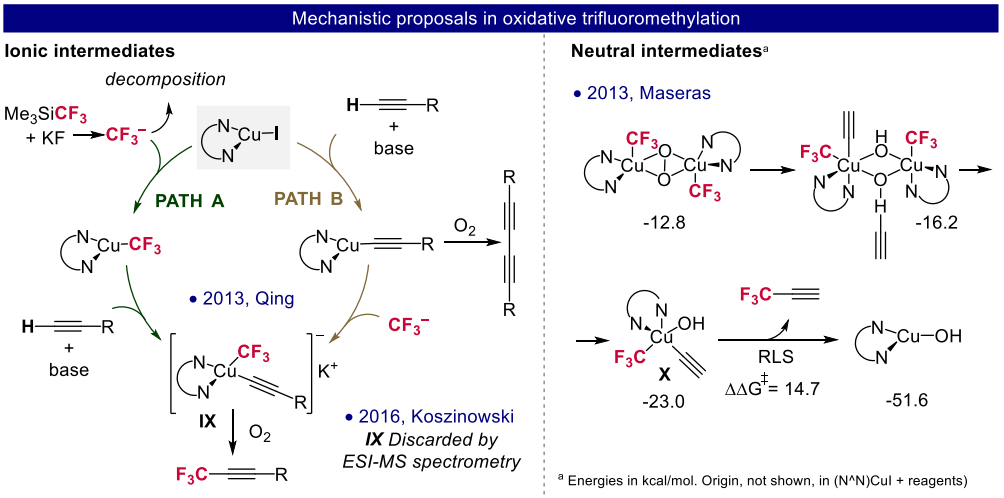

Scheme 5.10. Left: mechanistic proposals for the oxidative trifluoromethylation of alkynes involving ionic intermediates. Right: DFT-calculated mechanism for the same reaction involving neutral intermediates. RLS = rate-limiting step

Further mechanistic investigations using electrospray-ionization mass spectrometry (ESI-MS) by Koszinowski *et al.* aimed to shed light into the nature of the intermediates involved in these transformations.[24] On the one hand, in the absence of the alkyne component, the homoleptic ate-type complexes $[Cu(CF_3)_2]^-$ and $[Cu(CF_3)_4]^-$ were detected from the mixture of CuI, KF and Me_3SiCF_3 in different solvents such as acetonitrile, tetrahydrofurane or (*N*^*N*)-dimethyl-formamide. On the other hand, when adding the alkyne to the cuprate solution, the authors detected copper(III) species such as $[Cu(CF_3)_3(C{\equiv}CPh)]^-$, presumably the intermediate involved in the reductive elimination step. This is interesting since in these conditions the cuprates may be playing a role in the oxidative trifluoromethylation of terminal alkynes.

In the presence of (*N*^*N*)-bidentate-ligands, the authors were able to discard the intermediacy of $[(N\text{^}N)Cu(CF_3)(C{\equiv}CPh)]^-$, intermediate **IX**, previously proposed by Qing,[21] in the oxidative process on the basis of the unfruitful attempts to detect them even when modifying the ancillary ligand. Despite this remarkable mechanistic hint, a neutral (*N*^*N*)-bidentate-ligand-based mechanism, such as the one proposed by Maseras, mentioned above, could be simultaneously taking place and being overlooked using ESI-MS techniques.

23 Jover, J.; Maseras, F. *Chem. Commun*. **2013**, *49*, 10486.
24 Weske, S.; Schoop, R.; Koszinowski, K. *Chem. Eur. J.* **2016**, *22*, 11310.

- **Mechanistic proposals for the functionalization of aryl halides**

The potential mechanism for the trifluoromethylation of aryl halides has been a matter of discussion in the literature. In 2011, Goossen *et al.* provided a mechanistic proposal for the trifluoromethylation of aryl iodides considering $[Cu(CF_3)(I)]^-$ cuprate as active species.[13] This complex was observed when mixing potassium (trifluoromethyl)trialkoxyborates and CuI. They proposed that the CF_3 transfer occurs via σ-bond metathesis event from 'Cu(CF_3)' species (Scheme 5.11).

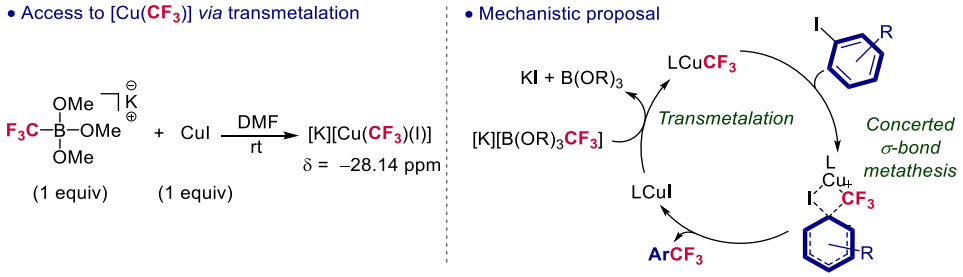

Scheme 5.11. Left: Synthetic pathway for accessing the heteroleptic cuprate. Right: mechanistic proposal for the Cu-catalyzed trifluoromethylation of aryl iodides.

In 2012, Shoenebeck *et al.* presented a new methodology combining Bu_3SnCF_3, as CF_3 source, and CuI/KF for the nucleophilic trifluoromethylation of aryl iodides (Scheme 5.12).[17] In this report, the authors explained that the trifluoromethylation reaction can be performed by both $Cu(CF_3)\cdot KBr$ and $[Cu(CF_3)_2]^-$ complexes based on ^{19}F NMR spectroscopy. In addition, radical mechanisms were discarded based on the lack of rearranged product when using radical clock substrates (Scheme 5.12). Although the complete mechanistic scenario for the formation of the C–C was not deeply discussed, a comparison between Me_3SiCF_3 and Bu_3SnCF_3 as transmetalating agents is presented. This is important since the efficiency in the transmetalation can be crucial for the development of Cu-catalyzed transformations as mention above for Qing's system.

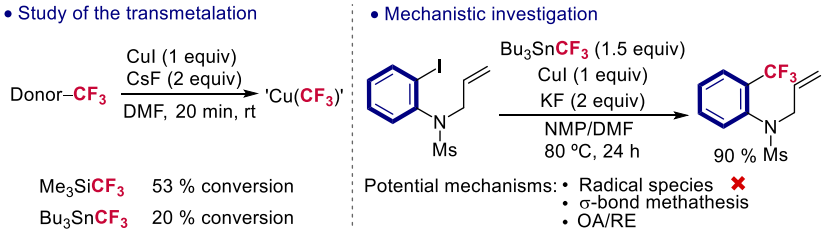

Scheme 5.12. Left: Study of the formation of [Cu–CF_3] species when using silanes and stannanes as transmetalating agents. Right: Mechanistic investigation for the dismissal of a radical-involving transformation.

Later, in 2013, Mikami described the trifluoromethylation of aryl and heteroaryl iodides catalyzed by copper(I) salt and phenanthroline using [Zn(CF_3)(I)], prepared *in situ* from trifluoromethyl iodide and Zn dust in DMPU (1,3-dimethyl-3,4,5,6-tetrahydro-2-(1*H*)pyrimidone).[15f] In order to gain insight into each step of the Cu-catalyzed Zn-mediated trifluoromethylation, they performed a ^{19}F NMR spectroscopic analysis, observing a Schlenk equilibrium of [Zn(CF_3)(I)] with [Zn(CF_3)$_2$] and [Zn(I)$_2$] (Scheme 5.13). The addition of CuI to this solution resulted in the transmetalation of the CF_3 group from zinc to copper observing two singlet peaks of the cuprate species, [Cu(CF_3)I]$^-$ and [Cu(CF_3)$_2$]$^-$ (Scheme 5.13). In this case, the neutral (DMPU)Cu(CF_3) species was not observed. The addition of aryl iodide to this mixture led to the formation of the trifluoromethylated organic molecule with the consumption of the cuprates [Cu(CF_3)I]$^-$ and [Cu(CF_3)$_2$]$^-$. The non-efficient and complex transmetalation reaction complicates the mechanistic picture and the real potential of both cuprate species in the trifluoromethylation of aryl halides was not clearly disclosed. Two year later, the same group provided a mechanistic proposal for the trifluoromethylation of aryl and heteroaryl iodides using isolated [(DMPU)$_2$Zn(CF_3)$_2$], involving a Cu$^{I/III}$ catalytic cycle (Scheme 5.13).[25] This proposal is in sharp contrast to the aforementioned σ-bond metathesis proposed by Goossen (Scheme 5.11).[13] Again, the impossibility to access selectively the copper species hampered the study of the real role of cuprates in the trifluoromethylation reaction.

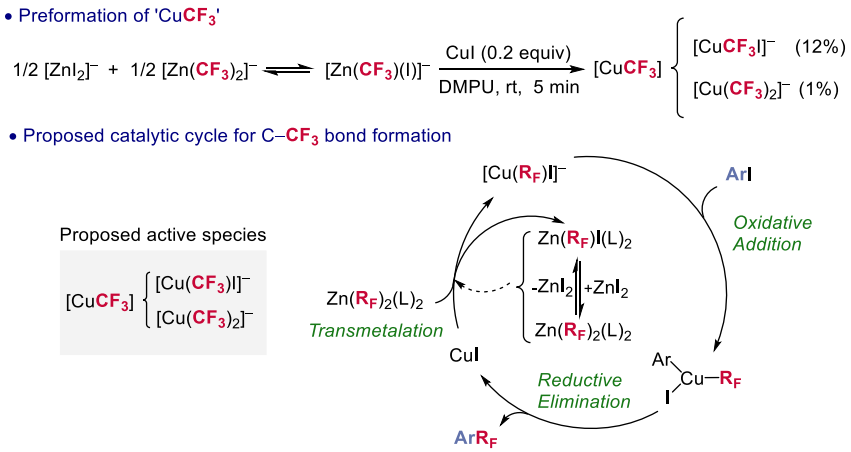

Scheme 5.13. Upper part, Schlenk equilibrium for trifluoromethyl zincates and transmetalation reaction towards copper(I). Lower part, scope of the trifluoromethylation of aryl iodides using zincates as CF_3 source and copper(I) as catalyst. The proposed mechanism involving Cu$^{I/III}$ intermediate is on the right.

In 2014, Grushin *et al*. performed an exhaustive experimental and computational study, in order to unravel the mechanism of the nucleophilic Cu-mediated trifluoromethylation using (DMF)Cu(CF_3), obtained directly from the cupration of fluoroform (Scheme 5.14).[26] Up until that

25 Aikawa, K.; Nakamura, Y.; Yokota, Y.; Toya, W.; Mikami, K. *Chem. Eur. J.* **2015**, *21*, 96.
26 Konovalov, A. I.; Lishchynskyi, A.; Grushin, V. V. *J. Am. Chem. Soc.* **2014**, *136*, 13410.

date, apart from the aforementioned proposals, only scarce mechanistic hints could be found in the literature: (i) the common rate trend when using different aryl halides (Ar–I > Ar–Br > Ar–Cl); (ii) the prevalent employment of DMF as solvent and (iii) the use of radical clock experiments that discarded a radical mechanism.[17,27] In this venue, Grushin performed an extensive mechanistic study. The most likely scenario involved an associative oxidative addition (OA), which is the rate determining step, of the aryl halide to the (DMF)Cu(CF_3) complex and, subsequently, the reductive elimination (RE) from the Cu(III) intermediate. This proposal is supported by the Hammett plot correlation (σ_p^-, ρ positive) and DFT calculations. Interestingly, almost perfect agreement was found between the experimental and calculated activation parameters ($\Delta G^{\ddagger}_{exp} \approx 24$ kcal·mol^{-1} vs $\Delta G^{\ddagger}_{DFT} = 21.9$ kcal·mol^{-1}). Further computational investigations were performed to evaluate other potential active species in the trifluoromethylation. This studies suggested that the oxidative addition of the substrate towards $[Cu(CF_3)_2]^-$ or $[Cu(CF_3)I]^-$ are less prompted to take place. However, this computational data was not supported by experimental evidences.

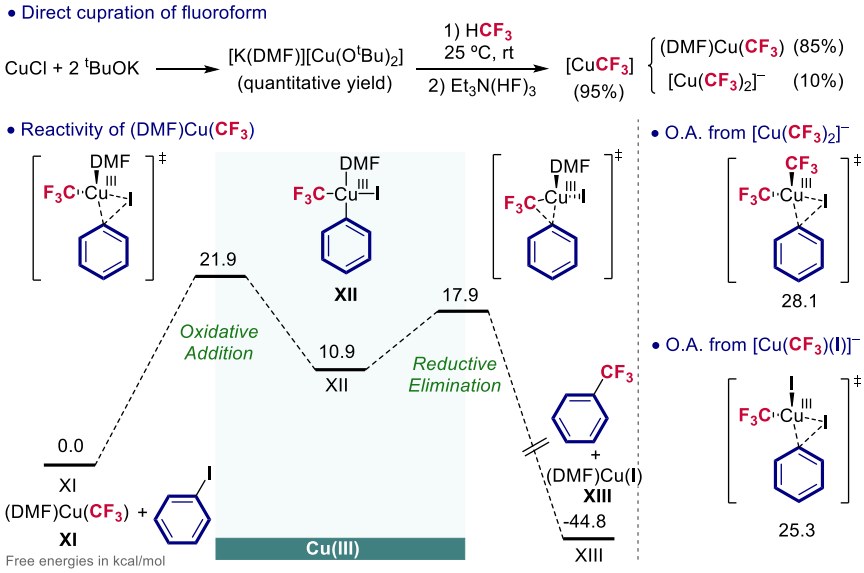

Scheme 5.14. Upper part, direct cupration of fluoroform. Lower part, DFT-calculated reaction mechanism involving an oxidative addition/reductive elimination sequence. On the right, alternative oxidative addition scenarios.

5.1.5. Bis-(trifluoromethyl) cuprates from the equilibrium of well-defined trifluoromethyl copper(I) species

Over the past decade, different literature precedents have demonstrated the exceptional activity of well-defined [(L)Cu(CF_3)] complexes, supported by ancillary ligands, in stoichiometric nucleophilic trifluoromethylation reactions. Most of these neutral copper(I) complexes are in

27 Morimoto, H.; Tsubogo, T.; Litvinas, N. D.; Hartwig, J. F. *Angew. Chem. Int. Ed.* **2011**, *50*, 3793.

equilibrium in polar solvents, commonly-used in these transformations, with salts containing the bis-(trifluoromethyl)cuprate as anion.

We have organized this section based on the nature of the ancillary ligand: (i) NHC-carbenes; (ii) bidentate nitrogen ligands and (iii) phosphines. Synthesis, reactivity and mechanistic hints are discussed for each particular case.

5.1.5.1. NHC-carbene copper (I) complexes

In 2008, Vicic *et al.* disclosed, for the first time, the synthesis of a well-defined trifluoromethyl copper(I) complexes using NHC-carbenes (SI^{i}Pr or IPr) as ancillary ligands (SI^{i}Pr = 1,3-Diisopropyl-4,5-dimethylimidazol-2-ylidene; IPr = 1,3-Bis(2,6-diisopropylphenyl)-1,3-dihydro-2H-imidazol-2-ylidene).[28] These stabilized copper complexes were synthetized by the treatment of *tert*-butoxide copper derivatives with Me_3SiCF_3, affording [(SI^{i}Pr)Cu(CF_3)] in 91% yield and a mixture of **A$_{IPr}$** and **B$_{IPr}$** copper complexes when L = IPr (Scheme 5.15). The authors tested their ability as trifluoromethylating agents, observing a higher activity when using the copper compound stabilized with the saturated ligand (SI*i*Pr). They observed a dramatic solvent effect, being DMF crucial to enhance the reactivity of the trifluoromethylation reactions.

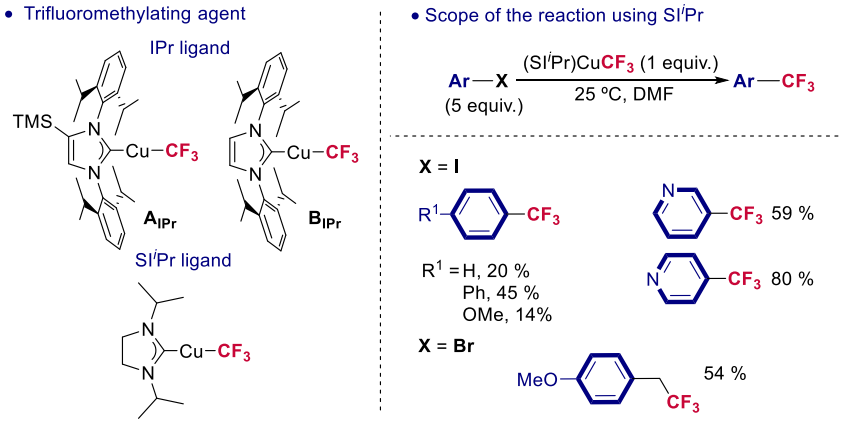

Scheme 5.15. Trifluoromethyl copper (I) species containing a NHC-carbene as ancillary ligand and scope of the trifluoromethylation reaction using them as nucleophilic CF_3 source.

The same year, modifications on the ligand led to the trifluoromethylation of electron-rich aryl halides by the use of [(SIMes)Cu(CF_3)] (**A$_{SIMes}$**) (SIMes = 1,3-bis(2,4,6-trimethylphenyl)- 4,5-dihydroimidazol-2-ylidene).[29] Interestingly, in THF, this neutral complex is in equilibrium with an ionic part, [(SIMes)$_2$Cu][Cu(CF_3)$_2$] (**B$_{SIMes}$**) that was characterized, for the first time, by X-ray diffraction. The mixture of **A$_{SIMes}$** and **B$_{SIMes}$**, in neat aryl halide or using as solvent mixture benzene:DMI, exhibited a superior activity than the previously described [(SI^{i}Pr)Cu(CF_3)]. They attributed the efficiency of this transformation to the superior activity of [(SIMes)Cu(CF_3)] (**A$_{SIMes}$**)

28 Dubinina, G. G.; Furutachi, H.; Vicic, D. A. *J. Am. Chem. Soc.* **2008**, *130*, 8600.
29 Dubinina, G. G.; Ogikubo, J.; Vicic, D. A. *Organometallics* **2008**, *27*, 6233.

based on kinetic studies and not to the ionic part ($\mathbf{B_{SIMes}}$). However, since $\mathbf{A_{SIMes}}$ and $\mathbf{B_{SIMes}}$ are presented in the reaction media is challenging to univocally stablish the origin of this outstanding performance.

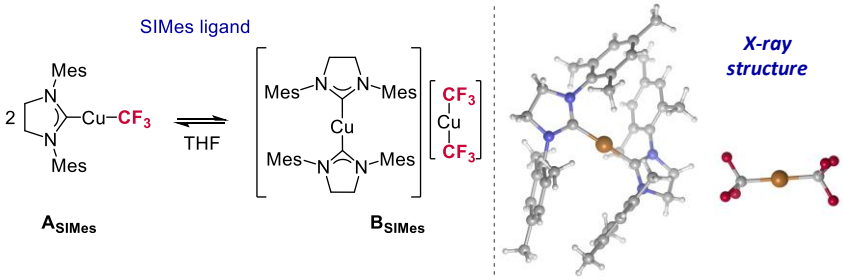

Scheme 5.16. Left: Equilibrium of (SIMes)Cu(CF_3) in polar solvent with [(SIMes)$_2$Cu][Cu(CF_3)$_2$]. Right: First X-ray structure of a bis-(trifluoromethyl) cuprate. Mes = mesityl.

5.1.5.2. (N^N)-bidentate copper(I) complexes

Bidentate ligands have been also used for the stabilization of '$CuCF_3$' species. In 2011, Hartwig *et al.* described the synthesis of [(phen)Cu(CF_3)] by the reaction of [CuO^{t}Bu]$_4$ with 1,10-phenantroline, followed by the addition of Me_3SiCF_3.[27] Although this species was previously proposed to be catalytically active in a seminal work of Amii *et al.*, in that work there was not any experimental evidence of its formation.[30] As described for [(SIMes)Cu(CF_3)], [(phen)Cu(CF_3)] ($\mathbf{A_{phen}}$) is in equilibrium with an ionic part, [(phen)$_2$Cu][Cu(CF_3)$_2$] ($\mathbf{B_{phen}}$), in polar solvents such as dichloromethane, tetrahydrofuran and DMF (Scheme 5.17). Conductivity and spectroscopic techniques were used to confirm the stoichiometric of the salt.

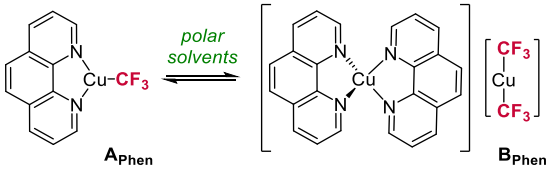

	A_{Phen}/B_{Phen} ratio	dipole moment (D)
DMF	21/79	3.82
THF	68/32	1.75
DCM	76/24	1.60

Scheme 5.17. Equilibrium of [(phen)Cu(CF_3)] with [(phen)$_2$Cu][Cu(CF_3)$_2$] in polar solvent. The ratios are shown in the right part at a concentration of 0.01 M.

This trifluoromethylating agent proved to be productive for the trifluoromethylation of aryl iodides and bromides in high yields. Regarding the mechanism, the use of radical clock experiments supported the absence of radicals during the transformation.

The same research group has also reported the functionalization of heteroaryl bromidesand the oxidative trifluoromethylation of arylboronate esters and aryl silanes (Scheme 5.18).[31] The

30 Oishi, M.; Kondo, H.; Amii, H. *Chem. Commun.*, **2009**, 1909.

31 a) Mormino, M. G.; Fier, P. S.; Hartwig, J. F. *Org. Lett.* **2014**, *16*, 1744. b) Litvinas, N. D.; Fier, P. S.; Hartwig, J. F. *Angew. Chem. Int. Ed.* **2012**, *51*, 536. c) Morstein, J.; Hou, H.; Cheng, C.; Hartwig, J. F. *Angew. Chem. Int. Ed.* **2016**, *55*, 8054.

arylboronate esters are generated by the reaction of arenes or aryl bromides with B_2pin_2 using iridium or palladium catalysts, respectively.

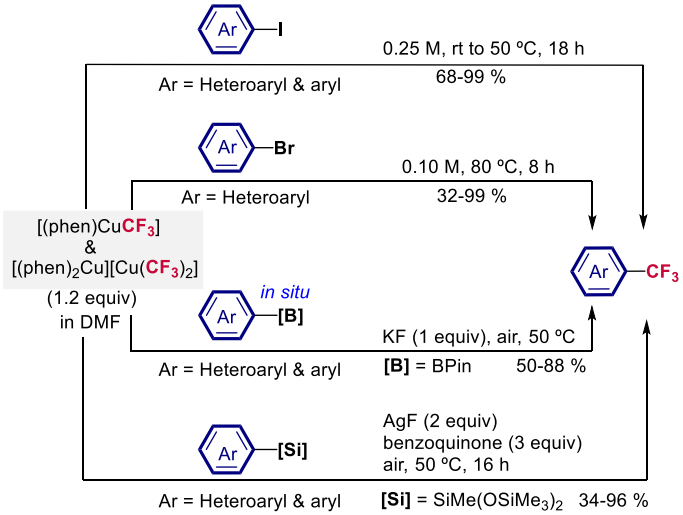

Scheme 5.18. Scope of the [(phen)Cu(CF_3)] as CF_3 source applied to different methodologies as trifluoromethylation of aryl halides, aryl boronates and silanes.

This new one-pot methodology permitted not only the regioselective functionalization of *in situ* generated arenes but also the expansion of the scope to aryl bromides. Regarding the aryl silanes, this new oxidative protocol was extended to pharmaceutically active molecules, inaccessible through other synthetic routes and using easily accessible starting materials. Remarkably, the broad applicability of [(phen)Cu(CF_3)] resulted in its commercialization, as Trifluoromethylator™.[32] It is worth mentioning that all the aforementioned described reactions were performed in DMF where there is a mixture $\mathbf{A_{phen}}$:$\mathbf{B_{phen}}$ (0.01 M, 21:79 respectively). Therefore, the participation of both complexes as trifluoromethylating reagents could not be completely ruled out.

5.1.5.3. Phosphine stabilized copper(I) complexes

In 2011, Grushin *et al.* reported an exhaustive study on the straightforward preparation of [(Ph_3P)$_3$Cu(CF_3)], previously described by Komiya *et al.*[33] and [(phen)Cu(PPh_3)(CF_3)], analogous to Hartwig's trifluoromethylator (see Scheme 5.17).[34] The later one is in equilibrium at room temperature with [(phen)$_2$Cu][Cu(CF_3)$_2$] and PPh_3 in CD_2Cl_2, analogous to the examples described by Hartwig.[27] Both complexes were exceptionally good as trifluoromethylating agents of aryl and heteroaryl iodides. In the case of [(Ph_3P)$_3$Cu(CF_3)], the addition of additives such as

32 https://www.sigmaaldrich.com/catalog/product/aldrich/777692?lang=es&region=ES
33 Usui, Y.; Noma, J.; Hirano, M.; Komiya, S. *Inorg. Chim. Acta* **2000**, *309*, 151.
34 Tomashenko, O. A.; Escudero-Adán, E. C.; Martínez-Belmonte, M.; Grushin, V. V. *Angew. Chem. Int. Ed*. **2011**, *50*, 7655.

phen, Bpy or ^{t}Bu-bpy favored the reaction, hampering the formation of side products like HCF_3 and $PhCF_2CF_3$.

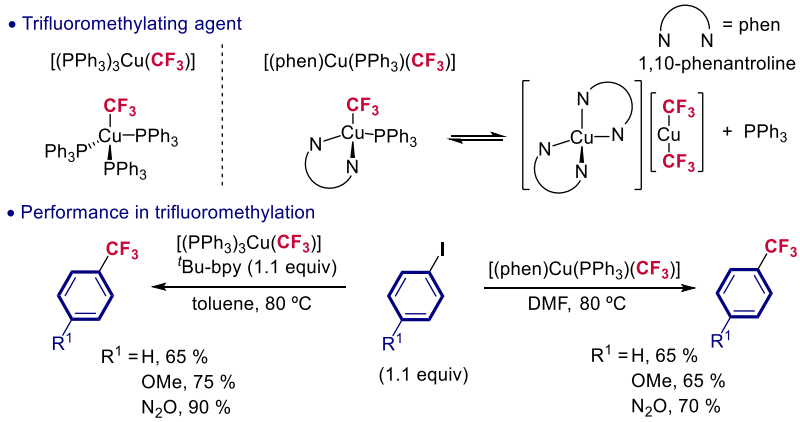

Scheme 5.19. Upper part, $[(Ph_3P)_3Cu(CF_3)]$ and $[(phen)Cu(PPh_3)(CF_3)]$ prepared by Grushin and co-workers as well-defined trifluoromethylating agents. Lower part, scope of the reaction for both complexes. ^{t}Bu-bpy = 4,4'-di-*tert*-butyl-2,2'-dipyridine.

5.1.6. Recent advances on the reactivity of different trifluoromethylation protocols

A mayor challenge for rationalizing the activity of the different $[Cu(CF_3)]$ species in the reaction media is the lack of standard conditions in the trifluoromethylation protocols. In 2017, Vicic *et al.* published an interesting work that compares the performance of previously described copper systems (Scheme 5.20).[35] In this report, the authors used as CF_3 sources not only well-defined trifluoromethyl copper reagents but also *in situ* generated 'Cu(CF_3)' by mixing $CuI/Me_3SiCF_3/KF$.[18,27,29,34] To that date, the described reaction conditions for the nucleophilic trifluoromethylation protocols were remarkably different hindering their comparison. In order to establish the relative reactivity between the copper systems, the authors selected as standard reaction conditions those described by Hartwig *et al.*, using 4-iodo-1,1'-biphenyl as model system and DMF as solvent. After 24 hours at 50 °C, the *in situ* generated $[(phen)Cu(CF_3)]$ exhibited the best performance as trifluoromethylating agent.

Moreover, the authors also performed the nucleophilic trifluoromethylation of 4-iodo-1,1'-biphenyl using the reported conditions for each protocol. This implies the employment of different solvents, temperature and concentrations. Under these different reaction conditions, the *in situ* generated $[(SIMes)Cu(CF_3)]$ showed the best performance, pointing out the crucial role of the solvent (benzene:DMI vs DMF). In general, the *in situ* formation of the complexes gave a better outcome than the corresponding isolated ones. Interestingly, when using the isolated or the *in situ* generated $[(SIMes)Cu(CF_3)]$ for the functionalization of electron-rich substrates, the authors observed induction periods in the kinetic profiles of the product formation

35 Kaplan, P. T.; Loyd, J. A.; Chin, M. T.; Vicic, D. A. Beilstein *J. Org. Chem*. **2017**, *13*, 2297.

(Scheme 5.20), suggesting a non-trivial behavior of these copper systems in solution. Based on their results, in this work, the authors encouraged the benchmarking in trifluoromethylation reactions to allow a fair comparison between new methods and the previously described ones under the same reaction conditions.

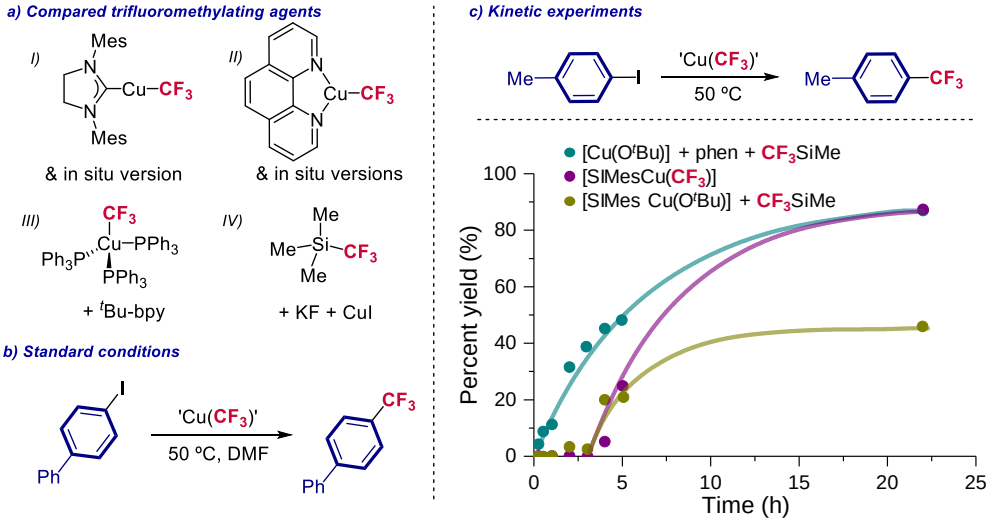

Scheme 5.20. Trifluoromethylating agents compared in the study of Vicic and definition of standard conditions to evaluate the potential of different trifluoromethyl copper species. Mes = mesityl. To the right, complex kinetics scenarios for electron-rich aryl iodide are shown.

Despite the tremendous efforts on providing a comprehensive mechanistic picture on Cu-mediated trifluoromethylation reactions, there is still a fundamental lack of knowledge about the potential performance of the bis-(trifluoromethyl) cuprates on the reaction.

5.2. Objectives

Trifluoromethyl coinage metal species have been proposed as key reactive intermediates in a wide variety of synthetic protocols involving the incorporation of CF_3 moiety into organic molecules. In this vein, bis-(trifluoromethyl) metallates (**1M**) are often neglected and, consequently, fundamental insights on their behavior, especially regarding their potential nucleophilic nature, are scarce in the literature. Among these ate-type complexes, bis-(trifluoromethyl) aurates have been recently isolated as a result of their stability. This has paved the way for reactivity studies from an organometallic perspective. In 2018, our group reported the synthesis of $[Cs][Ag(CF_3)_2]$ (**1Ag**) and studied its potential as transmetalating agent towards arylpalladium(II) complexes. However, copper congeners, ubiquitous in trifluoromethylation reactions, remains elusive due to their dynamic behavior in solution and inherent instability. Therefore, we envision that a selective route for accessing these ate-type complexes is needed. This would allow us to study their chemical behavior and get insights into the whole family of metallates (**1M**) in terms of fundamental knowledge and reactivity.

In this context, the main objectives of this Chapter 4 are the selective access to $[Cs][M(CF_3)_2]$ (M = Cu, Ag, Au) and the further comparison of the different coinage metallates (**1M**) from a structural and reactivity perspective under exactly the same conditions. To do so, the following points are pursued:

- Synthesis of $[Cs][M(CF_3)_2]$ (M = Cu, Ag, Au).
- Structural study of the different $[Cs][M(CF_3)_2]$ (M = Cu, Ag, Au).
- Study their relative reactivity as nucleophile towards selected electrophiles whose reactivity has been already reported for each coinage metal.

5.3. Results and discussion

5.3.1. Synthesis, characterization and theoretical analysis of different [Cs][M(CF$_3$)$_2$]

5.3.1.1. Synthesis and characterization of [Cs][M(CF$_3$)$_2$]

The synthesis of the family of [cat][M(CF$_3$)$_2$] metallates (**1M**) was intimately tied to our previously-described synthetic protocol for accessing [Cs][Ag(CF$_3$)$_2$] complex (**2Ag**).[2e] Using all the fundamental knowledge gained in this work as starting point (discussed in Chapter 2) we tested the transmetalation capability of [Cs][Ag(CF$_3$)$_2$] for generating the analogous bis-trifluoromethyl cuprate and aurate salts ([Cs][M(CF$_3$)$_2$] (M = Cu, Au)).

First, we targeted the access to [Cs][Cu(CF$_3$)$_2$] complex (**1Cu**). Gratifyingly, under argon atmosphere, the transmetalation reaction of [Cs][Ag(CF$_3$)$_2$] and CuI in a 1:1 molar ratio gave rise to the quantitative formation of **1Cu** in THF or DMF after 1 hour at room temperature (Scheme 5.21). Although **1Cu** is insufficiently stable for isolation as a solid,[36] we confirmed its structure by ^{19}F NMR spectroscopy, ESI-MS and single crystal X-ray diffraction. This result is particularly noteworthy considering the difficulties associated to the selective access [Cu(CF$_3$)$_2$]$^-$ species in solution, mentioned above.

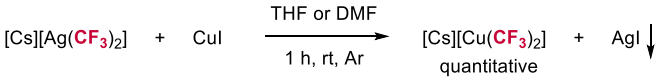

Scheme 5.21. Selective formation of **1Cu**.

Under identical conditions, the reaction between [Cs][Ag(CF$_3$)$_2$] salt and [AuCl·(SMe$_2$)] complex afforded a complex reaction mixture. Modifications of the conditions (temperature, ratio between complexes and time) were performed and, in all the cases, these reactions led to a mixture of species including the targeted [Cs][Au(CF$_3$)$_2$], **1Au**. However, after some experimentation, we found that the treatment of 1 equiv of [AuCl·(SMe$_2$)] with the combination Me$_3$SiCF$_3$/CsF (3.3/3) in THF afforded **1Au** as a stable blue solid in 85% isolated yield (Scheme 5.22). The resulting salt was fully characterized by NMR spectroscopy, ESI-MS and X-ray diffraction.

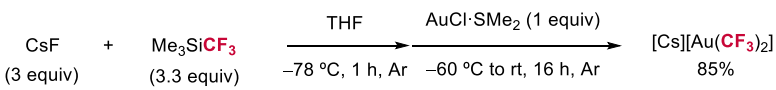

Scheme 5.22. Selective formation of **1Au**.

[36] In THF, the compound decomposes less than 10% after 15 days stored in the glovebox at –30 ºC. At room temperature, **1Cu** decomposes around 18% overnight. However, attempts to isolate complex **1Cu** as solid failed.

As mentioned above, we were able to determine the structure of **1Cu** and **1Au** by single crystal X-ray structure analysis at 100 K. The structure of these crystals, along with the one obtained for **1Ag** are shown in Figure 5.1, along with the most relevant parameters of the measured crystals.

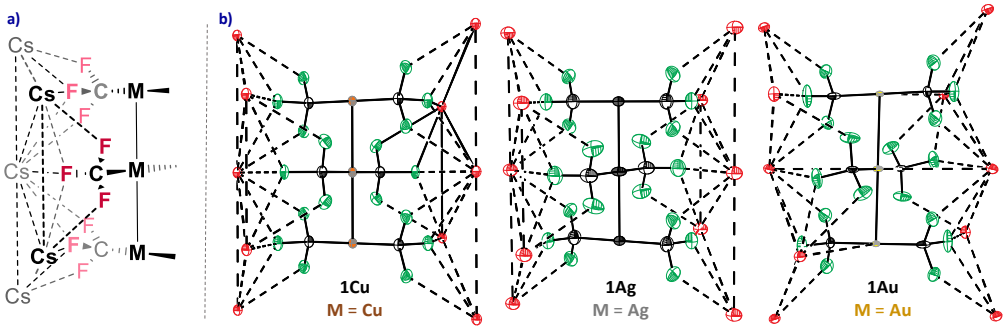

Distances (Å)	1Cu	1Ag	1Au
M–C	1.940(10)	2.123(9)	2.02(2)-2.07(2)
M–M	2.7193(8)	2.8830(4)	3.0138(3)-3.0254(4)
Shortest Cs–F	3.115(5)	3.101(9)	3.05(2)
Nº contacts Cs–F	12	12	12
Shortest Cs–M	-	-	3.929(3)
Angles (º)			
M–M–M	180.0	180.0	167.51(5)-172.56(2)

Figure 5.1. a) Measured crystal structures. b) ORTEP structures of **1Cu**, **1Ag** and **1Au** are shown with thermal ellipsoids set at 50% probability. The color code is described below: Red (Cesium), Grey (Carbon), Green (Fluorine), Orange (Copper), Black (Silver) and Yellow (gold). Most relevant parameters of the structures are shown in the table.

In all the metallates (**1M**), we observed a rather unique structure. Two CF_3 moieties are attached to the metal center and the cations are interacting with twelve different fluorine atoms from the CF_3 ligand. In fact, these numerous weak interactions could be involved in the stabilization of the isolated bis-(trifluoromethyl) complexes.[37]

[37] For representative examples of high Cs···F contacts, see: a) Pollak, D.; Goddard, R.; Pörschke, K.-R. *J. Am. Chem. Soc.* **2016**, *138*, 9444. b) Carreras, L.; Rovira, L.; Vaquero, M.; Mon, I.; Martin, E.; Benet-Buchholz, J.; Vidal-Ferran, A. *RSC Adv.* **2017**, *7*, 32833.

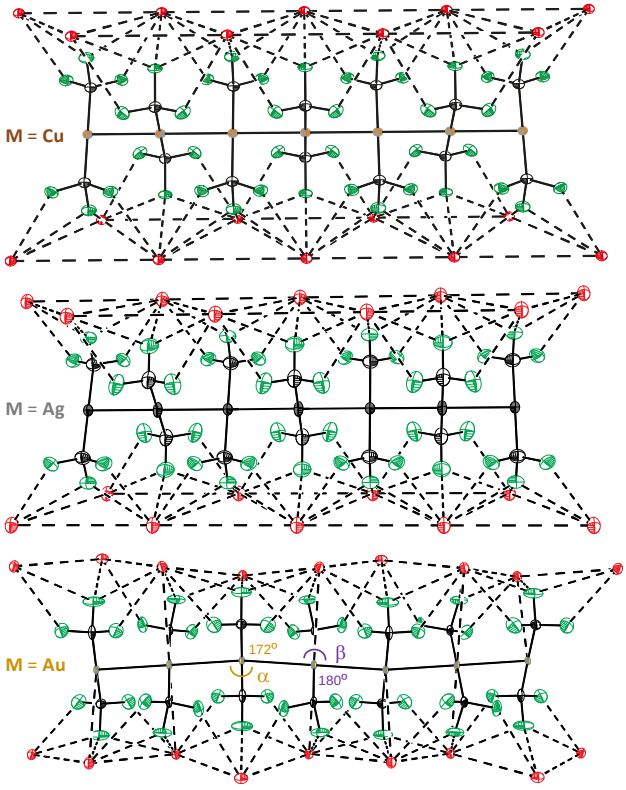

Figure 5.2. Representation of the linear chains with M–M contacts. The zigzag pattern in **1$_4$Au** is highlighted. In this case, only the α angle of 172º is represented and is not 167º (Figure 5.1).

The structure of **1Cu** is isostructural to the structure of **1Ag** while complex **1Au** crystallizes in a new unit cell within the space group, but showing a very similar packing to the others. In these series of Cs-salts, all the metal atoms are forming linear chains with M–M contacts along the structure, differing from other previously described $[M(CF_3)_2]^-$ anions.[1a,2f,29,38] Interestingly, **1Au** shows a zigzag pattern every three Au-atoms as we can see in Figure 5.2. Regarding the M–C bonds lengths, the Ag–C is the longest bond distance (2.12 Å), while the Cu–C the shortest with 1.94 Å. The Au–C bond distances are in the range of 2.04 - 2.07 Å and are comparable with previously described [cat][Au(CF$_3$)$_2$] salts.[1a,38] This shortening of the M–C bond distance, compared to **1Ag** and **1Cu**, is associated to the relativistic gold contraction effect.[39] Regarding the Cu–C bond distance, it is shorter than the only [cat][Cu(CF$_3$)$_2$] characterized by X-ray diffraction, [(SIMes)$_2$Cu][Cu(CF$_3$)$_2$] (1.94 vs 1.97 Å).[29]

5.3.1.2. DFT calculations on the electronic structure of bis-(trifluoromethyl) metallates

Next, we performed DFT calculations to gain insights into the electronic structure of the different metallates (**1M**). These calculations were carried out with the M06 functional with a

38 Martínez-Salvador, S.; Falvello, L. R.; Martín, A.; Menjón, B. *Chem. Eur. J.* **2013**, *19*, 14540.
39 Bayler, A.; Schier, A.; Bowmaker, G. A.; Schmidbaur, H. *J. Am. Chem. Soc.* **1996**, *118*, 7006.

double-ζ plus polarization basis set in gas phase (see Appendix for more details). We considered as model system the anionic version of the corresponding cesium bis-(trifluoromethyl) metallates.

We first analyzed the HOMO (Highest Occupied Molecular Orbital) energy to gain information about the nucleophilicity of these species. We observed that the energy of the HOMO decreases from copper to gold. The bis-(trifluoromethyl) cuprate anion is more nucleophilic than the argentate or aurate congeners. We then carried out Natural Bond Orbital (NBO) calculations to dig into the electronic structure of the metallate and the M–C bond situation. When evaluating the Natural Population Analysis (NPA) of the metal center for each metallate (Figure 5.3), we can observe that the values of the NPA over the metal center decreases from copper to gold (Figure 5.3). This points out that the M–C bond in the gold anion is less polarized towards the CF_3 ligand and, subsequently, it is expected to be a more covalent bond compared to the others.

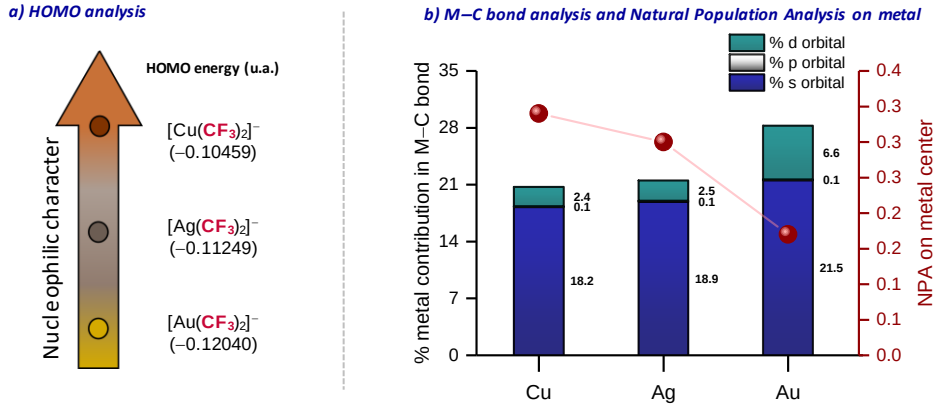

Figure 5.3. Left: HOMO energy values and nucleophilic scale for the different $[M(CF_3)_2]^-$. Right: Plot for the metal contribution (and the contribution of each orbital) in M–C bond along with NPA charge on the metal center.

NBO analysis was also used for the description of the σ-M–C bond. The main orbital contribution to the M–C bond comes from the carbon atom in all the cases (79.2% in Cu–C, 78.5% in Ag–C, 71.7% in Au–C, see Table A5.1). This is in line with the NPA charge distribution since the electronic density is mainly located on the CF_3 moiety. Interestingly, as we can see in Figure 5.3, the coefficient of the metal contribution on the M–C bond increase from copper to gold. We attributed this to the increase of electronegativity of the coinage metals from copper to gold (Cu = 1.90, Ag = 1.93, Au = 2.54). The more electronegative the coinage metal, the higher the contribution of the metal orbitals in the σ-M–C bond. This is also related to a mayor covalency of the bond since the charge is less localized over the CF_3. As result of a more covalent Au–C

bonds, the aurate **1Au** presents an exceptional stability compared to the argentate **1Ag** or cuprate **1Cu** analogues.

It should be emphasized the exclusive contribution of *s* and *d* orbitals of the metal to the bond M–C bond. As expected for the transition metals, especially for group 11, *p* orbitals have a small contribution since they are higher in energy than *d* or *s* orbitals. As expected, the contribution of *d* orbitals to the M–C bond in $[Au(CF_3)_2]^-$ anion is remarkably higher than in copper or silver analogues. This is in line with the stabilization and contraction of *s* and *p* gold orbitals and, subsequent expansion and destabilization of *d* and *f* orbitals, as consequence of relativistic effects.[40]

5.3.2. **Reactivity of [Cs][M(CF$_3$)$_2$]**

As mentioned in the introduction, the evaluation of the reactivity of the coinage metal bis-(trifluoromethyl) metallates (**1M**) have been limited to certain transformation but the three analogous have not been compared under the same conditions towards the same reaction. In the case of gold, oxidation to Au (III) with different electrophiles (X_2, XeF_2 or R^FI) has been deeply studied by Menjón and co-workers, as mentioned in the introduction.[1b,1c,1e] In the case of ate-type silver complexes, the reactivity studied has been exclusively devoted to the transmetalation in Pd/Ag systems (Chapter 3 and 4).[2e] In the case of copper, the knowledge about its reactivity, although it has been a matter of debate in the literature, is scarce and intimately tied to trifluoromethylation of organic substrate, essentially aryl halides.[3] In this context, we aim to carry out a unified reactivity study of the so-synthesized coinage metallates towards different electrophiles under the same reaction conditions in order to understand and compare the chemical behavior of these species as nucleophiles.

5.3.2.1. **Reactivity towards I$_2$**

Oxidative addition reactions using strong oxidating agents have been studied for bis-(trifluoromethyl)aurates, as discussed in the introduction.[1b,1c,1e] However, this reaction has not been reported for silver and copper, essentially due to the lack of protocols to access them in a selective fashion.

We first revisited the synthetic protocol for accessing [*trans*-$Au(CF_3)_2(I)_2]^-$ to form the corresponding cesium salt from $[Cs][Au(CF_3)_2]$ complex.[38] The reaction of **1Au** and I_2 in THF gave rise to the formation of the desired compound. The resulting salt was fully characterized by NMR spectroscopy, ESI-MS and X-ray diffraction. Diagnostic signal by ^{19}F NMR spectroscopy at δ = –13.0 ppm in THF was observed.

40 Schwerdtfeger, P. *Heteroat. Chem*. **2002**, *13*, 578.

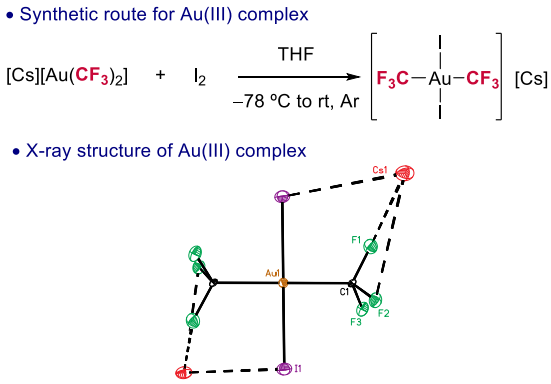

Scheme 5.23. Above, reaction of **1Au** with I_2 to form [Cs][*trans*-Au$(CF_3)_2(I)_2$]. Below, X-ray structure of [Cs][*trans*-Au$(CF_3)_2(I)_2$].

It should be noticed that the resonance of the fluorine atoms is shifted upfield (δ = –13.01 ppm) in comparison with [Cs][Au$(CF_3)_2$] (δ = –29.88 ppm) by the oxidation of the metal center. After 24h in solution, the complex started to decompose. Trifluoroiodomethane (CF_3I) was observed during the decomposition along with [Cs][Au$(CF_3)(I)$] suggesting a reductive elimination event.[41]

Regarding the silver metallate **1Ag**, the oxidation reaction using I_2 instantaneously formed a yellow solid (presumably AgI) along with CF_3I and small amounts of $[Ag(CF_3)_4]^-$ species. The formation of the corresponding cuprate was not successful, observing CF_3I and $[Cu(CF_3)_4]^-$ species as by-products of the reaction. These experiments suggested that $[M(CF_3)_2(I)_2]^-$ anions (M = Ag, Cu) are not as stable as Au(III) complexes and the formation of CF_3I is favored, potentially through a reductive elimination event.

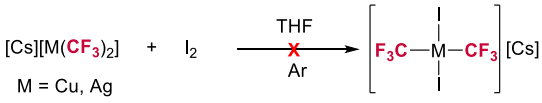

Scheme 5.24. Unfruitful attempts to obtain [Cs][*trans*-M$(CF_3)_2(I)_2$], (M = Cu, Ag)

5.3.2.2. **Reactivity towards [(dppp)Pd(Ph)(I)]**[42]

Bis-(trifluoromethyl) argentate (**1Ag**) proved to be an efficient transmetalating agent toward oxidative addition Pd(II) complexes. In this context, we wondered if the behavior of the whole family of coinage ate-type complexes as nucleophiles would be the same towards a benchmark electrophile arylpalladium(II) complex. As described in Chapter 2, the transmetalation reaction using [(dppp)Pd(Ph)(I)] and [Cs][Ag$(CF_3)_2$] (**1Ag**) leads quantitatively to [(dppp)Pd(Ph)(CF_3)] in less than 10 min at room temperature (Scheme 5.25).

41 Decomposition species were identified by ^{19}F NMR. This reductive elimination process is proposed to happen through a radical mechanism: Blaya, M; Bautista, D.; Gil-Rubio, J.; Vicente, J. *Organometallics* **2014**, *33*, 6358.

42 The results showed in this section have not been published yet and further studies are undergoing in our group.

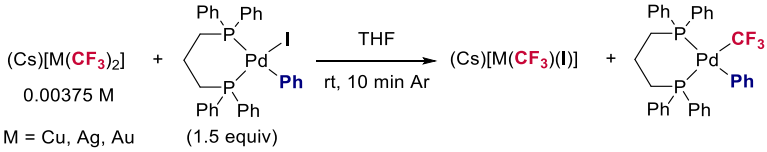

Scheme 5.25. Transmetalation model system of the different homoleptic metallates (**1M**) towards [(dppp)Pd(Ph)(I)] as benchmark palladium complex.

When performing the transmetalation reaction using [Cs][Au(CF_3)$_2$], no product formation was observed even after several days at room temperature or heating up to 120 ºC overnight. A reasonable explanation could be that this reaction is not thermodynamically favored due to the strength of the Au–CF_3 bond. Indeed, the transmetalation from aryl Au(I) complexes to organo-Pd(II) halides is well-known to be an endergonic process.[43]

We then studied the transmetalation capabilities of *in situ* generated [Cs][Cu(CF_3)$_2$] (**1Cu**). Interestingly, when performing the transmetalation reaction, the [(dppp)Pd(Ph)(CF_3)] product is formed in less than 10 min in quantitative yield. To gain insights into the cuprate **1Cu** behavior respect to the argentate **1Ag**, we run kinetic experiments by ^{19}F NMR spectroscopy at –20 ºC using both complexes as transmetalating agents for the model reaction with [(dppp)Pd(Ph)(I)] (Scheme 5.26).

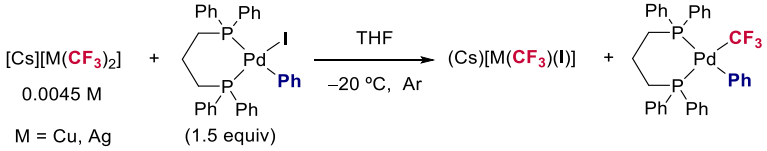

Scheme 5.26. Transmetalation model system for the kinetic experiment of the **1Cu** and **1Ag** towards [(dppp)Pd(Ph)(I)] at –20 ºC in THF.

As we can see in (Figure 5.4), the transmetalation reaction using [Cs][Cu(CF_3)$_2$] (**1Cu**) is much faster than the corresponding reaction using silver species **1Ag**. It should be mentioned that an induction period is observed during the first hour of this reaction. This could be related to the formation of more reactive species that promote the transmetalation reaction obeying the same behavior described for our studied Pd/Ag system in Chapter 4.

[43] Pérez-Temprano, M. H.; Casares, J. A.; de Lera, Á. R.; Álvarez, R.; Espinet P. *Angew. Chem. Int. Ed.* **2012**, *51*, 4917.

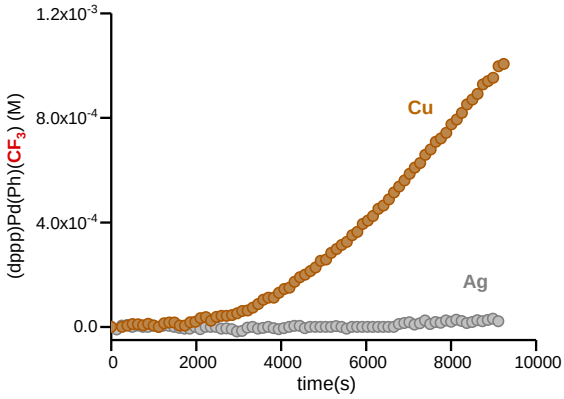

Figure 5.4. Evolution of the product concentration during the model transmetalation reaction of $[Cs][M(CF_3)_2]$ (M = Cu, Ag) towards [(dppp)Pd(Ph)(I)] in THF at –20 ºC.

Further studies to understand how the transference of the CF_3 moiety occurs and the influence of copper in the high performance are currently undergoing in our group.

5.3.2.3. Reactivity towards aryl halides

We next aimed to unravel the participation of these bis-(trifluoromethyl) metallates (**1M**) in the activation of aryl halides using 4-iodobiphenyl (**2I**) as benchmark substrate, a common electrophile in trifluoromethylation reactions (Scheme 5.27).[44]

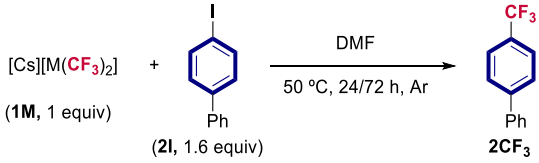

Entry	1M	2CF$_3$ (%)*
1	**1Au**	-
2	**1Ag**	-
3	**1Cu**	93

Scheme 5.27. Trifluoromethylation reaction of **2I** with **1Cu**, **1Ag**, **1Au**. *Yield obtained by ^{19}F NMR analysis using 4,4'-difluorobiphenyl as internal standard.

The reaction of **1Ag** or **1Au** with **2I** in DMF at 50 ºC during 24 hours did not provide the desired organic product, observing by ^{19}F NMR spectroscopy the starting materials and/or decomposition products.[45] Delightfully, **1Cu**, under the same reaction conditions, led to an excellent yield of 4-trifluoromethylbiphenyl (**2CF$_3$**, 93%) by ^{19}F NMR spectroscopy, along with the formation of $[Cs][Cu(CF_3)(I)]$ (**3Cu**) (Scheme 5.27 and Figure 5.5).

[44] We selected analogous reaction conditions to those reported previously by Vicic and co-workers. See ref. 35 for further details.

[45] Inspired by the work of Ribas *et al*. (Serra, J.; Parella, T.; Ribas, X. *Chem. Sci.* **2017**, *8*, 946), we tested the reaction of **1Au** with **4I** in DMF. Trace amount of the trifluoromethylated product was observed after heating the solution at 110 ºC after several days.

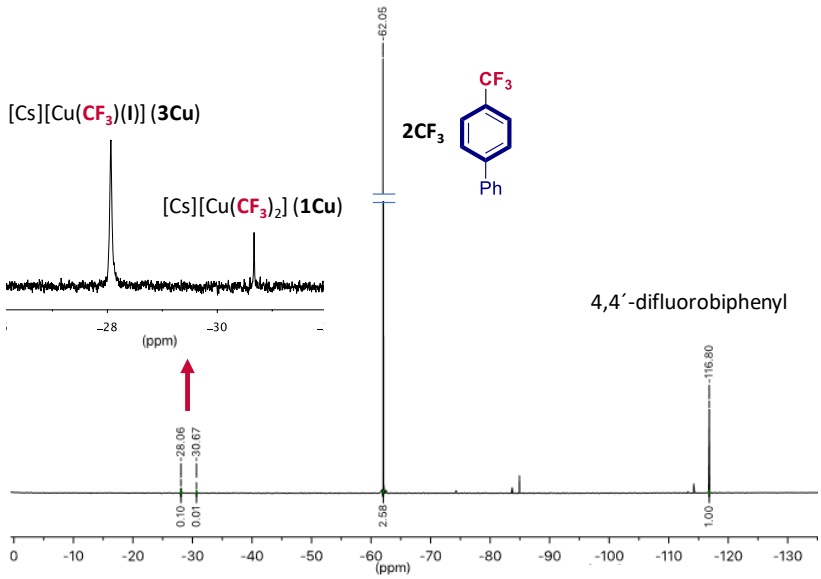

Figure 5.5. ^{19}F NMR spectrum in the region of 'CuCF$_3$' species after the trifluoromethylation reaction.

These preliminary results confirm, for the first time, the involvement of **1Cu** in the activation of **2I**, its capability to transfer the two trifluoromethyl groups, and highlights its remarkable performance compared to previously described Cu-mediated systems under analogous reaction conditions We next explored the reactivity of **1Cu** towards different representative organic electrophiles (Scheme 5.28) such as 10-iodobenzo*[h]*quinoline (**4I**), benzyl bromide (**5Br**) and methyl-6-bromopyridine-2-carboxylate (**6Br**). In all the cases, the yields were from moderate to excellent and comparable to the previously reported ones.[46] These results point out the capability of these bis-(trifluoromethyl) cuprate species to activate a variety of bonds such as Csp^2–I, Csp^2–Br and Csp^3–Br (Scheme 5.28).

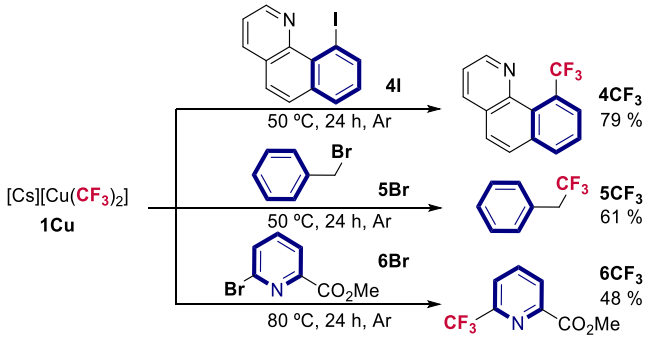

Scheme 5.28. Trifluoromethylation reactions using **1Cu** as nucleophile. Reaction conditions: **1Cu** (0.016 mmol), aryl halide (0.0256 mmol), DMF (0.6 ml), 50 ºC (**4I** and **5I**) or 80 ºC (**6Br**), 24 h under Ar. Yield calculated according to ^{19}F NMR spectroscopy using 4,4'-difluorobiphenyl as internal standard.

46 The yield for this product is lower than the reported in the literature. See ref. 31a.

5.3.2.4. Reactivity summary

To sum up the reactivity evaluation of the different bis-(trifluoromethyl) metallates (**1M**), we recovered the result for model reactions in Table 5.1.

The reaction **1Cu** and **1Ag** with I_2 did not give rise [Cs][*trans*-$M(CF_3)_2(I)_2$] (M = Cu, Ag). Instead, decomposition products including $[M(CF_3)_4]^-$ species or CF_3I (a potential reductive elimination product) were observed (Table 5.1), suggesting that those complexes, [Cs][*trans*-$M(CF_3)_2(I)_2$] (M = Cu, Ag), are not stable.

The transmetalation reaction of these metallates **1M** towards a organo-Pd(II) model system of **1Cu** and **1Au** were studied and compared to **1Ag**. Interestingly, we found that the reaction of **1Cu** and [(dppp)Pd(Ph)(I)] is faster than for **1Ag** while **1Au** is not reactive even increasing the temperature (Table 5.1).

The bis-(trifluoromethyl) cuprate (**1Cu**) promoted the trifluoromethylation reaction of aryl halides (**2I**) while silver and gold remained unreactive under the same reaction conditions (Table 5.1). We aimed at further mechanistic investigation to understand the efficiency of this cuprate **1Cu** compared to the lack of reactivity **1Ag** and **1Au** in the trifluoromethylation of aryl halides.

	Oxidation (I_2) (Scheme 5.27)	Transmetalation to (dppp)Pd(Ph)(I) (Scheme 5.25)	Trifluoromethylation of aryl iodide (**2I**) (Scheme 5.23)
[Cs][$Cu(CF_3)_2$]	Decomposition	Quantitative	93 %
[Cs][$Ag(CF_3)_2$]	Decomposition	Quantitative	-
[Cs][$Au(CF_3)_2$]	Quantitative	-	-

Table 5.1. Summary of the studied reactivity of the different coinage metallates **1M** in Chapter 4.

5.3.3. Mechanistic investigations on the reaction of [Cs][$Cu(CF_3)_2$] with aryl halides

Intrigued by spectacular performance of **1Cu** compared to its silver and gold congeners in the trifluoromethylation of aryl halides, and the experimental observation of other potentially reactive species such as **3Cu** (Figure 5.5), we decided to examine these intricacies through mechanistic studies.

5.3.3.1. Experimental mechanistic investigations

In order to evaluate the presence of radical species during the reaction, the trifluoromethylation reaction using cesium bis-(trifluoromethyl) cuprate (**1Cu**) with 1-(allyloxy)-2-iodobenzene (**7I**) was performed (Scheme 5.30). We selected this aryl halide as representative substrate due to the extremely fast cyclization reaction of the aryl radical derived from the iodoarene (Scheme 5.29).

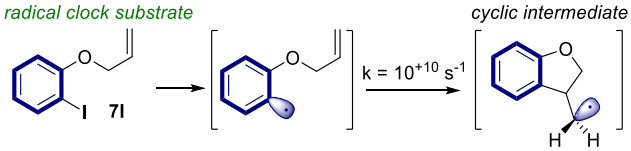

Scheme 5.29. Cyclization reaction after the formation of radical species from **7I**.

Therefore, given the fast reorganization of the radical intermediate, the presence of the corresponding cyclic product would indicate the intermediacy of radical species.[27,34,47] Under our standard conditions, we exclusively observed **7CF$_3$** (Scheme 5.30), which discards the participation of Cu(II) radical intermediates during the reaction.

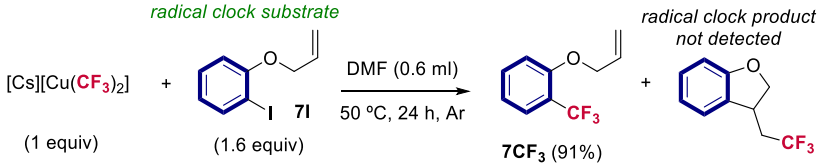

Scheme 5.30. Radical clock proof to discard the intermediacy of radical species. Yield calculated according to ^{19}F NMR spectroscopy using 4,4'-difluorobiphenyl as internal standard.

Another mechanistic information was obtained by carrying out the reaction of **1Cu** and **2I** in THF as solvent (Scheme 5.31). In this case, the formation of **2CF$_3$** was slower, leading to a 12% in 5 days at 50 ºC while this reaction takes 24 hours in DMF, as mentioned above. This suggests that the solvent may be playing a crucial role in the reaction mechanism. Indeed, as mentioned in the introduction, the use of DMF is common for the majority of Cu-mediated trifluoromethylation reactions.

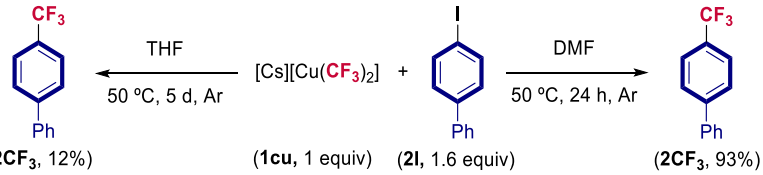

Scheme 5.31. Experimental evidence of the potential role of the solvent during the reaction mechanism.

5.3.3.2. DFT calculations on the mechanism reaction for the trifluoromethylation of aryl halides

With these pieces of information in hand, we next performed DFT calculations to uncover the mechanism that underlies this transformation.[23,26,48] Our computational study was carried out with the M06 functional with a double-ζ plus polarization basis set in a DMF continuum solvent. We used phenyl iodide as a model reagent and we did not include the countercation of

47 Abeywickrema, A. N.; Beckwith, A. L. J. *J. Chem. Soc. Chem. Commun.* **1986**, 464.
48 Yu, D.-H.; Shao, J.-N.; He, R.-X.; Li, M. *Chin. Chem. Lett.* **2015**, *26*, 564.

1M in the calculations for simplicity. Indeed, previous experimental and theoretical data for **1Ag**, analogous to copper complex, suggest no contribution of ion pairs in DMF.[49]

In alignment with the experimental results when using **7I** as substrate, preliminary calculations allowed us to rule out radical mechanisms with involvement of Cu(II) intermediates. These intermediates have been considered to be formed either through a Single Electron Transfer (SET) from the cuprate to the aryl halide or through a Halogen Atom Transfer (HAT). Both mechanism are depicted in Scheme 5.32 (further details can be found in the Computational appendix). As we can see, the free energy to reach those potential Cu(II) intermediates are restrictive at the working temperature (50 ºC).

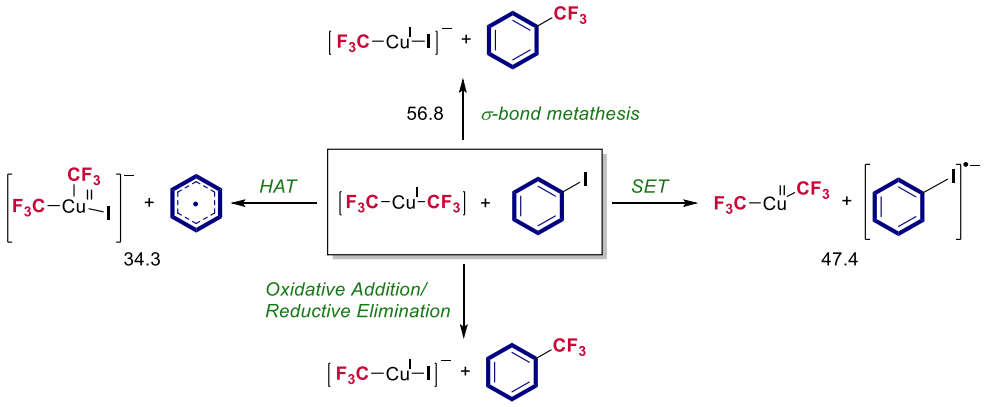

Scheme 5.32. Alternative mechanisms proposed for the trifluoromethylation of aryl halides when using cuprates. Free energies in kcal·mol^{-1}.

We also investigated the concerted σ-bond metathesis mechanism proposed by Goossen (Scheme 5.11).[13] This mechanism exhibited a free energy barrier of 56.8 kcal·mol^{-1}, even higher than the restrictive free energy differences for the radical mechanisms.

Our DFT calculations suggest that the Oxidative Addition (OA)/Reductive Elimination (RE) sequence is the most favorable pathway for this transformation and it will be discussed in more details below for each bis-(trifluoromethyl) metallate (**1M**).

- **Oxidative Addition/Reductive Elimination (OA/RE) sequence**

Our favored mechanism involves oxidative addition (OA) through a concerted transition state to form Cu(III) intermediates, as shown in Scheme 5.33 and Scheme 5.35. We first analyzed the direct involvement of species $[Cu(CF_3)_2]^-$, labeled as **I1Cu**, as the trifluoromethylating agent. The free energy profile, depicted in Scheme 5.33, shows a quite high barrier of 29.2 kcal·mol^{-1} for the oxidative addition step (**TS I1-I2Cu**), which would lead to an extremely slow trifluoromethylation process under the experimental conditions. Regarding gold and silver analogues (**I1Au** and

[49] Previous experimental and theoretical data for **1Ag** suggest no contribution of ion pairs in DMF. See Appendix chapter 2 for further details.

I1Ag), the oxidative addition processes are much higher in energy (5.2 and 16.2 kcal· mol^{-1}, respectively). Notably, although kinetically not accessible, Au(III) species (**I2Au**) is more stable than its copper (**I2Cu**) and silver (**I2Ag**) congeners.

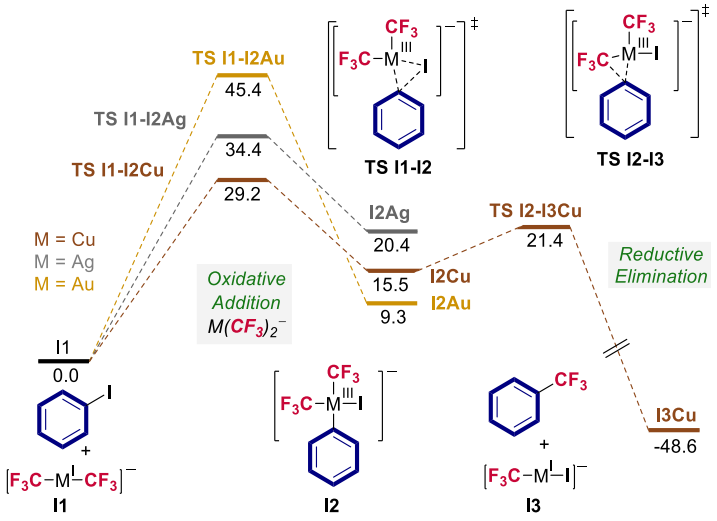

Scheme 5.33. Computed energy profile for the oxidative addition and reductive elimination sequence of different $[M(CF_3)_2]^-$ complexes. Free energies (kcal·mol^{-1}) are calculated using M06(SMD,DMF)/6-31+G(d,p)-SDD(Cu) at 50 ºC and 1M.

Since the oxidative addition step of iodobenzene to **I1Cu** is not able to explain the formation of α,α,α-trifluorotoluene in the reaction conditions, we investigated other potential reactive species such as $[Cu(CF_3)(I)]^-$, **I3Cu**, or [(DMF)Cu(CF_3)], **I4Cu**. The OA barrier of iodobenzene to **I3Cu** is 24.1 kcal·mol^{-1}(Scheme 5.33), still a high barrier and incompatible with the experimental reaction time. Interestingly, when considering, **I4Cu** the situation changes and the oxidative addition is an accessible event at the working temperature (50 ºC) with a barrier of 21.7 kcal mol^{-1}, **TS I4-I5Cu** (Scheme 5.35). It should be noticed that, although this copper species (**I4Cu**) is not among the initial species in solution, it can be generated efficiently during the trifluoromethylation reaction through the nearly thermoneutral equilibria outlined in reactions 1–3 (Scheme 5.34). The general mechanistic picture is explained below.

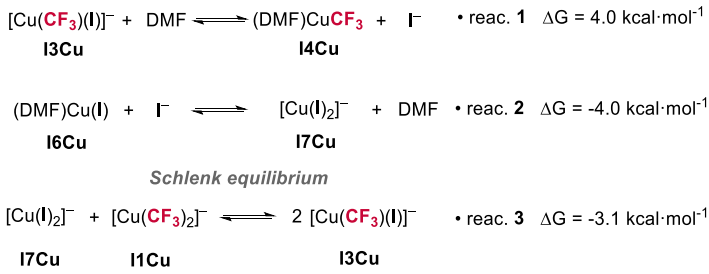

Scheme 5.34. Speciation of copper(I) complexes in the reaction media. Free energies in kcal·mol^{-1}.

The initial generation of **I4Cu** will come from ligand substitution in **I3Cu**, which is the side product in the initial, slow, trifluoromethylation process, shown in Scheme 5.33.[50] Once a critical concentration of **I4Cu** is reached, the second, faster, trifluoromethylation starts with an affordable barrier and this generates as the side product [(DMF)Cu(CF$_3$)], **I4Cu**, which, through the equilibria in reactions 2 and 3 (Scheme 5.34), can regenerate **I4Cu** and restarts the process. Interestingly, this proposed mechanism is in alignment with the beneficial effect observed when using DMF as solvent (Scheme 5.31).

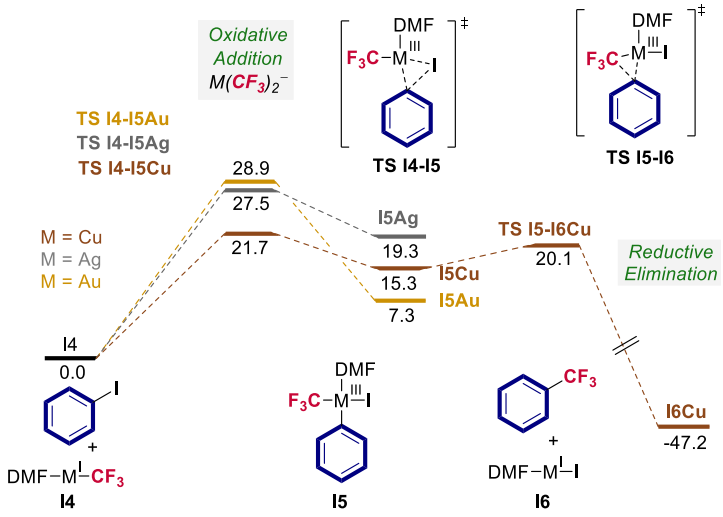

Scheme 5.35. Computed energy profile for the oxidative addition and reductive elimination sequence of different [(DMF)M(CF$_3$)] complexes. Free energies (kcal·mol^{-1}) are calculated using M06(SMD,DMF)/6-31+G(d,p)-SDD(Cu) at 50 ºC and 1M.

It is noteworthy that for silver and gold analogous systems (Scheme 5.33 and Scheme 5.35), we found that the paucity of reactivity towards the trifluoromethylation of aryl halides is related to a sluggish oxidative addition event regardless the speciation in DMF. The increased barrier when going from copper to gold correlates with the nucleophilic character of the different metalates, as shown in Figure 5.3.

50 The displacement of I$^-$ in this species has been proposed to occur by water in similar systems. See ref. 20.

- **Rationalizing the origin of the behavior of the different cuprates towards the OA.**

To a certain extent, it is counterintuitive that the neutral **I4Cu** species is a better trifluoromethylating agent than the anionic complex **I1Cu**, considering than the negatively charged **I1Cu** should stabilize a Cu(III) species, in high oxidation state (Scheme 5.33 and Scheme 5.35). For this reason, we analyzed in-depth which is the origin of the stabilization of the different Cu(III) species that could be formed in the reaction media (**Figure 5.6**).

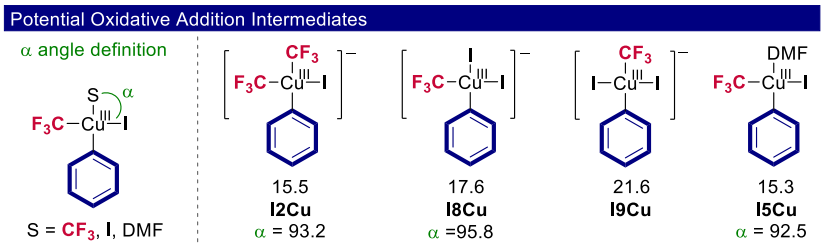

Figure 5.6. Relative stabilities for different Cu(III) complexes considering the origin of energy in the corresponding Cu(I) species plus PhI. Free energies in kcal·mol^{-1}.

Four different copper(III) species were considered bearing different ligands with different geometric isomerism which could be generated after the oxidative addition step. Among them, the most unstable is **I9Cu**. The mayor structural difference of this complex from the others is that the nearly linear {CF_3–Cu–I} moiety is not present (Figure 5.6), suggesting that this arrangement of the ligands can stabilize the other complexes.

Both the electronic and steric properties of the ligands have a role to play in the stabilization of the Cu(III) species (**I2Cu**, **I5Cu** and **I8Cu**). Specifically, CF_3 ligands have been described as strong σ-donor ligands with a strong *trans* influence. These ligands can donate electronic density to the metal center and stabilize Cu(III) intermediates.[51] If we compare **I2Cu** and **I8Cu**, we observe that the relative energy increases when the CF_3 is exchanged by an iodine atom. This happens because the iodine ligand, more polarizable, withdraw electronic density from copper metal center in high oxidation state. This makes **I8Cu** intermediate electronically more unstable. On the other hand, the steric hindrance of the iodine atom, bigger than the CF_3 group, could have also an influence in the destabilization of **I8Cu** intermediate. This effect can be seen in the α angle (Figure 5.6). The wider the angle, the bigger the steric hindrance.

It could seem counterintuitive that the neutral Cu(III) intermediate **I5Cu** is as stable as intermediate **I2Cu**, a negative complex. A reasonable explanation for this could be the release of the steric strain when a smaller and labile ligand, as DMF, replaces the iodide or trifluoromethyl group.

51 Algarra, A. G.; Grushin, V. V.; Macgregor, S. A. *Organometallics* **2012**, *31*, 1467.

Regarding the transition states, we looked for an explanation for the observed trend for **TS I1-I2Cu**, **TS I3-I8Cu** and **TS I4-I5Cu**. When comparing **TS I1-I2Cu** and **TS I3-I8Cu**, we found that the variation of the distance between the group *trans* to the phenyl moiety (labeled as S in Figure 5.7) and the metal center during the transition state (Δd) can explain the observed free energy barrier trend. We proposed that the iodide can partially decoordinate and easily accommodate the substrate during the transition state (Δd = 0.24). However, **TS I1-I2Cu** is unfavored because the CF_3 ligand remains anchored to the metal center during the OA step (Δd = 0.08). In the case of DMF, a labile ligand and smaller than iodide, the process is more kinetically favored (**TS I4-I5Cu**). The same trend for the oxidative addition barrier considering different 'Cu(CF_3)' species was previously reported by Grushin but further details were not discussed.

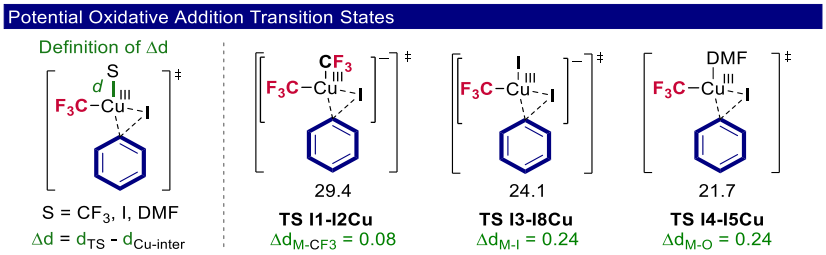

Figure 5.7. Oxidative addition barriers for considering as origin of energy the corresponding Cu(I) species + PhI. Free energies in kcal·mol^{-1}.

- **Microkinetic modelling considering the complex mechanistic scenario.**

Given the complexity of the system, our DFT proposal was surveyed by microkinetic modeling,[52] in which the evolution of concentrations through time is estimated from experimental initial concentrations and theoretically-computed rate constants (discussed in Chapter 1). The considered reactions for the microkinetic model and rate constants are depicted in Scheme 5.36.

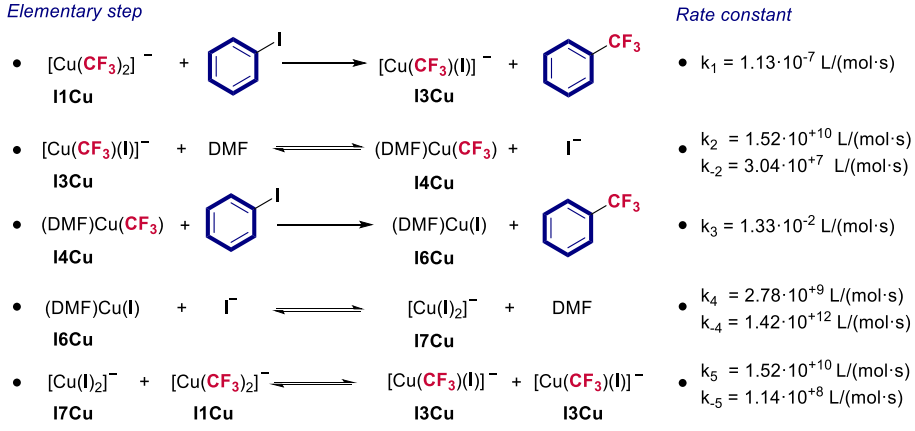

Scheme 5.36. Elementary steps for the formation of $PhCF_3$ considering as active species **I1Cu** and **I4Cu** considered in the microkinetic model.

52 Besora, M.; Maseras, F. *Wiley Interdiscip. Rev.: Comput. Mol. Sci.* **2018**, *8*, e1372.

Computationally, the microkinetic model predicts that the reaction starts in 4 hours and reach full conversion after 13 hours (Scheme 5.37). This result computed reaction time is comparable to the experimental data in spite of the high barrier of 29.2 kcal mol^{-1} for the first trifluoromethylation step (Scheme 5.33).[53] Interestingly, an induction period, required for the generation of [(DMF)Cu(CF_3)], is also predicted.

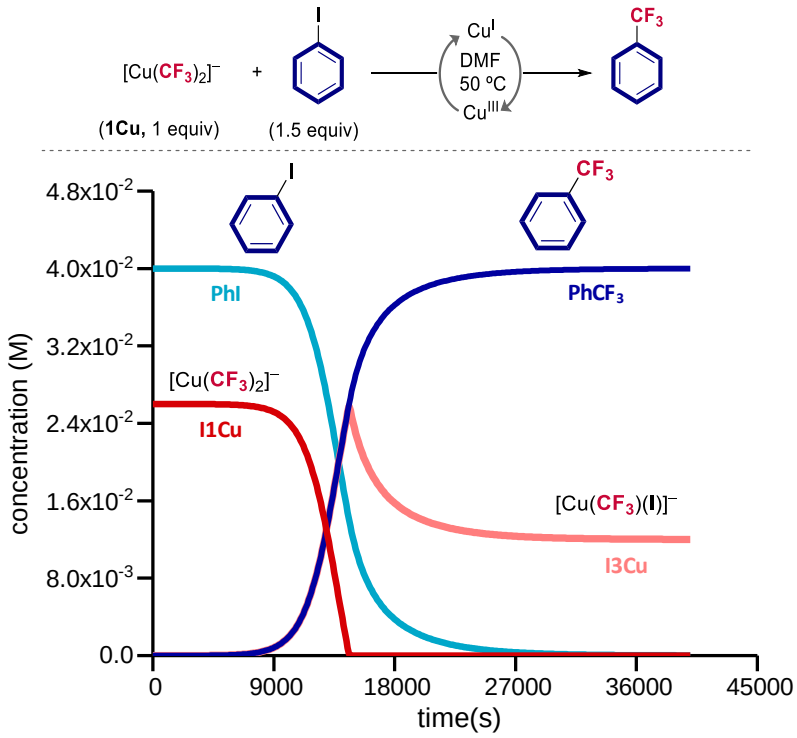

Scheme 5.37. Evolution of the concentration of different species according to the microkinetic model considering **I1Cu** and **I4Cu** as active species (Scheme 5.36).

Our DFT mechanistic proposal was supported by microkinetic modeling. Under our reaction conditions, **I1Cu** acts as CF_3 reservoir, in which [(DMF)Cu(CF_3)] is the most active species towards the oxidative addition step.[26] We then aimed to experimentally corroborate this theoretical mechanistic scenario with these two concatenated pathways and find the predicted induction period. To do so, we used ^{19}F NMR spectroscopy to monitor the trifluoromethylation reaction of **2I**, first forming a mixture of **1Cu** and **1Ag** (83:17) using substoichiometric amounts of CuI with respect to **1Ag**, and next adding excess of CuI. Our goal was to ensure that, initially, all the copper was speciated as **1Cu**. Based on reactions 1–3 (Scheme 5.34), in the absence of excess of I^-, **3Cu** (**I3Cu**) would not be formed, hindering the most facile route shown in Scheme 5.35 and observing a delay in the formation of **2CF₃** due to the proposed induction period. Under

[53] Regarding this scenario for silver, the reaction finishes after 12 years using the experimental concentration of the reagents.

these substoichiometric conditions, after 20 h at 50 ºC, we observed the trifluoromethylated product in only 4% yield.[54] As predicted by DFT, when we added an excess of CuI (4.2 equiv) a mixture containing **1Cu** along with $[Cu(CF_3)(I)]^-$ (**1Cu,** 33.3%; **3Cu**, 64.9%) is formed and we observed a dramatic increase in the yield of **2CF$_3$** (55% after approx. 4 hours). Moreover, we detected the appearance of not only [Cs][Cu(CF$_3$)(I)] (s, δ = –27.4 ppm), but also [(DMF)Cu(CF$_3$)] (broad signal, δ = –25.7 ppm; 1.8%), the reactive species based on our DFT calculations (Scheme 5.38 b)).[55]

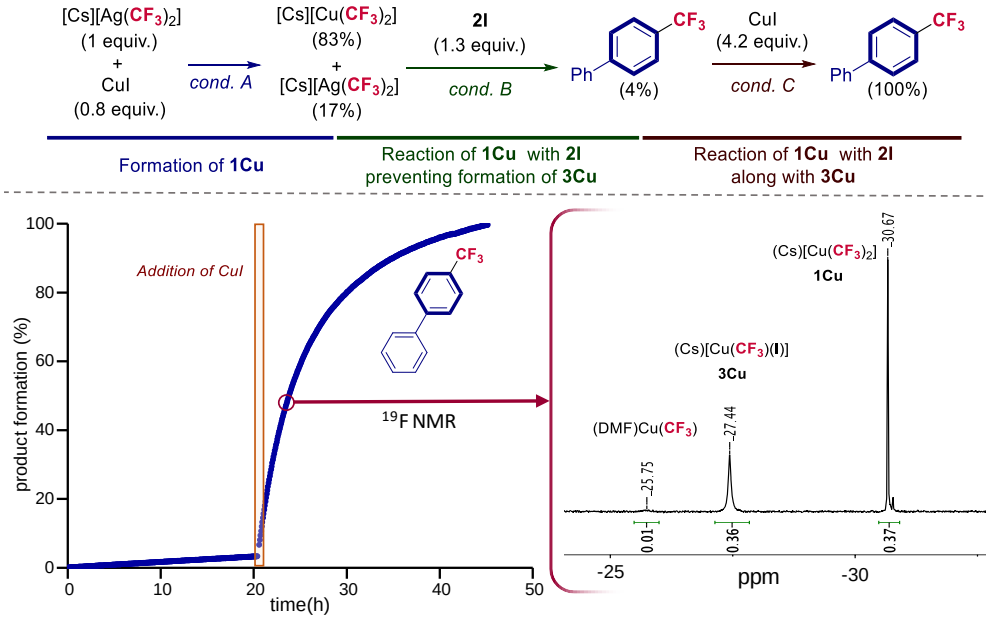

Scheme 5.38. Above, experimental sequence for verifying the DFT-suggested induction period. Cond. A: DMF, 30 min, rt, Ar; Cond. B: DMF, 20 h, 50 ºC, Ar; Cond. C: DMF, 24 h, 50 ºC, Ar. Below left: Kinetic experiment using **1Cu** before and after the addition of excess of CuI. Below right: ^{19}F NMR spectrum showing the different Cu(I) species present in the trifluoromethylation reaction of **2I**, 4 hours after the addition of CuI (**1Cu**, 33.3%; **3Cu**, 64.9%; [(DMF)Cu(CF$_3$), 1.8%)

This study is an example of the potential of combining DFT calculations and microkinetic modelling to predict experimental outcomes and validate reaction mechanisms. The selective access to the bis-(trifluoromethyl) cuprate (**1Cu**) allowed us to describe its nature as CF$_3$ reservoir in Cu-mediated trifluoromethylation reactions.

54 The different yield of **2CF$_3$** in comparison with the one obtained in Scheme 5.27 or Scheme 5.37 can be explained by two main reasons: i) No stirring in the reaction media and ii) the presence of **1Ag** that could avoid the generation of $[Cu(CF_3)(I)]^-$ or [(DMF)Cu(CF$_3$)].

55 We observed a variation in the chemical shift of $[Cu(CF_3)(I)]^-$ during the reaction, from –26.83 to –28.00 ppm, due to the formation of $[Cu(I)_2]^-$. This indicates a more complex scenario respect to the speciation of copper species as mentioned by Hu and co-workers (ref. 50) and the formation of species such as $\{[Cu(CF_3)(I)]_x\}^{x-}$ $\{[Cu(I)_2]_y\}^{y-}$.

5.4. Conclusions

In summary, in Chapter 4, we have discussed the synthesis of [Cs][M(CF_3)$_2$], (M = Cu (**1Cu**), Au (**1Au**)) and analyzed their structural features along with [Cs][Ag(CF_3)$_2$] complex (**1Ag**). Additionally, we have surveyed their electronic properties by DFT calculations, explaining the bonding situation of the σ-M–C bond and stablishing a scale of nucleophilicity.

We have further compared their reactivity towards different electrophiles. The reaction of **1Cu** and **1Ag** with I_2 to yield [Cs][*trans*-M(CF_3)$_2$(I)$_2$] failed, suggesting that those high-valent species are more unstable than [Cs][*trans*-Au(CF_3)$_2$(I)$_2$] complex. The transmetalation capabilities towards a organo-Pd(II) model system of **1Cu** and **1Au** were also studied and compared to **1Ag**. Additionally, we further discussed the potential implication of **1M** in the trifluoromethylation reaction of aryl halides, focused our attention on the homoleptic cuprate (**1Cu**). This allowed us not only to unravel the non-innocent role of **1Cu** in Cu-mediated trifluoromethylation reactions, but also to disclose a complex underlying $Cu^{I/III}$ reaction mechanism where [(DMF)Cu(CF_3)] intermediate is the most reactive species. DFT calculations, microkinetic modelling and experiments support our mechanistic proposal and explain the paucity of reactivity of silver and gold complexes.

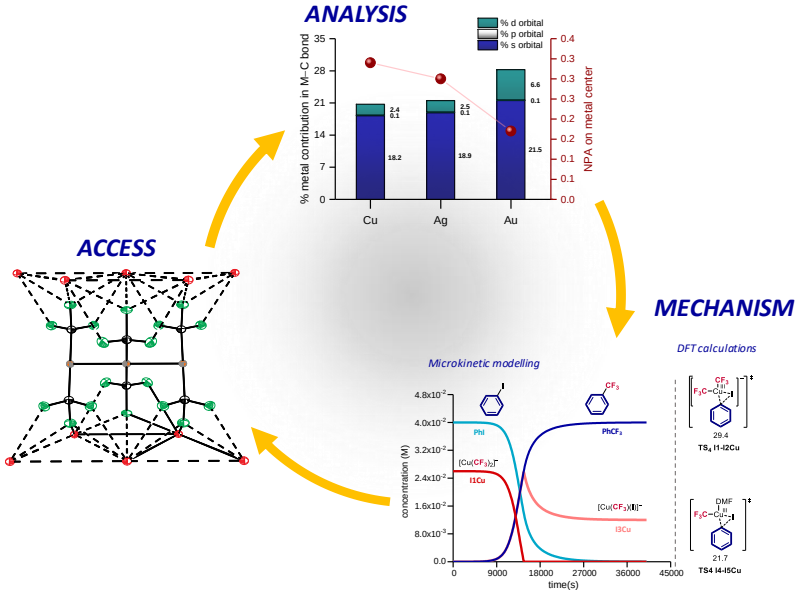

Figure 5.8. Graphical summary of the Chapter 5.

5.5. Appendixes

5.5.1. Experimental appendix

5.5.1.1. General procedures

All reactions were conducted in an argon-filled glovebox (mBraun Unilab 4420) with concentrations of O_2 and H_2O < 0.1 ppm or oven-dried glassware (at 100 ºC overnight and cooled under vacuum prior use) using Schlenk techniques under argon atmosphere (otherwise mentioned).

NMR spectra were obtained on a Bruker 400 MHz, a 500 MHz or a 500 MHz with cryoprobe spectrometers equipped with probeheads capable of producing gradients in the z direction with a maximum strength of 53.5 G·cm^{-1}. ^{1}H, ^{13}C and ^{19}F NMR chemical shifts are reported in parts per million (ppm), relative to tetramethylsylane (TMS) for ^{1}H and ^{13}C with the residual solvent peak used as an internal reference and relative to $CFCl_3$ (Freon) for ^{19}F. In the ^{19}F registered in non-deuterated solvents, a coaxial tube containing acetone-d_6 or dimethylsulfoxide-d_6 was used to maintain the lock ^{2}H signal. Multiplicities are reported as follows: singlet (s), broad singlet (bs), triplet (t), quadruplet of quadruplets (qq) and multiplet (m). The monitorization of the reaction and the product quantification were determined by on a Bruker 400 MHz internal calibration using 4,4'-difluorobiphenyl (–116.8 ppm), fluorobenzene (–113.15 ppm) and hexafluorobenzene (–164.9 ppm) with 32 scans for data acquisition. High Resolution Mass Spectrometry (HRMS) data was recorded on LCT-Premier (Waters) or a MicroTOF Focus (Bruker Daltonics) mass spectrometers using ESI ionization technique and dichloromethane, tetrahydrofuran, methanol or acetonitrile as solvent.

The details for the X-ray structure determination can be found in page - 300 -.

5.5.1.2. Materials and methods

Commercially available reagents AgOAc, CsF, CuI, $KAuCl_4$, fluorobenzene, 4,4'-difluorobiphenyl, hexafluorobenzene, 4-(trifluoromethoxy)anisole, Me_3SiCF_3, 4-iodobiphenyl, methyl-6-bromopyridine-2-carboxylate, benzyl bromide, 2-iodophenol, allyl bromide, dimethylsulfide and K_2CO_3 were used without further purification directly as received from the commercial supplier, and stored under inert gas and/or low temperature when required. If necessary, the solvents (MeOH, EtOH, Hexane, THF, CH_2Cl_2, toluene, Et_2O and DMF) were used from a solvent purification system *pure-solv* (SPS-400, Innovative Technology) and stored under argon over activated 4 Å molecular sieves. THF-d_8 was stored under argon over activated molecular sieves 4 Å. The compounds 10-iodobenzo*[h]*quinolone,[56] 1-(allyloxy)-2-

[56] Serra, J.; Parella, T.; Ribas, X. *Chem. Sci.* **2017**, *8*, 946.

iodobenzene,[57] AuCl·SMe_2,[58] [Cs][Ag(CF_3)$_2$] (**1$_{Ag}$**) and [(dppp)Pd(Ph)(I)][2e] were synthesized according to previous literature procedures.

5.5.1.3. *In situ* synthesis and characterization of 1Cu

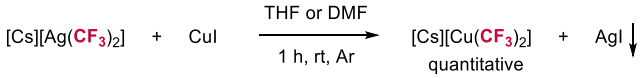

Scheme A5.1.Schematic for the formation of **1Cu**.

In an argon atmosphere glovebox, a crimped vial was charged with [Cs][Ag(CF_3)$_2$] (5.9 mg, 0.016 mmol, 1 equiv) and CuI (3.0 mg, 0.016 mmol, 1 equiv) and a known amount of the internal standard, 4,4'-difluorobiphenyl. The mixture was dissolved in 0.6 ml of THF or DMF and stirred at room temperature for 1 hour. The solution was then filtered using a PTFE 13mm 0.2µm NSTR syringe filter and transferred to a J-young NMR tube to be analyzed by ^{19}F NMR spectroscopy. In both cases, in THF or DMF, we observed full conversion into **1Cu**. Although this bis-trifluoromethyl ate-type complex of copper is highly unstable, crystals of **1Cu** were grown in a concentrated solution in DMF:THF:DCM (0.05:0.1:1) at –30 ºC inside the glovebox.

^{19}F NMR (470 MHz, acetone-d_6, 25 ºC): δ -30.71 (s) (THF) or -31.12 (s) (DMF) ppm. **^{13}C{^{1}H} NMR** was acquired during three days and no signal was detected due to the C−F coupling. **HRMS-electrospray (-) in DMF:THF:DCM (0.05:0.1:1) (m/z)**: $[M]^-$ calcd. for C_2CuF_6, 200.921 and 202.9182; found 200.9216 and 202.9194.

- **Preparation of a stock solution of 1Cu**

In an argon atmosphere glovebox, a crimped vial was charged with [Cs][Ag(CF_3)$_2$] (8.5 mg, 0.022 mmol, 1 equiv) and CuI (4.3 mg, 0.022 mmol, 1 equi.) and a known amount of the internal standard, 4,4'-difluorobiphenyl. The mixture was dissolved in 3 ml of THF and stirred at room temperature for 2 h and 30 min. The solution was then filtered using a PTFE 13mm 0.2µm NSTR syringe filter and transferred to another crimped vial that was stored at –30 ºC inside the glovebox. After 15 days, the solution of **1Cu** in THF loses around 10% of its mass balance with the appearance of $[Cu(CF_3)_4]^-$ in the ^{19}F NMR spectra.

57 Zhanga, H.; Huang, X.; *Adv. Synth. Catal.* **2016**, *358*, 3736.
58 Hooper, T. N.; Butts, C. P.; Green, M.; Haddow, M. F.; Mcgrady, J. E.; Russell, C. A. *Chem. Eur. J.* **2009**, *15*, 12196.

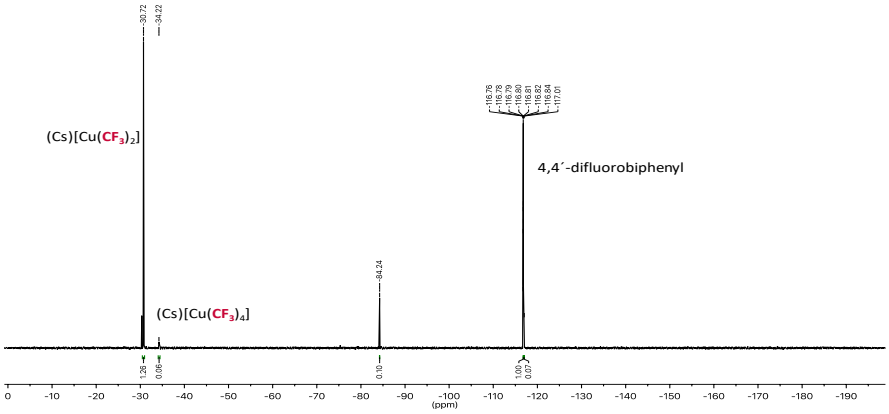

Figure A5.1. ^{19}F NMR spectrum of **1Cu** at 25 ºC in THF (acetone-d_6) measured after 15 days at -30 ºC.

- **Stability of complex 1Cu**

A J-young NMR tube was charged with **1Cu** (0.6 ml of a 0.0075 M stock solution, 0.0045 mmol) and left standing at room temperature. ^{19}F NMR spectra were acquired the next day and the mass percentage was determined by comparing the original mass of the sample to the number of moles of **1Cu** respect to 4,4'-difluorobiphenyl as standard. The solution of **1Cu** in THF loses around 18% of its mass balance after one night at room temperature.

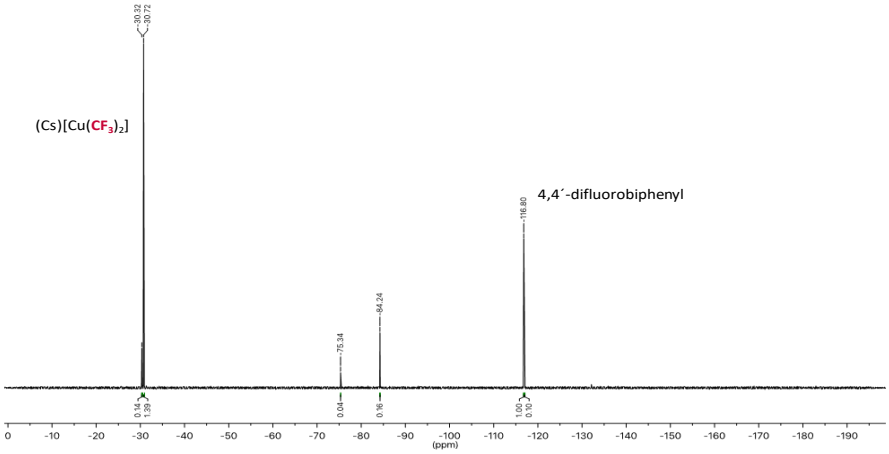

Figure A5.2. ^{19}F NMR spectrum of **1Cu** at 25 ºC in THF (acetone-d_6) measured after one day at room temperature.

5.5.1.4. **Synthesis and characterization of 1Au**

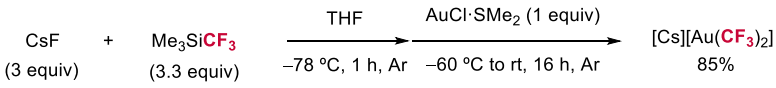

Scheme A5.2. Schematic for the formation of **1Au**.

In an argon atmosphere glovebox, a Schlenk flash was charged with CsF (154 mg, 0.99 mmol, 3 equiv) and Me_3SiCF_3 (162 μL, 3.28 mmol, 3.3 equiv) and it was dissolved in 5 ml of THF. The mixture was stirred during 1 h at –80 ºC. At this point, AuCl·SMe_2 (100 mg, 0.34 mmol, 1 equiv) was added at –60 ºC and the reaction was left stirring during 16 h while room temperature is achieved. The resulting white suspension was filtered through cannula and the solution was then reduced to dryness under vacuum at this temperature. The blue oily residue was recrystallized in a mixture of THF (1 ml) and hexane (20 ml) and the resulting blue solid was washed with hexane (2 x 10 ml). The blue solid (135 mg, 85% yield) is air and temperature stable. Crystals of **1Au** were grown in a mixture of THF and hexane at room temperature.

^{19}F NMR (470 MHz, THF-d_8, 25 ºC): δ –29.88 (s) ppm. **^{13}C{^{1}H} NMR** (126 MHz, THF-d_8, 25 ºC): δ 161.4 (qq, $^1J_{C,F}$ = 345.3 Hz, $^3J_{C,F}$ = 16.9 Hz) ppm.[59] **HRMS-electrospray (-) in MeOH (m/z)**: $[M]^-$ calcd. for C_2AuF_6, 334.9795; found 334.9579.

- **Unfruitful synthesis of 1Au using a transmetalation reaction**

AuCl·SMe_2 and [Cs][Ag(CF_3)$_2$] were mixed in THF under different conditions (temperature, ratio between complexes, time), but in all the cases these reactions led to a mixture of species including **1Au**.

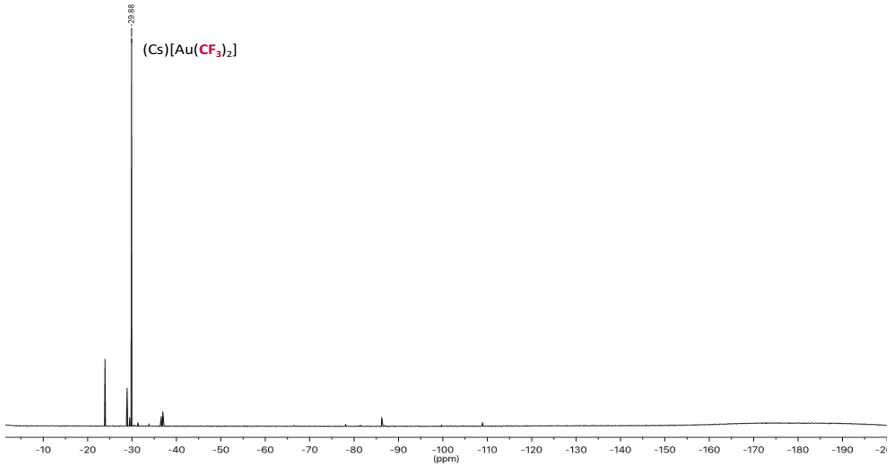

Figure A5.3. ^{19}F NMR of a transmetalation reaction between AuCl·SMe_2 and [Cs][Ag(CF_3)$_2$].

[59] This multiplicity is in accordance with the previously-described in ref. 1a. In Chapter 1, the ^{13}C spectrum of **1Ag** (specifically labelled $\mathbf{6}_{\mathbf{NBu4}}$ for being stabilized by NBu_4 cation) is described in detail.

5.5.1.5. Synthesis and characterization of [Cs][trans-Au(CF$_3$)$_2$(I)$_2$]

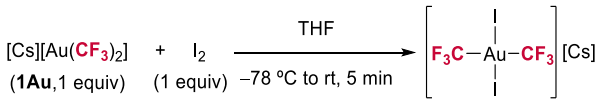

Scheme A5.3. Schematic for the formation of [Cs][*trans*-Au(CF$_3$)$_2$(I)$_2$].

Under air, a Schlenk flash was charged with **1Au** (11.2 mg, 0.024 mmol, 1 equiv) and I$_2$ (6 mg, 0.024 mmol, 1 equiv) and it was dissolved in 0.6 ml of THF at -80 ºC. Then, the mixture was stirred during 15 min at room temperature changing from a brown suspension to an orange solution that was precipitated using hexane (5 ml). The resulting orange solid was washed with hexane (5 x 10 ml). The orange solid (15 mg, 90% yield) is air and temperature stable. Crystals of [Cs][*trans*-Au(CF$_3$)$_2$(I)$_2$] were grown in a mixture of THF and hexane at room temperature.

^{19}F NMR (470 MHz, acetone-d_6, 25 ºC): δ –13.01 (s) ppm. **HRMS-electrospray (-) in MeOH (m/z)**: [M]$^-$ calcd. for $C_2AuF_6I_2$, 588.7659 found 588.7667.

Similar procedure was followed for the attempts to synthetize copper and silver analogous.

5.5.1.6. Reaction of the model substrate (4-iodobiphenyl) (2I) and the bis-(trifluoromethyl) metallate complexes

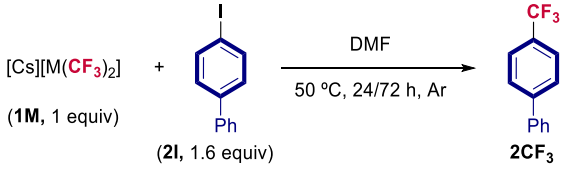

Entry	1M	2CF$_3$ (%)
1	**1Au**	-
2	**1Ag**	-
3	**1Cu**	93

Scheme A5.4. Schematic for the reaction of the different metallates towards 4-iodobiphenyl.

- **For 1Cu**

In an argon atmosphere glovebox, a crimped vial was charged with [Cs][Ag(CF$_3$)$_2$] (5.9 mg, 0.016 mmol, 1 equiv) and CuI (3.0 mg, 0.016 mmol, 1 equiv). The mixture was dissolved in 0.6 ml of DMF and stirred at room temperature for 30 minutes. The solution was then filtered using a 0.2 mm PTFE filter and transferred to another crimped vial, that contained the 4-iodobiphenyl (7.0 mg, 0.0256 mmol, 1.6 equiv) and a known amount of the internal standard, 4,4'-difluorobiphenyl. The mixture was stirred at 50 ºC during 24 hours and it was directly transferred to an NMR tube to obtain the ^{19}F NMR spectra. The yield was determined by comparing the original mass of the initial organic substrate (limiting reactive) to its number of moles versus the internal standard. This reaction was performed at least three times and the yield is the average of the different runs.

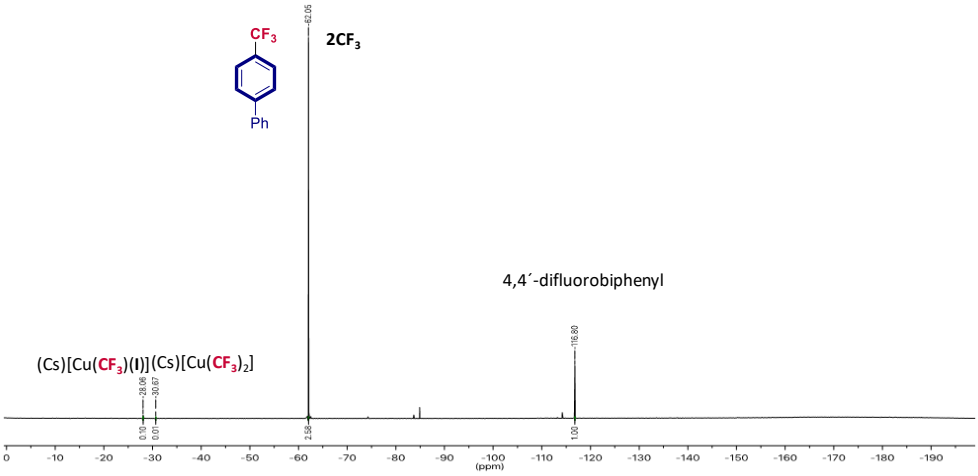

Figure A5.4. ^{19}F NMR spectrum of the reaction between **1Cu** and **2I** at 50 ºC in DMF (acetone-d_6) after 24 hours measured at room temperature.

When the same reaction of **1Cu** and **2I** was performed in THF as solvent the formation of **2CF$_3$** is really slow, leading to a 12% yield in 5 days at 50 ºC.

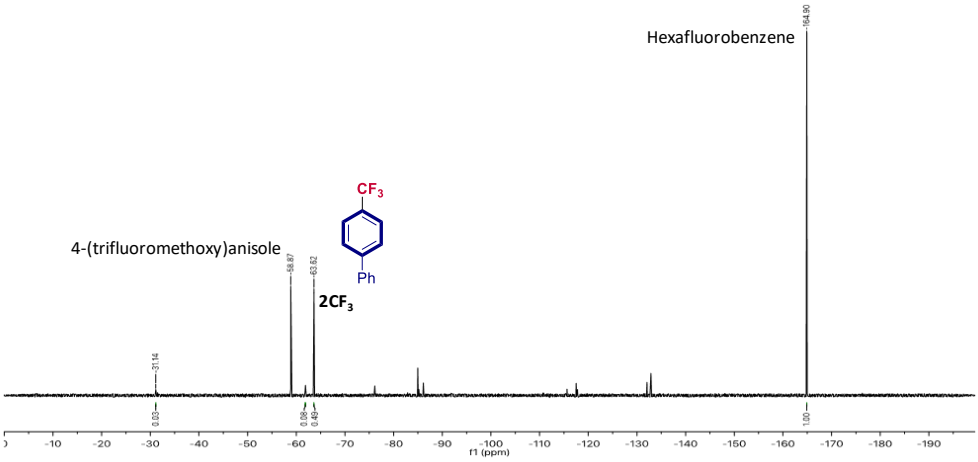

Figure A5.5. ^{19}F NMR spectrum of the reaction between **1Cu** and **2I** at 50 ºC in THF (acetone-d_6) after 120 hours measured at room temperature.

- **For 1Ag and 1Au**

In an argon atmosphere glovebox, a crimped vial was charged with [Cs][Ag(CF$_3$)$_2$] (5.9 mg, 0.016 mmol, 1 equiv) or [Cs][Au(CF$_3$)$_2$] (7.3 mg, 0.016 mmol, 1 equiv), 4-iodobiphenyl (7.0 mg, 0.0256 mmol, 1.6 equiv) and a known amount of the internal standard, 4,4'-difluorobiphenyl and it was dissolved in 0.6 ml of DMF. The mixture was stirred at 50 ºC for 72 hours and it was directly transferred to an NMR tube to obtain the ^{19}F NMR spectra. The yield was determined

by comparing the original mass of the initial organic substrate (limiting reactive) to its number of moles versus the internal standard. In both cases there is no reaction and the starting metallate complexes and/or decomposition products are observed in solution.

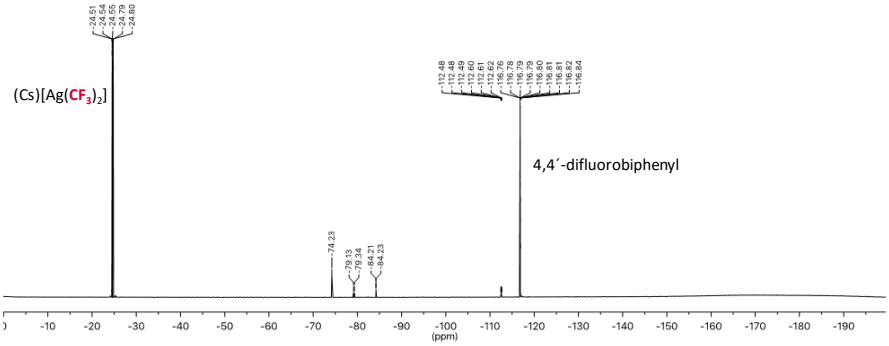

Figure A5.6.[19]F NMR spectrum of the reaction between **1Ag** and **2I** at 50 ºC in DMF (acetone-d_6) after 72 hours measured at room temperature.

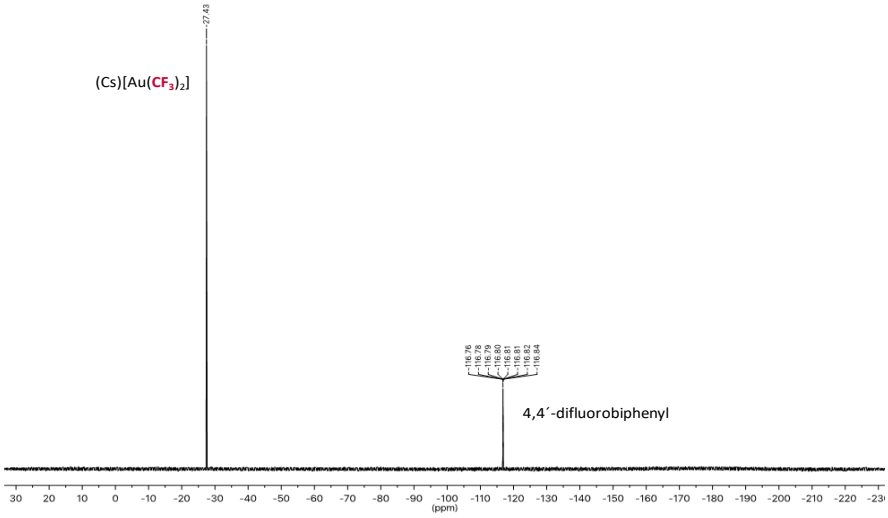

Figure A5.7.[19]F NMR spectrum of the reaction between **1Au** and **2I** at 50 ºC in DMF (acetone-d_6) after 72 hours measured at room temperature.

5.5.1.7. Characterization of organic compounds $4CF_3$, $5CF_3$, $6CF_3$ and $7CF_3$

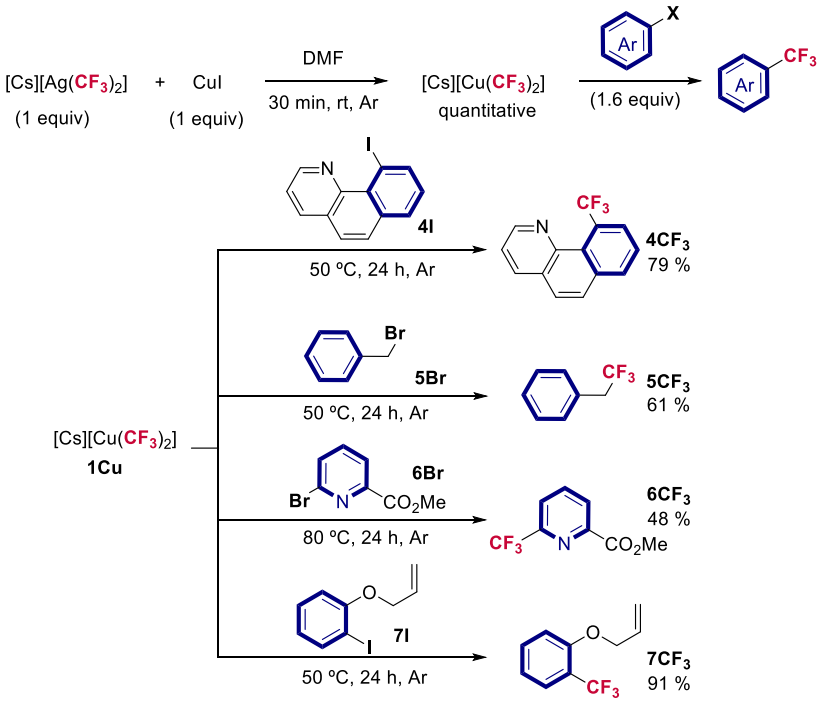

Scheme A5.5. Schematic for the scope of the trifluoromethylation of different aryl halides using the homoleptic cuprate **1Cu**.

In an argon atmosphere glovebox, a crimped vial was charged with $[Cs][Ag(CF_3)_2]$ (5.9 mg, 0.016 mmol, 1 equiv) and CuI (3.0 mg, 0.016 mmol, 1 equiv). The mixture was dissolved in 0.6 ml of DMF and stirred at room temperature for 30 minutes. The solution was then filtered using a 0.2 mm PTFE filter and transferred to another crimped vial, that contained the organic substrate (0.0256 mmol, 1.6 equiv) and a known amount of the internal standard, 4,4'-difluorobiphenyl. The mixture was stirred at 50 ºC (substrates **4Br**, **5Br** and **7I**) or 80 ºC (substrate **6Br**) for the corresponding time (24 hours) and it was directly transferred to an NMR tube to obtain the ^{19}F NMR spectra. The yield was determined by comparing the original mass of the initial organic substrate (limiting reactive) to its number of moles versus the internal standard. All the reactions were performed three times and the yield is the average of the different runs.

The reaction of **7I** with **1Cu** yielded exclusively **$7CF_3$** organic product. The organic product can be univocally detected by ^{19}F NMR since **$7CF_3$** appears as a singlet signal at –61.4 ppm, while the cyclic compound is represented by a triplet signal at –65.2 ppm.

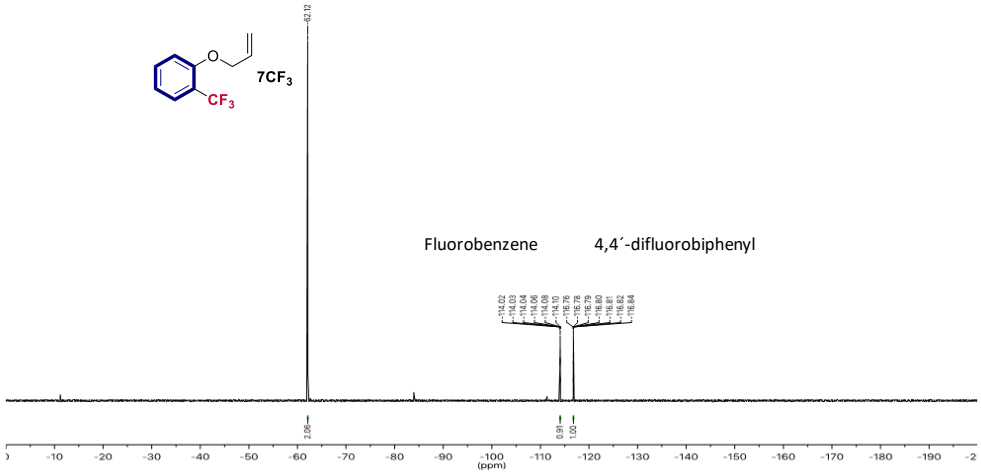

Figure A5.8.[19]F NMR spectrum of the reaction between **1Cu** and **7I** at 50 ºC in DMF (acetone-d_6) after 24 hours measured at room temperature.

5.5.1.8. Kinetic experiments of the reaction between 2I and 1Cu under substoichiometric conditions of CuI.

- **Formation of 1Cu preventing the formation of 3Cu**

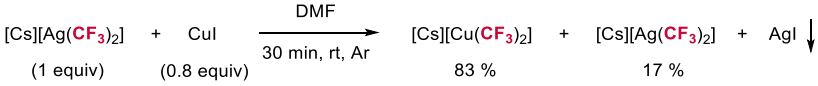

Scheme A5.6. Schematic for the formation of **1Cu** under substoichiometric conditions of CuI

In an argon atmosphere glovebox, a crimped vial was charged with [Cs][Ag(CF_3)$_2$] (**1Ag**, 9.1 mg, 0.024 mmol, 1 equiv), CuI (3.8 mg, 0.02 mmol, 0.8 equiv) and a known amount of the internal standard, 4,4'-difluorobiphenyl. The mixture was dissolved in 0.6 ml of DMF and stirred at room temperature for 30 minutes. The solution was then filtered using a 0.2 mm PTFE filter and transferred to a J-young NMR tube to be analyzed by [19]F NMR.

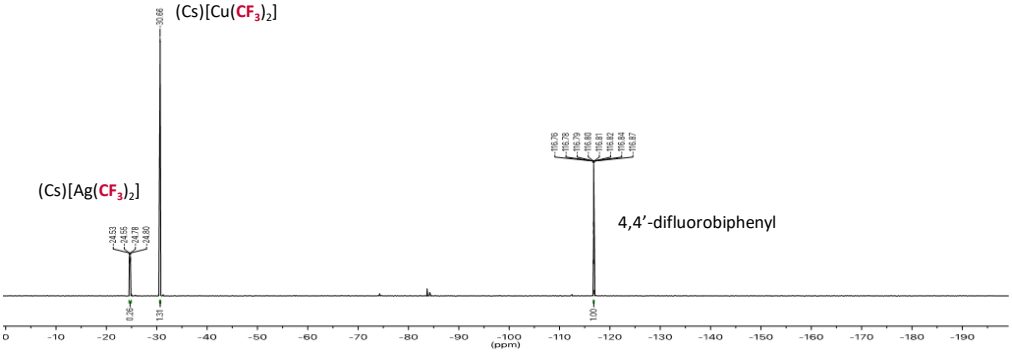

Figure A5.9. [19]F NMR spectrum of the reaction between **1Ag** and substoichiometric amounts of CuI in DMF (acetone-d_6) measured at room temperature.

- **Trifluoromethylation of 2I using the preformed mixture.**

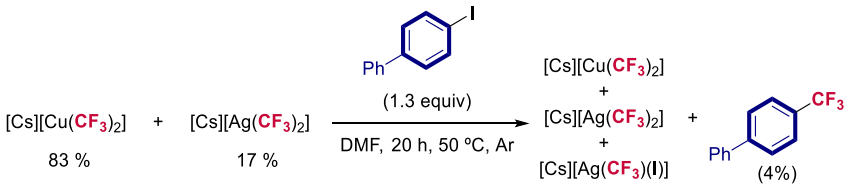

Scheme A5.7. Trifluoromethylation reaction of **2I** using the preformed **1Cu** under substoichiometric conditions

Once the ^{19}F NMR spectrum of the transmetalation has been recorded, inside the glovebox, a solution of the 4-iodobiphenyl (7.2 mg, 0.026 mmol, 1.3 equiv respect to the amount of [Cs][Cu(CF_3)$_2$]) in 0.3 ml of DMF was added to the solution of [Cs][Cu(CF_3)$_2$] and [Cs][Ag(CF_3)$_2$] in the J-young NMR tube. Immediately, the J-young NMR tube was taken out of the glovebox and directly put inside a cool bath at –50 ºC. All the ^{19}F NMR spectra (ns = 32) were measured at 50 ºC every 4 minutes and **2CF$_3$** was calculated by comparing the original mass of the 4-iodobiphenyl (limiting reactive) to its number of moles against the internal standard. At this point the amount of **2CF$_3$** is really low (4%) and in the ^{19}F NMR spectrum it is also observed the following species: [Cs][Cu(CF_3)$_2$], [Cs][Ag(CF_3)$_2$] and [Cs][Ag(CF_3)(I)]. The small amount of I^- that is formed after the first trifluoromethylation reaction could be in a complicated equilibrium with all the different species leading to, for example, the heteroleptic [Cs][Ag(CF_3)(I)] salt.

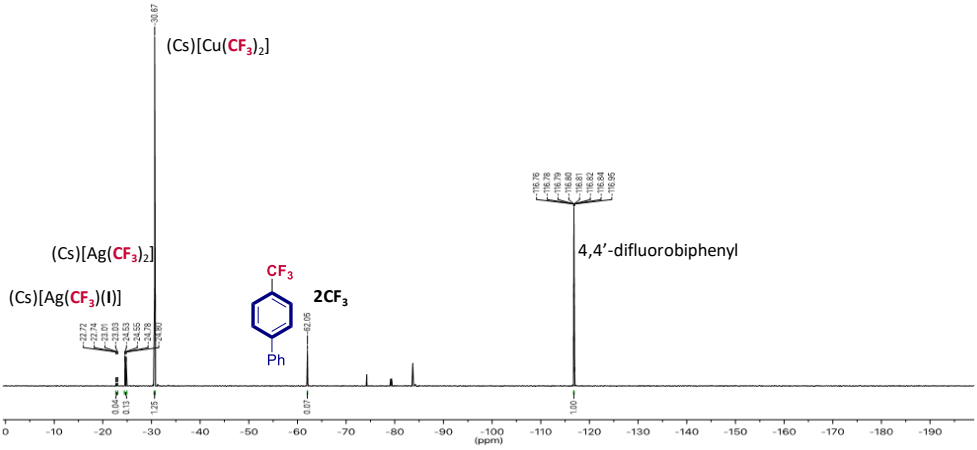

Figure A5.10. ^{19}F NMR spectrum of the reaction between **1Cu**, **1Ag** and **2CF$_3$** at 50 ºC in DMF (acetone-d_6) after 20 hours before the addition of CuI.

- **Addition of an excess of CuI**

After approximately 20 hours, the J-young NMR tube was directly put inside a cool bath at –50 ºC. Inside the glovebox, the solution was transferred to a crimped vial that contains an

excess of CuI (19.0 mg, 0.1 mmol, 4.2 equiv, respect to original [Cs][Ag(CF_3)$_2$]), the mixture was stirred 1 min and directly filtered using a 0.2 mm PTFE filter and transferred to another J-young NMR tube. Again, immediately, the J-young NMR tube was taken out of the glovebox and directly put inside a cool bath at –50 ºC. All the ^{19}F NMR spectra (ns = 32) were measured at 50 ºC every 4 minutes and **2CF$_3$** was calculated by comparing the original mass of the 4-iodobiphenyl (limiting reactive) to its number of moles against the internal standard.

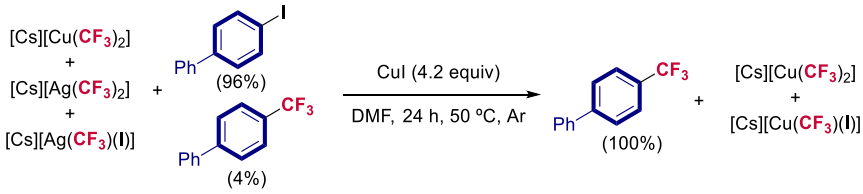

Scheme A5.8. Trifluoromethylation reaction after adding the excess of CuI.

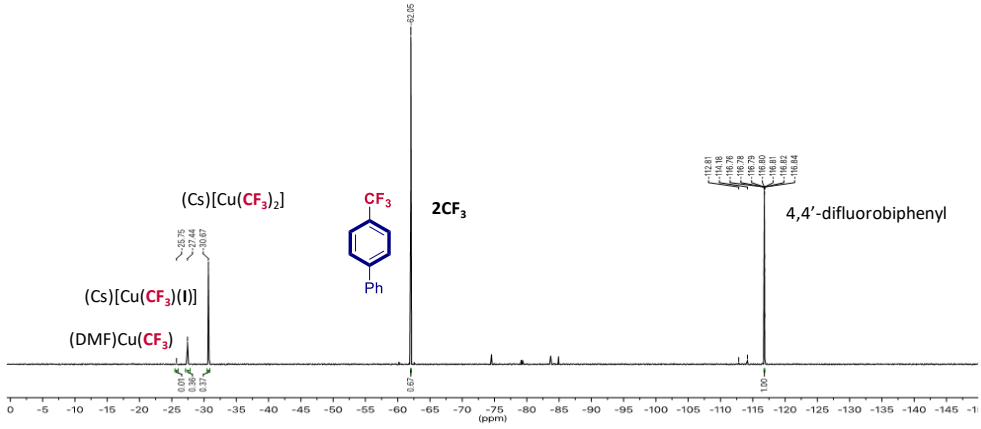

Figure A5.11. ^{19}F NMR spectrum of the reaction between **1Cu**, **3Cu** and **2CF$_3$** at 50 ºC in DMF (acetone-d_6) after 26 hours.

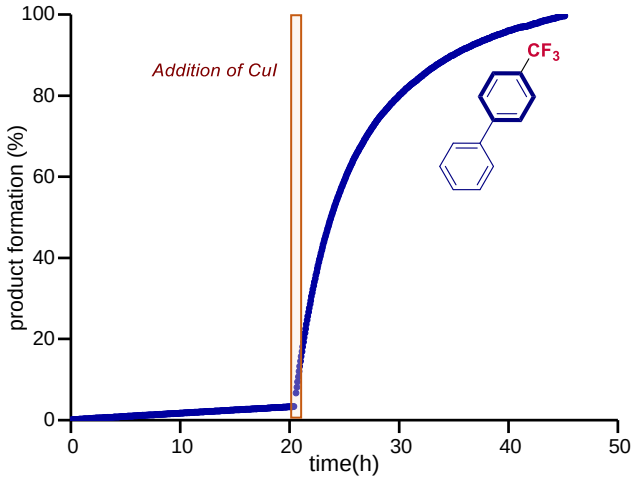

Figure A5.12. Conversion *vs.* time plot for the formation of **2CF$_3$** before and after the addition of an excess of CuI.

At the moment that the excess of CuI is added, the formation of [Cs][Cu(CF$_3$)(I)] (s, δ = –26.83 ppm) is observed by ^{19}F NMR spectroscopy. We detected an acceleration on the reaction rate, affording the formation of **2CF$_3$** in 61% approx. yield after 4 hours. Furthermore, we observed the appearance by ^{19}F NMR spectroscopy of [(DMF)Cu(CF$_3$)] (broad signal, δ = –25.75 ppm), the most reactive species based on our DFT calculations.

It is worth mentioning that we observed a variation on the chemical shift of [Cs][Cu(CF$_3$)(I)] (**3Cu**) during the reaction, from –26.83 to –28.00 ppm, due to the formation of [Cu(I)$_2$]$^-$. Hu and co-workers had already described that the amount of [Cu(I)$_2$]$^-$ can affect the chemical shift of **3Cu** type species, thus it is proposed that a more appropriate way of denominating these species would be {[Cu(CF$_3$)I]$_x$}$^{x-}$ {[CuI$_2$]$_y$}$^{y-}$.[20]

5.5.1.9. Reaction of [(dppp)Pd(Ph)(I)] and the bis-(trifluoromethyl) metallate complexes

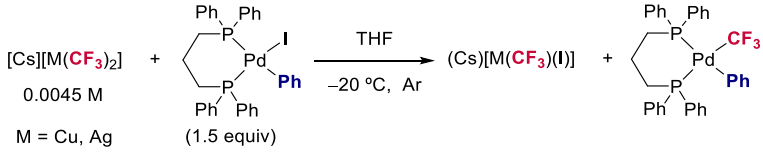

Scheme A5.9. Transmetalation study towards a palladium benchmark system using different bis-(trifluoromethyl) metallate complexes.

In an argon atmosphere glovebox, a crimped vial was charged with [Cs][Ag(CF$_3$)$_2$] (1.7 mg, 0.0045 mmol, 1 equiv) and CuI (0.85 mg, 0.0045 mmol, 1 equiv). The mixture was dissolved in 3 ml of THF and stirred at room temperature for 1 hour. The solution was then filtered using a 0.2 mm PTFE filter and 0.6 ml was transferred to a screw-cap NMR tube, that contained a known

amount of the internal standard, 4,4'-difluorobiphenyl. To a second vial, containing the palladium complex (1.5 equiv) we added 0.6 ml of THF. This solution was transferred to a syringe, protected from air (with a septum). The NMR tube and the palladium-containing syringe were taken out the glove box. The NMR tube was introduced in a cooling bath (–80°C) and the syringe was wrapped in aluminum foil with dry ice. At low temperature, the Pd-containing solution was injected in the screw-cap NMR tube. The mixture was shaken and immediately was introduced in the NMR instrument to study the kinetic evolution of the reaction.

Analogue procedure was followed for the kinetic experiment using silver complex **1Ag**.

5.5.2. **Computational appendix**

A data set collection of computational results is available in the ioChem-BD repository[60] and can be accessed via doi:10.19061/iochem-bd-1-111.

5.5.2.1. **Computational details**

DFT calculations were performed with the M06 functional,[61] using the Gaussian09 package.[62] The basis set was SDD plus pseudopotential for silver, copper and gold[63] and 6-31+G(d,p)[64] for the remaining atoms. All geometry optimizations were carried out in solution without symmetry restrictions. Implicit solvent was modeled through the SMD method.[65] calculations were carried out in DMF (ε = 37.22). Explicit solvent molecules were introduced when coordinating to the metal center. A correction of –4.0 kcal·mol^{-1} per explicit solvent molecule was applied based on previously studies on the use of cluster continuum model to simulate the bulk of the solvent.[4] All the energies reported are free energies at 50 ºC and 1 M in kcal·mol^{-1}. The correction to the translational entropy (from 1 atm to 1 M) has been performed by including 1.89 kcal·mol^{-1} to the free energy of each calculation. We are aware that 1 M is not the standard state for the solvent, but the concentration of the solvent is considered when

60 Álvarez-Moreno, M.; de Graaf, C.; López, N.; Maseras, F.; Poblet, J. M.; Bo, C. *J. Chem. Inf. Model*. **2015**, *55*, 95.

61 Zhao, Y.; Truhlar, D. G.; *Theor. Chem. Account.* **2008**, *120*, 215.

62 Gaussian 09, Revision D.01, Frisch, M. J.; Trucks, G. W.; Schlegel, H. B.; Scuseria, G. E.; Robb, M. A.; Cheeseman, J. R.; Scalmani, G.; Barone, V.; Mennucci, B.; Petersson, G. A.; Nakatsuji, H.; Caricato, M.; Li, X.; Hratchian, H. P.; Izmaylov, A. F.; Bloino, J.; Zheng, G.; Sonnenberg, J. L.; Hada, M.; Ehara, M.; Toyota, K.; Fukuda, R.; Hasegawa, J.; Ishida, M.; Nakajima, T.; Honda, Y.; Kitao, O.; Nakai, H.; Vreven, T.; Montgomery, Jr., J. A.; Peralta, J. E.; Ogliaro, F.; Bearpark, M.; Heyd, J. J.; Brothers, E.; Kudin, K. N.; Staroverov, V. N.; Keith, T.; Kobayashi, R.; Normand, J.; Raghavachari, K.; Rendell, A.; Burant, J. C.; Iyengar, S. S.; Tomasi, J.; Cossi, M.; Rega, N.; Millam, J. M.; Klene, M.; Knox, J. E.; Cross, J. B.; Bakken, V.; Adamo, C.; Jaramillo, J.; Gomperts, R.; Stratmann, R. E.; Yazyev, O.; Austin, A. J.; Cammi, R.; Pomelli, C.; Ochterski, J. W.; Martin, R. L.; Morokuma, K.; Zakrzewski, V. G.; Voth, G. A.; Salvador, P.; Dannenberg, J. J.; Dapprich, S.; Daniels, A. D.; Farkas, O.; Foresman, J. B.; Ortiz, J. V.; Cioslowski, J.; Fox, D. J. Gaussian, Inc., WallingfordCT, **2013**.

63 a) Dolg, M.; Wedig, U.; Stoll, H.; Preuss, H. *J. Chem. Phys.*, **1987**, *86*, 866; b) Andrae, D.; Haeussermann, U.; Dolg, M.; Stoll, H.; Preuss, H. *Theor. Chem. Accu.* **1990**, *77*, 123.

64 a) Hehre, W. J.; Ditchfield, R.; Pople, J. A. *J. Chem. Phys.* **1972**, *56*, 2257; b) Dill, J. D.; Pople, J. A. *J. Chem. Phys.* **1975**, *62*, 2921; c) Francl, M. M.; Petro, W. J.; Hehre, W. J.; Binkley, J. S.; Gordon, M. S.; DeFrees, D. J.; Pople, A. J. *J. Chem. Phys.* **1982**, *77*, 3654.

65 Marenich, S. A. V.; Cramer, C. J.; Truhlar, D. G. *J. Phys. Chem. B* **2009**, *113*, 6378.

performing the microkinetic modelling (see page - 297 - for further details). NBO analysis of optimized structures in gas phase was performed using version 6.0 of the software.[66]

5.5.2.2. Study of different bis-(trifluoromethyl) metallate anions by DFT

- **Metal carbon bond analysis**

	M = Cu (**I1Cu**)		M = Ag (**I1Ag**)		M = Au (**I1Au**)	
Metal contribution (%)	20.73	s(88.03) p(0.39) d(11.58)	21.52	s(87.81) p(0.46) d(11.73)	28.26	s(76.24) p(0.31) d(23.45)
Carbon contribution (%)	79.27	s(43.01) p(56.98)	78.48	s(41.69) p(58.31)	71.74	s(40.71) p(59.27)

Table A5.1. Percentage of the metal and carbon contributions in the σ-M–C bond for the different metallate **1M** (M = Cu, Ag, Au) anions in gas phase.

- **NPA analysis**

	M = Cu (**I1Cu**)	M = Ag (**I1Ag**)	M = Au (**I1Au**)
NPA (M)	0.34	0.30	0.17
NPA (CF_3)	–1.34	–1.30	–1.17

Table A5.2. NPA values for the metal center and both CF_3 moieties for different metallate **1M** (M = Cu, Ag, Au) anions.

- **Electrostatic potential**

The electron density surface was generated from total SCF density (mapped with electrostatic potential). To plot the surface, we used an isovalue of 0.02 and a range from –0.14 to –0.03. We can see how the charge is more delocalized in the gold complex, indicating a more covalency of the M–C bond.

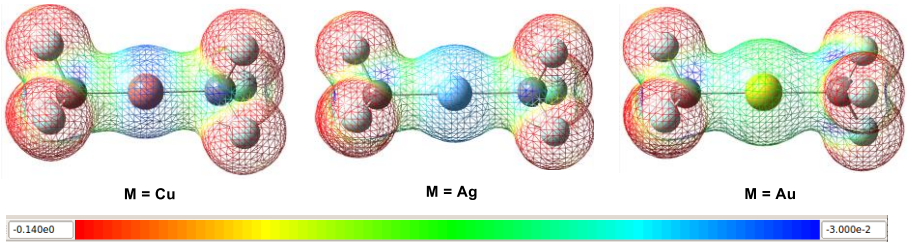

Figure A5.13. Representation of the electrostatic potential surface of the different bis-(trifluoromethyl) metallate **1M** (M = Cu, Ag, Au) anions.

66 Glendening, E. D.; Badenhoop, J. K.; Reed, A. E.; Carpenter, J. E.; Bohmann, J. A.; Morales, C. M.; Landis, C. R.; Weinhold, F. Theoretical Chemistry Institute, University of Wisconsin, Madison, WI, **2013**. http://nbo6.chem.wisc.edu/.

5.5.2.3. Trifluoromethylation reaction mechanism studies by DFT

- **Model species in solution**

The experimental part has been performed using the cesium derivative of the metallates. However, the simulation of this cation by DFT is challenging since it tends to be stabilized by solvent molecules. Tetrabutylammonium derivatives experimentally show the same performance in trifluoromethylation reactions and we decided to analyze these ammonium salts as initial model of our study since the simulation of the cation (as tetramethylammonium) is more reliable. As can be seen in Scheme A5.10, the dissociation of the ion-pair in the ionic part is favored in DMF. For this reason, all the calculations were performed assuming the free metallate anion.

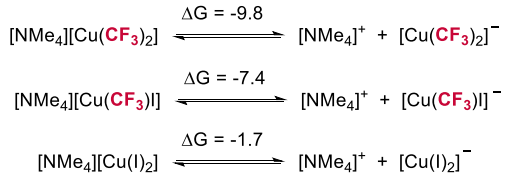

Scheme A5.10. Dissociation equilibrium of different copper ion-pair in DMF. Free energies in kcal·mol^{-1}.

Schlenk equilibrium and displacement of the iodide atom by solvent molecules were studied for copper, silver and gold complexes. Heteroleptic species are favored versus the homoleptic ones and the solvent tends to displace the halide. These calculated equilibria are a simplification since the existence of mixed species involving $[M(I)_2]^-$ and $[M(CF_3)(I)]^-$ cannot be discarded and the values should be taken as qualitative ones. Hu and coworkers proposed that a more appropriate way of denominating these species would be $\{[Cu(CF_3)I]_x\}^{x-}$ $\{[CuI_2]_y\}^{y-}$.[20]

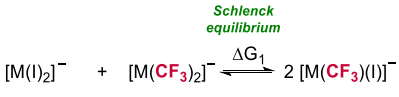

M	ΔG_1	ΔG_2	ΔG_3
Au	-5.3	-4.0	-4.0
Ag	-1.0	-4.0	-4.0
Cu	-3.1	-4.0	-4.0

Scheme A5.11. Schlenk equilibrium and displacement of iodide by DMF for different copper, silver and gold complexes. Free energies in kcal·mol^{-1}.

- **Oxidative Addition/Reductive Elimination for I3Cu.**

Scheme A5.12 displays the profile for the OA/RE to **I3Cu** copper complex.

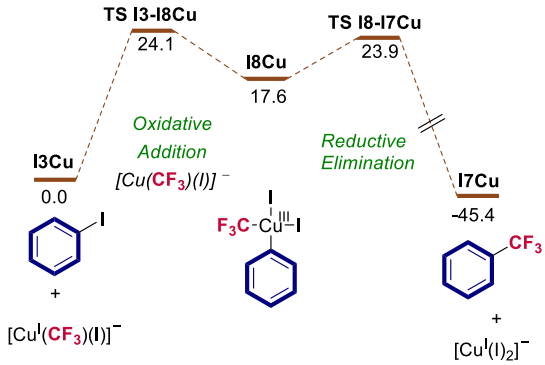

Scheme A5.12. Profile for the OA/RE considering **I3Cu** as active species. Free energies in kcal·mol^{-1}.

- **Alternative mechanisms for copper**

  - Outer sphere SET (Single Electron Transfer)

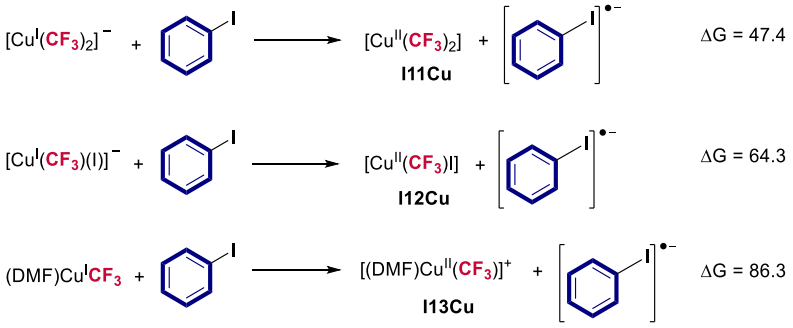

Scheme A5.13. Thermodynamic (free energy) for SET from different copper species. Free energies in kcal·mol^{-1}.

  - Halogen Atom Transfer

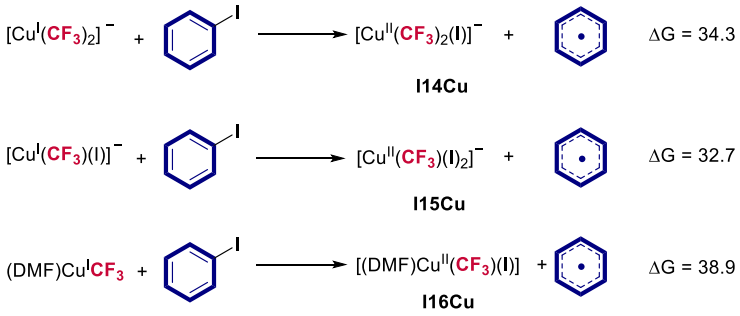

Scheme A5.14. Thermodynamic (free energy) for HAT from different copper species. Free energies in kcal·mol^{-1}.

- σ-bond metathesis

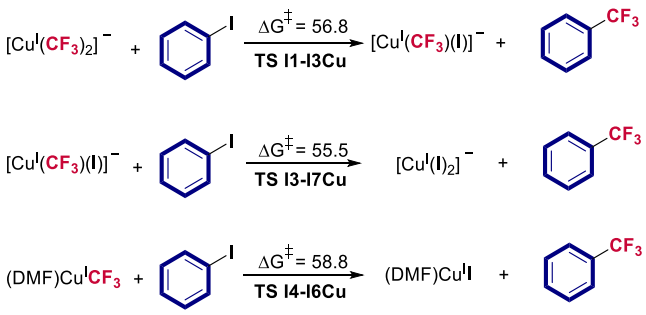

Scheme A5.15. Activation energies barriers for σ-bond metathesis from different copper species. Free energies in kcal·mol^{-1}.

5.5.2.4. Microkinetic modelling

- **General considerations**

We used COPASI 4.22 (Build 170) program package[67] for the microkinetic modelling. Deterministic method (LSODA) was used for the integration of the time-course simulation of the concentration of each species. Relative tolerance and absolute tolerance were fixed to $1 \cdot 10^{-13}$ and $1 \cdot 10^{-18}$, respectively. In the following sections, the considered elementary steps, free energy and rate constants for each kinetic model are specified.

The coordination or decoordination of ligands (i.e. solvent and iodide) that have been considered barrierless in the free energy surface in the aforementioned reactions, will be considered under diffusion-control for the microkinetic analysis. To do so, the rate constants for a diffusion control reaction is calculated using the Stokes-Einstein equation with the Smoluchowski relation.[52] This means that the diffusion rate constant for a bimolecular reaction is approximately defined by *eq.* 1 in L/(mol·s), where K_B is the Boltzmann constant, T is the temperature, η is the viscosity of the solvent at the given temperature and N_a, the Avogadro number.

$$k_{diff} = \frac{8K_B \cdot T}{3\eta} \cdot 1000N_a \quad (eq.1)$$

Regarding that the viscosity of DMF at 353.15 K is 0.47 mPa·s,[68] the conversion of the so obtained diffusion rate constant to free energy using the Eyring equation is 3.9 kcal·mol^{-1} at 323.15 K. When the equilibrium constant is defined by ΔG > 3.9 kcal/mol, the direct constant is calculated adding 1 kcal·mol^{-1} to the ΔG value that defined the equilibrium (see entry 5 and 6 in Table A5.4, microkinetic for the complete reaction).

67 Hoops, S.; Sahle, S.; Gauges, R.; Lee, C.; Pahle, J.; Simus, N.; Singhal, M.; Xu, L.; Mendes, P.; Kummer, U. *Bioinformatics*, **2006**, *22*, 3067.

68 Bernal-Garcia, J. M.; Guzmas-Lopez, A.; Cabrales-Torres, A.; Estrada-Baltazar, A.; Iglesias-Silva, G. A. *J. Chem. Eng. Data*, **2008**, *53*, 1024.

The reductive elimination step has not been considered in the kinetic simulations since this transformation is kinetically negligible.

The initial concentrations, according to the experimental conditions, are 12.9 M for DMF, 0.04 M for phenyl iodide and 0.026 M for $[M(CF_3)_2]^-$.

- **Combination of the oxidative addition to I1Cu and I3Cu**

The following equations were used to perform the microkinetic study of the reaction model 1:

MODEL 1

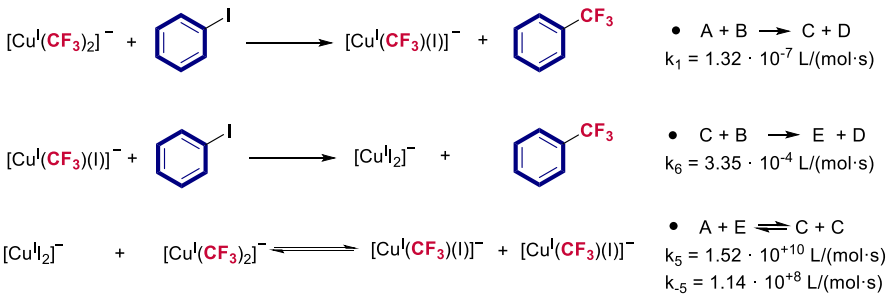

Scheme A5.16. Elementary steps for the formation of **2CF$_3$** considering as active species **1Cu** and **3Cu** (model 1).

Reactant(s)	Product(s)	Barrier ΔΔG (kcal/mol)	Rate Constant (k)		Corrected Barrier ΔΔG (kcal/mol)	Rate Constant (k)
A + B	C + D	29.2	$1.13{\cdot}10^{-07}$		29.2	$1.13{\cdot}10^{-07}$
C + B	E + D	24.1	$3.35{\cdot}10^{-04}$		24.1	$3.35{\cdot}10^{-04}$
A + E	C + C	0.0	$6.72{\cdot}10^{+12}$		3.9	$1.52{\cdot}10^{+10}$
C + C	A + E	3.1	$5.37{\cdot}10^{+10}$		7.0	$1.14{\cdot}10^{+08}$

Table A5.3. Calculated activation free energies and rate constant of kinetic model of the model 1.

Regarding this scenario, the reaction starts in 28 hours and there is product formation after 100 hours of reaction. This result is not comparable to the experimental data.

- **Combination of a first oxidative addition to I1M to generate a more reactive I4M species (M = Ag, Cu)**
  - COPPER

The following equations were used to perform the microkinetic study of the reaction model 2:

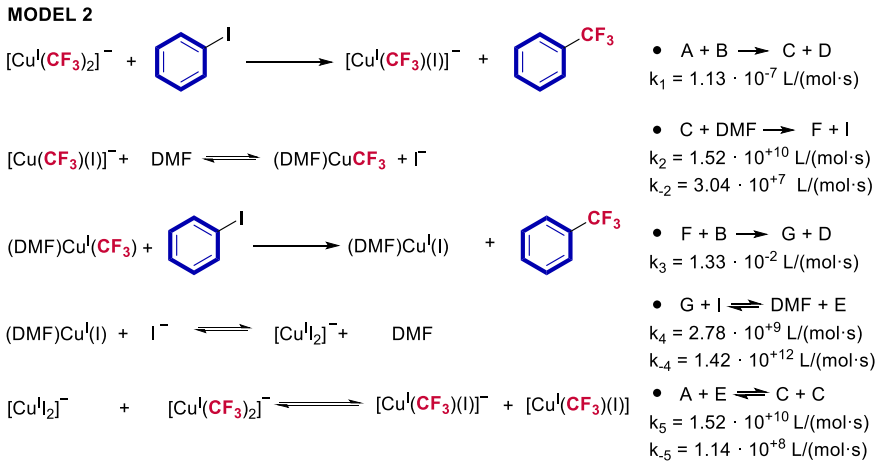

Scheme A5.17. Elementary steps for the formation of **2CF$_3$** considering as active species **1Cu** and **4Cu** (model 2).

Reactant(s)	Product(s)	Barrier ΔΔG (kcal/mol)	Rate Constant (k)		Corrected Barrier ΔΔG (kcal/mol)	Rate Constant (k)
A + B	C + D	29.2	$1.13{\cdot}10^{-07}$		29.2	$1.13{\cdot}10^{-07}$
C + DMF	F + I	0.0	$6.72{\cdot}10^{+12}$		3.9	$1.52{\cdot}10^{+10}$
F + I	C + DMF	4.0	$1.32{\cdot}10^{+10}$		7.9	$3.04{\cdot}10^{+07}$
F + B	G + D	21.7	$1.33{\cdot}10^{-02}$		21.7	$1.33{\cdot}10^{-02}$
G + I	DMF + E	4.0	$1.32{\cdot}10^{+10}$		5.0	$2.78{\cdot}10^{+09}$
DMF + E	G + I	0.0	$6.72{\cdot}10^{+12}$		1.0	$1.42{\cdot}10^{+12}$
A + E	C + C	0.0	$6.72{\cdot}10^{+12}$		3.9	$1.52{\cdot}10^{+10}$
C + C	A + E	3.1	$5.37{\cdot}10^{+10}$		7.0	$1.14{\cdot}10^{+08}$

Table A5.4. Calculated activation free energies and rate constant of kinetic model of the model 2.

Regarding this scenario, as mentioned above, the reaction starts in 4 hours and reach full conversion after 13 hours. This result is comparable to the experimental data.

- SILVER

The following equations were used to perform the microkinetic study of the reaction model 3:

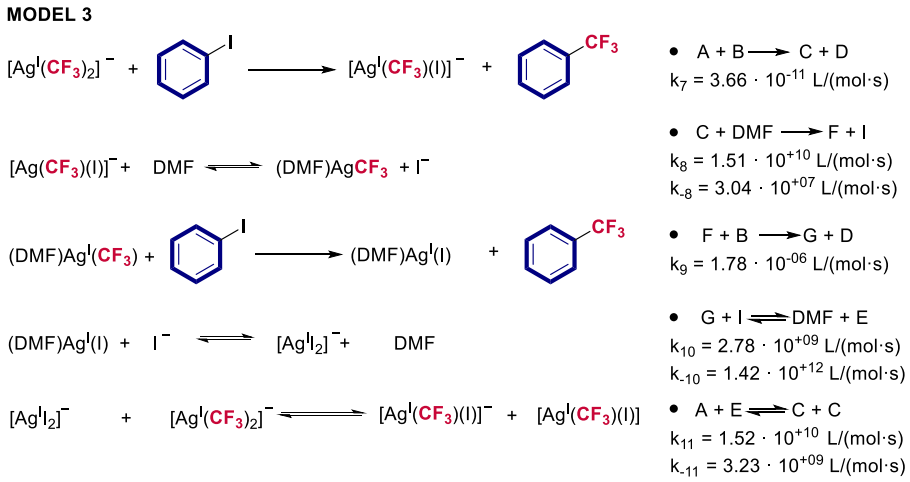

Scheme A5.18. Elementary steps for the formation of **2CF$_3$** considering as active species **1Ag** and **4Ag** (model 3).

Reactant(s)	Product(s)	Barrier ΔΔG (kcal/mol)	Rate Constant (k)		Corrected Barrier ΔΔG (kcal/mol)	Rate Constant (k)
A + B	C + D	34.4	$3.66\cdot10^{-11}$		34.4	$3.66\cdot10^{-11}$
C + DMF	F + I	0.0	$6.72\cdot10^{+12}$		3.9	$1.52\cdot10^{+10}$
F + I	C + DMF	4.0	$1.32\cdot10^{+10}$		7.9	$3.04\cdot10^{+07}$
F + B	G + D	27.5	$1.78\cdot10^{-06}$		27.5	$1.78\cdot10^{-06}$
G + I	DMF + E	4.0	$1.32\cdot10^{+10}$		5.0	$2.78\cdot10^{+09}$
DMF + E	G + I	0.0	$6.72\cdot10^{+12}$		1.0	$1.42\cdot10^{+12}$
A + E	C + C	0.0	$6.72\cdot10^{+12}$		3.9	$1.52\cdot10^{+10}$
C + C	A + E	1.0	$1.42\cdot10^{+12}$		4.9	$3.23\cdot10^{+9}$

Table A5.5. Calculated activation free energies and rate constant of kinetic model of the model 3.

The reaction finishes after 12 years using the experimental concentration of the reagents. The same behavior is expected for gold scenario.

5.5.2.5. X-ray structural determination for 1Cu, 1Ag, 1Au and [Cs][trans-Au(CF$_3$)$_2$(I)$_2$]

Crystal preparation: Crystals of **1Cu** were grown in a concentrated solution in DMF:THF:DCM (0.05:0.1:1) at –30 ºC inside the glovebox. Crystals of **1Cu** and [Cs][trans-Au(CF$_3$)$_2$(I)$_2$] were grown in a mixture of THF and hexane at room temperature under air. The crystals for **1Cu**, **1Ag**, **1Au**, and [Cs][trans-Au(CF$_3$)$_2$(I)$_2$] were selected using a Zeiss stereomicroscope using polarized light and prepared under inert conditions immersed in perfluoropolyether as protecting oil for manipulation.

Data collection: Crystal structure determinations for samples **1Cu**, **1Ag** and **1Au** were carried out using an Apex DUO Kappa 4-axis goniometer equipped with an APPEX 2 4K CCD area detector, a Microfocus Source E025 IuS using MoK_α radiation, Quazar MX multilayer Optics as monochromator and an Oxford Cryosystems low temperature device Cryostream 700 plus (T = –173 ºC). Crystal structure determination for sample [Cs][trans-Au(CF_3)$_2$(I)$_2$] was carried out using a Rigaku diffractometer equipped with a Pilatus 200K area detector, a Rigaku MicroMax-007HF microfocus rotating anode with MoK_α radiation, Confocal Max Flux optics and an Oxford Cryosystems low temperature device Cryostream 700 plus (T = –173 ºC). Full-sphere data collection was used with ω and φ scans. *Programs used:* Bruker Device: Data collection APEX-2,[69] data reduction Bruker Saint[70] V/.60A and absorption correction SADABS[71] or TWINABS.[72] Rigaku device: Data collection and reduction with CrysAlisPro[73] and absorption correction with Scale3 Abspack scaling algorithm.[74]

Structure Solution and Refinement: Crystal structure solution was achieved using the computer program SHELXT.[75] Visualization was performed with the program SHELXle.[76] Missing atoms were subsequently located from difference Fourier synthesis and added to the atom list. Least-squares refinement on F^2 using all measured intensities was carried out using the program SHELXL 2015.[77] All non-hydrogen atoms were refined including anisotropic displacement parameters. These data are provided free of charge by The Cambridge Crystallographic Data Centre. The corresponding code in the data base is shown in brackets next to the corresponding label in the next section.

Comments to the structures:

- **Comments on structure 1Cu (CCDC 1891323)**

This structure is shown in Figure 5.1. The asymmetric unit contains a half copper atom, a half cesium atom and one CF_3-group. Once symmetry is applied, the structure can be described as a Cu-complex in which one copper atom is connected to two CF_3-groups and it is contacting to two symmetry equivalent Cu atoms forming a monodimensional line of interconnected metal atoms. In each following Cu atom, the CF_3-groups are rotated in 90º. The cesium atoms are surrounding the complex and contacting the fluorine atoms of the CF_3-groups. In total each

69 Data collection with APEX II version v2013.4-1. Bruker (**2007**). Bruker AXS Inc., Madison, Wisconsin, USA.
70 Data reduction with Bruker SAINT version V8.30c. Bruker (**2007**). Bruker AXS Inc., Madison, Wisconsin, USA.
71 SADABS: V2014/5 Bruker (**2001**). Bruker AXS Inc., Madison, Wisconsin, USA. Blessing, *Acta Cryst.* (**1995**) A51 33-38.
72 TWINABS Version 2008/4 Bruker AXS; Blessing, *Acta Cryst.* (**1995**) A51 33.
73 Data collection and reduction with CrysAlisPro 1.171.39.12b (Rigaku OD, 2015).
74 Empirical absorption correction using spherical harmonics implemented in Scale3 Abspack scaling algorithm, CrysAlisPro 1.171.38.37f (Rigaku OD, **2015**)
75 SHELXT; G. M. Sheldrick, *Acta Cryst.* **2015** A71, 3.
76 SHELXle; C. B. Huebschle, G. M. Sheldrick, B. Dittrich, *J. Appl. Cryst.* **2011**, *44*, 1281.
77 SHELXL; Sheldrick, G. M. *Acta Cryst*. **2015** C71, 3. SHELXT.

cesium atom makes 12 contacts to fluorine atoms. This compound crystallized always forming multicomponent crystals. The measured sample was formed by three crystals (ratio 53:32:15) which were processed simultaneously with TWINABS taking in account overlapping reflections. This structure is isostructural to the Ag-complex published previously, but in this case the structure refined clearly in the space group C2/m and no disorder was observed. The structure is of good quality (no A- and B-alerts) with a R1-value of 5.7 %.

- **Comments on structure 1Ag (CCDC 1566839)**

This structure is shown in Figure 5.1.The asymmetric unit contains half Cs-cation and two quarters of $[Ag(CF_3)_2]^-$ anions. All the CF_3 groups are disordered in a minimum of two orientations. The cesium cation is disordered in two positions with a ratio of 57:43. The measured sample is formed by a minimum of two crystals with a ratio of 86:14. The data collected were processed with TWINABS taking in account overlapping reflections. The structure could be refined in the space groups *C*2/m, *C*2 (as a racemic twin) and *C*m (as a twin) with similar results. Finally, the higher symmetrical space group C2/m was selected which also gave the slowest R1 value. Structure solutions were also found using a larger monoclinic unit cell (a:17.00 b:5.77 c:16.12 β:119.57 instead of a:16.12 b:5.77 c:8.35 β:117.60) but the statics were worse so that they were not further used. The selected structure in the space group *C*/2m is of excellent quality and it does not show any A- or B-alerts.

- **Comments on structure 1Au (CCDC 1891324)**

This structure is shown in Figure 5.1. This compound crystallizes in the space group $P2_1/m$ and, although it is not isostructural to **1Cu**, it shows a similar packing. The asymmetric unit contains two gold atoms distributed in four positions (0.25:0.25:0.25:0.25), two Cesium atoms distributed in three positions (0.50:0.25:0.25) and four CF_3-groups distributed in six positions (1.0:0.5:0.5:1.0:0.5:0.5). Three of the refined Cs-positions and one of the Au-positions show a disorder (95:5) in which a side shift of around 0.5 Å can be observed. One of the CF_3-groups shows a rotational disorder (51:49). Each Au-atom in the structure is connected to two CF_3-groups and is contacting two Au-atoms forming a mono-dimensional line of interconnected metal atoms. The CF_3-groups of each following Au-atom are rotated 90º. The line formed by the Au-atoms shows every three Au-atoms an angle of around 170º, which gives a zigzag pattern. The structure shows high residual electron densities which can be explained by the presence in a high proportion of gold and cesium. Additionally, there were some additional factors which could generate these residual electron densities. The structure presents a disorder (94:6) in which most of the heavy atoms show a side shift of approx. 0.5 Å. By refining this disorder, the residual electron densities could be significantly improved but still some remained. Lighter atoms could not be included in this disorder, so some of the residual density may be generated by the

disorder described. Analyzing carefully the data, it could be observed that a second weaker crystal was present, but it could not be included in the integration. This may also affect the electron density map. Also, by analyzing the reflections measured, a weak pseudo-symmetry to higher symmetries probably induced by the heavy atoms was observed but attempts to use this higher symmetry were not successful. Measurements of alternative crystals did also not improve the presence of residual electron densities and they were mostly twinned or of lower quality. Different measurements were performed to improve the data and get completeness, but the quality of the different data collected was of lower quality. The best dataset obtained and finally selected was having a completeness of 0.957. Despite the fact that a small amount of reflections was missing to reach completeness and still some high residual electron densities were observed, it was considered that the structure had enough quality.

- **Comments on structure [Cs][trans-Au(CF_3)$_2$(I)$_2$] (CCDC 1891325)**

This structure is shown in Scheme 5.23. The asymmetric unit contains a half gold atom, a half cesium atom, one CF_3-group and one Iodine atom. Once symmetry is applied, the structure can be described as an Au-complex in which one gold atom is connected to two CF_3-groups and two iodine atoms forming a square planar geometry. The cesium atoms are surrounding the complex and contacting the fluorine atoms of the CF_3-groups. A weak interaction between iodine and cesium can also be observed. The CF_3-group is rotationally disordered in two orientations (ratio 63:37). The structure shows some high residual electron densities (B-alerts) which can be explained by the presence in a high proportion of gold, iodine and cesium. Additionally, the CF_3-group present in the structure is disordered in two positions, effect which may contribute in the presence of residual electron densities. Variations in the absorption correction or the measurement of alternative crystals did not improve the presence of the residual electron densities. It was considered that the structure had enough quality. The structure is of good quality (B-alerts are explained) and publishable with a R1-value of 2.99 %.

CHEMISTRY
A European Journal
www.chemeurj.org

A Journal of
ChemPubSoc Europe

2019-25/40

Supported by
ACES Asian Chemical Editorial Society

Cover Feature:
F. Maseras, M. H. Pérez-Temprano et al.
Exploring the Role of Coinage Metalates in Trifluoromethylation: A Combined Experimental and Theoretical Study

For the first time, the door to access selectively $Cu(CF_3)_2^-$ have been unlocked. These species, ubiquitous in trifluoromethylation reactions, displayed a superior reactivity towards aryl halides than its argentate and aurate congeners. Merging experimental and computational approaches, a complex mechanistic scenario is unraveled, through a $Cu^{I/III}$ process, with the participation of more reactive species such as $(DMF)Cu(CF_3)$, generated through multiple equilibria.

5.6. References and notes

1. *For representative examples on the synthesis and reactivity of* $AuCF_3$ *complexes, see: a)* Zopes, D.; Kremer, S.; Scherer, H.; Belkoura, L.; Pantenburg, I.; Tyrra, W.; Mathur, S. *Eur. J. Inorg. Chem*. **2011**, 273. b) Gil-Rubio, J.; Vicente, J. *Dalton Trans*. **2015**, *44*, 19432 and references therein. c) Pérez-Bitrián, A.; Martínez-Salvador, S.; Baya, M.; Casas, J. M.; Martín, A.; Menjón, B.; Orduna, J. *Chem. Eur. J.* **2017**, *23*, 6919. d) Levin, M. D.; Chen, T. Q.; Neubig, M. E.; Hong, C. M.; Theulier, C. A.; Kobylianskii, I. J.; Janabi, M.; O'Neil, J. P.; Toste, F. D. *Science* **2017**, 356, 1272. e) Pérez-Bitrián, A; Baya, M.; Casas, J. M.; Martín, A.; Menjón, B.; Orduna, J. *Angew. Chem. Int. Ed*. **2018**, 57, 6517.

2. *For representative examples on the synthesis and reactivity of* $AgCF_3$ *complexes, see*: a) Tyrra, W.; Naumann, D. *J. Fluorine Chem*. **2004**, 125, 823. b) Weng, Z.; Lee, R.; Jia, W.; Yuan, Y.; Wang, W.; Feng, X.; Huang, K.-W. *Organometallics* **2011**, 30, 3229. c) Hafner, A.; Jung, N.; Bräse, S. *Synthesis* **2014**, 46, 1440. d) Tate, B. K.; Jordan, A. J.; Bacsa, J.; Sadighi, J. P. *Organometallics* **2017** 36 964. e) Martínez de Salinas, S.; Mudarra, A. L.; Benet-Buchholz, J.; Parella, T.; Maseras, F.; Pérez-Temprano, M. H. *Chem. Eur. J*. **2018**, 24, 11895. f) Joven-Sancho, D. Baya, M.; Martín, A.; Menjón, B. *Chem. Eur. J.* **2018**, 24, 13098.

3. *For representative examples on the synthesis and reactivity of* $CuCF_3$*, see:* Mudarra, A. L.; Martínez de Salinas, S.; Pérez-Temprano, M. H. *Synthesis* **2019**, *51*, 2809 and references therein.

4. Naumann, D.; Wessel, W.; Hahn, J.; Tyrra, W. *J. Organomet. Chem*. **1997**, *547*, 79.

5. a) Hafner, A.; Bräse, S. *Angew. Chem. Int. Ed.* **2012**, *51*, 3713. b) Zhang; C.-P.; Wang, Huan; Klein, A.; Biewer, C.; Stirnat, K.; Yamaguchi, Y.; Xu, L.; Gomez-Benitez, V.; Vicic, D. A. *J. Am. Chem. Soc.* **2013**, *135*, 8141.

6. a) Ye, Y.; Lee, S. H.; Sanford, M. S. *Org. Lett.*, **2011**, *13*, 5464. b) Hafner, A.; Bräse, S. *Angew. Chem. Int. Ed.* **2012**, *51*, 3713. c) Wu, X.; Chu, L.; Qing, F.-L. *Angew. Chem. Int. Ed.* **2013**, *52*, 2198. d) Zeng, Y.; Zhang, L.; Zhao, Y.; Ni, C.; Zhao, J.; Hu, J. *J. Am. Chem. Soc.* **2013**, *135*, 2955. e) Wang, X.; Xu, Y.; Mo, F.; Ji, G.; Qiu, D.; Feng, J.; Ye, Y.; Zhang, S.; Zhang, Y.; Wang, J. *J. Am. Chem. Soc.* **2013**, *135*, 10330. f) Ye-bin Wu, Y.-b.; Guo-ping Lu, G.-p.; Yuan, T.; Xu, Z.-b. Wan, L.; Cai, C. *Chem. Commun*., **2016**, *52*, 13668.

7. a) Liu, J.-B.; Chen, C.; Chu, L.; Chen, Z.-H.; Xu, X.-H. Qing, F.-L. *Angew. Chem. Int. Ed.* **2015**, *54*, 11839. b) Teng, F.; Cheng, J.; Bolm, C. *Org. Lett.* **2015**, *17*, 3166.

8. Zhang, X. *Comput. Theor. Chem*. **2019**, *1158*, 15.

9. Tang, P.; Furuya, T.; Ritter, T. *J. Am. Chem. Soc.* **2010**, *132*, 12150.

10. Wiemers, D. M.; Burton, D. J. *J. Am. Chem. Soc.* **1986**, *108*, 832 and references cited therein.

11. Willert-Porada, M. A.; Burton, D. J.; Baenziger, N. C. *J. Chem. Soc., Chem. Comm.* **1989**, *21*, 1633.

12. Agnes, K.; Movchun, V.; Rodima, T.; Dansauer, T.; Rusanov, E. B.; Leito, I.; Kaljurand, I.; Koppel, J.; Pihl, V.; Koppel, I.; Ovsjannikov, G.; Toom, L.; Mishima, M.; Medebielle, M.; Lork, E.; Röschenthaler, G.-V.; Koppel, I. A.; Kolomeitsev, A. A. *J. Org. Chem.* **2008**, *73*, 2607.

13. Knauber, T.; Arikan, F.; Röschenthaler, G.-V.; Goossen, L. J. *Chem. Eur. J.* **2011**, *17*, 2689.

14. Zanardi, A.; Novikov, M. A.; Martín, E.; Benet-Buchholz, J.; Grushin, V. V. *J. Am. Chem. Soc*. **2011**, *133*, 20901.

15. a) Matsui, K.; Tobita, E.; Ando, M.; Kondo, K. *Chem. Lett.* **1981**, 1719. b) Chen, Q.; Wu, S. *J. Chem. Soc.*, *Chem. Commun.* **1989**, 705. c) MacNeil, J. G. Jr.; Burton, D. J. *J. Fluorine Chem.*, **1991**, *55*, 225. d) Duan, J-X.; Su, D-B.; Wu, J-P.; Chen, Q-Y. *J. Fluorine Chem.*, **1994**, *66*, 167. e) Prakash, G. K. S.; Hu, J.; Olah, G. A. *Org. Lett.* **2003**, *5*, 3253. f) Serizawa, H.; Aikawa, K.; Mikami, K. *Chem. Eur. J.* **2013**, *19*, 17692.

16. a) Kondratenko, N. V.; Vechirko, E. P.; Yagupolskii, L. M. *Synthesis* **1980**, 932. b) Kremlev, M. M.; Tyrra, W.; Mushta; A. I.; Naumann, D.; Yagupolskii, Y. Y. *J. Fluorine Chem.* **2010**, *131*, 212. c) Popov, I.; Lindeman, S.; Daugulis, O. *J. Am. Chem. Soc.* **2011**, *133*, 9286. d) Nakamura, Y.; Fujiu, M.; Murase, T.; Itoh, Y.; Serizawa, H.; Aikawa, K.; Mikami, K. *Beilstein J. Org. Chem.* **2013**, *9*, 2404.

17. Sanhueza, I. A.; Nielsen, M. C.; Ottiger, M.; Schoenebeck, F. Helv. Chim. Acta 2012, 95, 2231.

18. Urata, H.; Fuchikami, T. *Tetrahedron* **1991**, *32*, 91.

19. Lishchynskyi, A.; Novikov, M. A.; Martin, E.; Escudero-Adán, E. C.; Novák, P.; Grushin, V. V. *J. Org. Chem*. **2013**, *78*, 11126.

20. Hu, M.; Ni, C.; Hu, J. *J. Am. Chem. Soc.* **2012**, *134*, 15257.

21. a) Chu, L.; Qing, F.-L. *J. Am. Chem. Soc.* **2010**, *132*, 7262. b) Chu, L.; Qing, F.-L. *Org. Lett.* **2010**, *12*, 5060. c) Jiang, X.; Chu, L.; Qing, F.-L. *J. Org. Chem.* **2012**, *77*, 1251.

22. Carr, G. E.; Chambers, R. D.; Holmes, T. F.; Parker, D. G. *J. Chem. Soc., Perkin Trans. I* **1988**, *921*.

23. Jover, J.; Maseras, F. *Chem. Commun*. **2013**, *49*, 10486.

24. Weske, S.; Schoop, R.; Koszinowski, K. *Chem. Eur. J*. **2016**, *22*, 11310.

25. Aikawa, K.; Nakamura, Y.; Yokota, Y.; Toya, W.; Mikami, K. *Chem. Eur. J.* **2015**, *21*, 96.

26. Konovalov, A. I.; Lishchynskyi, A.; Grushin, V. V. *J. Am. Chem. Soc.* **2014**, *136*, 13410.

27. Morimoto, H.; Tsubogo, T.; Litvinas, N. D.; Hartwig, J. F. *Angew. Chem. Int. Ed*. **2011**, *50*, 3793.

28. Dubinina, G. G.; Furutachi, H.; Vicic, D. A. *J. Am. Chem. Soc.* **2008**, *130*, 8600.

29. Dubinina, G. G.; Ogikubo, J.; Vicic, D. A. *Organometallics* **2008**, *27*, 6233.

30. Oishi, M.; Kondo, H.; Amii, H. *Chem. Commun.*, **2009**, 1909.

31. a) Mormino, M. G.; Fier, P. S.; Hartwig, J. F. *Org. Lett*. **2014**, *16*, 1744. b) Litvinas, N. D.; Fier, P. S.; Hartwig, J. F. *Angew. Chem. Int. Ed.* **2012**, *51*, 536. c) Morstein, J.; Hou, H.; Cheng, C.; Hartwig, J. F. *Angew. Chem. Int. Ed.* **2016**, *55*, 8054.

32. https://www.sigmaaldrich.com/catalog/product/aldrich/777692?lang=es&region=ES

33. Usui, Y.; Noma, J.; Hirano, M.; Komiya, S. *Inorg. Chim. Acta* **2000**, *309*, 151.

34. Tomashenko, O. A.; Escudero-Adán, E. C.; Martínez-Belmonte, M.; Grushin, V. V. *Angew. Chem. Int. Ed*. **2011**, *50*, 7655.

35. Kaplan, P. T.; Loyd, J. A.; Chin, M. T.; Vicic, D. A. Beilstein *J. Org. Chem*. **2017**, *13*, 2297.

36. In THF, the compound decomposes less than 10% after 15 days stored in the glovebox at –30 ºC. At room temperature, **1Cu** decomposes around 18% overnight. However, attempts to isolate complex **1Cu** as solid failed.

37. For representative examples of high Cs···F contacts, see: a) Pollak, D.; Goddard, R.; Pörschke, K.-R. *J. Am. Chem. Soc*. **2016**, *138*, 9444. b) Carreras, L.; Rovira, L.; Vaquero, M.; Mon, I.; Martin, E.; Benet-Buchholz, J.; Vidal-Ferran, A. *RSC Adv.* **2017**, *7*, 32833.

38. Martínez-Salvador, S.; Falvello, L. R.; Martín, A.; Menjón, B. *Chem. Eur. J.* **2013**, *19*, 14540.

39. Bayler, A.; Schier, A.; Bowmaker, G. A.; Schmidbaur, H. *J. Am. Chem. Soc.* **1996**, *118*, 7006.

40. Schwerdtfeger, P. *Heteroat. Chem*. **2002**, *13*, 578.

41. Decomposition species were identified by ^{19}F NMR. This reductive elimination process is proposed to happen through a radical mechanism: Blaya, M; Bautista, D.; Gil-Rubio, J.; Vicente, J. *Organometallics* **2014**, *33*, 6358.

42. The results showed in this section have not been published yet and further studies are undergoing in our group.

43. Pérez-Temprano, M. H.; Casares, J. A.; de Lera, Á. R.; Álvarez, R.; Espinet P. *Angew. Chem. Int. Ed.* **2012**, *51*, 4917.

44. We selected analogous reaction conditions to those reported previously by Vicic and co-workers. See ref. 35 for further details.

45. Inspired by the work of Ribas *et al*. (Serra, J.; Parella, T.; Ribas, X. *Chem. Sci.* **2017**, *8*, 946), we tested the reaction of **1Au** with **4I** in DMF. Trace amount of the trifluoromethylated product was observed after heating the solution at 110 ºC after several days.

46. The yield for this product is lower than the reported in the literature. See ref. 31a.

47. Abeywickrema, A. N.; Beckwith, A. L. J. *J. Chem. Soc. Chem. Commun.* **1986**, 464.

48. Yu, D.-H.; Shao, J.-N.; He, R.-X.; Li, M. *Chin. Chem. Lett.* **2015**, *26*, 564.

49. Previous experimental and theoretical data for **1Ag** suggest no contribution of ion pairs in DMF. See Appendix chapter 2 for further details.

50. The displacement of I^- in this species has been proposed to occur by water in similar systems. See ref. 20.

51. Algarra, A. G.; Grushin, V. V.; Macgregor, S. A. *Organometallics* **2012**, *31*, 1467.

52. Besora, M.; Maseras, F. *Wiley Interdiscip. Rev.: Comput. Mol. Sci.* **2018**, *8*, e1372.

53. Regarding this scenario for silver, the reaction finishes after 12 years using the experimental concentration of the reagents.

54. The different yield of **2CF$_3$** in comparison with the one obtained in Scheme 5.27 or Scheme 5.37 can be explained by two main reasons: i) No stirring in the reaction media and ii) the presence of **1Ag** that could avoid the generation of $[Cu(CF_3)(I)]^-$ or $[(DMF)Cu(CF_3)]$.

55. We observed a variation in the chemical shift of $[Cu(CF_3)(I)]^-$ during the reaction, from –26.83 to –28.00 ppm, due to the formation of $[Cu(I)_2]^-$. This indicates a more complex scenario respect to the speciation of copper species as mentioned by Hu and co-workers (ref. 50) and the formation of species such as $\{[Cu(CF_3)(I)]_x\}^{x-}$ $\{[Cu(I)_2]_y\}^{y-}$.

56. Serra, J.; Parella, T.; Ribas, X. *Chem. Sci.* **2017**, *8*, 946.

57. Zhanga, H.; Huang, X.; *Adv. Synth. Catal.* **2016**, *358*, 3736.

58. Hooper, T. N.; Butts, C. P.; Green, M.; Haddow, M. F.; Mcgrady, J. E.; Russell, C. A. *Chem. Eur. J.* **2009**, *15*, 12196.

59. This multiplicity is in accordance with the previously-described in ref. 1a. In Chapter 1, the ^{13}C spectrum of **1Ag** (specifically labelled **6$_{NBu4}$** for being stabilized by NBu_4 cation) is described in detail.

60. Alvarez-Moreno, M.; de Graaf, C.; Lopez, N.; Maseras, F.; Poblet, J. M.; Bo, C. *J. Chem. Inf. Model*. **2015**, *55*, 95.

61. Zhao, Y.; Truhlar, D. G.; *Theor. Chem. Account.* **2008**, *120*, 215.

62. Gaussian 09, Revision D.01, Frisch, M. J.; Trucks, G. W.; Schlegel, H. B.; Scuseria, G. E.; Robb, M. A.; Cheeseman, J. R.; Scalmani, G.; Barone, V.; Mennucci, B.; Petersson, G. A.; Nakatsuji, H.; Caricato, M.; Li, X.; Hratchian, H. P.; Izmaylov, A. F.; Bloino, J.; Zheng, G.; Sonnenberg, J. L.; Hada, M.; Ehara, M.; Toyota, K.; Fukuda, R.; Hasegawa, J.; Ishida, M.; Nakajima, T.; Honda, Y.; Kitao, O.; Nakai, H.; Vreven, T.; Montgomery, Jr., J. A.; Peralta, J. E.; Ogliaro, F.; Bearpark, M.; Heyd, J. J.; Brothers, E.; Kudin, K. N.; Staroverov, V. N.; Keith, T.; Kobayashi, R.; Normand, J.; Raghavachari, K.; Rendell, A.; Burant, J. C.; Iyengar, S. S.; Tomasi, J.; Cossi, M.; Rega, N.; Millam, J. M.; Klene, M.; Knox, J. E.; Cross, J. B.; Bakken, V.; Adamo, C.; Jaramillo, J.; Gomperts, R.; Stratmann, R. E.; Yazyev, O.; Austin, A. J.; Cammi, R.; Pomelli, C.; Ochterski, J. W.; Martin, R. L.; Morokuma, K.; Zakrzewski, V. G.; Voth, G. A.; Salvador, P.; Dannenberg, J. J.; Dapprich, S.; Daniels, A. D.; Farkas, O.; Foresman, J. B.; Ortiz, J. V.; Cioslowski, J.; Fox, D. J. Gaussian, Inc., WallingfordCT, **2013**.

63. a) Dolg, M.; Wedig, U.; Stoll, H.; Preuss, H. *J. Chem. Phys.*, **1987**, *86*, 866; b) Andrae, D.; Haeussermann, U.; Dolg, M.; Stoll, H.; Preuss, H. *Theor. Chem. Accu.* **1990**, *77*, 123.

64. a) Hehre, W. J.; Ditchfield, R.; Pople, J. A. *J. Chem. Phys.* **1972**, *56*, 2257; b) Dill, J. D.; Pople, J. A. *J. Chem. Phys.* **1975**, *62*, 2921; c) Francl, M. M.; Petro, W. J.; Hehre, W. J.; Binkley, J. S.; Gordon, M. S.; DeFrees, D. J.; Pople, A. J. *J. Chem. Phys.* **1982**, *77*, 3654.

65. Marenich, S. A. V.; Cramer, C. J.; Truhlar, D. G. *J. Phys. Chem. B* **2009**, *113*, 6378.

66. Glendening, E. D.; Badenhoop, J. K.; Reed, A. E.; Carpenter, J. E.; Bohmann, J. A.; Morales, C. M.; Landis, C. R.; Weinhold, F. Theoretical Chemistry Institute, University of Wisconsin, Madison, WI, **2013**. http://nbo6.chem.wisc.edu/.

67. Hoops, S.; Sahle, S.; Gauges, R.; Lee, C.; Pahle, J.; Simus, N.; Singhal, M.; Xu, L.; Mendes, P.; Kummer, U. *Bioinformatics*, **2006**, *22*, 3067.

68. Bernal-Garcia, J. M.; Guzmas-Lopez, A.; Cabrales-Torres, A.; Estrada-Baltazar, A.; Iglesias-Silva, G. A. *J. Chem. Eng. Data*, **2008**, *53*, 1024.

69. Data collection with APEX II version v2013.4-1. Bruker (**2007**). Bruker AXS Inc., Madison, Wisconsin, USA.

70. Data reduction with Bruker SAINT version V8.30c. Bruker (**2007**). Bruker AXS Inc., Madison, Wisconsin, USA.

71. SADABS: V2014/5 Bruker (**2001**). Bruker AXS Inc., Madison, Wisconsin, USA. Blessing, *Acta Cryst.* (**1995**) A51 33-38.

72. TWINABS Version 2008/4 Bruker AXS; Blessing, *Acta Cryst.* (**1995**) A51 33.

73. Data collection and reduction with CrysAlisPro 1.171.39.12b (Rigaku OD, 2015).

74. Empirical absorption correction using spherical harmonics implemented in Scale3 Abspack scaling algorithm, CrysAlisPro 1.171.38.37f (Rigaku OD, **2015**).

75. SHELXT; G. M. Sheldrick, *Acta Cryst.* **2015** A71, 3.

76. SHELXle; C. B. Huebschle, G. M. Sheldrick, B. Dittrich, *J. Appl. Cryst.* **2011**, *44*, 1281.

77. SHELXL; Sheldrick, G. M. *Acta Cryst*. **2015** C71, 3. SHELXT.

CHAPTER 6. GENERAL CONCLUSIONS

The research presented in this Doctoral Thesis confirms the potential of coinage metals, namely silver and copper complexes, as reactive species in the context of C–C and C–N bond-forming reactions. The specific concluding remarks for each research chapter are the following:

Chapter 2. "*Unexpected cooperation in a bimetallic dual Rh/Cu catalytic system: DFT and microkinetic simulation as interrogating tools*". We clarified the mechanism for the Rh/Cu-catalyzed synthesis of isoquinolines by coupling of α-aryl vinyl azides and alkynes as a case study reaction of bimetallic dual catalysis in oxidative coupling. We demonstrated that evolution of concentrations through time is a valuable experimental observable to critically analyze a DFT-computed mechanism using microkinetic modeling. Thus, we proposed that the previously accepted mechanism of two independent cycles connected by a redox step is too simple and that a hetero-trinuclear species is likely to participate as catalyst for this transformation.

Chapter 3. "*New vistas in transmetalation with discrete Ag-CF_3 species: implications in Pd-mediated trifluoromethylation reactions*". We were able to design an efficient and unique [Cs][Ag(CF_3)$_2$] complex that circumvents unproductive transmetalation side reactions and allows the proof-of-concept $Pd^{0/II}$-catalyzed trifluoromethylation of aryl iodides for the first time. This work demonstrates the crucial role of the organometallic nucleophile in the success or failure of the coupling process and, therefore, the importance of the transmetalation step.

Chapter 4. "*Mechanistic studies on the transmetalation step in Pd/Ag bimetallic systems*". This study on the transmetalation reaction between aryl-Pd(II) complexes and trifluoromethyl silver(I) complexes reveals the remarkable influence of the ancillary ligand on the silver complex in the transmetalation mechanism and the complexity of their behavior in solution. We found that a common feature for these species is the conservation of the linear geometry of silver(I) complexes during the transmetalation and the generation of short-lived cationic palladium complexes stabilized by solvent molecules. As result of this investigation, we proposed a new chain mechanism for the transmetalation between palladium(II) and certain silver(I) complexes. This study not only demonstrates the common nature of the transmetalation step as a non-elementary step in Pd/Ag bimetallic systems but also highlights its complexity giving rise to the definition of new transmetalation reaction mechanisms.

Chapter 5. "*Exploring bis-(trifluoromethyl) coinage metallates landscape: a combined experimental and theoretical study*". We understood the different reactivity patterns of bis-(trifluoromethyl) coinage metallates towards different electrophiles. Moreover, in the context of

the trifluoromethylation of aryl halides, we demonstrated that bis-(trifluoromethyl) cuprates are active species in the incorporation of CF_3 moieties into organic scaffolds. Mechanistic studies, combining kinetic experiments, DFT calculations and microkinetic modeling, proved that these often overlooked ate-type cuprates play the role of CF_3^- reservoir and [(DMF)Cu(CF_3)] species is the most reactive intermediate in the $Cu^{I/III}$ scenario. This work reinforces the potential of using DFT calculation and microkinetic modeling as a mechanistic exploratory tool.

“A juí”

Eustaquio Mudarra Montero

UNIVERSITAT ROVIRA I VIRGILI
COINAGE COMPLEXES IN C-C AND C-N BOND-FORMING REACTIONS
Ángel Luis Mudarra Alonso